U.S. Department of Energy
Energy Efficiency and Renewable Energy
Bringing you a prosperous future where energy is clean, abundant, reliable, and affordable

AUTOMOTIVE LIGHTWEIGHTING MATERIALS

Less dependence on foreign oil, and eventual transition to an emissions-free, petroleum-free vehicle

FreedomCAR and Vehicle Technologies Program

2004 ANNUAL PROGRESS REPORT

21ST CENTURY TRUCK PARTNERSHIP

FreedomCAR & Fuel Partnership

U.S. Department of Energy
Office of Freedom Car and Vehicle Technologies
1000 Independence Avenue S.W.
Washington, DC 20585-0121

FY 2004

Progress Report for Automotive Lightweighting Materials

Energy Efficiency and Renewable Energy
FreedomCAR and Vehicle Technologies

Edward J. Wall
Program Manager, FreedomCAR and Vehicle Technologies

Rogelio Sullivan
Materials Technologies Team Leader

Joseph Carpenter
Technology Area Development Manager

April 2005

CONTENTS

1. INTRODUCTION 1

2. AUTOMOTIVE ALUMINUM R&D 7

A. Active Flexible Binder Control System for Robust Stamping 7
B. Warm Forming of Aluminum II 17
C. Electromagnetic Forming of Aluminum Sheet 31
D. Aluminum Automotive Closure Panel Corrosion Test Program 39
E. Development of the Infrared Thermal Forming Process for Production of Aluminum Vehicle Components 49

3. ADVANCED MATERIALS DEVELOPMENT 57

A. Low-Cost Powder Metallurgy Technology for Particle-Reinforced Titanium Automotive Components: Manufacturing Process Feasibility Study 57
B. Low-Cost Cast Aluminum Metal Matrix Composites 61
C. Structural Cast Magnesium Development 69
D. Magnesium Powertrain Cast Components 75
E. Low-Cost Titanium Evaluation 83
F. Structural Reliability of Lightweight Glazing Alternatives 87

4. POLYMER COMPOSITES R&D 95

A. Development of Manufacturing Methods for Fiber Preforms 95
B. Composite-Intensive Body Structure Development for Focal Project 3 103
C. High-Volume Processing of Composites 111
D. Development of Next-Generation Programmable Preforming Process 119

5. LOW-COST CARBON FIBER 125

A. Low-Cost Carbon Fibers from Renewable Resources 125
B. Low-Cost Carbon Fiber Development Program 133
C. Low-Cost Carbon Fiber Manufacturing Using Microwave Energy 143
D. Oxidative Stabilization of PAN Fiber Precursor 147

6. RECYCLING 153

A. Recycling Assessments and Planning 153
B. Baseline Assessment of Recycling Systems and Technology 157
C. Postshred Materials Recovery Technology Development and Demonstration 165
D. Development of Technology for Removal of PCBs and Other Substances of Concern (SOCs) from Shredder Residue 175
E. Compatibilization/Compounding Evaluation of Recovered Polymers 181

7. ENABLING TECHNOLOGIES 185

A. Durability of Carbon-Fiber Composites 185
B. Interphase Analysis and Control in Fiber-Reinforced Thermoplastic Composites 193
C. Low-Cost Test Methods for Advanced Automotive Composite Materials; Creep Compression Fixture 199
D. Intermediate-Rate Crush Response of Crash Energy Management Structures 205
E. Composite Crash Energy Management 211
F. Crash Analysis of Adhesively Bonded Structures (CAABS) 221
G. Long-Life Electrodes for Resistance Spot Welding of Aluminum Sheet Alloys and Coated High-Strength Steel Sheet (ORNL) 229
H. Long-Life Electrodes for Resistance Spot Welding of Aluminum Sheet Alloys and Coated High-Strength Steel Sheet (USAMP) 237
I. Plasma Arc Spot Welding of Lightweight Materials 245
J. Performance Evaluation and Durability Prediction of Dissimilar Material Hybrid Joints 247
K. Joining of Dissimilar Metals for Automotive Applications: From Process to Performance 255
L. Application of Thread-Forming Fasteners (TFFs) in Net-Shaped Holes 263
M. NDE Tools for the Evaluation of Laser-Welded Metals 267
N. NDE Inspection of Resistance Spot Welds in Automotive Structures Using an Ultrasonic Phased Array 277
O. Technical Cost Modeling 287

8. HIGH-STRENGTH STEELS 293

A. Evaluations of the Effects of Manufacturing Processes and In-Service Temperature Variations on the Properties of Transformation-Induced Plasticity (TRIP) Steels 293
B. High-Strength Steel Stamping Project 297
C. Strain Rate Characterization 301
D. Development of Advanced Tools for Energy Management 307
E. Lightweight Front Structures 315
F. Hydroform Materials and Lubricants Project 323
G. High-Strength Steel Joining Technologies Project 327
H. Sheet Steel Fatigue Characteristics 335
I. Tribology 339
J. Lightweight Closure Panels Project 343

Appendix A. ACRONYMS AND ABBREVIATIONS 347

1. INTRODUCTION

Automotive Lightweighting Materials R&D

As a major component of the U.S. Department of Energy's (DOE's) Office of FreedomCAR and Vehicle Technologies Program (FCVT), Automotive Lightweighting Materials (ALM) focuses on the development and validation of advanced materials and manufacturing technologies to significantly reduce automotive vehicle body and chassis weight without compromising other attributes such as safety, performance, recyclability, and cost.

The specific goals of ALM are to develop material and manufacturing technologies by 2010 that, if implemented in high volume, could cost-effectively reduce the weight of light-duty body and chassis systems by 50% with safety, performance, and recyclability comparable to 2002 vehicles.

ALM is pursuing five areas of research: cost reduction, manufacturability, design data and test methodologies, joining, and recycling and repair. The current Long-Range Plan for activities in these areas during the next 5 years is found at www.eere.enrgy.gov. Because the single greatest barrier to use of light-weight materials is their high cost, priority is given to activities aimed at reducing costs through development of new materials, forming technologies, and manufacturing processes. Priority lightweighting materials include advanced high-strength steels (AHSSs), aluminum, magnesium, titanium, and composites including metal-matrix materials and glass- and carbon-fiber-reinforced thermosets and thermoplastics. The inclusion of AHSSs is an example explaining the term "lightweighting" as opposed to just "lightweight" in order not to imply focus on just lower density materials.

Collaboration and Cooperation

ALM collaborates and cooperates extensively to identify and select its research and development (R&D) activities and to leverage those activities with others. The primary interfaces have been and still are with the Big Three domestic automotive manufacturers, namely the FreedomCAR Materials Technical Team, the Automotive Composites Consortium (ACC), and the United States Automotive Materials Partnership (USAMP). This collaboration provides the means to determine critical needs, to identify technical barriers, and to select and prioritize projects. Other prominent partners include such organizations as the American Iron and Steel Institute, the American Plastics Council, the Vehicle Recycling Partnership, and the International Magnesium Association. ALM also coordinates its R&D activities with entities of other U.S. and Canadian federal agencies. Interactions with the DOE Office of Industrial Technologies Program (ITP), FCVT's High-Strength Weight Reduction (HSWR) Materials effort, and the Department of Natural Resources of Canada (NRCAN) are especially important by virtue of overlaps of interests in lightweight materials. Contacts with similar efforts in other countries besides Canada are being pursued. Joint planning was done in FY 2004 with the U.S. National Science Foundation, and one project was jointly funded with the DOE Office of Science.

Project Selection and Stages

In cooperation with USAMP and the FreedomCAR Materials Technical Team, a procedure has been established to help facilitate the development of projects in order to help move high-risk leveraged research to targeted research projects that eventually migrate to the original equipment manufacturers (OEMs) or suppliers as application engineering projects. Technology research projects are assigned to one of three phases as depicted in the figure on the next page: concept feasibility, technical feasibility, and demonstrated feasibility. Projects are guided to meet the requirements of each phase before they are allowed to move on to the next phase. Definitions of the phases follow:

Concept Feasibility: Concept feasibility projects should contain a specific idea to address a need or to create something new. Projects are usually exploratory, small in monetary requirements, and short in length. Projects should provide a yes/no answer to the value of the idea. All projects are required to have a detailed research plan, budget, and timing. These projects are typically less than $200,000 and have a duration of 1–2 years. They can be ended before proceeding to technical feasibility if there is a lack of technical progress or if the preliminary business case turns out to be unfavorable. Successful concept feasibility projects can develop into technical feasibility projects.

Technical Feasibility: Technical feasibility projects should continue R&D for ideas with proven merit or potential. These projects should identify the key barriers to implementing the technology and focus on overcoming them. Technical feasibility projects should have well-defined OEM/industry supplier participation and pull. They are usually larger, longer term projects than the concept feasibility projects with typical research investment in the $1M to $2M range and length of 2–3 years. Technical feasibility projects can be ended before proceeding to demonstrated feasibility if there is a failure to overcome the key barriers to implementation or if the cost or business case does not develop as favorably as initially assessed.

Demonstrated Feasibility: Technology projects that need larger scale validation may become demonstrated feasibility projects. Not all technical feasibility projects will need a demonstration or validation program. These projects are few in number, much larger in scale, and may involve component or system fabrication and test. Support and leverage from the OEMs/industry is a key requirement for these projects.

Stage progression for project selection

Once selected, R&D projects are pursued through a variety of mechanisms, including cooperative research and development agreements (CRADAs), cooperative agreements, university grants, R&D subcontracts, and directed research. This flexibility allows the program to select the most appropriate partners to perform critical tasks. The ALM efforts are conducted in partnership with automobile manufacturers, materials suppliers, national laboratories, universities, and other nonprofit technology organizations. These interactions provide a direct route for implementing newly developed materials and technologies. Laboratories include Argonne National Laboratory (ANL), Lawrence Berkeley National Laboratory (LBNL), Lawrence Livermore National Laboratory (LLNL), Los Alamos National Laboratory (LANL), Oak Ridge National Laboratory (ORNL), Pacific Northwest National Laboratory (PNNL), and Sandia National Laboratories (SNL). PNNL manages the Northwest Alliance for Transportation Technologies, drawing on expertise and developments in the Northwest. ANL oversees recycling efforts and ORNL provides overall technical support and coordination, including for the DOE cooperative agreement with USAMP. The National Engineering Technology Laboratory (NETL) provides overall projects management.

Research areas and responsible organizations

Coordinated area	Organization
Production and fabrication of aluminum	HSWR, ITP, Natural Resources of Canada (NRCAN)
Production and fabrication of magnesium	International Magnesium Association, NRCAN, HSWR
Recycling, reuse, repair of automotive parts and materials	Vehicle Recycling Partnership, American Plastics Council
Fabrication of steel and cast iron	American Iron and Steel Institute, the Auto/Steel Partnership, HSWR
Fundamental materials research	DOE Office of Science, National Science Foundation
High-volume composite processing	Department of Commerce—National Institute of Standards and Technology's Advanced Technology Program
Materials research for defense applications	Department of Defense
Materials research for space applications	National Aeronautics and Space Administration
Crashworthiness	Department of Transportation
International vehicle material R&D	International Energy Agency
Production and fabrication of composites	American Plastics Council

FY 2004 Accomplishments

Recyclability is one of the five major R&D areas for the ALM. Recyclability of end-of-life vehicles (ELV) is presently limited by the lack of commercially proven technical capabilities to cost-effectively separate, identify, and sort materials and components and by the lack of profitable post-use markets. The automobile of the future will use significantly greater amounts of lightweight materials (e.g., advanced high-strength steels, aluminum, magnesium, plastics, and both metal- and polymer-based composites) and more sophisticated/
complex components (e.g., fuel cells). Researchers at ANL, in collaboration with the Vehicle Recycling Partnership and technology developers, are working to develop and demonstrate technology for the cost-effect recovery of materials from post-shred residues. A pilot plant for the processing of raw shredder residue was completed in early 2004. Various recovery technologies are being evaluated to determine the performance (e.g., yield, purity, efficiency and cost) so that an optimized and integrated process for recovering materials from shredder residue can be developed. In related projects, ANL is demonstrating the feasibility of materials recovery for reuse in automotive and other applications, chemical conversion of residue to fuels and chemicals, and energy recovery.

Magnesium is the lowest density structural metal, 30% less dense than aluminum. Magnesium components are envisioned to replace an equivalent volume of ferrous material with a mass reduction of 70–75% and aluminum with a reduction of 25–35%. Significant progress was shown by a USAMP team working on a project to demonstrate and enhance the feasibility and benefits of using magnesium alloys in place of aluminum in structural powertrain components. During 2004, the team has made excellent progress. Project accomplishments include the development and distribution of a comprehensive engineering property database for the high-temperature, creep-resistant magnesium alloys identified for use in the project; the selection of the appropriate alloys for the magnesium-intensive engine components (engine block, structural oil pan, and front engine cover); completion of the design and cost model to predict the cost-effective performance of the engine; and the selection and initiation of basic research projects to develop the understanding to fully implement magnesium alloys in powertrain applications.

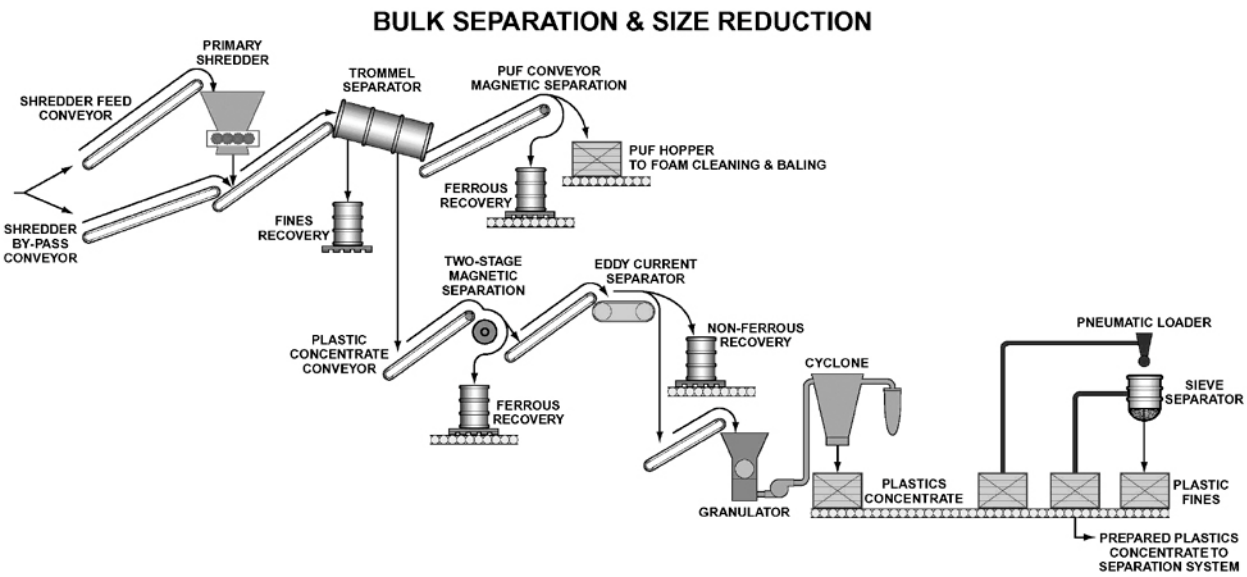

Schematic of the Argonne Pilot Mechanical Separation System for processing raw shredder residue.

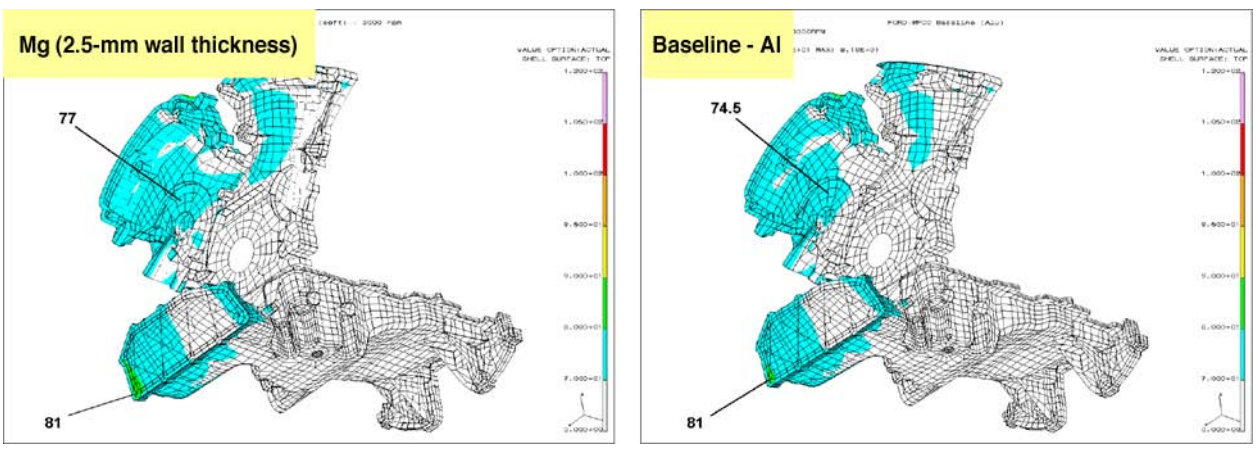

NVH (noise-vibration-harshness) analysis of the structural oil pan and front engine cover for octave band 250 Hz at 3000 rpm, comparing the soft magnesium design with the aluminum baseline.

Aluminum metal matrix composites (MMCs) possess both lightweight and high wear-resistance characteristics, making them desirable for a number of body, chassis, and powertrain applications, provided that performance and cost objectives can be reached. However, several barriers, including cost, durability, and manufacturability, have hindered the widespread use of these materials. With the overall goal of demonstrating cost-competitive aluminum MMC options for structural and powertrain components in general, PNNL, in collaboration with MC-21, USCAR, Visteon and others, focused efforts on a brake rotor as a target application. A lightweight rotor that is 60% lighter than a conventional four-door luxury sedan cast iron rotor was designed and manufactured. Initial phases of the project developed a lower cost material and a low-cost process for producing it. The thermal and structural properties of the new material were evaluated and found to be acceptable. More recently, a low cost manufacturing process was selected, and prototype full-scale, fully reinforced brake rotors were produced and dyno tested. The rotor performance meets the braking

requirements, with some future work still needed on friction materials to minimize noise and extend pad life. Work is ongoing to evaluate machining and tool life. The cost of the prototype rotor is estimated to be 1.5 times the cost of a cast iron rotor, compared to a figure of three times for prior aluminum MMC rotors.

Carbon-fiber-reinforced polymer-matrix composites (CFRPMCs) offer the potential to reduce vehicle weight by 50%. However, cost is a significant barrier to future implementation. Oxidative stabilization of polyacrylonitrile (PAN) precursor is a slow thermal process that typically consumes 70% or more of the processing time in a conventional carbon-fiber conversion line. ORNL is working on a rapid oxidation process that could dramatically increase the conversion line throughput and appreciably lower the fiber cost. They have demonstrated the ability, in atmospheric pressure plasma, to oxidize fiber in stages equivalent to conventional oxidation furnaces, identified key process parameters, modified the reactor to achieve stable operation, and identified the preferred range of feed gas compositions. Preliminary data suggest that the plasma oxidation process may allow earlier onset of carbonization, thus reducing oxidation residence even further. Early economic studies support the value of the research in reducing cost. Continued efforts will focus on continuous plasma processing of multitow precursors and characterization of fiber properties.

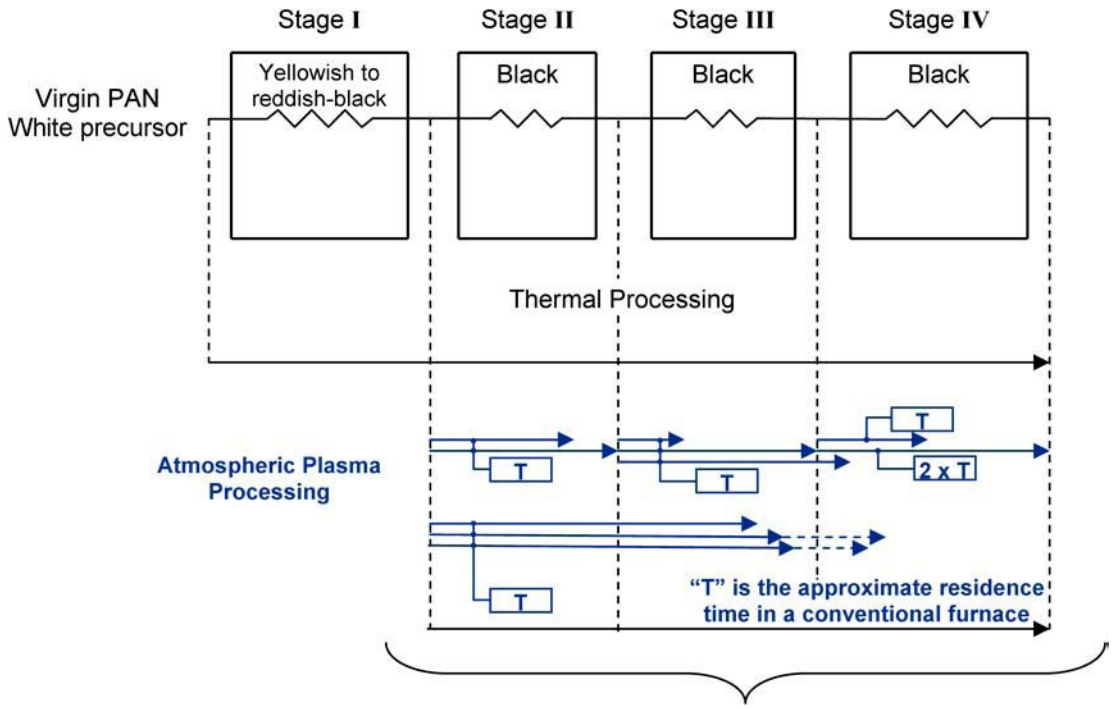

Schematic of conventional thermal oxidation process and progress in plasma oxidation process.

In addition to mass reduction, design optimization, high-volume manufacturing, and recycling, two key issues that need to be addressed are joining and crash energy management. ORNL is working to develop a comprehensive experimental and analytical methodology to analyze and design adhesively bonded automotive composite structures to sustain axial, off-axis, and lateral crash loads. The focus of the project is to develop the understanding of how critical joint design parameters affect the energy absorption. Significant progress has been made in characterizing the static response of bulk adhesive and braided carbon fiber substrates. In addition, preliminary dynamic stability tests on both bonded and unbonded tubes have been completed using the Test Machine for Automotive Crashworthiness (TMAC). The experimental results will be correlated with analytical results by developing finite-element-based tools with appropriate material models and progressive damage algorithms. The results of this project will be closely integrated with the experimental and analytical efforts undertaken by USCAR's Automotive Composites Consortium (ACC).

Future Direction

In FY 2002 and FY 2003, the FreedomCAR and Fuels Initiative formed from the 1994–2001 Partnership for a New Generation of Vehicles (PNGV) and thinking and planning on what replaces the ALM efforts that began in the PNGV in roughly 1999–2002, has continued since. The ALM and the FreedomCAR Materials Technical Team conducted a series of strategic reviews of various materials and manufacturing topics in FY 2004. Based on those reviews, CFRPMCs and magnesium will certainly be emphasized in the next few years as they have the greatest weight-reduction potential, but there will be some efforts on AHSSs, titanium, and metal–matrix composites because these will contribute in niche roles to the overall FreedomCAR weight-reduction and cost neutrality goals. Material-crosscutting work in general manufacturing will continue to increase in joining, nondestructive evaluation, and recycling. Though technical feasibility projects will dominate as before, base-technology, concept-feasibility and demonstrated-feasibility projects will also be pursued.

2. AUTOMOTIVE ALUMINUM R&D

A. Active Flexible Binder Control System for Robust Stamping

Principal Investigator: Tom Balun
Ford Motor Company
Vehicle Operations General Office
C290, 17000 Oakwood Blvd.
Dearborn, MI 48121
Phone: (313) 322-4951; fax: (313) 845-2647; email: tbalun@ford.com

Technology Area Development Manager: Joseph A. Carpenter
(202) 586-1022; fax: (202) 586-1600; e-mail: joseph.carpenter@ee.doe.gov
Field Technical Manager: Philip S. Sklad
(865) 574-5069; fax: (865) 576-4963; e-mail: skladps@ornl.gov

---

Contractor: U.S. Automotive Materials Partnership
Contract No.: FC26-02OR22910

Objective

- Build an advanced closed-loop flexible binder control system for installation in mechanical presses to actively control the sheet metal stamping process.
- Develop computer simulation with process optimization to predict blank holder force trajectories for each cylinder during the press cycle.
- Demonstrate that the system will improve quality, reduce variability, and maintain accuracy of stampings made from aluminum alloys and advanced high-strength steels.
- Demonstrate the economic feasibility of the system by showing that it will reduce time for tryouts and saves money on fine-tuning (welding/grinding), spotting, and setting of production tools.

Approach

- Apply binder control technology to mechanical presses.
- Build a new ten-cylinder flexible binder control unit with a closed-loop control system and pan tooling.
- Retrofit the 26-cylinder Erie flexible binder control unit with a nonlinear control system and liftgate tooling.
- Conduct open-loop control demonstration of the retrofit unit with the GM liftgate.
- Develop methodology and guidelines for designing and building flexible binders.
- Develop computer simulation and process optimization capabilities for flexible binders.
- Develop a closed-loop flexible binder control system with appropriate sensors.
- Demonstrate closed-loop control of the ten-cylinder flexible binder system.
- Evaluate technical and economic feasibility of flexible binder technology.

Accomplishments

- Completed retrofitting of the Erie Flexible Binder Control Unit with the appropriate real-time control system to achieve hydraulic pressure control in all of the 26 cylinders in a mechanical press. Retrofitting includes open- and closed-loop simulation studies, hydraulic reconfiguration, integration of dSPACE real-time control system with the binder control unit, electrical reconfiguration, verification of reconfigured electrical and hydraulic systems, and experimental implementation of pressure control for all 26 cylinders.
- Tested the electro-hydraulic/mechatronic system on the Erie Press Flexible Binder Unit and demonstrated closed-loop pressure control in multiple cylinders with different pressure trajectories. These tests were conducted without the binder or die installed.
- Conducted tryouts on the retrofitted Erie unit with the GM liftgate using bake hardenable steel (BH210), dual phase (DP500), and aluminum (A6111-T4). The control system hardware and software performed as desired.
- Successfully stamped BH210 steel liftgate part within about 8 hours of tryout, which included blank alteration, code modification, and conducting tests to determine that the upper was impacting the cushion before the binder. This is compared to an estimated 7 days needed for tryout using conventional methods.
- Built a new ten-cylinder flexible binder control system with special valves and controls for use in a mechanical press and set up for testing at the University of Stuttgart (IFU) in Germany. The associated tooling is based on a die design that included many features of automotive stampings (IFU pan). The unit has a feedback controller with three types of sensors and a touch screen to control pressure profiles in individual cylinders. The unit will be shipped to Detroit for tests and demonstration after functionality tests are completed at IFU.
- Used adaptive simulation and optimization methods, coupled with finite-element method (FEM) simulation, to predict optimum constant and variable blank holder force (BHF) trajectories in single and multicushion systems to reduce thinning and springback in the IFU pan, a fuel tank shield, an S-rail, and a General Motors (GM) rail. Simulation results showed that optimized BHF trajectories can reduce thinning and springback in the analyzed parts. Experiments were conducted to verify the predicted optimum BHF trajectories.
- Variable BHF trajectories improved the formability of conical cup drawing by about 9% compared with constant BHF trajectories. Adaptive simulation results can be used as an initial guess for optimization in reducing the number of iterative simulation runs and computation time.
- Developed procedure for modeling flexible binder in stamping simulation and updated optimization code to predict BHF for multipoint cushion systems.
- Determined that flexible binder simulation resulted in more uniform pressure distribution in the blank, resulting in more thinning and less draw-in and wrinkling compared to rigid binder.
- Established that optimum variable binder force (variable in space, constant in time) resulted in uniform reduction in thinning by 2% to 3%.

Future Direction

- Set up and conduct trials on the new IFU flexible binder control system to determine the benefits of using flexible binder control systems in improving part quality and consistency in automotive stampings.
- Run variable BHF in space and time using the sequential optimization technique for the IFU Pan and GM liftgate.
- Ensure that OEMs and suppliers will check and verify Ohio State University (OSU) results. Develop a mechanism to transfer technology from OSU to project team.
- Use optimized trajectories in stamping tryouts of the IFU pan and the GM liftgate with BH210, DP500, A6111-T4 and A5182-O.
- Determine that due to the difficulty in forming A6111-T4, it appears that finite-element analysis (FEA) simulation results would be critical in determining the required multicylinder BHF trajectories.

- Develop a Graphical User Interface (GUI) to download optimized trajectories obtained from FEA simulations to the real-time control system.

Participants

• Ford Motor Company	Lead project and determine its direction and benefits
• General Motors	Co-lead project and determine its direction and benefits
• DaimlerChrysler	Co-lead project and determine its direction and benefits
• U.S. Steel	Provide steels and technical support
• Rouge Steel	Provide steels and technical support
• ALCOA	Provide aluminum and technical support
• Pathway Technologies	Retrofit binder control unit and install control system
• Ohio State University	Provide simulation and optimization expertise
• University of Stuttgart	Build and ship new flexible binder unit to project
• NIST	Support forming and friction activities
• Troy Design & Manufacturing	Set up tooling and provide equipment for tryouts
• Erie Press Systems	Transfer binder control unit to project
• FormSys	Provide project administration and technical support
• Auto/Steel Partnership	Provide material and technical support

---

Introduction

Significant weight saving can be achieved by replacing parts made from mild steel with those made from lightweight materials (aluminum and magnesium alloys) and high specific strength materials (ultra high-strength and stainless steels). Such materials are less formable than mild steel and parts made from them lack dimensional control because of the significant amount of springback that they produce after forming.

Traditional stamping leaves no flexibility in the stamping process for using difficult-to-form materials and for responding to process variations (lubrication, material, die wear, blank placement) that can lead to stamping inconsistencies or even failure. It has been found that failure by wrinkling or tearing is highly dependent on the magnitude and trajectory of the binder force. Recently, dynamic variation of the binder force during the forming stroke has been shown to affect formability, strain distribution and springback. Optimal forming trajectories can be obtained under constant and variable binder force conditions, but there is no guarantee that process variables will remain constant during the stamping process. Specifying a binder force trajectory is not easy because the part shape changes during forming. Also, stresses in the part cannot be determined because the coefficient of friction is not a controllable quantity and it varies from location to location. Therefore, the forming process must be controlled, and a closed-loop system with an appropriate local control parameter (friction, draw-in) must be used to track a predetermined optimum control parameter trajectory.

The project uses flexible binder control technology in conjunction with innovative tool designs and closed-loop control to produce robust processes for stamping aluminum and high-strength steel automotive panels. The focus of this project is to implement binder and closed-loop process control in the stamping industry to increase the robustness of the forming process. This technology will use computer simulation and process optimization to predict optimum binder force trajectories that can be entered into programmable hydraulic cushions to control binder actions in mechanical and hydraulic presses.

Task 1: Conduct Open-Loop Control Demonstration of Flexible Binder Control Technology

A two-path approach is adopted to complete this task. The first one is to retrofit the existing Erie Unit with the appropriate real-time control system to achieve hydraulic pressure control in all of the 26 cylinders in a mechanical press environment. The second approach is to have the University of Stuttgart (IFU) build a more robust and smaller unit with only ten cylinders to accommodate a generic tool that captures the main features of industrial stampings.

1. Retrofitting the Erie Unit

Retrofitting the Erie Unit, shown in Figure 1, included the following:

- open and closed-loop simulation studies
- hydraulic reconfiguration,
- integration of the dSPACE real-time system with the binder control unit,
- electrical reconfiguration of the unit,
- verification of reconfigured electrical and hydraulic systems,
- demonstration of pressure control for all 26 cylinders. The unit was used, as previously planned, in conjunction with the liftgate tooling (Figure 2).

Figure 1. Erie binder control unit.

Figure 2. GM liftgate tooling.

Multicylinder Pressure Control Tests

A series of tests were conducted at Troy Design and Manufacturing (TDM) to demonstrate that pressure control can be achieved in multiple cylinders simultaneously using the nonlinear control algorithm developed during the course of this project and validated in single-cylinder tests. The controller parameters were tuned using data from open-loop tests and simulation studies. Low pass filters were digitally implemented to attenuate the sensor noise, and the system achieved stable pressure trajectory tracking (Figure 3).

The figure shows that multicylinder pressure trajectory tracking was achieved by using the nonlinear control algorithm in conjunction with a set of digital filters. The controller was able to deal with flow interaction between the cylinders.

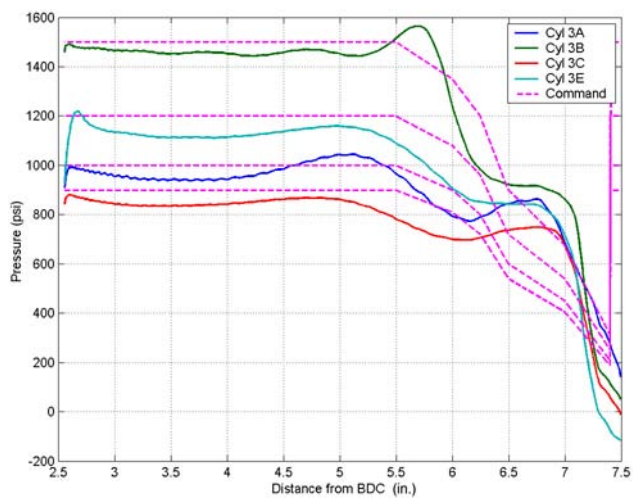

Figure 3. Stable pressure trajectory tracking with digital filtering for multicylinder system.

Tryouts

After achieving multicylinder pressure control with the system hardware and software, tryout tests of the control unit and liftgate die in the press were conducted at TDM. Figure 4 shows the unit and tooling installed in the press.

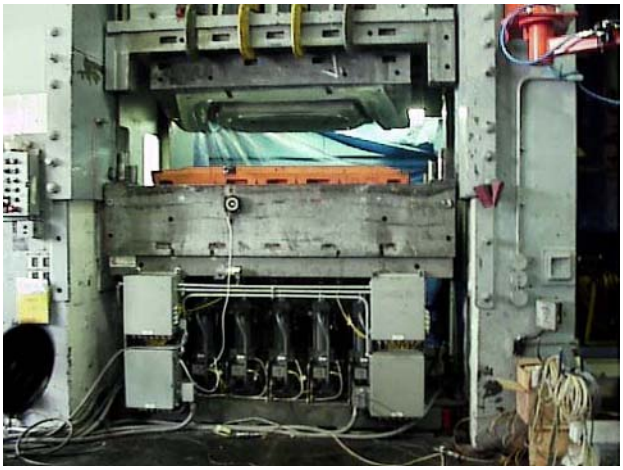

Figure 4. Flexible binder unit in press with tooling installed.

Following a complete system test with the tooling mounted, a number of tryouts were conducted on the GM liftgate using three sheet materials: bake hardenable steel (BH210), dual-phase steel (DP500), and aluminum alloy (A6111-T4).

Results of the tests are summarized:

- The BH part, shown in Figure 5, was successfully stamped within 8 hours of tryout, which included blank alteration, code modification, and conducting tests to determine that the upper was impacting the cushion before the binder. The current tryout period is extremely short compared to an estimated 7 days needed when using conventional tryout methods.
- Stamping of A6111-T4 proved to be difficult. A couple of defects were corrected, but a more structured tryout using finite-element analysis (FEA) simulation results would be required to successfully make the part.

2. Building a New IFU Unit

IFU collaborated with two prominent industrial suppliers in Germany, HYDAC and MOOG, to build the hydraulic and control systems for the binder control unit shown in Figure 6.

The IFU unit has state-of-the-art cylinders, valves, and controls. It accommodates three types of sensors for use in closed-loop control of the binder in a mechanical press environment. The closed-loop control system, shown in Figure 7, will automatically ensure that the desired binder forces are applied to the part by an electro-hydraulic actuation system during the forming process. The system will compensate for minor disturbances in the forming system caused by friction variation, inconsistent material properties, sheet thickness variation, die alignment problems, ram tilt, tool wear, blank placement, and press table deflection.

Feedback measurements are used to modulate the binder force in real-time to keep optimum binder force trajectories for each cylinder in the control

Figure 5. Successfully formed BH210 steel liftgate inner after tonnage adjustment.

Figure 6. IFU flexible binder control unit.

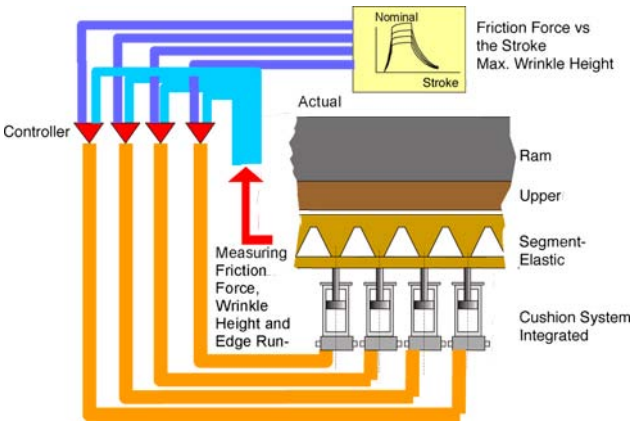

Figure 7. Closed-loop control system.

unit on target. The difference between the input signal and the output response is fed to the controller to reduce the error and bring the output of the process to a desired value. One of the control strategies that can be used would have the following scenario:

- Finite-element method (FEM) produces an optimum material flow/friction trajectory.
- Sensor measures actual material flow/friction.
- Controller manipulates binder to achieve material flow/friction compliance.

Success of the closed-loop control system in the IFU unit will also complete the objectives of Task 4. User interface with the system is accomplished through a touch screen where individual cylinder pressure can be selected.

The IFU unit is equipped and instrumented with a large collection of advanced features: 10 specially designed hydraulic cylinders, 12 proportional valves, 2 encoders for cushion position, 1 encoder for ram position; 4 punch force sensors, 1 wrinkle height sensor, 1 flow in sensor, and 1 friction sensor.

The IFU unit accommodates a generic tool, shown in Figure 8, which captures the main features of industrial stampings.

The test plan at IFU and at the press shop in Stuttgart includes the following:

- Track at least four pressure profiles (constant, ramp-up, ramp-down, and variable).
- Assess characteristics of the friction, draw-in, and wrinkle height sensors.

Figure 8. IFU pan.

- Test the stability of the closed-loop system.
- Optimize pin forces and trajectories for the part.
- Evaluate formed panels (dimensional quality, strain distribution, and surface quality).
- Assess costs to build a flexible binder control system.

The following sheet materials will be tested in Stuttgart and Detroit:

- Aluminum A5182-O, 1.0 mm
- Aluminum A6111-T4, 1.0 mm
- BH210 Steel, 0.8 mm
- DP500, 0.8 mm

After testing the IFU unit in Germany, the following steps are planned:

- Shipment of the die to Detroit. The modified system will be shipped to Detroit only after it has been thoroughly tested in Stuttgart and approved for transportation by a project delegate(s) who will review test results and arrange for shipping the unit to Detroit.
- Setting up and testing the die in the Detroit area in a mechanical press with support of IFU engineers.
- Demonstrate the functionality of the die with open- and closed-loop circuit control. The test plan in Detroit is similar to the test plan in Stuttgart. The experience of the previous tests in Stuttgart will be used for the tests in Detroit.
- Shipment of the die back to Stuttgart, Q205.

Task 2: Develop Computer Simulation and Process Optimization Capabilities for Flexible Binders

The blank holder (BH) applies appropriate restraining force on the sheet metal blank to suppress wrinkles and eliminate splits during forming. Many studies have shown that variable blank holder force (BHF) profiles increase the formability of stamped parts. In this task, Adaptive Simulation (AS) and Optimization (OPT) methods, coupled with FEM simulation, were developed and used to predict optimum, constant and variable BHF trajectories in single and multipoint cushion systems to reduce thinning and springback in the IFU part, the fuel tank shield, the S-rail and the General Motors (GM) structural rail.

Single-point cushions represent the traditional way of applying a constant or variable BHF on a rigid binder. Multipoint cushions represent flexible binders where a variable binder force in space/and or in time is applied to a segmented elastic BH. Differences in modeling the rigid and segmented elastic BH are shown in Figure 9.

Optimization code was updated to determine the BHF that varies in space using the segmented elastic BH for the IFU die. The segmented elastic BH was modeled as an elastic object in the finite-element (FE) simulation of the forming process to account for the deflection of the BH.

The AS technique requires only one simulation run to result in a "feasible" variable BHF profile, whereas the OPT needs many more iterative simulation runs to result in an "optimum" variable BHF profile. In this study, the resultant BHF profile from the AS was applied as an initial guess for the OPT. This resulted in reduced number of iterative simulation runs, which decreased the total computation time.

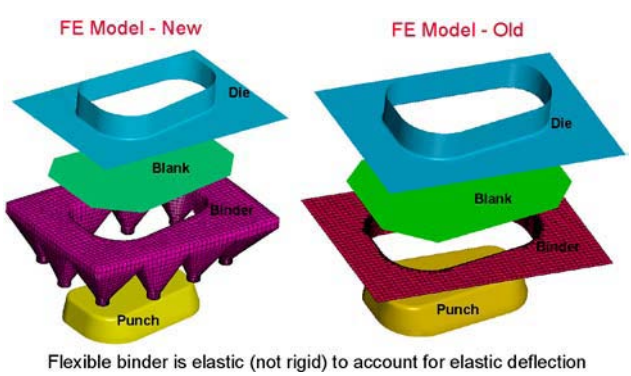

Figure 9. FEM models for rigid (old) and segmented elastic (new) BHs.

Single-Point Cushion Applications

Optimum constant and variable BHF were predicted using OPT and AS techniques for single-point cushion applications on the IFU pan, the fuel tank shield, the S-rail, and the GM structural rail.

Comparison of thinning distribution predicted by FE simulation for 0.92-mm A6111-T4 using three different BHF trajectories obtained from OPT and AS for the S-rail part at a depth of 30 mm is shown in Figure 10.

Figure 10 shows that using variable BHF from AS or OPT results in a decrease in maximum thinning from 34% to about 17% compared to the constant optimum BHF.

Figure 11 shows the BHF predicted by adaptive simulation with and without springback control.

Major conclusions drawn from applying predicted optimum constant and variable BHF using OPT and AS technique for single-point cushion applications on the IFU pan, the fuel tank shield, the S-rail and the GM structural rail are summarized:

- IFU pan—Thinning decreased by 3% for variable BHF from AS compared to optimum constant for materials A5182-O and A6111-T4.
- S-rail—Variable BHF predicted by AS reduced thinning from 34% to 17% compared to optimum constant BF. Springback was reduced ~50% by using variable BHF obtained with

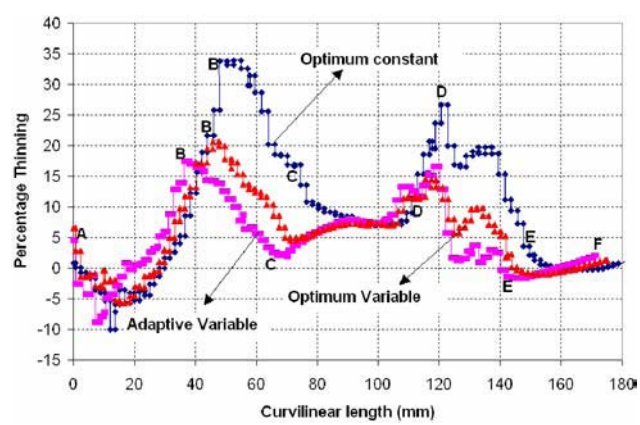

Figure 10. Thinning distribution predicted by AS and OPT for the S-rail.

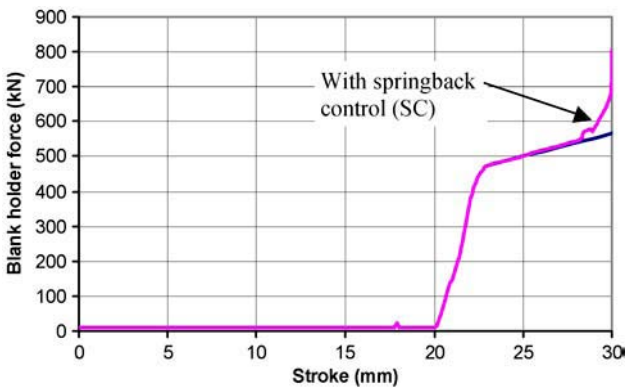

Figure 11. BHF with and without springback control.

springback control compared to variable BHF obtained without springback control.

- Fuel Tank Shield—Thinning decreased from 32% to 30% for variable BHF from AS compared to optimum constant.
- GM Structural Rail—Optimum variable BHF that minimized springback in the part reduced springback by 50% throughout the entire part compared to the variable optimum BHF profile that minimized thinning in the part.

Multipoint Cushion Application

A multipoint cushion system (flexible binder) is used to draw the IFU part. An FE model of the tool is shown in the left side of Figure 9. Materials used for the IFU part are 1.15-mm A5182-O and 1.0-mm-thick A6111-T4.

The IFU flexible binder die has ten independently controlled hydraulic cylinders to apply the BHF during forming. The location of the ten cylinders/cushion pins is shown in Figure 12.

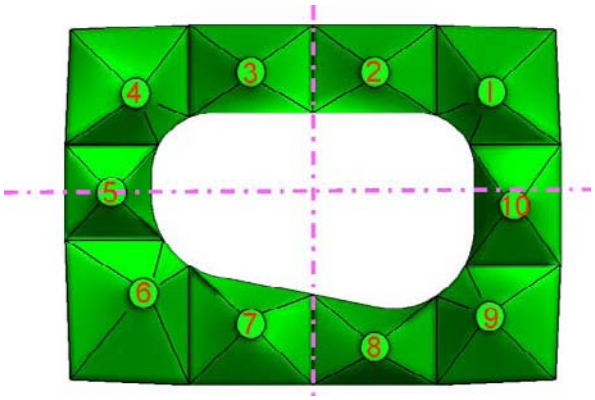

Figure 12. Location of the ten cushion pins in the IFU binder.

IFU pans from A5182-O were drawn to a depth of 75 mm, and those made from A6111-T4 were drawn to a depth of 60 mm to reduce thinning in the part.

Figure 13 shows a comparison between the optimum constant BHF and the optimum variable BHF (in space and constant in stroke) used in FEM simulation to assess thinning in the drawn IFU pan.

Thinning distribution obtained from FE simulations along two sections (Sections XX and YY, Figure 14) were compared for the constant optimum pin force in all the pins and constant optimum for individual pins.

A comparison of thinning distribution obtained for optimum constant pin force (constant in space and time) and optimum constant pin force in individual pins (variable in space and constant time) along section YY for the AA6111-T4 material is shown in Figure 15.

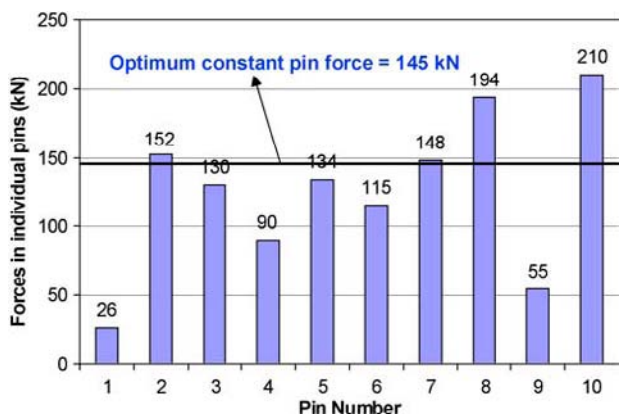

Figure 13. Optimum constant and variable.

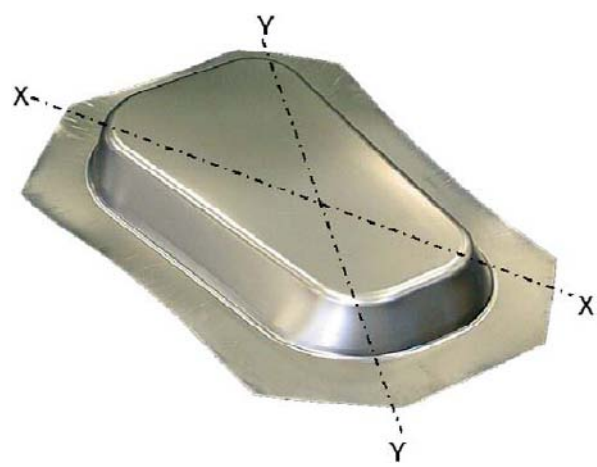

Figure 14. Sections along the IFU part used for thinning distribution comparisons.

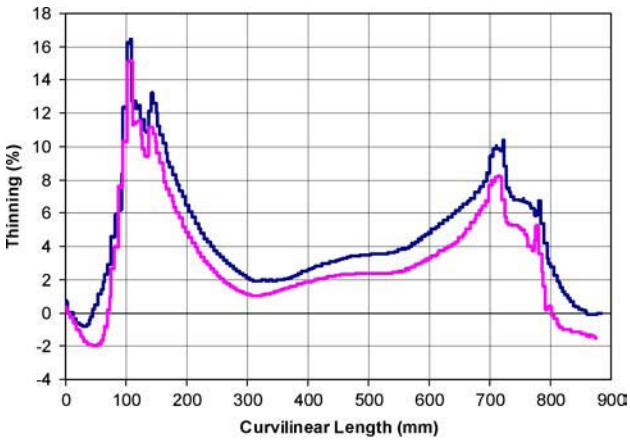

Figure 15. Thinning distributions predicted by FE simulation and optimization along section AA.

Figure 15 shows that by optimizing individual pin forces, maximum thinning in the part was reduced from 17% to 13%, thereby enhancing the drawability of the part.

Major conclusions from the IFU pan flexible binder simulation are summarized:

- Flexible binder resulted in more uniform pressure distribution in the blank, resulting in more thinning and less draw-in and wrinkling compared to the rigid binder.
- Flexible binder deforms elastically during forming simulation and remains in uniform contact with the nonuniform sheet thickness, thereby producing uniform contact pressure due to the applied BHF. Rigid binder, however, is in contact with the sheet at relatively thicker locations, thereby exerting a nonuniform pressure distribution due to the applied BHF.
- Thinning reductions from 17% to 13% were obtained by varying the forces in each pin (BHF varying in space and constant time) compared to the constant force in all the pins (BHF constant in time and space) for parts drawn from A6111-T4 to a depth of 60 mm. Reductions from 21% to 16% were observed for parts drawn from AA5182-O to a depth of 75 mm.

Summary

Highlights of the progress during FY 2004 follow:

- Retrofitted the 26-cylinder Erie Binder Control Unit by fixing its open-loop control and hydraulic problems. The Unit was successfully used in tryouts at TDM, and the control system hardware and software were shown to perform as desired.
- Built a new ten-cylinder IFU Binder Control Unit with closed-loop control and pan tooling.
- The electro-hydraulic/mechatronic system on the retrofitted Erie Press Flexible Binder Unit was tested, and closed-loop pressure control was demonstrated in multiple cylinders with different pressure trajectories. These tests were conducted without the binder or die installed.
- The system was tested with tooling installed, and synchronization algorithms to raise (and lower) the binder and inner cushion were validated as part of the control strategy.
- Actual tryouts for a liftgate inner were conducted with the unit using steel (BH210 and DP500) and aluminum A6111-T4.
- The steel (BH210) part was successfully made within about 8 hours of tryout (blank alteration, code modification, and conducting tests to determine that the upper was impacting the cushion before the binder) as compared to an estimated 7 days using conventional tryout methods.
- Initial attempts at stamping DP500 and A6111 proved to be difficult. A couple of defects were corrected, but a more structured tryout using FEA simulation results would be required to successfully make the parts.
- A few final mechanical modifications and hydraulic repairs need to be made before proceeding with tryout using A6111 and DP500.
- Current work involves addressing the mechanical issues, repairing and installing the missing cylinder, and designing a GUI to download trajectories obtained from FEA simulations to the real-time control system.
- AS and OPT programs to predict optimum constant and variable BHF profiles have been developed and successfully implemented on many parts (cylindrical cup, rectangular pan, IFU pan, S-rail, fuel tank shield, and structural rail).
- Procedure for modeling flexible binder in stamping simulation has been developed.
- OPT code was updated to predict BHF for multipoint cushions.
- Flexible binder resulted in more uniform pressure distribution in the blank, resulting in

more thinning and less draw-in and wrinkling compared to rigid binder.

- Optimum variable binder force (space) resulted in uniform reduction in thinning by 2% to 3%.

Conclusions

After facing some technical and organizational hurdles, retrofitting of the Erie Binder Control unit is now complete. The unit was successfully used in tryouts at TDM to stamp the GM liftgate. Also, similar delays were experienced during design and build of the IFU flexible binder control unit. The unit has finally been built. Its functionality is being evaluated in Germany before shipment to Detroit for testing and demonstration. The simulation and optimization task has proceeded according to plan. Three of the four major milestones are essentially satisfied.

Presentations and Publications

1. H. Palaniswamy, A. Thandapani, S. Kulukuru, and T. Altan, "Prediction of Blank Holder Force in Stamping Using Finite Element Analysis," presented at UNIFORM Conference, Columbus, Ohio, and presentation and publication at the SAE Congress, Detroit, Michigan, March 2004.
2. C. Du, J. Wu, M. Militisky, J. Principe, M. Garnett, and L. Zhang, "Springback Control With Variable Binder Force—Experiments and FEA Simulation," presented at the SAE meeting, Detroit, Michigan, and presentation and publication at the Numiform Meeting, Columbus, Ohio, May 2004.

B. Warm Forming of Aluminum II

Principal Investigator: Ken Oikarinen
DaimlerChrysler Corporation
2730 Research Drive
Rochester Hills, MI 48309
(248) 838-5221; fax: 248-838-5300; e-mail: kco3@daimlerchrysler.com

Principal Investigator: Peter Friedman
Ford Motor Company
Ford Research Laboratory
P.O. Box 2053, MD 3135/SRL
2101 Village Road
Dearborn, MI 48121-2053
(313) 248-3362; fax: (313) 390-0514; e-mail: pfriedma@ford.com

Principal Investigator: Paul Krajewski
General Motors Corporation
GM, R&D and Planning
Mail Code 480-106-212
30500 Mound Road
Warren, MI 48090-9055
(586) 986-8696; fax: (586) 986-9204; e-mail: paul.e.krajewski@gm.com

Project Administrator: Constance J. S. Philips
National Center for Manufacturing Sciences
3025 Boardwalk
Ann Arbor, MI 48108-3266
(734) 995-7051; fax: (734) 995-1150; e-mail: conniep@ncms.org

Technology Area Development Manager: Joseph A. Carpenter
(202) 586-1022; fax: (202) 586-1600; e-mail: joseph.carpenter@ee.doe.gov
Field Technical Manager: Philip S. Sklad
(865) 574-5069; fax: (865) 576-4963; e-mail: skladps@ornl.gov

---

Contractor: U.S. Automotive Materials Partnership
Contract No.: FC26-02OR22910

Objective

- Develop and demonstrate a production process for the warm forming (WF) of aluminum for automotive body structures and measure the economic feasibility of the WF process in a mass production environment.

Approach

- Develop individual elements of the WF process in a laboratory environment, including alloy characterization, lubricant development, and process thermal modeling.
- Develop full-size demonstration of WF process and run tests in a production environment. Integrate a blank preheater, blank transfer mechanism, lubricant application system, WF press with a modified thermal profile

controller, and lubricant removal step into production trials. Conduct production feasibility tests of the warm forming process at standard rates for current forming processes.

- Create a technical cost model that can generate cost comparisons between a warm-formed aluminum door inner and a same or similar door inner manufactured using conventional forming processes in steel and aluminum.
- Expect significant improvements in the formability of aluminum to be achieved through development of enabling WF process advancements, including:
  - Establishing the degree of improvement in formability of production-grade, commercial aluminum alloys.
  - Developing a cleanable lubricant suitable for use in a WF process.
  - Optimizing the temperature distribution of the die for improved thermal control and formability.
  - Evaluating rapid preheating systems for blanks.
  - Optimizing the process design and layout.
  - Applying the results of the cost model to optimize process design.
- Demonstrate the manufacturing feasibility and economic feasibility for a new mass production process such as the WF process, by defining the process flow and developing and applying a technical cost model that allows comparison of a product made in the WF process with a comparable component fabricated from aluminum/steel with deep draw using current processes.

Accomplishments

- Completed aluminum alloy characterization and laboratory-based WF process studies, including aluminum alloy sheet fabricated from custom-formulated 5000 series alloys and commercial alloys 5182-O, 5182-H18, 5754-O, and 5754-H18.
- Identified a suitable lubricant through extensive laboratory-based studies.
- Continued progress in the thermal analysis of the die through heat transfer analyses of the WF dies to be used in the WF process scale-up.

Future Direction

- Complete thermal studies and thermal models for finite-element analysis (FEA) for die heater optimization.
- Fabricate blank heating system to be used in production demonstration.
- Finish die refurbishment, and prepare it for use in production scale-up.
- Set up and conduct production scale-up and demonstration, and perform coupon evaluations.
- Employ the technical cost model to compare costs of WF process and alternative processes.

Introduction

The need to improve fuel economy has led automakers to explore lightweight materials such as aluminum for automobile body and closures. While attractive from a mass perspective, there are many challenges to the widespread use of aluminum:

- limited formability compared to steel,
- sliver management in trimming aluminum panels, and
- appearance problems in most 5000-series aluminum panels.

The Warm Forming of Aluminum, Phase II, project was initiated after the initial technical feasibility of forming complex shapes at elevated temperatures was previously demonstrated in Phase I. It is a 4-year development and demonstration program to establish the “production” feasibility of warm forming (WF) aluminum alloy blanks into automotive panels and to fully demonstrate a WF

process for cost-effectively manufacturing aluminum automotive panels that require a deep drawn shape.

This project focuses on the following objectives:

- Developing and demonstrating a WF process, including the materials, equipment, and heating processes that can cost-effectively expand the forming limits of aluminum sheet.
- Developing a technical cost model for the WF process to evaluate the economic feasibility of the WF process specific to component design.

The key enabling process improvements to make WF a production-capable process are the following:

- A high-temperature lubricant with good lubricity at WF conditions and preferably which is easy to clean prior to automotive painting.
- Temperature distribution management on the die surface during the forming operation.
- Effective preheating method for blanks.
- Identifying an optimum alloy for WF and characterizing its mechanical behavior at elevated temperatures.

Phase II Detail

Technical Cost Model: Camanoe Associates developed a detailed cost model based on a process sequence defined by the project team. Through use of the cost model, it was identified that aluminum alloy cost accounted for more than 70% of the cost of the end product. Thus, project research was refocused on commercially available alloys rather than "new" alloys with exotic alloying additions.

Alloy Selection: The University of Michigan completed analyses of the warm formability of commercial aluminum alloys and identified parameters affecting the sheet fabrication process for WF-capable aluminum sheet.

Lubricant Selection: The performance of selected lubricants under various temperature, travel time, and load pressures was evaluated at the University of Michigan in collaboration with General Motors (GM) and Fuchs' Lubricants.

Die Thermal Analyses: University of Michigan's S. Wu Manufacturing Center performed finite-element analyses of temperature profiles on the WF tooling for Neon door inners. Die geometry and heater location data were obtained from computer-aided design (CAD) models provided by Sekely Industries.

Blank Heating: Evaluations of infrared (IR) heating and a conduction heating methodology for heating laboratory-scale blanks were investigated at The University of Michigan and Ford Motor Company, respectively. The results assisted the team in selecting the preferred heating methodology for blank preheating for a WF production process.

Alloy Fabrication: Pechiney Rolled Products supplied the specified 5000 series aluminum sheet for these formability studies.

Full-scale Process Demonstration: With the individual component processes validated at laboratory level for technical and economic process feasibility, the full-scale WF demonstration using the Dodge Neon door inner stamping dies will be conducted starting in mid-2005. The process demonstration may be conducted in the local Detroit area, subject to acceptable vendor proposed terms.

Postprocess inspection and material analyses: Coupons from warm-formed parts will be cut out, and the materials properties will be evaluated by one of the original equipment manufacturers (OEMs). The typical properties to be evaluated will include strength, distortion, and corrosion.

Phase II Accomplishments

Alloy Characterization

This work was performed on Pechiney's Al-Mg alloys: 5182-O, 5182-H18, 5754-O and 5754-H18. Optical microscopy was performed at The University of Michigan. Cross-sectional photomicrographs of the 1-mm sheet alloys in the rolling-thickness planes are shown in Figure 1. The 5182-O alloy shows nearly equiaxed, annealed grains of average size of 7–9 µm, and the heavily rolled 5182-H18 alloy shows elongated grains that are 22 µm long and 2.6-µm average thicknesses. During polishing of the samples, second phase, coarse particles containing silicon, iron, and intermetallics fall off, leaving small pores; but in the H18 alloy, several particles, 15- to 20-µm size, are found severely damaged, and the matrix surrounding those particles severely deformed and cracked. From this information, it is understandable that formability of H18

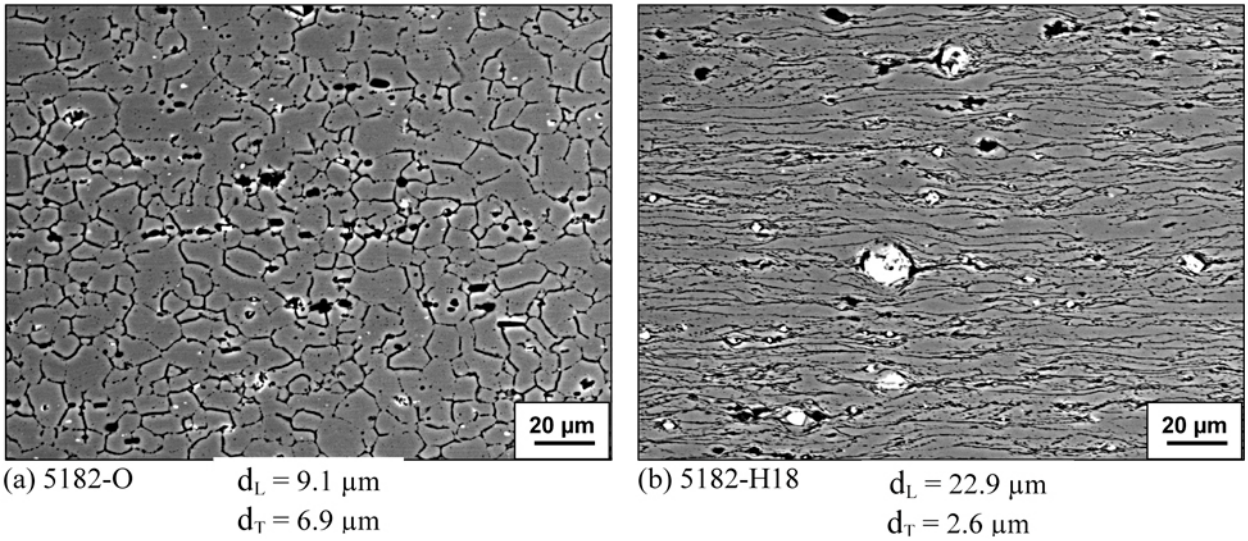

Figure 1. Microstructure of Pechiney alloys showing nearly equiaxed grain structure in the O-condition and elongated grains in the H-18 condition.

alloy would be severely impaired without a proper recrystallization and damage healing treatment. Alternatively, cleaner alloys with less content of large particles would be desirable. 5754-O and 5754-H18 alloys showed similar microstructures, but contained fewer particles.

Blank Preheating and Forming Studies

Blank preheating and forming studies were completed by the University of Michigan. A small laboratory-size IR heating oven (660 mm in length), manufactured by IR Heating Technologies, Inc., of Oak Ridge, Tennessee, was used to heat the sheets and convey them to the preheated laboratory cup-forming test machine. The IR heating equipment has a stainless steel chain belt system, driven by a variable-speed motor. The equipment did not come with a variable-speed control, which was subsequently installed by the University. Total IR heating power was approximately 20–24 kW, but the heating lamps were approximately 150 mm from the surface of the aluminum sheets, which minimized power coupling. The heat loss from the inlet and exit of the heater was significant. Insulation at the entry and exit was added to contain the heat within the furnace so that the IR lamps could effectively heat the sheet (blank).

The following experiments were conducted to determine the attributes of the IR heater capability and its effect on heating time, including the degree of recrystallization and forming performance of aluminum sheets:

1. effect of belt speed and temperature setting to reach various constant temperatures in the hot zone of the furnace;
2. the rate of temperature rise and exit temperature during passage of the sheet through the oven;
3. minimum time to reach 350°C exit temperature;
4. possibility of raising the sheet closer to the IR heating lamps;
5. degree of recrystallization of the alloys achieved upon exit from oven;
6. effect of preheating on the height of the formed cup;
7. role of lubricants, such as moly-disulfide, boron nitride, and Fuchs lubricants on cup height at fracture; and
8. cup height measurements on 5182-O, 5182-H18, 5754-O, 5754-H18, and also Alloy 725 used from an earlier WF study.

A variable-frequency potentiometer control was installed to drive the chain belt over a wide range of speeds with a maximum speed capability of 60 mm/s. A linear behavior between input power frequencies vs conveyor speeds is shown in the curves in Figure 2. Sheet samples were connected with thermocouples and traveled through the oven at various speeds at different temperature settings. It was anticipated that reaching a constant temperature

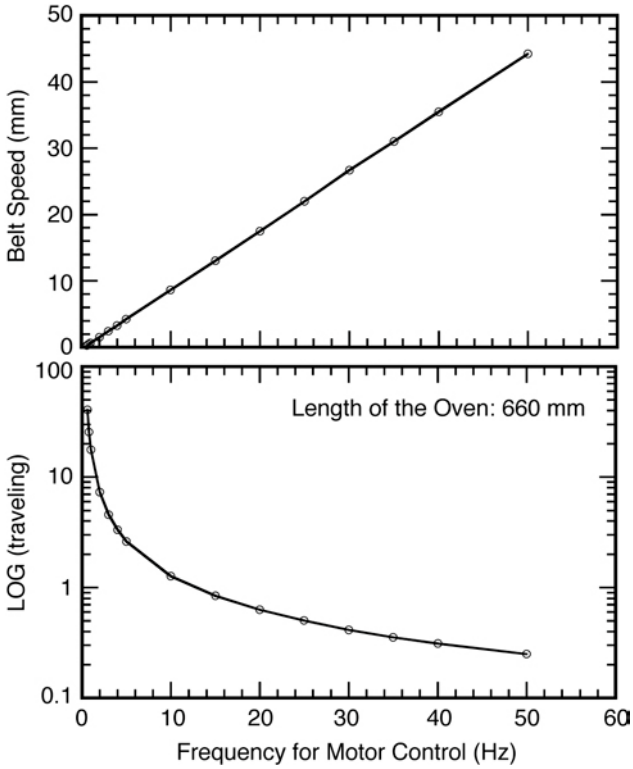

Figure 2. Belt speed control as a function of motor frequency and corresponding traveling time.

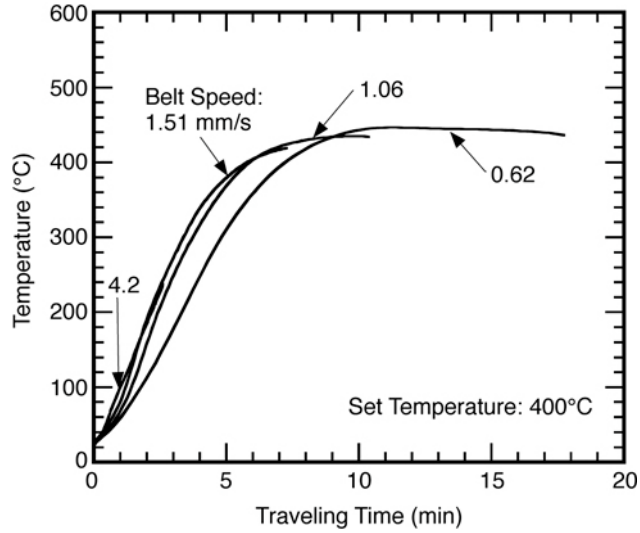

Figure 3. Sheet temperature as a function of time for three different belt speeds at an oven set temperature of 400°C.

profile within the oven was desirable to achieve uniform temperature over a period of time needed to anneal and recrystallize the hard temper aluminum sheets. However, for oxygen-temper sheets, the recrystallization step is not deemed necessary, and rapidly heating the sheet for minimizing forming time was needed. Initial experiments were performed at a 400°C furnace setting with a view to attain a constant temperature in the range of 350–400°C. Figure 3 shows temperature rise as a function of time of travel through the oven. These trials with the IR heater showed the time to heat the blank to 300°C was approximately 3 min at an oven temperature of 400°C.

The next series of experiments were performed with IR heater settings at 800–900°C to accelerate heating of blanks at rapid rates. A series of experiments was performed with specimens attached with thermocouples, each with a different conveyor speed such that the entry-to-exit time could be monitored. These experiments were performed to understand the general characteristics of these ovens and to examine alternative strategies where total residence time in the oven could be longer without compromising sheet exit rate. The rise in sheet temperature with various exit times is shown in Figures 4 and 5, with corresponding microstructural changes. Recrystallization effects are seen when the heavily deformed H18 microstructure is replaced by equiaxed grains.

Time to reach 300°C for these trials was closer to 35 and 25 s at 800°C and 900°C temperatures, respectively. This represents a significant improvement over the previous results at a set temperature of 400°C.

Recrystallization prior to forming is required to attain maximum formability. Material cost savings can be attained by using "hardened sheet" such as these instead of having the sheet batch-annealed at the aluminum manufacturing facility. However, for oxygen-temper sheets, a recrystallization step is not deemed necessary and rapid heating of the sheet was needed to minimize forming time.

While these trials demonstrated that an IR oven is capable of supplying ample heating for the WF process, it did not appear to be the best solution. Significant overheating appears to be necessary to achieve production feasible heat-up times. Additionally, overheating presents the risk of melting the sheet if the conveyer system were to stop for any period of time. Additionally, high emissivity of aluminum requires significant energy from the IR

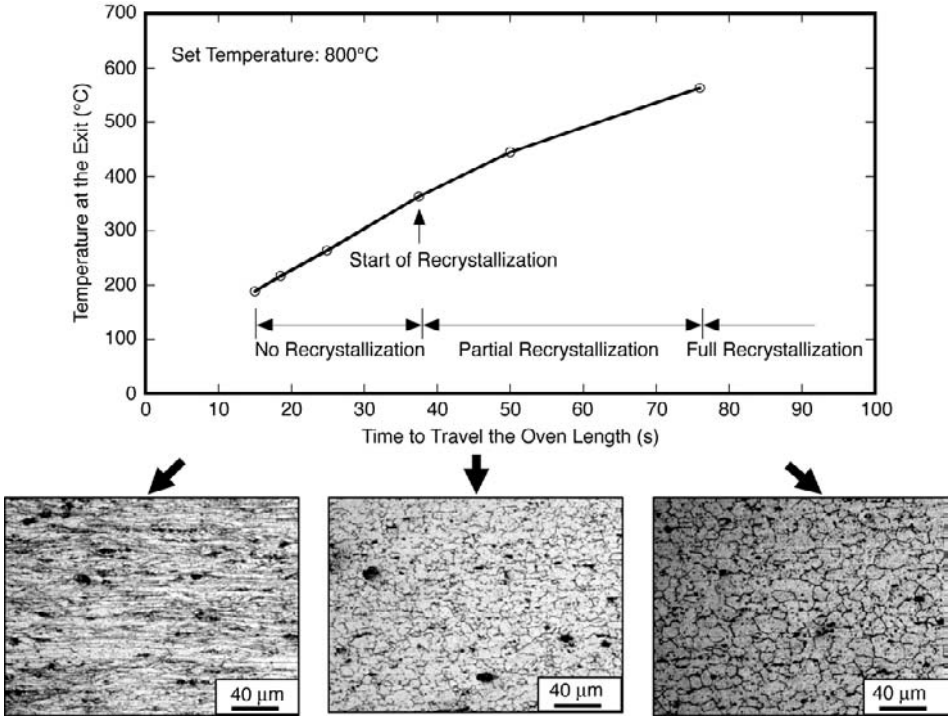

Figure 4. Heating and recrystallization of 5182-H18 alloy during passage through IR oven for various conveyor speeds (set temperature 800°C).

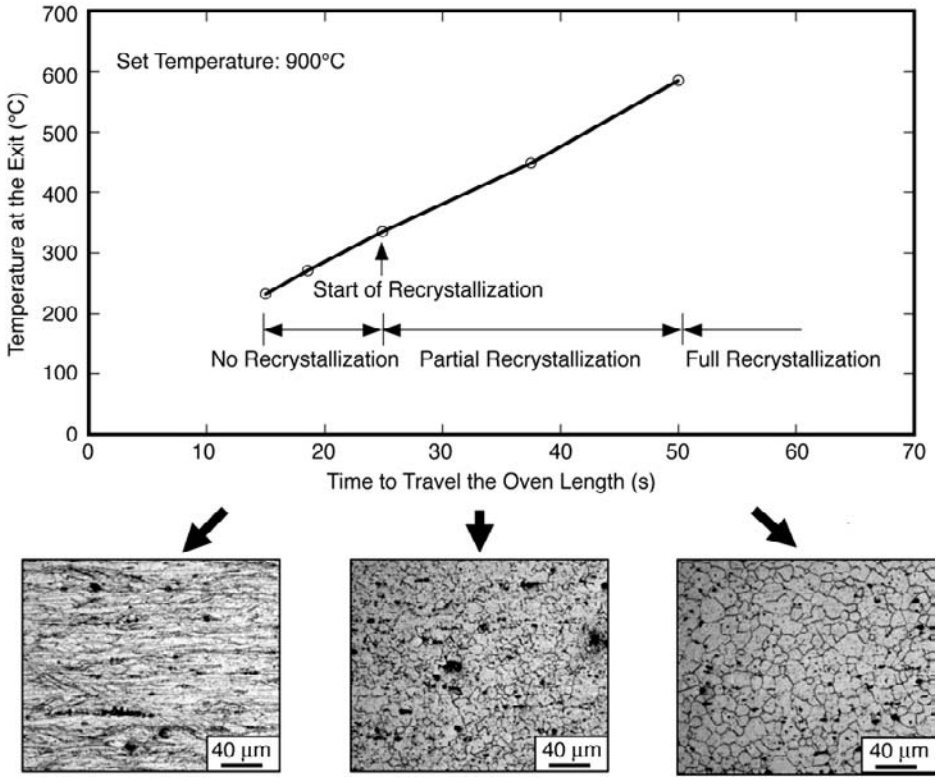

Figure 5. Heating and recrystallization of 5182-H18 alloy during passage through IR oven for various conveyor speeds (set temperature 900°C).

heater to reach target temperatures. For these reasons, the team decided to use a conduction heater in the scale-up of the WF process, which is thought to be a more cost-effective and robust method of heating aluminum sheet. Preliminary tests indicate that forming temperatures can be reached within seconds with this type of heater.

Biaxial Forming Tests, Forming Limit Measurement, and Lubricant Studies

Forming tests were performed on a heated rectangular die-punch apparatus designed and built at the University of Michigan, to simulate commonly observed biaxially formed parts and appropriate punch and die edge radii. Figure 6 shows a schematic diagram of the main part of the WF test device and a photograph of the die-punch configuration. Sheet blank size used in this work was 200 mm by 140 mm. Die opening area was approximately 110 mm by 50 mm including the die entry radius, and the overall punch size was 100 mm by 40 mm. Both the die edge and the punch had edge radii of ~5 mm.

The die and the punch were heated by embedded heating elements. Thermocouples inserted into different heating areas of the die and the punch permitted temperature control using proportional integral derivative (PID) devices, within a range of ±4°C. The punch-die device was mounted on an Instron-1116 testing machine with 250-kN capacity. The punch was actuated by moving the machine crosshead at predetermined speeds. The upper die plate was maintained in a fixed position in the die apparatus, while the lower die plate was moved upward by using the pistons of three ENERPAC hydraulic cylinders to clamp the sheet between them. The die and punch were preheated to desired temperature(s) and then the preheated sheet sample was moved into position marked on the lower die where a specified blank holding load (average pressure of 1.1 MPa) was applied to tightly clamp the sheet. The forming test temperature range was selected to be ~350°C, and room temperature tests were used as baseline references.

It was found that thermal equilibrium could be reached in just a few seconds. The punch advance speed was fixed at 10 mm/s, providing local strain rates in the small test sample close to commercial stamping strain rate. Load vs punch displacement curves were recorded using an X-Y data recorder, and the data were utilized to obtain the depth of a

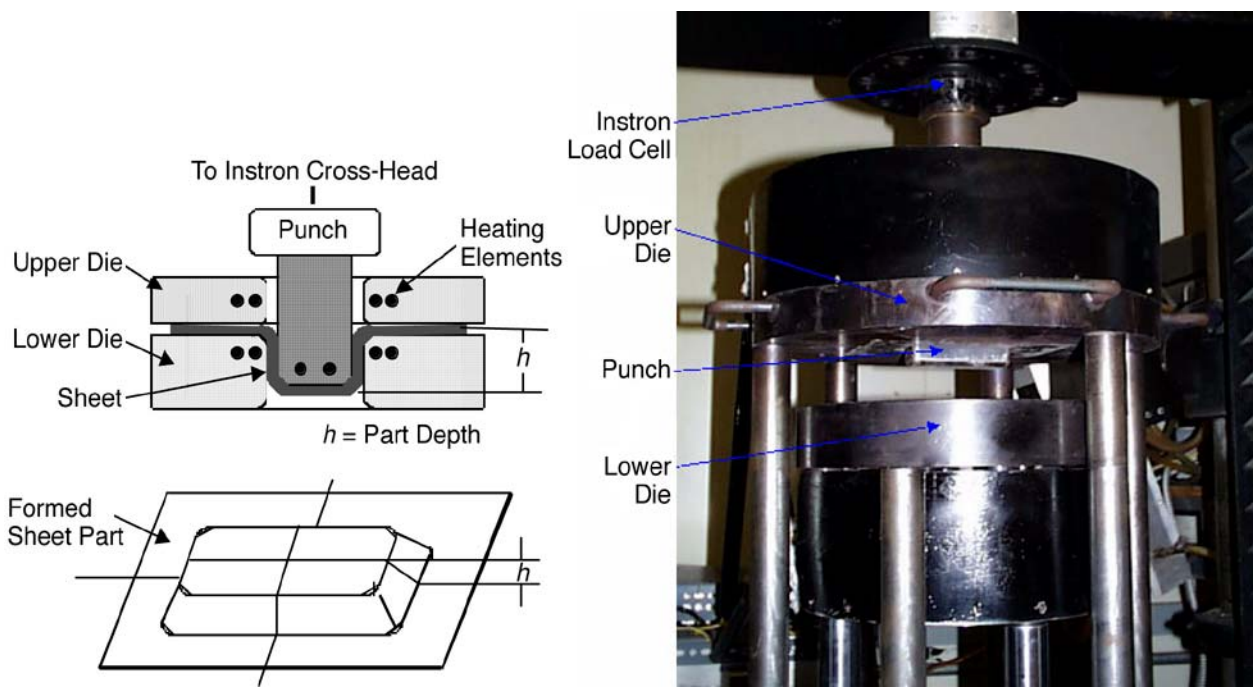

Figure 6. Schematic diagram of the main parts of the WF test device and a formed blank, and photograph of the rectangular die-punch apparatus with heated die set.

formed part at peak load (where necking occurred in the sheet). This part depth was used as the measure of formability.

To evaluate forming strain and to construct forming-limit diagrams (FLDs), the preetched grid size was measured using a video camera and digitally processed by a computer program (Scion Image) for the warm-formed rectangular parts. The measurements were made along both longitudinal and transverse axes and around the crack. Different lubrication and different blank holding pressure were utilized to permit failure in different regions of the formed cups such that the state of strain at failure could be altered, a requirement for determining the forming limit diagram. Grid strains were utilized for determining the FLD by using established techniques. The FLD of 5182-O aluminum was found to be lower in level compared to fine grain alloy 5182 + Mn and 5754 alloys studied previously during an earlier phase of the WF project (see website http://www.mse.engin.umich.edu/research/groups/ghosh/), also supported by the Department of Energy.

The effectiveness of lubrication was determined by measuring cup height from samples coated with different lubricants. In addition to spray coatings of boron nitride and molybdenum sulfide, synthetic lubricants supplied by Fuchs Lubricants were evaluated. The latter lubricants were evaluated in their "pure" state as well as after the addition of small levels of BN and MoS_2. Figures 7–9 shows cup heights at failure of samples tested with the various lubricants, under the same nominal test conditions.

In general, moly-disulfide lubrication produced equal or slightly inferior cup height in comparison to BN-coated samples, with values in the range of 18–21 mm. The Fuchs lubricant 216 gave the best performance when it contained some BN or moly-disulfide. The 216-BN was found to be the best lubricant, exhibiting a cup height of 25 mm. Without BN, the 216 lubricant was inferior to solid lubricants BN and moly-disulfide by themselves. A typical problem encountered with the use of Fuchs 216-based lubricants was a heavy, tenacious brown stain formation on the cup surface due to curing of the polymer base and bonding to aluminum.

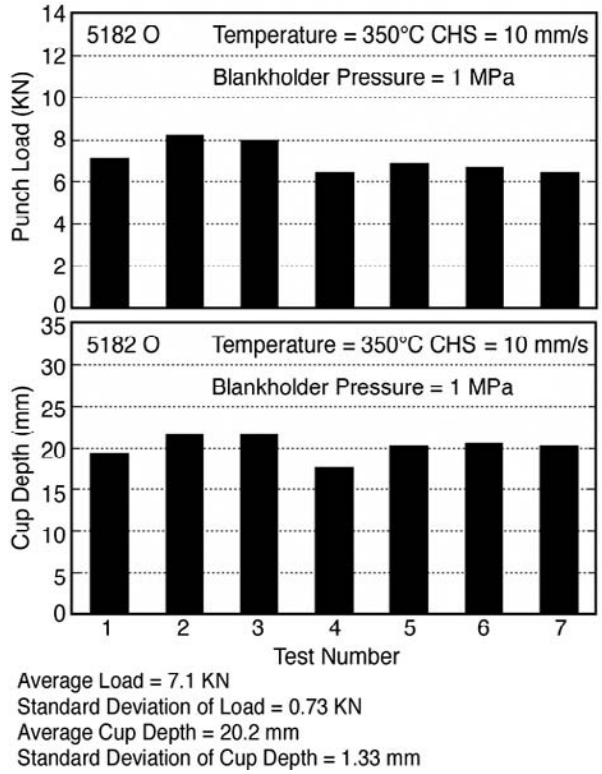

Figure 7. Variability in punch load and cup height, using moly-disulfide lubrication on 5182-O aluminum alloy.

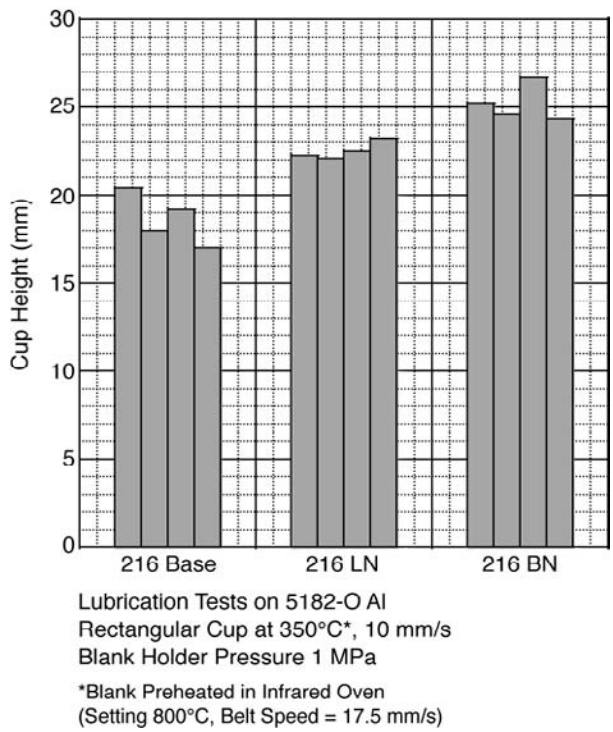

Figure 8. Cup height data, using various lubricants supplied by Fuchs Lubricants.

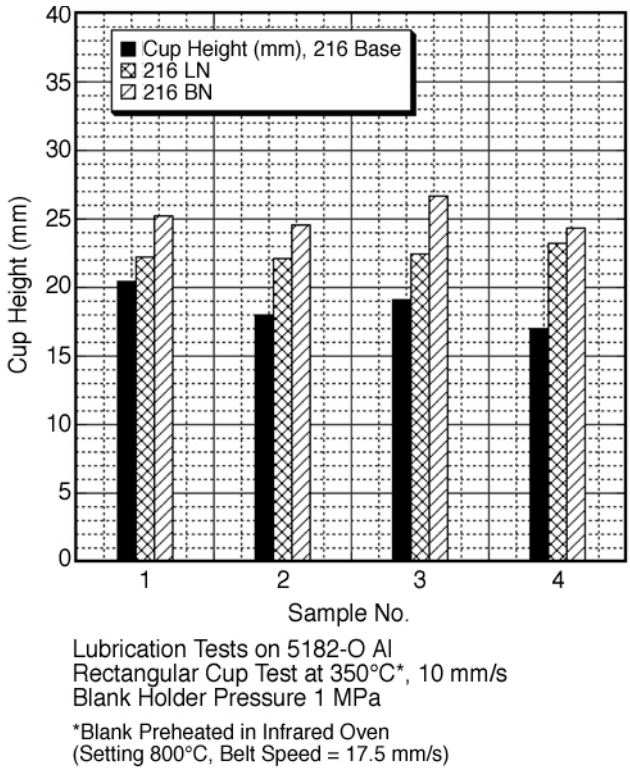

Figure 9. Data similar to that in Figure 8, showing superiority of lubricants containing small amount of BN over the base lubricant.

Tensile Deformation Behavior of 5182-O Aluminum Alloy after Preheating in an IR Heating Oven

Uniaxial tensile deformation behavior of 5182-O aluminum sheet alloy after preheating was studied in the temperature range from room temperature to 350°C and in the strain rate range of 0.015–1.33 s^{-1}. Strain rate, the relationship between stress and temperature, was studied. The total elongation in uniaxial tension is found to increase with increasing test temperature and to decrease with increasing test strain rates. The strain rate sensitivity (m value) is determined for the data produced at different strain rates. Also, the recovery effect during the tension test was investigated at different temperatures and strain rates based on the stress-strain curves obtained in the uniaxial tension test. It was found that total dynamic recovery effect in uniaxial tension increases with increasing temperature and decreases with increasing strain rate.

Findings from these studies include:

- Stress-strain relations—The tensile load-displacement data were processed to obtain true stress-true strain data. True stress-true plastic strain curves were obtained at four temperatures (25, 250, 300, and 350°C) and at three strain rates (0.015, 0.15, and 1.33 s^{-1}). Engineering stress-strain curves were obtained for the material at different strain rates and temperatures. For 5182-O aluminum sheet alloy, flow stress level increases with increasing strain rate but decreases with increasing temperature.
- Tensile elongation—In general, total elongation increases with increasing temperature and decreases with increasing strain rate. The enhanced total elongation becomes significant only above 250°C. Thus, 250°C appears to be the lower end of the WF temperature range. Tensile elongations in the range of 60–110% were achieved at 350°C. For strain to the maximum load, that is, uniform elongation, it was observed that the variation of uniform elongation does not follow a single trend against temperature or strain rate. In fact the value of uniform elongation actually increases with increasing temperature in some of the 5xxx alloys. Thus, the combined influence of temperature and strain rate may be complex.
- Strain rate sensitivity of flow stress—The strain rate sensitivity index of flow stress, m, is determined according to

$$m = d(\log \sigma)/d(\log \acute{\varepsilon}) \qquad (1)$$

where $\acute{\varepsilon}$ = strain rate. The value of m is an important material property in evaluating the formability of a sheet metal. Currently, there are different test methods to determine m value. The present tensile tests provided data of true stress-true plastic strain relations at each temperature. The m value is then calculated according to Eq. (1). The log σ-log $\acute{\varepsilon}$ relationships at different temperatures based on peak stress level (steady state) for each test were plotted, and the values of m were determined from the slopes of the curves. These m values are then plotted against temperature. It is found that m value increases markedly with increasing temperature. It is zero

at room temperature, 0.044 at 250°C, 0.099 at 300°C and 0.15 at 350°C. The reason for this is that at higher temperature atoms move more rapidly, and dislocation climb becomes easier. Climb and thermally activated glide lead to a higher m value with increasing temperature. We also can see that, the m value is not very high, for example, it is 0.15 at 350°C. The relatively low value of m indicates that the mixture of thermally activated glide and climb is the dominant deformation mechanism for 5182-O aluminum alloy. As for pure climb, the m value should be substantially higher, while for thermally activated glide, the m value is generally below 0.1. Because the higher value of m indicates larger elongation, the elongation will increase with the increasing temperature.

- Dynamic Recovery Effect—During the warm deformation process, two competing effects, strain hardening and dynamic recovery occur, leading to the attainment of a steady flow stress. On one hand, as the specimen is elongated, the dislocations in the material interact with each other and become tangled leading to a reduced effective distance between these obstacles, thereby increasing the resistance to the movement of subsequent dislocations. As a result, higher stress is needed to deform the specimen further.

  In contrast, because the specimen is deformed at elevated temperature, recovery and rearrangement of dislocations occur concurrently due to their greater mobility and annihilation of each other, therefore minimizing the stored dislocation density and increasing the spacing between the dislocations, thereby reducing deformation resistance. Reduced obstacle density tends to lower the flow stress leading to an equilibrium dislocation structure, and a steady state flow stress. Net hardening was found to increase with increasing strain rate, indicating that softening due to dynamic recovery is reduced at higher strain rates. Consequently, strain to maximum load increases as strain rate increases. The fact that uniform strain increases with increasing strain rate is a clear indication that dynamic recovery or softening is reduced at higher strain rates.

  The tendency for dynamic recovery is a critical indicator for warm formability and for the measured m values. To investigate the recovery effect due to temperature and strain rate, a method to quantify its extent was devised. For the tests, the change in the slope of the stress-strain curve, $\Delta(d\sigma/d\varepsilon)$, was compared to that at room temperature as a measure of recovery effect (at given values of flow stress, the state parameter for stored structure, and its deformation resistance). We define $\Delta(d\sigma/d\varepsilon)$ as the recovery parameter R. To determine the value of R, the reference value is either the elastic or the plastic slope: in this case, the Young's modulus E of 5182-O aluminum alloy at room temperature, S_1 = 69,000 MPa, and S_2, the slope of true stress-true strain curve at an elevated temperature at a specific stress level ($R = S_1 - S_2$).

  Figure 10 shows $\Delta(d\sigma/d\varepsilon)$ as a function of true stress at different strain rates at specific temperatures. The recovery effect increases with the increasing true stress level, because higher stored dislocation density drives faster recovery. Also at a specific stress level, the recovery effect increases with the decreasing strain rate. The reason for this is that at a lower strain rate, more time is available for dislocations to annihilate each other and more time is available for recovery. Thus, recovery effect is much more obvious at lower strain rate.

  Figure 11 shows $\Delta(d\sigma/d\varepsilon)$ as a function of true stress at different temperatures at a specific strain rate. At a specific stress level, the recovery effect increases with the increasing temperature. The reason for this is that at higher temperature, atomic transport is more rapid. Furthermore, faster deformation rates minimize the time available for dislocation annihilation and rearrangement. This reduces the degree of softening achievable by recovery.

For the 5182-O aluminum sheet alloys studied in the WF temperature range of 200–350°C and in

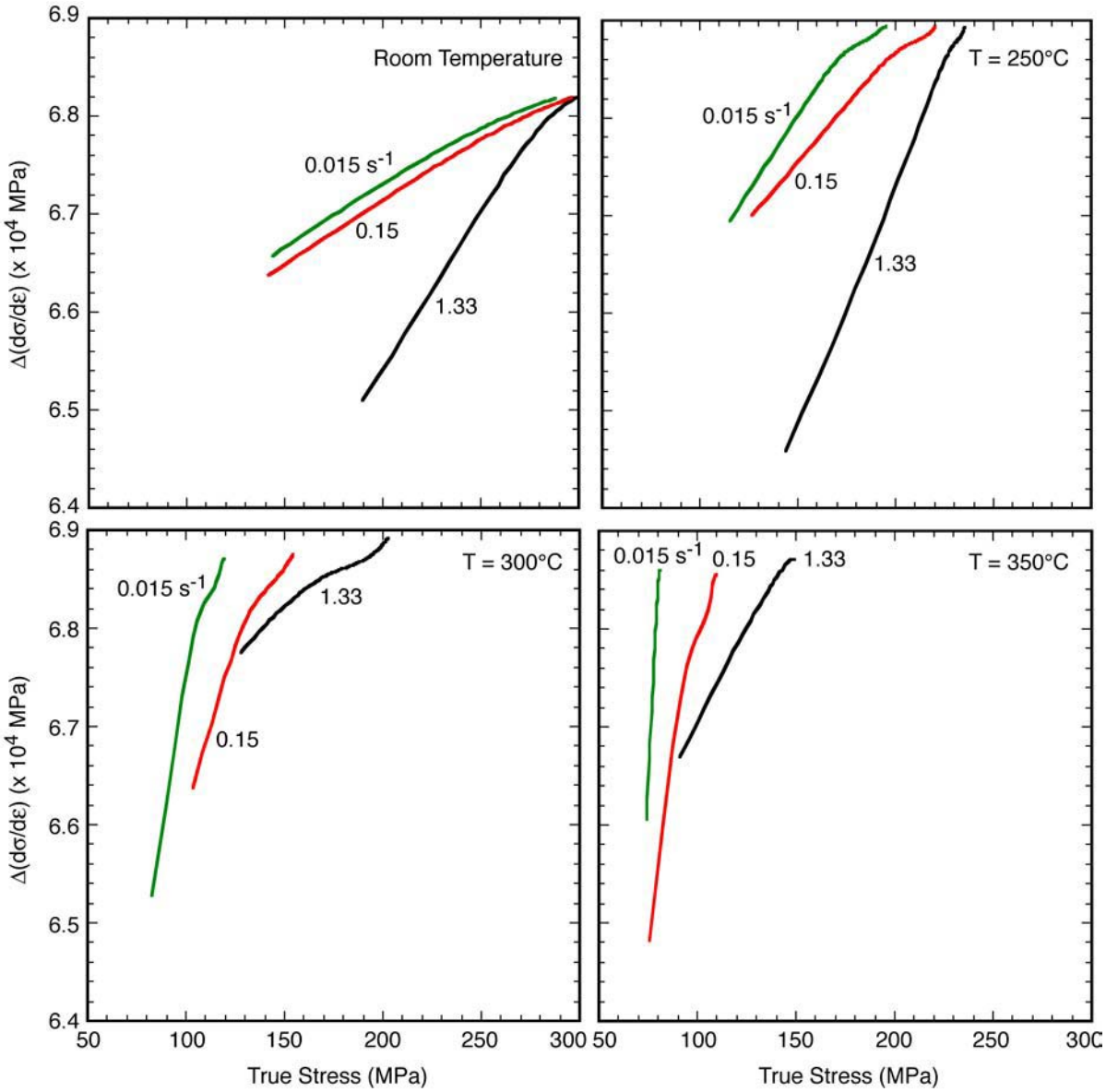

Figure 10. Recovery effect at different temperatures for 5182-O aluminum based on tensile test.

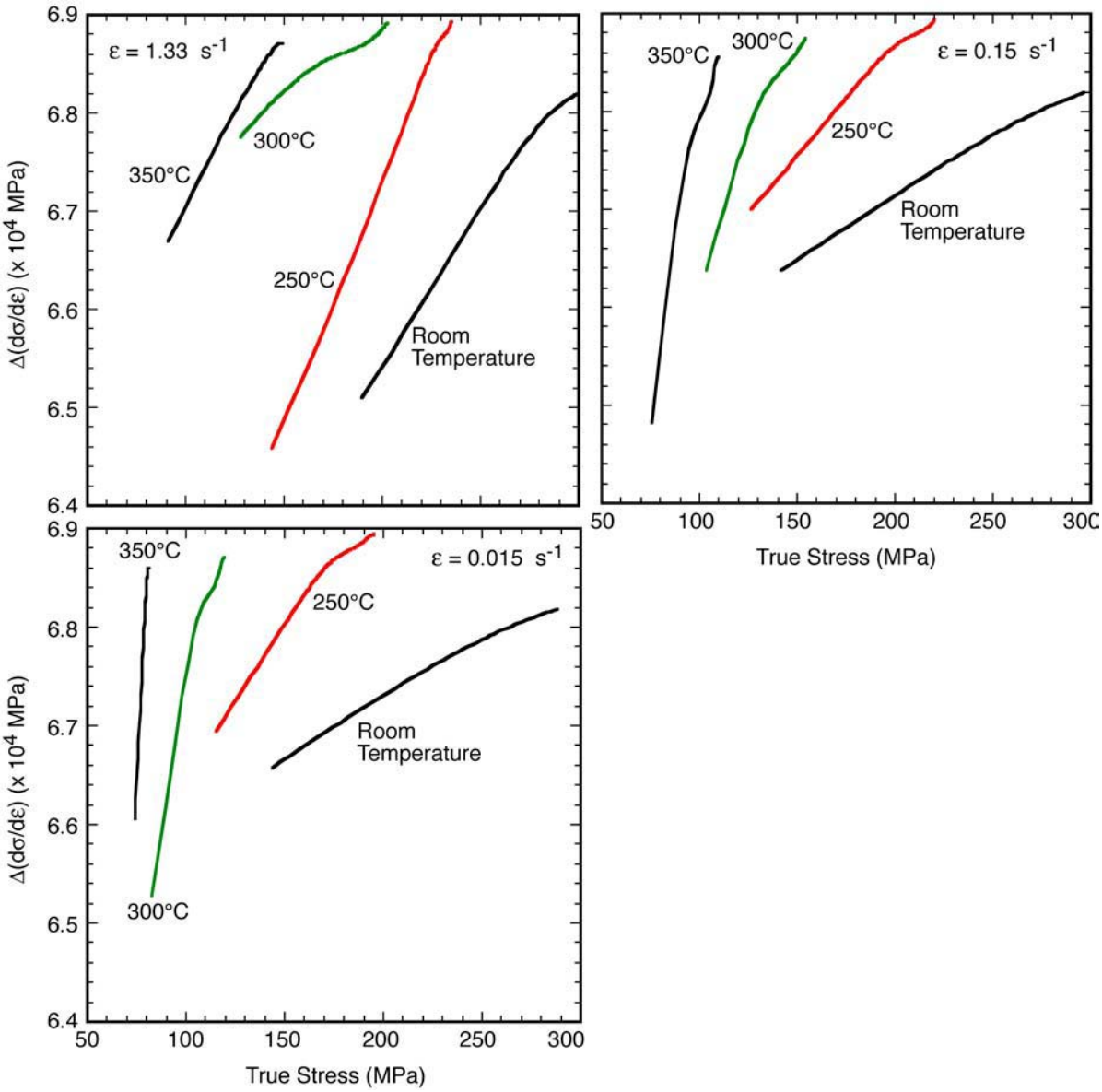

Figure 11. Recovery effect at different strain rates for 5182-O aluminum based on tensile test.

the strain rate range of 0.015–1.33 s^{-1}, the following conclusions can be drawn:

- Uniaxial tensile elongation increases with increasing temperature and decreases with increasing strain rate. The maximum tensile elongation observed ranged between 60–100% at 350°C.
- Strain rate sensitivity (m value) increases with increasing temperature, and the strain hardening rate increases with increasing strain rate in keeping with dynamic recovery effects. Strain rate hardening is deemed to play a dominant role in enhancing the elevated temperature plasticity in tensile deformation.
- Dynamic recovery effect [$\Delta(d\sigma/d\varepsilon)$ value] increases with increasing stress level. And at a specific stress level, the total amount of recovery effect increases with increasing temperature and/or decreasing strain rate.

Die And Blank Thermal Analyses

Positive progress was made during 2004 in the thermal analysis of the WF dies through a heat transfer analysis of the dies to be used in the WF

process scale-up. A preliminary finite-element analysis (FEA) model to study the heatup and cooling of formed parts and die components was defined by S. M. Wu Manufacturing Research Center, University of Michigan. The FEA model was then used to examine the effects of air vs water cooling on simple deep draw parts, the loss of temperature during sheet material transfer from preheater to die, and heat distortion effects on die and insert surfaces over time. Such information will be considered in the final process layout design.

Six parts (insert, lower holder, blank, upper holder, punch, and base) make up this complex die-punch process.

- In early simulations, heat fluctuation values for the die upper and lower holders, insert and punch were analyzed with and without a heater control scheme. Findings at that time concluded that desired steady state temperature values (350°C) can be achieved in significantly shorter time by using a heater control scheme. Additionally, steady state temperature can be maintained precisely through the use of a heater control scheme.
- The WF cycle was simulated using a sectional model. Findings indicate that the change in temperature of the upper and lower rings, insert and punch during a single forming cycle is negligible (±3°C).
- FEA with the heater control scheme on actual tooling was performed on the lower tooling, insert, and lower ring. Simplification of the models was done to reduce the model size and computational time. For example, the modified model for the insert reduced the number of nodes from 60,375 with 38,775 elements to 42,654 with 26,699 elements. Comparison of FEA and experimental results yielded these conclusions:
  - Using constant heat flux values, time to reach steady state temperature of 350°C takes 25 h and 10 h for the insert and lower ring, respectively.
  - Using the heater control scheme can reduce the time to reach steady state to ~2 h.
  - Vertical displacement distribution ranges from 0.68 to 0.8 mm in the insert, and 0.6 to 1.25 mm in lower ring.

Future work will complete FEA of the upper tooling with the heater control scheme and will verify FEA results against actual thermal data from the demonstration experiments. These data will then be incorporated into an FEA for determining optimal heater specifications for future tooling/process design.

Summary and Conclusions

Alloy Selection: 5182-O aluminum alloy has sufficient attributes for WF to support its use in the scale-up demonstration phase. Findings from the alloy characterization studies pertinent to the scale-up demonstration phase include the following:

- Full hard 5182 aluminum has observable rolling-induced damage, which is absent in 5182-O.
- Full hard 5182 alloy can be recrystallized by rapid heating; formability remains worse than 5182-O sheet.
- 5182-O alloy shows a cup height of 20 mm at 350°C.
- 5182-O alloy has a biaxial forming limit of 40% by 40% (approximately) at 350°C.

In the demonstration phase, magnesium sheet will be tested using the WF demonstration process and tooling to empirically evaluate the result. Magnesium behavior and blank forming results will help the OEMs determine what developmental work may be required to form magnesium.

Blank Preheating and Forming Studies: While our lab trials demonstrated that an IR oven is capable of supplying ample heating for the WF process, it does not appear to be the best solution. Significant IR lamp overheating appears to be necessary to achieve production-feasible heat-up times. Additionally, overheating presents the risk of melting the sheet if the conveyer system were to stop for any period of time. For these reasons, the team decided to fabricate a conduction heater for use in the scale-up of the WF process. It is thought to be a cost-effective and robust method of heating aluminum sheet. Preliminary tests indicate that forming temperatures can be reached within cycle time requirements.

In general, moly-disulfide lubrication produced equal or slightly inferior cup height in comparison to BN-coated samples, with values in the range of 18–21 mm. The Fuchs Lubricants 216 wax-based

varieties with BN or moly-disulfide produced the best results. 216-BN was found to be the best lubricant exhibiting a cup height of 25 mm. Because it is a wax-based lubricant, a heavy, tenacious brown stain forms on the cup surface due to curing of the polymer base and bonding to aluminum. Future work may consider development of economical cleaning solutions for this lubricant.

For the 5182-O aluminum sheet alloys studied in the WF temperature range of 200–350°C and in the strain rate range of 0.015–1.33 s^{-1}, the following conclusions can be drawn:

- Uniaxial tensile elongation increases with increasing temperature and decreases with increasing strain rate. The maximum tensile elongation observed ranged between 60–100% at 350°C.
- Strain rate sensitivity increases with increasing temperature, and the strain hardening rate increases with increasing strain rate in keeping with dynamic recovery effects. Strain rate hardening is deemed to play a dominant role in enhancing the elevated temperature plasticity in tensile deformation.
- Dynamic recovery effect increases with increasing stress level. And at a specific stress level, the total amount of recovery effect increases with increasing temperature and/or decreasing strain rate.

Lubricant Studies: Fuchs lubricant 216 BN produced the best cup height of all formulations studied, exhibiting a cup height of ~25 mm, and appears to be a feasible lubricant for use in the scale-up demonstration. Cleaning options and methodologies will be defined during the demonstration stage.

Die and Blank Thermal Analyses: Modeling performed to date represents positive progress toward development of an FEA for determining optimal heater specifications for future tooling/process design. Future work on this task will complete FEA of the upper tooling with heater control scheme and will verify FEA results against actual thermal data from the demonstration experiments. These data will then be incorporated into an FEA for determining optimal heater specifications for future tooling/process design.

C. Electromagnetic Forming of Aluminum Sheet

Richard W. Davies, Principal Investigator
Pacific Northwest National Laboratory
P.O. Box 999, Richland, WA 99352
(509) 375-6474; fax: (509) 375-4448; e-mail: rich.davies@pnl.gov

Sergey Golovashchenko, Technical Coordinator
Ford Motor Company
Ford Research Laboratory, Dearborn, MI 48121-2053
(313)-337-3738; fax: (313)390-0514; e-mail: sgolovas@ford.com

DOE Technology Area Development Manager: Joseph A. Carpenter
(202) 586-1022; fax: (202) 586-1600; e-mail: joseph.carpenter@ee.doe.gov
ORNL Field Technical Manager: Philip S. Sklad
(865) 574-5069; fax: (865) 576-4963; e-mail: skladps@ornl.gov

Participants

Vladimir Dmitriev, EMF R&D, Ford Motor Company
Dwight Rickel, EMF System Development, Los Alamos National Laboratory
James Sims, Coil Durability, Materials, and Design, Los Alamos National Laboratory
Andy Sherman, EMF R&D, Ford Motor Company
Jeffrey Johnson, EMF System and Control, Pacific Northwest National Laboratory
Jeff Bailer, EMF Capacitor Bank Control, Pacific Northwest National Laboratory
Gary Van Arsdale, EMF Coil Fabrication and Metal Forming, Pacific Northwest National Laboratory
Nick Bessonov, EMF Simulations, University of Michigan-Dearborn
Nick Klymyshyn, Computational Mechanics, Pacific Northwest National Laboratory
Dick Klimisch, Project Coordinator and Material Supply, Aluminum Association
Roy Cooper, Oxford Automotive Company, EMF Industrial Embodiment

---

Contractor: Pacific Northwest National Laboratory
Contract No.: DE-AC06-76RL01830

Objective

- Develop electromagnetic forming (EMF) technology that will enable the economic manufacture of automotive parts made from aluminum sheet. EMF is a desirable process because the dynamic nature of the deformation results in benefits including increased forming limits and reduced springback. These benefits would result in increased use of aluminum and, therefore, more fuel-efficient vehicles due to mass reduction.

Approach

- Address analysis methods for forming system design.
- Address development of durable actuators (coils).
- Address industrial embodiment of the EMF process.

Accomplishments

- Completed a literature search for information on EMF, coil materials, and coil design/durability.
- Completed design and assembly of a 150-kJ pulsed power unit (Figure 1) at Los Alamos National Laboratory (LANL).

Figure 1. Photograph of the capacitor bank and load cables connected to the forming coil.

- Found that Ford Motor Company designed an integrated forming coil system for high-volume automotive stamping.
- Established that LANL completed a literature review of patents, relevant coil materials, and the design of EMF coils.
- Installed the 150-kJ pulsed power supply at Pacific Northwest National Laboratory (PNNL), demonstrated operation, and installed an automated computer control system capable of automated cyclic testing and sheet metal forming.
- Completed fabrication of an experimental apparatus to evaluate coil durability.
- Established a Cooperative Research and Development Agreement (CRADA) that includes Ford, PNNL, and Oxford Automotive.
- Performed cyclic testing of an EMF coil assembly for durability assessment and achieved more than 5,000 cycles.
- Developed conceptual layouts for industrial embodiment of EMF process.
- Demonstrated ability to improve formability of aluminum sheet by a factor of 2-3 times more than conventional forming.
- Completed evaluation of EMF coil assembly cooling effectiveness.
- Observed that PNNL has fabricated an enhanced coil assembly for improved coil cooling and durability.

Future Direction

- Increase the cyclic testing rate to better evaluate the thermal characteristics of the industrial coil assembly.
- Scale-up laboratory testing to include commercially representative components.
- Further develop modeling capabilities that can assist in the design of EMF systems.
- Continue to investigate the industrial embodiment of EMF systems for automotive manufacturing.

Introduction

In the electromagnetic forming (EMF) process, a transient electrical pulse of high magnitude is sent through a specially designed forming coil by a low-inductance electric circuit. During the current pulse, the coil is surrounded by a strong transient magnetic field. The transient nature of the magnetic field induces current in a nearby conductive workpiece that flows opposite to the current in the coil. The coil and the workpiece act as parallel currents through two conductors to repel one another. The force of repulsion can be very high—equivalent to surface pressures on the order of tens of thousands of pounds per square inch. Thin sheets of material can be accelerated to high velocity in a fraction of a millisecond.

A recent interest in understanding the EMF of metals has been stimulated by the desire to use more aluminum in automobiles. The high workpiece velocities achievable using this forming method enhances the formability of materials such as aluminum. Also, the dynamics of contact with the forming die can help reduce or mitigate springback, an undesired effect that cannot be avoided in other forming techniques such as stamping. The commercial application of this process has existed since the 1960s. The large majority of applications have involved either the expansion or compression of cylinders (tubes). The forming of sheet materials is considerably more complex and has received relatively little attention.

Project Deliverables

At the end of this project, methods and data to assist the economical design of EMF sheet forming systems will be documented. This will include materials information and design methods for durable coils, coil durability test data for selected materials and design concepts, dynamic and hybrid formability data, methods for modeling the forming process, and concepts for the industrial implementation of the technology in an automotive manufacturing environment.

Approach

This project addresses three main technical areas. The first technical area involves establishing analysis methods for designing forming systems. These methods will be based on developed knowledge of forming limits and relations between electrical system characteristics and deformation response for specific aluminum alloys of interest. The second area of technical challenge is in coil durability. Existing knowledge of EMF and relevant knowledge from pulsed-power physics studies will be combined with thermo-mechanical analyses to develop durable coil designs that will be tested experimentally. Until a more thorough understanding is achieved of economic factors determining required durability, a nominal level of 100,000-cycle coil life will be the goal for this project. Finally, the third technical area involves the industrial embodiment of the EMF process. In this project, EMF is expected to be hybridized with conventional sheet metal stamping. Different approaches to hybridization will be analyzed for issues affecting the economic implementation in a modern stamping plant. Different system concepts are being developed and studied. Existing knowledge of the EMF process and technical achievements in this project will be combined to establish a methodology for designing hybrid forming systems that can be readily integrated into modern manufacturing facilities for the economic production of automotive sheet aluminum components. Some of the project focus areas and results are discussed in the following sections.

*EMF System Commissioning***.** The initial testing and trials of the new EMF system at PNNL were conducted in September and October 2001. The trials consisted of assembling the new EMF power supply system, load cables, and inductive load coil. The apparatus used to conduct the experiments is illustrated in Figure 1. This figure shows the four parallel coaxial conductors connected between the power supply and the EMF coil. The coil used was a single-turn, low-inductance aluminum alloy coil made from AA6061-T6. Not shown in the figure is the coil containment shroud and associated supports. The experiments involved multiple cycles of charging and discharging of the capacitor bank through the load coil at various known energy levels. The capacitor bank was controlled via the custom system developed for the unit. The sequence of testing consisted of charging the capacitor bank, isolating the charging power supply, triggering (releasing) the capacitor charge, and monitoring the response of the system. The system response was recorded using a high-speed digital oscilloscope. Figure 2 illustrates the typical response of the system during a 15-kJ discharge of the capacitor bank. This figure shows that the half-current (measuring half the total system current) of the system is approximately 86 kA, so

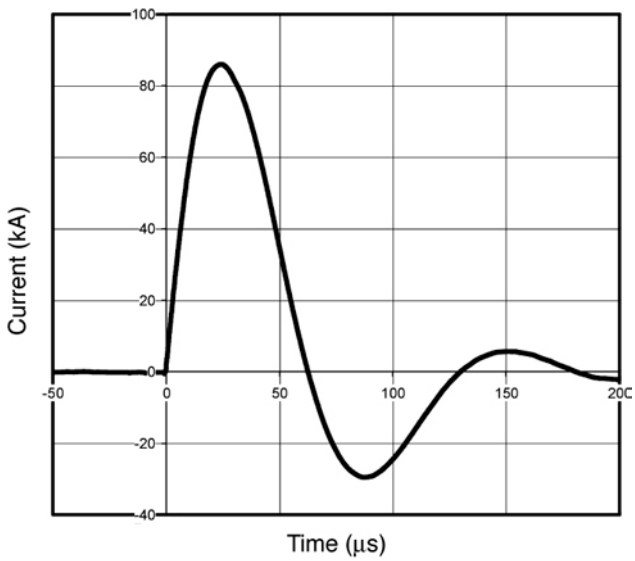

Figure 2. The current waveform that resulted during the initial system trials at PNNL.

that a total current of approximately 172 kA passed through the load coil. The system rise time was shown to be approximately 26 µs. This EMF system has been commissioned and demonstrated with an automated cyclic testing during sheet metal forming. During the first half of FY 2003, the EMF capacitor bank was demonstrated at current levels in excess of 225 kA. The system has also been cycled several thousands times at high current levels while supporting our coil durability experimental work. The custom-designed control system was also successfully demonstrated in automated cyclic loading operating modes. During the last half of FY 2004, the capacitor bank control system was upgraded to increase cycle-to-cycle reliability and to improve the efficiency of the data acquisition system used to sample the electrical response of the entire system as well as the changing response of the coil assembly.

Coil Design Concepts and Durability. During EMF, the high-intensity electromagnetic forces are applied to the turns of the coil. The coil, insulators, and support structure must resist these forces, as well as related thermal cycles, without significant permanent deformation or material failure. In contrast to typical cylindrical coils, sheet forming will require coils with general three-dimensional (3-D) shapes that are inherently less resistant to forces induced during forming. The key issues involve materials selection and design. Materials must be selected for both electrical conductivity and mechanical properties, and they must lend themselves to manufacturing. Materials may also need to be compatible with the presence of coolants and the forces generated during hybrid forming that combines conventional stamping and EMF. The design must integrate these elements while delivering the primary function of a spatial and temporal load distribution that achieves the desired deformations. Coil systems will have to be low-cost, modular, and have high durability (nominally 100,000 cycles) if they are to be relevant to automotive manufacturing.

During the second quarter of FY 2002, LANL generated a technical report containing a conceptual coil design to perform in a high-volume manufacturing system. This particular design is considered modular and would likely require multiple coils to execute any singular forming operation. This modular coil approach may require further study of coil-to-coil interaction and durability before it can be commercially implemented. In contrast, Ford Motor Company designed an integrated forming coil system for high-volume automotive stamping of complex components. This Ford-designed system has evolved into the system currently being tested for high-cycle forming trials at PNNL. The design integrates features that enhance the stiffness and durability of the coil during cyclic forming operations.

Beyond these trials on the Ford-designed coil system, PNNL has developed a system to evaluate these potential coil materials under high-cycle EMF conditions. PNNL has designed and fabricated a coil durability test apparatus, which was used early in the project for EMF testing. Figure 3 shows a photograph of the coil configuration that is part of the apparatus (copper alloy shown). Removed from this coil photograph (for clarity) are insulating sheets of Mylar that retard cross-coil sparking. This coil is connected to the EMF capacitor bank and control system via cables that connect on the bottom side of the coil shown. This coil is designed to be placed in close proximity to a stationary aluminum alloy plate and to be subject to cyclic pulse loading at different power levels and frequencies to determine the number of cycles to failure. The objective was to make coils from multiple materials and compare the coil durability across several samples from each population. This early work has evolved into testing of a full-scale coil assembly at PNNL.

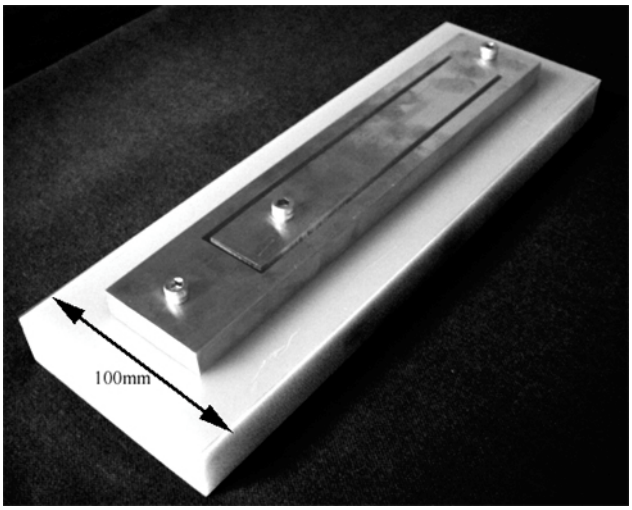

Figure 3. Photograph of the coil system originally used for testing different candidate coil materials.

<u>*Coil Durability Experiments*</u>. During the first half of FY 2003, PNNL evaluated the performance of the original coil assembly designed and fabricated under this project. The experiments consisted of evaluating the forming effectiveness, measuring the coil's thermal characteristics, and starting durability tests under cyclic loading of the coil system. Figure 4 shows a photograph of the Ford- and PNNL-designed coil assembly. Figure 5 shows photographs of the forming die used as well as the resulting formed aluminum sheet after testing. In this figure, the coil is directly below the aluminum sheet, and the holes in the die are 3 in. in diameter.

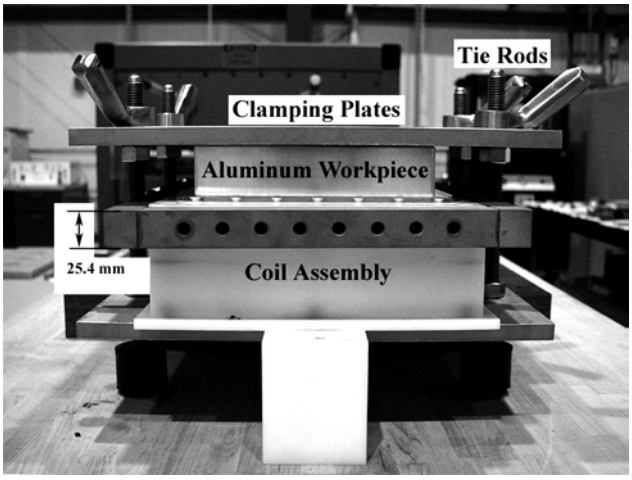

Figure 4. Photograph of the Ford and PNNL designed coil assembly. This assembly has undergone cyclic testing at PNNL and achieved greater than 5000 cycles with no signs of coil degradation.

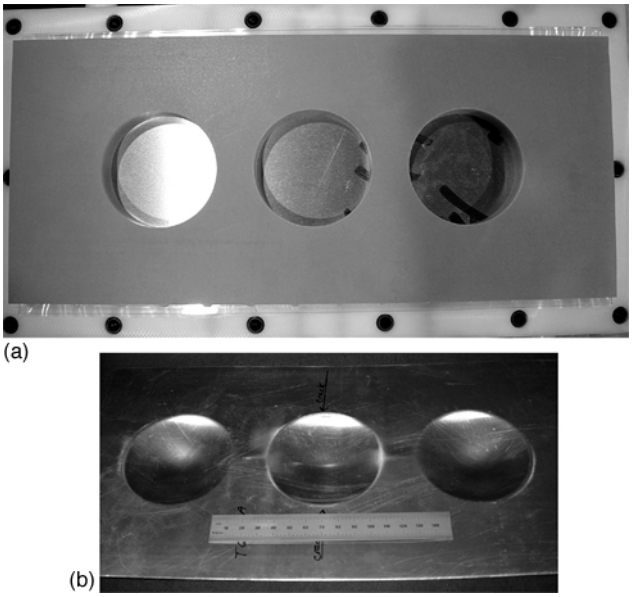

Figure 5. (*a*)Top view of the glass-fiber-reinforced plastic tooling on the coil assembly with aluminum sheet metal between the coil and the tool. (*b*) Photograph of the deformed sheet after one EM pulse through coil.

After a single EM pulse through the coil, the system forms three domes as shown in Figures 5 and 6. These forming experiments were conducted to learn the necessary pulse magnitude in order to effectively form aluminum sheet. Subsequent to determining this critical EM pulse magnitude, PNNL initiated cyclic loading experiments on the coil system to determine the thermal and mechanical characteristics of the coil assembly to determine long-term durability. This original assembly has undergone cyclic testing at PNNL and has achieved greater than 5,000 cycles with no signs of coil degradation.

The PNNL coil durability experiments have focused on increasing the frequency of capacitor discharge to simulate high-repetition rate of automotive manufacturing. PNNL has increased the charge rate of the capacitor bank and refined the control system to achieve cyclic discharge rates to fewer than 10 s. This has allowed the project team to evaluate the structural performance of the coil and better understand the effects of coil operating temperature. One major focus at PNNL during the first half of FY 2004 was investigating the influence of coil assembly temperature and the ability to remove heat from the coil. Figure 7 shows the results of experiments at PNNL to evaluate the

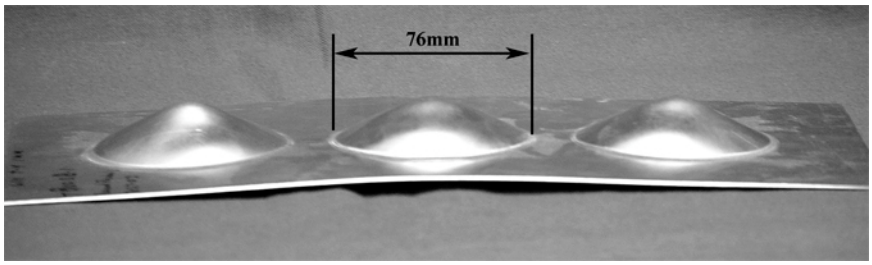

Figure 6. A formed aluminum sheet after a single EMF operation.

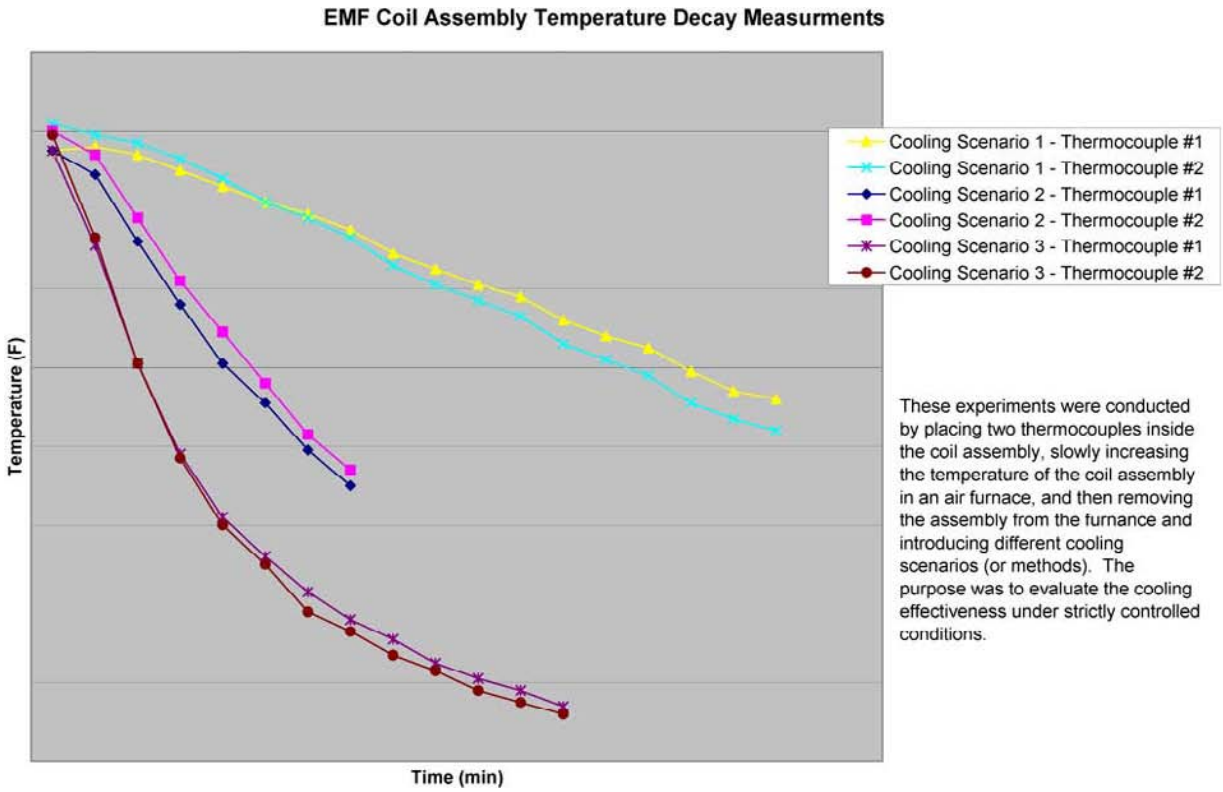

Figure 7. Plot showing the experimental results of heat removal from the coil assembly using three proprietary cooling scenarios. These experiments evaluated the rate of heat removal under controlled conditions to establish the effectiveness of each of the three cooling techniques.

ability to remove heat from the coil using various proprietary techniques.

In the second half of FY 2004, PNNL redesigned the original coil assembly to increase the efficiency of cooling. The original design had limited cooling capacity and included materials that had operating temperature ranges insufficient to support 10-s cycle times at high-energy capacitor bank discharge. The redesigned coil made a series of material substitutions and design refinements to increase the cooling efficiency, while attempting to retain the successful mechanical support from the original design. This second-generation design has been fabricated at PNNL. PNNL is currently evaluating the cooling efficiency of this second-generation design under short cycle times at high-energy capacitor bank discharge.

Formability of Aluminum During EMF. Ford Motor Company has conducted laboratory experiments to investigate the formability of aluminum alloy sheet during EMF. These laboratory experiments included free forming of domes and forming of sheet metal into v-shaped die cross-sections. Figure 8 shows a cross-section through a v-shaped

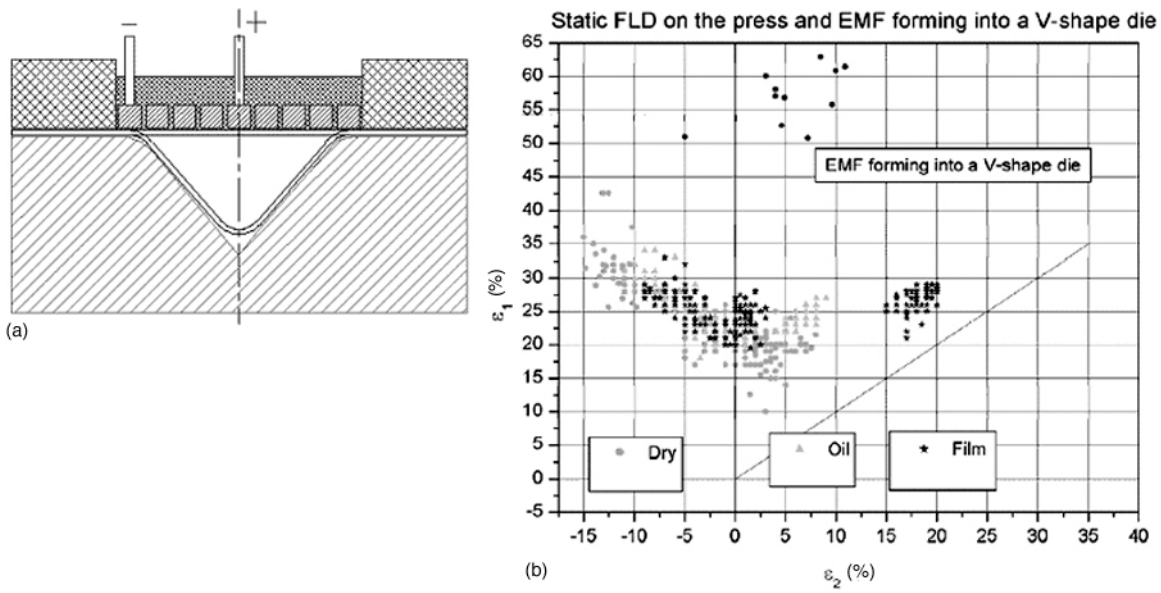

Figure 8. (*a*) A cross-section through a v-shaped die showing the coil, die, and workpiece before and after deformation. (*b*) Strain grid formability data showing the improvement in aluminum formability under these forming conditions.

forming die showing the coil, die, and the workpiece before and after deformation. This figure also shows the results of a typical strain grid analysis and the two to three times improvement in formability under these forming conditions. However, the experimental data have shown that the formability is sensitive to the shape of the die being used to evaluate the formability. Further investigation may be required in this area to better define the forming limits of the material under the varying biaxial and triaxial states of stress that develop during EMF.

Numerical Simulation of EMF Process. The EMF process is challenging to simulate due to the need to simultaneously model electromagnetic, thermal, and elastic-plastic deformation of materials. Many of the commercial research codes have serious limitations and an inability to accurately predict the results of EMF processes. This project has focused on integrating portions of existing commercial research codes to accurately predict the important characteristics of a 3-D EMF process. The current work involves collaboration with Dr. Nick Bessonov in cooperation with University of Michigan–Dearborn. Figure 9 illustrates an example of a 2-D simulation of EMF of aluminum sheet into a conical die with a fully coupled electromagnetic-elastic plastic model. These models are currently being extended for use as a fully 3-D numerical simulation approach.

Industrial Embodiment. Oxford Automotive completed a study of the industrial embodiment of the EMF process, which is designed to analyze the potential methods to incorporate EMF into the highly integrated manufacturing of automobiles. The study investigated integration into conventional sheet metal stamping production facilities and the

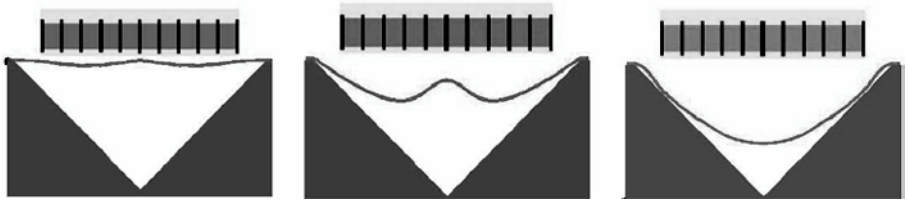

Figure 9. Example of a 2-D simulation of EMF of aluminum sheet into a conical die with a fully coupled electromagnetic-elastic plastic model. *Source:* Produced by Dr. Bessonov in cooperation with the University of Michigan–Dearborn.

potential to create an entirely new and separate production line based on EMF technology for aluminum alloy sheet. Several variations of industrial deployment were identified and studied. Figure 10 shows a conceptual industrial embodiment of the EMF process as produced by Oxford. The system shown involves an EMF station located in conjunction with conventional mechanical presses. In the scenario shown in Figure 10, the EMF system would be used as a separate forming station to perform a restrike function. This restrike operation would be employed to increase deformation in local regions requiring greater formability than conventional stamping will permit.

Conclusions

Technical feasibility of EMF for aluminum sheet in an automotive application has been demonstrated, during both this project and prior U.S. Council for Automotive Research projects. The durability of relevant coils systems and methods for the economical design, construction, and implementation of forming systems are yet to be demonstrated. However, the current project has made significant progress is demonstrating coil durability at commercially relevant conditions. There is also a need for additional dynamic formability data of relevant aluminum alloys. This project targets these issues. Progress has been made in assessing the current state of knowledge for materials, coil design, formability, and system design. Also, a pulsed power system has been designed and fabricated to serve in experimental testing of coil systems. This project has also shown that EMF can be performed using aluminum sheet while achieving intermediate coil life (~5000 cycles). As this project progresses, a balanced combination of analysis and experiment will be applied to demonstrate more durable coil systems that meet the performance requirements of automotive manufacturing.

Presentations and Publications

"Pulsed Electromagnetic Forming of Aluminum Body Panels." Accepted for publication by 2005 TMS Annual Meeting and Exhibition, San Francisco, California, February 13–17, 2005.

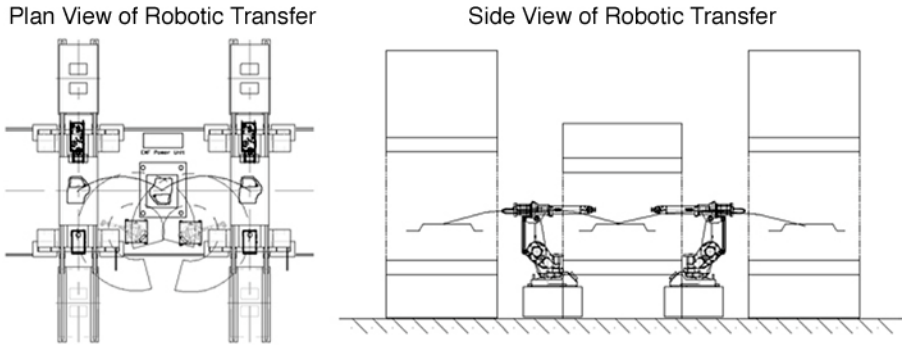

Figure 10. Conceptual industrial embodiment of the EMF process. The system shown involves an EMF station located in conjunction with conventional mechanical presses.

D. Aluminum Automotive Closure Panel Corrosion Test Program

Project Co-Chair: Tracie Piscopink-Jafolla
General Motors Corporation
Mail Code 483-370-101
3300 General Motors Road
Milford, MI 48380-3726
(248) 676-7014; fax: (248) 685-5279; e-mail: tracie.l.jafolla@gm.com

Project Co-Chair: Francine Bovard
Alcoa Technical Center
100 Technical Drive
Alcoa Center, PA 15069
(724) 337-3249; fax: (724) 337-2044; e-mail: francine.bovard@alcoa.com

DOE Technology Area Development Manager: Joseph A. Carpenter
(202) 586-1022; fax: (202) 586-1600; e-mail: joseph.carpenter@ee.doe.gov
ORNL Field Technical Manager: Philip S. Sklad
(865) 574-5069; fax: (865) 576-4963; e-mail: skladps@ornl.gov

---

Contractor: U.S. Automotive Materials Partnership
Contract No.: FC26-020R22910

Objective

- Develop a standardized cosmetic corrosion test for finished aluminum autobody panels that provides a good correlation with in-service testing and field performance.

Approach

- Define test matrix.
- Specify and obtain materials.
- Specify phosphate and paint system.
- Pretreat and paint large reservoir of test specimens.
- Conduct laboratory testing, outdoor exposures, test track exposures, and in-service testing.
- Evaluate test data to determine which accelerated tests correlate with in-service testing.
- Conduct second iteration of laboratory testing to determine reproducibility and repeatability of accelerated tests down-selected based upon initial data.

Accomplishments

- Completed test track exposures and initial laboratory tests.
- Exposed in-service tests for 2 years out of 5 planned.
- Completed initial evaluation of test track exposures laboratory test samples.
- Conducted corrosion product analyses for some laboratory tests.

Future Direction

- Complete analysis of initial laboratory test data and define second iteration of lab tests.
- Continue long-term in-service testing.
- Conduct corrosion product analyses for in-service tests.

Introduction

The use of aluminum closure panels such as hoods, deck lids, and lift-gates continues to increase as the need to lower overall vehicle weight and thereby improve fuel economy increases. One of the key requirements for closure panel materials is a very high degree of corrosion resistance and excellent paint durability. Although aluminum closures have been used for many years on a limited number of vehicles with satisfactory performance, the general level of confidence and ability to predict corrosion lifetimes in service remains uncertain. Over the years, many laboratory corrosion test environments have been developed to determine the performance of painted closure panels. Although the results of these tests are useful for relative comparisons of alloys or paint systems, the correlation of these lab test results with in-service performance has not been established in a systematic way. Extensive studies have been carried out in order to establish this correlation for finished cold-rolled and galvanized steel substrates[1] through cooperative efforts between the automotive companies and steel, pretreatment, and paint suppliers. With the increased use of aluminum, it was recognized that a program was required to establish the correlation between lab test results and in-service performance for finished aluminum closure panels.

In response to this need, a group composed of representatives from the auto companies, the aluminum industry, and associated suppliers was established in June 2000 to formulate a program that would provide this correlation. The establishment of a standard test method for corrosion of aluminum closure panels through this effort will accelerate the adoption of lightweight aluminum materials to lower overall vehicle weight and reduce manufacturing costs by eliminating multiple test programs. A single corrosion test accepted throughout the industry could also be used to allow rapid selection and verification of alloy, pretreatment, and paint performance. In this report, an outline of the test program, evaluation procedures, and discussion of the preliminary results from initial laboratory tests and test track exposures are presented.

Experimental

Reservoir of Painted Materials

In 2001, the first step in the development of a new cosmetic corrosion test occurred with the establishment of a reservoir of painted panels. These panels would then be used in the subsequent evaluation of all test methods. As listed in Table 1, the substrate materials, metal finish, and paint processing variables were selected to give a range of cosmetic corrosion performance. Several aluminum alloys used in the Unites States and in Europe, both current and historical, were included. Electrogalvanized steel and uncoated cold-rolled steel were included as reference materials. Two aluminum alloys were sanded to simulate metal finishing in an automotive assembly plant body shop.

The materials were painted with a typical automotive paint system. This paint system included zinc phosphate pretreatment, medium-build cathodic electrophoretic priming (e-coat), and spray painting with a primer surfacer and white basecoat—clear topcoat system for a total paint film thickness of approximately 100 μm. An additional set of 6111 panels was processed through the phosphate pretreatment with lower fluoride concentration (comparable to the fluoride level used for steel-only vehicles). Also, since qualification testing is often done on panels that are processed only through the electrophoretic primer (e-coat) step, another set of 6111 panels was processed only through the e-coat step, that is, standard fluoride for aluminum but no basecoat or clear coat applied.

Panels were prepared for testing with a single scribe penetrating through the coatings to the substrate. The painted and scribed samples were then sent to laboratories for testing in a variety of environments, including laboratory, static outdoor exposure, proving ground, and on-vehicle tests.

Table 1. Materials

	Alloy	Metal finish	Paint system
A	AA6111-T4PD	No	Standard
B	AA6111-T4PD	No	Low F-
C	AA6111-T4PD	No	E-coat only
D	AA6111-T4PD	Yes	Standard
E	AA6016	No	Standard
F	AA6022-T4E29	No	Standard
G	AA2036	Yes	Standard
H	Cold -rolled steel	No	Standard
I	EG 60 Steel	No	Standard

Evaluation Method

The evaluation of scribe corrosion has traditionally been performed visually with a simple ruler by measuring creepage distance. While this simple technique of measuring creepage distance has provided some quantitative measure of corrosion severity, the one-dimensional (1-D) interpretation (length only) of manual technique provides only a partial quantification of the two- (if not three-) dimensional (2- or 3-D) creepage phenomena. In the case of filiform corrosion found in aluminum substrate where creepage does not propagate uniformly along the scribe line, as in steel substrate, but rather forms threadlike, circuitous filament lines, this 1-D manual technique of measuring straight-line distance may incorrectly quantify corrosion.

Optical macro imaging is a proven instrumentation technology that, when applied to the evaluation of 2-D surface defects, provides more reliable and accurate measurements of geometrical shapes than are obtainable with traditional human visual evaluation methods or 1-D extrapolative analysis of 2-D shapes. For this study, an optical imaging system developed by Atlas Material Testing Technology, LLC, was employed to properly and quantitatively interpret the degree of filiform corrosion. (See Figure 1.) A state of the art imaging system such as VIEEW™ should employ controlled illumination conditions (geometry and intensity), high-resolution digital image capture and advanced algorithm-based image and data analysis methodologies. The use of optical imaging techniques eliminates the deleterious influences of human subjectivity by digitally capturing all sample images under the same enhanced illumination conditions and then subjecting them to a consistent image analysis administered by objective computer software.[2–6]

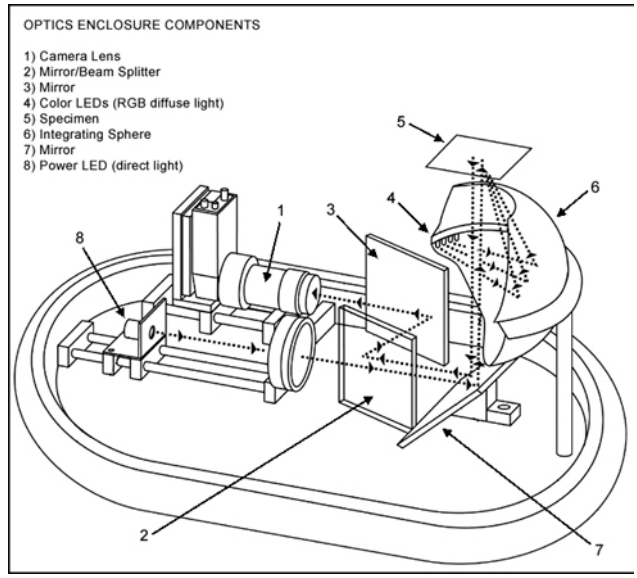

Figure 1. VIEEW™ System physical layout.

Application of the optical imaging system for the corrosion creepage analysis requires three functional steps to "train" the system for the specific test specimen topology: (1) selection of optimal illumination setting, (2) selection of region of interest setting, (3) selection of image processing routine. Once the steps are programmed into a macro function, the test is performed automatically. When so initiated, the instrument recreates the programmed conditions (illumination, region scanning, image processing, and detection) as a recurring process.

1. Selection of illumination setting: To detect the filiform or blisters on the reflective coating surface, direct illumination with a hint of monochromatic diffuse illumination should bring out the topological differences of the defect region from the flat background and identify the initial scribe line. (See Figure 2.) It is the contrast difference by the direct illumination that distinguishes the region of interest from the background. Once the optimal setting is chosen, it is saved as an illumination setting file.
2. Selection of region of interest setting: The X-Y automatic scanning stage can be programmed to scan only the region of interest. Because most corrosion testing is performed in a geometrically consistent manner, the automatic scanning mechanism is useful for multisample testing in the case of the scribe corrosion test. The automatic stage is indexed to successive X-Y coordinates, and the exact sample location is

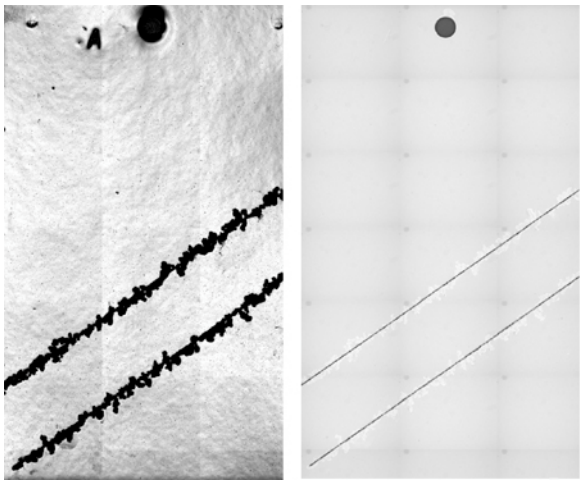

Figure 2. Filiform optically captured with direct illumination compared with common diffuse illumination.

reproduced as long as loading of the sample into the stage sample holder is performed in a consistent manner by users.

3. Selection of image processing routine: For the detection of filiform filaments, digitized gray images are divided into two gray regions: the corrosion region and the non-corroded background, through the use of a gray thresholding technique. During this step, the thresholding point (gray value) is recorded. As the subsequent samples are imaged with identical illumination geometry and intensity, the thresholding point allowed automatic determination of the region of interest. It is also at this step that the original image was digitally overlaid with a pseudo-color to more clearly identify the corrosion region. Once the region of interest is automatically detected, a few interactive processes takes place to "tell" the system where the scribe line is so that measurements can be made automatically. For this study, four geometrical attributes are measured: area of corrosion, maximum creepage, minimum creepage, and average creepage. Refer to Figure 3 for an example.

Evaluation of Existing Lab Tests

To evaluate existing cosmetic corrosion test methods, the Task Force decided to use triplicate sets of the standard materials chosen for evaluation. These materials were provided to the testing laboratories as shown in Table 2. Each test set also

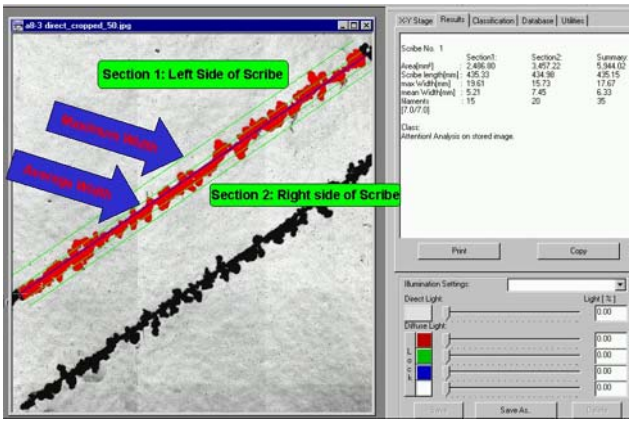

Figure 3. Automated corrosion measurement.

includes a minimum of two bare steel and two bare zinc mass loss coupons. There are laboratory (9), automotive proving grounds (3), and static outdoor tests (3) included in these evaluations.

As used in previous Society of Automotive Engineers (SAE) Automotive Corrosion and Prevention (ACAP) task force corrosion tests, these results will be quantitatively compared using scribe-creep results. The scribe-creep results will be compared to real-world standard results utilizing two methods; (a) coefficient of variation (COV) and (b) R^2 + C-ratio technique. A detailed description of these methods will be provided in subsequent presentations when enough field test data are available to compare to the laboratory test results.

In-Service (On-Vehicle) Cosmetic Corrosion Tests

It is critical when developing a laboratory-based test that test-to-field correlation be performed. In an effort to capture real-world data in developing this test, it is necessary to expose these panels to severe corrosive environments that represent real-world "worst case" scenario. Suitable environments exist in the northeastern United States, southeastern coastal areas of the United States, and southeastern Canada. The four sites selected for this study were (1) Detroit, Michigan; (2) Orlando, Florida; (3) St. John's, Newfoundland; and (4) Ohio–New York route.

Each site (two vehicles per site) will expose 4 sets of 24 test panels that are 2 in. by 4 in. with precut edges. Each set of 24 (3 each of 8 material variables) will be attached to a mounting panel (16 in. by 12 in.) using 3-M double-backed tape

Table 2. Cosmetic corrosion tests evaluated by the Corrosion Task Force

Accelerated laboratory tests			
SAE J2334—40, 60 and 80 cycles	General Motors Company	GM 9540—40 and 80 cycles	General Motors Corp.
Ford APGE—35 and 70 cycles	Ford Motor Company		
ASTM 2803—50, 80, and 100%RH	Alcan		
ASTM G85 Annex 2–3 weeks	Alcoa		
VDA 621-415	ACT		
ASTM B117	National Exposure Testing		
CCT 4	Ford Motor Company	HCL dip	Alcan
HCL dip	Alcoa		
Volvo Mud Test	Ford Motor Company		
Original equipment manufacturer (OEM) test track			
Chrysler Proving	Daimler Chrysler Corp.		
Ford Proving Ground	Ford Motor Company		
GM Proving Ground	General Motors Corp.		
Outdoor exposure site			
Miami, Florida			
Pittsburgh, Pennsylvania			
Cape Canaveral, Florida			
In-service (on-vehicle) exposure			
Orlando, Florida			
Detroit, Michigan			
St. John's, Newfoundland			
Cleveland, Ohio, to Massena, New York, truck route			

prior to mounting on vehicle. One set will then be on the hood of each vehicle (horizontal orientation) and one set on the right front door of each vehicle (vertical location). Each panel contains two diagonal scribe lines, which are 2 in. long and 1 in. apart. The panels will be exposed for 5 years of in-service exposure.

OEM Test Track Exposures

Proving ground tests have historical background and are based on extensive test-to-field correlation studies. The four proving grounds selected for this study were (1) GM—Milford, Michigan; (2) Ford—Flagstaff, Arizona; (3) DCX—Chelsea, Michigan; and (4) ARL—Aberdeen, Maryland.

Each site will expose two sets of 24 test panels that are 2 in. by 4 in. with precut edges. Each set of 24 (three each of eight material variables) will be attached to a mounting panel (16 in. by 12 in.) using 3-M double-backed tape prior to mounting on vehicle. One set will then be on the hood of each vehicle (horizontal orientation) and one set on the right front door of each vehicle (vertical location). Each panel contains two diagonal scribe lines that are 2 in. long and 1 in. apart. The panels will be run for a predetermined time that is representative of 10 years of field exposure.

Outdoor Exposures

In addition to on-vehicle and OEM test track exposures, static exposure for the products at the following three testing sites were elected for this study: (1) South Florida Test Services in Miami, Florida; (2) ARL Exposure Site in Cape Canaveral, Florida; and (3) Alcoa Exposure Site in Pittsburgh, Pennsylvania.

Each test site will expose 24 (3 each of 8 material variables) test panels that are 4 in. by 6 in. with precut edges and a 5/16-in. diameter hole for mounting. Each panel contains two diagonal and parallel scribe lines, which are 4 in. long and 1 in. apart. The panels will be exposed for 2 years of static outdoor exposure.

Corrosion Product Analysis

To state categorically that any lab test correlates well with in-service corrosion performance, it is essential that the chemical nature of the corrosion products formed on lab-tested materials match those on identically prepared materials exposed to in-service environments. Apart from the extent of corrosion found on painted coupons, the chemical composition of the corrosion products from lab and in-service exposure should be the same if a good correlation exists. To initiate this comparison, the corrosion products from samples of AA6111 that had been exposed to various corrosion test environments were analyzed using a variety of electron-optical techniques. This work was carried out in cooperation with the Surface Science group at the University of Western Ontario. A more complete description of this work is being presented at this year's SAE Congress.[7] In this paper, only a very brief description of this work will be provided.

Electron optical techniques were selected to do this analysis because the amount of corrosion product on aluminum closure panels is very small, making more traditional analytical procedures impractical. In addition, the use of these methods allows not only for a measurement of the chemical species present, but also for an analysis of the distribution of these species in and around the corroded area on the panel. Work to date has shown that some lab tests, such as the SAE J2334, result in corrosion product formation where high localized concentrations of certain elements such as chloride are found at the periphery of the corrosion site; whereas in other tests, such as the CCT IV, the distribution of chemical species is much more homogeneous throughout the corrosion product. It is anticipated that initial comparisons of corrosion product in lab tests and in-service environments will be carried out in 2005.

Results and Discussion

Nine different laboratory-accelerated corrosion tests were run by multiple test labs in an effort to determine both reliability and repeatability of the tests as well as the correlation of those tests to in-service exposure. The tests that were selected for this project are standard test methods that are requested by the automotive manufacturers as well as tests that the aluminum suppliers use to make decisions in their laboratories. They include salt spray tests and cyclical exposure tests.

One of the goals in the analysis of the accelerated corrosion tests was to identify the most reliable measure of corrosion on aluminum panels. A method used to identify a reliable measure was to analyze the variation in corrosion between the two scribes on the same panel and between the laboratories that were running the particular test.

The chart in Figure 4 shows the corrosion performance for two labs that ran the VDA test, measured by corrosion area. The corrosion area is consistent between the two scribes on the same panel for both labs that ran this test.

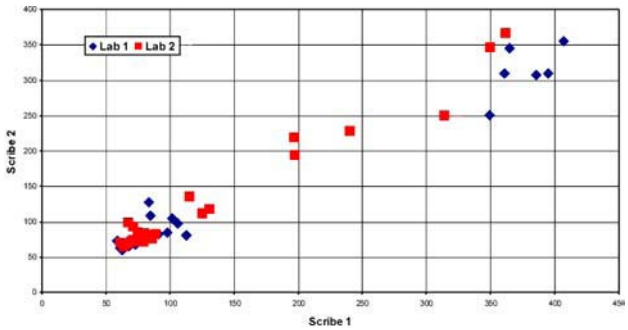

Figure 4. Lab-to-lab comparison for VDA test.

In Figure 5, there is also good correlation in the corrosion performance of the SAE J2334 test, as measured by corrosion area, between the scribes. The general trend for all of the accelerated corrosion tests run in this study is that corrosion area appears to be a reproducible measure of corrosion performance.

The standard measure of corrosion in the automotive industry is creepback from the scribe, primarily in terms of maximum creepback, or the maximum distance that corrosion has propagated from the scribe line. In general, the measure is

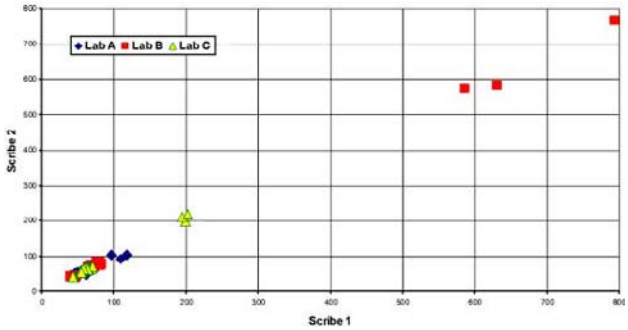

Figure 5. Lab-to-lab comparison for SAEJ2334.

subjective. The following charts exhibit the reliability of that measure.

Figure 6 shows the variation in maximum creepback between the two scribes on the same panels for the VDA test. It is obviously much more difficult to get a consistent measure of corrosion performance, even on the same panel.

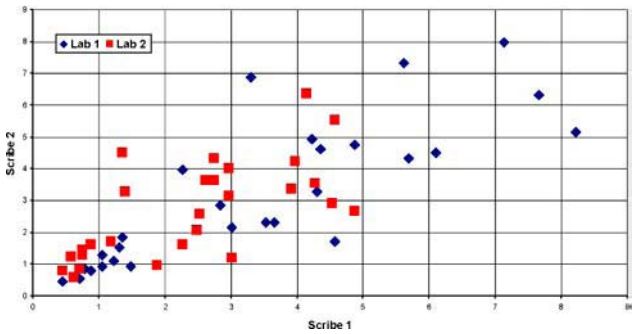

Figure 6. Variation in maximum scribe creepback between two scribes on the sample.

The chart in Figure 7 also shows the variation in corrosion performance, as measured by maximum length, for the SAE J2334 test. Again, it is difficult to get a consistent measure of corrosion performance, even on the same panel.

The results of all of the accelerated corrosion tests are similar to these two examples. It would appear that corrosion area is the preferred measure of corrosion performance, from a reliability perspective. But no conclusive judgments can be made until a correlation is found between the accelerated corrosion test results and the in-service exposure.

Steel panels were run in conjunction with the aluminum in the accelerated corrosion tests as a control. In most cases, the amount of corrosion on the aluminum was significantly less than that found on the steel. The chart in Figure 8 shows the disparity in corrosion performance.

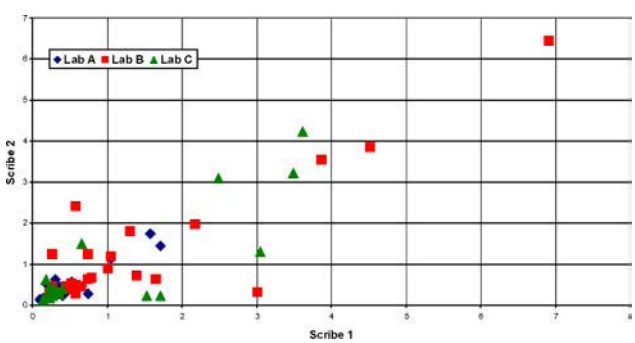

Figure 7. Variation in corrosion performance, as measured by maximum length, for the SAE J2334 test.

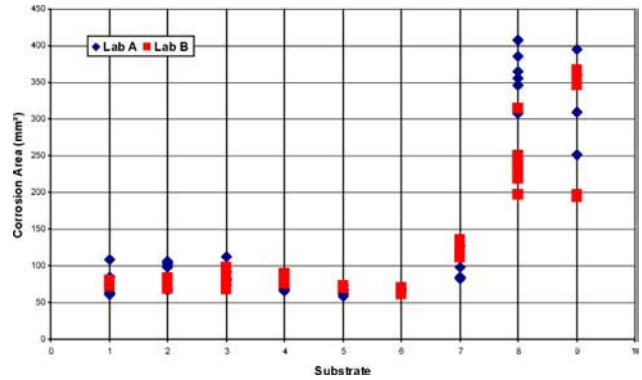

Figure 8. Disparity in corrosion performance of aluminum and steel substrates in VDA test.

Substrates 1 through 7 are aluminum, while substrates 8 and 9 are steel. Although this chart shows the results for the VDA test, the results are consistent for all of the accelerated tests run in this study. Only a few of the tests showed any significant differences in the aluminum substrates based upon the measurement of corrosion area or maximum length (creepback) using the Atlas Vieew technique.

At this point in the program, panels from the test tracks have been analyzed, and correlations between test tracks and the accelerated corrosion testing are currently being evaluated. Also at this point only a very limited amount of service-relevant results from the on-vehicle tests are available. From the preliminary on-vehicle results, it is qualitatively apparent that the panels with metal finishing (D & G in Table 1) have significantly more corrosion than the other substrates. Based on this preliminary observation, accelerated tests that also show a significant difference between the substrates with metal finishing (i.e. sanding) and those without metal finishing would appear to correlate better with the preliminary observations from on-vehicle testing. Many of the accelerated lab tests do not show a significant difference between the substrates with and without metal finishing. Of the laboratory test methods evaluated thus far in the program, only the HCl dip test, the ASTM G85-A2 test, and possibly the APGE test appear to show a significant difference in corrosion performance between the substrates with metal finishing (i.e., sanding) and those without metal finishing.

Similarly, test track or proving grounds tests that show a difference in performance related to metal finishing would qualitatively correlate better with the preliminary field test observations. One of the OEM test track exposures appears to exhibit differences in the performance of substrates with and without sanding that are consistent with the preliminary on-vehicle observations, but the other two OEM test tracks are not consistent with this difference as illustrated in Figure 9.

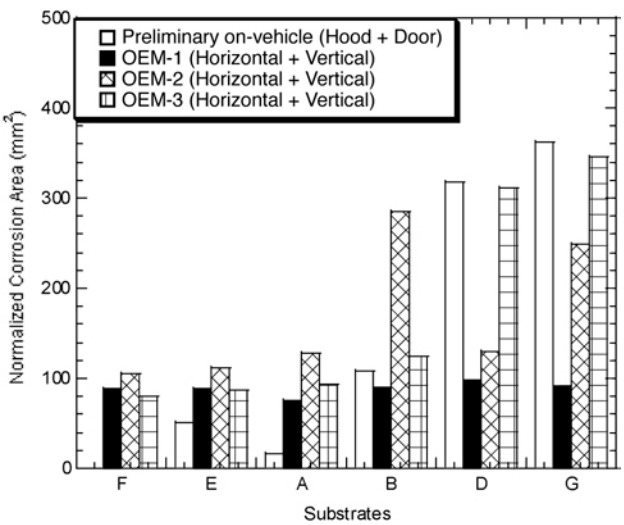

Figure 9. OEM test track and preliminary on-vehicle exposure results.

Summary and future work

Correlation of accelerated tests with on-vehicle exposures is critical for this test development effort. Accelerated tests that show signs of possible correlation with on-vehicle tests will therefore be selected for further evaluation in subsequent testing. The reproducibility of the tests is also an important consideration, which will require additional testing to evaluate. Most of the initial lab tests were run at two labs to provide an indication of reproducibility, but for those tests that are selected based on a possible correlation with on-vehicle results, testing will need to be conducted at a larger number of labs to better evaluate the lab-to-lab variability. Table 3 summarizes which tests appear to qualitatively correlate with the limited amount of in-service results available at this point in time and the reproducibility between labs as tested thus far. More in-service results are needed before decisions about selection of lab tests for further evaluation can be made. A large volume of lab test data has been generated. A more in-depth analysis of the lab test results is needed to compare corrosion morphologies and evaluate irregularities in the results (e.g. scribe-to-scribe and panel-to-panel variability for particular substrates).

Table 3. Qualitative summary of correlation with preliminary on-vehicle results and lab-to-lab reproducibility

Accelerated Test	Significant Difference With and Without Metal Finish? (Y or N)			Reproducible Lab to Lab
	Lab 1	Lab 2	Lab 3	
Lab tests				
ASTM G85-A2	Y	?		?
Ford APGE	Y	N		N
ASTM D2803 50%RH	N	N		Y
ASTM D2803 80%RH	N	N		Y
ASTM D2803 100%RH	N	N		N
ASTM B117	N	N		N
HCl Dip	Y	Y		Y
SAE J2334	N	N	N	Y
VDA 621-415	N	N	N	Y
CCT 4	N	N		N
GM 9540P	N	N	N	Y
Test Tracks	H	V/D		
OEM-1	N	N		
OEM-2	N	N		
OEM-3	Y	Y		

H = Horizontal or Hood
V/D = Vertical or Door

Acknowledgments

The authors express sincere appreciation to the U.S. Automotive Materials Partnership, the U.S. Department of Energy, the Automotive Aluminum Alliance, the Society of Automotive Engineers' Automotive Corrosion and Prevention Committee and to the many members of the Corrosion Task Force for their contributions and commitment.

References

1. SAE J2334, "Cosmetic Corrosion Lab Test," Society of Automotive Engineers, Warrendale, Pennsylvania, June 1998.
2. F. Lee, R. Ryntz, and D. Britz, "Analysis of Scratch Resistance Using Optical Imaging and

Automatic Classification," 4th International Coatings for Plastics Symposium, June 4–6 2001, Troy, Michigan.

3. F. Lee, B. Pourdeyhimi, and K. Adamsons, "Analysis of Coatings Appearance and Surface Defects Using Digital Image Capture/ Processing/Analysis," The International Symposium on a Systems Approach to Service Life Prediction of Organic Coatings, Breckenridge, Colorado, September 14–19, 1997.
4. B. Pourdeyhimi and F. Lee, *European Coatings Journal*, 11, 804 (1995).
5. G. Wypych, F. Lee, and B. Pourdeyhimi,. *Durability of Building and Construction Sealants*, Ed. A. T. Wolf, RILEM, 2000.
6. F. Lee, B. Pourdeyhimi, and J. Martin, "Comparative Study of Standard Weathering Test Methods Using Image Analysis," *Durability 2000: Accelerated and Outdoor Weathering Testing, ASTM STP 1385*, J. D. Evans and W. D. Ketola, Eds., American Society for Testing and Materials, West Conshohocken, Pennsylvania, 2000.
7. S. Ramamurthy et al., "Corrosion Product Analysis of Aluminum Closure Panels," SAE paper 05B-417, 2005.

E. Development of the Infrared Thermal Forming Process for Production of Aluminum Vehicle Components

Principal Investigator: G. Mackiewicz-Ludtka
Oak Ridge National Laboratory
P.O. Box 2009, Oak Ridge, TN 37831-6080
(865) 576-4652; fax: (865) 574-4357; e-mail: ludtkagm@ornl.gov

Technology Area Development Manager: Joseph A. Carpenter
(202) 586-1022; fax: (202) 586-1600; e-mail: joseph.carpenter@ee.doe.gov
Field Technical Manager: Philip S. Sklad
(865) 574-5069; fax: (865) 576-4963; e-mail: skladps@ornl.gov

---

Contractor: Oak Ridge National Laboratory
Prime Contract No.: DE-AC05-00OR22725

Objectives

- Implement infrared (IR) thermal forming as a preform method for aluminum tubes prior to hydroforming to reduce vehicle weight and achieve greater fuel economy.
- Verify initial IR thermal forming estimates to determine concept feasibility for aluminum tubes.
- Develop IR thermal forming process to form basic preform aluminum tubes for subsequent hydroforming trials.
- Evaluate IR thermally formed tubes after hydroforming.

Approach

- Initiate a 1-year feasibility study, followed by longer-term activities (based on favorable results from this feasibility effort) to address the following four primary process concerns: (1) a process that produces bends in the tubes, (2) a process that can meet production rates required for automotive needs, (3) an estimated cost associated with the process and how it compares to present processes, and (4) the influence of the process on the applications, that is, effects on material properties.

Accomplishments

- Verified, within the feasibility phase of this project, the relative order-of-magnitude for time estimates for thermal forming aluminum tubes using IR process trials.
- Calculated and determined the thermal flux necessary for forming aluminum tubes based on IR thermal experiments, utilizing thermal input results from laser forming experiments as a guide. Experiments determined that existing reflectors are not capable of providing the type of power distribution needed for forming aluminum tubes.
- Developed via collaborations with Vortek and N. A. Technologies, Inc., the initial design (optics) concept for a new reflector that can achieve the heat flux and IR arc profile needed for the pre-bending 4- to 5-in. diameter aluminum tubes. These tubes preforms are intended to be subsequently hydroformed as aluminum vehicle components. This optics design was based on our initial experimental and simulation modeling results. However, the cost of these optics exceeded the allotted project budget. Consequently, an alternate less costly approach was devised (see next item).
- Developed and designed, via collaborations with Vortek and N. A. Technologies, Inc., an alternative, less expensive, reflector design that utilized a current base reflector, but also incorporated a secondary reflector to

control and contour the thermal flux heat profile onto the tube to achieve the calculated/desired heat flux. Although this secondary reflector design was developed and was less costly than the new reflector, the cost associated with this option also exceeded the funding available for this project.

Conclusions

- Within the feasibility phase of this project initial IR trials, based on flat plates, for thermal forming aluminum tubes have verified the relative order-of-magnitude of time estimates using the IR process. Forming of a 45° bend is estimated to be achieved in 5–20 s. Results suggest that a minimum of ~5 s is required using optimized processing with cooling, a range of 10–20 s without cooling.
- Both experimental and simulation modeling results indicated that optics development and validation phases, in addition to cooling control, are necessary to achieve the power distribution required to conform larger tubes to the shape needed for hydroforming preforms.
- Several (new and modified) reflector designs have been proposed and developed that qualitatively provide the thermal flux contouring needed for preforming tubes for subsequent hydroforming.
- The cost estimates for both a new reflector design (optics) and the less expensive side-shield (secondary reflector) concepts exceed the budget allotted for this project, and therefore preclude the further development and implementation of this technology.
- Without additional funding, the reflector (optics) proposed and designed within this project that controls and contours the thermal flux heat profile onto the tube (to achieve the calculated/desired heat flux) can not be fabricated and implemented to demonstrate the success of the IR technology as a more cost efficient and lighter materials approach to pre-forming tubes for subsequent hydroforming.

Future Direction

- Secure additional funding for the reflector (optics) proposed and designed within this project to fabricate, implement, and demonstrate the success of the IR technology as a more cost efficient and lighter materials approach to preforming tubes for subsequent hydroforming.
- Pursue alternate heat sources, for example, induction thermal forming options for comparative costs.

Introduction

During the last 9 years, N. A. Technologies, Inc. (NAT) initiated thermal forming research utilizing the laser as the heat source. Using the laser, NAT has formed a wide variety of tubes in various sizes and materials. The laser thermal forming process has been found to work on both large and small aluminum tubes (see Figure 1). These experiments have demonstrated that the wall thickness of the outside bend of the tube is virtually unaffected, and the inside bend actually thickened in all cases. However, the cycle times required for laser forming are too long to be considered for high-volume applications. Based on some work done on plate-stock, NAT has shown that if the thermal input power level is scaled-up from 4 kW (characteristic of laser technology) to 300 kW (characteristic of IR plasma lamp), IR thermal forming works similarly, but much faster. However, this process still has to be proven for tubes. Consequently, the Vortek lamp that is installed at Oak Ridge National Laboratory (ORNL), with its inherent power levels, offers the potential to move the thermal forming process to speeds that are high enough to reach production rate levels. In fact, the higher power levels available with the Vortek lamp are key to taking this process from the “prototyping” or low-volume production stage, to the actual high-volume production stage. NAT has estimated that utilizing the power capacity of the Vortek lamp, the thermal forming process can be put into actual production (i.e., 60 units/h, as opposed to 2 units/h that can be achieved in the laser lab today). The key to tapping this higher

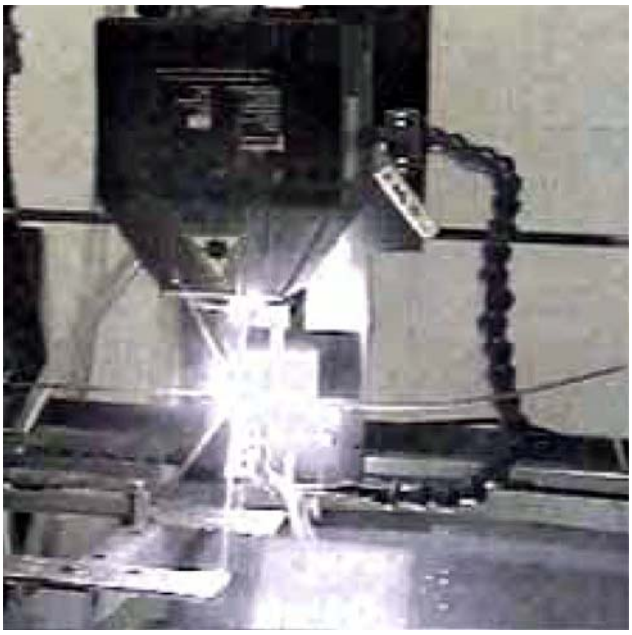

Figure 1. Laser thermal forming process demonstrated on small aluminum tubes.

power source to thermally form the tubes is to develop the correct heat distribution profile.

To date, a great deal of effort has been spent on finite-element modeling at Massachusetts Institute of Technology (MIT), Boeing, Rockwell, Penn-State, Ohio State, British Aerospace, and the best results (from MIT) provide predictions that are off by ±50%. These results emphasize the complexity of the IR thermal forming process. This complexity results directly from the extreme, transient nature of the process with continuously varying surface boundary conditions. Consequently, considerable work remains to be done to develop this process to distribute the heat properly around the tube. NAT has spent nearly a decade developing an understanding of the heat distribution needed to laser form a tube. Developing this process to distribute the heat from the Vortek heat source properly around the tube will be a significant effort. NAT is optimistic that, based on its success at scale-up of plate using the neural-network-based model,[1] developing the right thermal distribution with the Vortek lamp is possible. Success will be defined as demonstrating that the IR thermal forming process works and that it has the possibility of scale-up to real production.

Building on the NAT experience with laser forming and the results from the preliminary experiments involving the IR thermal forming process completed as part of the MPLUS program at ORNL, this project holds the promise of achieving DOE goals of reducing vehicle weight to realize greater fuel economy. The high thermal heat source of the IR lamp technology holds the key to unlock the potential in demonstrating that the IR thermal forming process is more than a laboratory demonstration so that the energy savings potential can be realized.

Status and Summary

Introduction and Background

From the onset of this project, as noted above, it has been known that developing the thermal forming process to properly distribute the heat flux around the tube would be a significant effort. However, based on NAT successful results using laser forming on small-diameter tubes, and its subsequent success at trial scale-up efforts for translating these results to plate, with the neural-network-based model developing the right thermal distribution with the Vortek lamp seems very viable. Consequently, a preliminary *feasibility study* was initiated. Due to the limited project budget available in the first year, the most cost-effective approaches were attempted first to verify the viability of utilizing IR thermal forming to form tubes. Several experimental approaches were attempted to determine the concept feasibility of utilizing IR thermal forming as a fixtureless preforming operation for subsequently hydroformed aluminum vehicle components. These approaches were (1) adapting a long (4-cm) stand-off reflector that was available, (2) modifying the hardware below the reflector to obtain a smaller thermally controlled heat flux zone (thermal footprint), and (3) developing and testing a thermal processing model to run process simulations to determine the appropriate reflector design needed to produce the correct heat flux distribution around the tube. These cost-efficient methods/steps were discussed in the FY 2003 annual report, but are included here for project clarity.

[1]Trained neural networks are attractive predictors for manufacturing processes because they can accurately capture material/process response without requiring actual physical data/models.

Hardware Modifications (FY 2003–FY 2004)

In the initial experimental attempts to form the aluminum tubes, the optics selected and utilized were those that enabled the largest (4-cm) stand-off from the work piece. To accomplish this, the already available 4-cm IR reflector optics were redesigned/reworked to attempt to provide the thermal flux and thermal footprint necessary to thermally bend tubes. Results from these experiments determined that a narrower beam and a higher heat flux are needed. To address this issue, a water-cooled, focusing plate was designed and fabricated to assist in controlling this heat input. The motive behind this inexpensive attempt was to constrain the heat flux at the surface of the tube by merely blocking and absorbing the heat outside of the targeted thermal footprint zone of the IR beam. Experimental trials, however, determined that not enough heat was available to form tubes because the thermal contour was not optimized yet for the tube geometry. However, these experiments did confirm the need to gain a more fundamental understanding of the heat flux required to design an IR thermal forming system to address the more complex case of thermally forming tubes. To accomplish this goal, an IR thermal forming system is needed to address several issues, including reflector shape, focal length, power density, and cooling. Consequently, some basic IR thermal forming trials were initiated to gain a more fundamental understanding of the thermal forming approach needed to bend the significantly more complex tube geometry and to gain a more basic understanding of how the heat flux distribution needs to be tailored to obtain the amount of tube bending necessary. Since these trials were described in detail in the FY 2003 annual report, the results from these experiments will only be summarized here.

Basic Experimental Trials and Modeling Simulations. Utilizing the data obtained from instrumented (thermocoupled) aluminum plates (Figure 2), thermal modeling simulations were run using the experimental parameters as a guide in setting up the modeling boundary conditions. Thermophysical parameters used for the simulations were obtained from the literature. The purpose of the experimental trials was first to obtain experimental temperature data to guide the selection

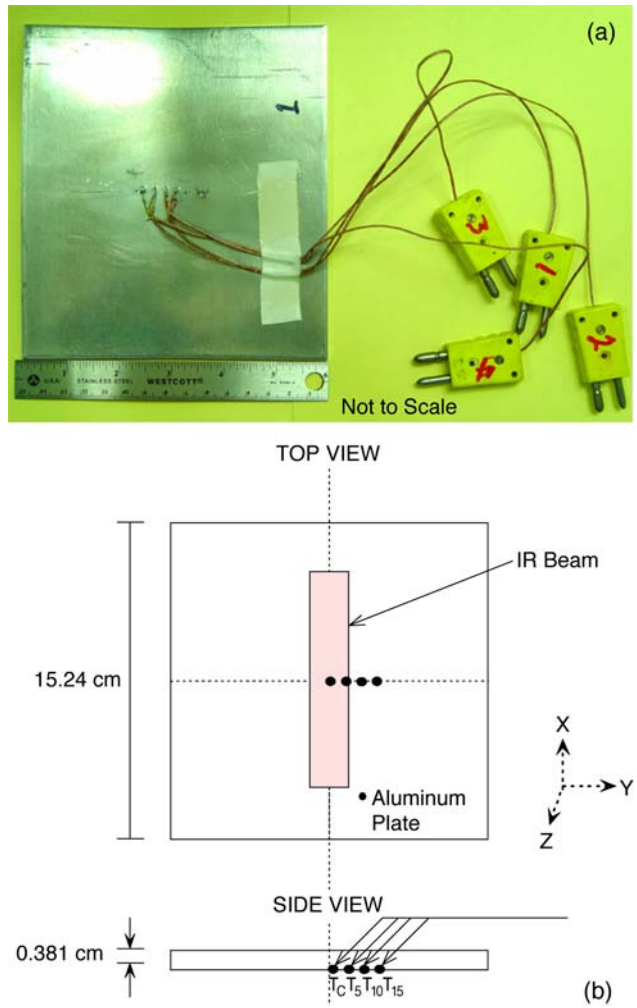

Figure 2. Experimental thermal forming specimens instrumented during trials to gain a more fundamental understanding of the IR thermal forming process.

of the heat flux needed to form aluminum plates and later extend this methodology to the more complex case of forming the tube geometry. The modeling results successfully predicted very similar thermal profiles, (Figure 3) and plate deflections (see Figure 4) with those experimentally measured/obtained from the initial basic experimental study trials. In addition, parametric studies were conducted to predict the effect of plate thickness on the thermal forming response. These results (Table 1) indicated (using these initial non-optimized experimental results) that as the maximum heat flux is increased, the deflection increases; and that as the plate thickness decreases, the plate deflects significantly more. Of course, the thicker plate also

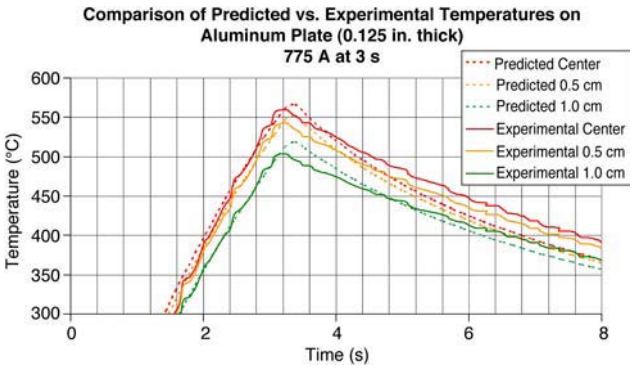

Figure 3. Experimental results and modeling simulation predictions that demonstrate excellent agreement.

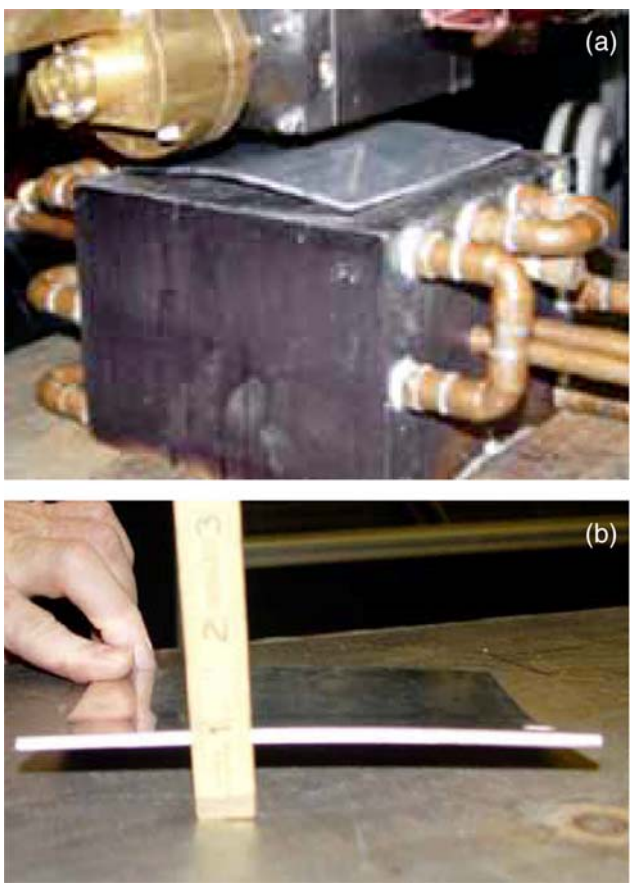

Figure 4. Examples of (*a*) the IR thermal forming setup and (*b*) the aluminum plate deflection observed during initial experimental IR thermal forming trials.

Table 1. Parametric modeling study results

Plate thickness (in.)	Maximum heat flux (W/mm^2)	Maximum temperature (^oC)	Maximum deflection (mm)
0.125	2.25	641	10.92
0.125	2.0	574	9.58
1.0	2.25	203	0.016
1.0	2.0	184	0.014

cools much more slowly, and additional localized cooling, applied immediately after heating likely would provide the necessary constraint to enhance bending. This would also be true for the thinner plate.

Both experimental and simulation modeling results indicated that further optics development and validation phases are necessary to achieve the power distribution required to conform larger tubes to the shape needed for hydroforming preforms.

Neural Net Modeling (NNM) simulations have also been utilized to gain some insight into what the optimized thermal processing parameters need to be to thermally form an aluminum plate. The model allows one to vary each of the three processing parameters independently, and/or as a group to assist in determining the most suitable set of processing parameters (IR power, the number of pulses to obtain a 45° deflection angle, and the total processing time) defined within the experimental data limits. Consequently, additional experiments are being planned to further optimize cycle times within broader processing limits.

Hardware Modifications

The existing reflectors at ORNL are not capable of this type of power distribution. The depths of field of the available reflectors are much narrower than needed; because of the angle of incidence of the energy on the side surfaces of the tube, a higher power density distribution is needed than what is available in the top 60° quadrant of the tube surface.

Consequently, the initial approach was to first develop a new reflector design (optics) based on the heat distribution experimentally determined in previous IR experiments and laser processing. A couple of reflector design concepts were calculated/developed based on this information and submitted to Vortek for review and to obtain cost estimates for these new reflector designs.

New Reflector—Proposed Design Concepts. Based on recent extrapolations from laser experiments, the power distribution needed on the tube surface that is expected to achieve the required 45° deflection angle for tube bending was estimated. While the ideal focus distance profile to provide the required power density distribution has been derived from our current knowledge-based experience on laser thermal forming experiments, in reality, it may be difficult to achieve the sharp profile changes that are needed at the far outer side wall limits of the tube. Consequently, another alternate power density, shown in Figure 5 may be easier to fabricate and is expected to get close enough to the ideal power density distribution to provide reasonable results for tube forming feasibility experiments.

For the currently available reflectors, the power density drops off to well below the ≥65% level needed for down the side wall of the tube. However, since laser processing produced good bending results without providing any power at all below the centerline of the tube, it is assumed that a modified (alternate) power density distribution would also provide good results using even an alternate design for the IR reflector (see Figure 5).

The proposed experimental setup to achieve this alternate power distribution is to orient the Vortek lamp/heat source so that the long axis of the heat lamp is perpendicular to the longitudinal axis of the tube to be formed. This is consistent with the LITS-Form approach, which was applied in the laser forming experiments. In this approach, a line source is moved along the longitudinal axis of the tube with the axis of the line heat source perpendicular to the longitudinal axis of the tube. This alternate reflector design concept also has a high probability of success (again, based on laser experiments) only if a variable focus lamp reflector can be designed and fabricated to provide the necessary power density distribution. The optimum focus profile is estimated to be similar to that shown in Figure 6. The quoted cost of this reflector, however, exceeded the allotted project budget.

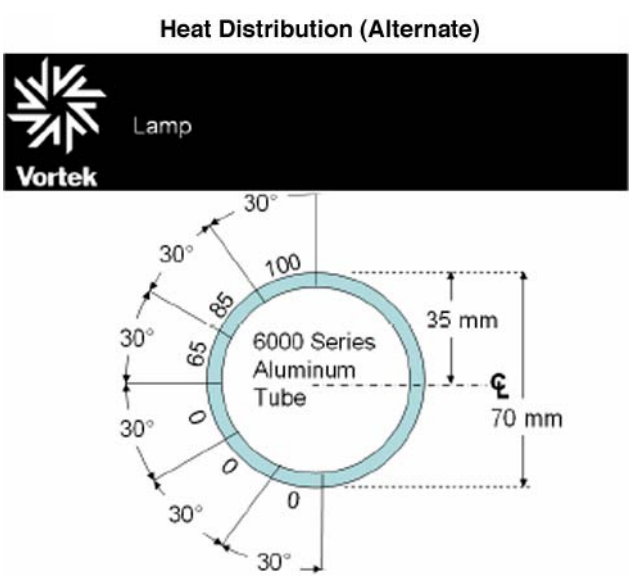

Figure 5. Schematic of modified (alternate) power density distribution needed to form aluminum tubes.

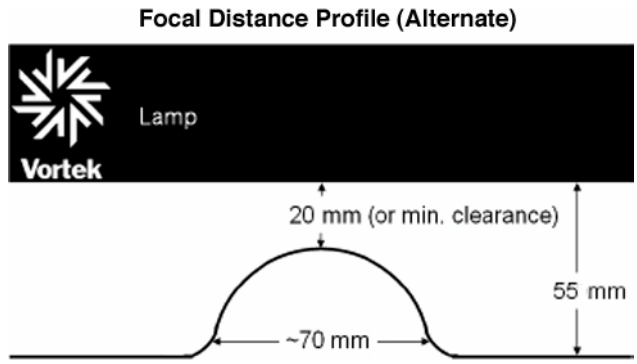

Figure 6. Schematic of the focus distance profile for the modified (alternate) power density distribution needed to form aluminum tubes.

Modified Reflector Optics—Proposed Design Concept. Consequently, an alternative reflector concept was devised. This proposed reflector was developed and designed so that a secondary reflector could be utilized in conjunction with our current *close coupled reflector*, thereby minimizing the reflector, and hence, project cost. A schematic view of this concept is presented in Figure 7. This alternative, less expensive, unoptimized reflector design was developed in collaboration with Vortek and NAT. The goal of this reflector option was to control the thermal heat flux and contour the heat input, but in a more cost-effective way. Several reflector designs were considered, and a final reflector concept was developed. The cost, however, of fabricating and implementing this secondary reflector to achieve the desired heat flux distribution and IR arc profile also exceeded the available funding allocated for this project.

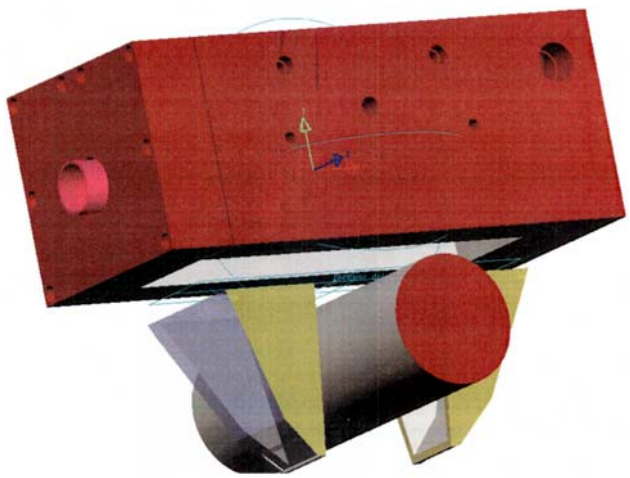

Figure 7. Schematic view of proposed secondary reflector.

Thermal Forming Reflector Design Results

Within the feasibility phase of this project, initial IR trials based on flat plates for thermal forming aluminum tubes have verified the relative order-of-magnitude of time estimates using the IR process. Forming of a 45° bend is estimated to be achieved in 5–20 s. Experimental results in conjunction with laser experience suggest that a minimum of ~5 s is required, using optimized processing with cooling and a range of 10–20 s without cooling.

Two proposed reflector (optics) design concepts for a "new reflector" were developed based on thermal flux calculations from past experimental results and laser processing experience. However, the cost estimates received from Vortek for fabricating the proposed "new reflectors" suggested that additional, less costly approaches needed to be considered. The alternate approach pursued was to develop and fabricate "side shields" that (based on Vortek's experience) would boost the power level to obtain a higher power density needed along the side surfaces of the tube. This approach promised to help experimentally establish/indicate that the higher power densities will achieve the power densities required for the full 45° bend. Because a higher power density can be achieved using the side shield approach, we requested a quote from Vortek. Vortek qualitatively verified that the estimated power distributions expected by incorporating these side shields into our current reflectors were favorable when they compared to the thermal flux requirements that we have calculated based on laser forming experience.

Conclusions

- Within the feasibility phase of this project initial IR trials, based on flat plates, for thermal forming aluminum tubes have verified the relative order-of-magnitude of time estimates using the IR process. Forming of a 45° bend is estimated to be achieved in 5–20 s. Results suggest that a minimum of ~5 s is required using optimized processing with cooling, a range of 10–20 s without cooling.
- Both experimental and simulation modeling results indicate that further optics development and validation phases, in addition to cooling control, are necessary to achieve the power distribution required to conform larger tubes to the shape needed for hydroforming preforms.
- Several (new and modified) reflector designs have been proposed and developed that qualitatively provide the thermal flux contouring needed for preforming tubes for subsequent hydroforming.
- The cost estimates for both a new reflector design (optics) and the less expensive side-shield (secondary reflector) concepts exceed the budget allotted for this project, and therefore preclude the further development and implementation of this technology.
- Without additional funding, the reflector (optics) proposed and designed within this project that can control and contour the thermal flux heat profile onto the tube (to achieve the calculated/desired heat flux) cannot be fabricated and implemented to demonstrate the success of the IR technology as a more cost-efficient and lighter materials approach to preforming tubes for subsequent hydroforming.

3. ADVANCED MATERIALS DEVELOPMENT

A. Low-Cost Powder Metallurgy Technology for Particle-Reinforced Titanium Automotive Components: Manufacturing Process Feasibility Study

Russell A. Chernenkoff
Ford Motor Company
SRL MD3135
2101 Village Road, Dearborn, MI 48124
(313) 594-4626; e-mail: rchernen@ford.com

Dr. William F. Jandeska
General Motors Corporation, GM Powertrain
895 Joslyn Ave., Pontiac, MI 48340
(248) 857-2184; e-mail: william.jandeska@gm.com

Dr. Jean C. Lynn
DaimlerChrysler
800 Chrysler Dr. East, CIMS 482-00-15, Auburn Hills, MI 48326
(248) 512-4851; e-mail: jcl6@daimlerchrysler.com

Technology Area Development Manager: Joseph A. Carpenter
(202) 586-1022; fax: (202) 586-1600; e-mail: joseph.carpenter@ee.doe.gov
Field Technical Manager: Philip S. Sklad
(865) 574-5069; fax: (865) 576-4963; e-mail: skladps@ornl.gov

---

Contractor: U.S. Automotive Materials Partnership
Contract No.: FC26-02OR22910

Objectives

- Demonstrate production-intent process scheme for fully densified titanium alloy powder metallurgy (PM) composite samples.
- Benchmark process capability using commercial-grade titanium powder feedstock, and follow with one of the proposed low-cost titanium powder materials. Blend additives to achieve final titanium alloy material with reinforcement.
- Perform microstructure characterization and interfacial studies.
- Confirm test specimens are crack-free by nondestructive evaluation method (Lawrence Livermore National Laboratory).
- Generate static mechanical properties and perform failure analysis.
- Perform a technical cost modeling study on the novel ADMA Products, Inc., process and establish sensitivity of each processing step for cost-effectiveness.

Approach

- Use titanium metal feedstock to produce blanks in simple shapes via the ADMA manufacturing process that will then be machined into coupons for mechanical property determination.

- Conduct microstructural and interfacial studies together with mechanical property testing.
- Perform a technical cost model on the ADMA manufacturing process.

Accomplishments

- Purchased and received raw materials required for the program.
- Produced powder blends of Ti-6Al-4V material from sodium-reduced titanium sponge fines without reinforcement (benchmark material) and Ti-6Al-4V without reinforcement from magnesium-reduced titanium sponge fines produced in Russia (lower cost alternative to benchmark material). Die-pressed powders in 0.500-in.-diameter carbide tooling to 0.500-in.-thickness for metallographic examination.
- Compacted and processed Ti-6Al-4V material from sodium-reduced titanium sponge fines into 3- by 5-in. blanks. Blanks were machined into tensile testing samples.
- Completed metallographic examinations on materials described above.
- Completed tensile tests on sodium-reduced material.

Introduction

The goal of this concept feasibility study is to develop a low-cost powder metallurgy (PM) manufacturing process to obtain fully dense parts based on current commercial-grade materials and a novel processing technology. The study will use particle-reinforced titanium metal feedstock in conjunction with PM press and sinter technology to manufacture simple parts for testing. A technical cost model will be performed to document the cost of the manufacturing process. The decision gate criteria are (1) a cost-competitive manufacturing process and (2) acceptable microstructure and mechanical properties that have been identified for connecting rods targeted for high-performance reciprocating engine applications.

Materials

Sample blanks (plates) have been manufactured using a baseline aerospace quality titanium material (RMI) and a low-cost Russian-grade material. Small samples of the materials were mounted and polished followed by etching for 8 s using Kroll's reagent. Photomicrographs were taken using a digital camera connected to a Leco metallograph.

Ti-6Al-4V from sodium-reduced titanium sponge fines (RMI "commercial" product): As-compacted density of the samples is 87%, and density after sintering at optimized temperature is more than 99% of theoretical. Metallographic analysis revealed homogeneous microstructure with a basket weave morphology (Figure 1). Level of detected porosity is less than 1%.

Ti-6Al-4V from innovative magnesium reduced-titanium sponge fines produced in Russia: As-compacted density of the samples is 84%, and density after sintering at optimized temperature is more than 99% of theoretical. Metallographic analysis revealed homogeneous microstructure with a basket weave morphology (Figure 2). Level of detected porosity is less than 1%.

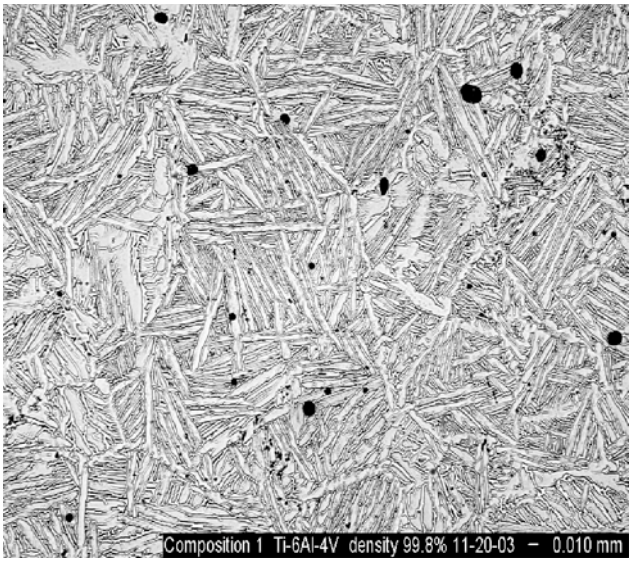

Figure 1. Ti-6Al-4V from sodium-reduced titanium sponge fines (RMI "commercial" product).

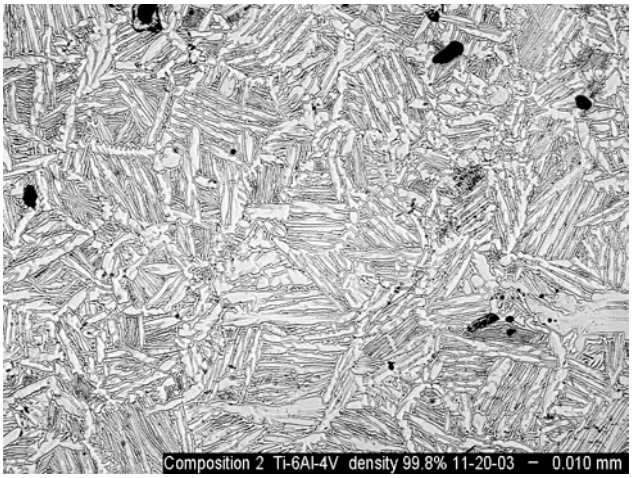

Figure 2. Ti-6Al-4V from innovative magnesium-reduced titanium sponge fines produced in Russia.

Mechanical Properties

Tensile test results shown in Table 1 are for Ti-6Al-4V sodium titanium powder without reinforcement. Both ultimate (UTS) and yield (0.2% YS) strength are higher than that specified by the American Society of Testing and Materials (ASTM) (UTS—130 ksi and 0.2% YS—120 ksi). Ductility is also higher than ASTM requirements (ASTM B348 for forged bars and billets specifies elongation—10%, RA—25% and ASTM B367 for castings specifies 6% elongation).

Ongoing—Future Work

- Manufacture blanks (plates) from Ti 6Al-4V sodium titanium powder with reinforcement. Heat treat to optimize mechanical properties.
- Manufacture blanks (plates) from International Titanium Powder, Inc. (ITP) ("low-cost" alternative) without reinforcement. Heat treat to optimize mechanical properties.
- Perform microstructural and interfacial characterization.
- Perform nondestructive evaluation to confirm tensile samples are crack free.
- Generate static mechanical properties.
- Perform failure analysis on tensile samples.
- Complete cost model on ADMA manufacturing process.
- Assess cost model and mechanical properties against decision gate criteria.

Table 1. Mechanical properties of Ti-6Al-4V without reinforcement

Composition	Sample No.	Tensile strength (ksi)	Yield strength (ksi)	Elongation (%)	Reduction of area (%)	Modulus of elasticity (msi)
Ti6A1-4V from sodium-reduced titanium sponge fines (RMI "commercial" product)	1	143.2	123.1	12.2	18.2	16.9
	2	143.6	123.7	13.8	19.6	18.3
	3	142.6	122.8	11.4	16.5	16.7
	4	142.7	123.1	11.8	23.3	16.8
Ti-6A1-4V from ASTM Standard B348-03 Grade F-5		130	120	10	25	

B. Low-Cost Cast Aluminum Metal Matrix Composites

Principal Investigator: Darrell R. Herling
P.O. Box 999/KZ-03, Richland, WA 99352
(509) 376-3892; fax: (509) 376-6034; e-mail: darrell.herling@pnl.gov

Technology Area Development Manager: Joseph A. Carpenter
(202) 586-1022; fax: (202) 586-1600; e-mail: joseph.carpenter@ee.doe.gov
Field Technical Manager: Philip S. Sklad
(865) 574-5069; fax: (865) 576-4963; e-mail: skladps@ornl.gov

USCAR Project Steering Committee:
Bruce Cox—DaimlerChrysler, e-mail: bmc8@daimlerchrysler.com
Rena Hetcsh—Ford Motor Co., e-mail: rhecht@ford.com
James Quinn—General Motors, e-mail: james.f.quinn@gm.com

Contractor: Pacific Northwest National Laboratory
Contract No.: DE-AC06-76RL01830

Objective

- Provide lightweight, cost-competitive, aluminum metal-matrix composite (MMC) options for future vehicles and hybrid structures, with a project application focusing on foundation brake system components. This project focused on three development tasks, which include (1) development of compositing technologies to produce low-cost MMC materials; (2) advanced shape-casting manufacturing processes; and (3) innovative designs for new brake rotor applications.

Approach

- Develop advanced MMC processing technologies and integrate these processes into an economical manufacturing cycle, including consideration of product design that accounts for material-specific characteristics and component performance. The specific major project tasks follow:
  - Develop rapid MMC mixing process and lower cost, castable aluminum MMC material
  - Evaluate mechanical and physical properties, as well as castability of this material
  - Friction and wear test sample products produced from the low-cost MMC material
  - Explore innovative casting and finishing options
  - Provide innovative brake system designs to utilize aluminum MMC materials
  - Prototype and full-scale test demonstration components (brake rotor)

Accomplishments

- Completed material property and foundry evaluation.
- Completed and validated cost modeling at pilot scale.
- Completed and prototyped evaluation of squeeze casting of fully reinforced rotor, and completed brake dynamometer testing.
- Completed centrifugal casting of selectively reinforced rotor prototypes and initiated dyno testing.
- Completed machining cost and tool life study.

Future Direction

- Complete economic evaluation of centrifugal casting for large volume production of aluminum components.
- Complete dynamometer testing of prototype, selectively-reinforced, aluminum MMC brake rotors.
- Pacific Northwest National Laboratory (PNNL) will investigate the use of centrifugal casting to demonstrate the production of a selectively-reinforced brake rotor caliper with the reinforcement located in the bridge region of the caliper.
- Draft final program report.

Introduction

The demand for better fuel economy is a major reason to reduce vehicle mass. In principle, the substitution of aluminum metal-matrix composite (MMC) material for steel components provides a significant opportunity to reduce vehicle mass in a number of automotive applications. Aluminum MMCs possess both light weight and high wear-resistance characteristics, making them desirable for a number of body, chassis, and powertrain applications, provided that performance and cost objectives can be reached. A brake rotor was selected as a demonstration piece for this project to show that the low-cost material developed in the initial phase of this project is viable for use in a challenging application that has potential for substantial mass savings.

While a number of niche automotive applications of aluminum MMCs have been made—including the Toyota diesel engine piston, Honda Prelude cylinder liner, General Motors (GM) S/T drive shaft, and rear brake rotors on the Plymouth Prowler, Lotus Elise, and Volkswagen (VW) Lupo—they have not seen widespread automotive application due primarily to cost and, in some cases, performance limitations. It was the purpose of this project to make a significant improvement in this situation.

With the overall goal of demonstrating cost-competitive aluminum MMC options for structural and powertrain components in general, the project focused its attention on a lightweight brake rotor as a target application. In cooperation with Visteon Corporation, a lightweight rotor that is 60% lighter than a conventional four-door luxury sedan cast iron rotor was designed and manufactured. Since the rotor is rotating, unsprung mass, the opportunity for improved fuel economy due to this substitution has been estimated to be on the order of 0.25 mpg from not only the direct weight reduction but also the resulting lower inertial forces. The cost of the prototype rotor is estimated to be 1.5 times the cost of a cast iron rotor, compared to a figure of three times or so for prior aluminum MMC rotors.

This project began with the development of a low-cost aluminum MMC material and process for making it. This venture was an industry-government collaboration between MC-21, Inc., U.S. Council for Automotive Research (USCAR), Pacific Northwest National Laboratory (PNNL), and the FreedomCAR Automotive Lightweighting Materials Program. While prior aluminum MMCs sold for prices of $2/lb or more, a more economical rapid mixing process for combining the aluminum and silicon carbide ceramic particles was developed. This process utilizes a modular mixing unit and lower cost raw materials, resulting in a projected material cost of $1/lb, which is more than a 50% savings. This process has been demonstrated at a 600-kg batch size level, which is suitable for production of 5 million pounds of aluminum MMC per year from one unit. Commercialization is under way with multiple licensing agreements complete or in negotiation.

The thermal and structural properties of new low-cost MMC materials have now been evaluated and found to be acceptable. Also, the cost model for the low-cost MMC material showing that $1/lb is feasible at pilot-scale volumes was validated by commercial entities. To demonstrate the material's potential, prototype full-scale, fully-reinforced brake rotors were produced by a squeeze-casting method. This method was selected as being the most economical of the several innovative shape-casting methods that were evaluated.

Computer simulations and brake dynamometer tests show that it is possible to achieve acceptable performance for either front or rear brakes of a mid-size sedan using the new low-cost aluminum MMCs. The novel brake rotor design enhances dissipation of

the heat generated during braking and prevents excessive temperature increase. Prototype castings of full-scale brake rotors based on the design and simulation results were produced and dyno tested by Link Engineering. A spider-chart representing the status of the major project tasks is shown in Figure 1.

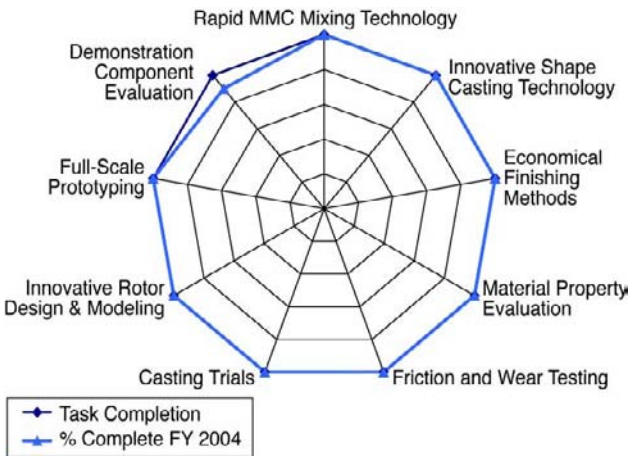

Figure 1. Status of project tasks and completeness.

Brake Rotor Prototyping and Dynamometer Testing

Having a low-cost material is a necessity, but it is not totally a sufficient condition to realize low-cost automotive products. With the success of the low-cost material development, the project team next addressed the secondary manufacturing cost issues. This also included identifying an innovative design for a brake rotor that would take into account the unique properties of MMC vs cast iron, such as higher thermal conductivity and lower maximum operating temperature capability. The patented externally vented rotor design shown in Figure 2, which was developed by Visteon, achieves the necessary thermal performance criteria based on brake dynamometer testing. Also shown in Figure 2 is the standard cast iron front disc brake rotor for the target four-door sedan as well as details on the physical differences and weight savings between the two. The rotor performance meets the braking requirements for a midsize sedan, with some future

Production rotor – four-door sedan	Aluminum MMC rotor (designed for same four-door sedan)
• 300-mm diameter by 30 mm wide	• 300-mm diameter by 32 mm wide
• Gray cast iron — green sand cast	• Aluminum with 20% silicon carbide — die cast or subliquidus cast (semisolid formed)
• Internally vented — 7.0-mm outer plate / 15.0-mm air gap / 8.0-mm inner plate	• Externally vented — alternating inboard (20) vents and outboard (20) external vents
• 6 Short and long alternating vanes	• Internal heat sink venting in hat section to better distribute heat
• Weight = 8.44 kg	• Weight = 3.32 kg

Figure 2. Comparison of production sedan rotor (left) and specially designed prototype lightweight aluminum-MMC front brake rotor (right).

work still needed on friction materials to optimize noise and pad life.

Working with team members THT Presses and Eck Industries, the externally vented rotor design was adapted for squeeze casting. Through this high integrity process, a number of features, including the mounting holes, can be produced in the casting process, which helps to minimize the need for extensive final machining. Current work with team member Kennametal is finalizing cutting tool materials and process parameters for production-scale machining of the rotors, recognizing the interrupted cut condition presented by the externally vented design.

Prototype brake rotors were produced for full-scale dynamometer evaluation of braking performance and durability. The tests were conducted by Link Engineering with the appropriate load and speed parameters that simulate front disc brake operation on a midsized four-door sedan, weighing approximately 3,700 lbs. The brake pad lining selected for testing is a commercially available formulation from Akebono that is used on other aluminum MMC brake rotors where the maximum operating temperature (MOT) is low, and application is for a rear brake only.

Of the six types of test profiles run for the evaluation, five of the six tests met the minimum performance requirements established and were given a passing grade, which is summarized in Table 1. The brake noise test was marginal in the evaluation with a final rating of 7 (Yellow), which is an industry index that designates an average noise level at the threshold for acceptability. The type of lining used for braking systems can have a significant effect on the amount of noise generated. Visteon feels this issue is correctable with different pad formulations, slight rotor geometry changes, or a combination of both.

Table 1. Results of initial prototype brake dynamometer testing

Test description	Pass/fail
Dyno simulation of AMS and fade test	Pass
Dyno simulation of Laurel Mountain hot roughness brake test	Pass
Brake lining wear vs temperature test	Pass
Brake noise test (with steady drag)	Marginal
Disc wear test (with low-pressure drag)	Pass
Brake effective test	Pass

Of more concern was the friction coefficient results during the fade and drag tests. The concluding remarks were that the high-temperature friction under extreme conditions was marginal. Although the rotor integrity was not compromised at the higher surface operating conditions (since the structural properties and microstructure were retained), the coefficient of friction was relatively low at an average of 0.25. The current desired target within the industry for automotive disc brakes is a friction coefficient between 0.35 and 0.45, with values in the 0.40+ range being comparable to a “European luxury vehicle brake pedal feel.” This pad formulation is indeed acceptable for lower MOT, but it was not necessarily designed to perform at the higher operating condition of the smaller rotor geometry. The Visteon rotor cannot be made larger to compensate for mass and surface area because the smaller conventional passenger vehicle wheel sizes limit the maximum rotor diameter that can be utilized.

Although the overall performance of the new aluminum MMC brake rotor exceeded expectations for the first round of testing, it is necessity to improve the friction coefficient in order for it to be considered for production vehicles. To that end, a review of brake pad manufacturers was made, and a pad formulation from TMD was identified for testing. According to TMD, this pad formulation (composition not disclosed) is designed to operate with braking surfaces (rotors) such as aluminum where the development and integrity of the friction film is more difficult to develop and needs to be more stable at elevated temperatures.

A second series of brake dynamometer tests was conducted at Link Engineering to evaluate braking performance with the TMD linings. The coefficient of friction during all of the tests was much higher than the first series with the Akebono linings, with values as high as 0.45. The average friction coefficient for this series of tests was within a desirable range, with values of 0.38–0.40. The same improved results also applied to the effectiveness curves and the rotor-speed-spread, pressure-spread, and temperature-spread data. In other words, this specific rotor and lining combination held up better under the higher temperature friction conditions.

The summary of results for the second series of testing is given in Table 2. Like previous test results,

Table 2. Results of brake dynamometer testing with TMD linings

Test description	Pass/fail
Dyno simulation of AMS and fade test	Pass
Dyno simulation of Laurel Mountain hot roughness brake test	Pass
Brake lining wear vs temperature test	Fail
Brake noise test (with steady drag)	Pass
Disc wear test (with low pressure drag)	Pass
Brake effective test	Pass

noise was an issue with a noise index rating of 5 (Red). Although the braking performance was significantly improved with the somewhat harder TMD lining, unfortunately the trade-off was more noise, which is a typical struggle for brake system designers. Visteon is confident that the level of noise and frequency is correctable with slight modifications to the rotor geometry, which should have little impact on thermal management and braking performance.

Machining Evaluation and Tool Life Study

The objective of this study was to determine tool material performance and machining parameters for turning aluminum (20 vol % SiC) MMC of representative brake rotor geometries. Diamond is clearly the tool material of choice for machining most MMCs; however, it was not clear whether diamond cutting edges could reliably withstand the very severe interruptions in the design of these rotors. An initial review of commercial and emerging tool materials determined that two types of diamond tool material commercially available from Kennametal, Grades KD100 and KD1405, would be pursued. KD100 is a 25-µm diamond-particle-size grade produced by the classic high-temperature/high-pressure process, which is a composite material consisting of bonded diamond particles and a small amount of cobalt catalyst. Polycrystalline diamond (PCD) tools of this type were among the first recommended for economically machining aluminum MMC materials. KD1405 is an essentially pure PCD tool fabricated by using chemically-vapor-deposited (CVD) diamond sheet material, ~400-µm-thick blanks at the cutting edge. In machining very abrasive, nonferrous workpiece materials, such as A390 (~18% silicon) aluminum, KD1405 typically exhibits two to three times the tool life of KD100 and provides superior workpiece finishes. However, KD100 typically shows better toughness in interrupted cutting applications.

Turning parameters for this study ranged from cutting speeds of 900–2000 surface feet per minute (sfm), feed rates from 0.005–0.020 inches per rotation (ipr), and depths-of-cut (DOC) of 0.020 in., thus providing material removal rates ranging from 1.08 to 9.6 in.^{3}/min. A total of 22 rotors with discontinuities in the cutting surface and two rotors with solid faces were supplied for the experiments, with the later rotors for use in evaluating tool wear under continuous cutting conditions. The setup used to machine the rotors included a Okuma LR35 lathe and KM50-CSKPL4 tool-holder, which imparts a +15° lead angle and a +5° rake angle to the diamond cutting edge. For each pass, cutting was initiated from the outside diameter of the rotor to the inside, while automatically adjusting the spindle revolutions per minute to maintain constant cutting speed. Flood coolant, Castrol–Syntilo 9904 at 5 vol %, was used throughout each test.

The first cut on each rotor was a clean-up pass of 0.020-in. DOC to remove surface nonuniformities and present a fresh surface to the cutting edge of the test insert. It was decided to use one test insert for each rotor, at a DOC of 0.020 in., which meant that the insert could be used for a maximum of 22 passes. Measurements of maximum nose wear and uniform flank wear were made after each of the first two passes and then after every other pass thereafter. Workpiece surface finish (µin.) measurements were made after each pass using a hand-held profilometer. The normal end-of-life (EOL) criteria for testing PCD tools in laboratory tests is 0.015-in. maximum nose wear, chipping, or cutting-edge breakage, whichever occurs first. However, because premature chipping or breakage was not observed in this test, there were insufficient rotors available to allow running each insert to EOL. Accordingly, linear regression analyses of the wear data were performed to calculate wear rates (µin./pass or µin./min) and an estimate of tool life for each insert at 0.015-in. maximum flank wear.

Results showed that there was no significant difference in tool performance between KD100 and KD1405 at the low-speed/low-feed and at the high-speed/high-feed cutting conditions studied. However, at low-speed/high-feed and high-speed/low-feed conditions, the KD1405 showed a significant tool life advantage of >4X, and greater cost

effectiveness at 900 sfm/0.020 ipr. As expected, smoother workpiece finishes (65 vs 350 µin. radius) were produced at the lower feed rate, but there was no significant difference in the finishes produced by the two types of tools. Typical wear characteristics in the cutting zone of the tools after interrupted cutting at 2000 sfm/0.005 ipr are shown in Figure 3 for KD100 and KD1405. Both tools showed abrasive wear patterns, but with no evidence of chipping. Mildly abraded regions are clearly evident in the chip-flow zone on the rake surface of the tools. Maximum wear occurred at the leading edge of the tool where it enters the cut, with generally uniform wear observed around the nose of the tool. Of the tools tested, only one, a two-nose radius KD1405 insert, chipped and fractured catastrophically on making an initial pass through the vented rotor. All others showed wear patterns similar to those illustrated in Figure 3.

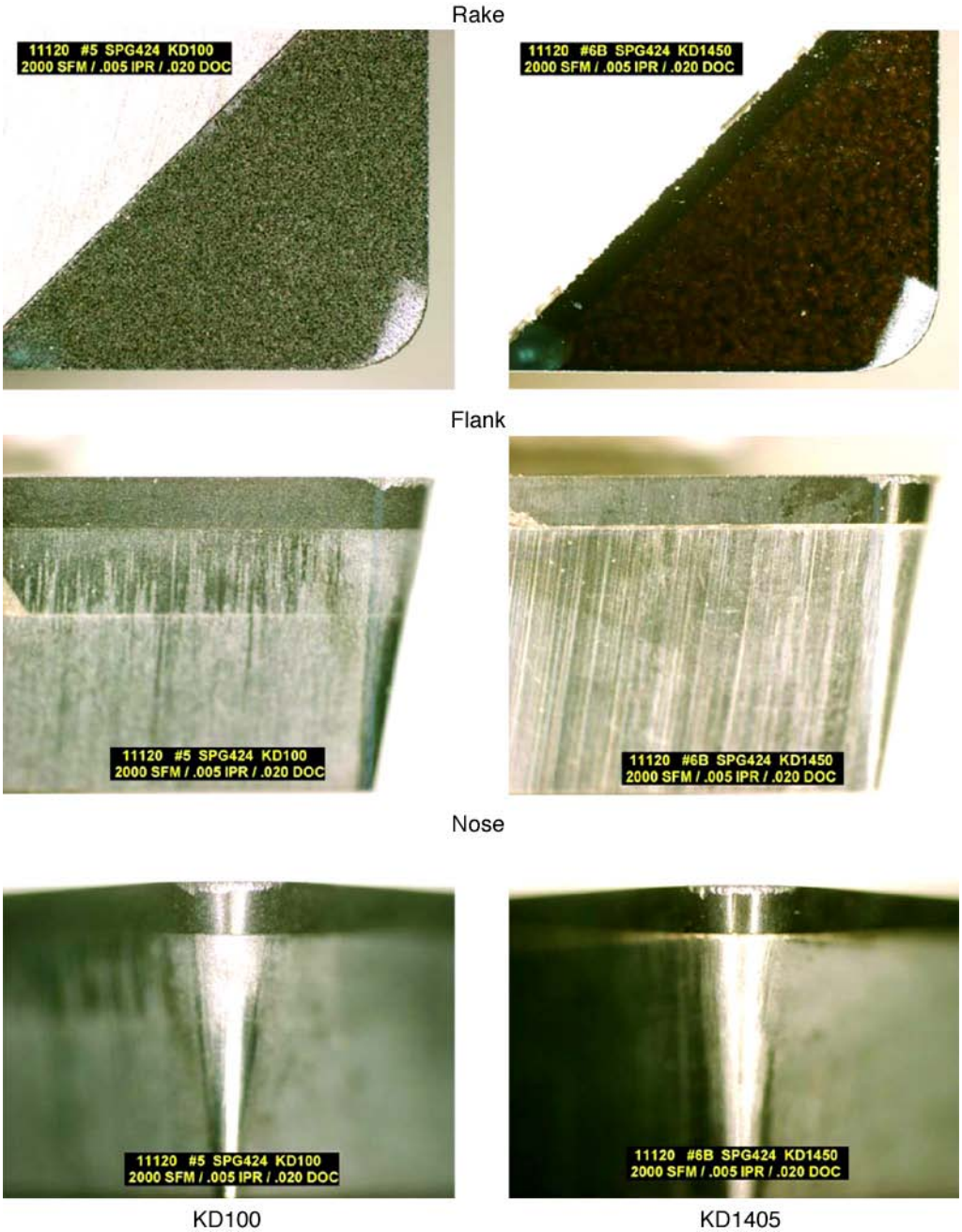

Figure 3. Wear zone of inserts after interrupted cutting at 2000 sfm/0.005 ipr.

On the basis of the estimated tool life data and the material removal rates corresponding to the machining parameters, the amount of workpiece material removed by KD100 totaled 824 in.^{3} and that for KD1405 amounted to 1353 in.^{3} At insert costs of $55 for KD100 and $105 for KD1405, the corresponding cutting edge costs under the test conditions are $0.067 vs $0.078/in.^{3} machined, respectively, giving a slight economic benefit to KD100.

Tool nose radius had an effect on tool life. Performance data for SPG422 and SPG424 inserts in grade KD1405 showed that the four-nose radius (0.0625-in.) tools had about 60% less tool life than the two-nose radius (0.0323-in.) tools. It is possible that higher tool pressures for the four-nose radius tools could account for the higher wear rates and decreased tool life.

In summary, PCD and CVD-diamond sheet tool materials (KD100, KD1405) were tested in facing operations of aluminum-MMCs, with discontinuous cuts in the brake rotor braking surfaces. Although both tool materials performed well over a wide range of cutting parameters, KD100 inserts in style SPG422 provided the most cost-effective performance. The greatest tool life is expected by using a proposed roughing pass at 2000 sfm, 0.020 ipr, and 0.015 DOC, followed by a finishing pass at 2000 sfm, 0.005 ipr, and 0.005 DOC.

Future Work

The remaining scope of work will focus on completing the economic analysis of commercial centrifugal casting and prototyping and dynamometer testing of selectively reinforced aluminum-MMC disk brake rotors. In addition, PNNL will investigate the use of centrifuge casting to demonstrate the production of a selectively reinforced brake rotor caliper with the reinforcement located in the bridge region of the caliper.

References

1. E. Oles, S. Etling, and J. Vankirk, *Machining Aluminum MMC Brake Rotors*, Project Report No.14245, Kennametal, November 2004.
2. D. Herling, *Full-scale brake dyno testing of automotive aluminum MMC brake system*, Project Milestone Report 15480, March 2004.
3. A. Hashmi and D. Myers, *Al-MMC Front Rotor: Testing Results Summary & Data*, Visteon, February 2004.

Presentations and Publications

1. D. R. Herling and W. H. Hunt, "Low-cost Cast Aluminum Metal Matrix Composites Have Arrived." In *Affordable Metal Matrix Composites for High Performance Applications II*, pp. 13–23 Minerals, Metals & Materials Society, Warrendale, Pennsylvania, 2004.
2. W. H. Hunt and D. R. Herling, "Applications of Aluminum Metal Matrix Composites: Past, Present, and Future," International Symposium of Aluminum Applications: Thrusts and Challenges, Present and Future, ASM International, Pittsburgh, Pennsylvania, October 2003.
3. W. H. Hunt and D. R. Herling, "Metal Matrix Composites," *Advanced Materials & Processes*, **162**(2), 39–42 (2004).
4. E. Oles, S. Etling, and J. Vankirk, *Machining Aluminum MMC Brake Rotors*, Project Report No. 14245, Kennametal, November 2004.
5. D. R. Herling, "Low-Cost Cast Aluminum Metal Matrix Composites Have Arrived," invited presentation at the 2003 TMS Materials Science & Technology Conference, Chicago, Illinois, November 2003.
6. W. H. Hunt and D. R. Herling, "Applications of Aluminum Metal Matrix Composites: Past, Present, and Future," keynote speaker presented at the ASM Fall Conference, Pittsburgh, Pennsylvania, October 2003.
7. J. F. Quinn, D. R. Herling, W. H. Hunt, and D. C. Myers, "USCAR Low-Cost Aluminum Metal Matrix Composite Program," GM Technology Showcase, Detroit, Michigan, September 2004.

Acknowledgments

The authors would like to thank G. Grant, M. Dahl, and K. Mattlin, Pacific Northwest National Laboratory, for their work in materials characterization, testing, and processing support. In addition, thanks go to W. Hunt, Aluminum Consultants Group; D. Myers, A. Hashmi, and A. Santavy, Visteon Corp.; D. Weiss, E. Industries; E. Oles, S. Etling, and J. Vankirk, Kennametal; and the OEM Steering Committee members for their contributions to the project activities and coordination.

C. Structural Cast Magnesium Development

Project Chairman: Richard J. Osborne
General Motors Corporation
Mail Code 480-210-3B1
30001 Van Dyke Road
Warren, MI 48090-9020
(586) 575-7039; fax: (586) 575-8163; e-mail: Richard.osborne@gm.com

Project Administrator: D. E. Penrod, P.E.
Manufacturing Services and Development, Inc.
4665 Arlington Drive
Cape Haze, Florida 33946
(941) 697-5764; fax: (941) 697-5764; e-mail: dep@gls3c.com

Technology Area Development Manager: Joseph A. Carpenter
(202) 586-1022; fax: (202) 586-1600; e-mail: joseph.carpenter@ee.doe.gov
Field Technical Manager: Philip S. Sklad
(865) 574-5069; fax: (865) 576-4963; e-mail: skladps@ornl.gov

---

Contractor: U.S. Automotive Materials Partnership
Contract No.: FC26-02OR22910

Objective

- Develop the science and technology necessary to implement a front structural cradle (with two different magnesium casting processes) that will interface with other concurrent magnesium programs proposed for the U.S. automotive industry.

Approach

- Improve our scientific understanding of magnesium alloys.
- Develop a cost model that compares cast magnesium chassis component costs to other materials and processing techniques.
- Provide comprehensive database and design guidelines.
- Develop improved casting processes.
- Identify and/or develop methods to improve corrosion resistance.
- Improve joining technologies.
- Transfer knowledge and lessons learned to industry.
- Complete all of the scientific project tasks relevant to microstructure-property modeling, corrosion mitigation, joining behavior, and nondestructive evaluation (NDE) methods.
- Convert existing aluminum cradle to magnesium and deliver parts ready for testing and approved for Corvette's Job 1 for 2006. Therefore, the industry part of this project cannot wait for all of the intricate scientific parts of the project to be understood before a process is chosen, tooling built, parts cast and the validation tests run. Both aspects of the project must be constantly aware of each other's needs and progress as shown in Figure 1.

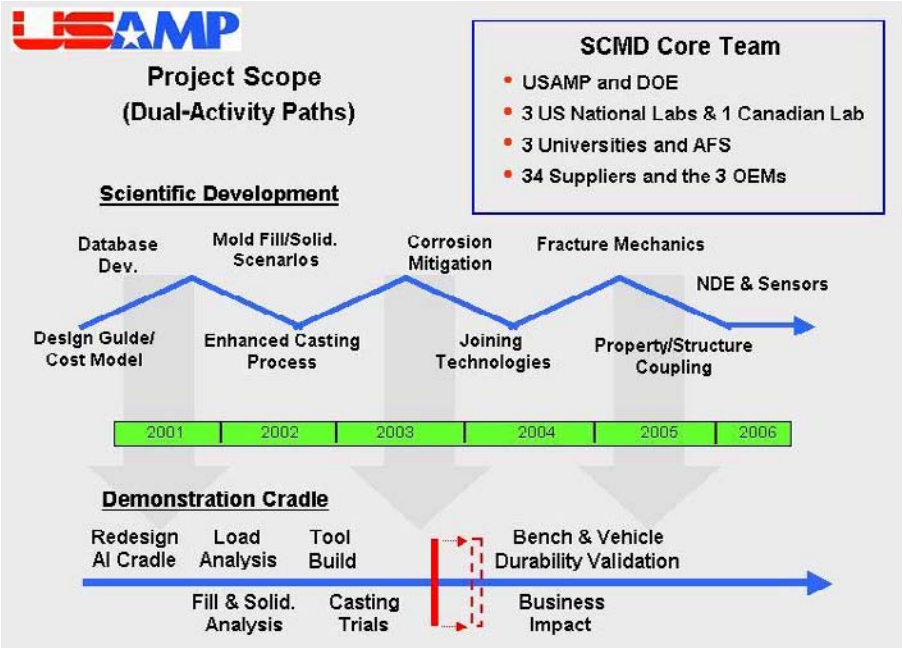

Figure 1. Dual-project path for science and magnesium demonstration casting validation activities.

Accomplishments

- Conducted material property evaluation of numerous magnesium alloy production castings for the development of the magnesium alloy database.
- Completed the design and building of the High-Pressure Die Casting (HPDC) tooling for the front engine magnesium cradle; cast several hundred HPDC magnesium castings and distributed them to key Structural Cast Magnesium Development (SCMD) project participants [and General Motors (GM) Corvette team] for validation, durability, and corrosion testing procedures. If the successful testing continues, this type of a magnesium cradle could possibly be included in one or more of GM 2006 models. This achievement alone is a major accomplishment for the magnesium industry of North America.
- Implemented new magnesium cradle casting parameters for HPDC magnesium casting process.
- Continued the corrosion and casting protection evaluation for specific cradle connectors, including new bolt load retention procedures.
- Continued the investigation of in-mold sensor applications and developed magnesium X-ray quality indicator.
- Initiated an alternative Low-Pressure Permanent Mold (LPPM) casting process for casting the same magnesium cradle. Achievement of this initiative will provide an alternative casting process for the magnesium industry for larger type magnesium castings.
- Continued characterization of AZ91D, AM50, AM60, and AE44 HPDC alloys by the Georgia Institute of Technology.
- Completed cost model and HPDC design guide.

Future Direction

- Continue the rigorous bench tests of the HPDC magnesium cradles that have been scheduled for actual vehicle road tests. There is a potential market for 45,000 vehicles by 2007 production, utilizing a magnesium front cradle (cross-member).

- Follow the SCMD Project's revised Statement of Work (SOW) to complete both the scientific and manufacturing aspects of the project.
- Continue to work with the industrial participants with the development of sensors, database, and practical casting applications developed by the SCMD project.
- Continue the investigation (and casting) of the additional LPPM casting process. Initial prototype LPPM castings have been reviewed at SCMD 2003 fourth-quarter project review meetings.
- Extended through 12/06 to complete additional testing and investigation of the two different types of magnesium castings (HPDC and LPPM) that have been included with the SCMD project. The tasks required by the Cooperative Agreement and CRADA participants were revised in the original SOW to reflect the required changes, and the final report will be issued to all participants at the conclusion of the project.

Introduction

The Structural Cast Magnesium Development (SCMD) project has focused on resolving critical issues that limit the large-scale application of magnesium castings in automotive components. The project activities combine the science and manufacturing technology necessary to implement front and rear structural cradles. Such components offer all of the difficult manufacturing issues, including casting process (high-pressure die, semisolid, low pressure, squeeze, etc) and joining, along with harsh service environment challenges, such as corrosion, fatigue, and stress relaxation associated with fasteners.

The project team includes personnel from

- the "Big Three" automotive companies,
- 34 companies from the casting supply base,
- academia ,
- independent testing and research labs,
- American Foundry Society (AFS),
- technical associations,
- Oak Ridge National Laboratory (ORNL),
- Sandia National Laboratories (SNL),
- Lawrence Livermore National Laboratory (LLNL), and
- Natural Resources Canada (CANMET).

Industry Participants

An existing aluminum engine cradle (that is currently in production use) has been redesigned for two different magnesium casting processes: High-Pressure Die Casting (HPDC) and Low-Pressure Permanent Mold (LPPM). Utilization of computer simulations (prior to tooling design) indicated good correlation of casting fill operation (and their effects) to actual production experiences (see Figure 2).

Tools and castings have been made for both processes. Several hundred HPDC production prototype castings have been distributed to SCMD project participants and to the GM Corvette Team for the vigorous testing procedures that are required for the HPDC cradle. Based on the results of the tests, the Corvette Team will determine what action (if any) will be required to meet the timing date of Job 1 for the 2006 production year. At the present time, the possibility of using the HPDC-type of a magnesium cradle appears to be very promising.

The LPPM cradle process [see Figure 3(*a*)—HPDC and Figure 3(*b*)—LPPM] and team experienced a facility problem (not related to the process or the cradle work that was in progress) that somewhat delayed additional casting of the LPPM prototypes. However, another facility has been located, and the recovery program of this process is proceeding on schedule.

Importance/Significance: Utilization of up-front computer modeling (used for both HPDC and LPPM processes) resulted in significant savings (time and costs) and eliminating casting defects in the initial castings. Based on the prototype castings produced by both processes, there is an estimated 35% weight saving in the magnesium cradle vs the current aluminum production part. This weight

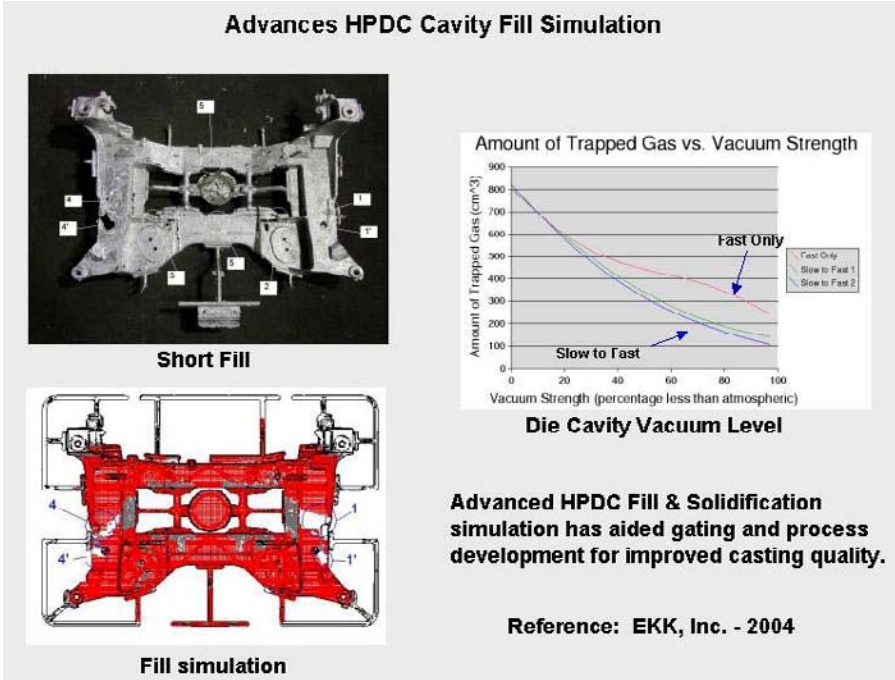

Figure 2. EKK, Inc. cavity fill simulations showing excellent correlation with short fill HPDC castings.

(*a*) (*b*)

Figure 3. (*a*) Initial machined HPDC cradle casting run and (*b*) initial LPPM magnesium cradle casting.

reduction (vehicle mass savings) will result in a reduction in fuel consumption, emissions, and less dependence on foreign oil. Cast magnesium structures have the potential to reduce 100 kg of vehicle mass, which could reduce emissions by 5% and reduce fuel consumption by approximately 1.0 mpg (ignoring secondary mass savings). The investigation of producing the same casting by the two different processes (HPDC and LPPM) has a great potential to enable existing aluminum casting companies to expand their operations into magnesium, without huge capital and facility expenditures.

Project Progress/Status vs Targets

Prototype HPDC magnesium alloy castings were provided to the Corvette C6 team before year end (2004) to coincide with the cradle validation schedule.

Remaining Technical Challenges and Plans

- Corvette has started the rigorous validation testing of the HPDC cradle designs. If acceptable, this design will be installed on a vehicle for actual road tests. There is a potential market for 45,000 vehicles for 2007.
- An investigation is ongoing into the effects of corrosion, coatings, and protection; long-range effects of bolt load retention are all being studied by CANMET (see Figure 4).

Milestones

Cooperative Agreement

- Magnesium front cradles have been cast by both of the chosen magnesium die cast processes.
- The Corvette Team is currently validating magnesium front cradles of the HPDC design.
- Detailed quantitative microstructural characterization continues for production components cast with AZ91D, AM 50, AM 60, and AE44 magnesium alloys.
- Actual casting results have coincided with predicted modeling techniques.
- Project Steering Committees are actively working with the project team and all industrial participants on major task issues.

Cooperative Research and Development Agreement (CRADA)

- **ORNL—**ORNL continues the investigation of modeling software from four of the supply teams. The results of the investigation will be applied to the ORNL models in current commercial software.
- **SNL/MSU—**SNL is coordinating and collecting all of the project data from all the testing sites and using the data to expand the mathematical "failure model" that was designed for the cast light metals (CLM) project. This information will be used for our multiscale fatigue model.

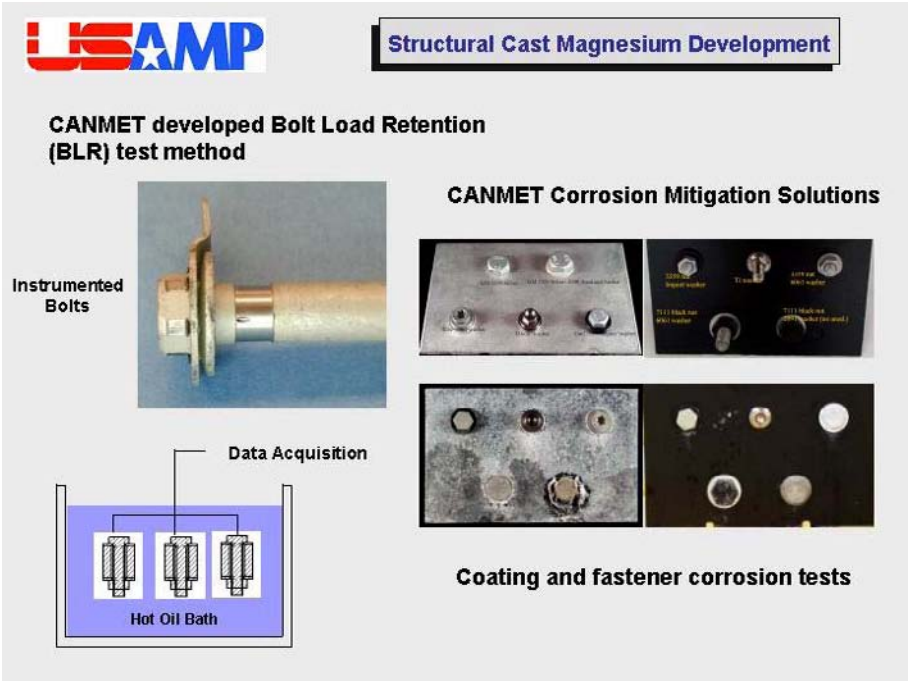

Figure 4 . CANMET bolt load retention (BLR) testing and corrosion studies developed knowledge required for product implementation.

- **LLNL**—Radiographic analysis of production parts and test samples will determine discontinuity types and grades at predicted high-stress locations. Investigation of the possibility of using fiber optics in-mold thermal monitoring system for HPDC continues in a high-volume production facility. Investigation and possible elimination of impurities in the metal charged into the furnace will reduce defects.

Project Benefit

Expected DOE and U.S. industry benefits derived from successful completion of this project would include the following:

- Vehicle mass savings for ground and air transportation will lead to reduction in fuel consumption, emissions, and less dependence on foreign oil.
- Automakers are under increasing pressure to reduce CO_2 emissions and increase corporate average fuel economy (CAFE). The North American auto industry currently uses approximately 70,000 MT/year of magnesium, which is equivalent to some 3.5 kg per vehicle.

  The ability to significantly increase magnesium usage will help the auto industry meet future Federal CAFE targets and reduce exposure to CAFE penalties. Cast magnesium structures have the potential to reduce vehicle mass by 100 kg, which could reduce emissions by 5% and reduce fuel consumption by approximately 1.0 mpg (ignoring secondary mass savings).
- Light metal alloys have greater recycling value with reduced energy consumption vs plastics (including melting, machining, handling, and transportation energy requirements).
- The Big Three competitive global postures will increase as a result of designing and manufacturing vehicles that offer greater consumer value. This can improve the U.S. trade balance with countries that market higher fuel efficiency vehicles than those produced in North America.
- Health and environmental issues for workers are reduced during light-metal casting operations when compared to ferrous foundries and polymer molding operations.
- It would provide national laboratories with valuable manufacturing development and product application experience.
- It has a dual-purpose role of providing the national laboratories an opportunity to develop math-based simulation models and NDE technologies that benefit both the auto industry and federal ongoing technology programs.
- The successful casting of a magnesium cradle (by low-pressure die casting) will indicate to the existing aluminum casting industry that the transfer of casting technology (aluminum to magnesium casting) can be achieved at a low facility cost.

Presentations or Publications

1. A. S. Sabau, “Predicting Interdendritic Cavity Defects during Casting Solidification,” *JOM*, Vol. **56**, 54–56 (2004).

D. Magnesium Powertrain Cast Components

Project Manager: Bob R. Powell
GM Research & Development Center
MC 480-106-212
30500 Mound Road
Warren, MI 48090-9055
(586) 986-1293; fax: (586) 986-9204; e-mail: bob.r.powell@gm.com

Project Administrator: Peter P. Ried
Ried and Associates, LLC
6381 Village Green Circle, Suite 10
Portage, MI 49024-2680
(269) 327-3097; fax: (269) 321-0904; e-mail: pried_imagineer@netzero.net

Technology Area Development Manager: Joseph A. Carpenter
(202) 586-1022; fax: (202) 586-1600; e-mail: joseph.carpenter@ee.doe.gov
Field Technical Manager: Philip S. Sklad
(865) 574-5069; fax: (865) 576-4963; e-mail: skladps@ornl.gov

---

Contractor: U.S. Automotive Materials Partnership
Contract No.: FC26-02OR22910

Objective

- Demonstrate and enhance the feasibility and benefits of using magnesium alloys in place of aluminum in structural powertrain components, thereby achieving at least 15% weight reduction of the cast components.

Approach

- Identify, benchmark, and develop a design database of the potentially cost-effective, high-temperature magnesium alloys and, using this cast-specimen database, select the alloys that are most suitable for the magnesium components. (Task 1)
- Design, using finite-element analysis (FEA), an ultra-low-weight engine containing potentially four magnesium components (cylinder block, bedplate, structural oil pan, and front engine cover) using the most suitable low-cost, recyclable, creep- and corrosion-resistant magnesium alloys. (Task 2)
- Create a cost model to evaluate alloy, manufacturing, and technology costs to predict the cost-effective performance of the engine. (Task 2)
- During the execution of Tasks 1 and 2, identify and prioritize the critical gaps in the fundamental science of magnesium alloys and their processing that are barriers either to the progress of the project or to the use of magnesium in future powertrain applications. Seed-fund the most critical research, and promote additional identified needs to support further development of the magnesium scientific infrastructure in North America, thereby enabling more advanced powertrain applications of magnesium. This will be one aspect of the technology transfer deliverables of the Magnesium Powertrain Cast Components (MPCC) Project. (Task 3)
- Refine the engine component designs as necessary (updating to match the properties of the alloy selected for each component), design and build tools and patterns, and cast the engine components. (Task 4)

- Excise specimens from the cast components and develop a full mechanical and corrosion design database for the alloys. Create an original equipment manufacturer (OEM)—common material specification for magnesium powertrain alloys. (Task 5)
- Assemble complete powertrains, dynamometer-test the components, and conduct end-of-test teardowns. Refine the cost model to support determining the cost-effective performance of the engine. (Task 6)
- Note that before addressing Tasks 4–6 and funding Task 3 research, an in-depth review of the engine design, including performance and durability predictions, alloy requirements and measured alloy properties, cost model, and predicted weight reduction will be conducted. Passing this gate review is necessary for entry into the second-half of the project, which has the goal of demonstrating/validating the engine design with respect to castability, manufacturability, performance, durability, and cost.

Accomplishments

- Conducted a successful gate review of the engine design.
- Completed the static and cyclic mechanical property testing of six high-pressure die casting (HPDC) alloys and three sand casting (SC) alloys.
- Rebuilt the architecture of the computer database to contain the above test results, populated the database with the test results, and distributed the compact disc (CD) containing the database to the Project Team.
- Created and used an analytical Pair-wise Analysis Comparison methodology to select the appropriate magnesium alloy for each engine component: the cylinder block, the structural oil pan, and the front engine cover.
- Revised the FEA designs for the structural oil pan and the front engine cover; assembled and issued purchase orders to the respective project teams to design and build the tools for HPDC these components. Design revisions also optimized each component for NVH and weight reduction. The design revisions of the cylinder block are ongoing.
- Defined an engine test matrix, which will be used to measure the performance and durability of the magnesium-intensive engine in dynamometer testing.
- Identified critical scientific needs for utilization of magnesium in powertrain applications and made this information public at a U.S. Council for Automotive Research (USCAR)-sponsored workshop and by presenting and publishing the findings at the 2004 TMS annual meeting. Received and reviewed 31 proposals and selected 5 for funding within the approved MPCC budget program.

Future Direction

- Complete necessary component design revision; freeze the design, and build tooling for SC of the cylinder block. Because of a fire in early 2004 at Eck Industries, that foundry will not be available to the Project as previously planned. Instead, the Project Team has been working with the Structural Cast Magnesium Development Project Team to cast the cylinder blocks at Denison Industries.
- Complete and implement cylinder bore treatment for the cast cylinder blocks.
- Document machining observations for each of the magnesium components to comprehend any potential differences between the chosen magnesium alloys and aluminum.
- Excise specimens from cast magnesium engine components and test to create an excised-specimen property database of the three selected magnesium alloys, which will complement the cast-specimen database completed during Phase I.
- Complete dynamometer testing, teardown, and analysis of the magnesium-intensive engines.
- Input data from all stages of the manufacture of the die cast oil pan and front engine cover and the sand-cast cylinder block into the cost model to determine the cost-effective performance of the magnesium-intensive engine.

- Initiate each of the five basic research projects, and complete each with one midpoint review.
- Deliver final reports for the project by June 30, 2006.

Introduction

In October 2003, the Magnesium Powertrain Cast Components (MPCC) project team successfully completed a review of the Phase I accomplishments and was given the go-ahead for Phase II, the completion of the project. The major accomplishments and ongoing activities in FY 2004 thus comprised: (1) completing and distributing the cast specimen mechanical and thermo-physical database for the alloys tested in Phase I, (2) selecting from those alloys the most appropriate alloy for each magnesium engine component, (3) completing the engine component design revisions based on the properties of the alloys selected for the respective components, (4) contracting the teams for tool design and build and casting of the engine components, (5) defining the test matrix for the component and engine dynamometer tests, and (6) selecting the Task 3 research projects for initiation in 2004.

Excellent progress was made in each area. However, a mishap at the foundry where the magnesium cylinder block was to be cast removed that capability. Accordingly, much activity by the MPCC and the Structural Cast Magnesium Development (SCMD) project teams has involved developing an alternative low-pressure casting site. This activity is continuing.

Mechanical Property Testing and Database Development

The property testing planned for Phase I of the project was completed, as was the architecture for the expanded computer database. The resulting information is the cornerstone of the alloy selection process, in particular because it was obtained from specimens that were separately cast and tested using identical protocols. The database was developed at Westmoreland Mechanical Testing & Research. The amount of data to be contained in the database required a substantial upgrade to the architecture. This and beta testing of the software was completed. Distribution of the compact discs (CDs) containing the complete database to the MPCC project team was begun. The property test matrix has been described in previous progress reports. Briefly, it was developed by consensus of the General Motors (GM), Ford, and DaimlerChrysler powertrain members of the MPCC Project. It represented, in their judgment, the most relevant tests and test conditions for the evaluation of materials to be used in the engine components: the cylinder block, the bedplate, the oil pan, and the front engine cover.

The alloy properties contained in the database include chemical compositions, Brinell hardness, corrosion behavior, compressive and tensile strengths, compressive and tensile creep behavior, density, modulus, and in some cases fatigue and fracture analysis. Also included in the database are the thermo-physical data for several of the alloys, including those which were selected for the engine components. This information (solidus and liquidus temperatures, fraction solid evolution through the mushy zone, molten metal viscosity, specific heat capacity, latent heat, thermal diffusivity and conductivity, density, and linear thermal expansion) is essential for fill and solidification modeling of the engine components, which in turn is essential for tool design and build.

Examples of the compressive yield strengths for the sand and die casting alloys are shown in Figures 1 and 2. For each value shown in the figures, the user will find in the database the following information: the specimen geometry and test procedure; the specimen casting and test history, and both the individual specimen test values and the statistical summary. Exportable stress-strain curves for each test are also contained in the database.

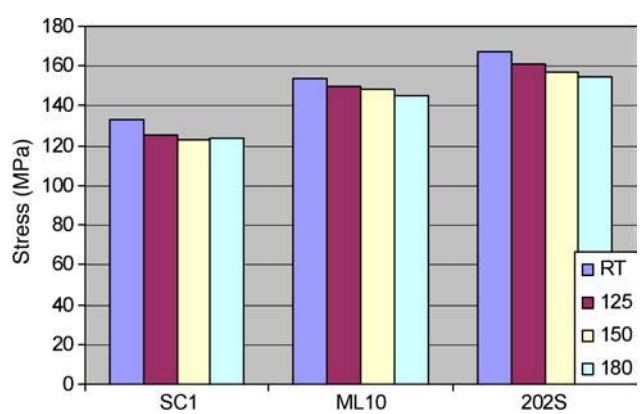

Figure 1. Compressive yield strengths of the SC alloys.

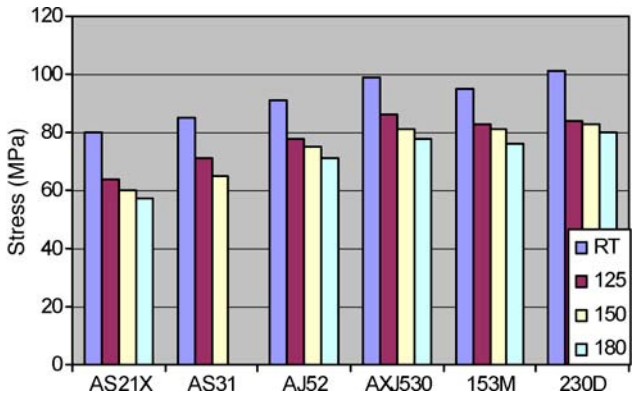

Figure 2. Compressive yield strengths of the HPDC alloys.

This database will be expanded in Phase II of the Project to include specimens excised from the cast components.

Alloy Selection—Pair-wise Analysis

Three major components of the Duratec engine were converted from aluminum to magnesium. One alloy was selected for each component. Having begun the project with seven high-pressure die casting (HPDC) alloys and three sand casting (SC) alloys, selection of the appropriate alloy for each component was a critical task of the project. To ensure objectivity of this process as much as possible, the project team used Pair-wise Analysis. This methodology involved identifying the most important criteria and categories for qualitatively and quantitatively rating the candidate alloys. The categories considered were mechanical properties, thermo-physical properties, corrosion behavior, and material and process cost. Within each category, specific criteria with component design-driven minimum or target values were identified against which to rate the alloys. For example, criteria deemed to be the most important among the block mechanical properties were the ultimate tensile strength, the high-cycle fatigue strength, the yield strength (stiffness) and the creep behavior. The criteria chosen for the other block categories were coefficient of thermal expansion and thermal conductivity (thermo-physical properties), salt-spray corrosion, heat-rejection surface corrosion in the coolant and galvanic corrosion in the coolant (corrosion behavior), and alloy cost and casting behavior (material and process cost).

Once the above categories and criteria were identified, a table was constructed to allow the relative importance of the each category to be compared and determined. Then, for each category a similar table was also created for determining the relative importance of the respective criteria within that category. Weighting was then calculated for each category and criterion, providing a relative, yet quantitative, level of importance for each. Having thus created the tables, rating of each alloy for each criterion was accomplished by comparing the measured property with the predetermined minimum or target property values previously specified. If a minimum property value was not achieved by a given alloy, then the alloy was eliminated from further consideration. Nevertheless, the category and criteria tables were completed for every alloy so that the alloy suppliers would have a complete picture of the relative performance of their respective alloys. Resultant scores for each criterion within each category were calculated and then summed to generate overall scores for each alloy, as is shown in Figure 3. Threshold tests were also performed on the resultant overall scores to determine whether the calculated scoring differences were significant. The process was repeated for each component: the sand-cast block, the die-cast oil pan, and the die-cast front engine cover.

The alloys thus selected were Australian Magnesium Corporation's SC1 for the cylinder block, Dead Sea Magnesium's MRI153M for the structural oil pan, and Dead Sea Magnesium's 230D for the

Criteria	Weights	Specification	Test Data	Alloy Rating	Score
Mechanical	33.333				41.80
UTS	0	235 MPa			
YS	8.889	120 MPa	123 MPa	3	26.40
Creep T	4.444	0.02%	5% at 100 hr	0	0.00
Creep C	2.222		Poor	0	0.00
Fatigue	10	75 MPa	tbd		
Modulus	7.778	45.7 Gpa	38.5 Gpa	2	15.40
Thermophysical	8.333				
CTE	4.167				
TC	4.167				
Corrosion	29.167				53.47
Salt	7.292	4 mils per yr	13.08	1	7.29
Galvanic	2.431	30 mg etc	35	3	7.29
Heat Rejection	19.444	1 mm etc.	5.87	2	38.89
Cost (29)	29.167				74.38
Alloy cost	2.917	AZ91D	5%	3	8.75
Solidification	8.750	1.75	1.9	4	35.00
Affinity/melt T	8.750	1.6 AZ	1.4	3	26.25
Hot tears	7.292	???			0.00
Recycling	1.458	AZ91D		3	4.38
Total	100.000				169.65

Figure 3. Pair-wise analysis of a candidate alloy.

front engine cover. Whereas the alloy selection criteria for the SC block and the structural oil pan were specific to those components, the criteria for the front engine cover were based on the requirements for a HPDC cylinder block, thus allowing a preliminary component-level evaluation of a third alloy.

The selected alloys will be used to cast the components, which will be tested in assembled engines. While each of these alloys was determined to have the best overall combination of available properties required for their respective component application, differences between alloys were often small. Consequently, the alloys selected for the magnesium-intensive V-6 engine represent the best collective engineering judgment of the Project Team. Because no single alloy was considered ideal, however, the Project Team expects that world-wide alloy development will continue until market forces determine a few standard powertrain alloys. The fact that several promising alloys are now available demonstrates the significant progress that has been made in magnesium.

Engine Component Design Revisions

The magnesium-intensive V-6 design, which was based upon the aluminum 2.5/3.0L Ford Duratec, exceeded the weight reduction target that was set by the Project Team at the start of the project. In postgate review activities, the Project Team further evaluated the engine design and design criteria using thermal, computational fluid dynamics, structural, durability, and noise, vibration, and harshness (NVH) performance criteria. The Phase I design of the engine was based on literature data. Having completed the property measurements and the selection of the alloys for the specific magnesium components, the focus of efforts in 2004 has been design revisions of the components for their respective alloys. In these activities, the goal was to optimize the designs for the aforementioned criteria and to take full advantage of the castability and other advantages of magnesium, relative to aluminum, to maximize weight reduction and the other performance criteria.

The design revisions for the structural oil pan and the front engine cover were completed. These were addressed first because of the lead time that will be necessary for die design and build. The cylinder block, which will be sand cast, is currently undergoing design revisions.

Optimized NVH performance was a major goal of the design revision effort for the oil pan and the front engine cover. Because of its lower modulus, and because the relationship between stiffness and NVH, it is generally thought that the weight reduction potential of magnesium is substantially nullified by the lower stiffness. In the design effort, two strategies were considered, a “soft” design which did not try to compensate for the less stiff magnesium, and a “stiff” design which did. Surface noise predictions were made for both design approaches over the full range of engine revolutions per minute and at several important regions in the acoustic spectrum. Figure 4 shows one set of results. In the

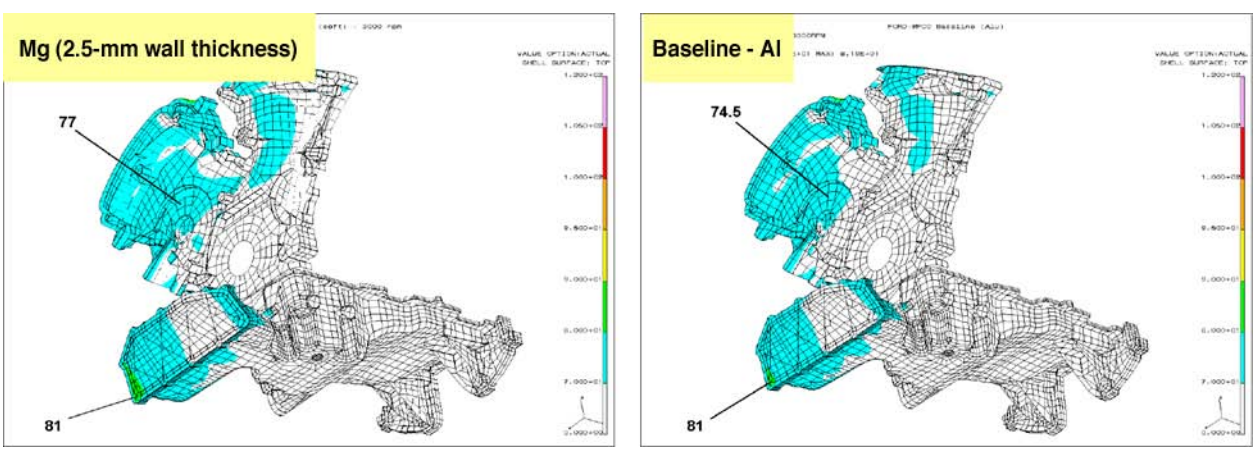

Figure 4. NVH analysis of the structural oil pan and front engine cover for octave band 250 Hz at 3000 rpm comparing the soft magnesium design with the aluminum baseline.

figure, the magnesium soft design version is compared with the aluminum components. The peak values for surface noise are labeled in each image. It is surprising that both versions show essentially the same NVH performance. As a result of these predictions, the Project Team elected to use the "soft" version, which would further lower the mass of the components. Predictions such as this challenge the prevailing notions about magnesium and designing with magnesium. These predictions will be thoroughly evaluated by the engine dynamometer testing planned for this engine.

Having completed the design revisions for the structural oil pan and the front engine cover, the computer-aided design (CAD) files were "handed off" to the die build team (see below), and work focused on completing the cylinder block design. It is expected to be completed in the first quarter of FY 2005.

Component Die Design and Build

Through competitive bidding, project teams for both the structural oil pan tool and the front engine cover tools were selected and contracts issued to them. The structural oil pan team comprises Technalysis, H. E. Vannatter, and Spartan Light Metal Products. These companies will design, manufacture, and use the tool, respectively. Sufficient oil pans will be HPDC to allow component and engine dynamometer testing and excising specimens for the mechanical property database. Exco Engineering and Intermet comprised the team to design, build, and use the front engine cover tool. Both sets of die casting tooling will use premium quality H-13 inserts. The MPCC Core Team chose H-13 over the less robust P-20 tool steel that is commonly used for prototype tools, so that tools could be made available to other alloy suppliers for casting trials and possibly for excised specimen testing once the engine test requirements have been met.

Once the cylinder block design is completed, a contract will be issued for tool build and low-pressure SC of the blocks. It was noted in the introduction, however, that the site where casting was to have taken place is no longer available to the Project. It was established during the castability trials of the SC alloys that low-pressure casting would be required to meet the melt quality requirements for the cylinder block. This is primarily due to the behavior of the grain refiners that these alloys require and, secondarily, to the recognized benefit of low-pressure casting for controlling metal fill of empty cavity molds. The MPCC project team is working with the SCMD project team to develop the capabilities of the Denison Industries for casting both the MPCC cylinder blocks and the SCMD engine cradles, both of which require high-temperature, creep-resistant alloys.

Engine Dynamometer Test Program

Just as the MPCC project team sought OEM consensus on the mechanical property test matrix, OEM consensus was used to develop the engine dynamometer test matrix. This matrix of tests will evaluate both the performance and durability aspects of the magnesium-intensive V-6 engine. The production Duratec (aluminum) will serve as the baseline for these tests. Testing will include block assembly and thermal distortion, thermal aging, hydraulic and thermal fatigue, hot scuff and cold scuff of the cylinder bores, NVH, and durability. Having defined the test matrix, the project will solicit bids for testing in 2005.

Critical Scientific Needs for Powertrain Magnesium Alloys

Phase I of the MPCC Project sought to determine the feasibility and practicality of producing a magnesium-intensive engine. Through the finite-element analysis (FEA) design activities, cost modeling, and extensive alloy casting and testing, the project team sought to quantify the technical and economic requirements of the V6 engine and which of the newly developed, high-temperature magnesium alloys best met those requirements. The additional objective of the project was to identify the fundamental scientific challenges of using magnesium alloys and casting processes in powertrain components both within the ongoing project and for more advanced powertrain components. This was accomplished by recognizing and documenting the critical scientific needs of the project as the Project Phase I was executed. The areas of critical scientific need are shown in Table 1.

During the reporting period these needs were compiled and rolled out to the North American scientific community in two ways. The first was a

Table 1. Areas of critical scientific need and MPCC project to address those needs

Area of need	Project	Principal investigator
Phase equilibrium and computational thermodynamics	Computational Thermodynamics and Alloy Development of Magnesium Alloys	Z. K. Liu Pennsylvania State University
Casting, solidification behavior, and microstructure	Hot Tearing Behavior of Magnesium Alloys	D. Emadi National Research Center of Canada
Alloy development and structure-property relationships	(No proposal selected)	
Creep and bolt-load retention	Creep, Bolt Load Retention, and Microstructural Analysis of High-Temperature Magnesium Alloys	W. Jones University of Michigan—Ann Arbor
Corrosion behavior and protection	Evaluation of Magnesium Corrosion by Various Methodologies and Surface Composition of Magnesium Alloys by Rutherford Backscattering Spectroscopy	P. Mallick University of Michigan—Dearborn
Alloy recycling	Fluxless Recycling Methods and Process Control for Creep-Resistant Magnesium Alloys	D. Schwam Case Western Reserve University

workshop held at the USCAR offices in Southfield, Michigan, to which representatives from universities and government laboratories were invited. The second was by presenting and publishing these needs at the Magnesium Technology 2004 Symposium, which was held at the TMS Annual Meeting in Charlotte, North Carolina, in March 2004.

Subsequent to the USCAR workshop, requests for proposals were solicited. Thirty-one proposals were received and evaluated by the project team. Using project funds allocated for this purpose in the original project budget, five of the proposals will be funded and initiated in 2005. These have been selected and the specifics of the work statements and funding are being finalized. A report was delivered to DOE, which contained all of the proposals with critiques by the MPCC Project Team. It is hoped that some of these additional proposals will be funded by other organizations. The projects to be executed within the MPCC activity are also shown in Table 1.

The newly developed, creep-resistant magnesium alloys are promising candidates for automotive powertrain applications. However, the limited amount of research and lack of understanding regarding these alloys remains a considerable obstacle to the full implementation of magnesium powertrain components. Conducting research in the areas shown in Table 1 will benefit both the short-term, immediate needs of the project in Phase II and will provide a long term legacy of the project by promoting new and strengthening existing research programs and thereby strengthening the scientific infrastructure for magnesium in North America.

Conclusions

The MPCC Project has made excellent progress since its inception in 2001. Project accomplishments include the science and engineering property database for the high-temperature, creep-resistant magnesium alloys; the selection of the alloys for the magnesium-intensive engine and the methodology used to make the selection; the engine design and cost model to predict cost-effective performance of the magnesium-intensive engine; and the selection and initiation of the basic science research projects. In fiscal year 2005, the project team expects to complete the technical work of the project. Completing of the research projects and documentation for the entire Magnesium Powertrain Cast Components Project will occur in 2006.

Acknowledgements

The success of this project is due to the dedicated efforts of a large number of team members, in particular the author's colleagues at Ford, DaimlerChrysler, and General Motors. The many other companies and organizations making up the project team were listed in the FY 2003 Progress Report. However, the author would like to acknowledge the MPCC core team for their work: John Allison, Joy Hines, and Robert McCune from Ford; Randy Beals and Lawrence Kopka from DaimlerChrysler; Larry Ouimet, James Quinn, and Grant Tappen from General Motors; and Peter Ried from Ried and Associates. The continuing support of our respective companies and the U.S. DOE is gratefully acknowledged.

Presentations and Publications

1. "Magnesium Powertrain Cast Components Project," B. R. Powell, presented at the AMD Board Casting Off-Site, September 29, 2004, Southfield, Michigan.
2. "Overcoming the Technical Barriers to a Magnesium-Intensive Engine," B. R. Powell, L. J. Ouimet, J. E. Allison, J. A. Hines, R. S. Beals, L. Kopka, and P. P. Ried, presented at the 10th Metal Casting Congress, sponsored by the American Foundry Society and the North American Die Casting Association, Rosemont, Illinois, June 12, 2004 (invited).
3. "USCAR Update on High Temperature Alloys for Magnesium Powertrain Cast Components Project," J. A. Hines, J. E. Allison, R. McCune, B. R. Powell, L. J. Ouimet, R. S. Beals, L. Kopka, and P. P. Ried, 14th Magnesium in Automotive Seminar, sponsored by the International Magnesium Association, Troy, Michigan, April 20, 2004 (invited).
4. "The Magnesium Powertrain Cast Components Project: Part II—Properties of Several New Creep-Resistant Magnesium Alloys," J. A. Hines, R. C. McCune, J. E. Allison, B. R. Powell, L. J. Ouimet, R. S. Beals, L. Kopka, and P. P. Ried, presented at the Magnesium Technology 2004 Symposium of the TMS Annual Meeting, Charlotte, North Carolina, March 15, 2004.
5. "The Magnesium Powertrain Cast Components Project: Part I—Accomplishments of Phase I and the Objectives and Plans for Testing the Magnesium Engine in Phase II," B. R. Powell, L. J. Ouimet, J. A. Hines, J. E. Allison, R. S. Beals, L. Kopka, and P. P. Ried, presented at the Magnesium Technology 2004 Symposium of the TMS Annual Meeting, Charlotte, North Carolina, March 15, 2004; also published in the symposium proceedings, pp 3-10 (2004).
6. "The Magnesium Powertrain Cast Components Project: Part III—Fundamental Scientific Needs for Magnesium Utilization in the Powertrain Environment," R. S. Beals, L. Kopka, J. A. Hines, R. C. McCune, J. E. Allison, A. A. Luo, B. R. Powell, L. J. Ouimet, and P. P. Ried, presented at the Magnesium Technology 2004 Symposium of the TMS Annual Meeting, Charlotte, North Carolina, March 15, 2004; also published in the symposium proceedings, pp. 11–18 (2004).
7. "Progress Toward a Magnesium-Intensive Engine: The USAMP Magnesium Powertrain Cast Components Project," B. R. Powell, L. J. Ouimet, J. E. Allison, J. A. Hines, R. S. Beals, L. Kopka, and P. P. Ried, presented at the Magnesium Technologies session of the 2004 Society of Automotive Engineers World Congress, Detroit, Michigan, March 9, 2004; also published as SAE Technical Paper No. 2004-01-0654 and to be published in *SAE Transactions* (2004).
8. "The USAMP Magnesium Powertrain Cast Components Project," B. R. Powell, published in *JOM*, **55**(11), 28–9 (2003).
9. "The Magnesium Powertrain Cast Components Project" B. R. Powell and P. P. Ried, Jr., presented at Advanced Technologies session at the 2003 North American Die Casting Association International Congress, Indianapolis, Indiana, September 15, 2003; also published as paper no. T03-28 in the NADCA Transactions (2003).

E. Low-Cost Titanium Evaluation

Principal Investigator: Curt A. Lavender
Pacific Northwest National Laboratory
Richland, WA 99352
(509) 372-6770; fax: (509) 375-4448; e-mail: curt.lavender@pnl.gov

Technology Area Development Manager: Joseph A. Carpenter
(202) 586-1022; fax: (202) 586-1600; e-mail: joseph.carpenter@ee.doe.gov
Field Technical Manager: Philip S. Sklad
(865) 574-5069; fax: (865) 576-4963; e-mail: skladps@ornl.gov

Participants:
Lance Jacobsen, International Titanium Powder, Inc., 20634 W. Gasken Drive, Lockport, IL 60441
Paul Jablonski, Albany Research Center, Albany, OR 97321
Mahi Sahoo, CANMET, Ottawa, Ontario Canada K1A 1M1
Nathan Canfield, Pacific Northwest National Laboratory, Richland, WA

Contractor: Pacific Northwest National Laboratory
Contract No.: DE-AC06-76RLO1830

Objectives

- Investigate alternate powder and melt processing methods for low-cost titanium materials.
- Evaluate processing methods to produce powder metallurgy (PM) titanium products with International Titanium Powder, Inc. (ITP) powder.
- Evaluate the suitability of emerging titanium technologies for the production of low-cost titanium products for automotive applications.

Approach

- Perform characterization and analysis of the sintering behavior of the ITP powder. Provide feedback of results to ITP for use in process design.
- Perform thin-section slab castings and roll to sheet to simulate and evaluate the use of continuous casting methods to produce sheet materials.
- Survey the emerging technologies for the low-cost production of titanium powders and evaluate for use in automotive applications.

Accomplishments

- Developed press and sinter cycles that produced greater than 97% dense plates of cold-pressed (CP) titanium from the ITP powder.
- Hot-rolled plates pressed and sintered from CP titanium ITP powder with a 2.5:1 reduction exhibited limited ductility in bend tests. Fracture surface evaluation showed that although densities were high, large amounts of the powder had not sintered.
- Designed and fabricated in cooperation with Albany Research Center (ARC) and CANMET, graphite molds for plate casting trials to determine the effect of solidification rate on the reduction of area required to produce wrought properties.

Future Direction

- Perform dilatometry, thermogravimetric (TGA), microstructural analysis, and XRD analysis to develop a sintering cycle that can eliminate sodium impurities and improve sinterability at lower pressing pressures.
- Continue the development of sintering cycles for the ITP powder with an emphasis on understanding the sintering mechanisms of the powder to increase ductility.
- Continue evaluations to determine the cause of the low ductility of compacted material produced with ITP powder.
- Evaluate alternate low-cost titanium feedstocks for powder or melt processing to wrought products.
- Evaluate mechanical properties of step-plate castings produced at ARC.

Introduction

An automobile design trend that has received much attention has been the reduction of vehicle mass. Reducing mass can improve both performance and fuel economy. While design changes can play a large role in reducing mass, large reductions ultimately will require the substitution of higher specific strength/stiffness materials in place of carbon steel. Primary contenders in this race are high-strength steels, aluminum, and fiber-reinforced polymer composites. One material not on this short list, but one that could provide further reductions, is titanium. Although titanium is light and strong, its role in the automobile has been almost nonexistent because of its exorbitant price. This high price is a direct result of the current production route, the Kroll process, which is time-consuming; energy-, capital-, and labor-intensive; and batch-based.

However, new technologies are emerging that may change the characteristics of the titanium market. In particular, these technologies may reduce the titanium price sufficiently to allow it to compete in high-volume markets, possibly even automotive. This project examines the powder metallurgy (PM) behavior of titanium powder produced by a new process being developed by ITP.

Approach

The production of low-cost titanium for automotive applications will require cost reductions in both raw materials and secondary processing operations. The approach to this project will be to evaluate the suitability of emerging titanium beneficial technologies and secondary operations, such as rolling to sheet by continuous casting and solid state methods. The ITP powder process produces an alloy powder with morphology very similar to the emerging technologies, FFC Cambridge and MER anodic reduction. Because ITP can produce powders in sufficient quantity for evaluation, the ITP process will be used as an evaluation of new secondary processing operations such as continuous rolling and solid-state sheet production.

Results and Discussion

Previous reports[1–3] of ITP powder processing indicated that sodium compounds were assumed to be limiting the density and tensile ductility of the sintered pressing. Thermo-gravimetric (TGA) results of ITP powders indicated that sodium compounds were present and began to decompose at temperatures near 500°C. Dilatometry of a pressed powder compact, given in Figure 1, showed that sintering of the compact initiated at 475 to 500°C.

Additionally, it was shown that vacuum distillation of NaCl from titanium sponge was a very slow process (which explains why titanium sponge

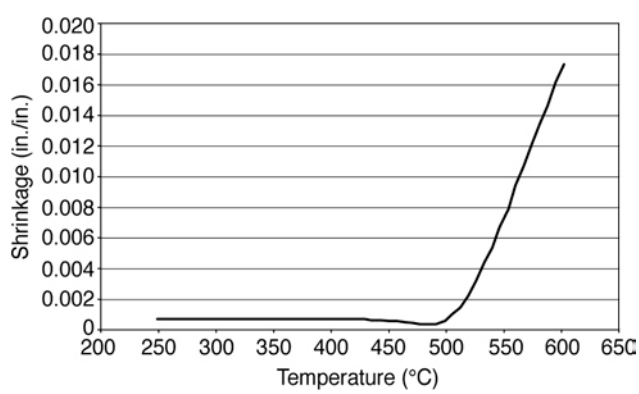

Figure 1. Sintering shrinkage of an ITP CP titanium powder pressed at 60,000 psi using a heating rate of 5°C/min.

produced by the sodium-reduced Hunter process was washed, and the magnesium-reduced Kroll processed sponge was vacuum distilled.)[4] The result of the combination of factors can result in sintering prior to complete removal of deleterious impurities such as sodium. Therefore, a sintering cycle was used at 1100°C that included an 8-h hold at 500°C to assist in distillation of any sodium compounds prior to excessive sintering. The result was a 97+% dense plate that, after rolling with 2.5:1 reduction, exhibited ductility in a bend test.

Analyses of the fracture surface and partially sintered powder, given by Figures 2(*a*) and 2(*b*), respectively, indicate that even with a high bulk density, a large quantity of the powder has not sintered and bonded.

This was not an expected result given the very fine size of the powder and the reactivity of titanium. When sintering of the ITP powder was performed, a relatively constant 11 to 15% density increase was observed; whereas atomized Ti-64 powder processed in parallel exhibited as much as a 30 to 40% density increase as illustrated here in Figure 3. At this point the sintering mechanism of the ITP powder particle must be studied to determine what process parameter must be modified to enhance particle growth and bonding. This can include sintering temperature, sintering atmosphere, and heating rate during sintering.

Increased compaction pressure, 75,000 psi, and slow heat times, 5°C/min, were used to produce powder compacts with densities in excess of 95%. The compacts processed using the exhibited limited ductility, 3%, did not show the regions of unsintered material observed in previous trials. Figure 4 has

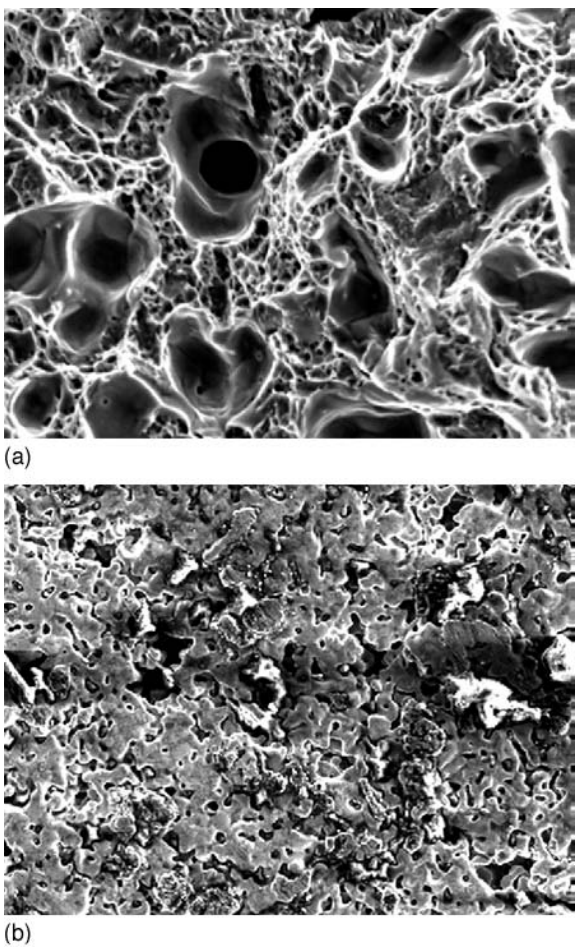

Figure 2. Fracture surface (*a*) and sintered structure (*b*) of sintered CP titanium powder indicate incomplete sintering even though bulk density was in excess of 97%.

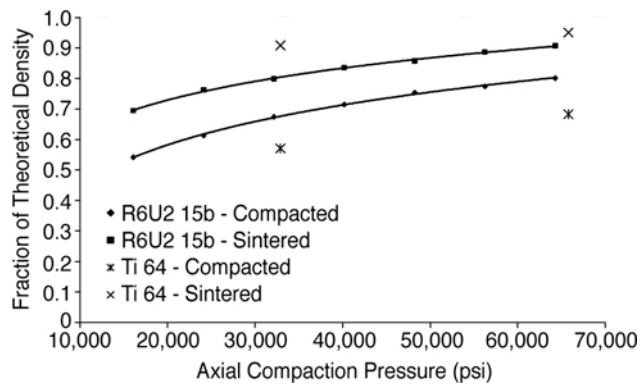

Figure 3. The fraction of theoretical density as a function of axial compaction pressure for ITP CP titanium and atomized Ti 6Al 4Vpowders.

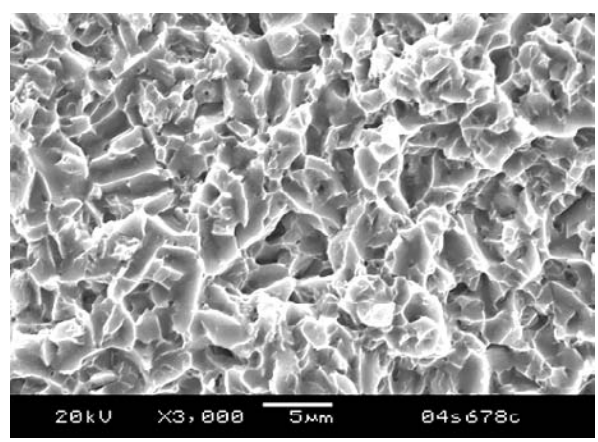

Figure 4. Fracture surface of sintered compacts of ITP powder processed at Pacific Northwest National Laboratory, indicating that relatively complete sintering of the compact has been achieved.

been included to illustrate the fracture surface observed in highly sintered ITP powder compacts, illustrating that relatively complete sintering has been achieved.

Progress was made in the development of the step-cast plates at Albany Research Center (ARC). Complete die fill was achieved through a series of design iterations on the mold. All cast plates have been delivered to CANMET for evaluation. Figure 5 has been included to illustrate the typical step cast plate developed by ARC and delivered to CANMET.

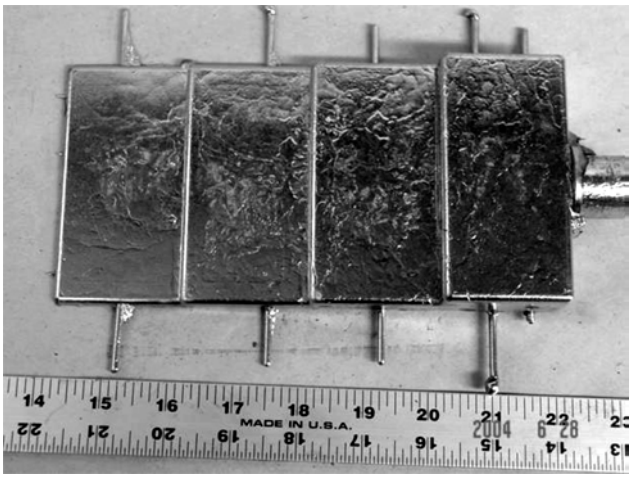

Figure 5. Step plate castings developed for evaluation at CANMET.

Conclusions

- Sintering conditions for the ITP can be developed to produce ductility. Optimization of the sintering cycle must be performed to maximize ductility.
- The sintering mechanism of the ITP powder is different than atomized powder, and conditions must be developed to maximize the volume of powder sintered.

References

1. S. Abkowitz, S. M. Abkowitz, H. Fisher, and P. Schwartz, Final Report of Contract No. 409117AU7, *Low-Cost Titanium Evaluation*, Dynamet Technology, Inc., November 29, 2002.
2. S. Abkowitz, S. M. Abkowitz, H. Fisher, and P. Schwartz, Final Report of Contract No. 7283, *Low-Cost Titanium Evaluation*, Dynamet Technology, Inc., July 29, 2003.
3. S. J. Gerdemann and D. E. Alman, *Characterization of a Titanium Powder Produced through a Novel Continuous Process*, Advances in Powder Metallurgy and Particulate Materials 2000, MPFI, Princeton, New Jersey.
4. S. D. Hill et al., "Heat and Mass Transfer in Kroll Process Titanium Sponge During Salt Evaporation," *Light Metals 1971: Proceedings of Symposia, 100th AIME Annual Meeting*, pp. 605.

F. Structural Reliability of Lightweight Glazing Alternatives

Principal Investigator: Moe Khaleel
Pacific Northwest National Laboratory
(509) 375-2438; fax: (509) 375-6605; e-mail: moe.khaleel@pnl.gov

PPG Project Manager: Jim Valimont
(412) 820-8731; fax: (412) 820-8705; e-mail: rueter@ppg.com

Visteon Project Manager: Mike Brennan
(313) 755-1879; fax: (313) 755-7485; e-mail: mbrenna1@visteon.com

Technology Development Manager: Joseph Carpenter
(202) 586-1022; fax: (202) 586-1600; e-mail: joseph.carpenter@ee.doe.gov
Field Technical Manager: Philip S. Sklad
(865) 574-5069; fax: (865) 576-4963; e-mail: skladps@ornl.gov

---

Contractor: Pacific Northwest National Laboratory
Contract No.: DE-AC06-76RL01830

Objectives

- Optimize glazing systems for cars of the future by decreasing sound transmission while maintaining structural rigidity.
  - Reduce sound transmitted through sidelights by 6 db by determining the effect of sidelight shape on sound transmittance, investigating sound-dampening materials for operating sidelight glazing, and quantifying the influence of alternate materials (e.g., laminated glass, bilayer glass) on sound attenuation.
  - Maintain the level of structural integrity while reducing glass thickness by validating the structural rigidity model for various types of urethane used in fixed glazing systems and by expanding/combining existing models to test various alternative constructions and glazing systems for side, rear, and roof windows.
- Reduce vehicle weight through alternate or thinner vision panels and/or by reducing the heat load transmitted through the glass. The goal is to improve the fuel economy of a car by requiring 30% less glass weight.
- Reduce side, rear, and potentially roof window glass weight while maintaining acoustics and minimizing price increases.
  - Consider several material options, including laminated glass, cast-in-place pseudo-laminated glass, and bi-layer materials.
  - Enhance fuel economy from reduced solar energy transmission.
  - Reduce solar energy transmission through glass by using absorbing substrates and reflective coatings.
  - Quantify gas mileage improvement opportunities from improvement in solar energy transmission.

Accomplishments

- Completed testing for demonstrating production compatibility using a resin injection method for side window laminations.
- Achieved 12-in. by 12-in. test panel interlayer fill times of 7–20 s, depending on viscosity.
- Fabricated 40 test windows with a new injection method for the cooperative research and development agreement (CRADA) partner to test interlayer material.
- Obtained preliminary test data from the CRADA partner showing successes and improvement areas.

- Completed and tested new tooling for ultraviolet (UV) and thermal curing of interlayer laminating resin.
- Characterized interlayer materials for accelerated curing for production.
- Demonstrated thermal and UV curing for continuous fill and cure laminating system.
- Demonstrated reduced infrared (IR) transmission up to 45% with alternative polymer systems.
- Characterized the sound transmission loss of the new lightweight laminated glass.
- Verified and extended the predictive sound transmission loss models to investigate the effect of the new polymeric materials.
- Completed the modeling of the acoustical response of glass.

Future Direction

- Develop lightweight side-door glass.
- Investigate the strength and thickness of new polymeric interlayer materials on overall side-door strength and performance.
- Investigate the overall thermal behavior based on the new interlayer materials, including the effect of laminated side-door glass.
- Fabricate newly designed tooling for complex automotive side window shapes and laminate with new interlayer materials.
- Investigate the use of nanomaterials for acoustic modification and UV resistance.
- Investigate multilayer interlayer for acoustic modifications.

Introduction

This project is a cooperative research and development agreement (CRADA) between the U.S. Department of Energy, Pacific Northwest National Laboratory (PNNL), Visteon Automotive Systems (Glass Division), and PPG, Inc. It started in June 2002.

The project will evaluate designs for optimized glazing systems to be used in cars of the future and will work to achieve the goals of FreedomCAR. The primary objective of the project is to reduce vehicle weight, improve fuel economy, and reduce vehicle emissions. However, to achieve these goals, it is necessary to consider the needs for high levels of structural reliability, competitive manufacturing costs, and passenger comfort from the standpoints of minimal acoustical noise levels and controlled interior temperatures. Energy savings will come from reducing weight by using thinner glazing; prior studies at PNNL have shown a potential for 30% reductions in weight from thinner glazing. Energy savings will also come from reducing interior heat loads; that, in turn, will reduce the demand for air conditioning. The evaluation of alternative glazing concepts will also seek means to improve acoustical characteristics that will minimize interior noise levels while maintaining glazing at minimal thickness and weight levels.

Lightweight Window Manufacturing

New lightweight window samples were fabricated using 1.6-mm and 2.3-mm glass plies (a conventional automotive glass ply has a thickness of between 2.4 and 2.6 mm. The new lightweight samples were formed and laminated at PNNL using several different types of polymer interlayers for comparison.

A new liquid control injection system was purchased for the scale-up effort for large windows. The new injection system allows for a continuous stream of mixed resin to be injected into the tooling for laminating. The fill rates and pressure can be controlled, and the system is flexible enough to be able to change resin systems that have significantly different resin ratios.

Testing was performed with the new injection system to determine whether mixing was adequate with the commercial static mixer tubes. The tubes purchased with the machine were determined to be

inadequate, and two alternative vendors were found to have better quality mixing tubes.

Several new lightweight laminated side glasses were fabricated using 2.3-mm plies. The new window glass samples that were constructed are 2.3-mm glass, 0.76-mm polymer interlayer, and 2.3-mm glass.

During FY 2004, researchers completed the demonstration of a production-compatible system. They conducted studies that demonstrated flow behavior, times to fill, curing studies, demold times, and material down-selection. The evaluation of optical properties was also addressed. Three of the commercially available materials were altered for specific characteristics in curing and hardness. Because the optical requirements for the sidelights are not as stringent as those for the windshield, other materials may prove to be more attractive and cost-effective.

Flow Behavior and Fill Time

A new aluminum fixture was designed and built to observe flow behavior in 12-in. by 12-in. glass panels working on UV curing of resins. Two new test fixture designs were used to hold the two glass plates against the fixture surface using vacuum and to control the separation for the interlayer to 0.5- and 0.75-mm gaps for resin filling. The gap is controllable with a spacer shim around the outside of the fixture.

The flow studies and measurements were performed using an 8-mm video camcorder with the clock on during taping. A ruler was laid across the glass plates before video taping, and the fill rate was determined based on the time to fill a particular length based on the flow front movement. The videos allowed for visualization changes in flow front profiles and time-to-fill measurements. Depending on the viscosity of the fluid, the flow front profile would vary from a parabolic flow front to a horizontal flow front. The low-viscosity materials demonstrated a horizontal flow, while the higher viscosity materials represented a parabolic shape. The shape of the flow fronts based on the viscosity of the material will help in predicting flow behavior in irregular-shaped windows and will determine the injection point of the part.

Previous flow studies used 8-in. head pressure to flow different materials and viscosities the length of the plates and tooling. The fill rates for this pressure and with viscosities as low as 123 cps had a fill rate of 14 in./min, while a viscosity of up to 3000 cps had a fill rate of 1.4 in./min.

Further testing with increased pressure shows that a 200-cps viscous material injected at 10 psi (70 kPa) fills the same areas and flows the same distance as the previously measured data in less than 5 s, which is equivalent to 3000-cps viscous material fills in 15 s. Table 1 illustrates the difference in pressure and viscosity affecting the fill rates.

Based on these fill rates, to fill a side window on an sports utility vehicle (SUV) of roughly 4200 cm^2 would take 25 to 70 s, depending on their viscosities.

Table 1. Fill rate comparisons with different viscosity resins and 0.60-mm interlayer thickness

Injection pressure	Viscosity (cps)	Time to fill (s)	Fill rate/length (mm/s)	Fill rate/area (mm^2/s)
8-in. head	123	49	5.96	1896
8-in. head	3000	492	0.59	189
70 kPa	123	5	58.40	18581
70 kPa	3000	15	19.47	6194

Material Curing Studies and Window Demold Times

With the validation of the injection process fill times, the focus changed on the cure times of resin. The cure times were evaluated on temperature and UV curing. The cure rates for thermal curing were based on temperature-controlled studies in a convection oven. The studies looked at demold times based on degree of cure. Further studies included Differential Scanning Calorimetry (DSC) that evaluated the resin mixtures at different isothermal temperatures. Figure 1 illustrates the reduction in cure times and increased temperatures. Even though the cure time can be significantly reduced, thermal oxidation of the material starts to occur and increases the yellowing of the cured material (which is undesirable) and reduces the light transmission. Demold times have been as low as 10 and 15 min, and additional curing took place at room temperature. The objective is to get the material to cure enough for handling and then allow the material to continue to cure after demolding. Cycle times of 20 min per fixture have been achieved.

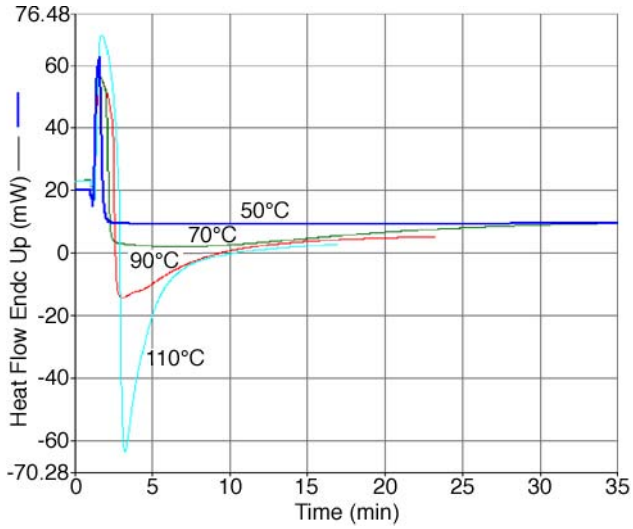

Figure 1. Epoxy isothermal DSC runs for cure times on mixed-resin system.

A new tool was fabricated for testing cure times using UV curing for polyester and acrylic resins. The UV testing shows promise, but some resin modifications are being worked on to help reduce masking affects. UV resins still look promising for production.

The UV-cured resin was modified with an accelerator and catalyst to partially cross-link the resin for demolding and then final cure with UV light. Figure 2 illustrates the reaction time for the resin at 93°C. The accelerators did not actually

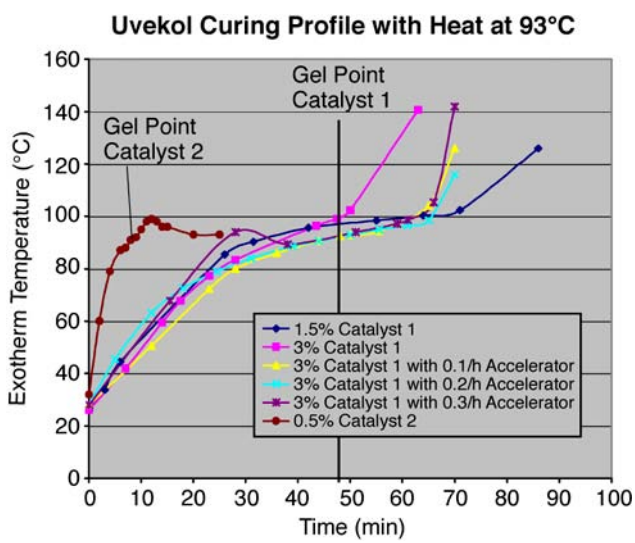

Figure 2. UV-cured resins with different ratios of catalyst and accelerators.

decrease the cure time; a reduction in the peak exotherm was reduced by 20°C. The reduction in exotherm helps reduce the overall shrinkage of the resin, which can impart temporary strain at the interface of the glass. Higher exotherms can also create resin boil because of the lower boiling point of the monomers, which can cause bubbles to form in the interlayer. Controlling the exothermic temperature can be just as important as decreasing the cure time.

Experiments on a second catalyst were conducted based on lessons learned from the first experiments. As indicated in Figure 2, a significant reduction in cure time and a significant reduction in peak exotherm were achieved. Further testing will be performed with this resin system.

Material Down-Selection

The materials down-selection led to polyurethane, acrylic, polyester, and epoxy. Testing conducted at PPG to further reduce the material down-selected was completed. The material has been down-selected to two final candidates that need further evaluation and optimization. Continued studies on the catalyst effects on the resin properties as well as the Society of Automotive Engineers (SAE) standards will assist in the final optimized material. Sound transmission loss is one of the important criteria, but it is difficult to find data on commercially available materials. Stress relaxation data are continuing to be collected on the two selected materials for use in the acoustic modeling of the sound transmission loss equipment. Furthermore, materials optimization for sound transmission loss is also being investigated. Several tests have been conducted based on the SAE Z26.1 criteria for side window laminations. PPG has done more total light transmission testing, UV and infrared (IR) testing, boiling water testing, humidity testing, and thermal cycling.

Transmittance Testing

To date, more than a hundred laminated glass panels have been fabricated and tested. The initial panels were used on the ring-on-ring testing, which demonstrated the adhesion properties. There were also initial transmittance spectrums using a UV-Vis spectrometer, which helped to determine the transmittance of the laminate. The U.S. requirement for total transmittance for sidelight windows is 70%. PPG has done some initial total transmittance testing

shown in Table 2. The total transmission test exceeds the 70% requirement for both tested materials. Material 1 has pretty much the same total transmission, and Material 2 is approximately 9% lower than the polyvinyl butyral (PVB). However, the UV transmission is lower in Material 1 and the same in Material 2 relative to the PVB standards. One of the most interesting results is the IR transmission. The PVB standards show a 71% IR transmission, and Material 2 is relatively close to that as well. However, there is almost a 50% drop in the IR transmission in Material 2. Finally, the total spectral transmission of Materials 1 and 2 shows a drop of less than 2% for the exposure. The glass substrates used for these test were all done on clear glass with no modifications for UV or IR. These differences are directly related to the interlayer materials.

The IR reductions in Material 2 can significantly reduce the heat load in the vehicle. This can further improve fuel economy by reducing the taxable horsepower from interior cooling and providing more comfort for the occupants.

Other Testing

Other testing being evaluated at PPG are boil, humidity, thermal cycling, and ball drop. The first round of boil testing was completed, and all specimens passed. The boil test submerges a 12-in. by 12-in. laminated glass panel in boiling water for 6 h.

The boil specimens were evaluated for delaminating, bubbles, and a cloud effect zone from the edge less than 12 mm. There were no issues from the boil test, and the material has passed that test.

The first humidity test results were marginal and needed further work to improve on the laminate. After some resin modification to optimize for the humidity, a significant reduction in the ESN total was observed; however, a total ESN number goal is zero. The initial ESN numbers were on the order of 2200, and we currently have ESN numbers around 100. This is a significant change, but further work will need to be accomplished to obtain a zero value.

The improved humidity-resistant resin also caused the material to fail the ball drop test. The initial ball drop testing passed with the previous formulations. It is now understood that a change as small as 5% in our resin formulation to improve humidity resistance had a detrimental effect on the ball drop. Ball drop testing properties are now being improved upon, and further testing is currently ongoing but has not been completed to date.

PNNL tested for stone impact and found some very unique differences compared to the PVB interlayer materials. The PVB had higher speed stone impact tolerance by about 10-15 mph; however, sidelight windows do not have criteria for stone impact. The evaluation was done to compare the difference between the materials being evaluated. Even though the speed was lower, the impact speeds were still satisfactory.

Acoustic Chamber Modeling and Testing

A coupled structural-acoustic modeling procedure was developed using commercial finite-element code ABAQUS to systematically study the structure vibration and acoustic behaviors of the injection-molded laminated glass. Our goal is to use the analytical modeling tool to examine the effects of resin properties on the acoustic performance of the laminated glass specimen.

To analyze the acoustic test chamber with an accurate-yet-efficient model, we initially assumed that the air layer 1 in. above the top glass surface (top microphone location) experiences incident waves of the same amplitude and frequency. An axisymmetric model was used for simplicity and the

Table 2. Spectral transmission average data

Material	Total transmission (%)	UV (%)	IR (%)	TSET (%)	Total transmission after UV exposure (%)
PVB Standard 1	88	NA	71	76	NA
PVG Standard 2	88	7	71	76	NA
Material 1	87	5	69	75	85
Material 2	79	7	38	53	78

foam supporting the glass boundary is modeled with two-dimensional (2-D) connector elements (see Figure 3). In Figure 3, the air layers are modeled with 4-node linear acoustic elements ACAX4R, and the glass and the resin layer are modeled with 4-node bilinear solid elements CAX4R with different materials properties. The interfaces between the air (acoustic elements) and glass (solid elements) are constrained at their abutting surfaces using the *TIE option. The thicknesses of both glass layers are set to be 2.3 mm, and the intermediate resin layer is 0.5 mm thick.

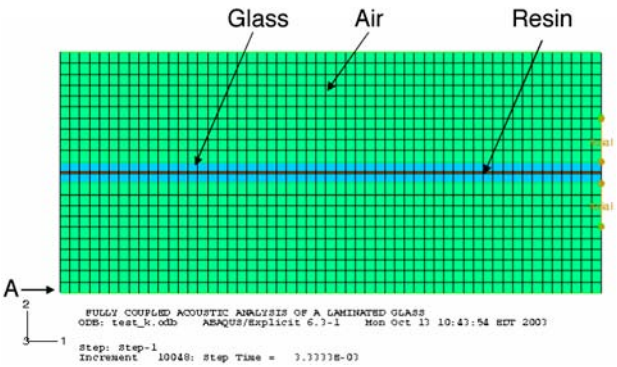

Figure 3. Coupled structural-acoustic finite-element model.

The incident wave comes from the top of the air layer with specified frequency and amplitude. The pressure response of the air at Point A, 1 in. below the glass center, is monitored as output of the analyses. Steady state dynamics procedures are used, and the final sound transmission loss values for different frequency levels were obtained through frequency sweep:

$$STL(dB) = 20\log\left(\frac{p_1}{p_{input}}\right) \quad , \qquad (1)$$

where p_1 is the response wave amplitude, and p_{input} is the input wave amplitude.

Figure 4 shows the predicted sound transmission loss (STL) values for the frequency sweep compared with discrete STL measurement from our experiments. Because the system has a natural frequency around 3500 Hz, we observe a dip in STL around 3440 Hz. This is very much consistent with our experimental findings in this study as well as other experimental findings reported in the open literature for architectural glass. In general, the predicted STL

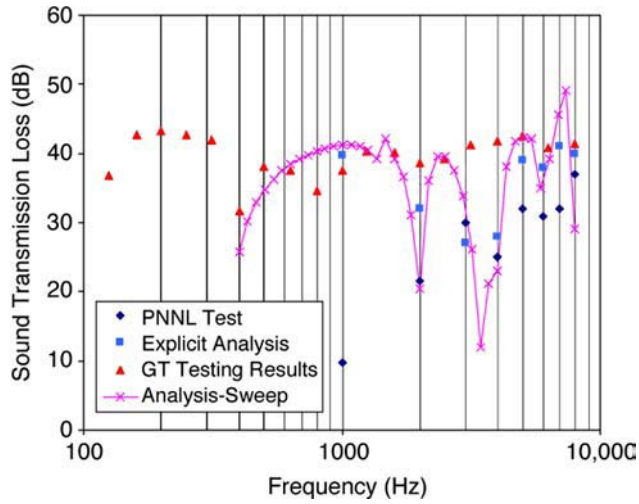

Figure 4. Predicted STL results compared with experimental results from different testing sources.

values compare reasonably well with the acoustic chamber measurement at frequencies higher than 2000 Hz. For frequencies lower than 2000 Hz, the prediction is higher than measurement.

To resolve the discrepancies between the predicted and measured STL values for low frequency levels and to better understand the sound transmission measurement, more acoustic measurements were carried out at the Georgia Institute of Technology (GT). Measurements of the sound noise reduction (in decibels) of four samples, 12-in. by 12-in., of laminated glass have been made in accordance to SAE J1400, in third-octave bands between 125 Hz and 8 kHz. The samples were mounted between the reverberant chamber and the semi-anechoic chamber of the Integrated Acoustics Laboratory (IAL) at GT. The results, together with the simulated results and the test results carried out at PNNL, are shown in Figure 4.

The measured STL values obtained at GT are generally higher than the ones obtained at PNNL. This is particularly true in frequency ranges lower than 1000 Hz. At frequencies higher than 400 Hz, the predicted STL values are in fairly good agreement with the GT measurements except for the fact that predicted results indicate more coincidence dips. It should be mentioned that very good repeatability has been found for both testing facilities at GT and PNNL. These results then indicate that caution should be exercised when comparing STL measurements from different experimental sources. More analytical work in this area will be pursued to

characterize the STL of laminated glass plates with different resin layers.

Future Work

Future work is focused on fabricating larger automotive side windows along with further testing by the PPG. The new tooling will be more automated and will be ready to simulate production runs of surface areas at least four times the current area. Further, 12-in. by 12-in. testing plates will continue to be made with other interlayer materials and given to PPG for further testing. The overall mechanical, thermal, and acoustical behavior of the new light weight glass will be evaluated using both experimental and analytical procedures. New experimental data from the humidity and acoustic testing allows focusing on specific changes needed to modify the material formulations that will maximize the system performance. Modeling efforts are continuing to focus on the effects of polymer properties on sound transmission loss.

Furthermore, work is beginning in nanocomposites for the interlayer and multiplayer features in the interlayer, which could further improve the acoustic properties.

4. POLYMER COMPOSITES R&D

A. Development of Manufacturing Methods for Fiber Preforms

Program Manager: Jeff Dahl
Ford Motor Company, Scientific Research Laboratory
P.O. Box 2053, MD 3135 SRL, Dearborn, MI 48121-2053
(313) 845-1039; fax: (313) 390-0514; e-mail: jdahl@ford.com

Project Manager: C. David Warren
Oak Ridge National Laboratory
P.O. Box 2009, Oak Ridge, TN 37831-8050
(865) 574-5069; fax: (865) 574-0740; e-mail: warrencd@ornl.gov

Technology Area Development Manager: Joseph A. Carpenter
(202) 586-1022; fax: (202) 586-1600; e-mail: Joseph.Carpenter@ee.doe.gov
Field Technical Manager: Philip S. Sklad
(865) 574-5069; fax: (865) 576-4963; e-mail: skladps@ornl.gov

---

Contractor: U.S. Automotive Materials Partnership
Contract No.: FC26-02OR22910

Objective

- Develop and demonstrate new fiber preforming processes to decrease cost, increase manufacturing rates, and improve reproducibility of large preforms for composite molding.
- Provide process development support to the Automotive Composites Consortium's (ACC's) Focal Project 3.

Approach

- Identify carbon fiber properties required to permit rapid processing and achieve desired performance levels.
- Investigate materials, process equipment, and tooling technology to further reduce the cost and enhance the quality of chopped fiber performs.
- Characterize chopped fiber preforms utilizing experimental carbon fiber rovings to determine important characteristics (permeability, light transmission, areal density distribution, etc.).

Accomplishments

- Obtained seven experimental rovings to investigate the effect of tow size on composite material performance; these were manufactured by Hexcel Carbon Fibers and delivered to the ACC.
  - Fabricated experimental light transmission analysis preforms using seven experimental carbon fiber rovings and sent them to Winona State University for analysis to determine the effect of tow size on material distribution.
  - Conducted preforming, molding, and mechanical testing using seven experimental carbon fiber rovings to determine the effect of bundle size on preforming, molding, and composite material performance.

- Established Fortafil carbon fiber roving development program, which is progressing with successful direct splitting of carbon fiber rovings.

Future Direction

- Evaluate experimental preforming and molding of mechanically split, low-filament-count, Fortafil carbon fiber rovings.
- Further characterize and investigate low-cost carbon fiber rovings with reduced individual bundle size.

Introduction

This project has focused on the development of the P4 process, a fully automated robotic preforming process. A prototype, two-station manufacturing cell was designed, fabricated, and installed at the National Composite Center (NCC) in Kettering, Ohio. This equipment is currently being utilized to support preforming and material development efforts within the Automotive Composites Consortium (ACC).

To obtain higher mass savings with composites relative to steel (50–70%), carbon fiber must be utilized as the reinforcing fiber. The extension of this technology to manufacture carbon fiber preforms is now in progress to support the development of ultra-lightweight vehicle structures. A major focus of this program is the development of a carbon fiber material suitable for chopped fiber processes; current production carbon fiber materials are not amenable. Advances in carbon fiber roving and preforming technology will be demonstrated in the structural automotive parts designed and prototyped as part of the ACC's Focal Project 3 (see 4.B).

Carbon Fiber Roving Development

To date, chopped carbon fiber preforming research and development has been limited due to material format and supply issues. To address fundamental material format issues present with current carbon fiber rovings, development programs have been initiated with two carbon fiber manufacturers (Hexcel and Fortafil) to expedite material research. The focus of these programs is to investigate the technology required to achieve a reduction in bundle size, to determine the effects of bundle size in the preforming/molding processes and to ascertain the effect on composite material performance.

Hexcel Carbon Fibers

A carbon fiber roving development program to investigate the effect of individual bundle size on preforming, molding, and composite material performance is currently under way using Hexcel Carbon Fibers.

The development effort is focused on assessing the effect of individual bundle size on P4 preforming, structural reaction injection molding (SRIM), and the resultant composite material performance. It is theorized that a reduction in bundle size will improve material distribution in the preforming process and, therefore, positively impact the mechanical performance of molded structures. The rovings will be tested and assessed within the preforming process, and flat panel preforms will be manufactured for in-plane permeability testing, light transmission analysis, areal density distribution testing, flat panel molding trials, and mechanical characterization. To investigate the effect of individual carbon fiber bundle size, the program calls for manufacture of seven different combinations of carbon fiber rovings. The details of these rovings are shown in Table 1.

As highlighted, the overall carbon fiber roving was kept constant at 36,000 filaments (i.e., 36k); however, a wide range of total individual bundles,

Table 1. Carbon Fiber Roving Types

Roving ID	Precursor type	Roving construction
1	Pilot	0.5k × 72 bundles
2	Pilot	1.0k × 36 bundles
3	Pilot	1.5k × 24 bundles
4	Pilot	3.0k × 12 bundles
5	Production	3.0k × 12 bundles
6	Production	6.0k × 6 bundles
7	Production	12.0k × 3 bundles

from 3 to 72, and filament counts within these bundles, from 0.5k to 12k, comprise each roving to determine the effect of bundle size on processing and composite material performance. Also note that two 3.0k × 12 rovings were manufactured, one using precursor fabricated on Hexcel's pilot line and one using precursor fabricated on its production line. This would serve as a control to ascertain potential differences between pilot and production line precursor materials in the final carbon fiber roving.

Hexcel Carbon Fibers manufactured the aforementioned materials under a subcontract with Oak Ridge National Laboratory (ORNL) for the ACC. Carbon fiber roving manufacture was completed in January of 2004, and the material was shipped to the ACC for evaluation. Approximately 70 kg of each roving type was manufactured and received for experimental evaluation in this program.

Light transmission preforms were fabricated at 500 g/m^2 to determine the light transmission and coverage characteristics for each of the seven carbon fiber rovings. All preforming process parameters were held constant with the seven different carbon fiber rovings being the only variable. To minimize fiber filamentization that can cause erroneous preform light transmission results, two processing parameters were controlled. First, a section of the existing material delivery system was bypassed to minimize friction on the carbon fiber roving and subsequently reducing bundle filamentization. Second, input air pressure to the fiber ejectors on the chopper gun was reduced from 3.0 bar to 1.0 bar, thereby minimizing fiber filamentization caused within the chopper gun. A total of 21 flat panels, 3 panels with each carbon fiber roving type, were fabricated for light transmission testing.

These panels were shipped to Winona State University for image analysis to determine the light transmission characteristics of each carbon fiber roving tested. To conduct the analysis, digital images of the preform on a light table were obtained for each preform type in question. Each preform was divided into four quadrants and an image acquired for each quadrant. Using the 3 preforms of each type that were fabricated, a total of 12 images were obtained for each preform type. Following image acquisition, the digital images were imported into image analysis software to determine the amount of light transmission for each quadrant. In this analysis, a histogram distribution, comprised of the gray scale where zero represents black (i.e., complete coverage) and 255 represents white (i.e., zero coverage), was constructed for each image. The image analysis software was then used to calculate the percent of the image within each of the 256 ranges in the gray scale relative to the entire image. Results from the 12 quadrants were then averaged for each preform type to obtain the average light transmission. For this analysis, the range from 205–255 was assumed to be regions of zero fiber content and would be used to report the light transmission for a given preform type. A representative preform light transmission section is shown in Figure 1.

Upon examination of the experimental data, differences were noted between carbon fibers manufactured using pilot line precursor and those using production line precursor. After additional investigation, it was found that a slight variation in processing conditions existed, causing the bundles to be either relatively round (pilot line precursor) or relatively flat (production line precursor). This bundle geometry characteristic caused notable differences in the material following preforming and during light transmission testing. Based on this fact, data from the two groups of materials were treated as separate data sets.

As previously theorized, a reduction in individual carbon fiber bundle size subsequently

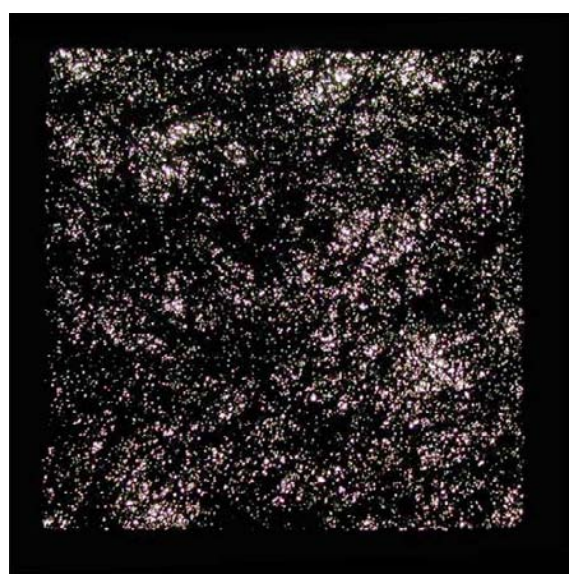

Figure 1. Representative preform light transmission image.

reduced the amount of light transmitted through a given preform. For example, the average light transmission for preforms manufactured using the 0.5k × 72 roving was 2.7 % vs 5.5% for preforms utilizing the 3.0k × 12 roving (Figure 2). In this instance, the reported light transmission is approximately two times, suggesting double the number of zero fiber content areas and higher areal density variability as a function of increasing bundle size. Because the quantity of light transmitted was reduced with smaller bundle sizes, the amount of zero fiber content regions were also reduced. This then suggests that a more uniform areal density distribution exists when utilizing carbon fiber rovings with smaller individual bundle sizes that should translate to more uniform mechanical properties. This same trend exists for both pilot and production line materials although the magnitude varies due to differences in the materials attributable to the carbon fiber manufacturing process.

To determine the effect of individual bundle size on composite material performance, flat panel preforms were manufactured and molded using SRIM. Following manufacture, the molded flat panels were mechanically tested to determine tensile and compressive properties.

Flat panels preforms were fabricated at 1260 g/m^2, corresponding to a fiber volume fraction of 35% for a 2.0-mm molded part thickness. All preforming and molding process parameters were kept constant throughout the trial with the only variable being the input carbon fiber roving. A total of 21 preforms were fabricated and molded using the seven Hexcel carbon fiber rovings (Table 1). Tensile samples were obtained from the molded panels and tested in accordance with American Society for Testing and Materials (ASTM) D-638. Eight samples from each panel were tested in both the 0° and 90° directions to determine tensile strength and modulus. A comparison of the 0° ultimate tensile strength for each of the seven carbon fiber rovings is shown in Figure 3.

The average 0° ultimate tensile strength for panels containing the 0.5k × 72 roving was nearly three times that of panels containing the 12k × 3 roving; 267 vs 90 MPa. Furthermore, the coefficient of variation (COV) was substantially reduced as a function of decreasing individual bundle size (Figure 4). The COV of 0° ultimate tensile strength for panels fabricated with the 12k × 3 carbon fiber roving was four times that of panels fabricated with the 0.5k × 72 carbon fiber roving (44 vs 11%). Average 0° tensile modulus was also higher in panels with the smallest individual bundles, but not nearly as significant as tensile

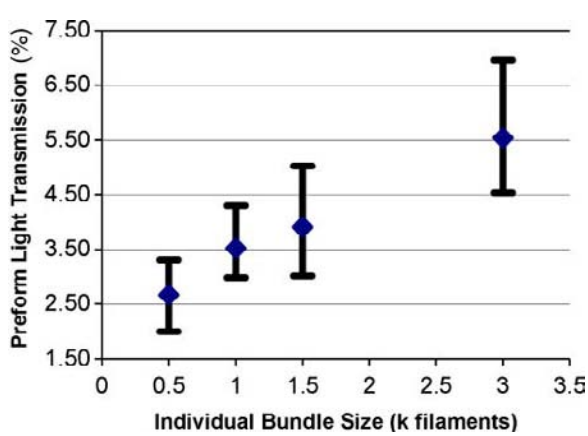

Figure 2. Light transmission vs bundle size.

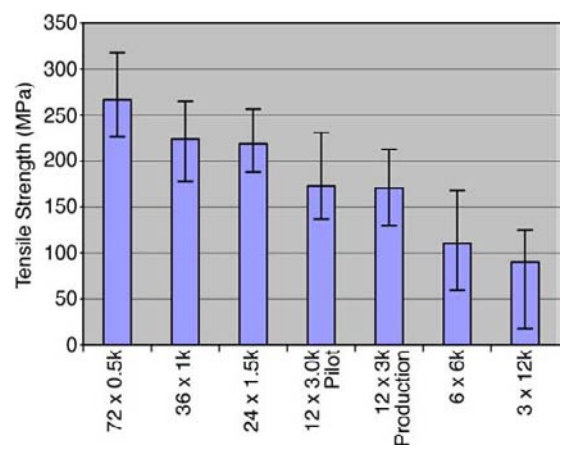

Figure 3. 0° ultimate tensile strength.

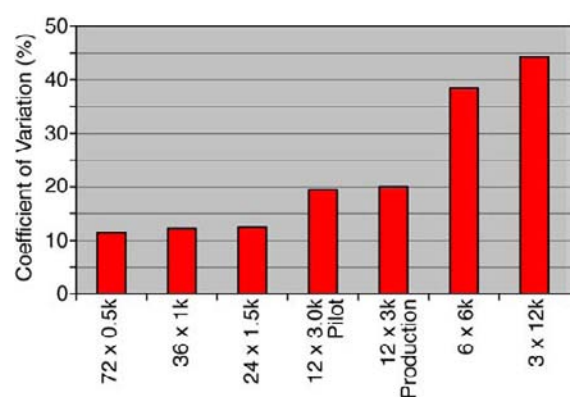

Figure 4. 0° ultimate tensile strength COV.

strength. For example, the average 0° tensile modulus was 27 GPa for the 0.5k × 72 fibers vs 22 GPa for the 12k × 3 fibers. However, the COV for tensile modulus was markedly different as a function of the particular carbon fiber roving. As shown in Figure 5, the COV for tensile modulus with panels containing 0.5k × 72 fibers and 12k × 3 carbon fiber rovings was 9% vs 33%, respectively.

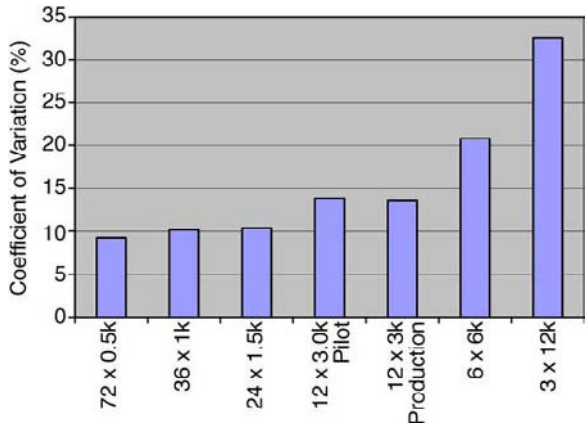

Figure 5. 0° tensile modulus COV.

As previously theorized and as the light transmission testing suggested, superior mechanical performance, both tensile strength and modulus, was evident in panels containing the smallest individual bundle sizes. In addition, the variability of these properties is also reduced with a reduction in bundle size. To be sure, a nearly identical trend was evident in the 90° tensile testing results. Furthermore, similar trends existed in both 0° and 90° ultimate compressive strength testing. Despite notable differences in the light transmission preforms between the control, 3.0k × 12 pilot and production line precursor/carbon fiber, no differences were evident in the mechanical properties as shown by the nearly identical tensile strength of both 3.0k × 12 carbon fiber rovings.

Based on the mechanical test data from this study, it can be stated that a reduction in individual bundle size both increases the magnitude of mechanical properties and reduces the variability of these properties within a panel. The data suggest that a reduction in bundle size within a carbon fiber roving will increase the mechanical performance of composite materials fabricated using chopped carbon fiber.

Fortafil Carbon Fibers

A research program to develop carbon fiber rovings more amenable to the P4 preforming process has been developed and initiated with Fortafil Fibers (now Teijin/Toho/Tenax). This program focuses on developing cost-effective methods to reduce the individual carbon fiber bundle sizes within a roving. A carbon fiber roving specification was developed jointly between the ACC and Fortafil as the target material for this program. The overall program is comprised of five phases and has an anticipated completion date of September 1, 2005.

The first phase of the program was to investigate whether splitting the precursor could give a final carbonized tow with fiber bundles of the desired dimensions. The initial technical efforts focused on methods to produce a stranded roving through modifications made to standard acrylic precursor. The work was carried out at the Acordis acrylic fiber production facility in Grimsby (United Kingdom). Technical resources were initially devoted to two major objectives. Firstly, the evaluation of mechanical techniques to introduce micro-splits in the precursor. And secondly, the identification and acquisition of candidate finishes to make splits in the acrylic strands permanent and able to survive the subsequent conversion to carbon fiber.

To address mechnical precursor splitting, stainless steel splitter bars to introduce the appropriate number of splits in the precursor were dimensioned to increment a subtow containing 80k filaments into 1k strands based on an operating subtow width of 9 in. Acordis concurrently identified candidate finishes with the properties necessary to hold the individual strands together while, at the same time, providing enough cohesion to maintain the integrity of the larger subtow during the crimping and packaging operations.

The first trials to produce stranded precursor were conducted in mid-October of 2004 using an 80k subtow. The splitter bar was evaluated at several locations, and a position immediately prior to the crimper hot plates proved to be the most effective. Split precursor samples were produced at the Acordis Grimsby site using a splitter bar to increment an 80k tow into approximately 2k filament strands and then “set” the strands by

applying sizings developed specifically for this purpose. Several samples of mechanically split precursor were fabricated and the most promising candidates were shipped to Fortafil in Rockwood, Tennessee (U.S.A.) for oxidation and carbonization. The first precursor samples containing mechanically introduced strands were evaluated in November. The two samples processed through the pilot line were designated as PT288 and PT290 (Figures 6 and 7).

In the carbon fiber pilot line trials, the high finish level on both samples caused interfilament sticking to occur in the first oxidation oven. Although a cold water wash applied to the tows prior to their entering the oven was effective in removing enough finish to eliminate the sticking, a loss of strand definition was observed in the downstream oxidation. Thus, the sizings alone do not appear to be adequate to preserve the strand character during subsequent processing. Due to these limitations, this pariticular approach was deemed to be unfeasible at this time.

Figure 6. PT288 split precursor.

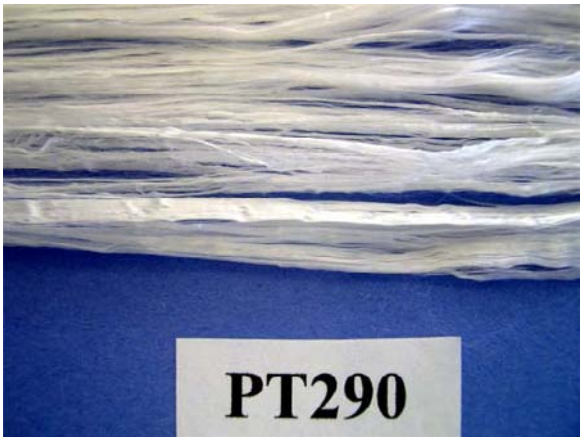

Figure 7. PT290 split precursor.

Upon completion of the mechanical bar slitting trials, work initiated on an air entanglement approach. The method adopted used compressed air, in conjunction with a splitter bar, to create strands within a tow by direct intermingling or entangling of the individual filaments. A first-generation “air splitter” device was fabricated in December of 2004 (Figure 8). Air entanglement produced by using dual splitters provided a precursor that was of sufficient quality to evaluate through carbonization. However, the splits were not sufficiently maintained through the carbonization step to warrant further work in this direction.

An alternative approach to producing a stranded roving involves first making a number of small strands and then ganging the strands to form a roving. Using readily available technology and a novel production approach, individual strands with filament counts as low as 500 were produced. The strands were then packaged into a roving containing 30 ends and shipped to the ACC for a P4 preforming trial. The trial showed specific directions for development and was overall very positive. However, cost analysis indicated that the developed material could exceed $10/lb, which was far enough over the cost target that it was decided to abandon this direction.

A fourth method of providing a split tow precursor is still under investigation. This involves spinning the precursor into split tows by manipulating the outlet hole pattern on the spinneret. Precursor strands have been fabricated that exhibit

Figure 8. Prototype air entanglement device.

appropriate splits. At the end of FY 2004, these samples were sent to Fortafil (Rockwood, Tennessee) and are awaiting carbonization.

The second phase of the program is to investigate techniques for direct creation of strands in a large carbon tow. This phase was initiated in April of 2004. Development efforts to date have concentrated on evaluating various machine geometries to obtain the cleanest and most scalable process to achieve the desired outcome. A preferred technology has been identified, and the optimum processing conditions are currently being established. The latest trials have generated promising results with rovings containing up to 30 ends. Quantities of stranded roving sufficient for evaluation in the P4 preforming process are expected by the second quarter of FY 2005. Figure 9 shows a sample of the stranded roving produced on the prototype development line.

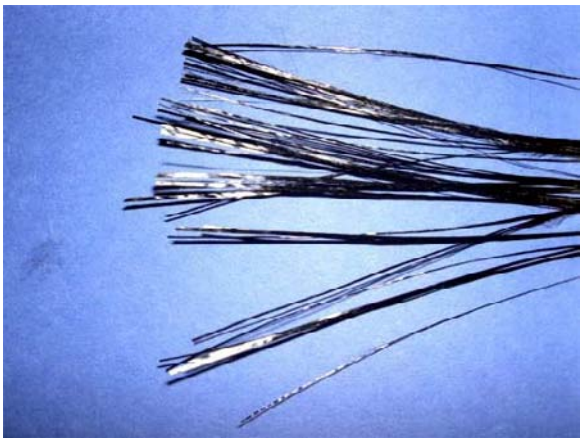

Figure 9. Stranded carbon roving produced on prototype development line.

Phase 3 is the development of appropriate fiber sizings for improved handling and fiber/matrix interface with a polyurethane resin system. This has been initiated in conjunction with the processing studies on the fiber slitting line.

The fourth phase is acquisition of a pilot line for fiber production, and the fifth phase is optimization of the pilot line, production of fibers for ACC evaluation, and assessment of manufacturing costs. Upon development of candidate carbon fiber rovings within this program, preforming and molding evaluations will be conducted by the ACC to determine the performance of these materials.

Conclusions

Carbon fiber roving manufacture for the development program with Hexcel Carbon Fibers was completed in January of 2004, and the material was shipped to the ACC for evaluation. Evaluation of the carbon fiber rovings is nearly complete with only preform permeability remaining. The experimental data generated to date clearly show increased mechanical performance with a decrease in the individual carbon fiber bundle sizes as previously theorized.

The first and second phases of the carbon fiber roving development program with Fortafil Fibers are under way. Progress has been made with regard to both precursor and carbon fiber mechanical splitting techniques along with fabrication of spun yarn rovings. Upon fabrication of prototype material in suitable test quantities, preforming and molding evaluation within the ACC will be conducted.

B. Composite-Intensive Body Structure Development for Focal Project 3

Nancy Johnson
GM Research & Development
MC 480-106-256
30500 Mound Road
Warren, MI 48090-9055
(586) 986-0468; fax: (586) 986-0446; e-mail: nancy.l.johnson@gm.com

Field Project Manager, Composites: C. David Warren
Oak Ridge National Laboratory
P.O. Box 2009, Oak Ridge, TN 37831-8050
(865) 574-9693; fax: (865) 574-0740; e-mail: warrencd@ornl.gov

Technology Area Development Manager: Joseph Carpenter
(202) 586-1022; fax: (202) 586-1600; e-mail: joseph.carpenter@ee.doe.gov
Field Technical Manager: Philip S. Sklad
(865) 574-5069; fax: (865) 576-4963; e-mail: skladps@ornl.gov

---

Contractor: U.S. Automotive Materials Partnership
Contract No.: FC26-02OR22910

Objectives

- Design, analyze, and develop the technology to build a composite-intensive body-in-white (BIW), offering a minimum of 60% weight savings over steel at a cost close to that of steel, while meeting manufacturing, assembly, and performance targets.
- Provide a focus for bringing together technology developed by each of the Automotive Composites Consortium (ACC) working groups through emphasis on carbon-fiber-reinforced composites and the use of hybrid materials, faster manufacturing processes, design optimization including crashworthiness, and rapid joining methods.

Approach

- Optimize the design and complete the finite-element analysis (Phase 1—completed).
- Build one part of the BIW to demonstrate high-volume processing methods, including the component as well as the needed assembly fixtures (Phase 2). Test the component before continuing with the construction of the complete BIW.
- Build the complete BIW (Phase 3). To reduce cost, not all parts will be made from production tooling; however, care will be taken to ensure that the properties of each part are consistent with those that will be obtained from production tools.

Accomplishments

- Conducted preforming and molding trials, which are ongoing.
- Fabricated second-generation preform tools, being used at NCC.
- Completed flow modeling studies for B-pillar.
- Completed cost modeling.

- Tested bonded parts successfully with pulsed thermography to check bondlines.
- Developed modeling approaches for joints.

Future Direction

- Complete the optimization of the B-pillar preforms with the second-generation preform tools.
- Develop mold filling flow model for the full bodyside design.
- Define a B-pillar structural test, develop a model for the test, and carry out the testing to confirm the model.
- Conduct preforming, molding, and mechanical testing evaluation of new low-cost carbon fibers.
- Complete B-pillar molding of carbon fiber preforms.

Introduction

All of the materials, manufacturing processes, and fabrication and assembly methods to be considered in this project are to be consistent with the following overall objectives:

- High-volume production techniques (>100,000 units per year)
- Cost parity with equivalent steel structures
- Overall 60% mass reduction relative to steel BIW structure
- Structural performance equivalent to or better than that of a steel structure
- Dimensional tolerance equal to or better than that of steel

We continue to develop the manufacturing processes necessary to build the body side. Preforming and molding trials continue with the B-pillar learning tool. For more details on the performing studies see the Automotive Composite Consortium (ACC) 040 annual report (4.A). For additional information on molding, see ACC 115's report (4.C).

B-Pillar Preforming Development

In support of the ACC's Focal Project 3 (FP3) program, researchers have been performing process development to facilitate manufacture of B-pillar inner and outer preforms.

Original B-Pillar Tooling

Preform development was conducted with the original B-pillar tooling that utilized the designed 'A' surface as the fiber deposition surface on both the B pillar inner and outer preforms. Extensive robotic programming efforts were performed in an attempt to achieve uniform areal density distribution throughout the parts. Despite these efforts, poor material distribution remained on both B-pillar inner and outer preforms when manufacturing preforms at a targeted fiber volume fraction of 40%. Material distribution issues were predominantly evident in 1.5-mm regions (Figure 1) of the components and in the 1.5-mm sections of thickness transition areas of 4, 6, or 8 mm to 1.5 mm.

Figure 1. Areal density distribution issues, 1.5-mm section.

Large areal density variability within the preform (±30%) has led to subsequent molding issues including fiber wash and dry regions in the parts. Excessive material density creates "dry spots" in the molded components, as highlighted in Figure 1, that are unacceptable. Additionally, incompatibility between the preform ('B' surface as the consolidation side) and the lower molding tool ('B' surface) created a less than optimum fit when

the preform was placed in the molding tool. Due to this issue, the preform was sheared along the edge of the part up to 5 mm during tool closure, thus creating "racetracking" and fiber wash in the mold tool leading to inconsistent filling of the preform.

Based on the aforementioned issues, researchers determined that a redesigned B-pillar preforming tool could possibly improve preform processing (robot reach) and preform characteristics (areal density distribution) and would ensure preform and molding tool compatibility (i.e., replication of the design B-surface in both lower tools).

Revised B-Pillar Tooling

A revised preforming tool was designed and fabricated in an inverted state relative to the original B-pillar preform tooling. In the revised tooling, the 'B' surface serves as the deposition surface and the 'A' surface as the consolidation surface. This configuration would allow easier robot access to deep draw sections of the part, thereby easing preform optimization efforts and improving areal density distribution. Additionally, a relatively rigid 'B' surface of the preform (i.e., deposition surface) will allow a more precise fit in the molding tool, thereby minimizing the preform and molding tool compatibility discrepancies and subsequent shearing of the preform edge during tool closure.

The revised preform tooling (Figure 2) was received and commissioned in the preforming machine located at NCC in Kettering, Ohio, during the third quarter of FY 2004. Robotic programs were developed using offline programming software and downloaded to the machine upon receipt of the tooling. Upon completion of tool commissioning, preforming development and robotic programming optimization efforts were initiated.

Although the preform and molding tool compatibility issue has been addressed with the revised preform tooling, the inverse orientation of the deposition surface has created unforeseen issues during the material deposition process. Excessive material density now exists in 1.5-mm regions, mainly the flange regions, immediately adjacent to thicker sections of the component (4, 6, and 8 mm). Areal density sampling data indicated regions exceeding 100% by volume for the target fiber volume fraction of 40% at a 1.5-mm thickness. In

Figure 2. Revised B-pillar inner/outer preforming tool.

the inverted tooling state, the high material density required for thicker cross sections requires material to conform on outside radii. These features were previously inside radii and more forgiving to the material deposition required for thicker cross sections in the original tooling configuration. Additionally, the inherent material deposition characteristics force material to be deposited beyond the outside radii and into regions not intended, thus creating both excessive and poor material distribution. Optimization efforts are ongoing in an attempt to resolve these issues.

Conclusions for Preforming

Extensive preforming development efforts were conducted using the original B-pillar preforming tools. However, a fully optimized preform could not be realized due to several issues including inadequate material distribution and preform-to-molding-tool incompatibility. A revised preform tool was designed and manufactured to address the previously mentioned issues. This tooling has been commissioned, and preforming development is ongoing. Based upon the preforming development performed to date using both preforming tools, the results suggest that a 1.5-mm part thickness at a fiber volume fraction of 40% is extremely challenging and may be at or beyond the current process capability.

Carbon Fiber Cost Modeling

A cost modeling study on carbon fiber manufacture and the effect of increased volume and

advanced technologies was carried out by Kline and Company. The three phases of the project were

1. review the existing baseline cost model from ORNL,
2. develop a cost model for increased volume production in higher capacity plants,
3. work with ORNL on the cost modeling of advanced technologies being developed for low-cost carbon fibers.

The baseline case assumes 50k PAN precursor in a 2-million lb/year plant, with a line speed of 1,378 ft/h, and uses conventional ovens for oxidation and carbonization. This shows variable costs (mostly PAN) of 55.2% of total, fixed costs (including labor, maintenance, and indirect overhead) of 29.5%, and depreciation of 15.3%, with a total production cost of $8.12/lb.

The high-volume case utilizes the same conditions as the baseline, except for a production volume of 24 million lb/year. Economies of scale decrease the total production cost to $7.00/lb, with variable costs 64% of the total, fixed costs 21.5%, and depreciation 14.5%.

For both of these scenarios, the precursor is the largest single element of the cost. Two alternative precursors that are being studied at ORNL were investigated. The modified commodity-grade PAN is not only less expensive than the baseline PAN, it also requires less residence time in the stabilization/oxidation oven. The lignin precursor is much less expensive than baseline PAN and may also have savings in the oxidation step. Adding the savings for these precursors to the high-volume case give production costs of $4.93/lb for the commodity-grade PAN, and $3.89/lb for the lignin.

The Microwave Assisted Plasma (MAP) has the advantage of reducing the carbonization time for the fibers, as well as reducing capital costs. Adding the savings from MAP to the savings from lignin, the high-volume case would have a production cost of $3.66/lb.

The use of microwave oxidation replaces the large conventional ovens with lower cost capital equipment. Combining the savings for the MAP and lignin with the microwave oxidation gives a high-volume production cost of $3.36/lb.

A summary of production cost improvements for the 2-million lb/year plant and for the 24-million lb/year plant are shown in Figures 3 and 4. The high-volume case also includes estimates for

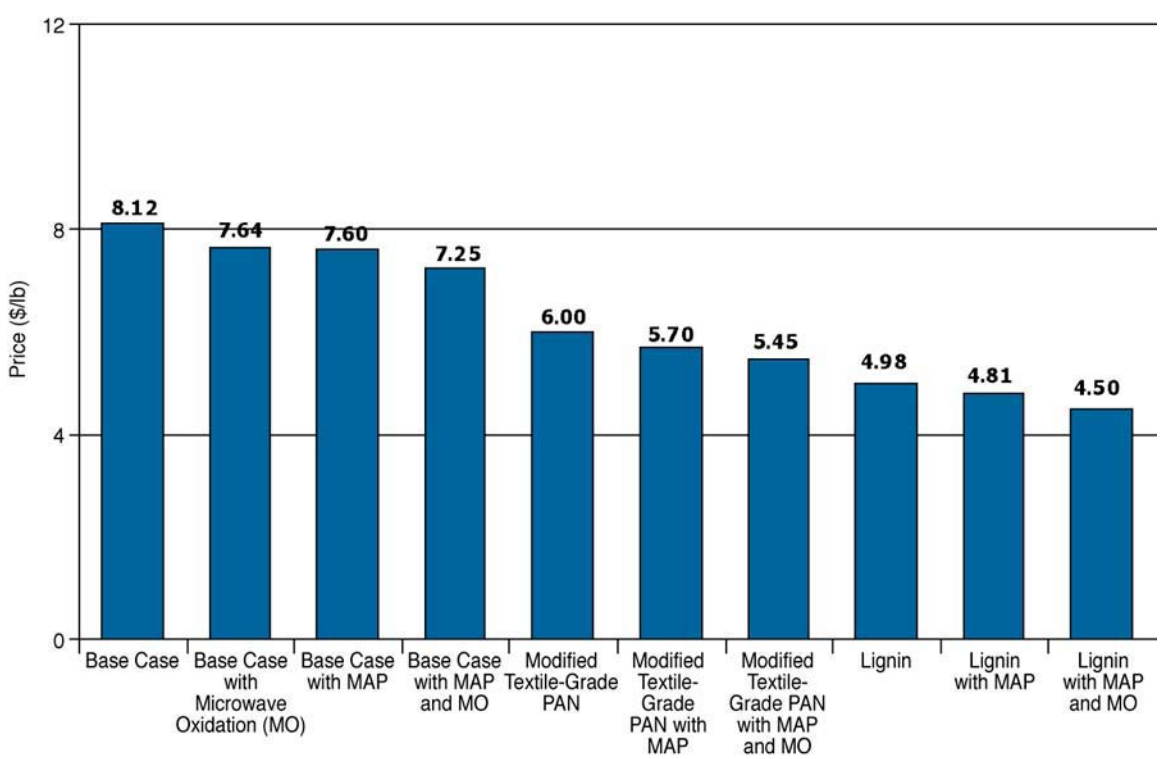

Figure 3. Summary of cost improvements for 2-million lb/year plant.

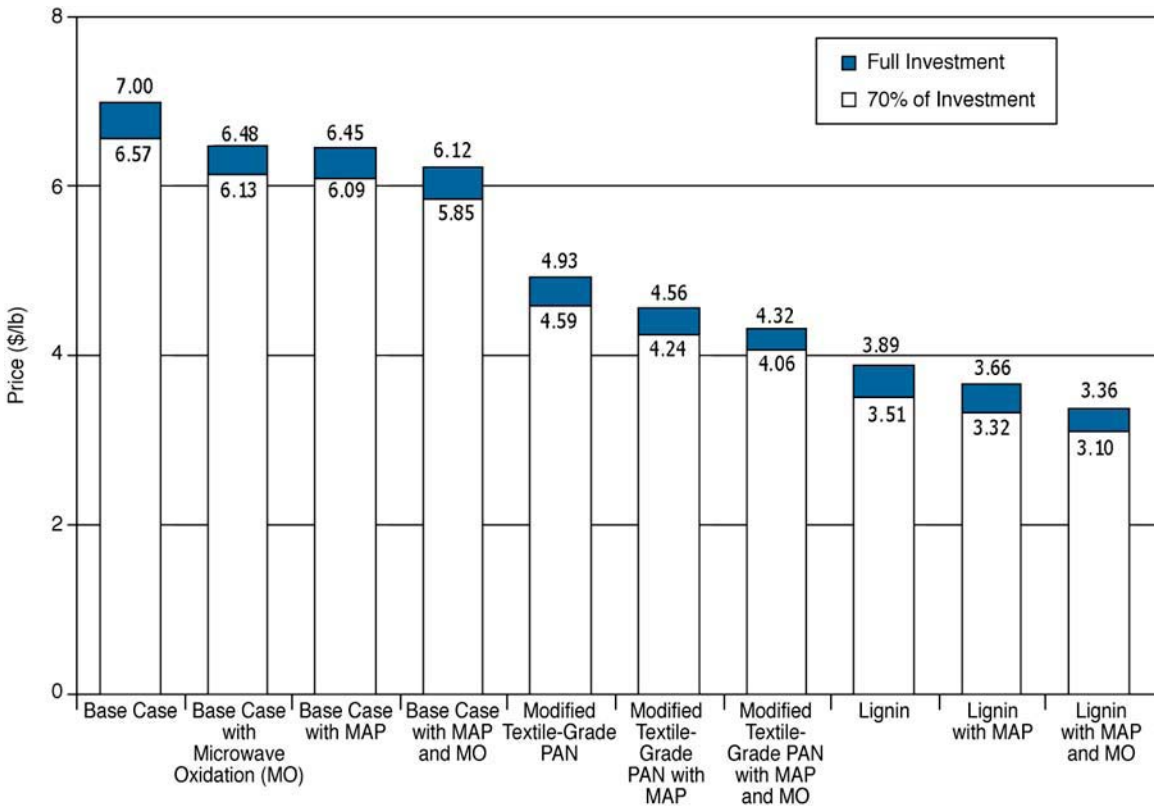

Figure 4. Summary of cost improvements for 24-million lb/year plant.

reduced capital costs (70%), which may be available due to synergies from producing multiple production lines at once. These charts show the compounding of all of these technologies, which taken together may give production costs as low as $3.10/lb.

Carbon fiber selling prices will also include costs for selling, administration, and research (SAR), as well as provide an acceptable return on investment (ROI). For the high-volume production, SAR is estimated to be about $0.20/lb. An acceptable ROI is usually 10%. Figure 5 shows that with SAR and ROI added to the production costs, the use of the lignin precursor and the alternative processing can give a selling price below $5.00/lb. Current selling prices are also included on this chart. (It should be noted that current selling prices are influenced by competitive pressures, and at least one producer is believed to be selling below cost.)

This study concluded that in order for carbon fiber to be sold profitably at less than $5/lb, the lignin precursor and the alternative processing methods will need to be used. The commodity-grade PAN may also give selling prices near the $5/lb level. As work continues on these processes, confirmation of the assumptions used in the study is advised.

Flow Modeling

Professor Suresh Advani of University of Delaware was contracted to develop a flow model for the injection-compression molding of the B-pillar. The intention was to develop and confirm a flow model, and then use this as a design tool assist in optimizing the location of the injection locations for the full-body side mold.

The starting point for this effort was the Liquid Injection Molding Simulation (LIMS) program that the Delaware team had already developed. To this was added the dynamics of the compression stage. In this problem, the resin is injected into the gap between the mold surface and the preform. Some of the resin penetrates into the preform. As the mold fully closes during compression, the resin progressively flows into the surrounding areas.

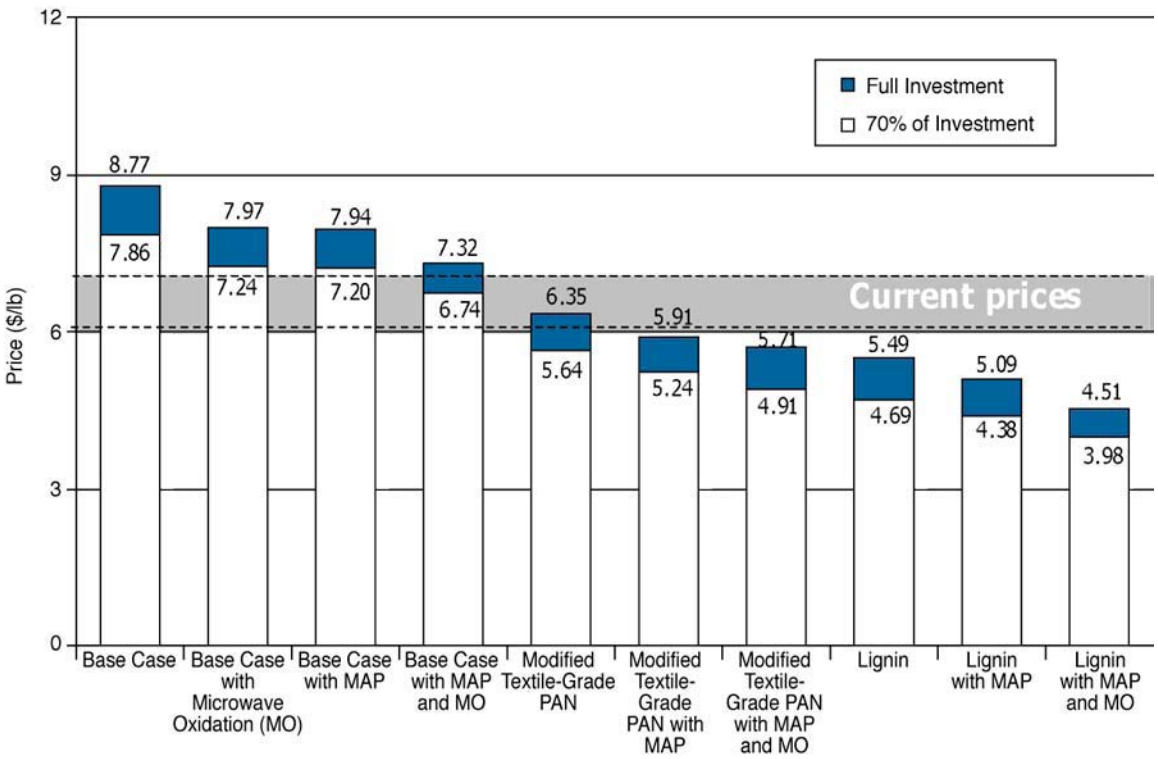

Figure 5. Estimated selling prices.

The solution approach was to model this problem in three phases. The initial phase was resin injection into the mold gap. The other phases were the initial and final compression stages and were modeled as a change in the cavity thickness and preform permeability as the mold closed.

Phase 1 is injection into the gap between the top of the preform and the mold cavity surface.

Phase 1

- Mold is stationary.
- Preform is modeled as three-dimensional (3-D).
- Gap is modeled as distribution media two-dimensional (2-D) with equivalent permeability.
- Injection conditions are as prescribed (any standard resin transfer molding option).

In Phase 2 the compression is started, and the gap above the preform closes.

Phase 2

- Mold starts closing.
- Gap thickness reduces with time, permeability changes and adequate flow source is created in filled nodes of gap.
- Preform deformation is neglected.
- Injection may be shut off.

Phase 3 is the completion of the compression stroke, with the preform being compressed into the final part thickness.

Phase 3

- Gap is closed; preform starts deforming.
- Fiber volume fraction and permeability of preform changes with time.
- Adequate flow source is created in filled nodes of gap.

This flow model did adequately represent the observed filling behavior for the B-pillar. We plan to apply it to the main fibers under consideration for the FP3 program. We intend to apply this flow model to the body side when the learnings from the B-pillar have been completed to the point that the team decides to fabricate the body side.

B-Pillar Bonding

The bonded B-pillars discussed in last year's report have been evaluated for bond quality by a

pulsed thermography nondestructive test method (Thermal Wave Imaging, Inc. of Ferndale, Michigan). The part is subjected to a high-intensity, short-duration flash of light, which heats the surface of the part. The heat flow away from the surface of the part is observed with an infrared (IR) camera, and the resulting time/temperature images are evaluated, pixel-by-pixel, with sophisticated thermal image analysis tools. In this way an image is created that can show any feature of the part (subject to part thickness and flaw size limitations) that causes a deviation in the heat flow. Voids, cracks, and other flaws in the bonds can cause such deviations. Thermographic analysis was performed prior to any mechanical testing of the parts and will be performed again once the parts have been subjected to mechanical testing. In this way, we can evaluate the quality of the as-bonded parts and correlate any questionable bonded areas with any failures during the subsequent mechanical testing. Then, we can recheck after mechanical testing for any additional or new damage to the bonds. Because this technique will allow us to determine if the mechanical testing caused any visually unobserved damage to the parts, thermal nondestructive testing (NDT) has the potential to be used for in-service testing of parts and components.

The four bonded B-pillar assemblies tested in preparation for mechanical testing showed, in general, good bonds. There were only a few regions, around curves of the parts, which showed thinner than optimal bond width. This occurred because the adhesive was laid down by hand (rather than by an automated, metered dispenser). These thin bond areas might be expected to be the first to show any damage (if it occurs at all) resulting from mechanical testing.

Generic Joint Modeling

Bonded (steel hat)/(steel flat) and (carbon composite hat)/(steel flat) parts have been tested at ORNL. The results have been evaluated in terms of agreement between simulations and test results. The modeling techniques needed to obtain simulations that correlated with the observed tests were, finally, finite-element modeling in conjunction with Virtual Crack Closure Techniques (VCCT) using a continually varying loading mode with increasing load (based on measured fracture envelopes). This resulted in a predicted failure load for the steel/steel part of 8225 lb compared to an average test value of 8484 lb (–3.1% difference). For the composite hat, failure load was predicted to be 3145 lb where the average test result was 3054 lb (+2.1% difference). This excellent agreement validates this approach for predicting failure under locally mixed-mode loading conditions. A report, "Failure Analysis of Adhesively Bonded Structures: from Coupon Level Data to Structural Predictions" is in progress. This will complete the original Phase 1 of this project.

In addition, as Phases 2 and 3 have progressed, several additional modeling approaches have been investigated (and reported on, see below) and a new set of tools is being explored for ease of use in automotive applications. This new method has been entitled Element Failure Approach (EFA); by the end of calendar year 2004 it should be known whether this approach will be effective.

Publications

1. D. Xie, A. M. Waas, K. Shahwan, J. A. Schroeder, and R. G. Boeman, "Computation of Energy Release Rates for Kinking Cracks based on Virtual Crack Closure Technique," submitted to *International Journal of Fracture*, January 2004.
2. D. Xie, A. M. Waas, J. A. Schroeder, K. Shahwan, and R. G. Boeman, "Fracture Criterion for Kinking Cracks in a Tri-Material Adhesively Bonded Joint Under Mixed Mode Loading Part 1: Experiment," submitted to *Journal of Engineering Fracture Mechanics*, June 2004.
3. D. Xie, A. M. Waas, K. W. Shahwan, R. G. Boeman, and J. A. Schroeder, "Fracture Criterion for Kinking Cracks in a Tri-Material Adhesively Bonded Joint Under Mixed Mode Loading Part 2: Analysis," submitted to *Journal of Engineering Fracture Mechanics*, May 2004.

C. High-Volume Processing of Composites

Principal Investigator: Stanley A. Iobst
General Motors R&D Center, MC 480-106-710
30500 Mound Road, Warren, MI 48090-9055
(586) 986-1223; fax: (586) 986-1207; e-mail: stanley.a.iobst@gm.com

Technology Area Development Manager: Joseph A. Carpenter
(202) 586-1022; fax: (202) 586-1600; e-mail: joseph.carpenter@ee.doe.gov
Field Technical Manager: Philip S. Sklad
(865) 574-5069; fax: (865) 576-4963; e-mail: skladps@ornl.gov

---

Contractor: U.S. Automotive Materials Partnership
Contract No.: FC26-02OR22910

Objective

- Develop and demonstrate high-volume manufacturing technology to produce lightweight composite automotive body structures.
- Achieve higher fiber volumes in thinner sections than were successfully achieved in Automotive Composites Consortium (ACC) Focal Project 2.
- Support the goals of ACC Focal Project 3.

Approach

- Investigate the structural reaction injection molding (SRIM) process at high fiber loadings using carbon fiber.
- Design and build a shape tool to investigate the complex preforming and molding processes required for the ACC Focal Project 3 program.
- Team with supplier partners to investigate alternative liquid molding processes.
- Assess the potential for the LFI (long fiber injection) process and materials to meet both the more demanding structural applications of Focal Project 3 and its potential to meet Class "A" automotive requirements.
  - Establish an ACCP "Surface Acceptance Standard" to gage progress of LFI development–benchmarking established Class "A" automotive exterior materials using known quantitative methods.
  - Conduct a series of designed experiments (DOE) to screen the parameters that contribute most significantly to surface quality.
  - Evaluate these plaques for physical properties to assess their potential for use as structural components.
  - Ultimately, lead the program to incorporate carbon fiber into the LFI for additional weight savings.

Accomplishments

- Continued B-pillar molding trials with 40% glass fiber preforms to evaluate and improve the preforming process and to produce panels for structural analysis.
- Conducted plaque molding evaluation of candidate Hexcel carbon fibers.
- Molded initial carbon fiber B-pillar panels.
- Completed the initial LFI molding trial.

- Assessed the effects of glass type, glass length, thickness, demold time, and surface veil via the experimental design.
- Constructed an LFI plaque tool based on an existing RRIM tool at Bayer but incorporated shear edges and a polished show surface.
  - Finish painted plaques and they were subjectively ranked by the ACC team.
    - Identified a "Surface Acceptance Standard" linked to specific quantitative techniques for use in subsequent studies based on extensive benchmarking of typical class "A" exterior substrates.
    - Agreed upon physical testing protocol. Mechanical property testing is completed, and data analysis is under way.
    - Designed a new LFI molding trial based on the observations of the first trial.

Future Direction

- Develop B-pillar modling process with Generation-2 preforms.
- Initiate carbon fiber B-pillar development when the fiber is available.
- Determine whether that process can be used for structural or structural cosmetic applications via the LFI program.

Introduction

The purpose of this project is to further develop the liquid composite molding technology previously demonstrated in the Automotive Composites Consortium (ACC) Focal Project 2 with the large structural truck box.[1–3] This project will extend the liquid molding process into more structurally demanding application of the ACC Focal Project 3 (FP3) body-in-white. This will be accomplished by using carbon fiber reinforcement at 40% by volume. To maximize the weight savings, the minimum section thickness will be reduced to 1.5 mm.

There will be two basic approaches running in parallel. The first is the extension of conventional structural reaction injection molding (SRIM) technology to carbon fiber preforms of reduced section thickness in support of the ACC FP 3. This involves both material and process evaluation. The ACC instrumented plaque mold is used for material and initial process evaluations. The ACC B-pillar mold is a shaped panel, which represents the B-pillar section of the FP3 body side. This mold has deep draws, and it is used for more detailed process studies of SRIM molding. This portion of the program is under the direction of, and includes direct participation of, ACC personnel.

The second approach will be to work with supplier-partners to adapt their liquid molding process toward being compatible with the material property and processing requirements of FP3. For this activity, a program was initiated with Bayer to investigate the feasibility of adapting the long fiber injection (LFI) process to the needs of the ACC.

The project team includes personnel from the Big Three automotive companies and Oak Ridge National Laboratory. The support team includes personnel from the National Composites Center (NCC). Bayer is a supplier-partner in the LFI portion of the program.

Carbon Fiber Plaque Molding and Data Acquisition

A new riser was built to use the ACC plaque mold in the 1000-ton French Oil press at NCC. Thus, for a plaque molding trial, the B-pillar mold can be parked on the press shuttle and not have to be removed from the molding cell. This allows for rapid switching between B-pillar and plaque molding. Figure 1 shows the new plaque molding setup at NCC. The molding data acquisition system was also upgraded to current generation computers.

Two separate plaque molding trials were performed in support of the Hexcel carbon fiber program. The first plaque trial was for different fiber volumes (ranging from 30 to 40%) and plaque thicknesses (1.5 to 3.0 mm). From this study, the

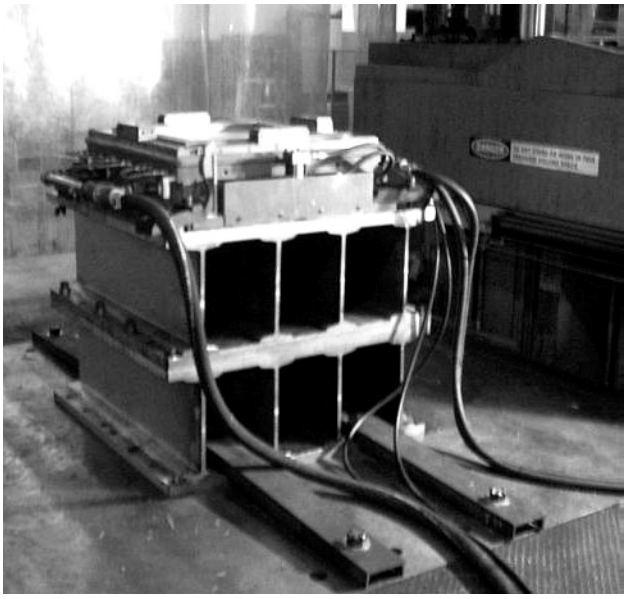

Figure 1. ACC plaque mold mounted on pedestal in 1000-ton press at NCC.

condition of 35% fiber and 2.0-mm plaque thickness was selected for the fiber size study. This was the condition of highest fiber volume and thinnest dimension that gave constant thickness plaques. Thinner plaques and higher fiber volume caused tool distortion, resulting in nonuniform plaque thickness.

The fiber-size-study rovings were constructed by combining smaller tows into 36K rovings. Preforms of rovings containing tow sizes of 0.5 to 12K were made and molded. Figure 2 shows typical molding traces from this trial, showing the pressure developed in the mold cavity from the mold closure and the resin flow. In general, as the fiber ends became larger, the pressure spike during compression became broader, but lower. The detailed results of this study are given in the "Development of Next-Generation Programmable Preforming Process" report (4.D).

All SRIM molding, both plaque and B-pillar, was by the injection/compression technique, where the polyurethane resin is injected into a partially open mold. As the mold closes fully, the compression stage, the resin is forced through the preform, filling out the mold. Thus, the observed cavity pressure is developed by the dynamics of the mold closing, and not the injection pressure.

B-Pillar Molding Program

Several B-pillar molding trials were carried out early in the year to support preform development. After satisfactory preforms were being delivered, a series of B-pillar sets were molded for the structural analysis group. Some of these B-pillars were also structurally bonded.

At this point it was judged by the preforming and molding teams that the quality of the preforms, primarily the fiber distribution uniformity, was not significantly improving. Fiber volume ranged from

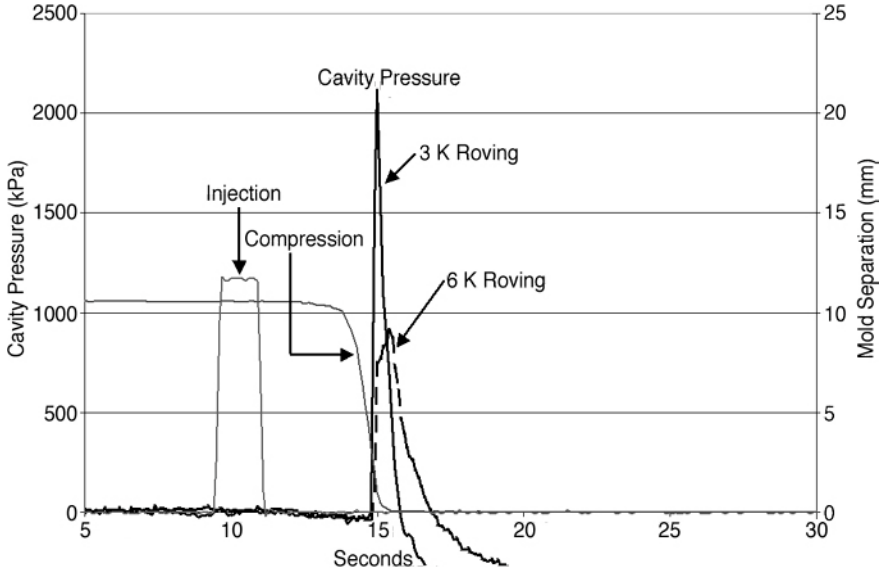

Figure 2. Molding data traces from Hexcel fiber size study showing pressure response for two fiber bundle sizes.

less than 20% to greater than 50% and is discussed in more detail below. A significant contributing cause to this broad range of fiber distribution was believed to be the geometry of the preforming screens. Some areas were difficult for the robotic arm to direct the fiber spray into, and others collected excessive overspray. Also, in the original screen design, the loft side of the preform was placed against the molding tool. This springy loft pushed the preform away from the side of the mold, and caused part of the flange area to be sheared off when the mold closed. Therefore it was decided to temporarily halt preform and molding development and design and build new preforming screens (discussed in 4.B). This shutdown time was used for the carbon fiber plaque study discussed above.

The new preforming screens were completed during the year, and the B-pillar mold has been reinstalled in the press. In a quick, initial look at the new preforms, the new preforms seem to fit into the molding tool better and do not have as much spring out.

B-Pillar Fiber Distribution

The distribution of the glass fiber content in a B-pillar inner and outer set molded in January of 2004 was determined by a series of burn-off tests. A chart of the overall fiber distribution is shown in Figure 3. Even though only one set of preforms was examined in detail, the robotic P4 process gives good reproducibility between preforms. In addition, sampling of other preforms and visual observations of the flow patterns support the repeatability of the fiber distribution results.

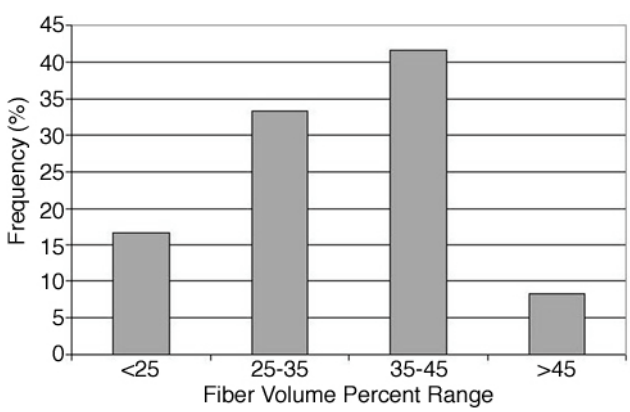

Figure 3. Fiber volume distribution in molded B-pillars with Gen-1 preforms.

The fiber content for the inner panel ranged from 13.5% to 55.0%, with a mean of 33.5% and a coefficient of variation of 29%. Although some areas of the part were within the target range of 35 to 45%, many other areas were not, as shown in the fiber distribution chart. At some points fiber content well above the target range was adjacent to areas of low fiber. Several instances of this occurred where the fiber was heavier around the corner and decreased on the walls and the flange.

The fiber content range for the outer panel was even larger, ranging from 3.2% to 60.7%, with a mean value of 38.2% and a coefficient of variation of 30%. Note that along the flanges of the molded part, the fiber was sometimes caught in the shear edge and torn away from the preform, causing the low fiber content. It is anticipated that the preforms from the new screens will have less spring-out and be less susceptible to this action.

The effect of the fiber content on molding can be demonstrated by two areas on the roof rail end of the B-pillar outer panel. One area of 47% fiber appeared to form a dam of denser glass, which impeded the resin from filling out the end of the roof rail, leaving an area of dry fiber, shown in Figure 4. In the other case, an area on the flange contained almost no fiber and acted as a runner during mold fill, allowing resin to flow preferentially to areas on the edges, and trapping air and causing unwet areas.

After this part was made, a great deal of effort went into tweaking the spray pattern of the P4

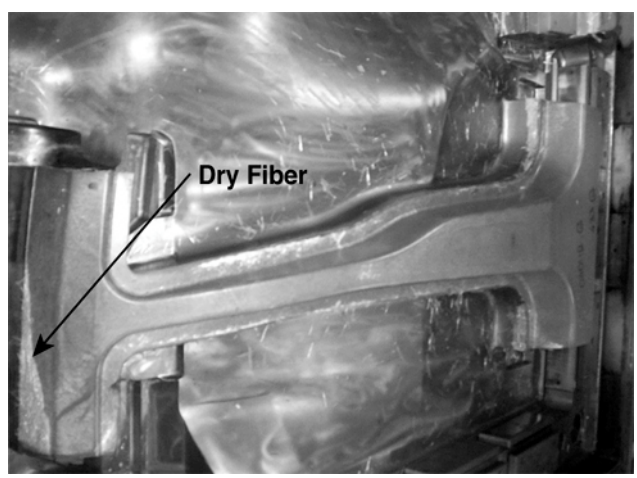

Figure 4. B-pillar molded from early Gen-1 preform showing an example of a dry area caused by flow restriction.

preformer. While the mean fiber contents for parts molded with this new spray pattern were similar (33.3% for the outer and 33.5% for the inner), the range was tighter. The outer range was 16 to 49%, and the inner range was 21 to 47%. While these ranges are an improvement, they are not yet acceptable. Work going forward will focus on a new set of screens, made to sit in the core position, instead of the cavity position as the current screens do.

Carbon Fiber B-Pillar Molding

Very little work has been done with molding of carbon fiber B-pillars to date, due to the shortage of the automotive-grade fiber. There was a brief look at two fibers, the Zoltek fiber being used in the ACC program for several years and a Hexcel fiber currently under development for this program. The preforms of the Zoltek carbon fiber had a very coarse fiber distribution, as was observed in the earlier plaque molding study with this fiber. There was some fiber wash with the preform tearing and resulting in resin-rich areas. Because the decision had already been made to build new preforming screens, it was decided to not use any more of the limited supply of the Zoltek fiber at that time.

A similar brief look was taken at the Hexcel fiber, which was preformed with the new screens. The 12 × 3K roving was preformed and successfully molded. While these performs were not at full weight, this result was very encouraging. Photos of perform and molded panel are shown in Figure 5. The molding chart in Figure 6 shows that carbon fiber preform had a much higher cavity pressure than did the glass at a similar fiber content. This is an indication of a higher resistance to flow with the carbon fiber preforms under this molding condition.

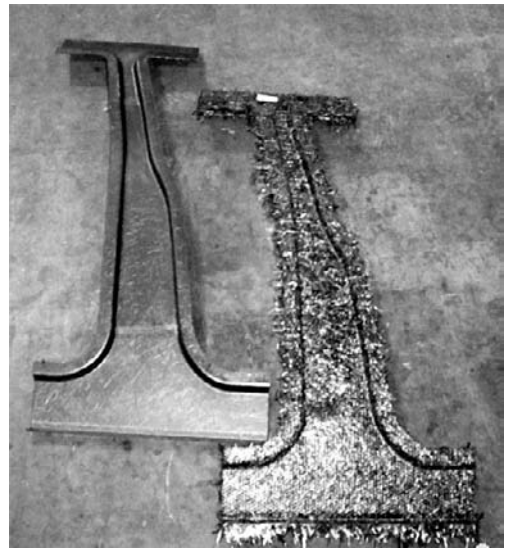

Figure 5. Hexcel carbon fiber preform and molded B-pillar.

Supplier-Partner Liquid Molding Program—LFI

The project team initiated a study of the LFI process, where the polyurethane resin and the chopped fiber are co-sprayed directly into the mold. The goals are to assess the potential for achieving a Class "A" exterior automotive surface and to characterize the material for its structural capability. The initial step for the team was to establish an "ACC Surface Acceptance Standard." After benchmarking a cross section of materials currently used for exterior Class "A" applications, Wavescan, QMS,

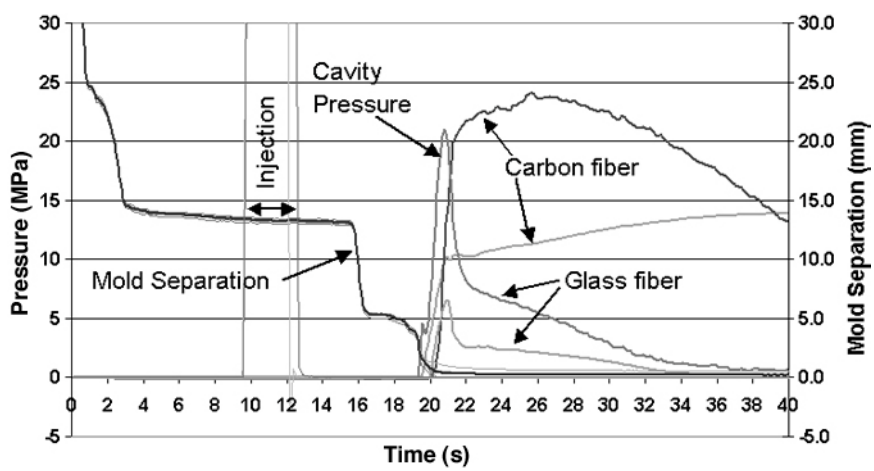

Figure 6. Carbon fiber and glass fiber performs cavity pressure profiles.

and jury evaluations were utilized to quantify and rank the samples. Consensus was reached on the following targets for this standard:

QMS: Combined score value > 65
Wavescan: Short-term waviness value < 20
Wavescan: Long-term waviness value < 5

These represent the lower range of values compiled in the benchmarking exercise.

Concurrently, the ACC had an existing Bayer SRIM plaque tool modified for LFI. The core surface was highly polished to a SPI A2 finish, and interchangeable stop blocks were built into the mold to vary plaque thickness. Figure 7 shows this tool prior to conversion.

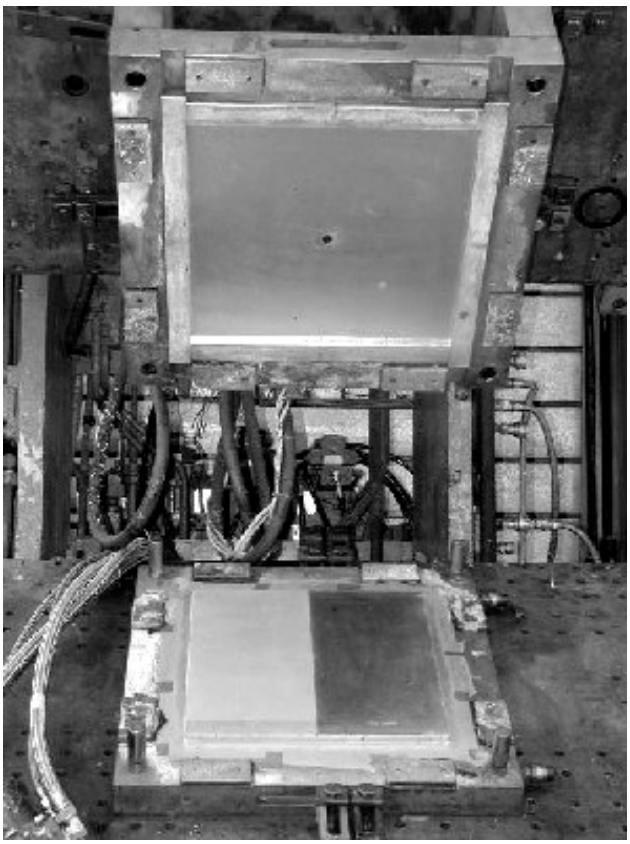

Figure 7. Plaque mold for LFI molding trials.

The next step involved an appropriate design of experiment (DOE) to evaluate the various design parameters that could potentially impact surface quality. Originally the proposal was to run two smaller DOEs sequentially. To save time and still attain statistically significant results, the DOEs were combined into one—a partial L32 Taguchi array. Variables included PUR density, glass type and length, glass content, plaque thickness, demold time, surface veil and postcure. Test plaques were painted using a low-bake (190°F) system.

The LFI team then used a jury evaluation to rank the plaques for surface appearance, ranging from best to worst. Generally, the strongest effects on surface were judged to be glass length, glass content, and the absence of a surface veil. Overshadowing these was postcure. Unfortunately, any real conclusive assessment of surface, especially using Wavescan or QMS methods, was not possible because air entrapment out-gassing was so extensive and resulted in an extremely poor overall surface quality. A directional statistical assessment based solely on subjective rankings resulted in the following conclusions:

Strongest effects:
- Glass length = 75 + 12.5 mm
- Glass content = 40%
- Surface veil = no
- Postcure = no

Because the surface quality of the initial DOE trial plaques was poorer than expected, the team focused its efforts for the balance of the reporting period on the elimination of the trapped air from the molded samples. Two potential approaches were considered. One was to design venting features into the ACC plaque tool shear edges. A second approach was to employ vacuum to evacuate the air during the molding process. When a separate existing sheet molding compound (SMC) plaque tool designed for vacuum became available, the team concentrated on adapting it to LFI. Preliminary results have been promising. Given that, the intent in the near term is to redirect the surface quality study and mold plaques using this vacuum setup.

Concurrently, the physical testing to characterize the LFI plaques from the initial DOE trial has been completed. The test program included tensile, compression, DMA, coefficient of linear thermal expansion, density, and glass content. All ACC team members, including our supplier partner, Bayer Polymers, participated in this physical testing phase. Data will be evaluated based on the statistical model used to structure the DOE initially. Results are expected in the late fall 2004.

While data analysis is continuing, some early observations can be made. The modulus depends strongly on the resin density and glass content. The molding experimental design utilized a low-density and a high-density resin and two levels of glass (25 and 40%) in each. The combination of resin density and glass content gave four levels of formulation density, target PFC (pounds per square foot). This is shown along with the tensile modulus values in the table below. The high-density, high-glass samples are about 2.5 times the modulus of the low-density, low-glass samples. The high-density, low-glass and low-density, high-glass samples fall between the other samples and have overlapping ranges of test values. The LFI samples all tested lower than expected for fiber content, so higher property values would be expected at the design-intent fiber levels.

Resin density	Fiber content (wt %)	Composite density (pcf)	Tensile modulus (GPa)
High	40	84	7.8
High	25	74	5.0
Low	40	59	4.5
Low	25	52	3.0

The next steps under consideration include further surface optimization, understanding the process variability that seems inherent to LFI, and studying the benefits of in-mold coatings. Ultimately, the team plans on addressing more complex molding features and replacing glass with carbon fibers.

Conclusions

During this year the molding of B-pillars with Gen-1 glass fiber preforms was completed. The B-pillar sets were provided to the adhesive bonding and structural analysis teams. There was limited molding of carbon fiber B-pillars, but much more work needs to be done in this area.

The LFI team completed the initial molding trial. Unfortunately, definitive conclusions could not be generated for surface appearance. Mechanical testing shows that a broad spectrum of properties can be generated with this process.

Presentations and Publications

1. D. L. Denton, C. H. Mao, D. E. Willertz, DaimlerChrysler Corporation, N. G. Chavka, J. S. Dahl, E. D. Kleven, Ford Motor Company, T. J. Dearlove, C. A. Di Natale, E. M. Hagerman, S. A. Iobst, J. A. Schroeder, General Motors Corporation, and R. A. Bergen, MSX International, “Development of a Cost-Effective SRIM Manufacturing Process for a Composite Pickup Truck Box,” presented at the SAMPE Advanced Composites Conference, Dearborn, Michigan, September 13–14, 2000.
2. S. A. Iobst (presenter), C. H. Mao, and D. L. Denton, DaimlerChrysler, “Use of Real Time Data Acquisition to Optimize the SRIM Process for a Pickup Truck Box,” presented at the SAMPE Advanced Composites Conference, Dearborn, Michigan, September 13–14, 2000.
3. N. G. Chavka and J. S. Dahl, “P4: Glass Fiber Preforming Technology for Automotive Applications,” 44th International SAMPE Symposium and Exhibition, May 23–27, 1999, Long Beach, California.

D. Development of Next-Generation Programmable Preforming Process

Co-Principal Investigator: Raymond G. Boeman
Oak Ridge National Laboratory
P.O. Box 2008, Oak Ridge, TN 37831-6053
(202) 586-0785; fax (202) 586-7409; e-mail: boemanrg@ornl.gov

Co-Principal Investigator; Robert E. Norris, Jr
Oak Ridge National Laboratory
P.O. Box 2008, Oak Ridge, TN 37831-6053
(865) 576-1179; fax (865)-574-8257; e-mail: norrisrejr@ornl.gov

Field Project Manager, Composites: C. David Warren
Oak Ridge National Laboratory
P.O. Box 2008, Oak Ridge, TN 37831-6065
(865) 574-9693; fax: (865) 576-4963; e-mail: warrencd@ornl.gov

Technology Area Development Manager: Joseph A. Carpenter
(202) 586-1022; fax: (202) 586-1600; e-mail: joseph.carpenter@ee.doe.gov
Field Technical Manager: Philip S. Sklad
(865) 574-5069; fax: (865) 576-4963; e-mail: skladps@ornl.gov

---

Contractor: Oak Ridge National Laboratory
Contract No.: DE-AC05-00OR22725

Objectives

- Develop the next-generation of low-cost fiber preforming technologies based on programmable, robotic-controlled, directed chopped-fiber processes for the application of
  - low-cost carbon fiber
  - reinforced thermoplastics
  - hybrid glass-carbon
- Develop supporting technologies required to successfully implement the process technology including
  - preform characterization (e.g., permeability, areal density uniformity)
  - preform process modeling for process effects analysis
- Conduct parametric process studies to investigate fundamental process effects and establish process-property relationships.
- Conduct requisite molding investigations—experimental and through modeling—to elucidate relationship between preform characteristics and moldability.

Approach

- Establish a base research programmable robotic preforming system for which advanced capabilities (e.g., new chopper designs) can be developed and evaluated.
- Establish a highly instrumented and controlled research molding capability to isolate and investigate the effects of process variables on moldability and mechanical properties.

- Develop new severing technology to facilitate the implementation of low-cost carbon, reinforced thermoplastics, and hybrid glass-carbon products.

Accomplishments

- Developed detailed specifications for a research-oriented programmable robotic preforming system.
- Executed a competitive solicitation to procure the preforming system.
- Held kick-off meeting and facility walkdown with preforming system vendor.
- Completed design for preforming system.
- Conducted literature and patent search on advanced fiber-severing technologies.
- Designed and constructed in-plane preform permeability measurement capability.
- Developed data acquisition and user interface for analysis of permeability data.
- Designed through-thickness preform permeability capability.
- Extended paper-making model to simulate the fiber preforming process.

Future Direction

- Conduct acceptance evaluation, disassemble, ship, and commission performer.
- Resolve sensor issues encountered with in-plane permeability rig and conduct measurements on preforms made by simulated split-tow products of varying tow-size.
- Evaluate preform process model relative to physical preform characteristics.
- Conduct initial preforming studies with low-cost carbon fiber.
- Construct and test through-thickness permeability rig.
- Finalize specifications and issue Request for Proposal for research molding press.
- Initiate bench-top studies of advanced severing technology.

Introduction

Polymer matrix composite materials offer a number of benefits in “lightweighting” of automotive and heavy vehicles, including greater stiffness and strength per unit weight than conventional materials, easier formability, less corrosion susceptibility, the ability to tailor properties to specific load requirements, and enhanced noise and vibration damping. However, widespread implementation of carbon fiber composites, which offer among the greatest mass savings potential, requires lower cost materials and processes than are currently available. Advanced preforming processes offer opportunities to facilitate the widespread use of carbon composites.

Robotic-controlled, programmable, directed-fiber preforming processes have demonstrated exceptional value for rapidly preforming large, glass-reinforced, automotive composite structures. Due to their unique features and flexibility and to their inherent low-scrap rate, they are the most viable candidate processes for making affordable carbon-fiber preforms for a variety of structural automotive components. The Automotive Composites Consortium (ACC) has implemented the Programmable Powdered Preform Process (P4), with glass fibers, very successfully in its truck box program—Focal Project 2 (FP2). Original equipment manufacturers (OEMs) have transferred the technology to commercial applications such as the General Motors (GM) Silverado pickup box and the Aston Martin Vanquish body-side.

Analyses have indicated a potential for greater than 60% mass savings for a carbon-fiber intensive body-in-white under the assumption of a thickness design constraint of 1.5 mm. The analyses also

indicate the potential of saving an additional 15% if the thickness constraint is reduced to 1 mm. Unfortunately, evidence suggests that 1.5 mm may be a practical limit for liquid molding. However, thermoplastics preforms, in which the matrix and fiber are both deposited in the preforming step, offer a potential path to obtaining thinner sections, and consequently additional mass savings as well as the potential for recyclability. Hybrid-fiber performs offer another potential benefit in terms of economics and property enhancement.

Approach

The objective of this project is to advance directed-fiber preforming processes to effect a further reduction in vehicle mass—relative to glass-fiber composites—while maintaining the economical advantages of net-shape preforming. The project will be executed in three phases corresponding to three materials systems: carbon fiber, reinforced thermoplastics, and hybrid glass-carbon fiber. Each phase will consists of four main tasks focused on (1) materials developments, including new fiber product forms and binders; (2) machine developments, particularly new severing technology; (3) process developments, for example, to control areal density uniformity and perform anisotropy; and (4) development of supporting technologies such as preform characterization techniques. Furthermore, this project will undertake to develop sufficient understanding of fundamental aspects of the process and their effect on preform quality and mechanical properties in the molded part. As such, this project will support, augment, and facilitate the current and future research activities undertaken in the "Development of Manufacturing Methods for Fiber Preforms" project (4.A).

Procurement of Preforming System

Central to this effort is the procurement of a research-oriented, robotic-controlled, programmable preforming system for installation in the polymer composites laboratories of the Metals and Ceramics Division at the Oak Ridge National Laboratory. This system will establish the base for future hardware developments as well as serve as a research instrument on which parametric process studies will be conducted. A competitive solicitation was issued in April 2004, vendor selection made in May 2004, and a purchase order let in June 2004. Applicator System AB of Mölnlycke, Sweden, was selected to design and build the system. System configuration and facility constraints were established during a kick-off meeting in July 2004. Detailed system design was complete in September 2004.

The system (see Figure 1) has a footprint of 9 by 15 m, contains a robot with 7 degrees of freedom and can produce preforms up to approximate dimensions 1 m × 1.2 m × 1.8 m. On the head of the robot is mounted a chopper unit that incorporates the main chopper for spraying the reinforcement fibers and a surface veil chopper. Fiber length is adjustable on-the-fly in two ranges, 20–85 mm and 90–200 mm, as well as continuous. Fiber output is variable and can be as high as 3500 g/min.

Future work will include modifications to the base system in facilitating advanced fiber product forms, including low-cost carbon, reinforced thermoplastics, and glass-carbon hybrids.

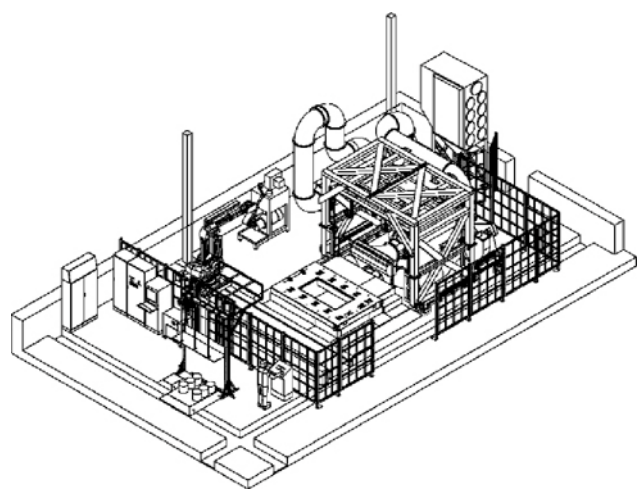

Figure 1. Schematic of the robot-controlled, programmable preforming system.

Fiber-Severing Technology

Due to significant differences in the physical properties of various reinforcement fibers as well as their available product forms, chopping technology that has been successful for glass fibers systems has demonstrated less-satisfactory results for the carbon-fiber products that are currently available. It is expected that similar results will occur for reinforced thermoplastics and hybrid glass-carbon products. Accordingly, consideration is given in this project to identifying alternative severing technology. A literature and patent search was undertaken to assess

promising technologies for bench-top investigation. Possibilities identified include mechanical-based, laser-based, CO_2 pellet, liquid nitrogen, water-jet, and ultrasonic. Based on the information available in the literature and personal contact, laser-based choppers appear to offer the most promise. However, further investigation as well as exploratory experiments are warranted before drawing firm conclusions.

Permeability Measurement

It has been found that injection-compression offers distinct advantages over injection-only liquid molding for the infiltration of high-volume fraction preforms. Consequently, both the in-plane permeability and the through-thickness permeability affect the moldability of the part. Accordingly, two novel research instruments are under development that will provide experimental data to characterize the three-dimensional permeability of the fiber mat preform (Figure 2).

The in-plane rig, shown in Figure 3, has a flow capacity of 0.33 gpm and a fluid capacity of 2 gal. It can be operated in either constant flow or constant pressure mode under feedback control. Maximum pressure and fluid viscosity is 100 psi and 5 poises, respectively. Both platens are instrumented with sensors—a total of 218 sensors—to monitor the flow-front with resolution of 0.25 in. The sensor

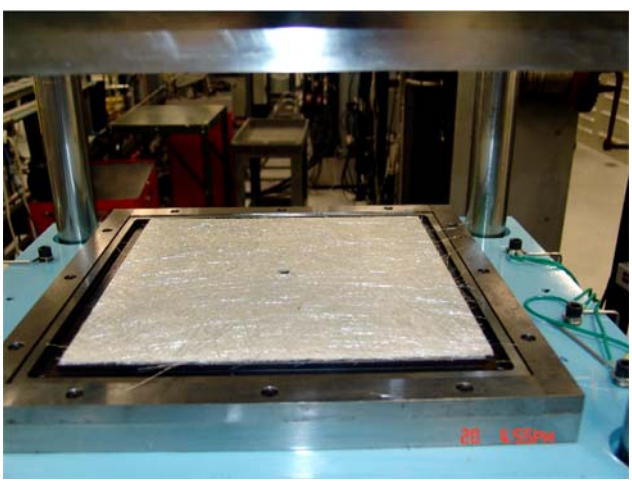

Figure 2. Glass preform sitting on bottom platen of the in-plane permeability rig.

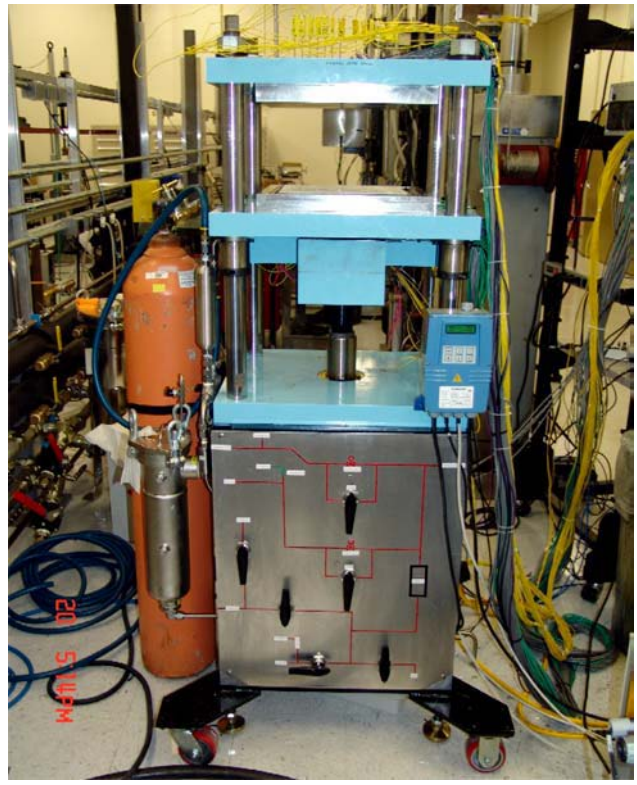

Figure 3. In-plane permeability rig with platen open.

concept was developed through subcontract to Prof. Richard Parnas at the University of Connecticut. It consists of a recessed insulated conductor that generates a voltage when the conductive fluid bridges the sensor and the metallic plate. Although the sensor appeared to work adequately in the University of Connecticut laboratory, it has been problematic when implemented in the system. Effort continues to improve the accuracy and reliability of the conductive sensor. Additionally, prototype thermocouple-based sensors have been developed and are being evaluated (Figure 4) .

A through-thickness rig has been designed (Figure 5) and fabrication initiated. Maximum pressure and viscosity are the same as the in-plane rig. The through-thickness rig has a flow capacity of 8 gpm. Through incorporation of a dynamic seal, preform thickness can be changed quickly for successive measurements to evaluate the influence of fiber volume fraction on permeability.

A data acquisition and control system has been developed based on National Instruments' PXI hardware and LabVIEW software. Stand-alone program modules have been written to evaluate the

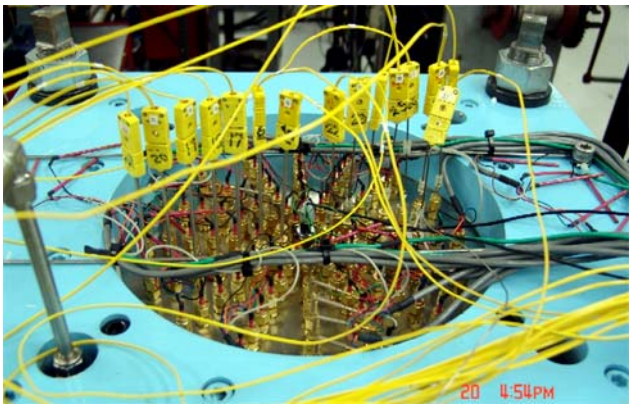

Figure 4. Top platen of the in-plane permeability rig with both conductive and thermocouple sensors installed for evaluation.

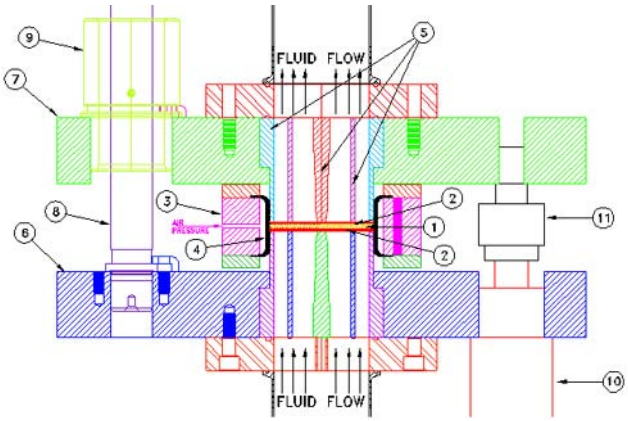

Figure 5. Through-thickness permeability rig consisting of a dynamic seal and thickness adjustment for fiber volume fraction studies. The preform is labeled 1.

sensor performance, to conduct the experiments, to analyze the collected data and calculate permeability value, and to review the experiment at reduced speed. The modules that monitor the sensors have been developed for both conductor and thermocouple-based sensors. An example of the real-time display is shown in Figure 6.

An analysis module that takes the elliptical flow front and calculates the in-plane components of the permeability sensor has been developed from expressions provided by Prof. Parnas. Full characterization of the analysis module will proceed following resolution of sensor reliability and accuracy issues.

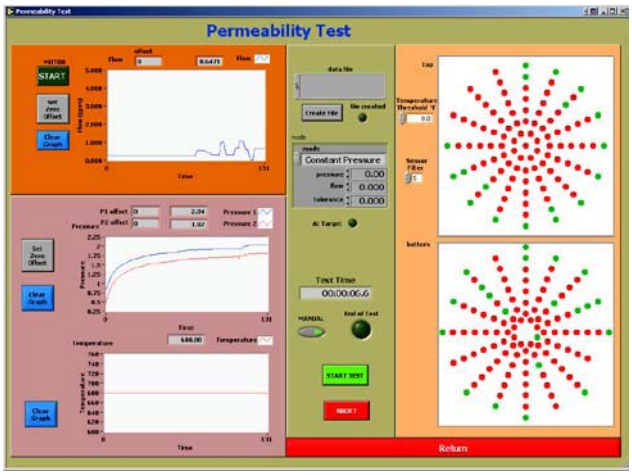

Figure 6. Real-time display indicating the progression of the flow-front during an in-plane permeability experiment. Tripped sensors change from green to red.

Modeling of Fiber Deposition

A C-based program is under development to analyze the affect of process variables on preform characteristics. The program, FNSim, will be used to evaluate preforms in terms of measures such as fiber run length, fiber connectivity, distribution of voids, etc. FNSim, when correlated with permeability data and areal density measurements, will provide an understanding of the effect of process variables on resulting preforms and their "moldability." Recent advancements to FNSim have included efficiency improvements such that it now can be used on desktop computers as well as the development of a new method of characterizing voids. Simulation of fiber deposition is illustrated in Figure 7.

Summary

A new project to develop the next-generation programmable preforming process was initiated in FY 2004. The research will build on past development and application of directed-fiber preforming processes, namely those of the Programmable Powdered Preform Process (P4), to extend the process to new material systems. Developments are expected to facilitate the use of low-cost carbon, reinforced thermoplastics, and glass-carbon hybrid materials as effectively as is the

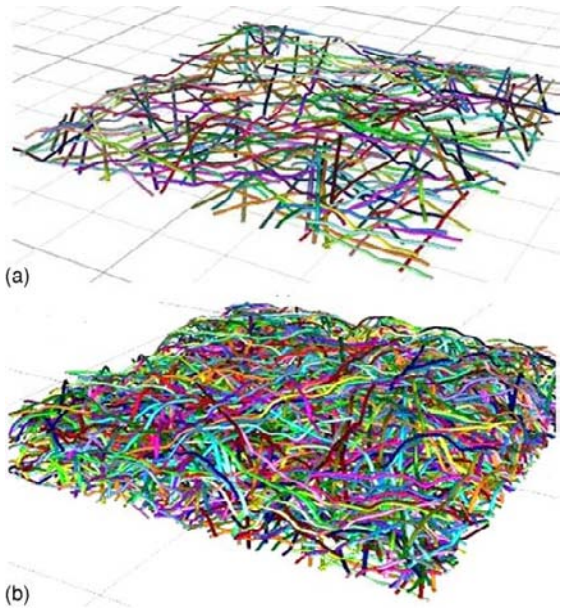

Figure 7. Progression of fiber deposition a predicted by FNSim.

current state-of-the-art with glass. Utilizing these materials is expected to lead to further reductions in vehicle mass in a more cost-competitive scenario than is currently possible. A preforming system, which will serve as the base for hardware developments, is under procurement and should be installed in the polymer composites laboratories at Oak Ridge National Laboratory in the second quarter of FY 2005.

The base system is designed around glass-fiber product forms. A literature review has identified alternate severing technologies that may prove more effective for "chopping" the carbon, reinforced thermoplastics, and glass-carbon hybrids under investigation in this effort.

Two novel permeability rigs are under development to characterize the preforms resistance to resin flow during the molding process. The in-plane rig has been constructed and experiments initiated. Issues with sensor reliability and accuracy have been identified, and effort is under way to resolve them. The through-thickness rig has been designed and hardware components purchased. A data acquisition, control, and analysis system has been developed for both rigs and is being used in the troubleshooting experiments. Together, the two rigs will provide the three-dimension permeability data required for the development of mold-flow models.

Modeling of the fiber deposition process is under way through the development of an in-house code. The program, FNSim, will be used to evaluate preforms in terms of measures such as fiber run length, fiber connectivity, distribution of voids, etc. Results will be correlated with permeability data and areal density data to assess the effect of process parameters on preform quality as well as the mechanical properties of molded parts.

Collectively, the technology under development in this project will advance low-cost processing on two fronts. First, it will provide the opportunity to employ additional materials in the net-shape preforming process, which is expected to lead to additional mass reduction and/or better performance. Second, it will provide the requisite tools to evaluate the affect of process parameters on the utility and performance of preforms and molded parts.

Presentations and Publications

1. R. Parnas, Q. Liu, K. Hoes, R. Boeman, and R. Battiste, "New Set-Up for Permeability Measurement," Invited Presentation, the Seventh International Conference on Flow Processes in Composite Materials, University of Delaware, July 7–9, 2004.
2. D. L. Denton, C. H. Mao, D. E. Willertz, DaimlerChrysler Corporation, N. G. Chavka, J. S. Dahl, E. D. Kleven, Ford Motor Company, T. J. Dearlove, C. A. Di Natale, E. M. Hagerman, S. A. Iobst, J. A. Schroeder, General Motors Corporation, and R. A. Bergen, MSX International, "Development of a Cost-Effective SRIM Manufacturing Process for a Composite Pickup Truck Box," presented at the SAMPE Advanced Composites Conference, Dearborn, Michigan, September 13–14, 2000.
3. S. A. Iobst (presenter), C. H. Mao, and D. L. Denton, DaimlerChrysler, "Use of Real Time Data Acquisition to Optimize the SRIM Process for a Pickup Truck Box," presented at the SAMPE Advanced Composites Conference, Dearborn, Michigan, September 13–14, 2000.
4. N. G. Chavka and J. S. Dahl, "P4: Glass Fiber Preforming Technology for Automotive Applications," 44th International SAMPE Symposium and Exhibition, May 23–27, 1999, Long Beach, California.

5. LOW-COST CARBON FIBER

A. Low-Cost Carbon Fibers from Renewable Resources

Project Contact: C. F. Leitten, Jr., W. L. Griffith, A. L. Compere
Oak Ridge National Laboratory
Post Office Box 2009
Oak Ridge, TN 37831-8063
(865) 576-3785; fax: (865) 574-8257; e-mail: leittencfjr1@ornl.gov

Technology Development Manager: Joseph A. Carpenter
(202) 586-1022; fax: (202) 586-1600; e-mail: joseph.carpenter@ee.doe.gov
Field Technical Manager: Philip S. Sklad
(865) 574-5069; fax: (865) 576-4963; e-mail: skladps@ornl.gov

---

Contractor: Oak Ridge National Laboratory
Contract No.: DE-AC05-00OR22725

Objective

- Demonstrate the use of new precursor materials that decrease the cost and increase the availability of carbon fiber, which meets the performance and price needs of the automotive market.
- Demonstrate that one or more renewable/recycled precursor formulations can be expected to produce industrial-grade carbon fibers at a cost of $3.00–$5.00/lb.

Approach

- Provide the data needed to scale processing up to industrial levels and to consistently achieve desired fiber properties at larger scale.
- Systematically develop the technical base needed to produce lignin-blend carbon fiber feedstocks at industrial scale:
  - Lignin production to obtain best molecular weight, low-volatile, low-salt material;
  - Spinning, oiling, and sizing technology;
  - Spinning technology, including production die structure, plasticizers, and nucleating agents;
  - Plasma treatment and sizing technology to make the fiber compatible with selected resin systems;
  - Selection of appropriate polyesters; and
  - Evaluation of properties and economics of fiber and composite systems.
- Work with industrial partners to scale and transfer the technology for the production of carbon fiber precursors from lignin-blend feedstock.
  - Evaluate melt-extrusion properties of lignin-based feedstock at increasing scale using near-industrial equipment that can be readily obtained by fiber manufacturers.
  - Evaluate production of carbon fiber using a research production line at an industrial facility.
  - Evaluate mechanical and composite compatibility properties of graphitized melt-spun lignin-blend fibers.
  - Work with partners to evaluate and develop process metrics and standards.
  - Work with partners to better define process economics.
- Transfer technology, including intellectual property, for the production of carbon fibers from lignin to industrial partners.

Accomplishments

- Demonstrated proof-of-concept of the melt extrusion of 28 filament tow of lignin-based fibers. This validated selected compositions, processing methods, and testing technologies. It also provided a basis for understanding the process improvements required for larger scale manufacture of lignin-based carbon fiber feedstocks.
- Showed from preliminary data that yields of 50%, consistent with those obtained commercially for lignin-based activated carbon, are feasible.
- Spun significant amounts of 28 filament tow successfully at the University of Tennessee (UT) using a two-step process. No sticking problems were apparent, and fiber diameter was reduced from ~45 μm to ~15 μm, with an apparent increase in mechanical properties.
- Discussed that preliminary evaluations of a plasma surface treatment + silanation for lignin-based fibers indicated a significant improvement in fiber-resin bonding over conventional carbon fibers.
- Made small epoxy resin composites using carbon fibers produced from UT 28 filament tow that showed composite mechanical properties.
- Determined sources of volatiles within lignin and developed purification methods that remove or mitigate volatiles.
- Developed of initial process control technologies.

Future Direction

- Develop methods for production of industrial-quality carbon fibers from lignin-blend feedstocks. Studies will include the following:
  - Optimization of lignin preprocessing to minimize contaminants (salts and particulates) and provide the best molecular weight.
  - Development of conditioning and spinning processes that remove water and volatiles prior to fiber production.
  - Selection and design of spinning dies that provide the best internal structure.
  - Selection of plasticizers and nucleating agents for lignin-polyester fiber blends.
  - Selection and development of techniques for spooling and oiling lignin blend fiber at each step.
  - Development of methods for surface treating and sizing the surface of carbon fibers to improve compatibility with proposed resin systems. This is particularly critical for chopped fiber–resin composites.
- Work with project partners to
  - address raw fiber production issues (lignin, preconsumer recycled polyesters, spinning and winding technologies); and
  - evaluate carbon fiber production from lignin-based multifilament tow using an industrial research process line.
- Transfer technology to industry.

Introduction

This project is developing methods for production carbon fibers from high-volume, low-cost, renewable and recycled feedstocks to reduce precursor and processing costs. Use of these materials also decreases sensitivity of carbon fiber cost to changes in petroleum production and in energy cost.

Proof-of-concept production of single fibers from a variety of high-volume natural, renewable, and recycled materials was demonstrated first. Single fibers melt spun from blends of Kraft lignin, an inexpensive, high-volume wood pulping by-product, with small amounts of routinely recycled polyolefins and polyesters could be processed using conventional stabilization (oxidizing atmosphere), carbonization, and graphitization (inert atmosphere) furnacing to yield carbon fibers. Fiber properties improved if the fibers were stretched during furnacing. Graphite content, measured with X-ray

diffraction, increased with increasing graphitization temperature. Carbon fiber yield from this lignin-blend feedstocks was ~50%, and the fibers were dense, smooth-surfaced, and round.

Larger amounts of a lignin-recycled polyester feedstock were melt extruded as a multifilament (4 to 28 fiber) tow using the University of Tennessee (UT) twin-screw Leistritz extruder to meet a September 2003 composite preparation and testing milestone. The U.T. Leistritz is the smallest member of a line of commercial melt extruders. Meeting this milestone showed that (1) lignin-blend fiber can be melt-extruded as a small tow using near-commercial spinning equipment, (2) composites made from graphitized lignin-blend fibers can be used in resin-fiber composites that have normal fracture patterns, and (3) although very smooth, lignin-blend fibers can be plasma treated and silanated to provide good fiber/resin adhesion.

Analysis of the samples obtained indicated that bubbles and inclusions were the major flaws in lignin-blend fibers. Flaws are known to decrease the strength of carbon fibers and are typically the initiation point for fiber breakage. The source of the bubbles was found to be volatiles from the lignin, and this year, methods were developed to mitigate these problems. Additionally, methods for controlling salt content in the fibers and for prefiltering black liquor prior to lignin production have been developed.

Project Deliverables

Goal: By the end of this multiyear program, production of one or more environmentally friendly, economically feasible carbon fiber precursors will be demonstrated and transfer of production technologies and any related intellectual property to industry initiated.

In FY 2004, major milestones, including the initial tests of the effect of lignin molecular weight on fiber properties (6/30/04) were completed on time.

FY 2005 milestones include development of a lignin feedstock specification to facilitate industrial production of carbon fibers meeting program goals (5/2005) and establishment of basic rheology for extruding and winding lignin bundles with improved handling characteristics (9/2005).

Planned Approach

Production of industrial-grade carbon fibers from a radically new type of feedstock requires the simultaneous development of methods for feedstock recovery, preparation, blending, spinning, handling, and spooling in addition to the furnacing, stretching/orientation, oiling, and sizing technologies required for conventional fibers. These are combined with evaluations of fiber quality and suitability for use in composites.

Because of high levels of emissions and costs typically associated with spinning of fiber from liquids, first priority was placed on development of melt-spinning techniques for fiber. Use of lignin and other non-nitrogenous feedstocks was preferred because it would eliminate cyanide emissions during furnacing. Use of modern furnacing techniques, such as hot-stretching and controlled atmosphere processing, are being evaluated to improve properties and yield of carbon fiber precursors from feedstock.

Industrial partners are increasingly involved in the development of process technologies. They have been working with project staff on the selection of blending polymers for lignin, purification of lignin, strategies for production of cleaner lignin, and spinning of fiber. In the later stages of the project, industrial partners will also assist in production of lignin-based carbon fiber using a research industrial production line.

Transfer of project technology, including any intellectual property, is planned.

Lignin Feedstock Quality

Lignin is an inexpensive, high-volume by-product of paper production. Although the bulk of Kraft lignin is burned to provide process energy, a fraction is recovered from black liquors. At acid pH, Kraft lignin forms a loose gel that is recovered, washed, dried, and marketed as a free-flowing powder. Softwood Kraft lignin forms the bulk of commercial materials, although hardwood lignin is also available. The current one-step precipitation process leaves several materials (e.g., particulates, cellulosics, water, volatile, and inorganic pulping chemicals) within the lignin gel. Although these are acceptable in the current product, which is marketed for applications such as cold-rolled asphalt, they

interfere with the production of satisfactory carbon fibers.

Developing cost-effective, industrially feasible methods for improving the quality of lignin as a carbon fiber feedstock has remained a major focus of this project. Removal of salts, particulates, and carbohydrates from lignin will be discussed below.

Control of Ash Levels in Lignin

To improve the strength of carbon fibers, it is desirable to minimize defects, such as inclusions. A typical alkaline pulping liquor contains ~10% salts, which can coprecipitate with lignin gel. When lignin is dried, extruded, and fired, these salts will create inclusions or, for fibers fired at temperatures in excess of 2000°C, voids. To minimize salts, lignins have been desalted by washing with slightly acidified water.

To develop an understanding of desalting, data on the salt concentrations of lignin and lignin wash waters were evaluated. As shown in Figure 1, there appears to be a good correction between the salt concentrations in the wash water and dried lignin across the likely range of process values. The ability to estimate salt concentration in lignin from that in wash waters will facilitate production of low salt lignins.

The major difficulty in desalting lignin was estimating the ash content of the resulting lignin. As shown in Figure 1, there is good correlation between the ash contents of lignin and wash water. A number of industrial technologies for measuring the dissolved inorganic solids, or ash, in water are available to industrial lignin producers, and the correlation should facilitate real-time process control.

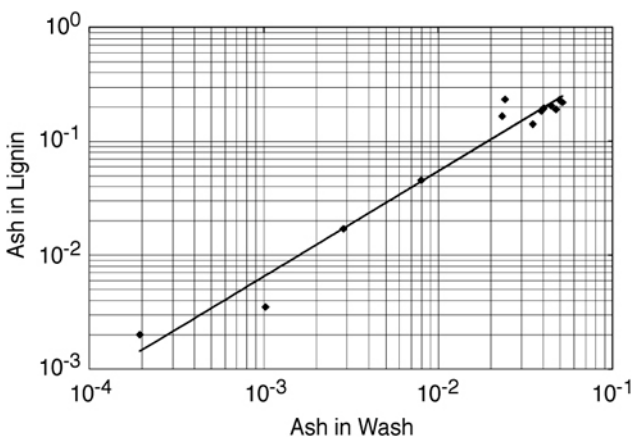

Figure 1. Ash (salts) content of dried lignin and water used to wash.

Black Liquor Filtration

Particulate contaminants, such as sand grains, diatoms, or bits of wood and paper, coprecipitated in the lignin gel cause difficulties in spinning. Although the black liquor from which lignin is precipitated is typically coarse-screened to recover wood and pulp, screens do not provide adequate removal of particulates in the 0.5- to 100-μm range, which could block spinning dies.

As the project scales up lignin production for use in fiber spinning, a filtration step could be inserted to decrease inclusions. Because the pulp and paper industry does not generally filter black liquor, a series of tests was performed to determine whether it would be feasible to use conventional submicron filtration prior to lignin precipitation. These tests were performed by obtaining black liquors made from several starting chemical concentrations and filtering them through 1-in. diameter, 0.45- or 0.2-μm filters, and measuring the flow rates or fluxes.

As shown in Table 1, the initial fluxes, or flow rates, of Kraft black liquor through various media were in an industrially feasible range. However, filtration rate was sensitive to both initial pulping chemical concentration, and to the type of filter used.

The most effective filter type was hydrophilic polypropylene. This material is particularly suited to use in carbon fiber precursor feedstock for two reasons. First, industrial polypropylene filters and filter cloths are readily available, inexpensive, and alkali resistant. Second, any residual filter material that became combined with the lignin would likely

Table 1. Filtration rate (cm/min) of Kraft black liquors

Filter material	Pore size (μm)	Pulping chemicals (% AA)		
		8	12	16
Polypropylene	0.45	9.2	12.2	18.3
Polysulfone	0.45	3.7	4.1	9.2
PVDF	0.45	4.3	6.1	7.3
Nylon	0.45	4.3	2.4	7.3
Alumina	0.20	6.9	7.6	4.4
PTFE	0.45	0.1	1.2	1.2

melt under the fiber extrusion conditions used. This would minimize blinding of spinning dies.

As the data indicated, use of submicron polypropylene cartridge filters and micron polypropylene filter felts has proven effective on high-volume black liquor samples processed to recover both high- and low-sulfur lignins from alkaline pulping.

Polypropylene filter felts can be used in a wide variety of industrial-scale filter configurations, such as belt filters or plate and frame filters. Although polypropylene filter felts are currently produced in the 1-μm and higher range, discussions with manufacturers indicated that felts capable of removing submicron particles are planned.

Purification to Decrease Volatiles

Bubbles in multifilament fibers could be produced in a number of ways: by release of sorbed water, by overpressurization of nitrogen during extrusion, by release of small volatiles in the feedstock, or by chemical breakdown of feedstock constituents. Some of these factors are best controlled during lignin preparation, others by modification of lignin purification and prespinning processing. For example, overpressurization during extrusion is likely due to the residual amount of particulate matter in the feedstock and will be controlled by the use of a feedstock that has been filtered prior to precipitation.

The color variation in as-spun raw fiber provided a valuable clue in understanding a major reason for die plugging and for volatile materials, including water, released during extrusion. Consideration of the spinning temperature, coupled with increased fiber darkening and carbon deposits noted on extruder cleanup, suggested that a material in commercial lignin was charring during long periods at processing temperatures of >225°C. Nuclear magnetic resonance profiles of desalted commercial lignin showed the presence of a significant amount of carbohydrate. Carbohydrate gels are hydrophilic, and additionally, carbohydrates may be carboxylated during the pulping process. Most of the carbohydrate occurs as beta-linked polysaccharides, and many carbohydrates are known to char.

Efficient separation of lignin-bound carbohydrates presents a significant technical challenge. The first method evaluated was enzyme hydrolysis of carbohydrates at pHs ranging from 3 to 8. However, enzyme treatments did not significantly reduce the amount of carbohydrate in commercial lignin samples.

The project staff were able to obtain experimental Kraft black liquors with varying pulping chemical levels from another Oak Ridge National Laboratory (ORNL) project. These liquors were to be used to prepare lignins. In conventional industrial lignin preparation, pH is dropped from ~13 to 3.5–4.5 in a single step. The lignin precipitates as a gel, which is washed and dried prior to use. However, this technique coprecipitates carbohydrates, such as short chain cellulosics, with the lignin.

An ORNL consultant suggested use of a modified version of a fractional precipitation technique used to separate Kraft lignin from black liquor for analysis. This technique takes advantage of the selective precipitation of cellulosic carbohydrates at pH 9–10.5. The cellulosic precipitate can be removed, and the liquid acidified to pH 3.5 to 4.5 to precipitate the lignin.

Figure 2 shows thermogravimetric analyses of three different types of lignins and the carbohydrate removed from a Kraft lignin. The cellulosic carbohydrate fraction has a significantly higher weight loss than do the lignins. Within the lignins, lignins from alkaline and organosolv pulping (Lignol Innovations) have the lowest weight loss. The alkaline pulping lignin was prepared using a two-step process in which the carbohydrate was first precipitated and removed, and then the lignin was precipitated.

Figure 3 shows a solid state nuclear magnetic resonance pattern (NMR) for carbohydrate removed in step precipitation. Carbohydrate removed in the first step was estimated to contain ~9% chemically bound lignin. Additionally, the carbohydrate contains a small amount of carboxylate. This is most probably due to changes that normally occur in wood carbohydrate during pulping.

Figure 4 shows the solid state NMR pattern of precipitated lignin that has been stripped of a portion of its carbohydate by fractional precipitation. This material has been reduced from 20–30% carbohydrate to estimated 12% carbohydrate.

At present, the bench-scale data discussed above have been evaluated during the processing of significant amounts of lignin from alkaline pulping black liquors. Although commercial lignins are relatively impure, having as much as 20–30% carbohydrate content, highly pure lignins, up to 97% as

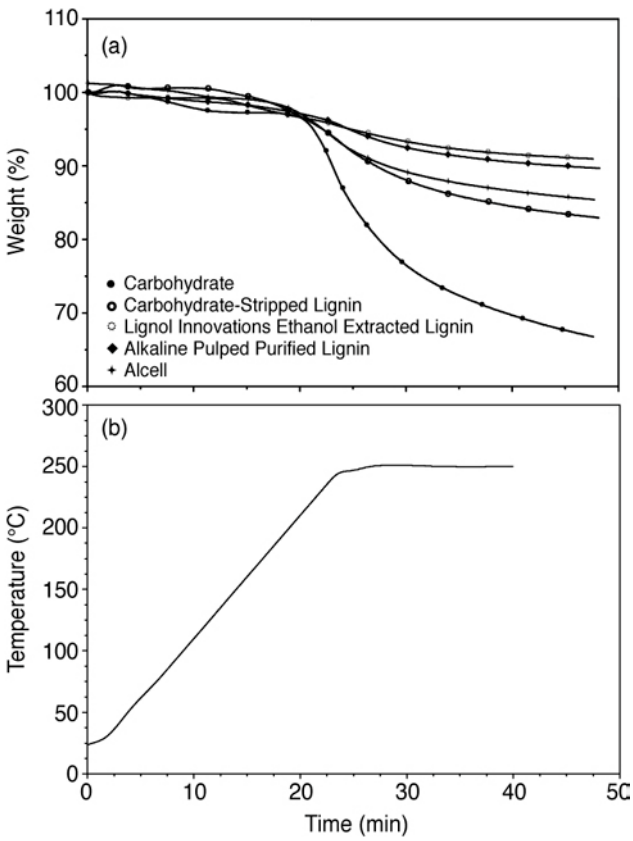

Figure 2. Thermogravimetric analysis of selected lignins and a lignin-derived carbohydrate: (*a*) weight loss curves and (*b*) temperature–time curve for the analysis.

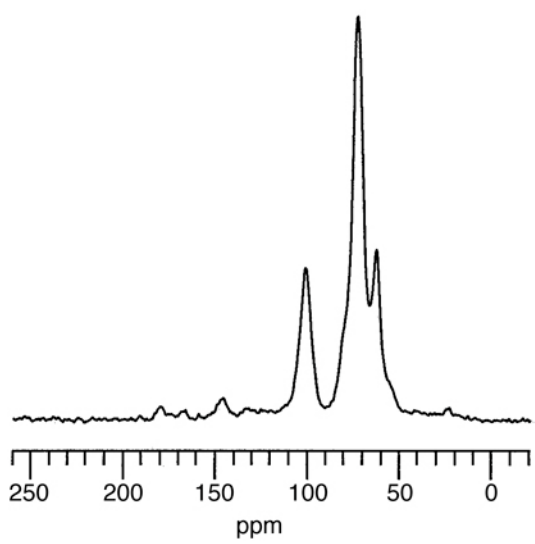

Figure 3. NMR analyses of celluloselike polymer removed from lignin by fractional precipitation.

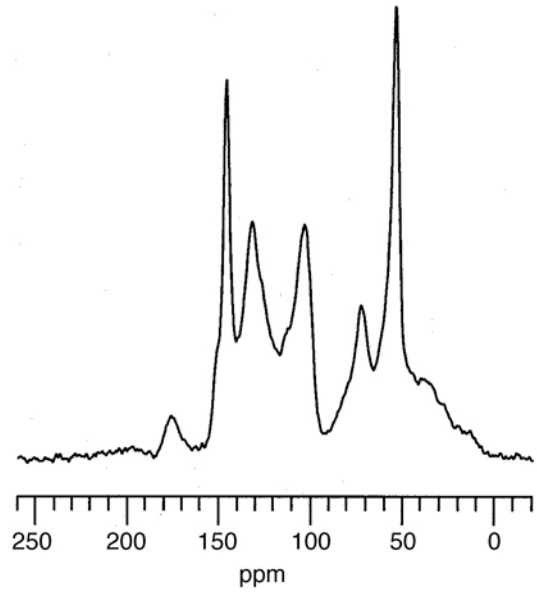

Figure 4. NMR analyses of Kraft lignins with reduced amounts of celluloselike carbohydrate after fractional precipitation.

measured by solution NMR, can be produced from black liquors.

The critical factor in recovering highly pure lignin appears to be effective removal of the carbohydrate. In early experiments, lignin and carbohydrate were separated by centrifugation. High-purity lignin required several purification steps, and the precipitates from both steps were both very small (around a micron) and quite gelatinous.

It was thought that this could be improved through the use of flocculants. The question was finding effective flocculants whose recycle would be acceptable to pulp and paper mills. Discussions with industrial partners, as well as industrial experience, indicated appropriate the levels and classes of flocculants.

Currently, two flocculants, applied at 10 ppm, are providing effective carbohydrate particulate aggregation. This permits use of a single filtration step for carbohydrate removal.

A combination of flocculants, applied at 10 ppm each, has also been used to improve the filterability of lignin aggregates.

Addition of small amounts of selected industrial enzymes to the lignin increases removal of residual carbohydrate from precipitated lignin during desalting.

The combination of coagulation and filtration is used effectively at industrial scale and the materials

and the enzymes used are standard commercial materials used by the forest products and food industries in other applications.

Removal of the carbohydrate, salt, and particulates changes the final lignin product. Commercial lignin with its associated carbohydrate functions as a liquid crystal surfactant. Carbohydrate-stripped lignin is significantly more hydrophobic. This will likely have the benefit of decreasing water sorption, but requires reformulation of the alloying polymers and plasticizers used in the lignin blend.

To minimize use of materials, fiber blends are currently being evaluated using a bench-scale melt extruder and winder.

Fiber Graphitization

As shown by wide-angle X-ray scattering, lignin-based fibers form graphene crystallites at temperatures as low as 1200°C. Figure 5 shows a typical wide-angle scattering pattern from a small bundle of carbonized lignin-blend fibers mounted across a pinhole. These data were obtained at the University of Tennessee Central X-ray Diffraction Facility Molecular Metrology Pinhole SAXS System equipped with a 120X, two-dimensional (2-D) detector.

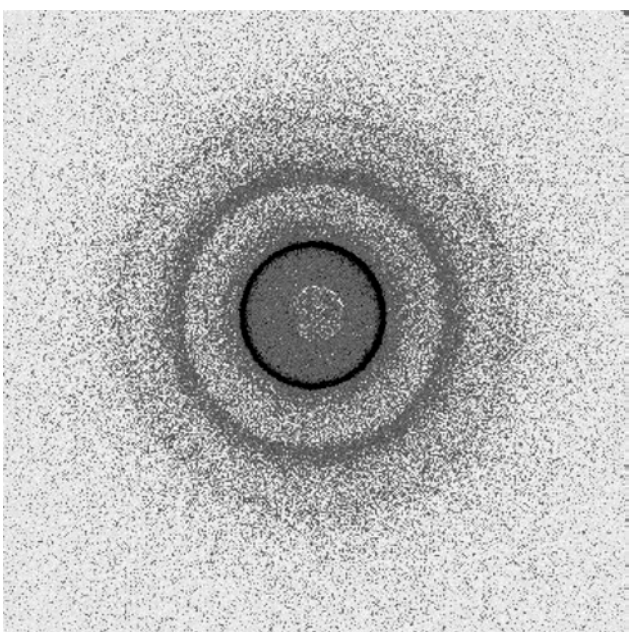

Figure 5. Wide-angle X-ray diffraction pattern showing the presence of graphene crystallites in lignin-based carbon fibers fired to 1200°C.

Future Directions

Significant production of lignin-based multi-filament (28 strand) tow and successful use of this material in small resin-fiber composites was demonstrated in FY 2003. This project was re-proposed and extended to permit evaluation of methods for producing high-quality lignin-based feedstocks for low-cost production of automotive carbon-fiber resin composites.

Having established proof-of-concept, the project staff is systematically addressing the technical issues required to produce industrial-grade, lignin-based carbon fiber at prices and properties meeting automotive need. Because the bulk feedstock used in this process is derived from alkaline (Kraft and soda) pulping, a major concern is developing methods for consistently recovering clean, high-quality lignin low in volatiles, water, particulates, and salts. Additionally, an understanding of the effect of pulping conditions on the molecular weight of lignin will be required to consistently produce industrial-grade carbon fiber and will be evaluated.

The purification and precipitation of carbohydrate and lignin is expected to evolve and improve. The goal is an industrially practicable method that permits one-step carbohydrate stripping and produces a material that can be directly reused in paper manufacture. If only small amounts of flocculants are used and if carbohydrate structure can be preserved, it is likely that the carbohydrate (and associated inorganics) can be directly recycled back to the pulp mill. The carbohydrate, which is primarily hemicellulose, can be used in several ways. First, it can be directly burned for mill energy. Second, it can be incorporated into the pulp produced by its original mill, by mills pulping a different furnish, or by mills pulping recycled fiber. This would be particularly advantageous because it would (1) significantly increase pulp yield and (2) significantly increase the tear and burst strength of papers and boards in which it is incorporated. It would also likely decrease the production cost for purified lignin because it would provide a second revenue stream, minimize waste production, and improve chemical return to the mill.

In addition to techniques for the production of lignin, fiber blends appropriate to the more hydrophobic purified lignin will be evaluated at bench and larger scales.

Spinning die designs for production of lignin-based fibers will be evaluated. Initial tests indicated that dies, similar to those use for spinning pitch-based feedstocks, which provide high shear, create a more uniform internal structure in the raw fiber. Spinning parameters, including rheology, of the blend will be optimized for multifilament production.

Production techniques that provide high-quality, handleable, spoolable, raw lignin-based fiber will be required and are being evaluated. These techniques include selection and evaluation of plasticizers and nucleating agents, as well as raw fiber coatings and oils. Spooling techniques will also be evaluated.

After lignin-based fiber is carbonized, it must be surface treated and sized to increase compatibility with the resin system. Fiber-resin compatibility is particularly critical in automotive applications because the current program plan calls for use of chopped, rather than woven or wound, fiber.

Throughout the period, a variety of analytical techniques, including physical property evaluations of fiber and resin, as well as X-ray diffraction and electron microscopic examination, will be used to assess fiber quality.

As studies proceed, project partners expect to become increasingly involved in research activities. These will include tests of the fiber on a research furnacing line of an industrial partner. In 2006, formal transfer of technology for production of carbon fiber from Kraft lignin-blend feedstocks will be initiated.

Partnerships

A number of different entities have been instrumental in development of this technology. North Carolina State University earlier spun a variety of lignin-blend polymers as single fibers. These were used in initial feasibility evaluations. At present, UT is working to prepare significant quantities of multifilament tow for project use.

Since its inception, this project has benefitted from participation of MeadWestvaco, the dominant domestic lignin producer, which has provided hundreds of pounds of softwood and hardwood lignins, including a wide variety of research lignins, for project use.

In FY 2004, this project attracted interest and participation from three other pulp and paper companies: Weyerhaeuser; Granit, S.A.; and Lignol Innovations. Their participation is broadening the variety of lignins available to the project. As was shown in Figure 2, this facilitates selection of lignins that have better melt spinning properties. Lignins from alkaline (sulfur-free) pulping and the ethanol extracted low-carbohydrate lignin (Lignol Innovations) have the lowest gas evolution. The participation of several lignin producers is welcomed because it improves feedstock selection and will likely increase the amount of carbon fiber feedstock.

Conclusions

In FY 2003, the project was reproposed and in FY 2004, retasked, to focus on larger scale production of carbon fiber precursor feedstocks. Relationships with MeadWestvaco and Eastman Chemical Company were formalized, and two additional pulp and paper companies have joined the project. A third paper company has informally sent significant samples of various black liquors from which lignins can be prepared.

During preparation of small lignin fiber tow, the project staff found that a combination of particulates in lignin and evolution of gas from lignin during spinning were significant problems. During this period, methods for addressing both of these concerns with technologies that can be used at industrial scale were developed. Carbohydrate, in the form of cellulosic polysaccharides that coprecipitate with lignin, was determined to contribute significantly to evolution of gas during spinning and also to produce char if held for long periods above 200°C. Carbohydrate-stripped lignins show significantly reduced volatile evolution between 150 and 250°C.

Methods for removal of carbohydrate from black liquor were developed and have been shown to be successful at increasing scale. These methods are industrially tractable. Filter materials that permit the removal of submicron particulates from black liquor were evaluated at bench scale and shown, at larger scale, to be effective in black liquor filtration. The most successful material is polypropylene, which has the additional advantages of acid and alkali resistance and melting below the temperatures at which lignin blends are typically spun.

B. Low-Cost Carbon Fiber Development Program

Program Manager: Mohamed G. Abdallah
Hexcel Corporation
P.O. Box 18748, Salt Lake City, UT 84118
(801) 508-8083; fax: (801) 508-8103; e-mail: mohamed.abdallah@hexcel.com

Project Manager, Composites: C. David Warren
Oak Ridge National Laboratory
P.O. Box 2009, Oak Ridge, TN 37831-8050
(865) 574-9693; fax: (865) 574-0740; e-mail: warrencd@ornl.gov

Technology Area Development Manager: Joseph Carpenter
(202) 586-1022; fax: (202) 586-1600; e-mail: joseph.carpenter@ee.doe.gov
ORNL Technical Program Manager: Philip S. Sklad
(865) 574-5069; fax: (865) 576-4963; e-mail: skladps@ornl.gov

Principal Investigators:
Harini Dasarathy, Carlos Leon y Leon, Stephen Smith, and Brent Hansen

---

Contractor: Hexcel Corporation
Contract No.: 450001675

Objective

- Define technologies needed to produce a low-cost carbon fiber (LCCF) for automotive applications at a cost of $3.00 to $5.00/lb for quantities greater than 1M lb/year. The required carbon fiber properties are tensile strength greater than 400 ksi, modulus greater than 25 Msi, and strain-to-failure greater than 1%.

Approach

- Develop new precursors that can be converted into carbon fiber at costs below the costs of current processes.
- Explore processing by methods other than thermal pyrolysis.
- Develop technologies leading to significant improvements in current production methods and equipment.
- Develop alternative methods for producing carbon fiber from pitch, polyacrylnitrile (PAN), or other precursors.
- Reduce precursor cost by the use of commercially available energy-efficient precursors and high conversion yields.
- Improve precursor production economies of scale and throughput.
- Introduce novel LCCF production methods.

Accomplishments

- Evaluated proposed research areas through laboratory trials and refinement of manufacturing cost analyses:
  - PAN-based precursors: large-tow benchmark, commodity textile acrylic tow, chemical modifications, acrylic fibers spun without solvents, and radiation and nitrogen pretreatment of PAN-based materials.
  - Precursors other than PAN: polyolefins—polypropylene (PP), linear low-density polyethylene (LLDPE) and high-density polyethylene (HDPE); polystyrene; and polyvinyl chloride (PVC) pitch.

- Scaled-up promising technologies to pilot line trials.
- Assessed the technical and economic feasibility of the proposed research areas.
- Down-selected the most promising technologies to meet the program objectives:
  - Commodity textile acrylic tow with chemical modification or radiation pretreatment.
- Developed detailed manufacturing cost models for the downselected technologies.
- Completed the engineering feasibility studies for large-scale production line.
- Completed the economic analysis to predict product production costs.
- Awarded a short-term (1-year) project to develop carbon fiber roving for the P4 process to meet the immediate needs of the Automotive Composites Consortium (ACC) development programs.
- Completed the program final report for Phase I project.
- Revised the Statement of Work (SOW) for a proposed long-term (3-year) follow-on project to distinguish development tasks from scale-up tasks and to reflect the cost sharing by Hexcel in the requested funding. The follow-on project is built on the results of the current LCCF project to develop product forms from commodity textile-acrylic-based carbon fiber for the ACC programs [under review by Oak Ridge National Laboratory (ORNL)].

Future Direction

- Start working on the proposed long-term Phase II project.
  - Long-term (3-year) program to build on the results of the LCCF program to develop product forms from commodity textile-acrylic-based carbon fiber for the ACC programs.
  - Support requests by ORNL and ACC development programs.

Introduction

The goal of this project is to define and demonstrate technologies needed for the commercialization of low-cost carbon fibers (LCCFs) to be used in automotive applications. Lighter-weight automotive composites made with carbon fibers can improve the fuel efficiency of vehicles and reduce pollution. For carbon fibers to compete more effectively with other materials in future vehicles, their cost must be reduced. Specifically, this program targets the production of carbon fibers with adequate mechanical properties, in sufficiently large quantities, at a sustainable and competitive cost of $3 to $5/lb.

Project Deliverables

At the end of this multiyear program, technologies for LCCF production will be defined. This definition will include the required materials and facilities and will be supported by detailed manufacturing cost analyses and processing cost models. Laboratory trials and pilot-scale demonstrations will be performed to support the defined technologies.

Planned Approach

This project was divided into two phases:

Phase I: Critical review of existing and emerging technologies, divided into two tasks:

Task I.1. Literature review and market analysis.

Task I.2. Laboratory-scale trials and preliminary LCCF manufacturing cost assessments of the proposed technologies. Phase I led to further refinement and down-selection of the most promising technologies for Phase II.

Phase II: Evaluation of selected technologies using pilot-scale equipment and cost models. Phase II was divided into three tasks:

Task II.1. Pilot-scale design for the evaluation of selected LCCF technologies. This included modifications of a polyacrylonitrile (PAN) spinning pilot line and two different carbon fiber conversion lines (a single-tow research line and a multitow pilot line) and the construction of continuous sulfonation processing equipment.

Task II.2. Experimental evaluation of down-selected LCCF technologies, including commodity textile-tow PAN (with chemical modification and radiation and/or nitrogen pretreatment) and polyolefins linear low-density polyethylene [(LLDPE) and polypropylene (PP)].

Task II.3. Large-scale feasibility study of selected LCCF technologies.

Conclusions of FY 2001 Results

(October 1, 2000 to September 30, 2001)

1. Further work on acrylic fibers spun without solvents, plasticized PAN, polyvinyl chloride (PVC), and polystyrene were halted because of technical, environmental, and cost issues.
2. The following most promising LCCF technologies for Phase II were evaluated and selected: commodity textile PAN-based precursors (as-received and with pretreatment using chemical modification, radiation, and nitrogen prestabilization technologies) and polyolefin precursors (LLDPE and PP).
3. A large-tow PAN precursor technology benchmark was used as a metric to evaluate the proposed technologies in terms of their potential to meet the LCCF program's cost targets. The difference between commodity textile PAN and large-tow precursor, based on carbon fiber cost, is approximately $1.80 vs $3.10/lb.

Conclusions of FY 2002 Results

(October 1, 2001 to September 30, 2002)

1. Demonstrated the technologies for using chemical modification and radiation pretreatments of commercial commodity textile (28K) tow to produce LCCF that meets the project targeted properties and estimated cost predictions.
2. Developed manufacturing recipes for the conversion of commodity textile acrylic fibers into LCCF, using the technologies of chemical modifications and radiation treatments.
3. Developed estimated carbon fiber cost projections using chemical modification and radiation pretreatments of commercial commodity textile acrylic fibers.
4. Demonstrated the conversion of LLDPE to LCCF that meet the targeted properties and estimated cost predictions. Due to the issues of sulfuric acid recycling and the available precursor, we concluded that the LLDPE-based technology would need more development efforts to compete with modified textile PAN-based technologies.
5. Commenced the engineering feasibility study of the production lines to produce LCCF based on commodity textile acrylic PAN using chemical modification and radiation pretreatment technologies.
6. Started the plans and statements of work (SOWs) for the long-term and short-term follow-up projects.
7. Updated and refined cost models to reflect the accomplishments in FY 2002.
8. Produced four papers [three published during Society for the Advancement of Material and Process Engineering (SAMPE) 2002, in Baltimore, Maryland, and one for the Global Outlook for Carbon Fiber 2002, in Raleigh, North Carolina] and a presentation during SAMPE 2002, in Long Beach, California.

Conclusions of FY 2003 Results

(October 1, 2002 to September 30, 2003)

1. We completed Task II.3, the large-scale feasibility study, for the selected technologies and the economic analysis for predicting product costs, based on subscale work done during this project using textile acrylic fiber, either chemically modified in an acrylic fiber manufacturing process or using radiation pretreatment in-line with the carbon fiber process.
2. We proposed a follow-on project built on the current project's results with the following goals:
   - Scale-up and verify the defined technologies.
   - Define product forms.
   - Develop and implement techniques to manufacture product forms.
   - Integrate results in ongoing automotive research with other activities by Department of Energy (DOE)/Oak Ridge National Laboratory (ORNL) and U.S. Council for Automotive Research (USCAR)/ Automotive Composites Consortium (ACC).

Conclusions of FY 2004 Results

(October 1, 2003 to September 30, 2004)

During this period we developed and completed two short-term projects for manufacturing and delivering carbon fiber roving to meet the immediate needs of the ORNL and ACC development programs for the P4 process. The first project was the manufacturing of 500 kg of AS4C-1925 (1.0%) 36K (12 × 3K). The second project was the spinning and manufacturing of 7 rovings of AS4C-1925 36K made from 0.5K, 1.0K, 1.5K, 3.0K, 3K, 6K, and 12K subtows (50 kg each).

The first project proved to be more time-consuming. This project turned out to be more difficult than expected due to problems experienced winding the 12 individual 3K tows to a single winder. The fiber was produced on the carbon fiber Pilot Line by running the AS4C 3K fiber through a sizing bath, then bundling the individual tows together, and collecting them as a 36K tow made up of 12 individual 3K tows. After a large amount of effort, the required 200 spools of 2.5 kg each were produced. A summary of the test results is shown in Table 1.

For the second project 500H (holes) and 1000H spinnerets were ordered. The 0.5K, 1.0K, 1.5K, and 3.0K PAN fibers were spun on the production line at Hexcel facilities in Decatur, Alabama. Then, 0.5K, 1.0K, 1.5K, and 3.0K fibers were converted to carbon fiber on Fiber Line 4 at Hexcel Carbon Fiber facilities in Salt Lake City, Utah (Table 2). The 3K, 6K, and 12K fibers were collected by running through a side-sizing bath during standard AS4 fiber production. The fibers were sized using 1925 size at 1.0% and collected on center pull cores into 72 × 0.5K, 36 × 1.0K, 24 × 1.5K, and 12 × 3.0K made from experimental PAN, and 12 × 3K, 6 x 6K, and 3 × 12K made from commercial PAN. The operability was good except for the 0.5K fiber. Also, the properties of the fiber were very good. The required numbers of spools were produced. A summary of the fiber properties is shown below.

Table 3 gives the fiber shipped to the National Composites Center (NCC).

These fibers were used for some pre-production trials and then in July 2004 were used to make flat panels for physical and mechanical testing. This work was directed by Jeff Dahl of Ford Motor Company. In September 2004, we received some results from the testing that had been done. A chart of the tensile strengths of the panels for the different fiber types is presented in Figure 1.

Table 1. Test results

Fiber lot No.	ST03026
Fiber density, g/cm^3	1.790
Fiber MPUL, g/m	0.201 (3K) 2.412 (36K)
Sizing content, %	1.01
Tow tensile strength, ksi	634
6-1 tow tensile modulus, Msi	32.8
Tow tensile elongation, %	1.76

Table 2. Line 4 run of P4 fiber—lot No. 2622-4A, AS-1925 36K

PAN filament count Lab request No.	**0.5K** D0245	**1.0K** D0246	**1.5K** D0237	**3.0K** D0248	**Std. ESAF 6K** D0256
Fiber density, g/cm^3	1.784	1.787	1.787	1.787	1.782
Fiber MPUL, g/m	0.2143	0.2222	0.2213	0.2188	0.7786
Sizing content, %	1.07	0.95	0.91	0.95	1.17
Tow tensile strength, ksi	638	642	635	653	661
6-1 tow tensile modulus, Msi	35.2	33.9	33.4	33.7	34.0
Tow tensile elong., %	1.69	1.74	1.75	1.78	1.78

Notes: (1) Tows bundled to 3K for testing (1 × 3.0K, 2 × 1.5K, 3 × 1.0K, 6 × 0.5K); (2) bundles for some of the 0.5K and 1.0K tows were not quite 3K; (3) standard ESAF 6K PAN was bundled to 12K before sizing. MPUL = mass per unit length.

Table 3. Test results

Fiber lot No.	Fiber type designation	Number of spools	Total weight (lb)	Total weight (kg)
2622-4A	AS-1925 36K (72 × 0.5K)	23	112.2	50.9
2622-4A	AS-1925 36K (36 × 1.0K)	23	140.8	63.9
2622-4A	AS-1925 36K (24 × 1.5K)	29	174.0	78.9
2622-4A	AS-1925 36K (12 × 3.0K)	28	172.9	78.4
2684-5E-P4	AS-1925 36K (72 × 0.5K)	21	102.7	46.6
2674-5E-P4	AS-1925 36K (12 × 3K)	29	155.7	70.6
26712-7J-P4	AS-1925 36K (6 × 6K)	30	142.0	64.4
	Total	183	1000.3	453.7

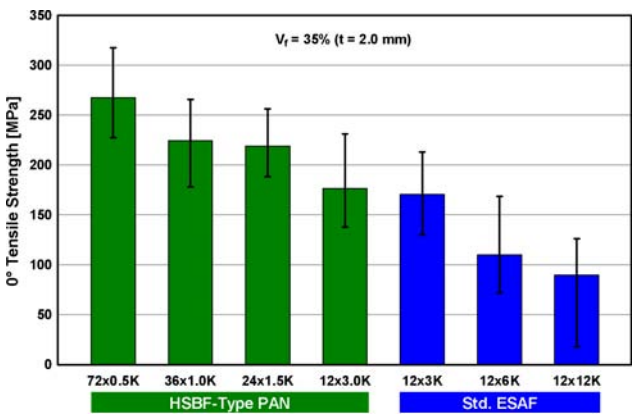

Figure 1. Tensile strength of different fiber types.

Figure 1 shows much higher tensile strength measured for panels made using the smallest filament bundle counts. The differences are quite dramatic, with the tensile strength of the 72 × 0.5K fiber being nearly three times greater than the tensile strength of the 3 × 12K fiber. While some differences were expected between the fiber types, this magnitude of difference was surprising. The differences are thought to be due to the quality of the composites made and the more uniform distribution of reinforcing filaments resulting from using the small bundle count fibers.

We completed an order for oxidized PAN fiber that was requested by ORNL. Three sets of four 2.3-lb spools were shipped to ORNL. Spools of partially oxidized fiber were collected on Line 4 and sent to ORNL to support its advanced oxidation project. ORNL had requested fiber with specific oxidized density ranges. A winder was placed at these locations and fiber collected. Four spools were collected at each location; each spool was about 2.3 lb.

Sample No.	Oxidation density
11365-54-1	1.245
11365-54-2	1.293
11365-54-3	1.335

The following is a summary of the efforts during this reporting period.

1. We completed the two short-term projects for manufacturing and delivering carbon fiber roving to meet the immediate needs of the ACC development programs.
2. We participated in meetings with Meridian Automotive systems, National Composites Center (NCC), ACC to provide input on the LCCF program status and LCCF applications for development programs that are supported by ORNL and DOE.
3. We are participating in the Delphi's Advanced Composite Support Structures (ACSS) Program. This is the development program for cross-members for Class-7 and -8 trucks. Our tasks are to support the program in material requirement and to advise based on Hexcel past experiences from the lessons that Hexcel gained in the development of the rails for Class-7 and -8 trucks.
4. We developed and provided partially oxidized PAN fiber to ORNL to support the microwave research efforts at ORNL.
5. We requested and we were granted a no-cost extension by ORNL.
6. We completed and submitted the mid-year and quarterly reports as requested by ORNL.
7. We completed and submitted the current project final report to ORNL in September 2004.

8. Based on the submittal of the initial follow-on project proposal, ORNL, after reviewing the Kline Report (see 4.B) and consultation with the material technology team, decided to consider the follow-on project. Therefore, we revised and submitted the SOW for the proposal to reflect the request by ORNL for cost sharing.

Final Report Executive Summary

In October 1999 the U.S. Department of Energy's Office of Transportation Technologies (DOE-OTT), through the Oak Ridge National Lab (ORNL), awarded Hexcel Corporation a multiyear contract to define and develop technologies needed for the commercialization of low-cost carbon fibers (LCCFs). The goal of the technical evaluation was to demonstrate a technology suitable for the commercial manufacture of $>10^6$ lb/year (>455 MT/year) of LCCFs with adequate mechanical properties for lighter weight, energy-saving automotive composite applications. Specific LCCF program targets follow:

- tensile strength > 2,800 MPa (400 ksi);
- tensile modulus > 172 GPa (25 Msi);
- strain to failure > 1%; and
- market price = $6.60 to $11/kg ($3 to $5/lb).

To meet the LCCF program targets, Hexcel developed a multistep, risk-mitigating approach (Phase I) that addressed three areas:

1. Identification of precursors and technologies that may lead to significant reductions in current carbon fiber production costs;
2. Demonstration of the selected technologies at research-scale and pilot-scale levels; and
3. Large-scale engineering feasibility studies of the technologies deemed most likely to meet LCCF targets.

A follow-up project would build on the results of this first project to develop production technologies and specific product forms required by DOE/OTT and various automotive manufacturers (USCAR/ACC).

Extensive internal and external literature searches uncovered a large number of materials and conversion technologies that could serve as potential LCCF development routes. The technologies identified fell in two broad categories: (1) those based on the use of polyacrylonitrile (PAN); and (2) those using polymer/precursor materials other than PAN. Among PAN-based routes, the use of low-cost textile acrylic fibers as LCCF precursors provided the most viable pathways. Among non-PAN-based routes, technical and cost considerations narrowed the choices to four candidates: polyethylene, polypropylene, polystyrene and polyvinyl chloride.

Research-scale trials and preliminary cost model estimates led to three viable routes for the development of continuous-tow LCCFs with mechanical properties meeting LCCF targets:

(1) Chemical modification of textile acrylic fibers. Uncollapsed textile acrylic fiber gels are exposed to an aqueous NaOH solution during the spinning process to induce functional group hydrolysis and hence speed up the stabilization process.

(2) Radiation pretreatment of textile acrylic fibers. This involves exposing textile acrylic fibers to an E-beam radiation dose of 30 Mrad prior to oxidation to induce stabilizing cyclization reactions.

(3) Sulfonation of polyethylene fibers. Commercial polyethylene fibers pass through a bath of hot concentrated sulfuric acid in order to induce cross-linking reactions that render the fibers infusible and carbonizable.

The technical viability of the textile acrylic fiber-based technologies was also demonstrated through pilot-scale experiments. Large-scale engineering feasibility studies defined manufacturing facility and processing costs needed to make 1,820 MT/year (4×10^6 lb/year) of LCCF in two carbon fiber production lines. Detailed economic analysis indicated that the carbon fiber manufacturing cost could be reduced from ~$13.20/kg (~$6.00/lb) for large tow textile PAN to ~$9.9/kg (~$4.50/lb) with either chemical or radiation pretreatments. These mill cost estimates are based on standard carbon fiber manufacturing model parameters, and exclude any return-on-investment (ROI). Should ROI be included, additional processing improvements would be needed to reach the LCCF cost targets in an economically sustainable manner.

Future Work

We will begin work on the proposed follow-on project when it is approved by ORNL. It is built on the results of Hexcel's LCCF current project with the following objectives: (1) scale-up and verify the defined technologies and (2) integrate into ongoing

automotive research activities by DOE/ORNL and USCAR/ACC. The goals of this future work follow.

1. Develop plans for integration of ongoing development activities that include the following subtasks: define requirements, finalize integration plans, and review and approval by all parties.
2. Scale-up and verification of chemical modification technology from the current project that includes the following subtasks: modification of textile acrylic fiber line at Sterling, verification of scaled-up chemical modification process, modification of carbon fiber pilot line at Hexcel, and verification of conversion of chemically modified acrylic tow.
3. Development of carbon fiber products forms that include the following subtasks: develop precursor materials for microwave processing, develop techniques to split textile acrylic tow, develop splitting techniques during/after carbon fiber conversion, and develop methods for manufacture of specific product forms such as chopped fiber, prepreg, fabric, and P4 roving.

A plan that addresses the above goals into three major tasks was developed. The following is a summary of these tasks.

LCCF Development Program—Follow-on; Major Tasks and Milestones

The major tasks and milestones are planned to provide the following:

1. Precursor fiber and carbon fibers for various applications as required by ORNL; for example, such as, precursor fiber for oxidation studies and oxidized/stabilized precursor for microwave processing.
2. Carbon fiber of various forms: continuous tow, chopped fiber, prepreg, woven fabric, and roving for P4 process for various automotive applications.

Three major tasks are outlined to meet the goals and objectives. The following are the tasks and milestones.

Task 1. Develop Plans for Integration of Ongoing Development Activities

The objective of this task is to develop the plans to integrate the SOW of this proposal with ongoing research activities by ORNL and ACC. In this task, the quantities, requirements, and specifications of various product forms will be identified and verified to meet the needs of ACC/ORNL development programs.

The following are the milestones for Task 1.

Task 1.1. Develop a Draft of the Integration Plans

The goal is to develop plans to assure that the needs of providing precursor materials and carbon fibers will meet the requirements of ongoing development work by ORNL and ACC. These plans will be developed first and approved by the all parties before commencing Task 2 and Task 3 of the proposal. The first step in developing the integration plan is defining the requirements.

Task 1.2. Define Requirements

First, the requirements for precursors and carbon fiber to meet the needs of the ongoing research activities by ORNL and ACC will be defined. These requirements will address the identification and specifications of the following materials forms:

1. Precursors for oxidation studies and oxidized/stabilized precursors for microwave processing.
2. Carbon fiber product forms (continuous, chopped, roving, etc.) for the automotive industry that includes surface treatment, sizing systems for above product forms, and make-up and packaging.

Task 1.3. Finalize Integration Plans

In this subtask the drafted integration plans will be provided to team members for review and comments before a formal presentation and review meeting.

Task 1.4. Review Meeting

Task 1 will be concluded with a review meeting of the team members for approval of the integration plans and the detailed SOW for Task 2 and 3. This will give the “green-light” for commencing Task 2 for the scale-up and verification of the chemical modification technology from the current project, and Task 3 for the development of the product forms for automotive applications.

Task 2. Scale-up and Verification of Chemical Modification Technology

Task 2 objectives are the scale-up demonstration and verification of production technologies for producing the textile fiber with chemical modification and the conversion into carbon fibers.

Task 2.1. Modification of Textile Acrylic Line (Sterling)

This subtask consists of the modification of Sterling's textile line to implement and incorporate the application of chemical modification in-line. Within the scope of this task, the engineering design requirement for installation will be developed, and modification equipment will be integrated in the line before verification and scale-up trials run are performed.

Task 2.2. Verification of Scaled-up Chemical Modification Process

Once the modification of the textile line is completed, and equipment is debugged to ensure operational performances, the next step is to verify scale-up of the chemical modification processing on the large textile fiber. Several trials will be performed to verify processing conditions, develop manufacturing procedures, and to manufacture materials for conversion into carbon fiber at Hexcel facilities.

Task 2.3. Modification of Carbon Fiber Pilot Line (Hexcel)

In a parallel effort, modifications of Hexcel's Carbon Fiber Pilot Line (which is a semiproduction line) will be implemented to handle textile acrylic fiber. Equipment operational and processing procedures will be developed for the conversion of the chemically modified textile fiber to carbon fiber.

Task 2.4. Verification of Conversion of Chemically Modified Acrylic Tow

Once the implementation and the equipment modifications at the two facilities are completed, verification trials will be performed to establish the operating procedures for conversion of the chemically modified textile fiber at Sterling facilities into carbon fiber at Hexcel facilities. First, the converted carbon fiber will be characterized to verify that it meets the mechanical and physical properties established in the current project.

Task 2 will include preproduction verification trials to ensure that the scale-up process produces modified textile and carbon fibers that will meet the objectives and requirements for Task 3, the development of carbon fiber product forms.

Task 3. Development of Carbon Fiber Product Forms

Task 3 objectives will be planned and directed based on the integration plans that were developed and approved by the team members in Task 1. The scope for Task 3 will include the development and providing of textile precursor fiber and carbon fiber for the integration into ongoing activities by ACC and ORNL. Precursor fibers will be manufactured to support ongoing research activities for oxidation studies and oxidized/stabilized precursors using microwave processing. Carbon fiber products of various forms such as continuous tow, chopped fiber, prepreg, woven fabrics, and roving for P4 process are expected to be supplied to support development activities for automotive components as defined in Task 1. The development of splittable tow to produce carbon fiber roving for the P4 process will be the major effort in this task. The results of the ongoing evaluation of various roving configurations for the P4 process will guide the carbon fiber roving development effort in this task. The following are the milestones for Task 3.

Task 3.1. Develop Precursor Materials for Microwave Processing

Based on the conclusion of the integration plans of Task 1, the requirements (quantities, forms) of the textile fiber for the microwave processing will guide the scope of work for this subtask. Precursor materials will be manufactured at Sterling, and any other preprocessing (stabilization) will be performed by Hexcel to meet ORNL requirements. The scope of this subtask will be developed and defined for integration into ongoing research activities for oxidation studies and oxidized/stabilized precursors for microwave processing as would be required by ORNL. This subtask may depend on the next subtask efforts of developing techniques to split textile acrylic tow.

Task 3.2. Develop Techniques to Split Textile Acrylic Tow

Subtask 3.2 will focus on developing technology to split large textile acrylic tow into small tows that may meet some of the product forms requirement as defined in Task 1. The challenge in this subtask is the feasibility of integrating precursor tow splitting technologies within the precursor manufacturing process and equipment. Equipment configurations and processing methods will put constraints and limitations on the tow size that can be achieved. Hexcel will work with Sterling Fiber to direct, develop, and plan these efforts. The results of subtask 3.2 will have a direct impact on the efforts in subtask 3.1 and subtask 3.3

Task 3.3. Develop Splitting Techniques During/After Carbon Fiber Conversion

Depending on the results of subtask 3.2 and requirements for the products forms as defined in Task 1, the scope of this subtask will be defined in order to develop technologies and methods for splitting tows during/after carbon fiber conversion. The requirement for the specific automotive carbon fiber products forms (subtask 3.4) will direct the scope of work for subtask 3.3.

Task 3.4. Develop Methods for Manufacture of Specific Carbon Fiber Product Forms (Chopped Fiber and Prepreg, Fabric, P4 Roving)

This subtask will concentrate on the development of methods for manufacturing carbon fiber for specific automotive carbon fiber products forms such as continuous tow, chopped fiber, prepreg, woven fabrics, etc. The defined/selected carbon fiber product forms (Task 1) for automotive applications will focus the scope of this subtask and the technology development for splitting the modified textile tow during/after carbon fiber conversion. Textile and carbon fiber conversion trials will be performed to manufacture the specific carbon fiber product forms to meet the integration plans as will be defined in Task 1.

The SOW and the estimated request for funding proposal for the follow-on project, including the cost share by Hexcel, were revised and submitted to ORNL for consideration and evaluation. The proposal is for 3 years. Hexcel planned this follow-on project scope based on input and results of the joint working relationship with Sterling Fiber of Pace, Florida, during the LCCF project. [Editor's note: In December 2004, DOE and ORNL decided not to pursue the follow-on project at this time and to concentrate DOE's funding of the longer-term higher-risk but potentially lower-cost option discussed in 5.A.]

C. Low-Cost Carbon Fiber Manufacturing Using Microwave Energy

Principal Investigator: Felix L. Paulauskas
Oak Ridge National Laboratory
Oak Ridge, TN 37831-8048
(865) 576-3785; fax: (865) 574-8257; e-mail: paulauskasfl@ornl.gov

Project Manager, Composites: C. David Warren
Oak Ridge National Laboratory
P.O. Box 2008, Oak Ridge, TN 37831-6065
(865) 574-9693; fax: (865) 576-4963; e-mail: warrencd@ornl.gov

Technology Area Development Manager: Joseph A. Carpenter
(202) 586-1022; fax: (202) 586-1600; e-mail: joseph.carpenter@ee.doe.gov
Field Technical Manager: Philip S. Sklad
(865) 574-5069; fax: (865) 576-4963; e-mail: skladps@ornl.gov

Participants
Terry L. White, Oak Ridge National Laboratory
Kenneth D. Yarborough, Oak Ridge National Laboratory
Professor Roberto Benson, University of Tennessee

Contractor: Oak Ridge National Laboratory
Contract No.: DE-AC05-00OR22725

Objective

- Investigate and develop a microwave-assisted technical alternative to carbonize and graphitize polyacrylonitrile (PAN) based precursor.
- Prove that carbon fiber with properties suitable for use by the automotive industry can be produced inexpensively using microwave-assisted plasma (MAP) processing.
- Demonstrate that MAP processing can produce acceptably uniform properties over the length of the fiber tow.
- Show that for specified microwave input parameters, fibers with specific properties may be controllably and predictably manufactured using microwave furnaces.
- Demonstrate the economic feasibility for producing approximately 30-Msi modulus fibers at a significant cost reduction relative to those produced conventionally.

Approach

- Demonstrate the ability to deliver high fiber mass throughput by increasing line speed and tow count.
- Conduct parametric studies on the continuous carbon-fiber processing pilot unit to continually improve the system design, process parameters, and fiber properties.
- Characterize MAP-processed carbon fibers to confirm that they satisfy program requirements.
- Continually evaluate, develop, and characterize “spin-off” technology, hardware, and ideas that improve upstream or downstream processing, or facilitate more efficient utilization of fiber.

Accomplishments

- Carbonized 50 K PAN fiber tows successfully at three-tow line speeds up to 13 in./min.
- Determined that improved generator matching and longer plasma length are needed to increase line speed beyond 13 in./min; designed and procured the necessary hardware.
- Investigated the effects of varying fiber tension during carbonization.
- Commenced surface treatment studies in which initial results suggest that MAP-carbonized fibers may accept a higher level of surface treatment than conventionally carbonized fibers.
- Co-authored two papers for 2004 SAMPE Symposium and Exposition, and the principal investigator was the lead author on the 2004 SAMPE Symposium's Outstanding Technical Paper.

Future Direction

- Increase 3-tow line speed to 40 in./min.
- Continue parametric studies and fiber characterization to better understand process effects and processing window and to quantify fiber properties.
- Achieve integration with other carbon-fiber technology developments, for example, new precursors, rapid oxidation/stabilization processes, advanced surface treatment, advanced downstream formatting, and/or component manufacturing processes.
- Develop and demonstrate related technologies in the area of carbon-fiber manufacturing (e.g., advanced characterization, surface treatment, sensing and control technology, recovery and reuse) as resources and time permit.
- Develop partnership(s) to commercialize the technology.

Introduction

The purpose of this project is to investigate and develop a microwave-assisted technical alternative to carbonize and partially graphitize the polyacrylonitrile (PAN) precursor. The project is to prove that carbon fiber with properties suitable for use by the automotive industry can be produced inexpensively using microwave-assisted plasma (MAP) processing. It is to be demonstrated that MAP processing can produce acceptably uniform properties over the length of the fiber tow. The project is also to show that for specified microwave input parameters, fibers with specific properties may be controllably and predictably manufactured using microwave furnaces. Lastly, but most importantly, this project is to demonstrate the economic feasibility for producing approximately 30-Msi modulus fibers at a significant cost reduction below those produced conventionally.

Project Deliverables

At the end of this project, a continuous, multiple-tow, scalable, high-production line speed MAP carbon fiber prototype unit will have been developed, constructed, and tested. A final report will be issued with the test results of the carbon fibers processed with this unit. Appropriate industry briefings will be conducted to facilitate commercialization of this economically enabling technology.

Fiber Properties

A key goal of this project is to demonstrate that carbon fibers with satisfactory material properties can be produced by the MAP process. Program goals established for fiber properties are 25-Mpsi tensile modulus, 250-ksi ultimate tensile strength, and 1.0% ultimate strain. Mechanical properties are shown in Figures 1–3. Mechanical property results generally satisfied the specified requirements, except

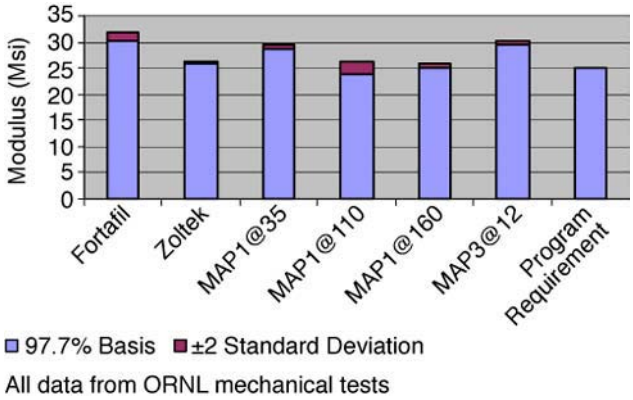

Figure 1. Carbon fiber tensile modulus.

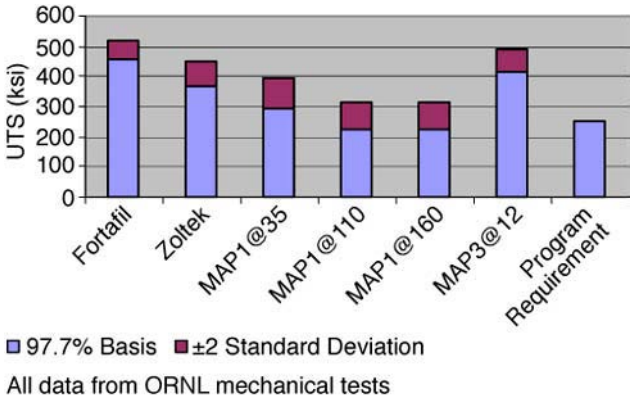

Figure 2. Carbon fiber ultimate tensile strength.

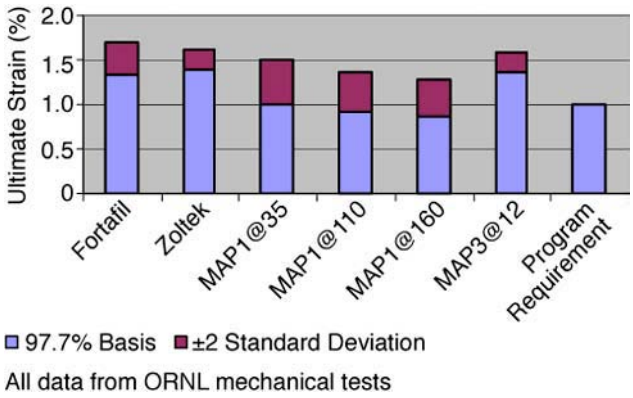

Figure 3. Carbon fiber ultimate tensile strain.

that the ultimate tensile strength was slightly deficient at the highest single-tow line speeds. This is attributed to the fiber transport and tensioning system that was not designed for high line speeds. To resolve this problem, a commercial, high-speed, fiber transport and tensioning system was installed during the upgrade to three-tow capacity.

In Figures 1–3, 97.7% basis means that 97.7% of property data should exceed the indicated value. The 97.7% basis value is the mean less two standard deviations. Labels indicate fiber processing, number of tows, and line speed. For example, MAP3@12 indicates three tows MAP processed at 12 in./min.

Throughput

The economics "figure of merit" is cost per unit throughput. Increasing throughput usually reduces unit cost. Hence the MAP process must be operable at production line speeds and "bandwidth" (number of tows) comparable to or exceeding those of conventional fiber manufacturing lines if it is to realize the desired cost effect. Conventional large-tow carbon fiber manufacturing lines normally run at line speeds in the 90- to 120-in./min range, with about 100 tows per line (a typical line is rated at nominally 1M lb/year when processing 50 K tows).

The researchers have previously demonstrated single-tow operation at line speeds to 200 in./min. The present focus is to achieve high line speed with a three-tow line configuration. Maximum three-tow speed achieved to date was 13 in./min. The limiting factors appear to be generator matching and plasma length. Higher power will be required to run at higher speeds, but raising the power has produced arcing in the waveguide system. Improved generator matching should resolve this problem. Also, the current configuration produces a compact plasma (short length), which results in a severe processing gradient. A simple applicator modification was tried, but it lengthened the plasma by only a small amount.

A major applicator modification is under way, based on scalable mathematical and physical simulations that correlated satisfactorily. The applicator was completely redesigned, and the design was verified by simulation on the subscale physical model shown in Figure 4. Upon completion, the modified applicator should lengthen the plasma processing region by ~6X. New hardware was fabricated and delivered during the last half of FY 2004 and is now ready for assembly.

Parametric Studies

The fiber properties are affected by many processing parameters such as temperature, pressure, power, plasma density, line speed, and tow tension.

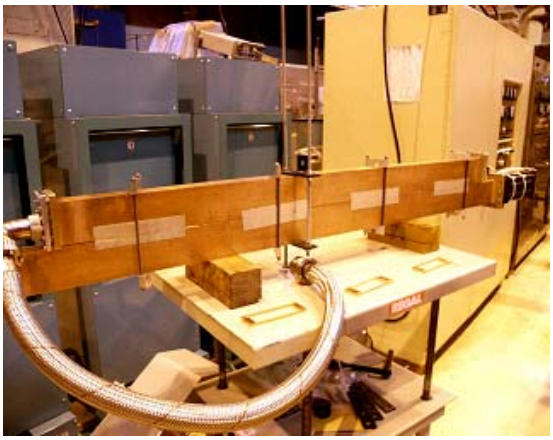

Figure 4. Subscale applicator simulation hardware.

During FY 2004, the effects of tow tension were investigated. The results are not published for patent protection and export control purposes.

Surface Treatment

MAP carbonized fibers were ozone surface treated by the same process as conventionally carbonized fibers. The MAP carbonized fibers consistently exhibited 75%–80% higher concentration of oxygen on the surface than did conventionally carbonized, commercial-grade fibers.

Economics

During FY 2004, Kline and Company completed a cost study of the Department of Energy's (DOE's) entire carbon fiber development program, estimating profitable selling prices for baseline technology and determining if various technologies under development were implemented. Kline's estimates generally indicated that MAP carbonization and graphitization should reduce the fiber selling price by about 10%. These estimates, however, were based on a line speed comparable to that of conventional conversion lines. Rough calculations suggest that if we can achieve much higher line speeds, the savings could increase dramatically. We have not discovered any inherent physics limits that would prevent us from achieving a large increase in conversion line speed using plasma oxidation and MAP carbonization.

Education

The materials characterization, notably utilizing scanning electron microscopy (SEM) and spectroscopy methods such as x-ray photoelectron spectroscopy (XPS), has been conducted in partnership with the University of Tennessee's Materials Science Department. A doctoral candidate provided characterization support to the project. This work forms the basis of her doctoral thesis.

Conclusions

The development of MAP carbonization and graphitization technology has progressed well. Fiber properties have generally satisfied or exceeded targets, and the process knowledge database continues to grow. The three-tow line has been operated at 13 in./min, with modifications underway that should enable operation at 40 in./min or higher line speed.

Presentations and Publications

1. F. L. Paulauskas and T. L. White, "Temperature-Dependent Dielectric Measurements of Polyacrylonitrile Fibers During Air Oxidation," 49th International SAMPE Symposium 2004, May 16–20, 2004, Long Beach, CA (2004).

D. Oxidative Stabilization of PAN Fiber Precursor

Principal Investigator: Felix L. Paulauskas
Oak Ridge National Laboratory
Oak Ridge, TN 37831-8048
(865) 576-3785; fax: (865) 574-8257; e-mail: paulauskasfl@ornl.gov

Project Manager, Composites: C. David Warren
Oak Ridge National Laboratory
P.O. Box 2008, Oak Ridge, TN 37831-6065
(865) 574-9693; fax: (865) 576-4963; e-mail: warrencd@ornl.gov

Technology Area Development Manager: Joseph A. Carpenter
(202) 586-1022; fax: (202) 586-1600; e-mail: joseph.carpenter@ee.doe.gov
Field Technical Manager: Philip S. Sklad
(865) 574-5069; fax: (865) 576-4963; e-mail: skladps@ornl.gov

Participants
Terry L. White and Kenneth D. Yarborough, Oak Ridge National Laboratory
Professor Joseph Spruiell, University of Tennessee
Daniel Sherman, Atmospheric Glow Technologies

Contractor: Oak Ridge National Laboratory
Contract No.: DE-AC05-00OR22725

Objectives

- Develop an improved technique for oxidizing carbon fiber precursor with increased line speed, reduced carbon fiber cost, and reduced equipment footprint.
- Verify that produced fiber properties satisfy automotive and heavy-vehicle manufacturers' requirements.
- Conduct a preliminary evaluation of the new oxidation technique's cost impact.

Approach

- Develop plasma process for oxidation in an atmospheric-pressure plasma reactor.
- Develop fiber handling protocols for continuous processing.
- Conduct parametric studies to correlate processing parameters and fiber properties.
- Characterize fibers to confirm that they satisfy program requirements.

Accomplishments

- Demonstrated the ability, in atmospheric-pressure plasma, to oxidize fiber in stages equivalent to conventional oxidation furnaces.
- Identified key process parameters, critical operating range, and modified the reactor to achieve stable operation in the required parametric space.

- Identified preferred range of feed gas compositions.
- Improved dielectric properties monitoring technology and presented a conference paper on that topic.

Future Direction

- Continue refining the reactor design and processing protocols to achieve rapid, single-stage fiber oxidation.
- Develop "prestabilization" technique.
- Develop continuous processing protocols.
- Conduct parametric studies and fiber characterization to better understand process effects and the processing window and to quantify fiber properties.
- Conduct rate-effect studies and update cost analysis.

Introduction

The purpose of this project is to investigate and develop a plasma processing technique to rapidly and inexpensively oxidize a polyacrylonitrile (PAN) precursor. Oxidative stabilization is a slow thermal process that typically consumes 70% or more of the processing time in a conventional carbon fiber conversion line. A rapid oxidation process could dramatically increase the conversion line throughput and appreciably lower the fiber cost. A related project (5.C) has already demonstrated the potential for greatly increasing line speed in the carbonization and graphitization stages, but the oxidation time must be greatly reduced to fully exploit faster carbonization and graphitization. This project intends to develop a plasma oxidation module that integrates with other advanced fiber processing modules to produce inexpensive carbon fiber with properties suitable for use by the automotive industry. Critical technical criteria include (1) 25-Msi tensile modulus, 250-ksi ultimate strength, and 1.0% ultimate strain in the finished fiber; (2) acceptably uniform properties over the length of the fiber tow; (3) repeatable and controllable processing; and (4) significant unit cost reduction in comparison to conventional processing.

Project Deliverable

At the end of this project, we will have demonstrated satisfactory fiber oxidation in a multiple-tow plasma oxidation module operating at line speed exceeding that typical of conventional carbon fiber conversion lines.

Technical Approach

We are investigating PAN precursor fiber oxidation by "direct exposure" in a nonequilibrium, nonthermal plasma at atmospheric pressure, with the fiber transported through the plasma. Plasma processing is thought to enhance oxygen diffusion and chemistry in the PAN oxidation process. Atmospheric pressure plasma provides better control over the thermal environment and reaction rates than does evacuated plasma, in addition to eliminating the sealing problems accompanying evacuated plasma processing. Various fiber characterization tools and instruments are used to conduct parametric studies and physical, mechanical, and morphological evaluations of the fibers to optimize the process. An evacuated plasma reactor is useful for bench-scale studies because it allows a greater degree of manipulation and control over reactive species and related parameters. Early in the project, processing tests were conducted in an evacuated plasma reactor, and that same reactor is now used for conducting the bench-scale parametric studies.

Atmospheric-Pressure Plasma Processing Results

Exposure in plasma at or near atmospheric pressure provides superior thermal control because the gas flow should convectively heat or cool the fibers. This is deemed particularly important to avoid fiber melting from the exothermic reactions associated with the PAN cross-linking that occurs during stabilization. However, the mean free path of the chemically reactive species is shorter by orders of

magnitude than it is in an evacuated environment, and this makes it very difficult to find a combination of process parameters that will oxidize the fibers with acceptable residence time.

Conventional PAN oxidation is typically accomplished in three or four thermal stages (stages can be physically separate furnaces or zones in a single physical furnace) in air, at temperatures increasing from about 200°C to 250°C. In FY 2004, the researchers demonstrated the ability to reproduce the oxidation advancement in each of conventional furnaces two, three, and four. The virgin PAN is chemically fragile; hence, we have not yet discovered a satisfactory nonthermal processing protocol that reproduces the oxidation advancement in the first conventional furnace. Subsequent experiments have demonstrated the ability to advance the oxidation from the beginning of furnace two through the exit of furnace three in a single, uninterrupted process. These processing results are schematically illustrated in Figure 1.

A potentially very important discovery was that the cores of plasma-oxidized fibers are more chemically stable than are those of conventionally processed fibers. Figure 2 illustrates the advancement of oxidation and stabilization through a filament cross-section. Most of the fiber must be oxidized, as represented by the outer region, before it can withstand carbonization. In thermal oxidation, the outer stabilized and oxidized region grows inward slowly, purely by diffusion. However in plasma oxidation, we have observed that oxidation over the filament cross-section is much more uniform, and the entire fiber becomes highly oxidized at a lower fiber density (fiber density is normally used as an indicator of degree of oxidation advancement). This suggests that plasma oxidation may allow onset of

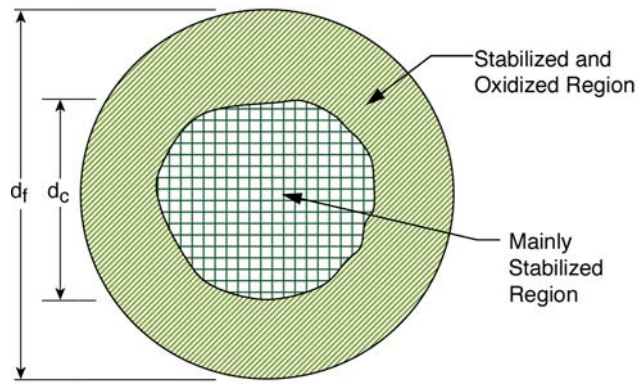

Figure 2. Illustration of advancing oxidation and stabilization through filament cross-section.

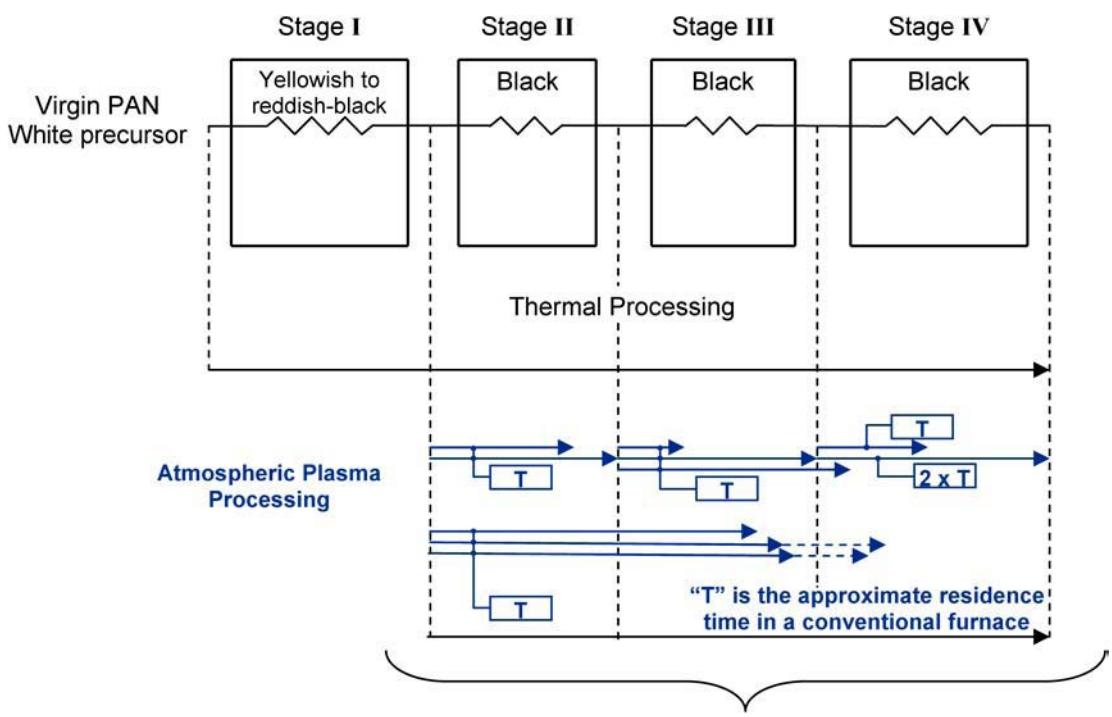

Figure 1. Schematic of conventional thermal oxidation process and progress in plasma oxidation process.

carbonization at a lower fiber density, a thesis that will be experimentally tested in future work. If carbonization can indeed commence at a lower fiber density, this could significantly reduce the residence time required for oxidation.

The researchers have made good progress toward identifying the parameters that most affect the oxidation rate and optimizing those parameters within the reactor. For patent protection and export control reasons, the detailed results are not published but are periodically disclosed to the relevant program managers in oral briefings.

Feed Gas Composition

The researchers investigated the effects of plasma oxidation with various gas compositions. It was confirmed that the chemistry can be quite sensitive to feed gas composition, as illustrated in Figure 3. A wide range of feed gas compositions were investigated and the results recorded. Specific compositions and processing parameters are not published for patent protection and export control reasons.

Instrumentation

During this reporting period, the researchers continued developing techniques and hardware for measuring the fiber dielectric properties over a selected range of oxidation processing conditions. A dielectric measurement system, shown schematically in Figure 4, was validated. Several temperature control problems were identified and corrected by adjusting control and operational parameters, modifying hardware, and changing the PAN cross-section in the instrument chamber. A large number of runs were conducted with PAN partially oxidized to differing degrees. The real and imaginary parts of the dielectric constant correlated well with the degree of PAN oxidation. A paper on this topic was presented at the 2004 SAMPE Symposium and Exposition in Long Beach, California.

The researchers began creating a dielectric properties database for 3k and 80k PAN fiber tows that were partially oxidized in varying degrees by conventional means. Plasma-oxidized fiber properties can later be compared against this database as a selector for fiber specimens that will be further characterized by more time-consuming spectroscopy techniques.

The researchers need a rapid turnaround technique for indicating oxidation trends, to quickly assess whether various parametric processing trials have successfully advanced the oxidation. Density measurements are frequently used by fiber manufacturers. In this project, dielectric measurement

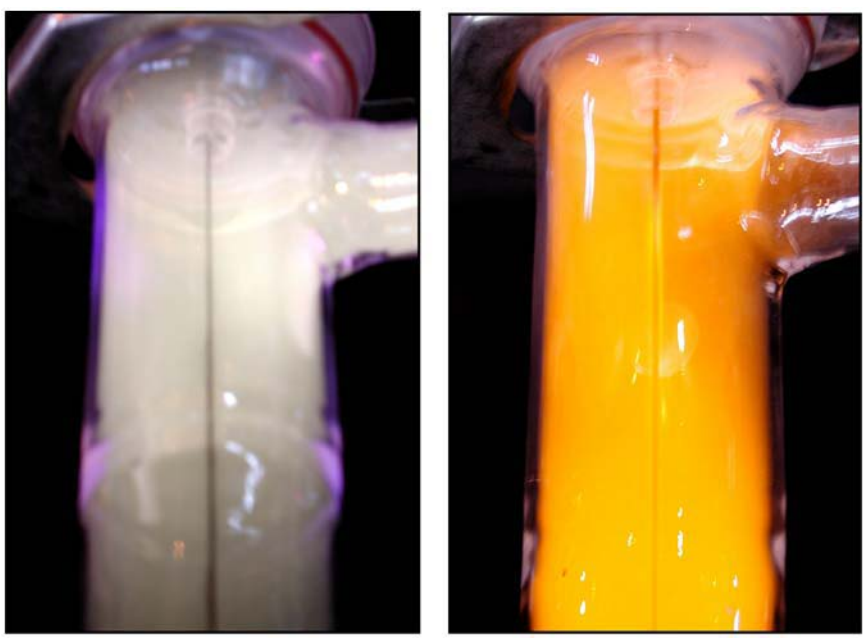

Figure 3. Plasma with two different feed gas compositions in evacuated plasma reactor.

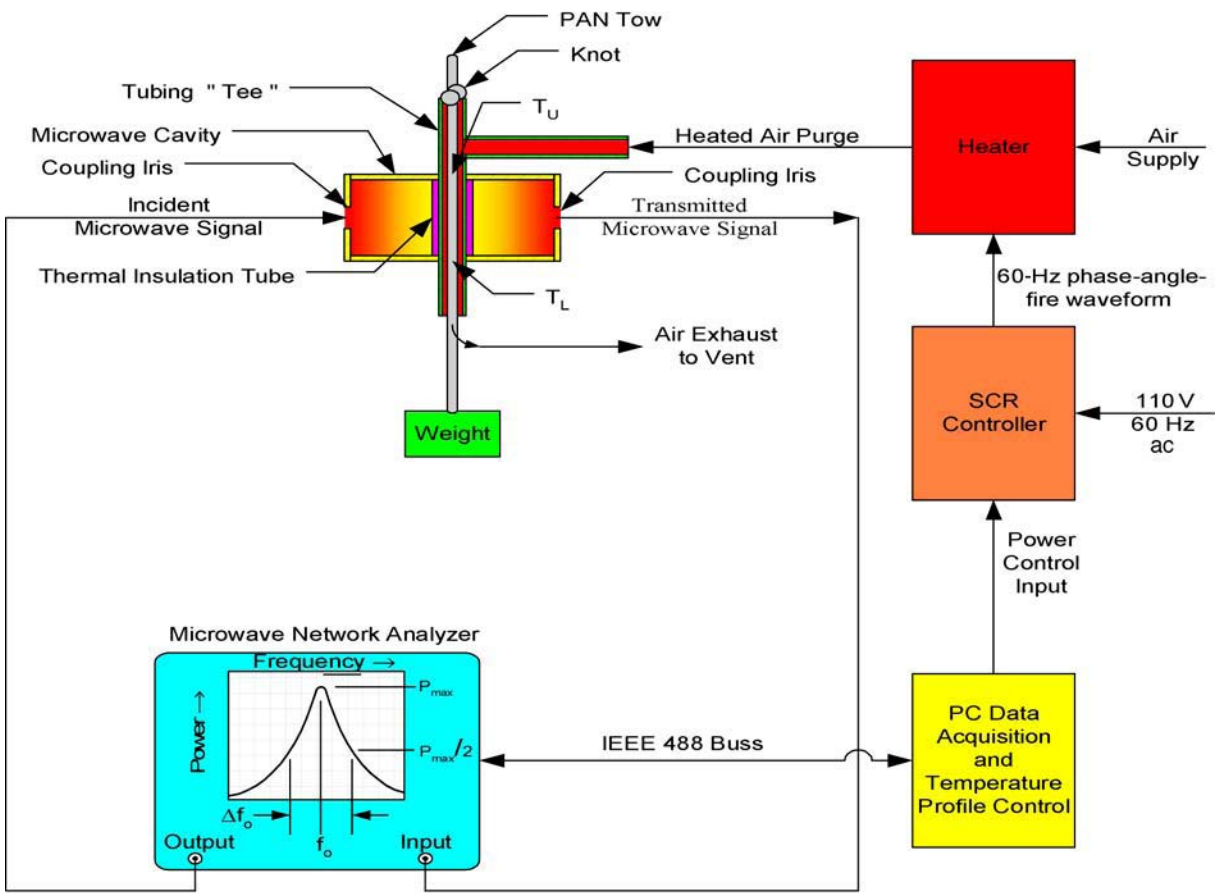

Figure 4. Dielectric measurement system schematic.

equipment and techniques have been successfully developed and validated, and morphology measurements are also used to characterize the fibers. However density, dielectric, and morphology measurements all have turnaround times of hours to days because of measurement duration, instrument cost and location, required operator skill, and/or instrument time-sharing. The fiber changes color, starting from white and successively darkening until it turns completely black after it is about 10–20% oxidized. Therefore, color is a reasonable progress indicator in early oxidation, but another technique is needed for the remainder of oxidation. The researchers investigated direct current (dc) electrical resistance measurement as an oxidation progress indicator. The very high tow resistance (10^{12}–10^{15} Ω) is beyond the capability of most resistance meters and can be accurately measured only under exceedingly well-controlled environmental conditions. A high resistance meter was purchased and tested. The PAN fiber must present the most conductive path between measurement terminals to achieve accurate resistance measurement. Because moisture, and even air, can provide a conductive "short," the researchers concluded that dc resistance measurements are too unreliable, even with ultra-high-resistance rated meters. The researchers are still searching for a good, inexpensive, and rapid turnaround technique for monitoring the relative oxidation progress.

Economics

During FY 2004, Kline and Company completed a cost study of DOE's entire carbon fiber development program, estimating profitable selling prices for baseline technology and if various technologies under development were implemented (see 4.B). Kline's estimates generally indicated that advanced oxidation techniques should reduce the fiber selling price by about 6%–8%. These estimates, however, were based on a line speed comparable to that of conventional conversion lines. Rough calculations suggest that if we can achieve much higher line speeds, the savings could increase dramatically. We have not discovered any inherent physics limits that

would prevent us from achieving a large increase in conversion line speed using plasma oxidation and microwave-assisted plasma carbonization.

Education

The materials characterization has been conducted in partnership with the University of Tennessee's (UT's) materials science department. Two UT graduate students were engaged to provide characterization support to the project.

Partners

Oak Ridge National Laboratory (ORNL) gratefully acknowledges contributions to this project by Fortafil and Hexcel. Both have generously provided raw materials and offered technical consultation. An updated materials transfer agreement was executed with Hexcel during this reporting period. Additionally, technical and programmatic consultation has been provided by U.S. Council for Automotive Research's (USCAR's) Automotive Composites Consortium and by Delphi Corporation.

Conclusions

The development of plasma-based oxidation technology has achieved a major milestone by demonstrating feasibility of plasma processing to oxidize PAN precursor fibers. Preliminary data suggest that the plasma oxidation process may allow earlier onset of carbonization, thus reducing oxidation residence time. Understanding of the parametric processibility space has grown substantially during this period. Preliminary economics studies support the value of research in advanced oxidation. The researchers expect to demonstrate continuous plasma processing, and continue growing our understanding of the plasma oxidation process and its benefits in FY 2005.

6. RECYCLING

A. Recycling Assessments and Planning

Principal Investigator and Field Project Manager: Edward J. Daniels
Argonne National Laboratory
9700 S. Cass Ave., Argonne, IL 60439
(630) 252-5279; fax: (630) 252-1342; e-mail: edaniels@anl.gov

Technology Area Development Manager: Joseph A. Carpenter
(202) 586-1022; fax: (202) 586-1600; e-mail: joseph.carpenter@ee.doe.gov
Field Technical Manager: Philip S. Sklad
(865) 574-5069; fax: (865) 576-4963; e-mail: skladps@ornl.gov

Participants:
This project is conducted as part of the CRADA between Argonne, USCAR's Vehicle Recycling Partnership, and the American Plastics Council
CRADA Partner Principal Investigators:
Michael Fisher, American Plastics Council, (703) 741-5599; e-mail: mike_fisher@plastics.org
Gerald Winslow, VRP, DaimlerChrysler Corp., (248) 512-4802; e-mail: grwx@DCX.com
Claudia Duranceau, VRP, Ford Motor Co., (313) 390-0504; e-mail: cdurance@ford.com
Candace Wheeler, VRP, General Motors Corp., (586) 986-1674; e-mail:candace.s.wheeler@gm.com

---

Contractor: Argonne National Laboratory
Contract No.: W-31-109-Eng-38

Objectives

- Ensure that any real or perceived recycling barriers that might preclude the use of advanced lightweighting automotive materials are removed.
- Enable the optimum recycling of all automotive materials, current and future, thereby obviating the need for legislative recycle mandates.
- Assess the critical needs for cost-effective recycling of automotive materials and components.
- Establish research priorities to enable cost-effective recycling of advanced automotive technology materials and components.
- Communicate a collaborative industry/government approach to automotive materials recycle issues.
- Coordinate research with other agencies and stakeholders in the United States, Europe, and Asia.

Approach

- Consult with automotive manufacturers and recycling industries, the U.S. Council on Automotive Research (USCAR) and its affiliates, national laboratories, universities, and other relevant organizations to assess critical recycling needs/barriers.
- Develop a recycling research plan that will serve as a "working document" to guide the U.S. Department of Energy (DOE) in establishing priority goals, with an initial emphasis on lightweight body and chassis materials.

- Establish an outreach/communication function to enable cooperation and leveraging of resources with all stakeholders and with the international community.
- Assist DOE in establishing advanced recycling research and development (R&D) initiatives and provide technical oversight to ensure that priority objectives/goals are accomplished.

Accomplishments

- Prepared *A Roadmap for Recycling End-of-Life Vehicles of the Future*.
- Prepared a draft 5-year research plan based on the recommendations and priorities identified in the Roadmap and based on an initial planning meeting with the management council of the Vehicle Recycling Partnership (VRP) of USCAR.
- Negotiated a Cooperative Research and Development Agreement (CRADA) with the VRP, the American Plastics Council (APC) and Argonne National Laboratory (ANL), as partners; effort under the CRADA was initiated in August 2003.
- Held a CRADA announcement event at Argonne on December 2, 2004; the event was attended by representatives of the press, industry, and government.
- Presented a co-authored DOE, USCAR, and APC keynote paper entitled "Market Driven Recycling in North America" at the 2004 International Car Recycling Workshop in May.
- Held a meeting with the CRADA partners and representatives of the Institute of Scrap Recycling Industries (ISRI) in August; the CRADA team was invited to make a presentation to ISRI's Shredder Committee meeting upcoming in Dallas.

Future Direction

- Continue development and management of the research plan with the CRADA partners.
- Continue ongoing efforts toward the milestones and objectives of the CRADA statement-of-work.
- Develop a joint "US ELV CRADA" Team presentation kit and brochure and establish a US ELV CRADA Team Web site to publicize the approach and work of the partners.
- Continue outreach efforts to broaden the basis for cooperation among stakeholders.
- Continue ongoing project efforts to assist DOE in preparation of planning documents, priority recycling R&D needs, proposal reviews, and related tasks.
- Update the ELV Roadmap.

Summary

The objective of this project is to establish priorities and develop cost-effective recycling technologies and strategies in support of the U.S. Department of Energy (DOE) FreedomCAR Vehicle Technology (FCVT) long-term objectives and goals. The major goals of this research are to (1) enable the optimum recycling of all automotive materials, (2) ensure that advanced automotive materials that improve the life-cycle energy use of vehicle are not precluded from use due to a perception that those materials are not recyclable, and (3) continue to enable market-driven vehicle recycling.

Today, cars that reach the end of their useful service life in the United States are profitably processed for materials and parts recovery by an existing recycling infrastructure. That infrastructure includes automotive dismantlers who recover useable parts for repair and reuse; automotive remanufacturers who remanufacture a full range of components, including starters, alternators, and engines to replace defective parts; and ultimately the scrap processor who recovers raw materials such as iron, steel, aluminum, and copper from the remaining auto "hulk" after components have been recovered for recycling.

Today, more than 75% of the materials from obsolete cars is profitably recoverable for recycling.

The recyclability of end-of-life vehicles (ELVs) is presently limited by the lack of commercially proven technical capabilities to cost-effectively separate, identify, and sort materials and components and by the lack of profitable postuse markets. During the next 20 years, both the number and complexity of ELVs are expected to increase, posing significant challenges to the existing recycling infrastructure. The automobile of the future will use significantly greater amounts of lightweighting materials (e.g., ultra-light steels, aluminum, plastics, and composites) and more sophisticated/complex components.

Roadmap Recommendations

A roadmap was developed with input from key stakeholders to guide DOE's recycle research. The key recommendations from the roadmap follow:

- Come together as a unified recycling community to cost-share the development of required new technology.
- Incorporate reuse, remanufacturing, and recycling into the design phase for cars whenever possible.
- Recycle as early in the recycling stream as possible, while relying on the market to optimize the value and amount recycled at each step.
- Maintain a flexible recycling process that can adapt to diverse model lines fabricated with different techniques and materials from various suppliers.
- Develop automated ways to recover bulk materials.
- Emphasize R&D on postshred material identification, sorting, and product recovery.
- Focus R&D efforts on materials not recycled today by sorters (e.g., postshred glass, rubber, fluids, textiles, plastics).
- Develop uses for recovered materials (whether in the same or different applications) and testing specifications.
- Encourage investment in the infrastructure needed to achieve the recyclability goal. Build on the existing infrastructure.
- Develop a means to prevent the entry of polychlorinated biphenyls and other hazardous materials into the recycling stream and promote acceptable limits in shredder residues.
- Consider the recycling requirements of new technologies entering fleets as early as possible.

The 5-Year R&D Plan

Based on the roadmap and continuing discussions with key stakeholders, a 5-year research plan has been prepared. The plan includes the following three focus areas:

Area 1. Baseline Technology Assessment and Infrastructure Analysis

The focus of the work under this activity will be to develop the tools and document the information necessary to make effective decisions relative to technology needs to facilitate sustainable future vehicle recycling and to make effective decisions regarding allocation of R&D resources.

Area 2. Materials Recovery Technology Development and Demonstration

Research to be conducted in this area will initially focus on addressing technology needs for postshred materials recovery, including mechanical recycling and conversion to fuels and chemicals. Projects that enhance preshred recovery, including disassembly for materials recovery and direct reuse and remanufacturing of components, will also be considered. In the long term, components such as fuel cells, advanced batteries, and hydrogen reformers are more likely to enter the recycle stream through preshred recovery for remanufacturing, repair, and materials recovery. Research will be undertaken to determine the technology needs to ensure the recyclability of these very advanced automotive components.

Area 3. Recovered Materials Performance and Market Evaluation

Understanding and enhancing recovered materials performance is an essential ingredient to a successful recycling program. This is especially true in automotive systems when the materials and components that are recovered have been in use for an average of from 10 to 15 years. This area will include projects to quantify the relative performance of recovered materials vis-à-vis new or virgin mate-

rials; research on compatibilization of recovered polymers to improve performance properties; development of technologies to upgrade the recovered materials, such as separation of fibers from polymeric substrates; and development of applications for other recovered materials, such as rubber and glass.

CRADA Projects

A collaborative research and development agreement (CRADA) among Argonne, the Vehicle Recycling Partnership of U.S. Council for Automotive Research (USCAR), and the American Plastics Council (APC) has been structured to provide a core team of expertise and the resources to enable the optimum recycling of all automotive materials.

The CRADA team's R&D agenda focuses on the following key objectives:

- Develop and demonstrate sustainable technologies and processes for ELV recycling.
- Demonstrate the feasibility of resource recovery from shredder residue, including materials recovery for reuse in automotive and other applications, chemical conversion of residue to fuels and chemicals, and energy recovery.
- Develop viable strategies for the control and minimization, or elimination of substances of concern.
- Benchmark recycling technology and provide date to stakeholders.
- Stimulate markets for reprocessed materials to support economic collection, processing, and transportation.
- Transfer technology to commercial practice.

This project provides for the overall management of the CRADA team activities and for communication and advocacy with other organizations. The other major projects that have been initiated under the CRADA follow:

- Baseline Assessment of Recycling Systems and Technology
- Postshred Materials Recovery Technology Development and Demonstration
- Development of Technology for Removal of PCBs and Other Substances of Concern from Shredder Residue
- Compatibilization/Compounding Evaluation of Recovered Polymers

The objectives and progress on these projects are discussed in their respective sections of this report. Effort under the CRADA was initiated in the fourth quarter of FY 2003.

Outreach Efforts

While the CRADA team provides a core of expertise, cooperation with other organizations is key to achieving the overall program objectives. In the United States, a market-driven recycle infrastructure is in place. The team is actively pursuing cooperation with the organizations and companies that are a part of that infrastructure. Cooperation with other stakeholders is also essential.

Papers outlining the industry/government collaboration have been presented at international conferences. A joint DOE, USCAR, and APC paper on "Market Driven Recycling in North America" was presented as the keynote paper at the recent 2004 International Car Recycle Congress in Washington, D.C. A paper entitled "Sustainable End-of-Life Vehicle Recycling: R&D Collaboration between Industry and the U.S. DOE" appeared in the August 2004 issue of the JOM.

An initial meeting with representatives of the Institute of Scrap Recycling Industries (ISRI) was held in August to brief ISRI on the CRADA objectives and projects and to elicit ISRI participation. Representatives of the CRADA team will make a presentation to the ISRI Shredder Committee meeting upcoming in October 2004 to develop a relationship with this organization.

To further communicate the U.S. approach to ELV recycling, a one-page CRADA summary has been developed, a CRADA brochure is under development, and a U.S. ELV CRADA Team Web site is being developed.

B. Baseline Assessment of Recycling Systems and Technology

Principal Investigator and Field Project Manager: Edward J. Daniels
Argonne National Laboratory
9700 S. Cass Ave., Argonne, IL 60439
(630) 252-5279; fax: (630) 252-1342; e-mail: edaniels@anl.gov

Technology Area Development Manager: Joseph A. Carpenter
(202) 586-1022; fax: (202) 586-1600; e-mail: joseph.carpenter@ee.doe.gov
Field Technical Manager: Philip S. Sklad
(865) 574-5069; fax: (865) 576-4963; e-mail: skladps@ornl.gov

Participants
This project is conducted as part of the CRADA between Argonne, USCAR's Vehicle Recycling Partnership and the American Plastics Council
CRADA Partner Principal Investigators:
Michael Fisher, American Plastics Council, (703) 741-5599, e-mail: mike_fisher@plastics.org
Gerald Winslow, VRP, DaimlerChrysler Corp., (248) 512-4802, e-mail: grwx@DCX.com
Claudia Duranceau, VRP, Ford Motor Co., (313) 390-0504, e-mail: cdurance@ford.com
Candace Wheeler, VRP, General Motors Corp., (586) 986-1674, e-mail: candace.s.wheeler@gm.com
.
Recyclability Studies P.I., Roy Muir, USCAR, VRP

Contractor: Argonne National Laboratory
Contract No.: W-31-109-Eng-38

Objective

- Establish the baseline or state-of-the-art for automotive materials recovery/recycling technology.

Approach

- Review the state-of-the-art of worldwide automotive materials recovery/recycling technologies.
- Develop technology profiles of emerging automotive materials recycle technology.
- Review international, federal and state regulatory information regarding vehicle recyclability, substances of concern, and recycle laws and mandates.
- Conduct life-cycle studies to quantify the environmental burdens associated with various end-of-life recycling technologies.
- Conduct reference case end-of-life recyclability studies.

Accomplishments

- Conducted a literature search that identified technologies that are being classified as mechanical, thermo-chemical conversion and energy recovery, and technology profiles are being developed.
- Characterized the existing U.S. recycling infrastructure and derived estimates of automotive recycle rates from the literature.

- Initiated a review of global regulatory requirements regarding end-of-life vehicle recycling; the review includes not only recycle mandates but also proposed and existing requirements regarding handling of substances of concern.
- Initiated life-cycle studies of selected alternative recycle technologies; the initial studies will provide a comparison of alternative mechanical recycle technologies relative to technologies proposed for the thermo-chemical conversion of shredder residue to fuels.
- Conducted reference recyclability calculations for reference cases and three lightweight alternatives: lightweight steel, composite, and aluminum.

Future Direction

- Prepare database of recycle technologies.
- Conduct CRADA-led visits to evaluate state-of-the-art material and energy recovery technologies, as appropriate in Japan and Europe.
- Continue life-cycle comparisons.
- Plan additional recyclability evaluations using the current study as a starting point for assessing recyclability of vehicles of the future.

Summary

The objectives of this project are to benchmark the automotive materials recycling industry and to compile information in an accessible format regarding the status of existing and emerging recycling technology and research.

The focus of the work under this activity will be to develop the tools and document the information necessary to make effective decisions relative to technology needs to facilitate sustainable future vehicle recycling and also to make effective decisions regarding allocation of R&D resources.

The state-of-the-art of worldwide automotive materials recovery/recycling technologies and associated resource recovery infrastructures will be reviewed to identify technology gaps and needs and to identify differences in automotive recycling strategies between the United States, Europe, and Japan. Technologies that will be included in this review include, but are not limited to, postshred materials recovery technologies, preshred materials recovery technologies, materials identification technologies, automated dismantling technologies, bumper recycle processes, fuel tank recycle technology, and thermochemical conversion technology.

Life-cycle analyses of alternative recycle technologies will be conducted to identify differences of technologies such as mechanical recycling vis-à-vis thermochemical recycling relative to energy and environmental benefits.

Regulations at the international, federal, and state level will be reviewed to identify the impact that proposed and existing regulations may have regarding recycling of automotive materials.

Reference case recyclability calculations will be undertaken to quantify the expected recyclability of alternative vehicle designs.

Infrastructure

The North American recycle infrastructure has been characterized (Figure 1). Material flows within the existing infrastructure are being quantified.

Technology Profiles

The recent literature has been reviewed, and summaries and profiles of available and emerging recycle technologies are being compiled into a database.

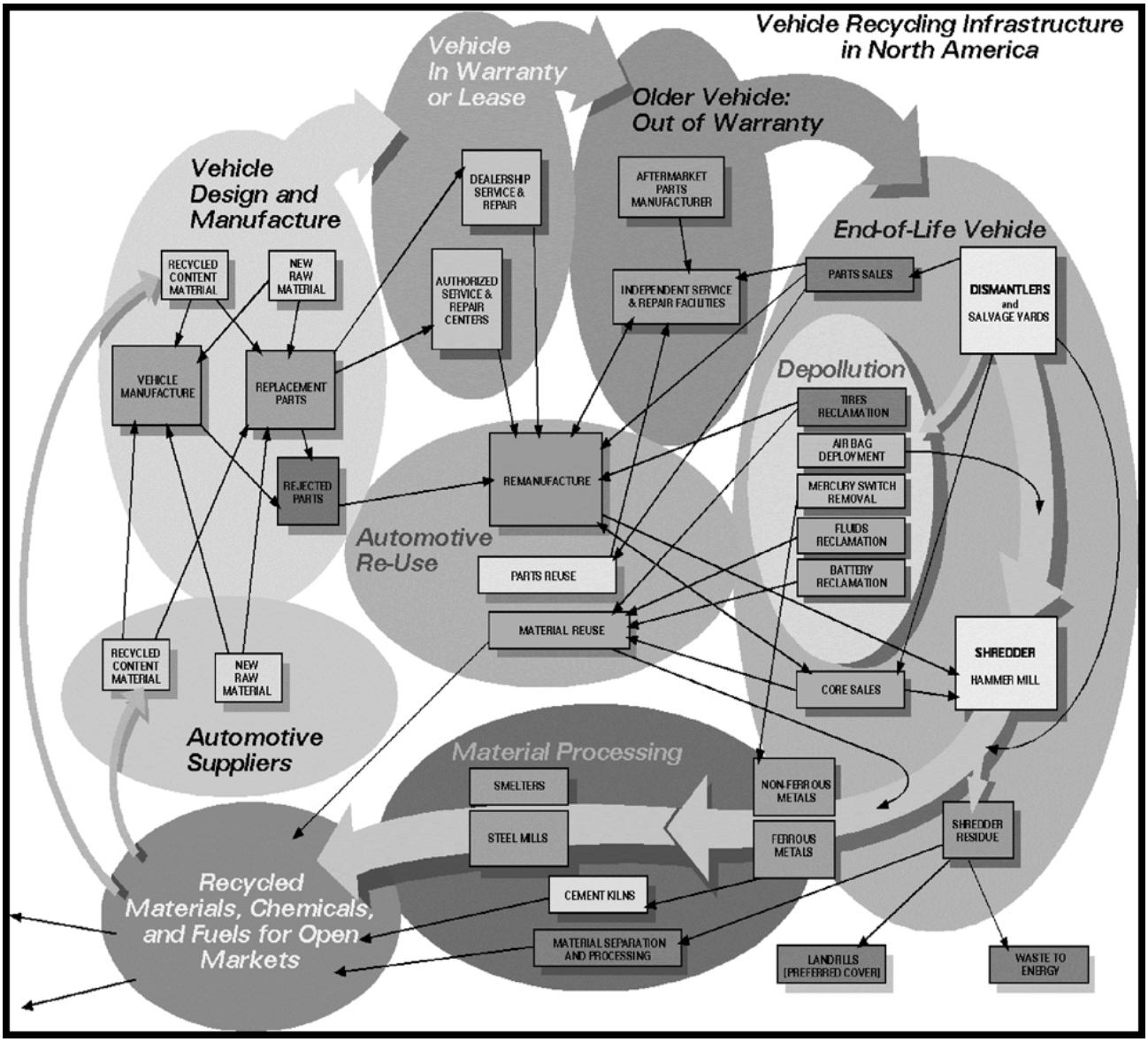

Figure 1. Representation of the North American recycle infrastructure.

A bibliography of abstracts of papers that discuss automotive recycling issues has been compiled. The bibliography is organized in the following sections:

- Recycle infrastructure
- Design for recycle
- Legal and regulatory issues
- Life-cycle analysis
- Research programs
- Substances of concern
- Disassembly technologies and case studies
- Reuse of automotive parts and subassemblies
- Remanufacturing
- Mechanical separation technology
- Thermochemical conversion technology
- Energy recovery technology
- Other technology
- Advanced materials recycle technology
- Case studies of materials recycled for auto applications

The bibliography was compiled from the following primary sources:

1. Society of Automotive Engineers (International) World Congresses from 1997 to 2004
2. Environmental Sustainability Conference and Exhibition, 2001
3. Society of Plastics Engineers
   - Automotive Research Consortium ’98 Conference
   - Automotive Research Consortium’99 Conference
   - GPEC 2002 Conference
   - GPEC 2003 Conference
4. Other conference proceedings
   - International Automobile Recycling Congress 2002
   - TMS Fourth International Symposium of Recycling of Metals and Engineered Materials, 2000
   - Ecomaterials and Ecoprocesses, The Conference of Metallurgists, COM 2003

Conference proceedings from the International Automobile Recycling 2001, 2003, and 2004 conferences have been ordered as have been the ARC 2000 proceedings for inclusion of relevant papers into the bibliography. At present, the bibliography includes 110 citations (Table 1).

Table 1. Citations included in the recycle bibliography (as of September 2004)

Bibliography section	Number of citations
Recycle infrastructure	4
Design for recycle	1
Legal and regulatory issues	16
Life-cycle analysis	5
Research programs	7
Substances of concern	2
Disassembly technologies and case studies	6
Reuse of automotive parts and subassemblies	1
Remanufacturing	0
Mechanical separation technology	13
Thermochemical conversion technology	5
Energy recovery technology	7
Other technology	17
Advanced materials recycle technology	7
Case studies of materials recycled for auto applications	18
Total citations	110

Regulatory Situation

The European Union has issued End-of-Life Vehicle Recycle Directives. The enforcement of these directives is, however, the responsibility of each member state. The status of the member states’ position relative to the directives and the policies for implementing the directives are under review. While the United States has not developed a federal policy or mandate, regulations at the federal and state level can impact the technology needs for recycling automotive materials. For example, U.S. Environmental Protection Agency (EPA) regulations regarding polychlorinated biphenyl (PCB) disposal limits the concentration of PCB on recycled materials to below 2 ppm. State regulations regarding mercury and polybrominated diphenyl ethers (PBDEs) can also impede materials recycling. A review of the regulatory arena is ongoing to identify the impacts of regulations relative to technology options for recycling.

Life-Cycle Studies

The objective of this project is to use life-cycle analysis to assess the environmental impacts of various mechanical separation technologies and alternative end-of-life recycling technologies used with automotive shredder residue. This information will then be used to create a flexible, computerized, life-cycle inventory model, which is process specific and yet can be modified to include additional recycling technologies and various material inputs. Life cycle involves assessing all of the upstream burdens associated with the production of the materials and energies used in the process, including the transport of all materials to the facility.

The Vehicle Recycling Partnership (VRP) contracted PE Europe GmbH, a company that is experienced in conducting life-cycle assessments and in model development using their own GaBi (Ganzheitliche Bilanzerung) software, to assess Salyp NV’s mechanical separation process and create a flexible end-of-life module based on this scenario.

Salyp NV's separation process, the first technology examined as part of this project, combined equipment developed by Argonne National Laboratory and others to create a facility that currently separates shredder residue into discrete fractions of metals, foam, mixed plastics, fiber-rich, and dust streams.

Because a life-cycle inventory requires the collection of primary data on each process, including all energy, water, and material inputs plus data on emissions to air and water, wastes, and products produced, these data were collected for the Salyp separation process and then input into the GaBi software to create a flexible model of the process. Table 2 shows the percentages used for the creation of the model, and Figure 2 shows the mass flow of the material as depicted in the GaBi software.

Table 2. Average shredder residue composition: basis used for LCA modeling

Material	ASR (%)
Plastic	34.0
Ferrous metals	33.4
Sand, dirt	15.7
Unknown	4.0
Glass	3.4
Wood	2.8
PU foam	2.8
Nonferrous metals	2.2
Copper	1.1
Stainless steel	0.6

Three different scenarios for handling the various materials recovered from the separation

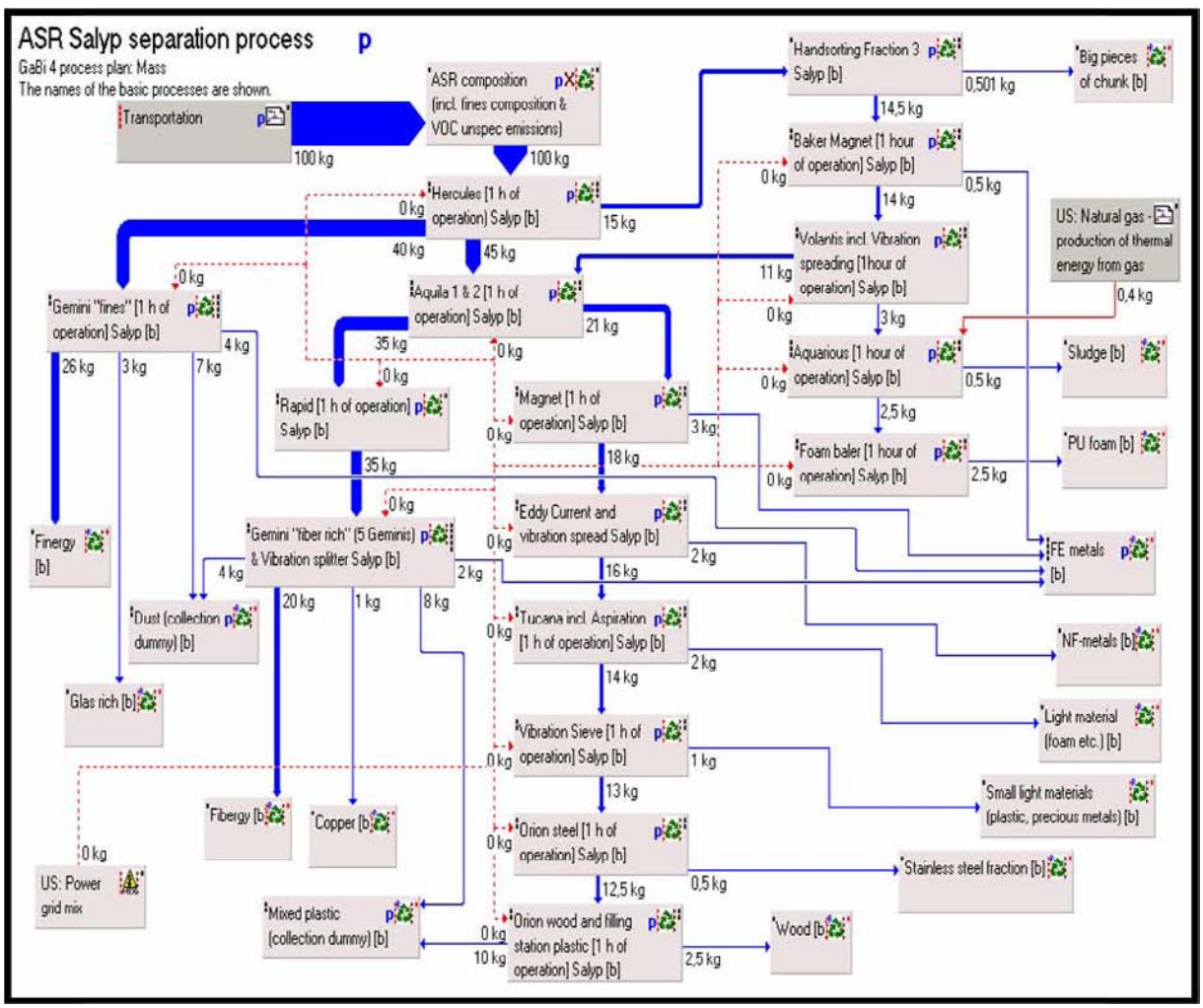

Figure 2. Life-cycle analysis mass flow representation of Salyp separation process.

process were determined along with their market values. These included waste treatment such as material recovery, energy recovery, turning specific material fractions into oil for cement kilns, as well as material substitution using mixed plastics to replace products such as wood pallets and polypropylene (PP) pellets. GaBi allows for the analysis of the various scenarios in a range of impact categories, including primary energy demand, photochemical ozone creation potential, and CO_2 emissions. All of these scenarios can be changed within the GaBi software to account for different or new types of treatments that arise in the future, which could lead to different impacts on the environment.

The model allows the user to run simulations on shredder residue separation within different boundary conditions. The following boundary conditions can be modified: (1) shredder residue composition, (2) location of the facility, (3) type and distance of transportation, (4) market values for the separated fractions, (5) new potential applications for separated fractions, and (6) utilization ratio of the facility.

Additional life-cycle studies are underway to compare mechanical separation to other thermal/chemical conversion technologies. When completed, the goal is to have a comprehensive end-of-life model that will allow us to rapidly and accurately assess the potential environmental impact of various material/design changes in our future vehicles.

Recyclability Studies

Recyclability studies are being conducted to examine the effect of using automotive lightweighting material on recyclability. A Toyota Prius hybrid was selected for a reference case. This vehicle is a second-generation hybrid with a gas/electric powertrain. Evaluating the recyclability of this vehicle and its new technology will be a step in identifying changes that will impact end-of-life recycling of vehicles of the future.

In collaboration with Johnson Controls, Inc. (JCI), the VRP dismantled the vehicle according to VRP procedures to single material components and entered data for each part into a database. A material list that identified the breakdown of materials into separate classifications such as ferrous and nonferrous metals, as well as composte materials and plastics was prepared. The materials breakdown is summarized in Table 3 and shown in Figure 3. In comparison, the materials composition of a production Ford Taurus is summarized in Table 4 and Figure 4.

Table 3. 2004 Toyota Prius materials breakdown

Materials	Mass (kg)	Percent
Ferrous metals	776.94	60.55
Nonferrous metals	229.99	17.92
Plastics	154.85	12.07
Elastomers	39.66	3.09
Inorganic material	34.71	2.71
Other	28.21	2.20
Organic materials	18.84	1.47
Vehicle mass (less fluids)	1283.1	100.00

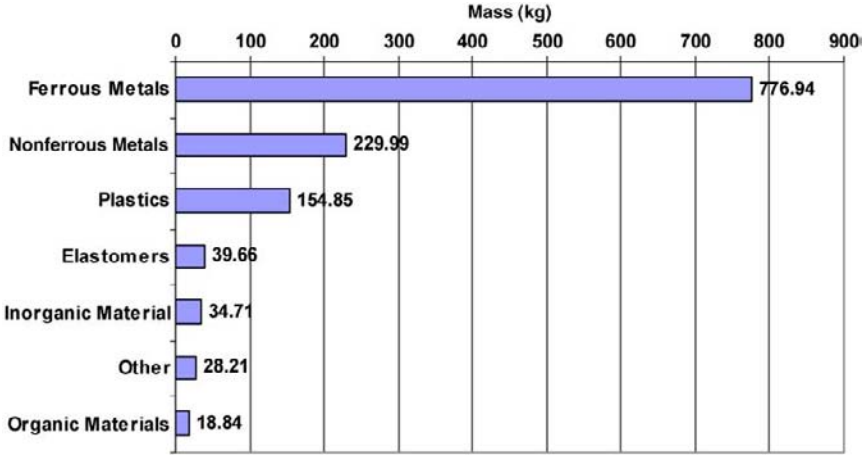

Figure 3. 2004 Toyota Prius materials breakdown.

Table 4. 2004 Ford Taurus materials breakdown

Materials	Mass (kg)	Percent
Ferrous metals	1008.28	70.37
Plastics	154.41	10.78
Nonferrous metals	141.43	9.87
Elastomers	68.71	4.80
Inorganic material	40.91	2.86
Other	17.45	1.22
Organic materials	1.66	0.12
Vehicle mass (less fluids)	1432.86	100.00

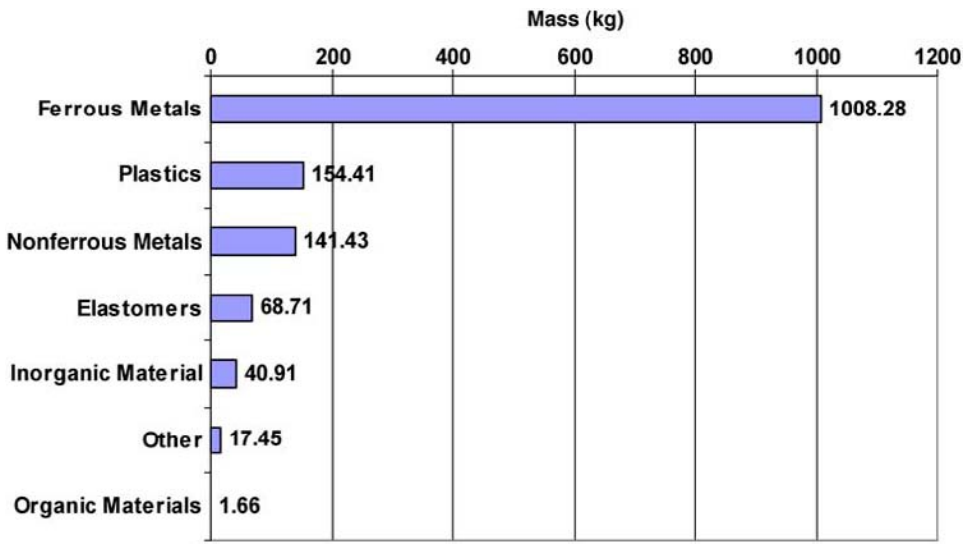

Figure 4. 2004 Ford Taurus materials breakdown.

Three different recyclability calculations were made (Table 5). The Federal Trade Commission (FTC) recyclability number is the percentage by weight of the material that is currently being recycled, and it includes metals, fluids less fuel, and batteries. The European guidelines include FTC materials plus fuel at 90% of a full tank, plastics that could be recycled, and up to 10% by weight energy recovery. Note that Europe requires 95% recyclability for new vehicles. The feasible-to-recycle number includes the FTC materials plus plastics that can be recycled. Changes to the current infrastructure would be required to increase recycling beyond the current FTC percentage.

Table 5. Reference case recyclability: 2004 Toyota Prius

Federal Trade Commission	80.86%
European	97.61%
Feasible to recycle	85.58%
Ref. 2000 Ford Taurus Federal Trade Commission	80.50%

To establish an indication of the impact of lightweight materials on the reference case recyclability calculations, the production Toyota Prius is compared to a proposed aluminum-intensive lightweight vehicle and a proposed composite lightweight vehicle based on the 2004 Toyota Prius. The production 2004 Toyota Prius hybrid vehicle body was steel with aluminum hood and decklid. The suspension was of steel except for an aluminum steering knuckle on the front suspension. This was used as the base for this study.

The aluminum alternative is for a 2004 Toyota Prius with an aluminum body and magnesium engine cradle and rear axle substituted for the pro-

duction parts. In addition, seat frames, body brackets, and the instrument panel cross car beam have been changed from steel to aluminum. As a result the weight has been reduced by approximately 630 lb or 21%. Because the weight reduction is entirely in the currently recycled portion of the vehicle, the recyclability is adversely affected and is reduced from 80.86% to 76.10%. No changes were made to the currently nonrecycled portion of the vehicle. Aluminum replaced steel at 50% by weight of the original steel.

The composite alternative is for a 2004 Toyota Prius with a carbon fiber body with 40% carbon fiber and 60% thermoset polyurethane/urea resin by volume, 49.72% carbon and 50.28% thermoset polyurethane/urea resin by weight, and magnesium engine cradle and rear axle substituted for the production parts. In addition, seat frames, body brackets, and the instrument panel cross car beam have been changed from steel to composite. As a result the weight has been reduced by approximately 711 lb or 24%. Because the weight reduction is entirely in the currently recycled portion of the vehicle, the recyclability is adversely affected and is reduced from 80.86% to 57.20% if none of the composite is recycled or 74% if all of the composite material is recycled. No changes were made to the currently nonrecycled portion of the vehicle. The composite material replaced steel at 40% by weight of the original steel.

There are reductions in all three recyclability calculations for lightweighted vehicles, even though there is no change to the rest of the vehicle (Table 6). Where the aluminum and composite material is being recycled, the same amount of material would be landfilled in each of the three scenarios. The only difference is that the recycled portion of the lightweighted vehicles would be lighter. While the recyclability would be less, there would be no difference in landfill, and the lighter vehicles would use less fuel during their life. As can be seen, lightweighting presents challenges in the European market. Note that these calculations do not take into account downweighting of related components that would accompany any lightweight vehicle, such as powertrains, brakes, tires, etc. Because the downweighted components are high in metallic content, downweighting will further reduce recyclability and make it difficult to meet the European 95% requirement.

Table 6. 2004 Toyota Prius recyclability, reference case vs aluminum and composite body materials

	As produced (%)	Aluminum body (%)	Composite body (%)
FTC	80.9	76.1	74.0[a]
European	97.6	96.0	94.5[a]
Feasible to recycle	88.3	85.6	83.9[a]

[a]If the composite material were not recycled, then the numbers would be FTC—57.2%, European—78.2%, and Feasible to Recycle—67.1%. Recycling of the composite material would require significant changes in the current recycling infrastructure. In addition, a market for the recycled carbon fibers would need to be developed. Current technology for recycling carbon fibers results in a 20% loss in fiber length and properties, which would limit their reuse in the original applications.

In conjunction with this study, additional evaluations are planned using these data as a starting point for assessing recyclability of cars of the future. The impact of vehicle lightweighting and material selection on recyclability will be evaluated. In addition, powertrain changes including hybrid and fuel cell alternatives will be compared to current vehicles. An assessment of various alternatives on recycling and the effect on the current recycling infrastructure will be produced. No downsizing of other components was included in this study. Future studies will reflect downweighting of powertrains, brakes, tires, and other components in recyclability calculations. Items requiring further study resulting from these assessments will support future projects to determine the feasibility of various alternative vehicle configurations and material selection choices.

C. Postshred Materials Recovery Technology Development and Demonstration

Principal Investigator and Field Project Manager: Edward J. Daniels
Argonne National Laboratory
9700 S. Cass Ave., Argonne, IL 60439
(630) 252-5279; fax: (630) 252-1342; e-mail: edaniels@anl.gov

Technology Area Development Manager: Joseph A. Carpenter
(202) 586-1022; fax: (202) 586-1600; e-mail: joseph.carpenter@ee.doe.gov
Field Technical Manager: Philip S. Sklad
(865) 574-5069; fax: (865) 576-4963; e-mail: skladps@ornl.gov

Participants
This project is conducted as part of the CRADA between Argonne, USCAR's Vehicle Recycling Partnership and the American Plastics Council
CRADA Partner Principal Investigators:
Michael Fisher, American Plastics Council, (703) 741-5599; e-mail: mike_fisher@plastics.org
Gerald Winslow, VRP, DaimlerChrysler Corp., (248) 512-4802; e-mail: grwx@DCX.com
Claudia Duranceau, VRP, Ford Motor Co., (313) 390-0504; e-mail: cdurance@ford.com
Candace Wheeler, VRP, General Motors Corp., (586) 986-1674; e-mail: candace.s.wheeler@gm.com

The Association of Plastics Manufacturers of Europe provided cost-sharing for the Salyp NV process evaluation.
Changing World Technologies is cost-sharing on the evaluation of their thermal depolymerization process.
The Polyurethanes Recycle and Recovery Council (PURCC) is also participating and cost-sharing on the evaluation of the Troy Polymers, Inc., polyurethane glycolysis process.

Contractor: Argonne National Laboratory
Contract No.: W-31-109-Eng-38

Objective

- Develop and demonstrate technology for the cost-effective recovery of materials from postshred residues.

Approach

- Characterize shredder residues from a number of sources to determine composition variability.
- Conduct bench-scale and large-scale process/technology tests to benchmark technology.
- Build and operate a shredder residue separation pilot plant to produce samples of recovered materials for market evaluation.
- Conduct costs and performance analysis of alternative technologies to establish the business case for the technologies and to identify technology gaps.

Accomplishments

- Completed characterization of five shredder residues; two European and three United States.
- Completed large-scale tests of Salyp's "thermoplastics sorting" technology using residue from two European and one U.S. location as feed materials.

- Completed construction in the first quarter of FY 2004 of a large-scale pilot separation facility at Argonne National Laboratory; shakedown of the facility occurred during the second and third quarter, production campaigns have been started.
- Completed bench-scale testing of Changing World Technologies (CWT) thermal depolymerization process; test runs have been initiated using 3000 lb of bulk shredder residue.
- Started bench-scale testing of a glycolysis process for conversion of polyurethane foam to polyol initiators.
- Developed an Excel-based process cost model that incorporates two primary modules for recovery of automotive plastics: the first module includes the unit operations required for recovering a plastics concentrate from shredder residues, and the second module includes the unit operations required to recover selected plastics from the mixed plastics concentrates.

Future Direction

- Continue characterization of shredder residue.
- Complete CWT thermal depolymerization tests; evaluate process economics; define path forward.
- Complete Polyventure/TPI glycolysis bench-scale tests; evaluate process performance; define path forward.
- Complete Argonne froth flotation campaigns, evaluate process performance and economics; define path forward.
- Update process cost analysis model.
- Review/critique technology developments with representatives of the automotive shredding industry.

Summary

The objective of this project is to develop and demonstrate technology for the cost-effective recovery of materials from postshred residues.

A wide range of materials recovery technologies is at various stages of development. Certain of those technologies specific to recovery of materials from postshred materials streams will be evaluated and demonstrated to fully understand the commercial viability of those processes.

The objective of this project is to determine the performance (e.g., yield, purity, efficiency, and cost) of these emerging technologies such that an optimized and integrated process for recovering these materials from shredder residue can be developed.

Research conducted in this project will provide data essential to establishing a business case for sustained recycling of automotive materials from postshred residue.

Research has been completed on the Salyp N.V. physical separation/thermosorting process. Research is ongoing on the Argonne physical separation/froth flotation process, the Changing World Technologies (CWT) thermal depolymerization process, and The Polyventure/Troy Polymers process for glycolysis of polyurethane foam.

Characterization of Shredder Residue

To facilitate the development of technology for recovery of materials and resources from shredder residue, characterization of shredder residue from different sources has been conducted by MBA Polymers. Small (2-kg) samples of shredder residue from five sources have been characterized to date: two European and three American. Samples of shredder residue from other sources will be analyzed as appropriate throughout the course of the project.

In general, while there are some differences in the composition of the shredder residue from each source, the differences do not yet appear to be significant in terms of the design constraints of recovery technology. The bulk composition of the residue samples is compared in Table 1. The composition of the plastics fraction for each sample is compared in Table 2.

Table 1. Bulk composition of European and U.S. shredder residue (*Basis*: small sample, ~1 kg, analysis)

Materials	Europe 1	Europe 2	U.S. 1	U.S. 2	U.S. 3
Fines (<1/8 in.)	18.0	4.9	37.5	32.8	5.3
Residual metals	3.0	6.4	9.3	7.1	15.5
Foam	36.8	31.6	21.3	26.6	26.9
Wood	0.4	3.2	7.2	4.0	1.9
Rubber	17.3	22.5	4.9	9.3	27.7
Stone, fiber, other	10.1	0.0	7.4	8.9	5.5
Plastics	14.4	31.4	12.4	11.3	17.2

Table 2. Composition of the plastics fraction of European and U.S. shredder residue (*Basis*: small sample, ~1 kg, analysis)

Plastic	Europe 1	Europe 2	U.S. 1	U.S. 2	U.S. 3
Polypropylene	41.4	31.9	26.3	41.0	33.3
Polyethylene	3.7	17.3	6.6	7.0	5.3
High-impact PS	4.9	3.3	25.9	15.2	28.1
ABS	8.8	11.5	17.1	22.2	11.8
PA	11.8	2.1	2.9	3.7	10.7
PVC	0.7	10.4	0.0	0.0	1.9
Rigid urethane	18.9	13.4	4.1	0.5	4.1
PC/PBT	6.6	4.2	1.9	2.7	4.4
Other	3.2	5.9	15.2	7.6	5.7

Argonne Pilot Plant

Construction of the pilot plant at Argonne was completed in the first quarter of FY 2004. The facility will be used to

1. conduct optimization/integration studies,
2. provide a production capability to produce large samples of recovered materials for market evaluation,
3. demonstrate the effectiveness of alternative separation technologies and systems, and
4. serve as a user/demonstration facility to conduct separation tests for residue from specific sources.

The pilot plant consists of two major unit operations. The first is a mechanical separation facility; the second is a wet-density/froth-flotation separation facility.

The mechanical separation facility is shown schematically in Figure 1. An overview of the facility is shown in Figure 2. The mechanical separation facility processes the raw shredder residue to yield a "plastics concentrate." The raw shredder residue is separated into the following fractions:

- oversize tramp material,
- fines (–5/16 in.),
- oversize [polyurethane foam (PUF), fiber, etc.],
- nonferrous,
- ferrous,
- small fluff and other light materials,
- other reject, and
- middling/plastics concentrate.

The "middling" fraction is further processed for size reduction in a small shredder to produce the plastics concentrate.

The wet density/froth-flotation facility is shown schematically in Figure 3. An overview of this pilot plant is shown in Figure 4. It includes six continuous stages for separation and recovery of targeted materials from the plastics concentrates derived from shredder residue.

The first stage cleans the plastics concentrate and also recovers the lighter olefins for further processing. The second stage drops out heavy

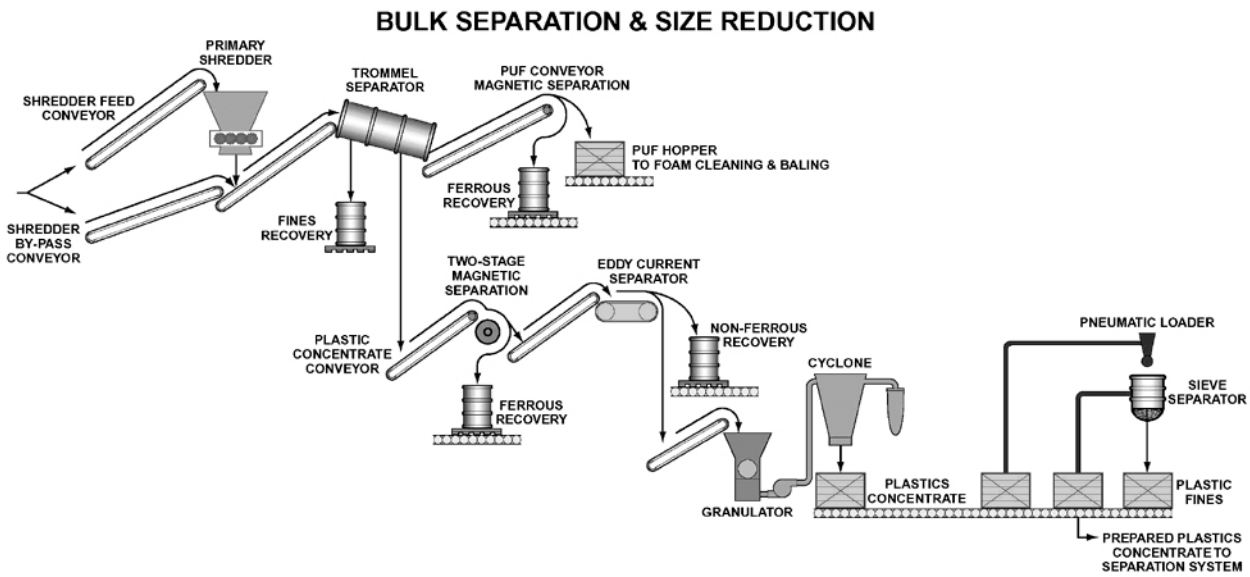

Figure 1. Schematic of the Argonne Pilot Mechanical Separation System for processing raw shredder residue.

Figure 2. Overview of the Argonne Bulk Separation Pilot Plant.

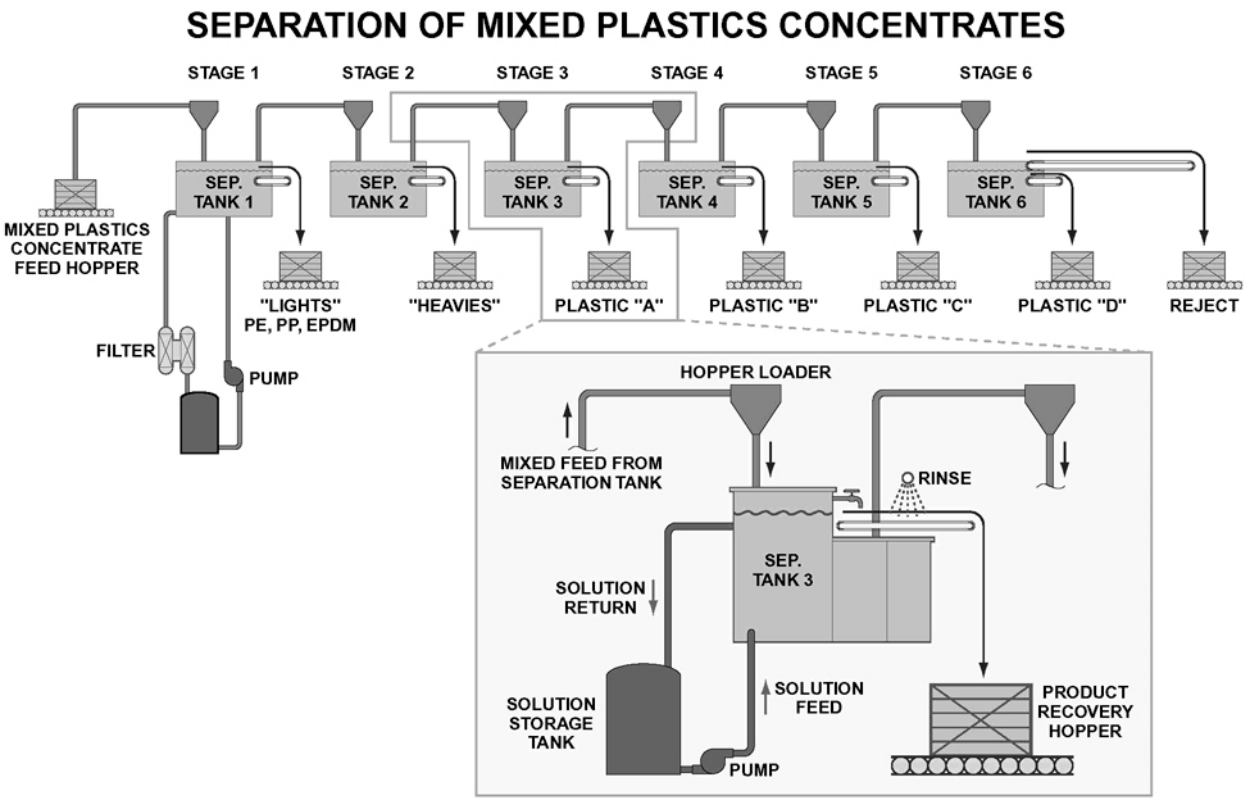

Figure 3. Schematic of the Argonne Pilot Wet Separation System for recovery of plastics from shredder residue.

Figure 4. Overview of the Argonne Froth-Flotation Pilot Plant.

materials, including any residual metals that remain in the concentrate.

The following four stages will process the balance of the concentrate for recovery of the following targeted materials:

- acrilonitrile-batadiene-styrene (ABS),
- high-impact polystyrene (HIPS),
- nylon, and
- polyvinyl chloride (PVC).

Depending on recovery rates and yield, other polymer cuts may be explored to define the overall best strategy for separation and recovery of the materials from the concentrates.

Shakedown of the wet density/froth-flotation facility was conducted during the second quarter of FY 2004. Shakedown was conducted using about 4000 lb of postconsumer electronics and appliance mixed plastics because the composition of these materials is much less variable than the composition of plastics concentrate from shredder residue. The composition of a feed material for the shakedown trials is shown in Figure 5. The shakedown tests were conducted using four of the six froth-flotation stages targeting recovery of the ABS and HIPS from the feed material. In these trials, approximately 75% of the feed material HIPS was recovered in a single fraction at a purity of 97% (Figure 6). The ABS yield was lower at about 55%; however, the purity of the ABS was 98%. Physical properties of the recovered materials were consistent with a range of "virgin" or primary grades of HIPS and ABS,

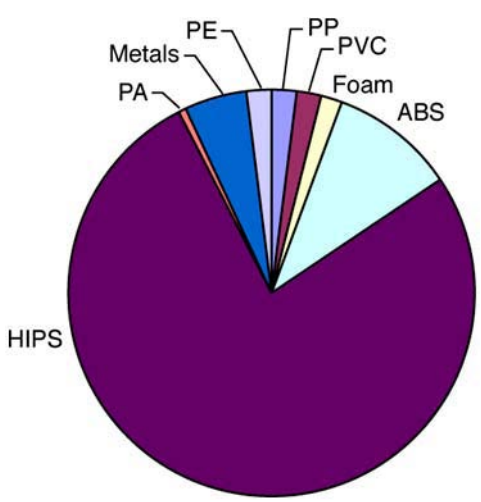

Figure 5. Composition of postconsumer mixed plastics used in Argonne Froth-Flotation Pilot Plant shakedown trials.

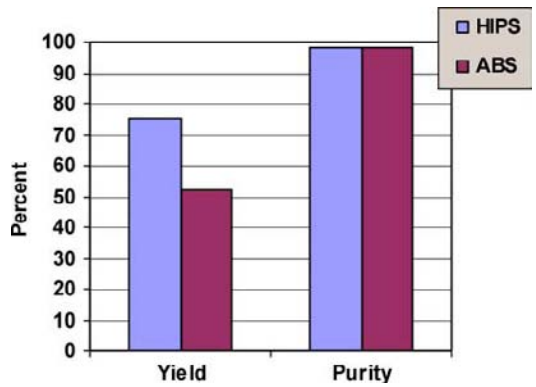

Figure 6. Percentage of HIPS and ABS recovered (yield) and purity of the recovered HIPS and ABS.

respectively. (See Compatibilization/Compounding Evaluation of Recovered Polymers annual report, see 6.E)

Following shakedown of the froth-flotation system, shakedown and debottlenecking of the bulk separation pilot plant was undertaken during the third quarter of FY 2004.

During the fourth quarter, campaigns were undertaken that resulted in the physical/bulk separation of about 60,000 lb of shredder residue (6 campaigns). The average yield of plastics concentrate from these campaigns was about 17% (Figure 7). The composition of the recovered plastics concentrate is, of course, much more complex than the plastics fraction from just appliance or electronics scrap (Figure 8).

The initial froth-flotation campaigns run with the shredder residue plastics concentrate showed that the process could recover a concentrated

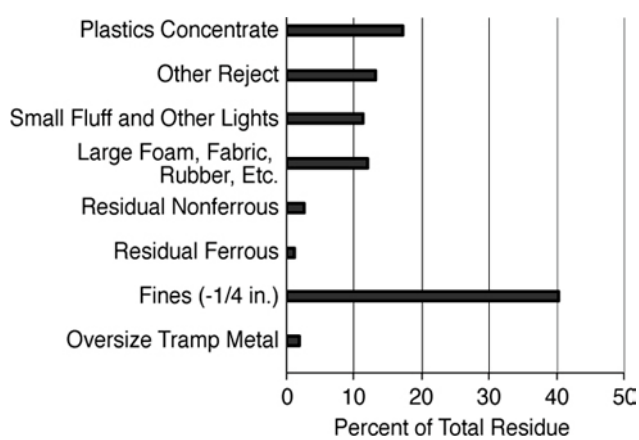

Figure 7. Bulk composition of shredder residue processed in Argonne's Bulk Separation Pilot Plant. (*Basis*: 60,000 lb, six campaigns.)

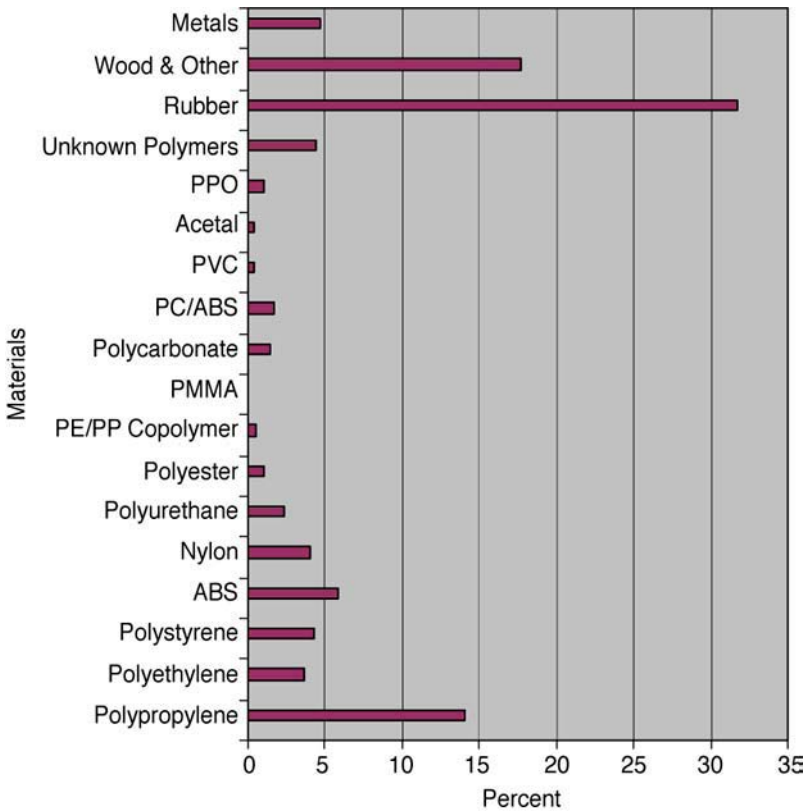

Figure 8. Average composition of the plastics concentrate fraction recovered from shredder residue. (*Basis*: 60,000 lb, six campaigns.)

polyolefin's fraction and a concentrated ABS fraction, but that these materials contained a significant amount of residual wood and rubber. The effectiveness of the froth-flotation process is dependent on the ability to isolate these materials from the balance of the plastics concentrate. The technical feasibility of conventional separation equipment such as gravity tables, mineral jigs, and hydrocyclones in isolating the wood and rubber from the plastics concentrate will be evaluated as the research on mechanical separation continues. Alternative operating conditions for the froth-flotation system are also being evaluated.

Salyp Thermo-Plastics Sorting Technology

Salyp N.V., a Belgium company has developed and integrated a full recycling line using different sorting technologies, which processes and recycles various material fractions from shredder residue. The key objective of the project was to determine the feasibility of a mechanically automated, near industrial recovery of various mixed engineering plastics into individual plastic streams.

Salyp processed three different shredder residues totaling 100 metric tons that included one U.S. shredder and two European shredders. Each shredder selected sent approximately 33 metric tons of shredder residue to Salyp for processing.

Results from this study indicated that Salyp was able to separate different material streams that included

- metals,
- fibers,
- foam (using Argonne's technology),
- fines, and
- plastic concentrates.

The economics of shredder residue separation were determined, and the following costs were defined.

- Investment cost for machinery and equipment to process 40,000 tons of shredder residue per year is estimated at $3.6M.
- Cost for separation of a mixed plastic stream is estimated at 13¢/lb.

Salyp's near-industrial sorting line was able to recover a mixed plastics fraction. However, sorting the mixed plastic fraction into individual plastic streams could not be accomplished.

Changing World Technologies

Changing World Technologies, Inc. (CWT) has developed a two-stage thermal conversion process that converts organic material into fuels, gases, and solids. CWT's first commercial facility based on this technology was commissioned in April 2003 and converts 200 tons/d of turkey offal into fuels and fertilizers. This installation is a joint venture partnership with ConAgra and CWT. The thermal conversion process should be able to process the organic materials in shredder residue.

CWT's research and development center is located at the Philadelphia Naval Yard where they have a 7-ton/d pilot plant (Figure 9).

The CRADA team funded a study on a limited basis to CWT titled "Protocol Testing Shredder Residue Project." This study focused on a select sampling of two different types of shredder residue. Results from this initial study indicated that the CWT process was able to convert the shredder residue samples to three product fractions: an oil, a gas, and a carbon char. The resultant oil product characteristics are summarized in Table 3.

Based on the results of this initial project testing, CWT has offered to process 3,000 lb of shredder residue to further confirm the technical and economic feasibility of this process.

At the completion of this study, CWT will prepare a final report for the CRADA team; it will include a Performance Cost Analysis that defines converting plastics from shredder residue into fuels and chemicals. Additionally, the output products will also be made available to the CRADA project members for further analysis and testing.

If the results look promising, the CRADA team will investigate further funding opportunities that will aid in the launch of a scale-up study.

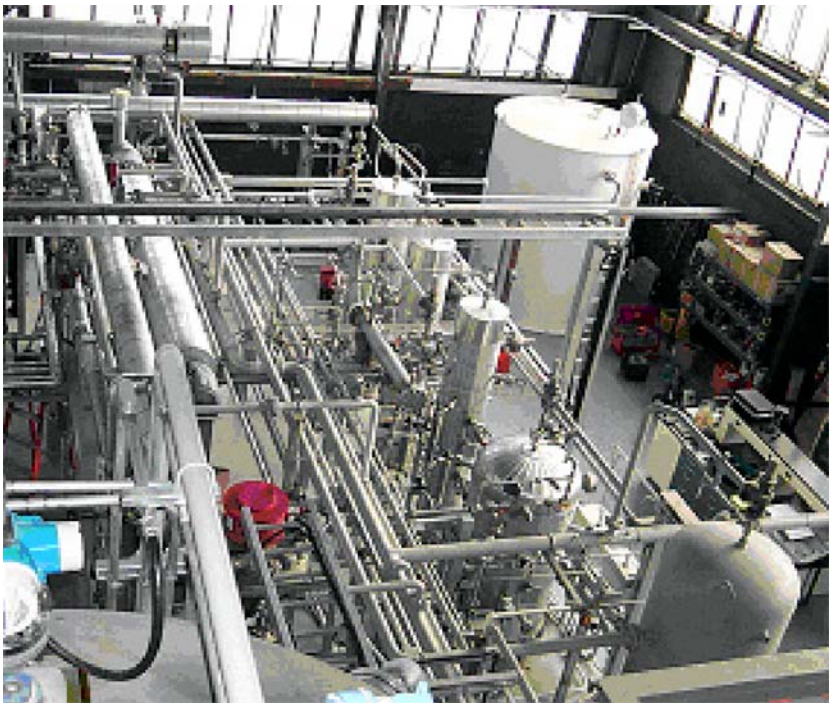

Figure 9. Overview of the CWT Thermal Conversion Pilot Plant.

Table 3. CWT oil characteristics from shredder residue feedstock

Method	Test	SR bucket 1	SR bucket 2
D-287	API@60°F	37.6	40.7
D-93	Flash point, °F	<72	<72
D-86	Distillation, °F		
	IBP	200	119
	10%	320	234
	50%	460	451
	90%	668	652
	FBP	712	691
D-4294	Sulfur, wt %	0.125	0.124
D-97	Pour point	–38°F/–39°C	–38°F/–39°C
D-482	Ash, wt %	0.004	0.003
	Carbon, %	86.38	85.30
	Hydrogen, %	13.47	14.54
	Nitrogen, %	<0.1	<0.1
D-240	Heat content		
	Btu/lb	19,094	18,622
	Btu/gal	133,046	127,409

Troy Polymers Process for Glycolysis of PUFs

Troy Polymers, Inc. (TPI) has developed a patented glycolysis process (assigned to TPI and Polyventure, Inc.) for the conversion of mixed PUFs into polyol initiators (Figure 10). The process concept can recycle foam collected at shredders and convert the recovered PUF into polyol initiators, which can then be utilized to produce new urethane products (Figure 11).

Working with the Polyurethane Recycle and Recovery Council (PURRC), bench-tests to establish proof-of-concept were undertaken. The tests demonstrated the technical feasibility of the process in converting mixed clean PUFs from shredder residue to polyol initiators at a yield of about 88% (Table 4). Dirty foam was converted to polyol initiators at a yield of about 72%. However, the product from the dirty foam required more extensive filtration because of the solid residue contained within the foam.

Preliminary characterization of the products was also performed. The OH number, which is an indicator of molecular size (412 for the polyol initiator derived from clean foam and 570 for the polyol initiator derived from dirty foam), proves that the foam has been broken into smaller molecules. Commercially produced initiators can have OH numbers from about 100 to 1000 mg KOH/g. The OH numbers from the bench-test indicate that propoxylation of these intermediate products to produce polyols with OH numbers between 42 and 56 mg KOH/g, as commonly used in industry, is feasible. Obviously other characteristics of the polyols such as acid number, water content, color,

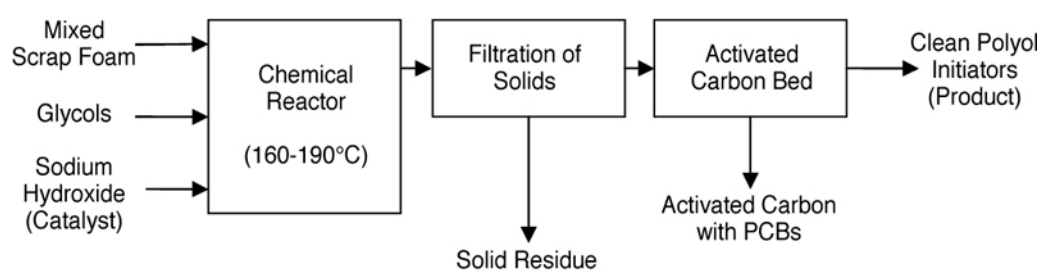

Figure 10. Glycolysis process conceptual process flow sheet.

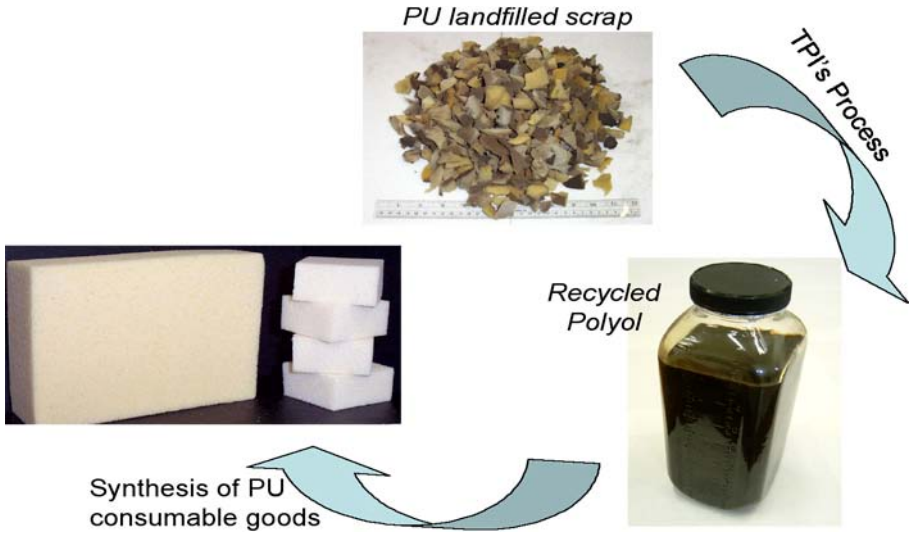

Figure 11. Glycolysis process concept.

Table 4. Glycolysis reaction input materials and product yield

Designation	Clean PUF	Dirty PUF
Starting Materials		
Diethylene glycol, g	1200	1200
NaOH, g	12.0	12.0
Foam scrap, g	1800	1800
Product yield		
Weight of products after glycolysis, g	2750	2762
Percent of recovered materials, %	91	92
Liquid fraction in products after filtration, %	96	79
Solid fraction (reside) in products after filtration, %	4	21
Yield of liquefied fraction, g	2640	2182
Yield of liquefied fraction (mass of liquid product)/ (mass of total input materials)*100	88	72
OH number (mgKOH/g)	412	570
Viscosity (cPs)		
• @23°C	350	500
• @50°C	200	300
• @77°C	100	—

pH, content of terminal unsaturation, acid and alkalinity content, amount of peroxide and carbonyl groups, amount of antioxidant and residual solvent, will have to be determined and controlled. The viscosity values of the polyol initiator products are also typical of the initiators used by industry. The greater viscosity of the product recovered from dirty foam indicates that further filtration of the product may be necessary.

As a result of this initial phase study, the CRADA team has agreed to fund a larger study at TPI. The study will include processing approximately 1,000 lb of dirty foam and produce about 50–100 gal of polyol for market evaluation. The polyurethane industry producers BASF, Bayer, and Dow have agreed to evaluate the polyol initiator product and identify potential applications.

D. Development of Technology for Removal of PCBs and Other Substances of Concern (SOCs) from Shredder Residue

Principal Investigator: Bassam Jody
Argonne National Laboratory
9700 S. Cass Ave., Argonne, IL 60439
(630) 252-5279; fax: (630) 252-1342; e-mail: bjody@anl.gov

Field Project Manager: Edward J. Daniels
Argonne National Laboratory
9700 S. Cass Ave., Argonne, IL 60439
(630) 252-4206; fax: (630) 252-1342; e-mail: edaniels@anl.gov

Technology Area Development Manager: Joseph A. Carpenter
(202) 586-1022; fax: (202) 586-1600; e-mail: joseph.carpenter@ee.doe.gov
Field Technical Manager: Philip S. Sklad
(865) 574-5069; fax: (865) 576-4963; e-mail: skladps@ornl.gov

Participants
This project is conducted as part of the CRADA between Argonne, USCAR's Vehicle Recycling Partnership and the American Plastics Council
CRADA Partner Principal Investigators:
Michael Fisher, American Plastics Council, (703) 741-5599; e-mail: mike_fisher@plastics.org
Gerald Winslow,VRP, DaimlerChrysler Corp., (248) 512-4802; e-mail: grwx@DCX.com
Claudia Duranceau, VRP, Ford Motor Co., (313) 390-0504; e-mail: cdurance@ford.com
Candace Wheeler, VRP, General Motors Corp., (586) 986-1674; e-mail: candace.s.wheeeler@gm.com

The Polyurethane Recycle and Recovery Council (PURCC) is also participating and cost-sharing in this project.
PURCC Project Lead: Steve Niemic

Contractor: Argonne National Laboratory
Contract No.: W-31-109-Eng-38

Objective

- Develop viable strategies and technology for the control and minimization or elimination of polychlorinated biphenyls (PCBs) and other substances of concern (SOCs) from recycled automotive materials.

Approach

- Identify efficient and environmentally acceptable process solutions for removal of contaminants, including PCBs from materials recovered from shredder residue.
- Conduct large-scale washing/cleaning tests using plastics from shredder residue in commercially available equipment.
- Identify necessary modifications to existing equipment to improve its performance and/or economics.
- Examine variances in analytical procedures/test results for PCB analysis.

Accomplishments

- Completed bench-scale screening of 11 surfactants and 3 organic solvents for removal of PCBs and other contaminants from polymers derived from shredder residues and specified preferred surfactant/cleaning solutions.
- Reviewed and identified commercially available washing equipment that can be adapted to a commercial-scale recycle process.
- Conducted trials of selected equipment; performed analyses of samples of cleaned product.
- Conducted laboratory tests to develop an understanding of the variability inherent in the analytical procedures for PCB analysis.

Future Direction

- Complete the large-scale cleaning tests using commercially available equipment and systems.
- Identify necessary modifications to existing equipment for most efficient and economical operation.
- Prepare a cost analysis of modified systems.
- Complete laboratory tests to quantify variability in PCB analytical procedures.

Summary

The objective of this project is to develop techniques and/or technology to identify and/or cost-effectively remove polychlorinated biphenyls (PCBs) and other substances of concern (SOCs) from recycled automotive materials.

SOCs can impact the recyclability of automotive materials in a number of ways. Certainly, their presence in either recycled materials and/or materials source stream impact the overall costs of recovering recyclable materials. In some cases, their presence at parts-per-million levels, such as PCBs, can prevent the reuse of the recovered materials such as polymers and polyurethane foams.

The strategy that is required for control of the SOCs may vary regionally. For example, requirements are different in Europe, North America, and Asia for various SOCs. Strategies for control of SOCs can also depend on the technology that is being proposed for recycling the automotive material.

The presence of SOCs in current vehicles and/or in other durable goods that are presently recycled with end-of-life vehicles is likely to impact the materials recycle stream for the foreseeable future. Consequently, control of certain SOCs will require technology that will effectively remove the SOCs from recovered materials consistent with current regulatory requirements and consistent with the market requirement for the recovered material.

The initial focus of the work in this project is on the development of options and technology for removal of PCBs from potentially recyclable materials recovered from shredder residue. PCBs, at parts-per-million levels, are routinely found in shredder residue. The source of the PCBs is not completely understood but historically has been associated with liquid PCB-containing capacitors and transformers that inadvertently escape the scrap inspections and control process at the shredders.

Bench-scale screening of commercially available surfactants and large-scale testing of commercially available equipment for cleaning of recovered materials has been conducted.

Laboratory experiments have also been performed to develop an understanding of the variability in PCB analytical procedures.

Bench-Scale Screening of Commercially Available Surfactants for Removal of PCBs

Working with Argonne, Troy Polymers, Inc. (TPI) completed the bench-scale screening of 11 surfactants and 3 organic solvents for removal of PCBs and other contaminants from polymers derived from shredder residue. Multiple samples of mixed plastics and polyurethane foam that were

recovered from shredder residue were used in the study.

The surfactant TRITON RW 50 was found to be the most efficient surfactant among the ones tried. PCB concentrations in the plastics and foam samples that were washed with this surfactant were reduced to below 2 ppm (Table 1).

The three organic solvents were also effective but were precluded from further consideration due to environmental considerations and cost.

Evaluation and Testing of Commercially Available Equipment

Technologies that can potentially be adapted for cleaning/washing of plastics from shredder residue fall into three major categories:

1. conventional methods that include mechanical transport of material through a cleaning solution through an agitation and/or scrubbing process by rotating drums and/or auger systems,
2. ultrasonic systems with and without agitation, and
3. centrifugal systems.

TPI undertook a review of the commercially available equipment, including the following:

- GraPar Corporation, Warren, Michigan. The company's expertise is in the design and manufacturing of aqueous cleaning equipment and systems.
- Almco, Inc., Industrial Finishing Systems, Albert Lea, Minnesota. The company's expertise is in the design and manufacturing of aqueous washers, dryers and liquid filtration systems).
- CarolMac Corporation, Greenville, North Carolina. The company markets centrifuge washers built by SeKoN, Bergamo, Italy.
- RANSOHOFF, Cincinnati, Ohio. The company's expertise is in the design and manufacturing of agitating ultrasonic washers.
- RG Hanson Co., Inc., Bloomington, Indiana. This is a testing lab for developing cleaning specifications and selecting cleaning equipment.
- JTW International, Inc., Lawrenceville, Georgia. The company's expertise is in the design and manufacturing of size reduction, separation, cleaning, and preparation of postconsumer plastic scrap.
- Greco Brothers Incorporated, Providence, Rhode Island. The company's expertise is in the design and manufacturing of aqueous ultrasonic cleaning systems.
- MTA Technical Cleaning, Reseda, California. The company's expertise is in the design and manufacturing of aqueous and ultrasonic parts cleaning equipment.
- Sanborn Technologies, Walpole, Massachusetts. The company's expertise is in the design and manufacturing of separation, ultra-filtration and nano-filtration and in fluid management and disposal issues.
- SeKoN, Italy. The company's expertise is in the design and manufacturing of aqueous washing using centrifugation equipment.

Table 1. Concentration of PCBs in plastics and foam before and after washing, bench-scale tests for surfactant selection

Designation	PCBs before washing (ppm)	
Plastics	2.8 ± 1.4	
Foam	27.2	
Surfactant or solvent used	PCBs in plastics after washing (ppm)	PCBs in foam after washing (ppm)
Triton DF-12	<1	2.4
Triton RW-100	<1	2.7
Tergitol TMN-6	<1	4.1
Bio-Terge Pas-8S	3.2	6.0
Triton RW-50	<0.08	2.0
Triton RW-75	—	4.7
No surfactant used	—	6.2

Preliminary large-scale cleaning/washing experiments were conducted using plastics from shredder residue in the following equipment to identify the limitations of various types of existing equipment: ALMCO rotary drum washer, equipped with a dryer, and SeKoN centrifuge equipment. The tests were carried out on approximately 100 lb of plastic chips each. The particle sizes were between 0.2 and 0.5 in. In each of these large tests, the washed material was "visually" clean as far as dirt and oils are concerned. However, the results for the PCB analyses indicated that the tests were not successful in meeting targets for residual concentrations under the test conditions (residence times, surfactant loading). Analysis of residual heavy metals is not yet complete.

Evaluation and testing of the commercially available equipment, to date, suggests that existing equipment may require modification to efficiently and economically clean plastics that are recovered from shredder residue.

Modifications that are suggested are intended to address two issues: (1) the dirt and oil are not evenly distributed on the plastics; (2) plastics are generally hydrophobic in nature and therefore have the tendency to re-adsorb oils and other organics. Key modifications involve (1) ensuring that the washed material does not come in contact with the liberated oil and dirt that is floating on or dispersed in the wash tank, as the washed material is removed from the tank; (2) ensuring that adequate agitation is provided so that the heavier plastics that will tend to sink stay afloat to achieve adequate mixing and contact between the plastics and the washing solution in the tank; (3) ensuring rapid and adequate removal of the oils and dirt from the wash solution to minimize or eliminate readsorption on the plastics; and (4) rinsing of the washed plastics as they exit the wash tank.

Based on these considerations, GraPar Corp. built a pilot-scale test stand. Controlled tests are planned in the GraPar machine at TPI to further delineate the issues (e.g., surfactant loading, residence times, etc.) with regard to effective cleaning of recovered materials so that more effective evaluations of commercially available equipment can be undertaken.

Evaluation of the Variability of PCB Analytical Procedures

In the large-scale washing tests, there was a significant degree of apparent inconsistency in the analytical results of residual PCB concentrations on the washed materials. Evaluation of these results suggested that this variability may be due to a number of factors including

1. sample size,
2. plastics particle size,
3. PCBs extraction procedure,
4. analytical procedures, and
5. interference from other compounds.

To begin an investigation of the effect of these factors, a series of controlled laboratory experiments were conducted at TPI, to investigate sample size, extraction procedures, plastics particle size, and analytical procedures.

In these experiments, samples of plastics were sent for direct PCB analysis to three different laboratories. Split samples of about 300 g each were extracted in hexane at TPI, and the resultant extract was analyzed for PCB concentrations. Typically, analysis of materials for PCBs is done using samples of only few grams of material.

The split samples were extracted with hexane nine times each in exactly the same manner. Three equivalent sets of these samples were then analyzed by three different laboratories using standard PCB analysis techniques. Preliminary results follow:

1. The three laboratories produced fairly consistent results for each set of samples.
2. Direct analysis of the samples, from the three labs showed that the PCBs concentration in the granulated plastics was about 5 ppm, while the concentrations reported for the ungranulated samples were about 10 ppm. Because the granulated samples have larger surface area per unit mass than the other samples, a more efficient extraction of PCBs from the plastics would be expected in the case of the granulated chips. These apparently inconsistent results are an indication of the variability that can be encountered with direct analysis of the plastics.

3. Calculation of the PCBs concentration in the 300-g samples based on hexane extractions showed concentrations of PCBs in the granulated samples to be comparable to the ungranulated samples. These results indicate that the PCB contamination is a surface contamination and that the PCBs have not been absorbed below the surface of the plastics.

Two of the laboratories identified Aroclor 1242 as the only PCB present, while the third laboratory identified Aroclors 1232 and 1254 as the only two present, and all three labs reported about same overall PCB concentrations. Each of these Aroclors consists of a multiple of congeners, and assignment of the PCB to a particular Aroclor is based on the measured distributions of specific congeners present as interpreted by the analysts. This is an indication of the complexity of the PCB analysis in these samples.

Analyses of samples using GC-ECD (gas chromatography-electron capture detector) and GC-MS (gas chromatography-mass spectroscopy) methods were conducted to compare these techniques. Results from the two methods are in good agreement, even though the GC-MS method seems to consistently predict slightly higher values.

Based on the results of these experiments, the cooperative research and development agreement (CRADA) team is planning a seminar to discuss PCBs analysis with expert chemical analysts to determine whether further work is needed or recommended with regard to analytical procedures.

E. Compatibilization/Compounding Evaluation of Recovered Polymers

Principal Investigator: Bassam Jody
Argonne National Laboratory
9700 S. Cass Ave., Argonne, IL 60439
(630) 252-5279; fax: (630) 252-1342; e-mail: bjody@anl.gov

Field Project Manager: Edward J. Daniels
Argonne National Laboratory
9700 S. Cass Ave., Argonne, IL 60439
(630) 252-4206; fax: (630) 252-1342; e-mail: edaniels@anl.gov

Technology Area Development Manager: Joseph A. Carpenter
(202) 586-1022; fax: (202) 586-1600; e-mail: joseph.carpenter@ee.doe.gov
Field Technical Manager: Philip S. Sklad
(865) 574-5069; fax: (865) 576-4963; e-mail: skladps@ornl.gov

Participants:
This project is conducted as part of the CRADA between Argonne, USCAR's Vehicle Recycling Partnership and the American Plastics Council
CRADA Partner Principal Investigators:
Michael Fisher, American Plastics Council, (703) 741-5599; e-mail: mike_fisher@plastics.org
Gerald Winslow, VRP, DaimlerChrysler Corp., (248) 512-4802; e-mail: grwx@DCX.com
Claudia Duranceau, VRP, Ford Motor Co., (313) 390-0504; e-mail: cdurance@ford.com
Candace Wheeler, VRP, General Motors Corp., (586) 986-1674; e-mail: candace.s.wheeler@gm.com

---

Contractor: Argonne National Laboratory
Contract No.: W-31-109-Eng-38

Objective

- Evaluate the market opportunity of polymers recovered from shredder residue.
- Identify limitations to the re-use of the materials as recovered and determine the need for postprocessing technology to upgrade the recovered materials to meet the requirements of the market.

Approach

- Specify standard protocols for material testing, content characterization, and performance properties.

Accomplishments

- Established a test protocol for material testing, content characterization and physical properties testing of polymeric materials.
- Issued a contract to Midland Compounding to evaluate the properties of polymers that are recovered as part of the technology demonstrations that are being conducted under the project "Postshred Materials Recovery Technology Development and Demonstration."
- Initiated physical properties testing of recovered samples.

Future Direction

- Continue physical properties testing of recovered polymers.
- Evaluate the market potential for clean mixed plastics streams recovered from shredder residue.
- Establish a database of properties of recovered polymers vis-à-vis general purpose virgin polymers.
- Identify candidate automotive applications for recovered polymers.
- Conduct mold trials using recovered polymers.

Summary

The objectives of this project are (1) to characterize the properties of potentially recyclable automotive materials and (2) to confirm the technical and economic feasibility of using those materials in value-added applications.

The project will initially focus on establishing the properties of polymeric materials that are recovered as part of the Post-Shred Materials Recovery Technology Development and Demonstration project.

Regardless of the effectiveness of any automotive materials recovery technology, the materials that will be recovered will be on average 10 to 15 years old. In this project, the performance properties of recovered polymers will be compared vis-à-vis new or virgin materials to establish a database of the properties of recovered automotive polymers. At present, there are few data concerning the physical properties of polymers recovered from postconsumer durable goods. Absent such data, it is unlikely that sustainable applications for recycled materials will be either identified or developed.

Blending and compounding tests will be done, as required, to achieve desired performance properties of the recovered materials for target applications. Mold trials may also be conducted to confirm the technical and economic feasibility of using recycled polymers in specific applications.

Physical properties testing is conducted by Midland Compounding, Inc. Midland will also run composition testing for comparison with compositional analysis done on recovered materials by Argonne.

Three other companies, Collins and Aikman Corporation, Enviro-Plas Corporation, and Mayco Plastics, Inc., have agreed to evaluate, compound, and run mold trials using recovered materials subject to the physical properties of the recovered materials.

Polymer Physical Properties and Materials Composition Analysis

Typically, 10-lb samples of recovered materials are utilized to define physical properties and to characterize the composition of the material.

To quantify physical properties, the sample is extruded on a single-screw extruder, melt screened through a 40-mesh screen, molded into American Society for Testing and Materials (ASTM) test bars and plaques, and tested. The molded parts and a random selection of regrind chips from each sample are evaluated for material identification on a Bruker P/ID 28 IR machine.

Physical properties that are measured for each sample include the following:

— melt flow rate,
— Izod impact,
— flexural modulus,
— tensile strength at yield,
— tensile strength at rupture,
— elongation at rupture,
— deflection temperature,
— Gardner impact, and
— specific gravity.

Physical properties of the high-impact polystyrene (HIPS) and the acrilonitrile-butadienestyrene (ABS) materials recovered during the shakedown tests of the Argonne froth-flotation process are summarized in Table 1. The shakedown trials were conducted using postconsumer shredded electronics and appliances scrap, not plastics from a typical automotive shredding

Table 1. Physical properties of HIPS and ABS recovered during Argonne froth-flotation shakedown trials

Properties	HIPS 1	HIPS 2	ABS
Melt flow rate, g/10 min, 200°C, 5 kg	5.4	5.5	5.2
Izod impact, ft-lb/in., 73°F	1.6	1.6	1.6
Flex modulus 1% secant, psi	248,662	262,939	341,543
Tensile strength at yield, psi	3,068	3,091	5,242
Tensile strength at rupture, psi	3,082	3,137	5,035
Elongation at rupture, %	38	41	33
Deflection temperature under load, 264 psi, °F	147	153	165
Gardner impact, 73°F, in.-lb	12	20	4
Specific granty, g/cm^3	1.05	1.05	1.08

operation. (See the Annual Report, "Postshred Materials Recovery Technology Development and Demonstration, see 6.C.)

A comparison of the physical properties of the recovered HIPS to various primary or "virgin" grades of HIPS indicates that the properties of the recovered postconsumer material are within the ranges of the "virgin" grades (Table 2).

Polymer Physical Properties Database

A physical properties database is being compiled to provide comparison of the physical properties of the recovered polymers vis-à-vis general purpose virgin polymers. The Vehicle Recycling Partnership had previously compiled physical properties data on selected polymers that were recovered during the U.S. Field Trials. These materials were recovered by disassembly. These data will also be included in the database to provide a comparison between the physical properties of materials recovered by disassembly relative to materials that are recovered from postshred operations.

General purpose physical properties have been compiled from the literature for the following plastics:

- ABS,
- nylon (6 cast, 6/6 extruded, 30% glass filled),
- PPO (unfilled, 30% glass filled),
- polycarbonate,
- polyethylene (LDPE, HDPE, UHMW),
- polypropylene,
- polystyrene (general purpose, high impact), and
- polyvinyl chloride (PVC).

Other polymer specifications may be added to the database as appropriate.

Table 2. Comparison of "recycled" and "virgin" grades of HIPS

Properties	HIPS 1	HIPS (natural)	Dow 484 HIPS (natural)
Generic material description	As received	Range	Typical HIPS
MFR, g/10 min, 200°C, 5 kg	5.7	2–14	2.8
Izod impact, ft-lb/in., 73°F	1.8	1–4	2.1
Flex modulus, 1% secant, psi	275,927	240,000–430,000	277,000
Tensile strength at yield, psi	2,660	2200–4500	2,800
Tensile strength at rupture, psi	3,033	2100–4500	3,500
Elongation at rupture, %	48	25–70	52
DTUL, 264 psi, °F	178	157–199	165
Gardner impact, 73°F, in.-lb	14	10–330	160
SG, g/cm^3	1.053	1.04	1.04

7. ENABLING TECHNOLOGIES

A. Durability of Carbon-Fiber Composites

Dan J. Naus (Principal Investigator), J. M. Corum, R. L. Battiste, C. Janke, J. Spruiell, L. Klett, Y. J. Weitsman, A. Ionita, J. Cao, H. Lin, M. Davenport
Oak Ridge National Laboratory, P.O. Box 2009
Oak Ridge, TN 37831-8056
(865) 574-0657; fax: (865) 574-6098; e-mail: nausdj@ornl.gov

Technology Area Development Manager: Joseph A. Carpenter
(202) 586-1022; fax: (202) 586-1600; e-mail: joseph.carpenter@ee.doe.gov
Field Technical Manager: Philip S. Sklad
(865) 574-5069; fax: (865) 576-4963; e-mail: skladps@ornl.gov

---

Contractor: Oak Ridge National Laboratory
Contract No.: DE-AC05-00OR22725

Objective

- To develop experimentally-based, durability-driven design guidelines to ensure the long-term (15-year) integrity of representative carbon-fiber-based composite systems that can be used to produce large structural automotive components. Durability issues being considered include the potentially degrading effects of cyclic and sustained loadings, exposure to automotive fluids, temperature extremes, and low-energy impacts from such events as tool drops and kickups of roadway debris on structural strength, stiffness, and dimensional stability.

Approach

- Characterize and model the durability behavior of a progression of three representative carbon-fiber composites, each with the same thermoset urethane matrix but having a different reinforcement preform: (1) continuous fiber, ±45° crossply; (2) continuous fiber, quasi-isotropic; and (3) random chopped fiber.
- Replicate on-road conditions in laboratory tests of each composite to generate durability data and models.
- Subsequently shift focus to suitable thermoplastic composites, for which durability issues are generally more significant.
- Develop and publish durability-based design criteria for each composite.

Accomplishments

- Published report addressing mechanical response of randomly-reinforced, chopped-fiber composites (MABE03-1.0-CM, University of Tennessee, October 2003).
- Completed draft report assessing the effects of processing on poly(phenylene sulfide) (PPS) crystallinity and the relationship between crystallinity and properties (ORNL report, August 2004).
- Completed testing to determine baseline tensile and compressive properties and effect of specimen orientation and annealing on these properties.
- Completed testing to investigate effect of thermal exposure and thermal cycling on tensile and compressive properties.

- Completed in-air, room temperature, tensile creep-rupture testing.
- Completed impact testing (pendulum, air-gun, and brick drop tests) and compression- and tension-after-impact testing.
- Completed testing to evaluate damage tolerance to circular holes and cracks.
- Completed testing to evaluate effect of specimen width on tensile properties.
- Published report on the nonlinear response of quasi-isotropic laminates (*Composite Science and Technology*, Vol. 64, pp. 1577–1585, Elsevier, 2004).
- Published report on properties, failure, and aspects of material design for randomly-reinforced composites. (Report MABE04-3.0-CM, Mechanical, Aerospace and Biomedical Engineering Department, University of Tennessee, Knoxville, August 2004.)
- Input carbon-fiber composite data directly into the planning and analysis for the Focal Project III carbon-fiber body-in-white.

Future Direction

- Publish report on relationship between processing of PPS materials and crystallinity as well as relationship between crystallinity and material properties.
- Complete durability assessment of carbon-fiber-reinforced PPS material.
- Publish durability-driven design criteria documents for representative thermoplastic composites suitable for automotive structural applications.

Introduction

Before composite structures will be widely used in automotive applications, their long-term durability must be assured. The Durability of Carbon-Fiber Composites Project at the Oak Ridge National Laboratory (ORNL) was established to develop the means for providing that assurance. Specifically, the project is developing and documenting experimentally-based, durability-driven design criteria and damage-tolerance assessment procedures for representative carbon-fiber composite systems to assure the long-term (15-year) integrity of composite automotive structures. Durability issues being considered include the potentially degrading effects of cyclic and sustained loads, exposures to automotive fluids, temperature extremes, and incidental impacts from such things as tool drops and kick-ups of roadway debris. Research to determine the effect that these environmental stressors and loadings have on structural strength, stiffness, and dimensional stability is being conducted. The project is carried out in close coordination with the Automotive Composites Consortium (ACC).

It is envisioned that about 15% of the Focal Project III (4.C) carbon-fiber-composite body-in-white will utilize directed continuous-fiber reinforcement architectures, while the remainder will employ random chopped-fiber reinforcement. The approach to investigating durability has thus been to address a progression of thermoset composites, each of which has the same urethane matrix:

- reference $[\pm 45]_{3S}$ crossply composite,
- $[0/90/\pm 45]_S$ quasi-isotropic composite, and
- Randomly-oriented chopped-carbon-fiber composite.

Characterization of the first two, continuous-fiber composites has been completed, and design criteria documents published. In mid-FY 2002, the focus turned to chopped-carbon-fiber composites. Characterization of the randomly-oriented chopped-carbon-fiber composite was completed in FY 2003. Also in FY 2003, investigation of carbon-fiber-reinforced thermoplastic materials for structural automotive applications was initiated. Primary activities associated with evaluation of the thermoplastic material have addressed thermoplastic

material characterization, baseline property determination, environmental and sustained-loading effects testing, and damage-tolerance assessments.

Thermoplastic Material Characterization

The ACC has supplied 43 plaques, 510 mm by 610 mm by about 3-mm thick, for use in durability studies. Plaque reinforcement is symmetrical and consists of 16 plies of carbon-fiber unidirectional tape, [0/90/±45]2S. PPS is the matrix material.

Processing conditions are very important because they affect the crystallinity of a semicrystalline polymer such as PPS. Crystallinity changes of thermoplastic materials can result in significant changes in the mechanical behavior of composites containing them, particularly with respect to matrix-dominated properties such as compressive strength and creep. For this reason, the ability to precisely characterize the polymer crystallinity in a thermoplastic material becomes an important requirement. Unfortunately, due to the proprietary nature of the material processing, only limited information has been provided by the material supplier on processing of the as-received material.

Differential scanning calorimetry (DSC) results, over the temperature range from 40 to 320˚C, have been obtained from several samples of the quasi-isotropic material to investigate crystallinity of the as-received material. The first scan indicated that the degree of crystallization was less than optimum—about 85% of maximum crystallinity or about 32% crystallinity assuming a 40% resin content. The crystallization peak was not present during the second scan, indicating a higher degree of crystallinity due to the first scan test temperature. Additional ramp-and-hold experiments were run in which samples were either heated from 40 to 90°C at 20˚C/min, held at 90°C for 60 min and then permitted to return to room temperature; or heated to 120°C and held for 60 min prior to cooling to room temperature. After the 90°C ramp, the scan (sample ran at 40 to 320°C at 20°C/min) showed a T_g and crystallization peak signifying less than an optimum degree of crystallinity. The second scan exhibited a flat baseline indicating a high degree of crystallinity. Additional testing conducted by the University of Tennessee using X-ray diffraction produced crystallinity results in agreement with those obtained at ORNL.

A review of literature and contacts with industry has been conducted to provide data and information that addresses the relationship between processing of PPS materials and crystallinity as well as the relationship between crystallinity and material properties. Results of this review are provided in a report that has been prepared.[1]

Baseline Property Determination

Tests to establish room-temperature tensile and compressive properties of as-received material as well as material that has been annealed at 230°C for 2 h in an attempt to enhance the as-received material crystallinity, have been completed. Investigation of specimen orientation effects also has been completed.

Table 1 summarizes tensile and compressive properties obtained to date for the as-received material. Tensile results represent tests of 128 specimens that were obtained from 24 plaques. Compressive results represent tests of 46 specimens obtained from 8 plaques. Tensile and compressive properties for material that had been annealed at 230°C for 2 h are summarized in Table 2. Results for specimens tested at room temperature indicate that annealing produced little change in tensile or compressive properties compared to results from as-received material.

The effect of specimen orientation was investigated. Tensile and compressive test specimens were machined having their major axis

Table 1. Baseline properties: as received material

Property	Tension	Compression
Strength, MPa	540	294
Modulus, GPa	36.44	34.40
Failure Strain, %	1.51	0.94

Table 2. Baseline properties: annealed material

Property	Tension	Compression
Strength, MPa	539	292
Modulus, GPa	37.38	35.09
Failure strain, %	1.42	0.92

oriented either at 0°, 22.5°, 45°, or 90° relative to the long direction of the plaque. Test results are summarized in Table 3. Tensile strength results for each orientation were fairly consistent except for the 22.5° orientation, which is the only orientation that does not coincide with a carbon fiber direction. Compressive strength results were maximum at a specimen orientation of 45°. The carbon-fiber reinforcement tends to have the greatest influence on tensile properties, and the matrix material has added significance relative to compressive results. The tensile and compressive moduli of elasticity for both tensile and compressive testing did not exhibit an orientation effect. Tensile and compressive strains at failure exhibited similar trends to the tensile and compressive strength results. Tensile and compressive results obtained from annealed material exhibited similar trends to the as-received material.

Table 3. Effect of specimen orientation

Property	Orientation[a]			
	0°	22.5°	45°	90°
Tensile				
Strength, MPa	546	383	618	614
Modulus, GPa	37.3	36.7	37.0	40.0
Failure strain, %	1.43	1.07	1.65	1.48
Compression				
Strength, MPa	254	335	369	336
Modulus, GPa	33.8	34.9	34.6	36.5
Failure strain, %	0.83	1.07	1.23	0.98

[a]0° is in long direction of the plaque.

Environmental and Sustained-Loading Effects Testing

Three series of tests were conducted that address environmental and sustained-loading effects: elevated temperature, thermal cycling, and creep rupture.

The effect of elevated temperature on tensile and compressive properties was evaluated by subjecting specimens to preconditioning temperatures of either –40, 70, 90, or 120°C for 1 h prior to testing. For each preconditioning temperature, half the specimens were tested at temperature with the other half permitted to return to room temperature prior to testing. This series of tests involved material in the as-received condition as well as material that had been annealed.* Figures 1 and 2 present tensile strength results as a function of preconditioning temperature for as-received and annealed materials that had been either permitted to return to room temperature prior to testing or tested at temperature, respectively. Similar results were provided for both the as-received and annealed materials because the tensile strength tended to increase slightly with preconditioning temperature for specimens permitted to return to room temperature prior to testing and decrease slightly when specimens were tested at temperature. Modulus of elasticity results for both materials were relatively unaffected by preconditioning temperature for specimens either permitted to return to room

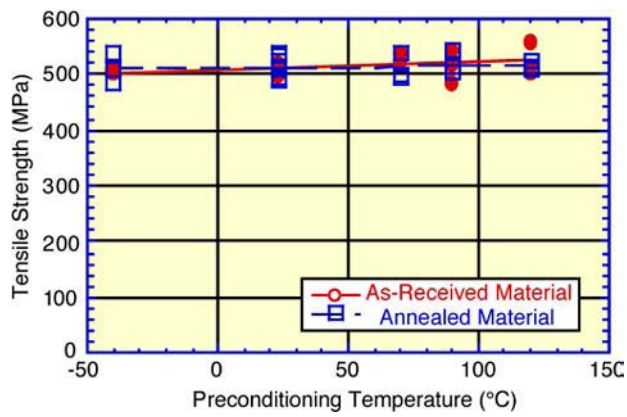

Figure 1. Effect of preconditioning temperature on tensile strength: room temperature tests.

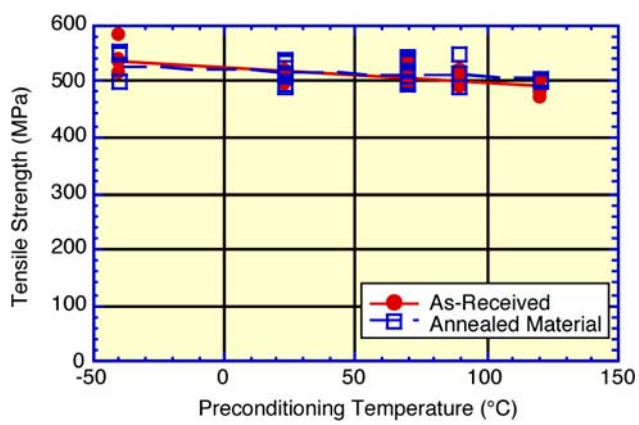

Figure 2. Effect of preconditioning temperature on tensile strength: tests at temperature.

*Specimens were tested having major axis orientations of 0° and 22.5°. Only 0° orientation results are presented.

temperature prior to testing or tested at temperature. The effect of preconditioning temperature on compressive strength of as-received material tested either at temperature or permitted to return to room temperature prior to testing is presented in Figure 3. Results for both test environments were fairly consistent up to a preconditioning temperature of 70°C; however, at higher temperatures the compressive strength of specimens permitted to return to room temperature prior to testing was consistently higher than that obtained from specimens tested at temperature. Compressive modulus of elasticity was relatively unaffected by the preconditioning temperature and test environments (Figure 4). Compressive strength results for the annealed material tested at temperature also tended to decrease with increasing preconditioning temperature; however, the tensile strength results for the annealed material tested at room temperature exhibited a trend to increase slightly with preconditioning temperature.

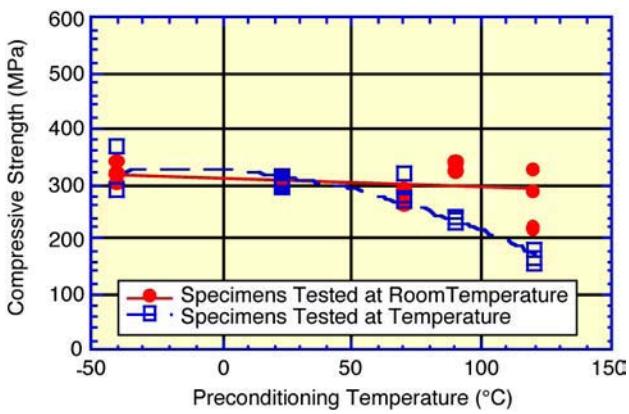

Figure 3. Effect of preconditioning temperature on compressive strength: as-received material.

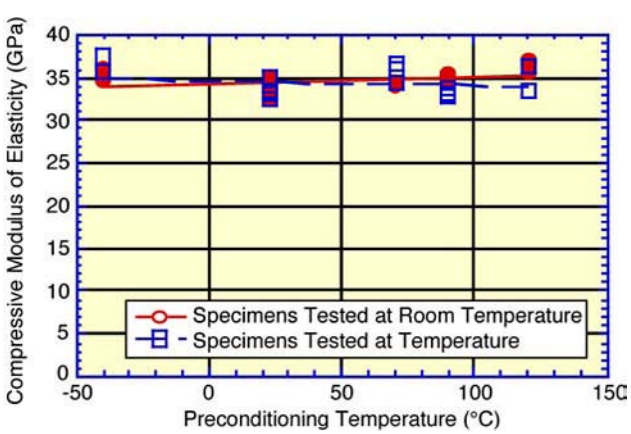

Figure 4. Effect of preconditioning temperature on compressive modulus: as-received material.

The effect of prior thermal cycling on tensile and compressive properties was also investigated. Prior to testing, specimens were subjected to either, 1, 5, 10, or 25 thermal cycles from 23°C to 120°C to –40°C to 23°C. Results, summarized in Table 4, indicate that for the temperature range and number of thermal cycles investigated, there was a slight increase in tensile strength resulting from the thermal exposure; however, little change in other tensile and compressive properties resulted relative to the baseline data.

Table 4. Effect of thermal cycling

Property	Number of thermal cycles				
	0	1	5	10	25
Tensile					
Strength, MPa	520	568	551	555	532
Modulus, GPa	36.3	35.9	36.1	35.3	35.1
Failure strain, %	1.37	1.47	1.48	1.45	1.42
Compression					
Strength, MPa	323	296	322	316	311
Modulus, GPa	34.6	39.1	34.4	33.4	33.7
Failure strain, %	1.05	0.83	1.04	1.03	1.02

Sustained-load tests (creep rupture) were conducted as part of an overall assessment of the PPS composite material's ability to sustain constant loads for long time periods. Twenty-three in-air room temperature tests were conducted in which tensile specimens were loaded to nominal values representing 80.0 to 95% of the material's ultimate tensile strength. The specimens remained under load until either they failed or the test was terminated. Failure times ranged from less than 2 h for specimens loaded to 95% ultimate tensile strength to 500 to 2000 h for specimens loaded to 86% ultimate tensile strength. No failures were observed for specimens loaded to ≤ 84% ultimate tensile strength. Seven in-air, elevated-temperature (120°C) creep rupture tests are under way.

Damage Tolerance Assessments

Damage tolerance assessments have addressed both damage resistance (impact tests) and damage tolerance (holes and cracks). Both of these aspects are important because it is desired that an automotive composite be resistant to formation of

damage as well as tolerant of any damage or defect that is present.

Forty-two impact tests have been conducted as part of an assessment of the ability of the PPS composite material to continue to perform its function in the presence of damage. Air-gun and pendulum tests were performed both at room temperature and at low temperature (–40°C) (Figure 5). Also, a series of brick-drop tests was performed at room temperature. The impact tests were performed to address potential service-induced damage resulting from events such as kick-ups of roadway debris, tool drops, and events of interest to pickup truck boxes. The tests utilized material in the as-received condition as well as material that had been annealed prior to testing. Impact parameters (e.g., velocity or drop height) were selected to inflict damage ranging from slight to severe. Ultrasonic "C" scans of the specimens were used to determine the damage area in each of the specimens. Figure 6 presents time-of-flight results for an air-gun impact specimen tested at –40°C, indicating that damage occurred at different depths in the material thickness. After conduct of an impact test and assessment of the damage areas, each specimen was cut into three test specimens to be used for compressive or tensile tests: specimen containing impact damage, specimen for baseline testing, and specimen containing a circular hole having roughly the same area as the

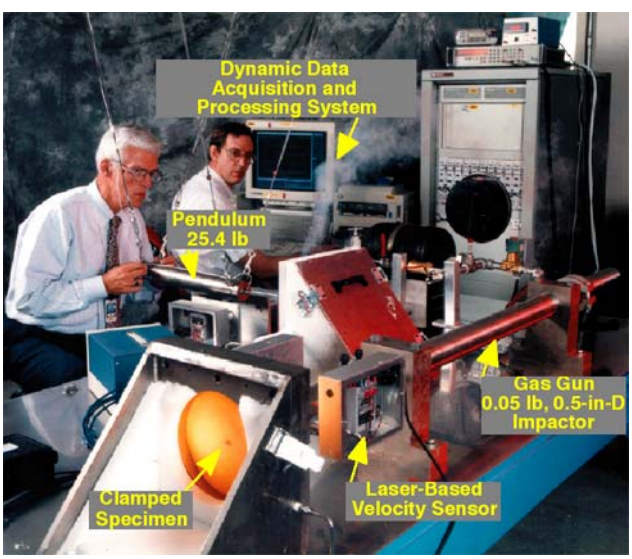

Figure 5. Air gun and pendulum impact test facility.

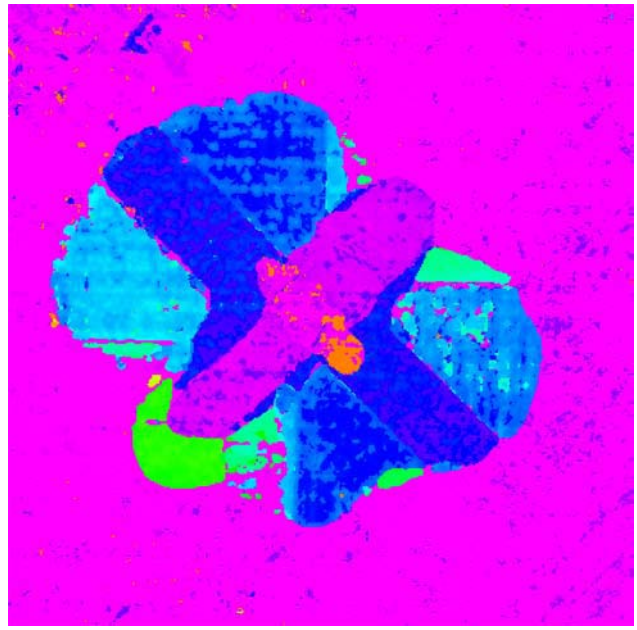

Figure 6. Time-of-flight ultrasonic results: Spec. T7-27.

corresponding impact damage. Figure 7 presents damage area vs kinetic energy for the pendulum and air gun impact tests and compares it to a thermoset quasi-isotropic material tested previously (Note: quasi-isotropic thermoset is 2.2-mm thick vs 2.8-mm thickness of thermoplastic). Results indicate that the air gun produced larger damage areas than the pendulum for a given impactor energy. Compression-

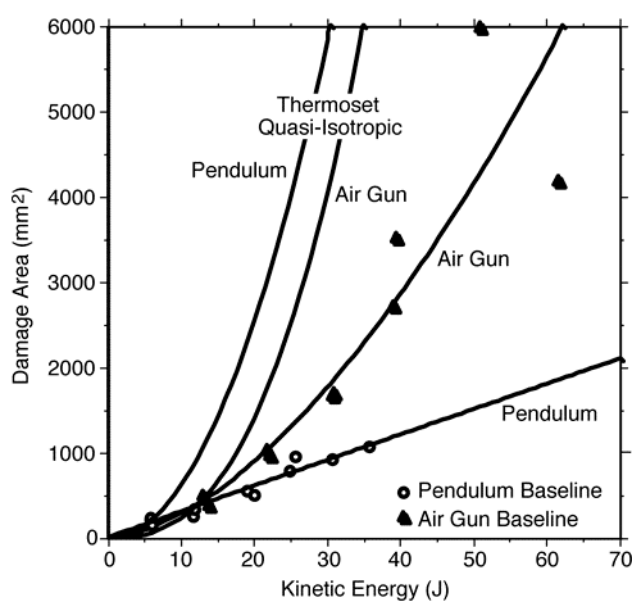

Figure 7. Impact test results: damage area vs kinetic energy.

and tension-after-impact tests indicate that compressive strength reduction was greater than tensile strength reduction.

Additional information on damage tolerance was provided by testing tensile specimens that contained center holes and cracks. Figure 8 presents notch strength (gross stress in an infinitely wide plate away from hole or crack) normalized for plaque ultimate tensile strength as a function of hole diameter or crack length. Crack results agree closely with those obtained from holes and tend to be in agreement with fracture-mechanics relationships.

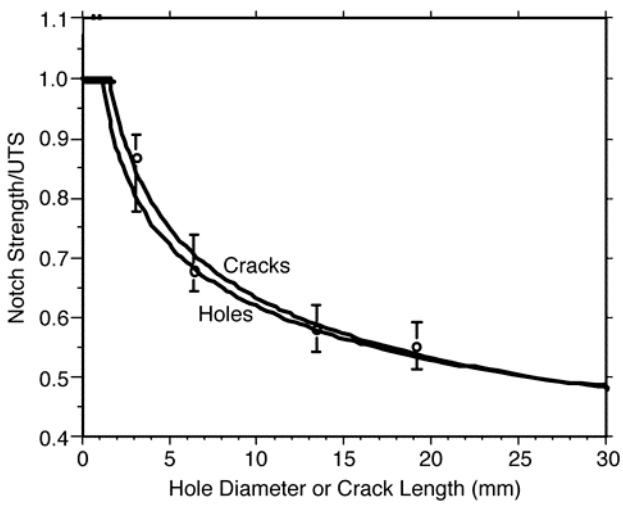

Figure 8. Impact test results: damage area vs kinetic energy.

Summary

A quasi-isotropic carbon-fiber-reinforced PPS material is being investigated. This is the first thermoplastic material to be studied under the durability program. The ACC has supplied 43 plaques, 510 mm by 610 mm by about 3-mm thick, for use in durability studies. Plaque reinforcement is symmetrical and consists of 16 plies of carbon-fiber unidirectional tape, $[0/90/\pm45]_{2S}$. Processing conditions for these plaques are very important because they affect the crystallinity of a semicrystalline polymer such as PPS, which can result in significant changes in the mechanical behavior of composites containing them. Because precise processing information on the plaques is not available due to the proprietary nature of the processing, the crystallinity of the material was investigated. DSC and X-ray diffraction have been utilized to investigate the as-received material crystallinity, and results indicate that the material has a crystallinity that is about 85% of maximum. A report has been prepared that presents data and information on the relationship between processing of PPS materials and crystallinity as well as the relationship between crystallinity and material properties.

Tests to establish baseline room-temperature tensile and compressive properties of the PPS composite material have been completed. The effect on tensile and compressive properties of annealing at 230°C for 2 h to increase crystallinity of the as-received material has been investigated. Testing to evaluate specimen orientation effects for the as-received and annealed material has been completed. The effect of thermal exposure at temperatures up to 120°C for 1 h prior to testing on tensile and compressive properties has been evaluated. Testing to investigate the effect on tensile and compressive properties of applying up to 25 thermal cycles from room temperature to 120°C to –40°C to room temperature prior to testing has been completed. In-air, room-temperature sustained tensile loading (creep rupture) tests have been completed. Damage tolerance assessments have been completed that address both damage resistance (impact tests) and damage tolerance (presence of holes and cracks).

Results presented above in addition to subsequent testing to be conducted will be used to develop recommended durability-based design properties and criteria for the quasi-isotropic carbon-fiber-reinforced PPS composite for possible automotive structural applications. Durability issues being addressed include the effects on deformation, strength, and stiffness of cyclic and sustained loads, automotive fluid environments, and low-energy impacts. Guidance will be developed for design analysis, time-dependent allowable stresses, rules for cyclic loadings, and damage-tolerance design guidance.

Reference

1. J. E. Spruiell and Chris J. Janke, A Review of the Measurement and Development of Crystallinity and Its Relation to Properties in Neat Poly(Phenylene Sulfide) and Its Fiber Reinforced Composites, ORNL/TM-2004/304, Oak Ridge National Laboratory, Oak Ridge, Tennessee, August 2004.

B. Interphase Analysis and Control in Fiber-Reinforced Thermoplastic Composites

Principal Investigator: Jon J. Kellar
Department of Materials and Metallurgical Engineering
South Dakota School of Mines and Technology
501 E. St. Joseph Street
Rapid City, SD 57701-3901
(605) 394-2343; (605) 394-3369; e-mail: jon.kellar@sdsmt.edu

Technology Area Development Manager: Joseph A. Carpenter
(202) 586-1022; fax: (202) 586-1600; e-mail: joseph.carpenter@ee.doe.gov
Field Technical Manager: Philip S. Sklad
(865) 574-5069; fax: (865) 576-4963; e-mail: skladps@ornl.gov

---

Contractor: South Dakota School of Mines and Technology
Contract No.: DE-FG02-04ER46117, jointly funded by DOE Office of Science and Office of Energy Efficiency and Renewable Energy under the Experimental Program to Stimulate Competitive Research (EPSCoR)

Objectives

- Develop the science underlying the formation and effects of transcrystalline regions in carbon-fiber-reinforced thermoplastic matrix composite systems.
- Exploit the understanding developed from the research described above to allow controlled tailoring of the interphase transcrystallinity for specific applications.
- Analyze processing parameters in new thermoplastic matrix composite technologies, specifically the DRIFT (Direct Reinforcement Fabrication Technology, Southern Research Institute) and the P4 [Programmable Powered Preform Process, Department of Energy (DOE)/Oak Ridge National Laboratories (ORNL)] processes.
- Generate composites with tailored interphases for specific applications of laminates produced by the DRIFT and P4 processes in the FreedomCar and other DOE initiatives in lighter weight vehicles.

Approach

- Choose matrix materials relevant to the FreedomCar and DOE automotive lightweight materials initiatives.
- Characterize the chosen matrix materials with respect to mechanical properties and crystallinity.
- Determine the thermodynamic and practical adhesion between the chosen matrix materials and carbon fibers. The carbon fibers will be both sized and unsized.
- Identify and control the presence and size of transcrystalline regions in the matrix material adjacent to the carbon fibers.
- Manufacture laminates using the DRIFT and P4 processes having controlled transcrystalline regions.
- Perform mechanical testing, including tensile testing, impact testing, and indentation testing of the laminates having controlled interphases.

Accomplishments

- Chose matrix materials—polypropylene (PP), poly(phenylene) sulfide (PPS).
- Manufactured axisymmetric microbond test fixture for practical adhesion measurements.
- Created carbon fiber resistivity/temperature calibration curves and heating device.
- Gave presentation at South Dakota EPSCoR (Experimental Program to Stimulate Competitive Research) Conference.
- Began mechanical testing of component materials.

Future Direction

- Conduct thermodynamic and practical adhesion measurements of PP and PPS with carbon fibers having various (including no) sizings.
- Perform indentation testing of initial DRIFT laminates with Dr. Edgar Lara-Curzio of ORNL and with a new nanoindentation machine recently purchased by the South Dakota School of Mines and Technology (SDSM&T).
- Continue mechanical property determination of matrices and fibers. Much of this work will be performed at SDSM&T, but some single-fiber testing work will be performed at ORNL.
- Begin measurement of the extent of transcrystalline regions in test pieces using a new acoustic force atomic force microscope accessory, to be purchased with funds from this grant.
- Perform static and dynamic mechanical testing of DRIFT and P4 laminates.
- Send at least one student and two of the Principle Investigators to ORNL and the University of Alabama-Birmingham to procure samples, perform testing, and better understand the processing techniques used to fabricate samples.

Introduction

During the past decade, considerable effort has been expended to develop a new generation of vehicles that are lighter and more fuel-efficient than today's vehicles. In addition, these vehicles should retain crashworthiness and be of relatively low cost. Targets include reduction in overall weight of approximately 50%, primarily achieved through lighter body and chassis materials. Polymer matrix composites (PMCs) have reached this target with a potential weight savings of 70%. At the current time, PMC technology has, in general, been deemed too costly, because carbon-fiber-based PMCs can cost ten times as much as steel parts. Some of this increased cost is due to the high price of carbon fibers and some due to limitations in the manufacturing process. Many of the problems in the manufacturing process are caused or exacerbated by lack of fundamental scientific knowledge of the interactions between the fibers and matrix materials.

This research is of significance to the Department of Energy (DOE) Automotive Lightweighting Materials Program because it will help develop the necessary science base to allow greater exploitation of PMCs having thermoplastic matrices. Traditionally, these materials have trailed the use of PMCs having thermoset matrices, because of processability issues stemming from the low viscosity and wetting of the thermoplastic matrix material. In addition, thermoplastic matrices are generally less strong and less stiff than thermoset matrices. This liability is further compounded by the fact that most fiber reinforcements associated with thermoplastic matrix PMCs are of fairly short length, mainly because of the processing limitations mentioned earlier. This latter aspect is relevant because short-fiber reinforcements do not carry load as well as long or continuous fiber reinforcements. From the automotive perspective, short-fiber-reinforced PMCs are therefore most utilized in nonstructural components. Further comparisons between thermoplastic and thermoset matrix PMCs

are warranted here to highlight the focus of this research project, namely the role of the interface/ interphase region between the fiber and the matrix.

The development of the interphase in thermoplastic PMCs is quite different from that of thermosetting matrices, which tend to be amorphous in nature. Rather, in thermoplastic PMCs, the interphase development is generally due to nucleation and growth of crystallites from the fiber surface rather than actual chemical reactions within the interphase. The interphases formed in these systems are termed transcrystalline regions, reflecting their dependence upon the thermoplastic crystallinity. There has been much speculation in the literature as to the cause for the formation of the transcrystalline region and its role in bulk composite properties. Several conclusions can be reached. First, the transcrystalline region can grow in size to tens of microns, depending upon such parameters as fiber type, morphology, and fiber surface treatments such as sizings. Second, the transcrystalline region can significantly affect properties such as the strength and impact resistance. Also, in some cases different types of transcrystalline interphases may be formed. For instance, both α and β transcrystalline regions were produced around natural fibers in polypropylene matrix composites. These regions could be altered by inclusion of maleic anhydride in the polypropylene or on the fiber.

With respect to these novel processing routes, two examples are of particular interest to this research. The first is a low-cost process to produce continuous reinforcing fibers with thermoplastic matrices, called the **D**irect **Rei**nforcement **F**abrication **T**echnology (DRIFT) developed by the Southern Research Institute (SRI). PMCs produced by this continuous fiber technology could serve as metal-replacements in structural applications, specifically for the automotive industry. Keys to optimal utilization of the DRIFT process are fiber wetting, and ultimately adhesion, of the thermoplastic matrix. Traditionally, sizings are applied to the fibers to help prevent abrasive damage, and assist with lubrication. A major component of the sizing is a coupling agent that aids in wetting, adhesion, and hygrothermal stability of the composite. Research conducted in this program will utilize thermoplastic matrix PMCs produced by SRI using the DRIFT process. The second novel processing route of interest is the **P**rogrammable **P**owered **P**reform **P**rocess (P4). While the P4 technology does allow control over fiber length, its main potential benefit is its ability to circumvent previous PMC process limitations through robotic control. To our knowledge, no fundamental analysis of PMC interphases formed by the P4 technology has been undertaken.

This research program builds upon a multidisciplinary effort with a vast background in interphase analysis and control in thermosetting PMC systems and applies this wealth of experience to new thermoplastic matrix PMC systems critical to the future success of the Automotive Lightweighting Materials Program. The research will investigate model systems deemed of interest by members of the Automotive Composites Consortium (ACC) as well as samples at the forefront of PMC process development (DRIFT and P4 technologies). Finally, the research will investigate, based upon the fundamental understanding of the interphases created during the fabrication of thermoplastic PMCs, the role the interphase plays in key bulk properties of interest to the automotive industry.

Project Deliverables

This research will provide a better understanding of the science, particularly with respect to adhesion, of thermoplastic matrices with fiber reinforcements. The adhesion data will be used to identify processing parameters for thermoplastic matrix composites to tailor transcrystalline interphase formation. Transcrystalline interphases are generally quite large (>10 μm) and can be stronger and stiffer than the matrix material or tougher and with greater work of fracture than the matrix. In addition, this work will produce composite samples using new processing technologies and the scientific knowledge gained with respect to adhesion and interphase formation. These test protocols are important to possible end uses for the tailored PMCs in automotive applications.

Accomplishments

Research accomplishments during the past year occurred in three primary areas: adhesion, mechanical property determination, and extent of crystallinity as a function of formation conditions. Progress in each of the three areas is described below.

Adhesion

Adhesion research was divided into two areas, thermodynamic adhesion and practical adhesion. Thermodynamic adhesion includes the measurement of the work of adhesion between each polymer and fiber combination through the determination of the drop geometry and hence three-phase contact angle. Practical adhesion is the polymer/fiber adhesion measured through micromechanical testing such as the microbond test or the microindentation test. In thermodynamic adhesion progress, drop shapes for a variety of polymer beads on carbon fibers have been measured and the contact angles found. A typical drop is shown in Figure 1. This work is ongoing. In addition, methods of heating the fiber, as in the DRIFT process, have been developed. Also, techniques for measuring the fiber temperature were derived. Currently, the best method involves resistively heating the fibers through the application of an applied voltage. This process was modeled through a finite-difference, heat-transfer model. The model is used to back calculate the temperature, as the resistance as a function of temperature for the fibers has been measured experimentally.
Figures 2–4 contain graphs of the fiber resistivity curve, the fiber temperature as a function of length, and power vs temperature for a resistively heated fiber. In Figure 2, the resistivity was found to vary with the length of the fiber used, but the slope of the resistivity was relatively constant for all fiber lengths until fiber oxidation began at about 250–300ºC. In Figure 3, the temperature distribution away from the heatsink at a fiber end was found using the equations listed with the figure. Within 2 μm from the heatsink, the fiber has achieved a constant temperature. In Figure 4, a carbon fiber was resistively heated and the temperature predicted from the data in Figure 2. A small polypropylene (PP) chevron was placed on the fiber during heating, and the point of PP melting was found from visual observation. The PP melting point was slightly higher than measured in bulk PP, which could be due to heat transfer effects, differences between the types of fibers used, or the method of observation.

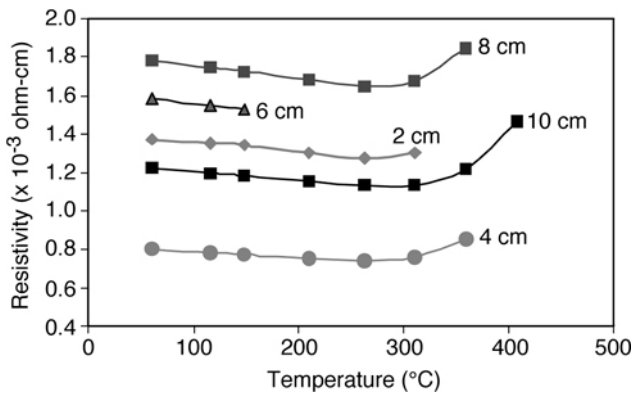

Figure 2. Measured carbon fiber resistivity as a function of applied temperature.

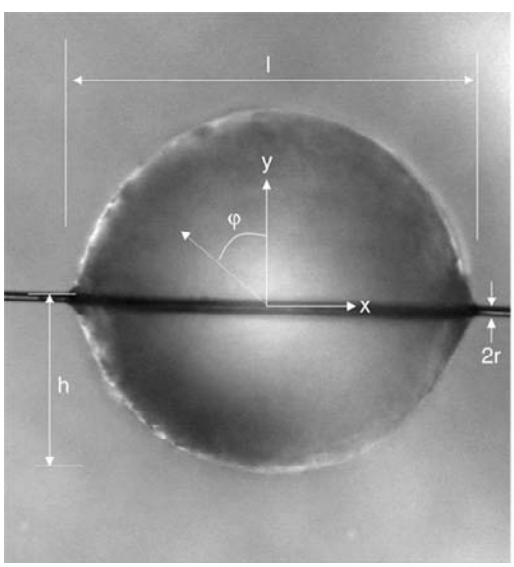

$x = \pm[arF(\varphi, k) + hE(\varphi, k)]$,

$y^2 = h^2(1 - k^2\sin^2\varphi)$,

a = f (contact angle, geometry)
h = f (geometry)
k = f (a, h)
F, E are Legendre integrals

$y_{max} = h$
$x_{max} = 1/2$

Figure 1. Polypropylene bead on carbon fiber.

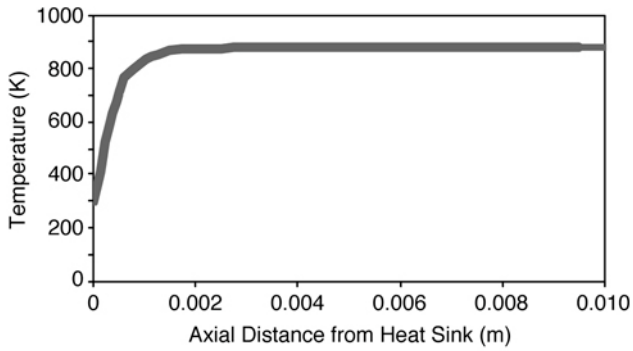

$$k\frac{\partial^2 T}{\partial x^2} - \frac{2}{r}\left[h(T - T_{air}) + \sigma\varepsilon(T^4 - T_{air}^4)\right] + \iota^2\rho = 0$$

$$T(0) = const \qquad T'\left(\frac{L}{2}\right) = 0$$

Figure 3. Predicted temperature profile of carbon fiber away from heatsink. Equations at bottom of figure were those used to make the profile prediction.

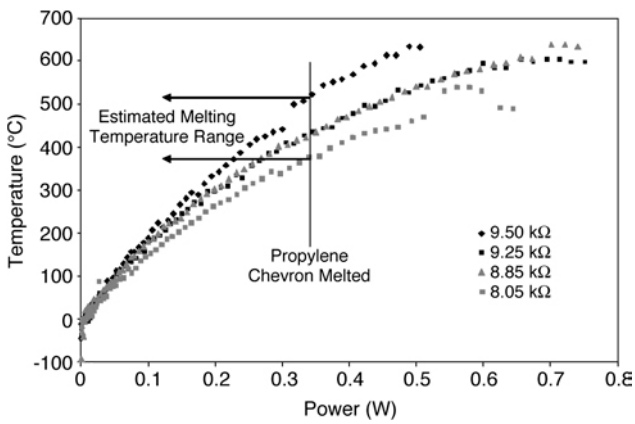

Figure 4. Predicted temperature versus applied voltage for carbon fiber. The data in Figure 2 was used to predict the temperature.

For practical adhesion, a new device for performing the microbond test has been developed to take advantage of the load resolution of our new dynamic mechanical analysis (DMA) equipment. The load resolution of our new system is approximately 2 orders of magnitude better than our previous device. In addition, the new device utilizes a laser-fabricated circular aperture to allow the force to be distributed more evenly on the bead than the previous parallel vise setup. Consequently, the new device yields a less complex stress distribution that is also more readily modeled using finite-element analysis, resulting in more meaningful test results. This new device is currently being evaluated with a variety of systems including PP/carbon fiber that had been manufactured for thermodynamic adhesion measurements.

Mechanical Property Determination

The mechanical properties of the component materials were examined during year 1. With respect to the matrix materials, DMA of the PP has been conducted. This was used to determine the storage and loss modulus of the materials as a function of temperature. Tensile testing of the PP material has been initiated. Thus far, these experiments have been conducted as a function of strain rate for PPs having little crystallinity. With this strain rate knowledge, tensile testing using biaxial or rosette strain gages is being conducted to simultaneously determine the Young's modulus, yield strength, postyield behavior, and the Poisson's ratio. For fiber testing, a new device for testing single fibers has been made. This device is similar to that mentioned in the adhesion discussion because it uses the DMA to achieve good force resolution. As this device is undergoing final testing to ensure its proper functioning, fiber tensile testing is set to begin within the next few weeks.

Extent of Crystallinity as a Function of Formation Conditions

The research conducted in this area over the past year has been primarily aimed at determining conditions by which transcrystalline regions are formed in the PP-carbon fiber systems. The initial work in this area was to perform differential scanning calorimetry (DSC) to determine the extent of crystallinity of the initial material and the effect of cooling rate on crystallite formation. Figure 5 shows a standard DSC curve for the PP used herein. In Figure 5, the degree of crystallization is relatively constant for three different cooling rates, probably due to using the same time at the melting temperature for all samples. This research is ongoing as additional parameters such as time in the melted state and temperature difference between the maximum test temperature and the melting point are important to crystallite formation. In addition, the best methods for obtaining surfaces suitable for atomic force microscopy, both acoustic and phase

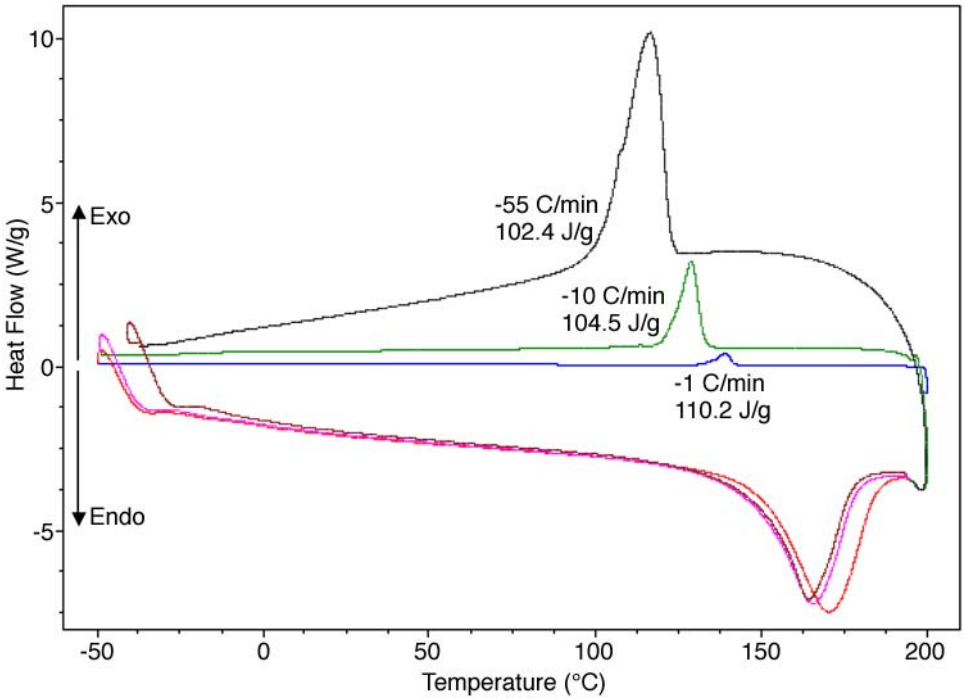

Figure 5. Differential scanning calorimetry curves for polypropylene at various cooling rates.

imaging, are currently under investigation. In particular, the behavior of carbon fibers during microtoming may result in damage to the near-fiber region, inhibiting the finding and interrogation of transcrystalline regions. Therefore, this may necessitate a change in AFM sample preparation.

Summary

Highlights of our FY 2004 research include:

1. Chose matrix materials—PP and PPS.
2. Manufactured axisymmetric microbond test fixture for practical adhesion measurements.
3. Created carbon fiber resistivity/temperature calibration curves and heating device.
4. Presented initial work at South Dakota EPSCoR Conference.
5. Began mechanical testing of component materials.

Presentation

1. T. Engstrom, S. Bickett, J. Ash, W. Cross, L. Kjerengtroen, J. Kellar, and R. Norris, "Interphase Analysis and Control in Fiber Reinforced Thermoplastic Composites," presented at the South Dakota EPSCoR Annual Meeting, September 2004.

C. Low-Cost Test Methods for Advanced Automotive Composite Materials; Creep Compression Fixture

John M. Henshaw
The University of Tulsa
600 South College
Tulsa, OK 74104
(918) 631-3002; fax:(918) 631-2397; e-mail: john-henshaw@utulsa.edu

Kenley McQueen
The University of Tulsa
e-mail: kenley-mcqueen@utulsa.edu

Ronald P. Cooper
The University of Tulsa
e-mail: ronald-cooper@utulsa.edu

ACC Project Contact: Dan Houston
Ford Motor Co.
20000 Rotunda Dr., MD 3182 SRL, P.O. Box 2053
Dearborn, MI 48121-2053
(313) 323-2879; fax: (313) 323-0514; e-mail: dhousto2@ford.com

Technology Area Development Manager: Joseph A. Carpenter
(202) 586-1022; fax: (202) 586-1600; e-mail: joseph.carpenter@ee.doe.gov
Field Technical Manager: Philip S. Sklad
(865) 574-5069; fax: (865) 576-4963; e-mail: skladps@ornl.gov

---

Contractor: U.S. Automotive Materials Partnership
Contract No.: FC26-02OR22910

Objectives

- Design and develop low-cost, reliable fixtures and methods for the characterization of compression creep behavior of automotive composites with and without environmental exposure. Confirm results generated by the new fixture with those from conventional testing systems.
- Incorporate the fixtures and methods in the above objective into industry-standard test methods for automotive composites.
- Using results of short-term tests, develop predictive models for lifetime property degradation.
- Investigate the fundamental damage mechanisms in polymer-matrix, carbon-fiber, and E-glass composites as a function of specific, varied mechanical loading with concurrent environmental exposure.

Approach

- Design and develop a compact compression creep test fixture system and confirm its performance.
- Use the new fixture system to develop a compression creep database.
- Develop a standard procedure for compression creep testing using the new system.

Accomplishments

- Developed and fabricated third-generation fixture prototype.
- Conducted extensive, varied testing of third-generation prototype that shows validity of design concept.
- Documented minor suggested improvements.
- Implemented new Data Acquisition System.

Future Direction

- Complete design and fabrication of third-generation prototype fixture. Evaluate fixture performance; determine if fixture modification is required.
- Conduct compressive creep evaluation of candidate composite materials using final creep compression fixture.
- Establish project end date: December 31, 2005.

Introduction

Because of insufficient information on the long-term durability of lightweight composite materials, reliable methods and models requiring relatively short-term tests are essential to composites achieving their full potential in the automotive industry. The purpose of this project is to develop simple, low-cost fixtures and methods for the creep and creep-rupture characterization of automotive composites and confirm the in-situ creep test fixture results with those obtained using conventional testing methods.

Initial Design Concept For The Compression Creep Fixture

Several design specifications were targeted when developing the initial prototype fixture during the first year of this project. The creep compression fixture must simulate in-service loading conditions by allowing the specimen to be exposed to various automotive environments. The fixture must also be lightweight, compact, relatively inexpensive, and portable compared to industry-standard dead weight creep testing fixtures. Lastly, the data generated by the fixture should be of design quality while comparing favorably to Oak Ridge National Laboratory (ORNL) and literature data. A successful fixture will also be corrosion-resistant, capable of testing American Society for Testing and Materials (ASTM) standard compression coupons, and exhibit no signs of specimen buckling.

Prototype 3 Design Details

The third-generation prototype currently under development utilizes a four-pin design where the specimen fits inside two compression blocks that are pressed toward each other by load reversing pins (Figures 1 and 2). The ends of the pins are threaded into a connecting bracket that, in turn, mounts to either a clevis joint on a spring-loaded moment arm or into a standard load frame (Figure 3). Prototype 3 is capable of testing compression specimens that are 5 in. long, which is near the recommended ASTM D3410 standard length. Earlier prototypes utilized an undersized specimen.

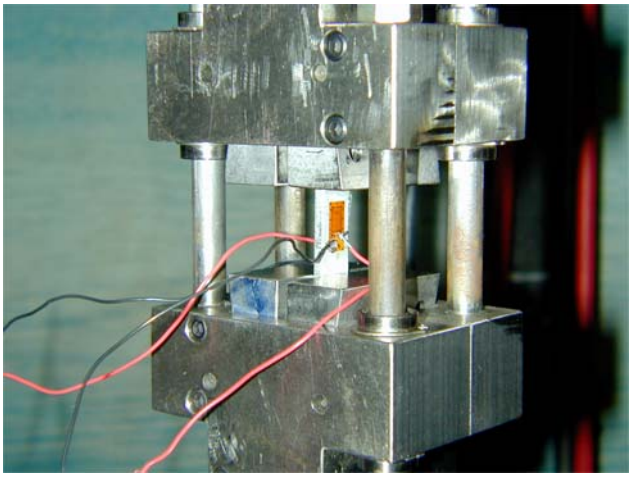

Figure 1. Third-generation creep compression prototype shown during a compression test.

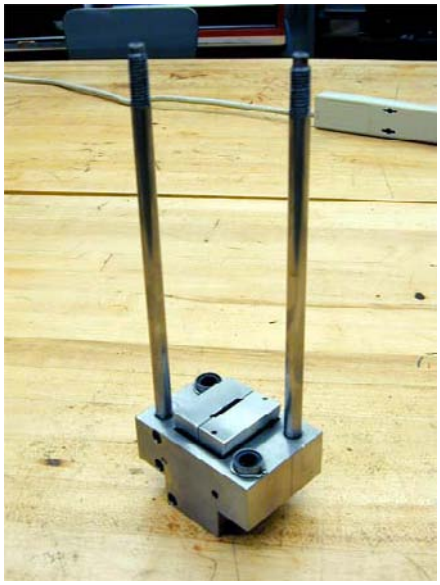

Figure 2. Disassembled creep compression fixture showing load block, load reversing pins, and slot for inserting specimen.

Figure 3. A creep compression test using the third-generation prototype. For this test, the fixture is pulled in tension in a standard load frame.

Prototype 3 Test Results

Initial testing of P4 (Programmable Powdered Preform Process) manufactured glass-reinforced polymer-matrix composite with the first-generation prototype showed compression creep behavior very similar to the compression creep curves generated by ORNL. Results of these tests were included in the 2003 annual report. As noted in that report, a problem with the earlier prototype was the difference in strain levels between opposite sides of the specimen. Such a strain difference indicates a bending load being induced on the specimen. ASTM requires compression tests to exhibit less than 5% bending. Because bending loads were frequently excessive on the old prototype, a new design was required.

The second-generation prototype, whose design was detailed in the 2003 annual report, showed improved test results, but several more modifications were desired, resulting in a third-generation prototype (as shown in Figures 1–3).

Test results with the new prototype (third-generation) have been extremely encouraging. The results of a typical test are described below and shown in Figures 4–7. For these tests, a standard-sized aluminum compression specimen (5 in. long by 1 in. wide by 1/8 in. thick), strain-gaged front and back, is loaded into the fixture, which is then pulled in tension in a standard MTS load frame (Figure 3). Various tests have been performed using this setup as part of the fixture development and prove-out process. One such test, the results of which are shown in Figures 4–7, consists of cycling the fixture from zero load to a maximum load (about 950 lb in this case) and back to zero. For the test described herein, this load cycle was performed ten times, as shown in Figure 4. (The maximum load of 950 lb was chosen in this case because that represents a typical maximum load for a carbon-fiber automotive composite tensile test.)

During these loading cycles, strain on both sides of the specimen is measured continuously. Figure 4 shows both the load in pounds during the test (compression loads are shown in pounds on the positive y-axis of the graph). Figure 4 also shows the compressive strain (in microstrain on the negative y-axis) for the same ten loading cycles. Two strain channels, for both sides of the creep-compression specimen, are shown in Figure 4. Because the two channels of strain data are so similar, they cannot be distinguished in Figure 4.

Thus, Figure 5 shows the variation in strain, expressed as the percent difference between the front and back of the specimen vs time. Figure 5 has the same time scale (x-axis) as Figure 4 to show that the percent difference is greatest at the beginning and end of each load cycle—that is, when the loads are the smallest.

Figure 6 replots the data for all ten load cycles as percent strain difference vs load; thus, all ten load cycles are superimposed on each other. Figure 6

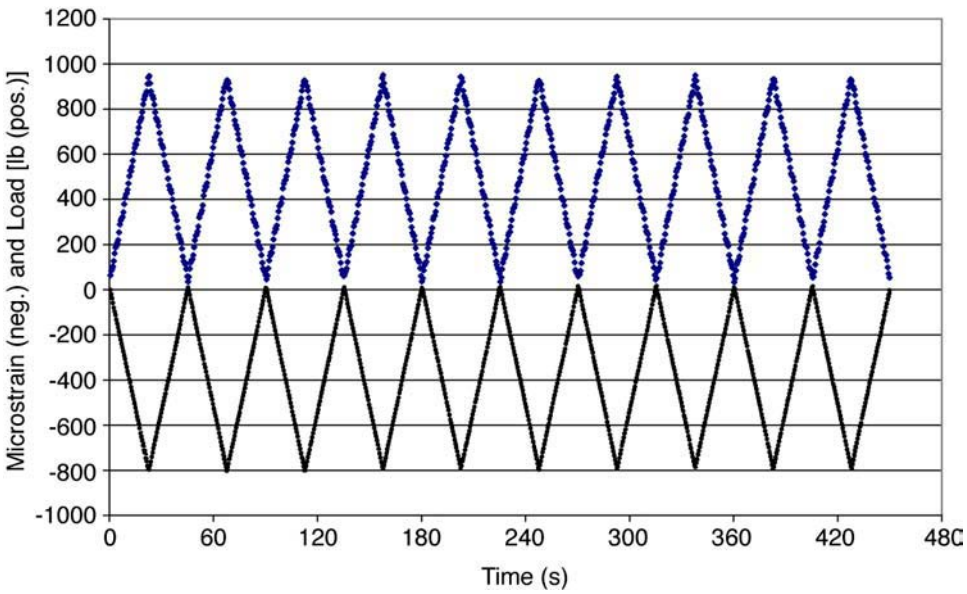

Figure 4. Load and strain for a typical creep-compression fixture development test. Ten load cycles (from zero to about 950 lb and back to zero) are shown. For each load cycle, two channels of strain (front and back of specimen) are shown. The strain data channels lie on top of one another and cannot be distinguished in this graph (see Figure 5).

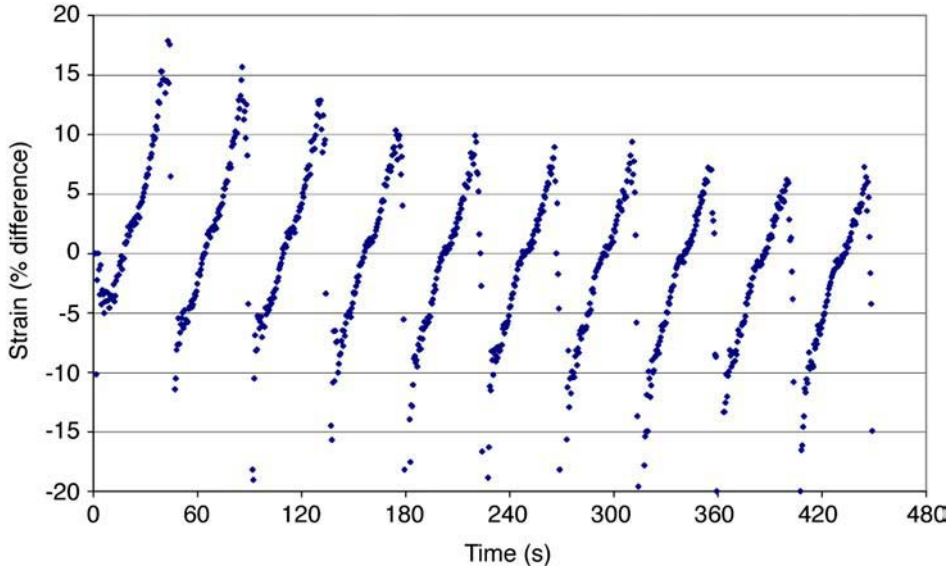

Figure 5. The percent difference in strain measurements, vs time, for the two channels of strain shown in Figure 4. Note that the percent differences are small (within ±5%) except for the beginning and ending of each load cycle, when the loads (and strains) are also small.

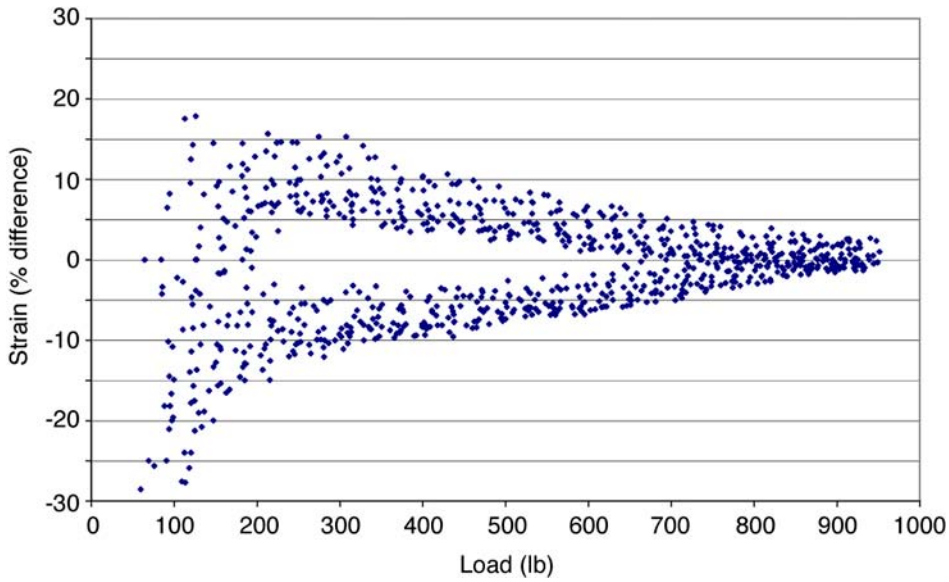

Figure 6. The data from Figures 4 and 5 plotted as percent difference (between the two sides of the creep compression specimen) vs load. Data from all ten loading cycles are superimposed.

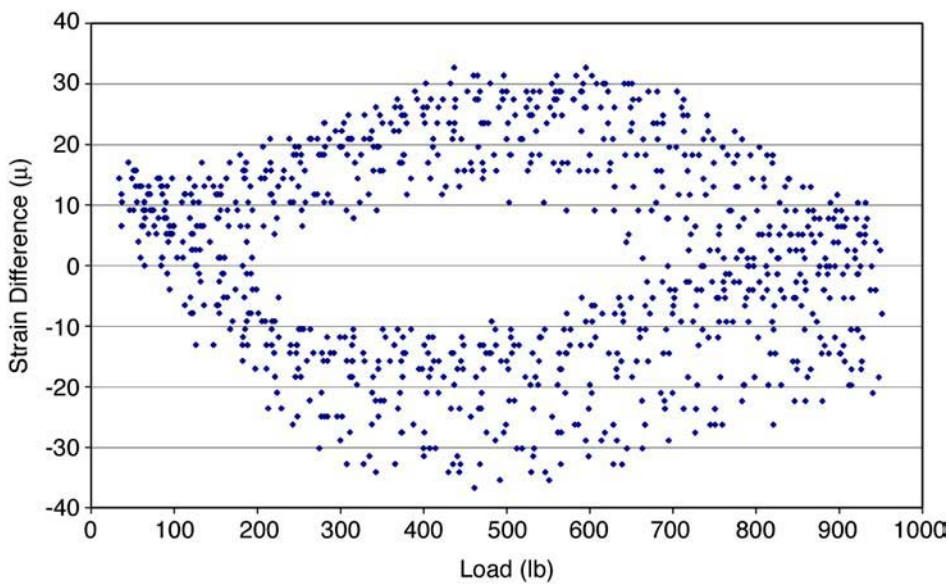

Figure 7. Data from Figure 6 replotted as the absolute strain difference in microstrain (between the two sides of the creep compression specimen) vs load for all ten loading cycles.

shows clearly that the percent strain difference decreases as load increases and that the percent difference is below the ASTM limit of 5% for loads above about 600 lb.

That the percent difference in strain is above 5% for lower loads may be at least partially explained by the low absolute strain levels at those low loads (the maximum strain levels for these tests, at applied loads of about 950 lb, are about 800 microstrain; at lower loads the strains are proportionally lower). At the lower strains, the absolute difference in strain can thus be relatively small and still result in a per-

cent difference greater than 5%. As shown in Figure 7, the absolute difference in strain for all ten loading cycles is always below 40 microstrain.

Another important aspect of this creep compression fixture is its ability to transfer load to the specimen. Test results show that the third-generation fixture consistently transfers over 90% of the load from the load frame to the specimen, for loads in excess of about 300 lb. From these results it is concluded that the efficiency of the fixture is acceptable and that the new fixture will be able to be successfully adapted to spring-loaded, in-situ fixtures developed in earlier projects.

Test results for the third-generation creep compression prototype, as exemplified by those shown reported herein, are thus extremely encouraging.

Prototype 3 Improvements

Several minor improvements to the third-generation creep-compression fixture are envisioned. These involve design details intended to further simplify the specimen loading procedure and to further reduce specimen bending, especially at low loads.

Other Ongoing/Future Work

Continued evaluation of prototype 3 performance through short-term tests using composite and aluminum specimens is ongoing.

The minor design modifications noted above are being incorporated into a final prototype able to meet all design requirements and criteria. This will be followed by fabrication of that final prototype.

Fabrication of several such compression fixtures will then allow statistical evaluation, by researchers at several facilities, of creep compression properties of polymer composite material systems.

Conclusions

1. A third-generation compressive creep prototype has been designed, fabricated, and extensively tested.
2. Test results with this prototype are extremely encouraging, in terms of (a) the ability of the fixture to minimize the percent difference in strain from one side of a specimen to the other, and (b) the ability of the fixture to efficiently transfer load to the specimen.
3. Cyclic loading of specimens in the fixture shows excellent repeatability: the difference in front-to-back strain is below 5% for loads more than about 600 lb.
4. The fixture easily and repeatedly achieves maximum design loads of about 950 lb.

D. Intermediate-Rate Crush Response of Crash Energy Management Structures

Co-Principal Investigator: Raymond G. Boeman
Oak Ridge National Laboratory
P.O. Box 2008
Oak Ridge, TN 37831
(202) 865-0785; fax: (202) 586-7409; e-mail: boemanrg@ornl.gov

Co-Principal Investigator: J. Michael Starbuck
Oak Ridge National Laboratory
P.O. Box 2009, Oak Ridge, TN 37831-8048
(586) 576-3633; fax: (865)-574-8257; e-mail: starbuckjm@ornl.gov

Project Manager, Composites: C. David Warren
Oak Ridge National Laboratory
P.O. Box 2008, Oak Ridge, TN 37831-6065
(865) 574-9693; fax: (865) 576-4963; e-mail: warrencd@ornl.gov

Technology Area Development Manager: Joseph A. Carpenter
(202) 586-1022; fax: (202) 586-1600; e-mail: joseph.carpenter@ee.doe.gov
ORNL Field Technical Manager: Philip S. Sklad
(865) 574-5069; fax: (865) 576-4963; e-mail: skladps@ornl.gov

---

Contractor: Oak Ridge National Laboratory
Contract No.: DE-AC05-00OR22725

Objectives

- Develop unique characterization facility for controlled progressive crush experiments, at intermediate rates, of automotive materials (polymer composites, high-strength steels, and aluminum) and structures.
- Study the deformation and failure mechanisms of automotive materials subjected to crush forces as a function of impact velocity.
- Obtain specific energy absorption and strain data, and correlate with deformation and failure mechanisms to describe the unknown transitional effects from quasi-static to high loading rates for polymer composites.
- Characterize the strain rate effects for metallic materials and components.
- Provide access to unique test capability to university, industry, and government users for collaborative research.

Approach

- Develop a unique high-force (270-kN), high-velocity (8-m/s) servo-hydraulic machine to conduct progressive crush experiments on structural components at intermediate rates.
- Use high-speed imaging to observe and document deformation and damage mechanism during the crush event.
- Conduct strain measurements at discrete locations and explore full-field measurements of strains and curvatures.
- Coordinate polymer composites investigations with the Automotive Composites Consortium (ACC) Energy Management Group.
- Coordinate steel investigations with the Automotive/Steel Partnership.

Accomplishments

- Completed design modification and fabrication to achieve increased performance (125%) up to 8 m/s.
- Completed installation and initial operator training at the National Transportation Research Center (NTRC).
- Completed new acceptance tests on-site to demonstrate enhanced performance.
- Completed design and fabrication of test fixtures for testing five different tube geometries.
- Completed integration of high-speed data acquisition with test operation.
- Completed vendor demonstrations on four high-speed video systems.
- Completed a total of 38 shakedown tests as part of high-speed video assessments, capability demonstrations, and machine commissioning.
- Held official dedication ceremony in August 2003.
- Completed 60 tests to characterize glass fiber composites tubes at 5 different velocities.
- Completed carbon-fiber tube and strip tests for Ford Motor Company under the User's Facility Agreement.
- Completed parametric studies on tuning parameters to qualitatively and quantitatively determine their effect on the velocity drive file.
- Completed full-field measurement demonstration using digital image correlation techniques.
- Completed 47 tests on steel tubes in support of the Auto/Steel Partnership Program.

Future Direction

- Procure high-speed video.
- Explore techniques for full-field measurements of strains and curvatures.
- Develop User Interaction Plan.
- Support user collaboration as required.

Introduction

Progressive crush is an important mechanism by which the kinetic energy of a traveling automobile is dissipated in a collision to protect the safety of occupants. Unfortunately, the mechanisms governing the progressive crush response of some emerging automotive materials are not well understood. Additionally, many of these materials are known to exhibit responses that are sensitive to rate of loading.

Understanding the influence of impact velocity on the crush response of materials and structures is critically important for crashworthiness modeling inasmuch as collisions occur at a range of velocities. Additionally, from a structural standpoint, the deformation (or strain) rate is generally not unique from either a spatial or temporal standpoint. Consequently, it is important to quantify the behavior of materials at various strain rates.

Test Machine for Automotive Crashworthiness (TMAC)

Typically, standard test machines are employed for experiments at quasi-static rates, whereas drop towers or impact sleds are the convention for dynamic rates. These two approaches bound a regime within which data, for experiments at constant impact velocity, are not available by conventional experimental practice. This regime is termed herein the intermediate-rate regime and is defined by impact velocities ranging from 1 m/s to 5 m/s. Investigation of rate effects within this regime requires experimental equipment that can supply a large force with constant velocity within these rates. Using a drop tower or sled at intermediate rates, although technically possible, is problematic due to the prohibitively large mass required to maintain constant velocity during the crush. Consequently, the Oak Ridge National Laboratory (ORNL) and the Automotive Composites Consortium (ACC) collabo-

rated to define specifications for a unique experimental apparatus that mitigates the shortcomings of existing equipment. MTS Systems Corporation designed and built the servo-hydraulic test machine, referred to as the TMAC. As shown in Figure 1, TMAC is uniquely capable of conducting controlled progressive crush tests at constant velocity in the intermediate velocity range (i.e., less than 5 m/s) because of the large energy available at those rates and to the sophisticated simulation and control software that permits velocity uniformity to within 10%.

The new experimental facility will be used to understand the crush behavior between the static and dynamic (8-m/s) conditions. The installation of the TMAC at its National Transportation Research Center (NTRC) Knoxville, Tennessee, location is shown in Figure 2.

Status

Since the last reporting period, a set of baseline cases were run using the Advanced Drive File Generator (ADFG). The purpose of these dry-fire tests, that is, tests without specimens, was to archive the machine performance for future maintenance checks and/or troubleshooting. Cases from 1 m/s up to 8 m/s were run with various initial accelerations.

After completing the baseline cases, parametric studies were done to determine the influence that different tuning parameters had on generating

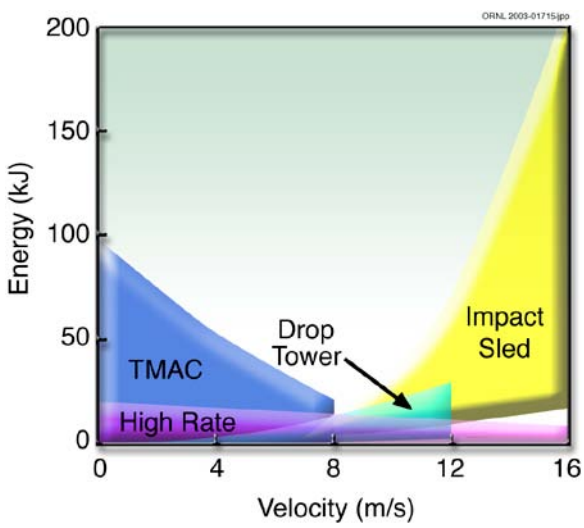

Figure 1. Energy plot indicating TMAC's unique capability of supplying enough energy at the intermediate rates for controlled, constant-velocity crush tests.

Figure 2. TMAC installation at NTRC.

constant velocity profiles. The parameters that were adjusted were the initial acceleration, zero offset, velocity trim, and acceleration trim. It was determined that up to approximately 4 m/s, it was possible to achieve constant velocity profiles without adjusting the baseline parameters and without iterating using the inverse model. Beyond the 4-m/s regime, additional work is required to fully understand the relative effect each parameter has on the ability to achieve a constant velocity profile. It was also apparent that several iterations would be required at these higher velocities to achieve the desired result of a constant velocity over at least a 100-mm crush length.

A test matrix on glass-fiber reinforced composite tubes was completed, and the experimental data were supplied to the ACC. The tubes were approximately 50 mm by 50 mm square and used an internal plug with a radius as an initiator. The test setup is shown in Figure 3. A total of 60 tests were conducted: 6 specimens/velocity/material; and there were 5 velocities (5 mm/s, 1000 mm/s, 2000 mm/s, 3000 mm/s, and 4000 mm/s); and 2 materials (1 braided and 1 fabric). All target velocities were achieved within a ±3.5% range without having to iterate or define a specimen. By using a revised test setup that moved the specimen higher up in the load train, the constant velocity was achieved over a 140-mm crush length. All of the drive files were created by trying different initial accelerations for the different test velocities and conducting dry-fires to compare the physical response with the expected response. The experimental data are currently being analyzed and reviewed by the ACC. Photographs that depict typical failure modes for this composite are shown in Figures 4 and 5. Figure 4 was actually taken during a test at the quasi-static rate of 5 mm/s. A typical force and velocity vs time plot is shown in Figure 6 for a 4000-mm/s test.

The first User Facility Agreement for work on TMAC was completed. This work was performed for Ford Motor Company and is described in the following paragraphs.

Characterizing composites for energy management for automotive applications is frequently performed by testing tubular structures. The technical approach for this research was to develop simple coupon tests that quantified the relative energy absorption of each energy absorption mode that was identified in the tube tests. Testing would then be performed dynamically and quasi-statically. Ford had already identified the different modes and performed the quasi-static tests, but it needed the dynamic test results to complete the research project.

Figure 3. Test setup with internal plug.

Figure 4. Specimen failure during 5-mm/s test.

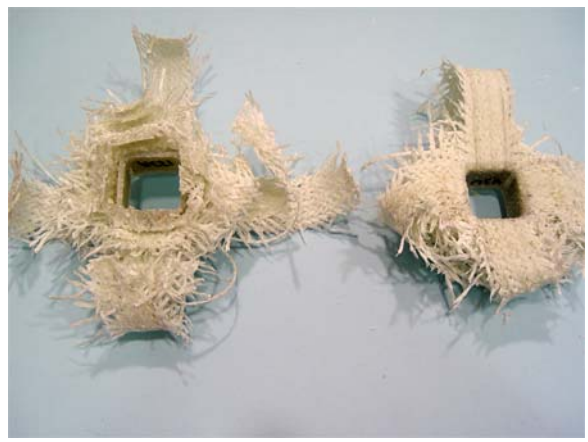

Figure 5. Progressive crush failure modes in glass-fiber reinforced composite tubes.

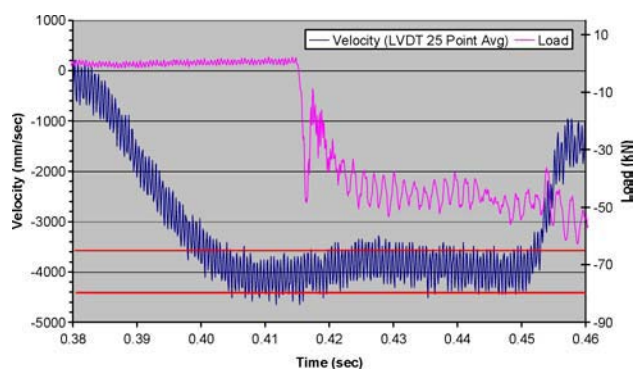

Figure 6. A 4-m/s velocity profile and force vs time plot of a glass-fiber reinforced composite tube.

The testing consisted of crushing square cross section graphite composite tubes at an impact velocity of 2–4 m/s using the TMAC. The test setup is shown in Figure 7. Also, the test plan included crushing graphite composite strips using a test fixture supplied by Ford and adapted for use on the TMAC (see Figure 8). These tests were conducted at the same impact velocity as the tubes. Figure 9 shows a typical failure mode for the composite tubes. The displacement and load data for each test in a format that Ford could process to extract energy absorption was supplied to the Ford engineer that was present on-site during the testing. Ultimately, the data will be used to separate energy absorption due to bending damage of the composite and friction. When these data are compared with the quasi-static data, the goal is to be able to develop a theory to explain the difference in specific energy absorption between dynamic and quasi-static tests on otherwise identical test specimens.

Figure 7. Test setup for graphite fiber composite tubes tested under the Ford User Facility Agreement.

Figure 8. Test setup for composite strips tested under the Ford User Facility Agreement.

Figure 9. Typical failure for a progressively crushed carbon fiber composite tube.

The use of digital image correlation techniques as a full-field measurement of strains during dynamic testing was explored by conducting a demonstration. Correlated Solutions completed the demonstration at NTRC in collaboration with Vision Research and their Phantom line of high-speed video cameras. The digital image correlation technique is based on random speckle pattern recognition and tracking the motion of these patterns in space with respect to time. For the out-of-plane displacement associated with a tube crushing experiment, this is a three-dimensional displacement field, and two high-speed cameras are required to resolve the pattern motions. The demonstration was completed using steel tube samples that were approximately 100 mm in diameter and 200 mm long. The specimens were first cleaned and coated with a white flexible coating call SEM Color Coat. They were then oversprayed with a black flexible coating to produce a speckle pattern. Specimens were tested in TMAC and imaged with Phantom high-speed cameras. One Phantom V5 model and one Phantom V7 model were used. Correlated Solutions' software, VIC-3D, was used to reduce the image data to strain and displacement fields. Figure 10 shows an example of the speckle pattern that was sprayed on the tube and then overlaid with a calculated axial strain field resulting from precrushing the tube. The overall results from the demonstration were sufficient to show the capability of VIC-3D for testing with the TMAC.

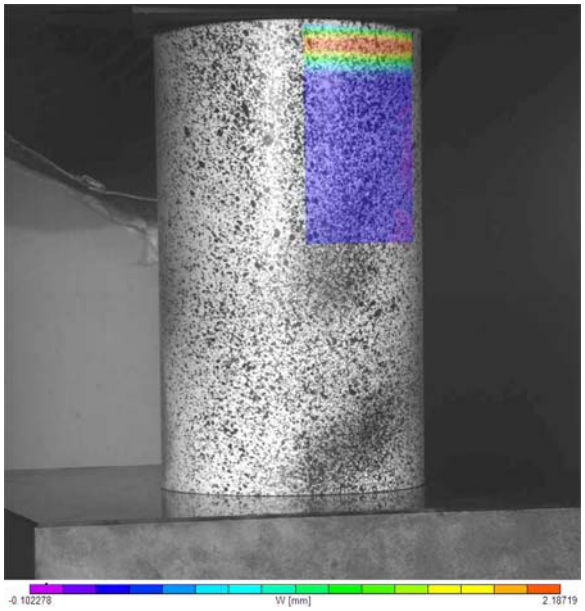

Figure 10. Axial strain in steel tube measured using digital image correlation.

Conclusions

TMAC provides a unique capability to measure the specific energy absorption on crush tubes and other specimen geometries as a function of (constant) impact velocity within a range from quasi-static to 8 m/s.

During the past reporting period, 60 tests were conducted to characterize glass fiber composite tubes at 5 different velocities, and the test data were provided to the ACC. These tests provided critical data in the velocity range of 0.5 to 4 m/s that was previously unavailable using other test methods. Also, carbon fiber tube and strip tests were completed for Ford Motor Company under the first User's Facility Agreement on TMAC. In support of the Auto/Steel Partnership Program, 47 tubes were testing to determine strain rate sensitivities in new high-strength steel alloys.

To gain a better understanding of the TMAC operational characteristics, parametric studies were completed on tuning parameters to qualitatively and quantitatively determine their effect on the velocity drive file. The results showed that iterating on the tuning parameters to achieve a constant velocity profile really becomes an important part of the operation at velocities above 4 m/s. Additional work is required to refine the data acquisition, particularly with regard to comparisons of the two data acquisition cards, filtering of data, and determination of velocity from accelerometer signals.

The full-field measurement technique of digital image correlation was qualitatively demonstrated and showed the potential for being a powerful method of measuring strains in progressive crush experiments at dynamic loading rates.

E. Composite Crash Energy Management

Principal Investigator: Richard Jeryan
Ford Research Laboratories
2101 Village Road
MD3137 SRL
Dearborn, MI 48124-2053
(313) 594-4903; fax: (313) 337-5581; e-mail: rjeryan@ford.com

Field Project Manager: C. David Warren
Oak Ridge National Laboratory
P.O. Box 2009, Oak Ridge, TN 37831-8050
(865) 574-9693; fax: (865) 574-4963; e-mail: warrencd@ornl.gov

Technology Area Development Manager: Joseph Carpenter
(202) 586-1022; fax: (202) 586-1600; e-mail: joseph.carpenter@ee.doe.gov
Field Technical Manager: Philip S. Sklad
(865) 574-5069; fax: (865) 576-4963; e-mail: skladps@ornl.gov

---

Contractor: U.S. Automotive Materials Partnership (cooperative agreement) Automotive Composites Consortium Energy Management Working Group
Contract No.: FC26-02OR22910

Objectives

- Determine experimentally the effects of material, design, environment, and loading on macroscopic crash performance to guide the design and the development of predictive tools.
- Determine the key mechanisms responsible for crash energy absorption and examine microstructural behavior during crash to direct the development of material models.
- Develop analytical methods for predicting energy absorption and crash behavior of components and structures.
- Conduct experiments to validate analytical tools and design practices.
- Develop and demonstrate crash design guidelines and practices.
- Develop and support design concepts for application in demonstration projects.

Approach

- Conduct experimental projects to increase understanding of the global and macro influences of major variables on crash performance.
- Use the data from these experiments to create crash intuition, guidelines, and rules of thumb and data for the validation of analysis developments.
- Conduct microscopic experimental characterization to define the mechanisms that occur during and as a result of the crash process.
- Develop and validate analytical design tools to predict structural crash performance based on both phenomenological and micromechanical approaches to material and crash mechanism modeling.

Accomplishments

- Completed high-rate compression tests to demonstrate that shear transfer between fiber tows and matrix is reduced at higher strain rates.
- Completed static and dynamic tests to determine effects of friction during sliding and bending.
- Completed static and dynamic tests to determine Mode I and Mode II adhesive fracture properties.
- Completed down-selection of composite sandwich face/core configurations and initiated second phase of testing.
- Implemented cohesive zone models into finite-element analysis codes and demonstrated good agreement with experimentally determined behavior of bulk adhesive.
- Characterized in-situ and bulk composite matrix material properties and examined details of the fiber architecture of molded specimens to understand anomalies in material properties and energy absorption of braided composites.
- Completed the analysis of the fracture of a composite strip under a combined bending and compression load. Experiments are being conducted to validate the analytical results.

Future Direction

- Continue the development and validation of both micromechanical and phenomenological analytical design tools to predict structural crash performance.
- Expand micromechanical approaches to model material and crash mechanisms and explore novel multiscale approaches.
- Expand focus on design tools suitable for use with random chopped carbon-fiber-reinforced composites.
- Continue the characterization of the energy absorption mechanisms of carbon-fiber-reinforced composites.
- Characterize the critical physical parameters required for analytical model development. Develop test methods to obtain the stress-strain response beyond the peak stress of the materials and expand the current experimental methods to more fully characterize the dynamic material and physical properties needed to advance the modeling capability.
- Determine the effects of manufacturing features and environmental and loading factors, for example, minor field damage, abrasion, fatigue, and cumulative effects, on the macroscopic crash performance of carbon and carbon/glass hybrid reinforced composites. These results will establish design guidelines and guide the development of predictive tools.
- Develop relationships to implement analytical tools for commercial use.

Introduction

The purpose of the Crash Energy Management Program is to develop and demonstrate the technologies required to apply production-feasible structural composites in automotive crash and energy management applications. Projects within the program are intended to understand the mechanisms of polymer composite crash, develop analytical tools for use in vehicle design, and build a knowledge base for the vehicular application of lightweight polymer composites. The projects relate to materials, molding, and assembly process and design configurations that are useful in realistic applications. Design analysis methods will be developed that can be used at the several different steps in the design process. These steps require different levels of precision and speed of use, and the appropriate tools are expected to include both micro-mechanical and phenomenological approaches.

Static vs Dynamic Performance

This project's objectives are to experimentally determine the microstructural factors and behaviors that lead to decreased energy absorption when crushing tubes dynamically. In this study, the strain rate effects of a braided carbon fiber composite are investigated at the specimen level. The goal is to determine the source of rate effect using specimen-level tests and develop experimental methods by which candidate materials for energy absorption can be evaluated for their rate sensitivity. The results of this study will be used to develop and enhance analytical models that will need to take into account rate-sensitive material behavior.

Material properties of the two composite material systems were measured. This included the virgin and the in-situ properties (i.e. matrix properties within the composite) of the resins. The results showed that in-situ properties were much lower than the virgin properties. This suggests that virgin properties of the resins are not useful for characterizing the composite material properties or behavior. Mode I and II fracture toughness tests were carried out on thick specimens at both static and dynamic loading rates, Figures 1 and 2. The results showed that for both Mode I and II, increasing loading rates resulted in lower fracture toughness. In addition, high-rate compression tests were conducted to characterize the rate-dependent inelastic response. The results showed that shear transfer between the fiber tows and matrix was reduced at higher strain rates. This implies that the load carrying capacity of the fibers is lower at high strain rates.

Friction Effects on Crash Performance

The objectives of this work are to (1) experimentally determine the relative energy absorption due to each mode of a progressively crushed composite tube and isolate that portion of energy absorption due to friction and (2) evaluate differences in friction energy absorption between quasi-static and dynamic crush.

All dynamic and static testing has been completed for tubes and strips. The dynamic testing was performed on the National Transportation Center Test Machine for Automotive Crashworthiness (TMAC). The specific energy absorption (SEA) was 23% lower for dynamic loading than static loading. Results show that for static loading friction accounted for 30% of SEA and only 13% when tested dynamically. More than 80% of the difference in SEA between static and dynamic loading is attributable to friction.

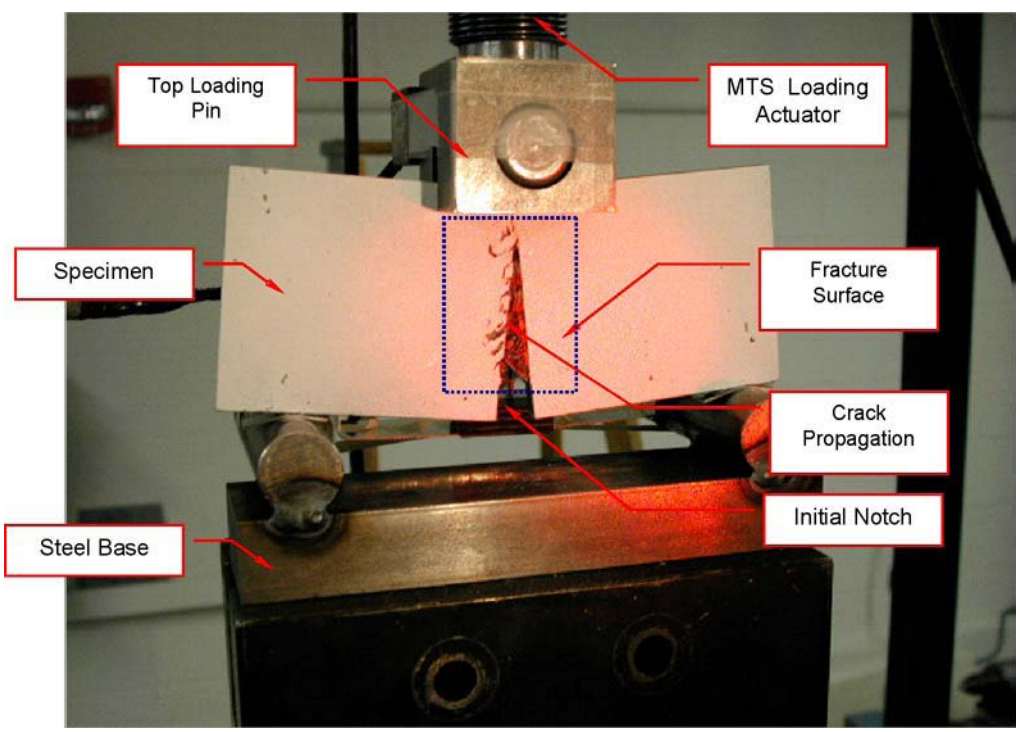

Figure 1. Three-point bending test setup for Mode I fracture toughness measurement.

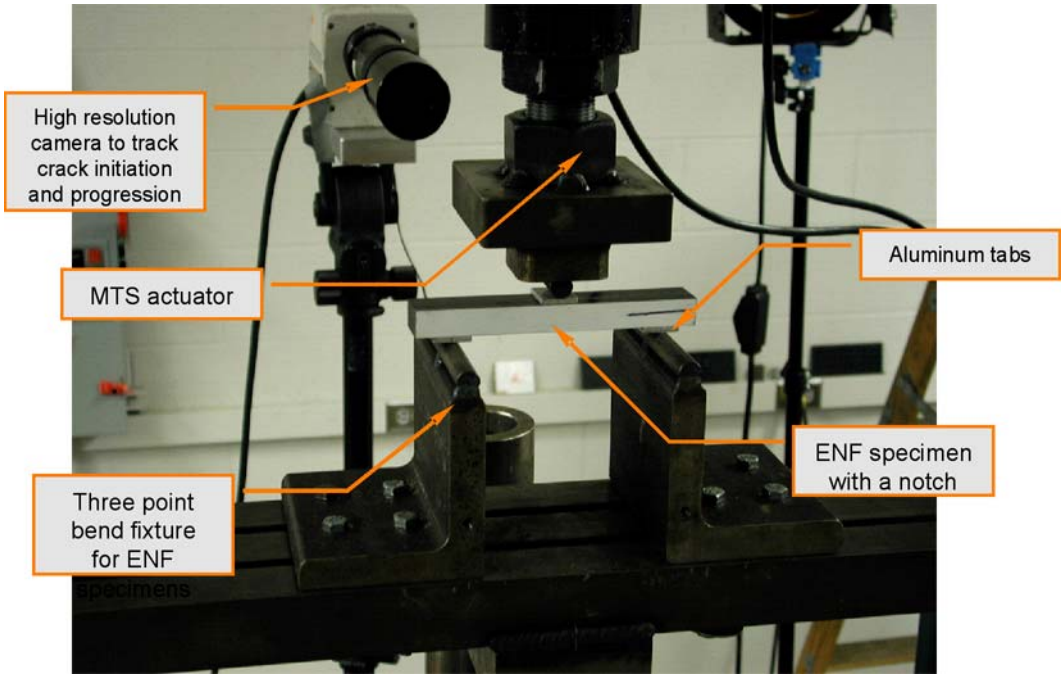

Figure 2. End-notched fracture (ENF) test setup for Mode II fracture toughness measurement.

Impact Performance of Bonded Structures

The objectives of this effort are to (1) evaluate the performance of bonded structures under crash loads; (2) examine the influence of bond design concepts, impact velocity, and other material issues; and (3) fabricate new molding tools to produce simulated automotive structures. Visteon Corporation, a Tier I automotive supplier, is leading this effort jointly with Focal Project 3 and the Automotive Composites Consortium (ACC) Energy Management and Joining Work Groups.

An integrated computational and experimental study of the dynamic response and behavior of an adhesively bonded, automotive substructural component under impact loading is undertaken here. The approach consists of characterizing the dynamic fracture of the adhesive material under various mode mixities. Numerical constitutive models of the adhesive are developed and validated. The numerical constitutive model of the adhesive will be implemented in the LS-DYNA software package to simulate the tube crush tests. Corroboration of the test results with the simulation will be used to assess the computational modeling methodology.

In the experimental part, the test methods for measuring the fracture parameters under dynamic Mode I, II, and mixed-Mode I/II, loading were established. Data analysis methods for Mode I and II were developed. Static and dynamic fracture tests, Figure 3, were conducted using both aluminum and composite adherends. The results for Mode I and II tests are presented in Figure 4 and Table 1.

In the computational effort, the CZM (cohesive zone model) constitutive law was used to study the dynamic crack propagation in adhesively bonded structural joints. There is a nonlinear relationship between the interfacial tractions and the relative displacements of the upper and lower surfaces of a crack. The law for mode I fracture initiation and crack propagation is shown in Figure 5, where T1 denotes the normal traction component, or peel component, and Δ denotes the opening displacement. The CZM law was implemented in an interface finite element, which is located between either two-dimensional (2-D) or three-dimensional (3-D) bulk material elements. In 2-D models the interface element is a line in the undeformed geometry, and in 3-D models it's a surface. The element level matrices were formulated, and the element was incorporated into ABAQUS® using the User-defined Element (UEL). The CZM law was further modified to incorporate rate-dependent behavior in the interface element. The comparison of the numerical results, using both rate-independent and rate-dependent CZM laws and experimental data for

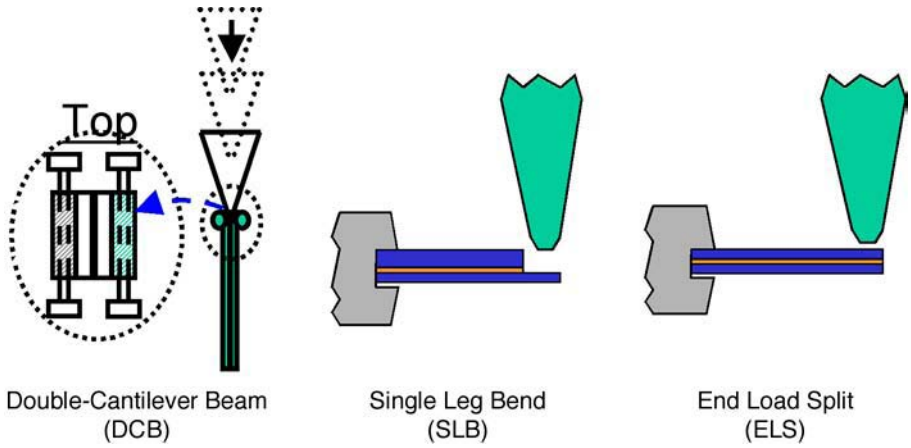

Figure 3. Static and dynamic fracture test configurations.

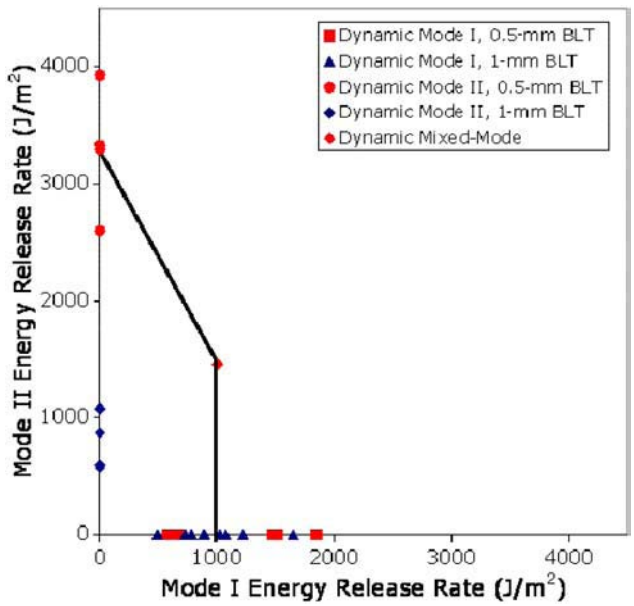

Figure 4. Mode I and II fracture test envelop for the adhesive.

Table 1. Mode I and II energy release rates for adhesive

Mode I/II energy release rates			
Adherent		Peak/initiation (J/m^2)	Average (J/m^2)
6.4-mm aluminum DCB	Static	1800	610
	Dynamic	1900	N/A
36-ply composite DCB	Static	1200	440
12-ply composite DCB	Static	2700	510
	Dynamic	1400	N/A
12-ply composite DCB	Dynamic	3100	N/A
12-ply composite SLB	Mode I	1000	N/A
	Mode II	1400	N/A

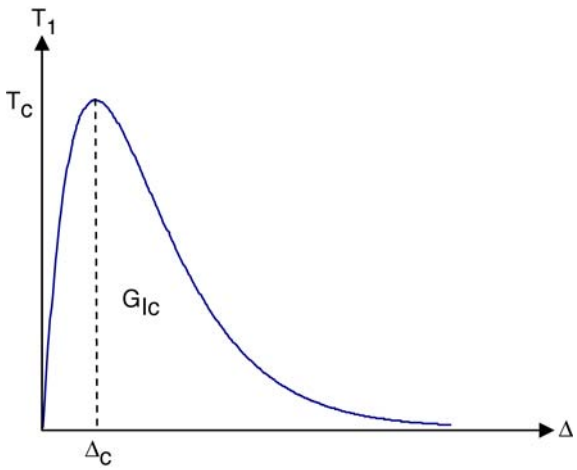

Figure 5. Nonlinear behavior of the traction opening displacement curve.

double-cantilever beam (DCB) specimens is shown in Figure 6.

Next, the interface element was implemented in LS-DYNA using the user-defined material (UMAT) option. The traction-displacement law from the interface element has been modified to a stress-strain law for use in the UMAT subroutine. The UMAT was implemented using the standard library 8-noded solid brick element. Preliminary results for a DCB analysis were obtained using the newly implemented CZM law in LS-DYNA analysis and are compared with ABAQUS® as shown in Figure 7.

Performance of Novel Sandwich Composites

The objective of this project is to investigate the viability and crashworthiness of novel sandwich composite concepts for automotive applications.

Topics such as wrinkling, face-sheet debonding, Poisson's effects and core-skin property mismatch, load rate effects, impact damage modes, and energy absorption were identified as part of the research effort. The research work being performed at the University of Utah is split into three phase-specific objectives:

Phase I: To evaluate candidate materials, concepts, and manufacturing methods for automotive sandwich composites. This two-round experimental evaluation of energy absorption, damage mechanisms, and mechanical properties will be used to identify the best-suited sandwich composite concepts for further investigation in the second phase.

Phase II: To develop an understanding of the structural response of selected sandwich composite concepts identified in Phase I. This investigation will focus on damage modes and energy absorption mechanisms during impact loading as well as static loading.

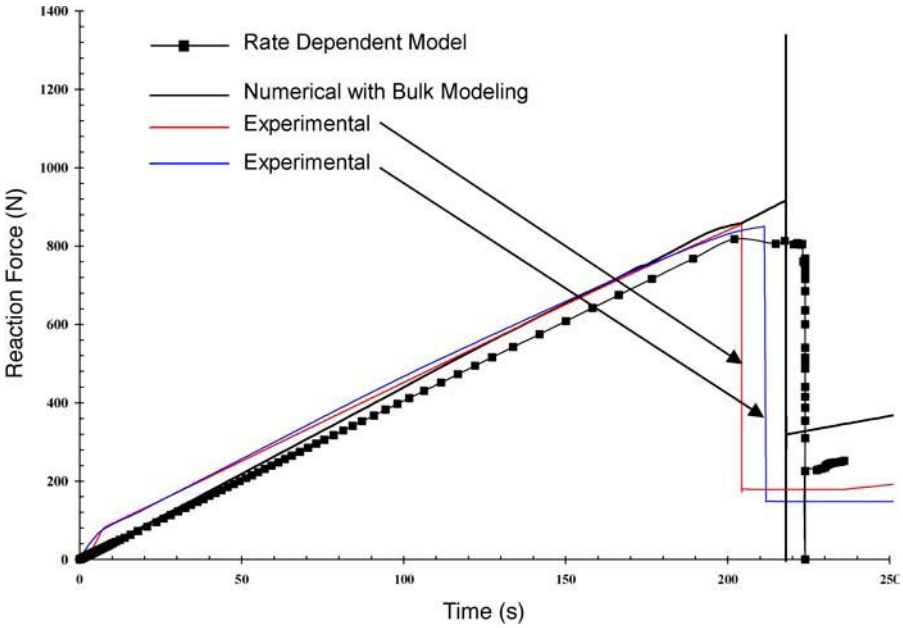

Figure 6. Tip reaction forces for DCB specimen using rate-dependent law and bulk adhesive modeling.

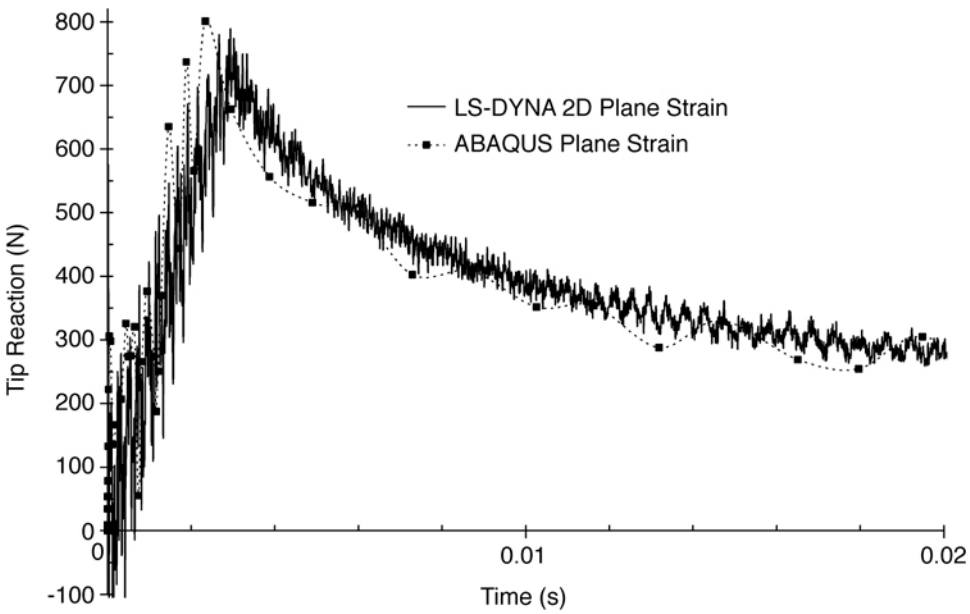

Figure 7. Comparison of results for DCB analyses using CZM law as implemented in LS-DYNA and ABAQUS.

Phase III: To develop and validate finite-element (FE) based methodologies for predicting damage formation and energy absorption in candidate sandwich composite concepts identified in the first two phases of the program.

The Phase I has been completed. Thirteen different sandwich configurations were subjected to three types of testing viz., flat-wise tensile, three point bending, and edgewise compression. The configurations tested included both thermoset and thermoplastic facesheets and had an overall thickness of 15 mm. Five sandwich configurations were chosen for the second round of tests including flexural creep, edgewise impact, flexural impact, and interlaminar shear tests. Four configurations were selected for evaluation in Phase II based on the criterion of mechanical performance, manufacturing ease, and cost. These facesheet/core configurations were Carbon-Epoxy/Balsa, Carbon-Epoxy/Polyurethane foam, P4 Carbon-Epoxy/Polyurethane foam, and P4 Carbon-Epoxy/Balsa.

Postpeak Response Characterization of 2-D Triaxially Braided Composites

The objectives of this project are to (1) computationally demonstrate postpeak softening (PPS) observed with single unit cell structural models on multicell structural models; (2) computationally investigate how the hierarchy of behavior modes and the number/arrangement of unit cells affect PPS predictions; (3) computationally investigate how the variation in degree of imperfection in the microarchitecture affects the derived structural properties of the 2-D Triaxially Braided Composite (2DTBC); and (4) experimentally test multiunit cell structural specimens to reflect, refute, or support the findings of the above objectives.

In the approach to this project, scalability of macroscopic structural stress-strain relations in 2DTBC will be investigated and studied. Computational models will be employed to demonstrate PPS observed with single-unit cell structural models on multicell unit structural models. The results of such analyses are directly applicable to the development of structural properties of 2DTBC for large-scale FE simulations that are needed to assess energy absorption in 2DTBC structural components. Using laser extensometer and speckle photography (for full field strain measurements), experimental tests to measure PPS on single and multicell 2DTBC will be performed. Further, computational models that incorporate cohesive zones (CZs) within the cell in order to capture experimentally observed tow/matrix separation will be developed and analyzed including the effect of CZ on PPS. Finally, the computational analyses will be carried further to study and characterize the effects of measured architecture imperfections on the single-unit cell and multicell structural stress-strain properties of 2DTBC, including the

effects of different types and distribution of imperfection on PPS.

The primary materials (Hetron and Epon) were experimentally characterized by measuring their pure (virgin) properties, performing coupon tension tests (with 0, +45/–45 tow orientations), and then using data reduction techniques back-calculated to in-situ material properties. It was found that in-situ matrix properties differ from pure matrix properties, and hence, the in-situ properties (not pure) should be used for subsequent FE analyses.

Because axial fiber tows are the dominant load-carrying component of the braided composite architecture, statistical scanning electron microscopy (SEM) in conjunction with photo-stitching techniques were performed on the Hetron- and Epon-based composites. From the detailed specimen preparation and subsequent SEM images, it was found that unwetted regions inside the tows needed to be accounted for (e.g., FE analysis) by a reduction in tow cross-sectional area and/or material constants. Such regions that reduce the fiber volume fraction exist in the Hetron-based composite and are usually associated with microcracking. However, detailed SEM images of Epon-based composite show that the tows are fully wetted and microcracks are minimal. Such a difference might explain (at this early stage in the study) the higher energy absorption capacity of the Hetron-based system as compared with the Epon-based one as reported in the literature.

A detailed FE model has been developed encompassing several unit cells of the above braided architectures and material systems and is currently being analyzed and compared with experimental data.

The Principal Investigator and his team have investigated and tested several laser extensometers and are in the final stages of making the purchase decision. This will be used in tracking deformations that are intra-unit cell as well as inter-unit cells (in specimen with several unit cells).

Energy Absorption of Triaxially Braided Composite Tubes

The objective of the project is to develop a predictive tool for the crush analysis of triaxially braided composite structures under dynamic loads based on a smeared micromechanics model developed in an earlier project that specifically targeted static loading. The smeared micromechanics model meant for static analysis was simplified to improve computational efficiency, without loss of precision.

The effects that were considered as significant role players were stress concentration, fiber tow scissoring, and rate dependency. The scissoring was introduced based on the assumption that once the matrix fractured in a unit cell, the tows could scissor under a constant tow load until the tows jammed against one another. This phenomenon was observed experimentally, and the tow rotation measured in the experiments was predicted using the FE analysis in a static mode. The effect of delay in damage propagation as a result of stress concentration was captured using the fiber bundle theory of Tsai and Hahn specialized for the triaxial braid situation.

The effect of stress-concentration was demonstrated by comparing experimental and numerical results in case of a tensile specimen with a hole. The critical damage area approach based on Tsai-Hahn fiber bundle theory was found to be very effective. The effect of strain rate on the damage evolution was introduced based on Sun et al.'s approach of anisotropic viscoplasticity. It was demonstrated on dynamic crushing of square tube with ±45° layup.

The constitutive model with scissoring, stress-concentration, and rate dependency has been implemented as a user material subroutine in the explicit version of ABAQUS. The user material needs to be tested thoroughly against several tube tests at different rates of loading.

Lateral Impact Study

The objective of the project is to achieve a fundamental understanding of the energy-absorbing mechanisms in triaxially braided composites subjected to lateral bending and impact. A combined experimental and analytical approach has been planned and implemented for this purpose. The analytical study has applied the smeared micromechanics material model previously developed in the Energy Management Program, available as a user subroutine with ABAQUS®. Based on the study of a simple test specimen, a specimen representative of an automotive component such as a B-pillar will be proposed.

The overall study involves three distinct phases: smeared micromechanics material model of composite strips under lateral bending, validation of the model using experimental data, and extension of the model for designing automotive components

such as the B-pillar of a passenger compartment. Phase I of the project has been finished with modeling and analysis of a $[0_{80k}/\pm45_{12k}]$ triaxial carbon fiber braided composite strip subjected to off-axis compressive loading. Damage initiation and accumulation at the midlength of the strip have been observed with identification of many energy absorption modes. Principle modes observed include tow splitting—in-plane and out-of-plane, axial tow compression, matrix cracking, and interply delamination, which all contribute to some degree to material degradation/softening in the strip subject to lateral bending. The axially braided composite exhibits, as observed in the micromechanics model, a phenomenon in which the material within Representative Unit Cell (RUC) can regain a prominent stiffness even after a peak load point. This would be caused by a dramatic change of stiffness distribution in a RUC as a certain scale of accumulated micromechanics damage zone has been reached

Project activity in Phase II is being carried out to pursue experimental investigation into the composite strips for validating the model effectiveness and competitiveness, including model capabilities for characterizing mechanical properties of the unit cell structure in the braided composite. Atkins & Pierce was selected to provide the braided raw materials (production code 4374-2) for plaque molding. The molded plaques were then provided to the university contractor for specimen cutting and testing in July 2004. Guidelines on procedures for all the tests, including material test matrix and specimen cutting layout were established for research contractors to follow to acquire proper experimental data for validation. Total of 90 specimens were planned on characterizing properties of triaxially braided composites in tensile, compression, pure bending, and lateral bending. The tests started in the fourth quarter of FY 2004 and are projected to be finished in the first quarter of FY 2005.

Summary

The Crash Energy Management Program develops and demonstrates technologies that are required to apply production feasible structural composites in automotive crash and energy management applications. Projects within the program are intended to understand the mechanisms of polymer composite crash, develop analytical tools for use in vehicle design, and build a knowledge base for the vehicular application of lightweight polymer composites. The FY 2004 experimental projects follow:

- High rate compression tests were completed to demonstrate that shear transfer between fiber tows and matrix is reduced at higher strain rates.
- Static and dynamic laboratory tests were completed to determine effects of friction during sliding and bending.
- Mode I and Mode II adhesive fracture properties were determined in both static and dynamic tests.
- Composite sandwich face/core configurations were evaluated, and the down-select was completed to initiate the second phase of testing.
- In-situ and bulk composite matrix material properties were characterized, and details of the fiber architecture of molded specimens were examined to understand anomalies in material properties and energy absorption of braided composites.

The analytical studies indicated the following:

- Cohesive zone models were implemented into FE analysis codes and demonstrated good agreement to experimentally determined behavior of bulk adhesive.
- The analysis of the fracture of a composite strip under a combined bending and compression load was completed using a code previously developed in the program. Experiments were initiated to validate the analytical results.

Presentations and Publications

1. A. G. Salvi, A. M. Waas, and A. Caliskan, “Rate-Dependent Compressive Behavior of Unidirectional Carbon Fiber Composites,” *Polymer Composites*, **25**(4), 397–406 (August 2004).
2. A. G. Salvi, A. M. Waas, and A. Caliskan, “Specimen Size Effects in the Off-axis Compression Test of Unidirectional Carbon Fiber Tow Composites,” *Composites Science & Technology*, **64**(1), 83–97 (January 2004).
3. R. K. Kapania, D. P. Makhecha, E. R. Johnson, J. Simon, and D. A. Dillard, “Modeling Stable And Unstable Crack Growth Observed In Quasi-Static Adhesively Bonded Beam Tests,” IMEC204-59765, *Proceedings of IMECE’04*, 2004 ASME International Mechanical

Engineering Congress and Exposition, Anaheim, California, U.S.A., November 13–16, 2004
4. J. C. Simón, D. A. Dillard, and E. R. Johnson, "Characterizing the Impact Fracture Properties of Structural Adhesives," Presented at the 27th Annual Meeting of Adhesion Society, Wilmington, North Carolina, U.S.A., February 15–18, 2004.
5. A. L. Van Otten, N. S. Ellerbeck, D. O. Adams, C. L. Nailadi, and K. W. Shahwan, "Evaluation of Sandwich Composites for Automotive Applications," *Proceedings of the 2004 SAMPE Conference, Long Beach, California*.
6. N. D. Flesher and F-K. Chang, "Modeling the Response of Braided Composites with Stress Concentrations," 11th U.S.-Japan Conference on Composite Materials, September 9–11, 2004, Yonezawa, Japan.
7. N. D. Flesher and F-K. Chang, "Effect of Cross-Section Configuration on Energy Absorption of Triaxially Braided Composite Tubes," 18th Annual Technical Conference American Society for Composites, October 19–22, 2003, University of Florida.
8. N. D. Flesher and W. Cheng, "Evaluation of STCrush for Characterization of Crushing Behavior of Composite Tubes, 10th U.S.-Japan Conference on Composite Materials," September 16–18, 2002, Stanford University.
9. S. C. Quek, A. M. Waas, K. W. Shahwan, and V. Agaram, "Compressive response and failure of braided textile composites: Part 2—computations," *Int. J. Nonlinear Mech.*, **39**(4), 650–663 (June 2003).
10. S. C. Quek, A. M. Waas, K. W. Shahwan, and V. Agaram, "Compressive response and failure of braided textile composites: Part 1—experiments," *Int. J. Nonlinear Mech.*, **39**(4), 635–648 (June 2003).
11. S. C. Quek, A. M. Waas, K. W. Shahwan, and V. Agaram, "Analysis of 2D Flat Triaxial Braided Composites," *Int. J. Mechanical Sciences*, **45**(6–7), 1077–1096 (2003).
12. S. C. Quek and A. M. Waas, "Micromechanical Analyses of Instabilities in Braided Glass Textile Composites," *AIAA J*, **41**(10), 2069–2076 (October 2003).

F. Crash Analysis of Adhesively Bonded Structures (CAABS)

Co-Principal Investigator; J. Michael Starbuck
Oak Ridge National Laboratory
P.O. Box 2009, Oak Ridge, TN 37831-8048
(865) 576-3633; fax: (865) 574-8257; e-mail: starbuckjm@ornl.gov

Co-Principal Investigator: Raymond G. Boeman
Oak Ridge National Laboratory
P.O. Box 2008, Oak Ridge, TN 37831-6472
(865) 946-1204; fax: (864) 946-1214; e-mail: boemanrg@ornl.gov

ACC Collaboration Contact: Naveen Rastogi
Visteon Corporation
6100 Mercury Drive, #SW61-025, Dearborn, MI 48126
(313) 755-6264; fax: (313) 755-4229; e-mail: nrastogi@visteon.com

Project Manager, Composites: C. David Warren
Oak Ridge National Laboratory
P.O. Box 2008, Oak Ridge, TN 37831-6065
(865) 574-9693; fax: (865) 576-4963; e-mail: warrencd@ornl.gov

Technology Area Development Manager: Joseph A. Carpenter
(202) 586-1022; fax: (202) 586-1600; e-mail: joseph.carpenter@ee.doe.gov
Field Technical Manager: Philip S. Sklad
(865) 574-5069; fax: (865) 576-4963; e-mail: skladps@ornl.gov

---

Contractor: Oak Ridge National Laboratory
Contract No.: DE-AC05-00OR22725

Objectives

- Develop a comprehensive experimental and analytical methodology to analyze and design adhesively bonded automotive composite structures to sustain axial, off-axis, and lateral crash/impact loads.
- Determine the rate sensitivity of bonded tubes to crush through experiments on the Oak Ridge National Laboratory (ORNL) Test Machine for Automotive Crashworthiness (TMAC).
- Determine influence of critical joint design parameters, for example, bond length, bond thickness, and fillet, on specific energy absorption.
- Experimentally determine the full-field deformations at joint discontinuities for validation of analytical/numerical results.

Approach

- Coordinate with the bonded joint experimental and analytical efforts undertaken in the Automotive Composites Consortium (ACC) project "Composite Crash Energy Management."
- Select a substrate, adhesive, and representative subcomponent joint geometry for evaluation.
- Characterize substrate material, adhesive material, and coupon level joints under static and dynamic loads.
- Build and test unbonded and bonded rail components under static and dynamic crush loads.

- Correlate experimental results with analytical results by developing finite-element-based tools with appropriate material models and progressive damage algorithms.
- Enhance the understanding of joint performance by conducting full-field deformation measurements using moiré interferometry.

Accomplishments

- Fabricated near void-free bulk adhesive panels and cylindrical rods for adhesive characterization studies.
- Characterized tensile and compressive response and fracture toughness of bulk adhesive at quasi-static load rates.
- Characterized static behavior of the braided carbon fiber substrate under uniaxial tension and compression loads.
- Completed preliminary dynamic stability tests on both unbonded and bonded tubes using TMAC.
- Designed and a fabricated a slack adapter for conducting dynamic coupon-level tests.
- Completed preliminary static tests on specimens having single lap joint geometry to determine influence of critical joint design parameters on specific energy absorption.
- Completed limited dynamic tests on the braided carbon fiber substrate and the bulk adhesive.

Future Direction

- Procure new high-rate test apparatus for conducting coupon-level dynamic tests.
- Complete static and dynamic testing of substrate, bulk adhesive, and coupon-level joints.
- Install and set-up moiré interferometric test equipment for characterizing full-field deformation patterns in adhesive joints.

Introduction

The objective of this project is to develop a comprehensive experimental and analytical methodology to analyze and design adhesively bonded automotive composite structures to sustain axial, off-axis, and lateral crash loads. This direct-funded project will be closely aligned with the experimental and analytical efforts undertaken by the Automotive Composites Consortium (ACC) for composite substrates (see 7D of this document). The focus of this work, however, will be restricted to the adhesive joint related issues. The key to the methodology development is the understanding of how critical joint design parameters, for example, bond length, bond thickness, and fillet, affect the energy absorption. Recent investigations at ORNL have provided valuable insight toward the understanding of composite joint performance and composite crashworthiness. The next logical step is determining the correlation between measurable adhesive joint parameters and their influence on the structure to dissipate energy and ultimately predict crashworthiness for a particular composite design.

Experimental tasks include material testing under quasi-static and dynamic loads for substrates, adhesives, and joints; full-field deformation mapping of joints with moiré interferometry for correlation with computational results; strain-rate sensitivity studies; fracture toughness testing; and test method development as required. These experimental results will provide the building blocks for model developments—first at the coupon level, then progressing in complexity to component level. Correlation with experimental results will provide the basis for which the analytical developments, including development of constitutive laws, materials models, damage algorithms, and new finite elements will be made. Structural tests will be conducted on the new intermediate-rate test machine [Test Machine for Automotive Crashworthiness (TMAC)] at ORNL.

Project Deliverables

At the end of this multiyear program, joint parameters that have significant influence on energy dissipation will be identified, and their influence quantified, using appropriate analytical models and experimentation. In collaboration with the ACC Composite Crash Energy Management project, a predictive capability for joint performance will be demonstrated, and the validity of the prediction will be assessed through structural crash testing.

Approach and Results

The technical approach involves both experimental and analytical tasks. There are four main tasks:
Task 1—Materials Selection and Screening,
Task 2—Material Characterization,
Task 3—Component Testing, and
Task 4—Computational Tools Development.

Task 1 was completed and reported on in the FY 2002 annual report. The selected chopped carbon fiber prepreg material system was characterized from flat plaques provided by the vendor. Discussions with the vendor led to an overly optimistic view of the suitability of the material for this project. Additionally, delays in receipt of the material from the supplier resulted in consideration of a carbon fiber sheet molding component (SMC). Both materials are unsatisfactory due to processing difficultly and material variability. As a result of the variability in the initial material screening tests and difficulty in fabricating tubes with this material, the substrate material was changed to a carbon fiber braided system. The woven fabric prepreg is comprised of T300B carbon fiber with a tow size of 3K and 42% (by weight) epoxy resin.

Task 2 was initiated during FY 2002 and was originally scheduled to be completed in the third quarter of FY 2003. The schedule has been adversely impacted by several factors, including delays in substrate material acquisition due to supplier manufacturing constraints and then actually changing the substrate (discussed previously), laboratory-initiated relocation of test facilities from the Y-12 National Nuclear Security Complex to ORNL, operation constraints on TMAC pending pressure vessel certification, and budget constraints. A new schedule is being prepared that takes into account the impact of all these factors.

The substrate will be fully characterized by conducting tension, compression, and in-plane shear tests. The degree of anisotropy in the material will be qualified by testing specimens that are machined from two different orthogonal directions in the panels. This work will be contracted out to an independent testing laboratory by the ACC with a limited set of comparison tests being conducted by ORNL.

Characterization of the tensile and compressive static responses of the substrate material is complete. Tensile and compression testing of specimens that were machined from two different orthogonal directions in the panels indicates similar properties in both directions. Tensile results for five samples, each from two different orthogonal directions in the panels tested at 0.02 mm/s, indicate that average ultimate strength and modulus for the substrate are 70.4 ksi and 5.8 Msi, respectively. Coefficients of variability (COVs) for the strength and modulus results are 3.6% and 1.3%, respectively, which is very good. A typical tensile stress strain curve for this substrate is shown in Figure 1. Compressive results for five samples, each from two different orthogonal directions in the panels tested at 0.02 mm/s, indicate that average ultimate strength and modulus for the substrate are 61.4 ksi and 5.6 Msi, respectively. COVs for the strength and modulus results are 3.9% and 3.2%, respectively. A typical compressive stress strain curve for this substrate is shown in Figure 2. Tests for five substrate samples at 100 mm/s resulted in a decrease in the average ultimate strength to 65.6 ksi, but the average modulus remained the same at 5.9 Msi. COVs for the strength and modulus results

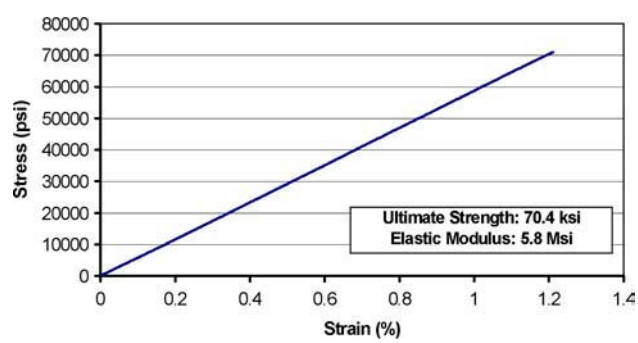

Figure 1. Typical tensile stress-strain curve for the substrate.

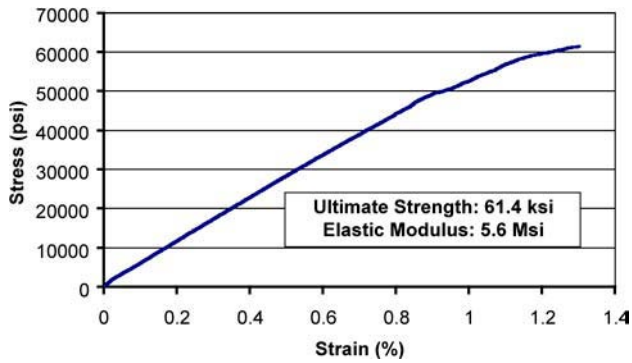

Figure 2. Typical compression stress-strain curve for the substrate.

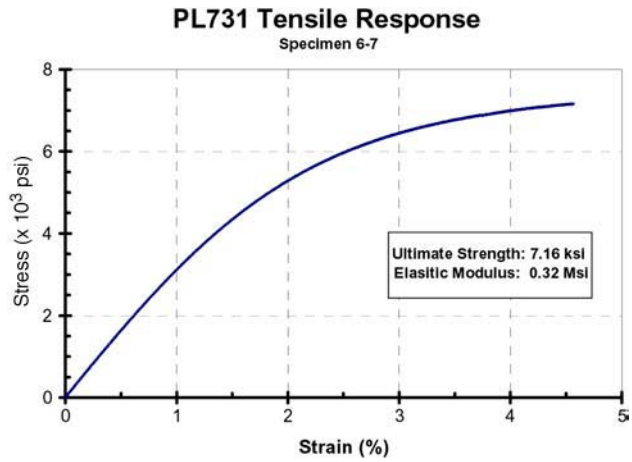

Figure 3. Typical tensile stress-strain curve for the bulk adhesive.

are 4.3% and 0.8%, respectively, which is also very good.

The adhesive used in this study is an epoxy paste designated as Sovriegn PL731 and is used in many of the research projects within the ACC. The bulk adhesive testing consists of tension, compression, shear, and fracture toughness. In addition, DSC/DMA tests will be conducted to verify the degree of cure. The key to this task is the successful fabrication of high-quality specimens (e.g., low void content) to accurately quantify the bulk adhesive mechanical properties. The compression and shear testing will be accomplished using cylindrical rod specimen geometries. Cylindrical rod specimens were fabricated using centrifugation and glass test tubes as molds. Initial difficulties in producing flat plaques were alleviated by developing a mold-filling process that uses an adequate supply of excess adhesive under pressure to back fill the mold cavity. High-quality specimens for all bulk adhesive tests were fabricated with these two approaches.

Characterization of the tensile and compressive static responses is complete and indicates excellent consistency from specimen to specimen and from plaque to plaque. Tensile results for 18 samples from two different plaques indicate average ultimate strength and modulus for the adhesive are 7.3 ksi and 0.31 Msi, respectively. COVs for the strength and modulus results are 4.8% and 1.6%, respectively, which is excellent. A typical tensile stress strain curve for this adhesive is shown in Figure 3.

Eight cylindrical samples—25-mm long and 12-mm diameter—were subjected to compressive loads (ASTM D695) up to strains of 22% without global failure. Compressive modulus for the adhesive, taken from a range of 1% to 2% strain, is 0.31 Msi, identical to the tensile value. The COV is 1.6%, consistent with the tensile results. Figure 4 depicts representative "failed" test samples that indicated plastic deformation with small local cracks being present in some samples. Figure 5 illustrates the consistency of the compressive response out to more than 20% strain.

A preliminary shear test for the bulk adhesive was conducted by applying a torsional load to a solid cylindrical rod specimen. The rod was 12 mm in diameter and 100 mm long. Figure 6 shows the measured shear stress-strain response. This specimen did not fail, and the maximum shear strain of almost 13% corresponded to a 60° rotation of the specimen, which was the maximum capability of the test equipment. To achieve a more uniform shear stress distribution and possibly produce an ultimate failure the solid rod specimen geometry was modified to a hollow cylinder. The specimens were manufactured by drilling and reaming the solid rods.

Figure 4. Typical post-test condition of compression samples, indicating plastic deformation and local cracking associated with large strains.

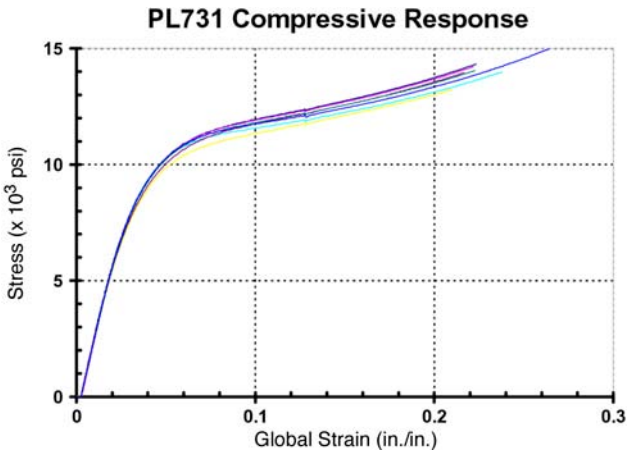

Figure 5. Combined compressive stress-strain curves for the bulk adhesive (eight samples).

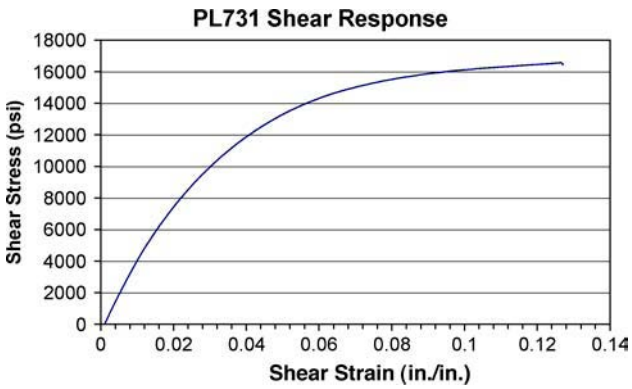

Figure 6. Shear stress-strain curve for bulk adhesive.

The hollow cylindrical specimen still did not fail before exceeding the maximum capability of the test equipment. Hence tests are being planned by the V-notched beam method to determine the shear properties of the bulk adhesive.

Preliminary quasi-static and low-speed dynamic fracture toughness tests were completed using the compact tension specimen geometry. The specimens were machined from an 8-mm-thick bulk adhesive plaque per the geometry specified in ASTM D5045. The technique developed for making near void-free 3-mm-thick plaques was also used for making these plaques. The tests were conducted on a conventional closed-loop, servo-hydraulic machine at rates of 0.02, 2.5, 25, and 1000 mm/s with three specimens tested at each rate. An untested and a tested specimen are shown in Figure 7. From these initial tests, there appeared to be an initial drop in the fracture toughness as a function of load rate, but the initial quasi-static value appeared to be much greater than

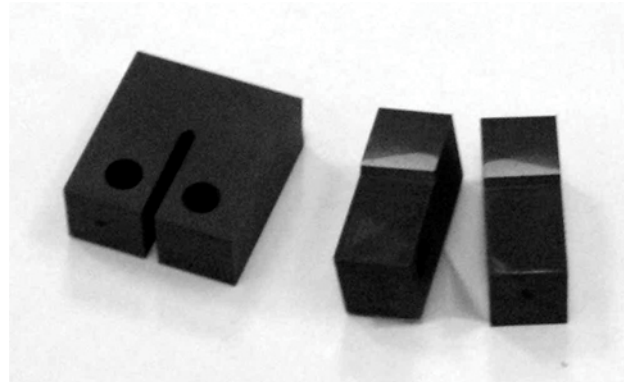

Figure 7. An untested and a tested bulk adhesive compact tension specimen.

typical values for epoxy systems. The experimental data and test methodology were evaluated for their validity, and it was determined that the target velocities were not achieved prior to load application. Consequently, the test setup was modified to include a slack adapter, and the tests were repeated at 0.02, 100, 500, and 1000 mm/s. Check-out tests were completed, and it was determined that the target velocities could be achieved prior to the load application. There was a drop in fracture toughness as loading rate was increased from 0.02 to 100 mm/s. At rates of 500 and 1000 mm/s it was difficult to discern the relatively small loads generated by the test specimen from the contributions of the momentum generated by the 10-lb slack adapter (see Figure 8). Hence, use of alternate specimen geometries like the single-edge notch bend (SENB) to determine fracture toughness at 500 and 1000 mm/s are being investigated.

Figure 8. Slack adapter.

Coupon-level joint configurations will consist of double-notch shear (DNS) and single-lap shear (SLS) test specimen geometries. Joint parameters that will be investigated are the adhesive thickness, overlap length, and fillet geometry. Moiré interferometry will be used to study the full-field deformation pattern in the bond-line during static testing of the SLS joint specimens. The crack growth characteristics of an adhesive joint will be quantified by conducting Mode I, Mode II, and Mixed Mode fracture tests using double-cantilever beam (DCB), end-notch flexure (ENF), and mixed-mode bending (MMB) specimen geometries, respectively. SLS tests were conducted at 0.02 mm/s on specimens with adhesive thickness and overlap length of 0.6 mm and 12.7 mm, respectively. Two types of adhesives were used: one that was subjected to heat treatment, and the other that was not heat treated. The SLS specimens having the adhesive not subjected to heat treatment recorded higher shear strength values (22.56 MPa) when compared to the ones that went through heat treatment (18.78 MPa). More SLS and DNS test specimens with different overlap lengths and thicknesses are currently being prepared.

Component testing in Task 3 was scheduled to commence in the last half of FY 2004 but will likely be delayed due to the issues stated above. Component testing will consist of unbonded and adhesively bonded upper rail sections. The testing will include static and dynamic crush loads, and axial and lateral impact loads. The TMAC at ORNL and test sleds will be used for the dynamic testing. The unbonded tests are to establish a baseline, and then the results from Task 2 will guide the joint design such that bonded sections will be built to either fail or not fail in the joint. Some of these tests will be repeated using scaled geometries to get an initial look at scale effects.

To determine if the baseline tube geometry would have any stability problems, that is, tube buckling would be the failure mode instead of a progressive crush, two unbonded tubes and two bonded tubes were tested at 500 mm/s and 4000 mm/s using TMAC. The tube geometry was square with nominal dimensions of 100 mm × 100 mm × 2 mm, and the length was 380 mm for the unbonded tube and 300 mm for the bonded tube. The bonded tubes were fabricated by using two c-channels having ply drop-offs to form a stepped scarf joint. The results are shown in Figures 9–12

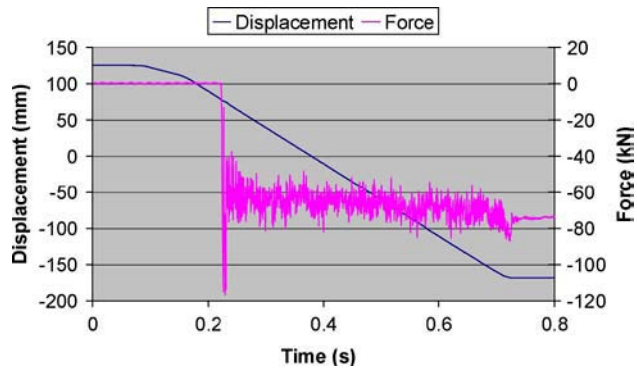

Figure 9. Unbonded tube tested at 500 mm/s.

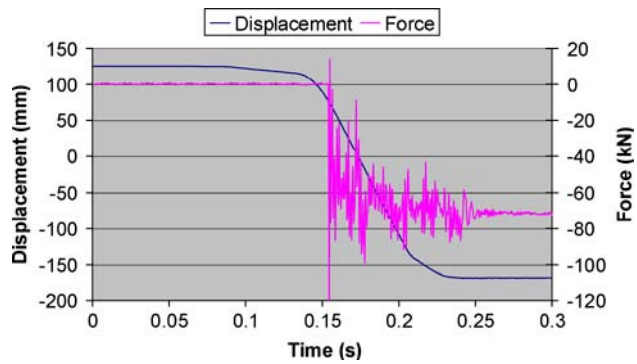

Figure 10. Unbonded tube tested at 4000 mm/s.

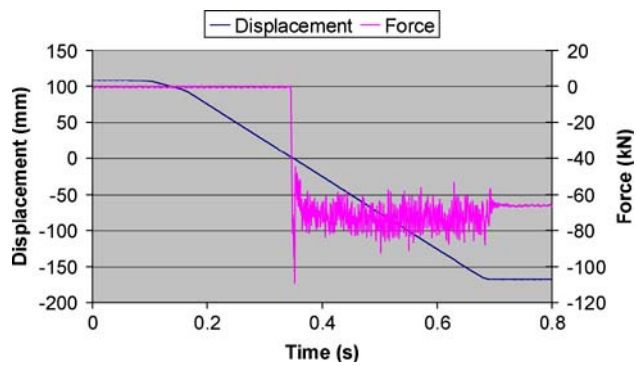

Figure 11. Bonded tube tested at 500 mm/s.

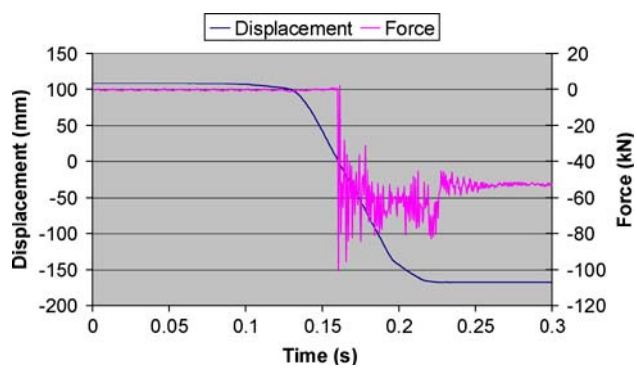

Figure 12. Bonded tube tested at 4000 mm/s.

and indicate a very well behaved progressive crush response with little difference between the bonded and unbonded tube responses. The substrate failed in a brittle fashion and literally exploded into tiny pieces (see Figure 13).

In Task 4, the computational tools development will consist of analyzing the test geometries at both the coupon level and component level, developing new material models, and developing new test methods to support the model development. This task is conducted in parallel with Tasks 2 and 3. The coupon- and component-level analyses will be completed using existing material models that are available in finite-element analysis (FEA) tools such as ABAQUS and LS-DYNA. The bond-line deformations predicted by the analyses will be compared with the Moiré experimental results. Also, the effects of bond-line thickness and length, fillet, and loading rate on the stress distribution in the joint will be correlated with the experimental results. The model development effort will consider new constitutive laws, progressive damage algorithms, new finite elements for modeling the adhesive layer, and new computationally efficient techniques. In support of this effort, new test methods will be developed for characterizing strain-rate effects and dynamic fracture.

Figure 13. Progressive crush failure of unbonded tube tested at 4000 mm/s.

Summary

Highlights of the progress during this reporting period follow:

1. Manufactured all bulk adhesive samples for tension, compression, shear, and fracture tests.
2. Completed bulk adhesive tensile and compression tests. Results indicate excellent consistency. Data have been supplied to the ACC partners for implementation in the FEA.
3. Completed preliminary shear and fracture toughness tests on bulk adhesive, and the results are being reviewed by the project team for their validity.
4. The chopped carbon fiber substrate material was replaced with a carbon fiber braided material as a result of excessive variability in the chopped fiber material data and inability to fabricate high-quality tubular specimens.
5. Machined all substrate material samples for tension, compression, and shear tests.
6. Characterized static behavior of the braided carbon fiber substrate under uniaxial tension and compression loads. Results indicate excellent consistency. Completed limited dynamic tensile tests on the braided carbon fiber substrate.
7. Completed preliminary static tests on specimens having single-lap joint geometry.
8. Completed stability testing for progressively crushing both bonded and unbonded tubes at dynamic rates.

G. Long-Life Electrodes for Resistance Spot Welding of Aluminum Sheet Alloys and Coated High-Strength Steel Sheet (ORNL)

Principal Investigator: S. S. Babu
Metals and Ceramics Division, Oak Ridge National Laboratory
Building 4508; Mail Stop 6096; 1, Bethel Valley Road, Oak Ridge, TN 37831-6096
(865) 574-4806; fax: (865) 574-4928; e-mail: babuss@ornl.gov

Technology Area Development Manager: Joseph A. Carpenter
(202) 586-1022; fax: (202) 586-1600; e-mail: joseph.carpenter@ee.doe.gov
Field Technical Manager: Philip S. Sklad
(865) 574-5069; fax: (865) 576-4963; e-mail: skladps@ornl.gov

Participants:
Michael L. Santella, Oak Ridge National Laboratory
W. Peterson, Edison Welding Institute

Contractor: Oak Ridge National Laboratory
Contract No.: DE-AC05-00OR22725

Objective

- Understand the mechanisms of copper electrode wear used in spot-welding of high-strength steel sheets used in automotive industries.
- Evaluate the fundamentals of physical processes that lead to deformation and chemical attack, and model the same using thermo-mechanical-metallurgical models.
- Apply the models to design new electrode material—geometry—process parameter combinations that may mitigate excessive electrode wear.
- Characterize the mechanical properties of electrodes at high temperatures as input to the computational models and also to evaluate the softening resistance of different electrodes.
- Explore the possibility of electrode softening on the overall electrode wear characteristics.
- Provide support to the team lead by automotive industries in the implementation of these new computational models.

Approach

- Perform critical review of literature to evaluate the conditions that determine the mode of electrode wear, that is, either deformation or chemical attack due to zinc coating present on the coated steel sheets.
- Develop simple and phenomenological models that can capture the electrode wear characteristics by welding engineer in the automotive industry.
- Measure the stress-strain characteristics of candidate copper electrode materials at different temperatures, and describe them using well-established analytical equations.
- Measure the spatial hardness variations in copper electrodes at different stages of their useful life during a typical resistance welding operation.

- Measure the extent of chemical attack by molten zinc by isothermal exposure test on candidate copper electrode materials.

Accomplishments

- Identified the conditions at which either deformation or chemical attack can occur during resistance spot-welding through exhaustive review of the literature. The hypotheses were validated with results from sequential life test experiments performed at Edison Welding Institute.
- Identified the spatial softening of copper electrodes as a function of electrode life in conventional electrodes due to metallurgical changes.
- Developed a simple, but powerful, phenomenological model that captures the sequential deformation of copper electrodes as a function of electrode mechanical properties and resistance spot-welding process parameters.
- Applied computational thermodynamic and diffusion-controlled growth models to describe chemical attack of copper electrode by zinc. The modeling results successfully identified that the copper electrodes will wear at rapid rates when they are exposed to molten zinc due to dissolution of copper.
- Both deformation and chemical model results were in agreement with experimental results from Edison Welding Institute and Oak Ridge National Laboratory.
- Based on the above modeling work, possible concepts for improving the life of copper electrodes were devised in collaboration with an industrial team.
- Published the results in a internationally reputed sheet metal welding conference, which is attended by a wide range of automotive industry personnel, including original equipment manufactures and suppliers. The paper was well received, and the audience agreed with the findings and indicated the applicability of the computational models to their industrial setting.

Future Direction

- The deformation model will be made accessible to the automotive industries for plant-specific applications after rigorous validation with the new industry data.
- Participate in the "beta-site" testing and evaluation of the results from new sets of experimental electrode materials and different geometry.
- Disseminate the knowledge to a wide range of audiences by publishing in international welding journals.

Introduction

The introduction of galvanized high-strength steels has led to increased demands on the performance of copper electrodes used in resistance-spot welding of these steel sheets. Resistance spot welding relies on rapid generation of heat due to resistive heating. The heating is proportional to I^2R, where I is welding current, and R is the electrical resistance of the steel. When the steel sheets are galvanized, the zinc coating provides a very low resistance compared to the bare steel. Consequently, resistance spot welding of galvanized steels requires higher welding currents. The higher welding currents produce higher temperatures and temperature gradients in the copper welding electrodes (shown schematically in Figure 1). As a result, the electrodes deteriorate by both deformation and chemical reactions**.** These deteriorations slowly increase the diameter of the copper electrode until it reaches a critical value after making 1000–2000 welds. At this critical diameter, the current density becomes too low to make an acceptable weld between the zinc-coated steel sheets. This condition signals the end of life for the electrodes. In general, the life cycles of copper electrodes used in coated steels are lower than electrodes used on bare steels.

Until now, the above problem has been addressed by trial and error experiments with different types of electrodes (geometry and

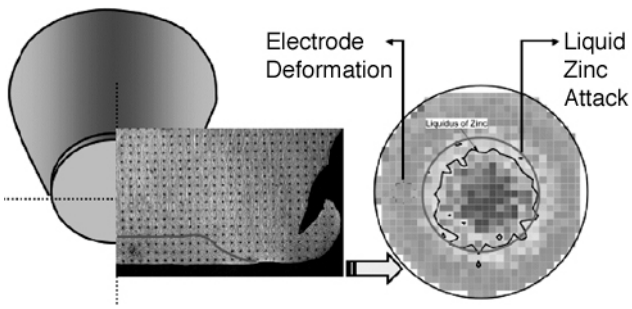

Figure 1. Schematic illustration of copper electrode wear mechanisms through deformation and chemical attack.

composition) and zinc coatings (composition and thickness), and by modification of resistance spot welding parameters. However, there is a need to develop a more systematic framework for evaluating various candidate electrode materials and accelerating the selection of improved electrodes for the various requirements of the automotive industry.

The goal of this collaborative research project with Edison Welding Institute (EWI), automotive industrial members, and electrode suppliers was to develop a mathematical model to describe the deterioration of copper electrodes as a function of electrode properties and welding process parameters.

Earlier Research

In earlier research, Oak Ridge National Laboratory (ORNL) and EWI, through a collaborative project, developed a coupled thermal, electrical, mechanical, and metallurgical model to evaluate the weld formation, deformations in both electrode and sheet, microstructure formation in welds and performance of welds, in bare steels.[1–3] The model was able to consider the complex interplay between welding loads, welding current, contact resistance, and strength of materials. It was able to capture all the physical phenomena that occur within the time scale of one spot weld. In principle, this finite-element-based model can be extended to simulate electrode deterioration by repeating the procedure as a function of 1000 or 2000 welds. However, there are major issues with doing this. One is that the simulation for each spot weld takes up to 10 h of computing time on average. Consequently the simulation of 2000 spot welds will take 833 d! Another problem is that the electrode shape will change with each successive weld. The new electrode shape will require a new mesh. This is another time-consuming activity. Therefore, the existing model, and others like it, was not an efficient solution in terms of both time and cost for optimizing electrode materials and geometries over wide ranges of process conditions. This was the challenge posed to ORNL at the beginning of the research project.

Experimental Measurements of Electrode Wear

The results from an electrode life test conducted according to the American standards are shown in Figure 2. The data show that as the number of spot welds increases, the electrode face diameter also continuously increases. Because the welding current is kept constant in these tests, the increase in electrode face diameter leads to a reduction in current density. Eventually the current density is reduced below the critical value needed to produce the required minimum weld button size. This event signals the end of electrode life.

Figure 2 illustrates the importance of current density on electrode life. It is well known that the current density is directly related to the peak temperatures achieved at the sheet/sheet and electrode/sheet interfaces. The electrode face temperatures will decrease with increasing electrode face diameter for a fixed current level. The face temperature will determine the rates of deformation and chemical attack at the electrode/sheet interface. Therefore, an analytical model was needed to relate the electrode face diameter to electrode face temperature.

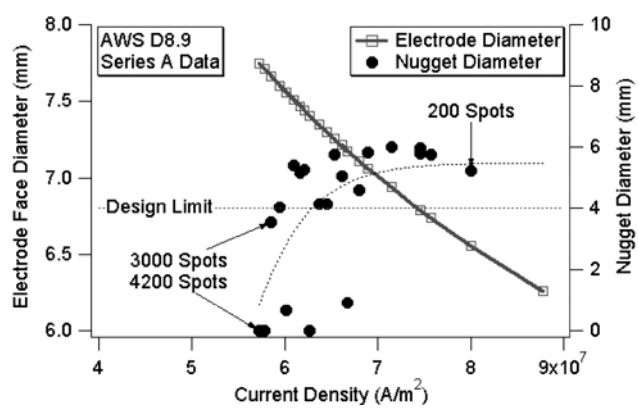

Figure 2. Experimentally measured electrode face diameter of a standard electrode tip and weld nugget diameter as a function of current density.

Localized Softening of Copper Electrode During Welding

For the model development, it was speculated that the regions of the electrodes near their faces would soften during welding operations. This softening may be related to metallurgical changes that cumulatively occur due to thermal cycling experienced during each spot weld. The spatial variation of Vickers microhardness of the CuCrZr electrode alloy was also measured at various stages of electrode life, and microhardness maps are presented in Figure 3. The maps were done on only one-half of the sectioned surfaces because of axial symmetry. Figure 3(*a*) shows that the hardness of the electrode alloy near the tip was 120 kg/mm^2 after 100 welds, while the bulk of the electrode exhibited a hardness of 180 kg/mm^2. This confirms that softening occurs fairly rapidly in the cold-worked, precipitation-hardened electrode alloy as has been observed in other work. The hardness distributions after 500 welds and at the end-of-life stage are shown in Figure 3(*b* and *c*). As life testing proceeded, microhardness values near the electrode tip fell to as low as 70 kg/mm^2. However, the hardness distribution did not change significantly after 500 welds. These results demonstrate that an assumption of constant room temperature strength is not valid, and the model to be developed in this work needs to consider this phenomenon.

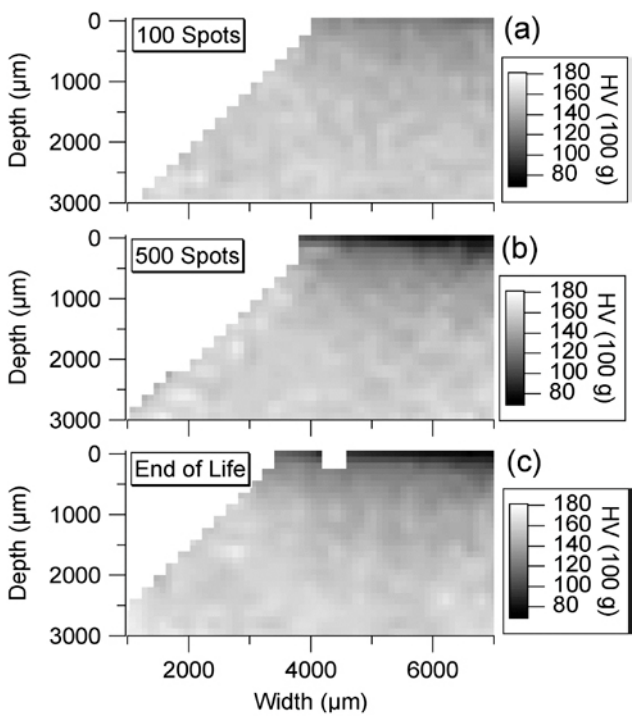

Figure 3. Measured spatial variation of hardness in copper electrodes after (*a*) 100 welds, (*b*) after 500 welds, and (*c*) at the end of life showing progressive softening at the electrode face.

Model for Predicting the Electrode Deformation

The deformation model must consider the physical processes as follows: (1) thermal cycles at the copper electrode—steel sheet interface; (2) stress-strain characteristics as a function of temperature, (3) softening characteristics as a function of weld numbers; and (4) progressive electrode deformation. The methodologies to describe each of the four phenomena are briefly outlined below.

(1) Thermal cycle prediction: Although sophisticated finite-element or finite-difference methods can be used to estimate these temperatures, to allow for rapid calculations, an empirical sigmoidal equation was used to relate the electrode face temperature (T, in Kelvin) to electrode face diameter (d, in mm).

(2) Stress-strain characteristics: The tensile properties of CuCrZr class 2-electrode alloy were measured as a function of temperature to provide input for the deformation analysis. The specimens had gage dimensions of 6.35-mm diameter by 31.75-mm length. They were tested at a nominal strain rate of 6.7×10^{-4} s^{-1}. All of the elevated temperature tests were conducted in still air. The data were then represented in the form of a simple analytical equation.

(3) Electrode softening: The softening characteristics measured (see Figure 3) were represented in the form of an analytical equation. Ability to change the softening resistance was considered in this equation.

(4) Progressive deformation: The descriptions of temperature variation at the electrode face, temperature-dependent tensile properties, and softening behavior were then combined into a simple model of electrode deformation. The model assumes that the deformation is confined to a disc of material at the electrode tip. The deformation of the disc will

eventually cease when the pressure associated with welding equals the yield strength of the alloy. At that point, mechanical equilibrium is achieved at the electrode face.

The model was calibrated to a set of experimental data. The comparisons of measured and predicted data are shown in Figure 4 and demonstrate the validity of the model. There is no question that this model greatly simplifies the mechanical and metallurgical issues associated with the electrode deformation process. However, as details are added to improve technical precision, the complexity of the analysis and the demand for computation time increases.

Our intention was to provide an engineering tool that would be capable of guiding electrode alloy development efforts and selecting welding parameters and one that was relatively accessible to a wide range of potential users. This personal-computer-based deformation model satisfies that objective.

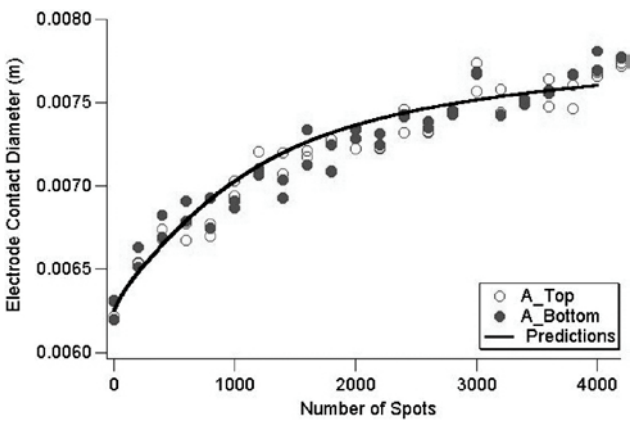

Figure 4. Comparison of predictions using Eq. (4) and experimentally measured face diameters from top and bottom electrode as a function of number of welds.

Methodology for Predicting the Chemical Attack by Zinc Coating on Steel

Clearly any general model of resistance spot welding electrode deterioration must account for chemical attack mechanisms. This aspect of electrode deterioration is being addressed through application of diffusion-controlled growth analysis. One-dimensional diffusion (analogous to the axial direction in an electrode tip) in a material couple between copper and zinc is being considered. The chemical activity of zinc at the copper/zinc interface is held constant at unity, which is equivalent to assuming there is an infinite reservoir of zinc . This is reasonable for describing conditions over typical electrode lives of 1000s of welds.

Two simulation conditions are considered: (1) a peak temperature close to the melting point of zinc, and (2) a peak temperature above the melting point of zinc. The analyses are based on somewhat arbitrary temperature profiles with durations of 0.5 s. The calculations were performed with DicTra™ software[4] assuming a diffusivity of copper in liquid zinc of 10^{-8} m^2/s.

The results are presented in Figure 5. The case where the zinc does not melt was based on the thermal cycle shown in Figure 5(*a*) in which the temperature increases from room temperature to near the melting point of zinc (693 K) in 0.4 s and cools back to room temperature in 0.1 s. Because zinc does not melt, only solid-state diffusion occurs across this copper/zinc interface and the profile of zinc concentration in the copper is shown in Figure 5(*b*). For these conditions, the diffusion distance for zinc into the copper is less than 1 nm, a miniscule amount.

The thermal cycle for the case where zinc melting is permitted is shown in Figure 5(*c*). The initial temperature is just above 693 K. It increases to a maximum of 1000 K in 0.4 s, and then decreases back to 693 K in 0.1 s. For these conditions copper dissolves into the zinc and the copper/zinc interface rapidly penetrates into the copper. The profiles for zinc penetration into the copper are shown in Figure 5(*d*) for this case. The maximum extent of the zinc penetration was about 500 nm.

These results are consistent with the conclusion that it is the reaction of liquid zinc with copper alloy electrode tips that dominates the chemical attack process. Subsequent solidification of the copper-rich liquid at the copper/zinc interface will result in the formation of brass layers on the electrode tip.

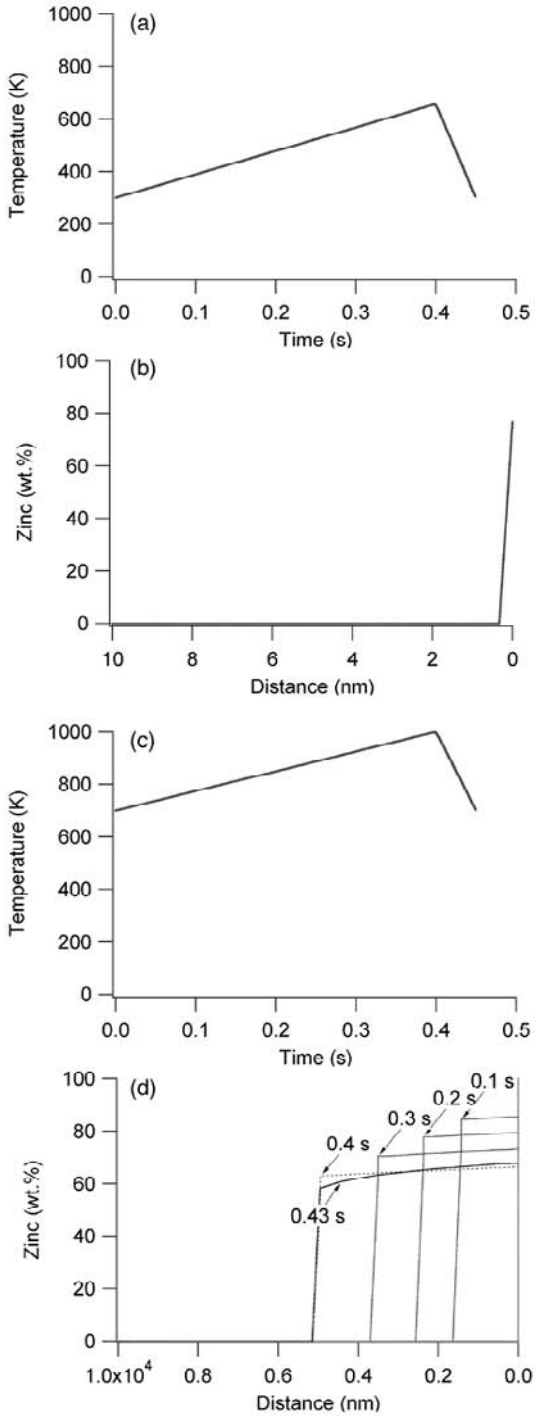

Figure 5. Predictions of a model that considers chemical attack by zinc: (*a*) assumed temperature profile with a peak temperature less than melting point of zinc, (*b*) calculated solid-state diffusion profile in the copper block, (*c*) assumed temperature profile with a peak temperature higher than melting point of zinc, and (*d*) calculated penetration depth of liquid zinc into copper block.

Experimental Evaluation of Chemical Attack by Molten Zinc

A simple melting experiment was done to illustrate the rate of reaction between liquid zinc and copper. An OFHC copper specimen with dimensions of 12 × 12 × 3 mm was heated in high-purity argon atmosphere to 440°C on a hot plate with digital temperature control. A 0.25-g pellet of high-purity zinc was then placed on the copper. The zinc melted within several seconds, and then the specimen was removed from the hot plate and rapidly cooled to room temperature. The total contact time between the liquid zinc and copper could not be accurately determined, but it was very brief, less than 30 s. An optical micrograph of the zinc droplet that solidified on the copper surface is shown in Figure 6(*a*). Reaction of the zinc with the copper surface is illustrated in Figure 6(*b*) where the original position of the copper surface is indicated by the line. Penetration of the liquid zinc into the copper surface is evident. Also, the yellow layer of α-brass indicates diffusion of zinc into the copper. Identical results were obtained when this experiment was repeated using CuCrZr rather than OFHC copper.

Ongoing Work

Analyses of the chemical aspects of electrode deterioration are continuing with one objective being development of a predictive capability similar to the deformation model. Whether deformation or chemical attack dominates, deterioration is not clear. Certainly both deterioration mechanisms are operating in resistance spot welding electrodes, and either could be dominant under specific welding conditions or during different periods of the typical electrode life behavior.

For instance, in the early period of life, electrode diameters are relatively small resulting in relatively high current densities and contact pressures. The higher current densities will increase temperatures at the electrode/sheet interfaces, and this will promote deformation. Higher contact pressures will also make deformation at the electrode tip more likely. In later life, as face diameters enlarge, current densities and contact pressures will decrease, thereby reducing the probability of further deformation. In contrast, the formation of liquid

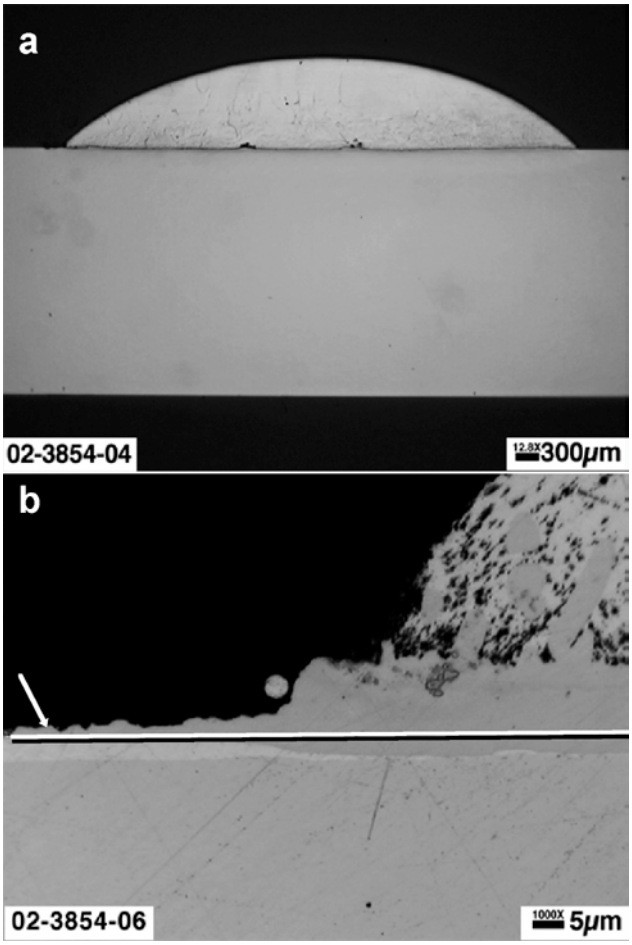

Figure 6. (*a*) Optical macrograph showing the presence of solidified zinc layer on top of the copper electrode and (*b*) high-magnification micrograph showing the presence of different brass layers with different shades indicating different zinc concentrations. The horizontal line shows the original position of the surface before the chemical attack.

zinc at electrode/sheet interfaces is likely to occur irrespective of electrode tip diameter.

Consequently, it may be that deformation is more important as an electrode deterioration mechanism in the early stages of life, while chemical attack is nearly constant throughout. Developing an improved generalized model of electrode deterioration, even of a simplified variety like the present case, will require a better understanding of the deterioration mechanisms and their interrelationships.

Conclusions

An analytical model that relates the electrode face diameter, welding load, welding current, mechanical properties as a function of temperature, and material degradation to electrode wear was developed. The model suggested that the life of resistance spot welding electrodes can be increased by enhancing their softening resistance rather than their absolute strength. A diffusion-controlled growth model showed that if the electrode face temperature is higher than the melting point of zinc, there is a probability of significant penetration of liquid zinc into copper. The predicted rate of liquid zinc penetration into copper was 500 times more than the rate of solid-state diffusion. Melt drop experiments confirmed that liquid zinc penetration into copper readily occurs and will lead to the formation of different brass reaction layers.

References

1. Z. Feng, J. E. Gould, S. S. Babu, M. L. Santella, and B. Riemer, "An incrementally coupled electrical-thermal-mechanical model for resistance spot welding," *Proc. Intl. Conference on Trends in Welding Research, Pine Mountain, Georgia*, 1–5 (1999), ASM International, p. 599.
2. M. L. Santella, S. S. Babu, B. Riemer, and Z. Feng, "Microstructure development in resistance-spot steel welds," *Proc. Intl. Conference on Trends in Welding Research, Pine Mountain, Georgia*, 1–5 (1999), ASM International, p. 605.
3. S. S. Babu, M. L. Santella, Z. Feng, B. W. Riemer, and J. W. Cohron, "An empirical model of the effects of pressure and temperature on the electrical contact resistance of metals," *Science and Technology of Welding and Joining*, 2001, **6**, 126–132.
4. J.-O. Andersson, L. Höglund, B. Jönsson, and J. Agren, "Computer simulations of diffusional transformations in steel," pp. 153–163 in *Fundamentals and applications of ternary diffusion*, ed. G. R. Purdy, Pergamon Press, 1990.

Presentations and Publications

1. S. S. Babu, M. L. Santella, and W. Peterson, "Modeling Resistance Spot Welding Electrode Life," *Proc. of Sheet Metal Welding Conference XI, Sterling Heights, Michigan, May 11–14, 2004*.
2. S. S. Babu, M. L. Santella, W. Peterson, and J. E. Gould, "Modeling resistance spot welding electrode life," AWS Welding Show, April 2004, Chicago, Illinois.

H. Long-Life Electrodes for Resistance Spot Welding of Aluminum Sheet Alloys and Coated High-Strength Steel Sheet (USAMP)

Principal Investigator: Warren Peterson
Edison Welding Institute
1250 Arthur E. Adams Drive
Columbus, OH 43221-3585
(614) 688-5261; fax: (614) 688-5001; e-mail: warren_peterson@ewi

Project Manager: Eric Pakalnins
DaimlerChrysler Corporation
Body Materials Engineering
800 Chrysler Dr.
CIMS 482-00-15
Auburn Hills, MI 48326-2757
(248) 576-7454; fax: (248) 576-7490; e-mail: ep18@daimlerchrysler.com

Technology Area Development Manager: Joseph A. Carpenter
(202) 586-1022; fax: (202) 586-1600; e-mail: joseph.carpenter@ee.doe.gov
Field Technical Manager: Philip S. Sklad
(865) 574-5069; fax: (865) 576-4963; e-mail: skladps@ornl.gov

Participants:
Mike Santella and Suresh Babu, Oak Ridge National Laboratory
Randy Bowers, University of Windsor
Jerry Gould, Edison Welding Institute
Peter Sun, General Motors
Arnon Wexler, Ford Motor Company
Brian Swank and Paul Ruess, Outokompu-Nippert
David Fleckenstein, CMW
Bill Brafford and Chuck Pfister, Tuffaloy
Nigel Scotchmer, Huys
Prabhjit Sidhu, Tower Automotive
Tom Natale, AK Steel

Contractor: U.S. Automotive Materials Partnership
Contract No.: FC26-02OR22910

Objectives

- Survey the currently available technology for achieving long electrode life.
- Comparatively test a broad selection of existing and developmental electrode technologies that have technical merit.
- Investigate the electrode wear process through a combination of testing, metallography, and computer modeling.
- Evaluate a “best practice” electrode(s) through beta-site automotive production testing.

Approach

- Conduct benchmarking (Phase 1). The open literature and available corporate literature will be reviewed along with interviews of industry experts in an effort to produce a state-of-the-art report on electrode wear. This phase has been completed.
- Conduct testing (Phase 2). This involves screening of candidate electrode technologies, in-depth testing of electrodes, and beta testing of selected electrode technologies in a production environment.
- Conduct computer modeling (Phase 3) of the electrode metallurgical and mechanical changes that occur as a result of electrode wear. The models will be used to define the mechanism(s) of electrode wear.

Accomplishments

- Finished metallographic investigation of the wear process through a sequential examination of electrode wear for three electrodes using two standard electrode geometries.
- Finished development of computer models to predict electrode life. This includes wear due to both electrode deformation and chemical attack.
- Developed initial description of electrode wear mechanism.
- Continued initial beta site test planning.

Future Direction

- Produce the five electrodes selected for beta site testing.
- Complete planning and execution of beta site tests on hot dip galvanized and galvannealed steels.
- Complete final report on project.

Introduction

Resistance spot welding (RSW) has been heavily adopted by the automotive industry due to its relatively low capital and operating costs and the capacity to support high production rates. RSW is commonly used to weld high-strength steel (HSS) and aluminum in vehicle construction. These materials are commonly selected to reduce vehicle weight and thus improve fuel economy and reduce greenhouse gas emissions. However, electrode wear of coated steels and aluminum continues to be a significant issue. Electrode wear adversely affects the cost and productivity of automotive assembly welding due to reduced weld quality, reliability, and robustness. This mandates increased inspection rates and greater control of welding parameters. Consequently, large potential cost savings and quality improvements are expected from substantial improvements in electrode life.

As technology has developed, few engineering solutions have been successfully introduced into the manufacturing process to manage electrode wear. Weld current steppers and electrode cap dressers have been used for many years, but these techniques do not resolve the underlying causes of electrode degradation. More recent efforts to remedy electrode wear have resulted in innovative electrode technologies, such as new material compositions, material inserts at the electrode face, surface-coated electrodes, and nontraditional electrode geometries (P-, G-, and S-nose). The scope of the present investigation is to objectively evaluate existing and developmental electrode material and geometry technologies to improve electrode life in production.

However, due to technical roadblocks to the development of new electrode materials for aluminum the focus of this year has concentrated on the electrode life of hot dip galvanized (HDG) HSS.

The activities in Phase I, II, and III have been completed this year, and five electrode materials/designs have been identified for limited automotive production trials (beta site tests). The initial planning for these tests is under way.

Previous progress reports have described the results of electrode screening tests on electrode materials/designs that demonstrated improved elec-

trode life under laboratory conditions. This report describes the metallographic results of more detailed sequential life tests, completion of deformation and chemical models describing electrode wear, a description of the mechanisms of electrode wear, and selection of the five electrodes identified for beta site production testing.

Metallographic Evaluation of Sequential Electrode Life Tests on HDG Steel

Sequential evaluation of the stages of electrode wear has been completed for CuZr and two developmental electrode materials (identified as M and R series). An example of the sequential life test results are shown in Figure 1.

Sequential life testing involves the production and metallurgical evaluation of electrodes tested to progressively longer electrode lives. The electrodes were removed after 25, 50, 100, 250, 500, 1000, and 2000 welds and the end-of-life condition. These electrodes were prepared for metallographic examination to show the stages of electrode wear. Optical and scanning electron microscope (SEM) evaluation of the brass phases on the electrode surface were tracked as a function of depth from the electrode face for each electrode. A plot of average brass phase thickness vs number of welds for CuZr E-nose electrodes is shown in Figure 2.

A summary of the brass alloy thickness data is plotted against numbers of welds for each electrode in Figures 3, 4, and 5 for the β brass, γ brass, and total alloy thickness respectively.

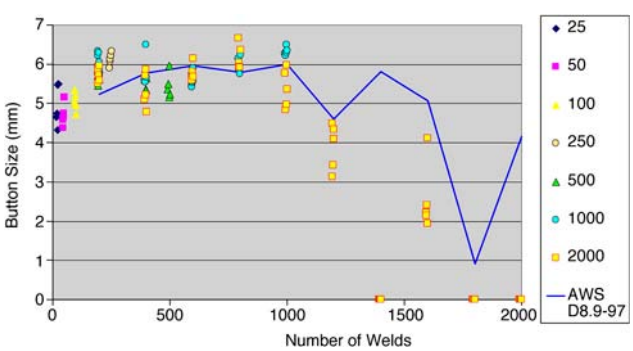

Figure 1. Button size measured during interrupted electrode life tests with CuZr electrodes on 1.1-mm, 350-MPa HDG steel (solid line indicates AWS D8.9 results).

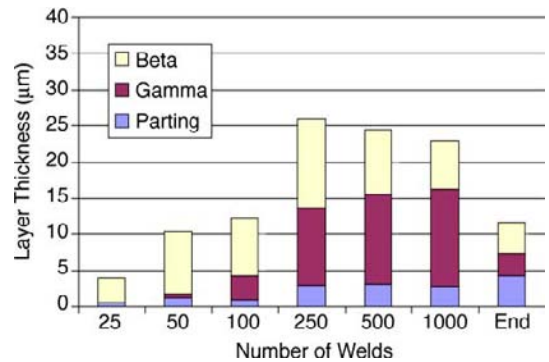

Figure 2. Total alloy thickness present on the electrode face after sequential life testing CuZr E-nose-style electrodes (Series A) on 1.1-mm HDG HSS. (Electrode life tests were interrupted, and the electrodes were extracted for metallographic examination after predefined numbers. Brass phase identification was made using EDAX. Brass phase thickness was made using SEM.)

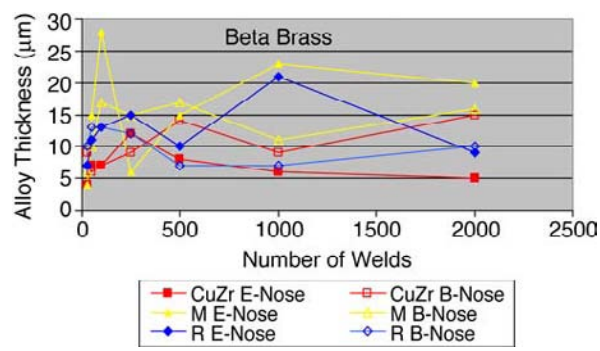

Figure 3. Summary of β brass alloy layer thickness plotted as a function of numbers of welds for CuZr, M, and R materials. (Filled symbols are E-nose-style, and open symbols are B-nose-style electrodes.)

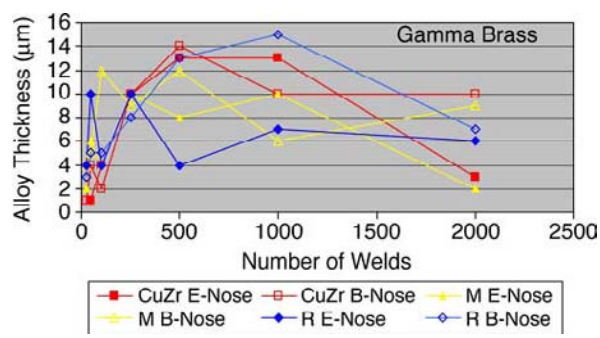

Figure 4. Summary of γ brass alloy layer thickness plotted as a function of numbers of welds for CuZr, M, and R materials. (Filled symbols are E-nose-style, and open symbols are B-nose-style electrodes.)

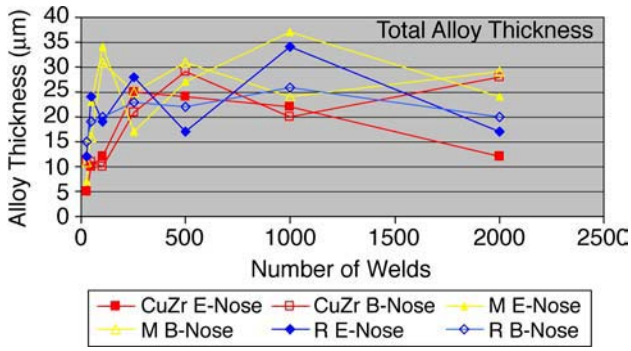

Figure 5. Summary of total alloy thickness plotted as a function of numbers of welds for CuZr, M, and R materials. (Filled symbols are E-nose-style, and open symbols are B-nose-style electrodes.)

The β brass on the electrode face forms first, followed by the γ brass. Between 250 and 500 welds, all of the electrodes had reached equilibrium. The average maximum thickness of the β brass occurred at about 100 welds, while the average maximum thickness of γ brass occurred at about 250 welds.

The ratio of β brass to γ brass thickness after 1000 welds ranked well with both overall electrode life and the onset of button size instability measured during the AWS D8.9 tests. This is the result of thermal conditions on the electrode face. It appears that γ brass is favored for electrodes that operate at higher interface temperatures or exposed to more severe service conditions. Beta brass is softer than gamma brass, and the data suggest that softer brass phases on the electrode face may decrease resistive heating and extend electrode life.

This analysis is further amplified by plotting microhardness contours across ½ of the electrode face for the CuZr and M electrodes. Examples of the hardness matrices after 500 welds of wear are shown in Figures 6 and 7. Figure 6 shows that softening is largely limited to 500 µm below the electrode face for the CuZr electrode, with extreme softening at the face. Heavy softening occurred along an elliptical contour with the greatest softening at the centerline and the least softening at the electrode edge. The hardness along the outside surface of the electrode body remains hard, except near the electrode face.

Hardness contour for the M electrode after 500 welds in Figure 7 shows that the overall hardness is

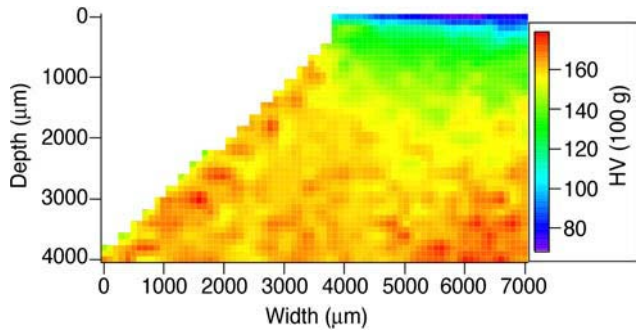

Figure 6. Contour plot of microhardness measurements systematically made over half of the sequential life test CuZr E-nose-style electrode extracted after 500 welds. (Color scale represents hardness as a function of depth from the electrode face and distance from the centerline.)

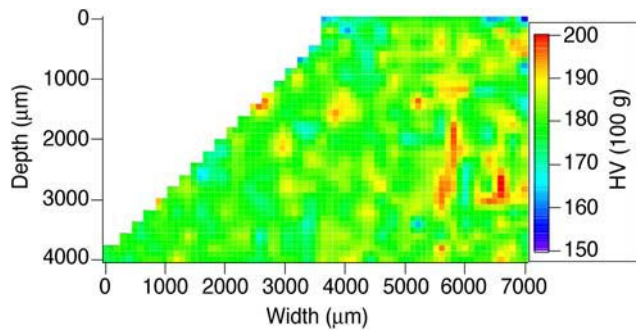

Figure 7. Contour plot of microhardness measurements systematically made over half of the sequential life test M material E-nose-style electrode extracted after 500 welds. (Color scale represents hardness as a function of depth from the electrode face and distance form the centerline.)

much greater than the CuZr electrode at room temperature. This electrode is characterized by hard and soft randomly spaced regions. The electrode face does not exhibit any significant softening as observed on the CuZr electrode. The centerline of the electrode appears to have strengthened during electrode life with some very hard regions directly below the electrode face.

Optical metallographic examination of the M electrodes showed a few instances of deep cracks oriented along the body and emanating from the electrode face. These cracks appeared after 500 and 1000 welds of wear. Zinc was shown to flow into the cracked regions. Another observation characterizing the M electrodes was the apparent intermixing

of β and γ brass layers at specific points on the electrode face.

The R material showed typical alloy layers characteristic of CuZr electrodes. However, this material showed excessive pitting. In several instances, metal flow into pits was observed. Compared to M material, the β and γ brass alloy layers for the R electrodes were well delineated.

Models of Deformation and Chemical Attack of Electrodes on HDG Steel

Electrode face enlargement was modeled as both electrode deformation (extrusion) and surface chemical erosion. These two modes were identified to provide significant contributions to electrode wear.

Electrode deformation contributes to electrode face enlargement through incremental flow of electrode material from the face during welding. Analytical expressions of stress-strain characteristic as a function of temperature, degradation of material properties with numbers of spot welds, and variation in peak temperature at the electrode surface were coupled to predict the growth of electrode face diameter as a function of numbers of welds. Using the deformation models, predictions of electrode face diameter can be made for various electrode material properties and welding conditions. The applied stress from the electrodes and the weld time are integrated into the model. The strain in the copper electrode at the electrode-sheet interface during one spot weld was estimated. The strain from subsequent welds accumulates with a specific efficiency. The amount of strain was related to the stress-strain characteristic and its measured tempering behavior. The model assumes that the deformation is limited to a small disk of material at the electrode face. The size of the disk increases with progressive electrode wear. Deformation of the disk ceases when the applied stress at temperature falls below the yield stress at temperature. Although it ignores many of the numerous intricacies of the mechanical deformation process, the predicted change in face diameter is in good agreement with typical test data and practical experience. The model was a useful tool for predicting "what if" scenarios during analysis of the sequential life data.

The chemical effects were calculated from diffusion-controlled growth models assuming the copper is in contact with an infinite supply of zinc. Appropriate temperature dependencies were applied to the one-dimensional diffusion model. Two cases were considered: face operating temperatures below and above the melting point of zinc. For the first case, solid state diffusion was found to be much too slow to describe the rate of brass alloy formation shown in Figure 2. For the second case, the zinc diffuses rapidly into the zinc/copper interface, which rapidly penetrates into the copper. The resulting brass layers formed close to the rate of brass formation depth found in this program as shown in Figure 2. An example of brass formation at 450°C is given in Figure 8.

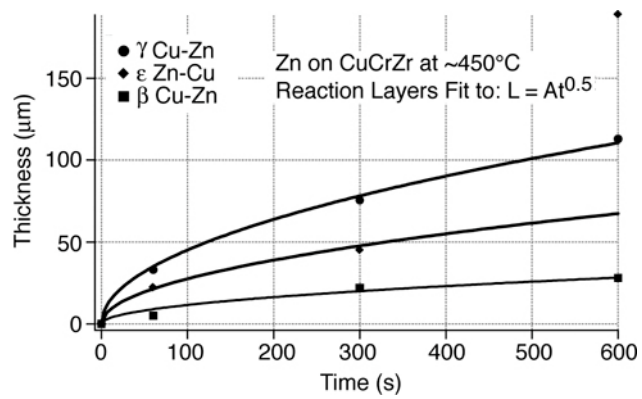

Figure 8. Plot of β, γ, and ε brass thickness as a function of time at 450°C.

Mechanisms of Electrode Wear

The electrode wear process in RSW of galvanized HSS was shown in this program to be limited by

1. current density, and
2. weld nugget instability.

These two factors combine to produce the rapid degradation of button size often observed at the end of electrode life.

The typical weld setup produces a large weld with fresh caps. First, electrode face diameter enlargement decreases the current density and decreases the size of the weld. Large welds are relatively insensitive to the factors that contribute to weld nugget establishment. However, as the weld size decreases toward minimum button size, weld size is controlled more by nugget establishment factors and less by maximum nugget growth factors (retention of the molten weld nugget without weld metal expulsion). This makes the weld very sensitive

to bulk and interface resistance heating and to the increase in heat extraction due to electrode face enlargement. (This was tracked to a decrease in nugget penetration for one electrode, suggesting that extraction of heat from the sheet surfaces limited nugget penetration and made weld establishment less stable as predicted from one deformation model.) Because nearly all of the typical welding process factors contribute to nugget establishment and early growth, the nugget becomes instable and thus exhibits the tendency for precipitous drops in weld button size.

Two approaches were envisioned to improve electrode life. These were based on

1. maintaining a low electrode-sheet interface temperature, and
2. sacrificial electrode nose.

Both approaches were found to improve electrode life in these tests. These two approaches operate on very different principles, and the beta site tests will largely focus on the first approach.

The second approach was found to offer the best performance of any of the electrodes tested. The benefits of this approach were shown to occur through the development of a "protrusion" on the face of the electrode. This protrusion enhances and maintains current density during electrode wear. It occurs for electrodes with very high electrode-sheet interface operating temperature. The exact mechanism responsible for maintaining the protrusion is not fully understood at present.

Electrodes for Beta Site Tests

Stepper-current type electrode life will be evaluated in the beta site tests. The conclusions from this work and taking into account the type of galvanized sheet and application-specific characteristics were combined to recommend five electrodes for beta site production testing:

- G-cap or P-cap electrodes produced from M or oxide-dispersion-strengthened electrode material,
- E-cap electrodes produced from M electrode material with reduced face thickness,
- B-cap electrodes produced from M electrode material with reduced face thickness,
- E-cap electrodes produced from CuZr material with reduced face thickness and internal fins, and
- B-cap electrodes produced from CuZr material with reduced face thickness and internal fins.

All of the electrodes will be produced as female caps in a 16-mm body with a 6-mm face diameter. These electrodes follow the principles governing the two approaches for improving electrode life listed earlier.

Conclusions

The completion of Phases I, II, and III of this program have yielded several electrode materials and electrode designs that will be tested in automotive production environments. These electrodes were selected based on a hypothesis of electrode wear in HDG steels. This hypothesis is based on a progressive loss in current density and development of weld nugget instability due to the governing welding conditions and enhanced heat extraction from enlarged electrode face diameter.

Extension of electrode life of aluminum is possible, but fell outside the scope of this program. Electrode life on aluminum is fundamentally different from welding coated steels. The development of effective electrodes for aluminum will require more study involving more than modified electrode material and geometry.

Future Work

The electrode life models developed in this program should be further refined. The extrusion and chemical dissolution models should be coupled into a single model that incorporates welding parameters. These changes should greatly enhance the combined models predictive capability and make it much more useful for predicting such things as optimized weld schedules.

Optimization of the electrode composition and design was not possible in this study. However, the critical electrode material characteristics have been identified. Further copper alloy development on targeted copper systems should prove invaluable in producing an "ideal" electrode material. Additionally, optimization of the electrode design would include engineering heat flow to the water-cooling channel and define the rate of electrode face enlargement.

The mechanics of copper extrusion and brass alloy formation should be studied more systemati-

cally to better describe the events contributing to electrode face enlargement and nugget stability. The electrodes and the steel sheets should be instrumented, and these dynamic measurements used as inputs to computer models to validate the end-of-life test conditions.

These tests should extend to steels outside of the steel gauge, coating type, and power supply type used in this program. The welds should be metallographically examined to further understand the nugget stability conditions at the end of electrode life.

The development of protrusions on the electrode face should be studied further to optimize the sacrificial behavior and perhaps incorporate this into standard electrode cap designs. This would be done by better understanding the nature of extrusion and the equilibrium conditions that interact to produce the protrusion. Because the weld face runs very hot in this style of electrode, the effect of face temperature on nugget formation should be further evaluated.

Presentations and Publications

1. M. Gallagher, K. S. B. Athwal, and R. Bowers, "Electrode Wear Characterization in Resistance Spot Welding," *Proc. of Sheet Metal Welding Conference XI, Sterling Heights, Michigan, May 11–14, 2004*.
2. W. Peterson, J. Gould, R. Bowers, M. L. Santella, and S. S. Babu, "Evaluation of Electrode Design and Materials for Improved Electrode Life," *Proc. of Sheet Metal Welding Conference XI, Sterling Heights, Michigan, May 11–14, 2004*.
3. S. S. Babu, M. L. Santella, and W. Peterson, "Modeling Resistance Spot Welding Electrode Life," *Proc. of Sheet Metal Welding Conference XI, Sterling Heights, Michigan, May 11–14, 2004*.
4. S. S. Babu, M. L. Santella, W. Peterson, J. E. Gould, "Modeling resistance spot welding electrode life," AWS Welding Show, April 2004, Chicago, Illinois.

I. Plasma Arc Spot Welding of Lightweight Materials

Principal Investigator: William A. Marttila
DaimlerChrysler Corporation
800 Chrysler Drive
CIMS 482-00-11
Auburn Hills, MI 48326
(248) 576-7446, fax (248) 576-7490, e-mail wam8@dcx.com

Technology Area Development Manager: Joseph A. Carpenter
(202) 586-1022; fax: (202) 586-1600; e-mail: joseph.carpenter@ee.doe.gov
Field Technical Manager: Philip S. Sklad
(865) 574-5069; fax: (865) 576-4963; e-mail: skladps@ornl.gov

Participants
R. V. Hughes—Arc Kinetics LLC, AKLLC@Hotmail.com
M. G. Poss—GM Corporation, Michael.g.Poss@GM.com
T. Hanel—Ford Motors, T.Hanel@ford.com
F. G. LaManna—LaManna Enterprises, Fglamanna@comcast.net

Contractor: U.S. Automotive Materials Partnership
Contract No: FC26-95OR22910

Objective

- Develop and verify the welding technology required for the joining of lightweight materials (aluminum and magnesium) using Plasma Arc Spot Welding technology.
- Develop the necessary weld parameters and techniques required for a robust joining process.

Approach

This project was divided into three phases: testing, analysis, and summary.

- Produce approximately 6000 material coupons to be used for tensile, shear, and metallurgical analysis and testing (Phase I).
- Determine the material alloys based on Phase I results (Phase II).
- Produce guidelines for welding parameters and quality control (Phase III).

Accomplishments

- Successfully completed fatigue testing at Coventry University.
- Completed data comparison (plasma arc spot welds, resistance spot welds, and rivets).
- Adapted plasma arc spot weld process to join magnesium sheet stock with filler wire.
- Developed guidelines for testing mechanical properties of the new technology that are appropriate for the various applications.

Future Direction

- Complete project and produce Final Report for presentation to U.S. Automotive Materials Partnership

---

Introduction

The overall deliverable for this project is a robust process to join lightweight materials economically. Current technology relies heavily on conventional resistance spot welding. High maintenance, tip wear, and accessibility continue to be major concerns. Rivets and/or mechanical clinching are costly alternatives that require high capital investment. The viability of plasma arc spot welds has been validated through the efforts of Arc Kinetics, Ltd., which developed a single-sided plasma arc spot welding process for Jaguar. It was used for joining the sheet metal floor pan assembly, which was not accessible with conventional resistance spot welding equipment. Arc Kinetics also developed a process called aluminum plasma arc welding (APAW). By combining the two processes (single-sided spot welding and APAW), Arc Kinetics developed a process that demonstrates excellent potential for joining lightweight materials.

Status

- Coupon production complete.
- Fatigue testing complete.
- Modified equipment to trial joining magnesium sheet stock AZ31A utilizing TIG filler wire AZ92A. (Spooled magnesium wire cost prohibited if available.) Due to timing and funding constraints, magnesium investigation was terminated.
- Project complete.
- Preparing final report (available first quarter 2005).

Conclusions

- Absorbed hydrogen compounds (i.e., hydrated oxides) in the surface films of sheet aluminum and magnesium at present require a phosphoric acid-based pretreatment prior to plasma arc spot welding to eliminate haloes.
- The addition of appropriate amounts of 4047 grade filler wire appears to eliminate microcracking within the spot welds.
- Destructive testing of spot welds by torsional shear is valuable for assessing the likely strength, degree of macroporosity, and material thinning through the outgassing effects of the welds.
- Plasma arc spot welds typically offer tensile shear strengths 40% higher than those of competitive technologies.
- Under ac welding conditions used in this project, use of a convex radiused tip geometry prevents damage to the plasma torch nozzle through double arcing.
- Service intervals in excess of 3000 welds can be achieved for the consumables associated with plasma arc spot welding. This greatly exceeds service intervals associated with resistance spot welding of lightweight materials.
- Hard anodizing of an aluminum shield cup of appropriate design can produce a cup that is lower in cost and more robust than the ceramic-coated copper alloy shield cups previously associated with the process.
- A flat-surfaced backup positioned between 0.75 mm and 1.0 mm below the lower sheet surface gives better performance in terms of weld quality than do alternative geometries.

J. Performance Evaluation and Durability Prediction of Dissimilar Material Hybrid Joints

D. L. Erdman
Oak Ridge National Laboratory
P.O. Box 2009, Oak Ridge, TN 37831-8048
(865) 574-0743; fax: (865) 574-8257; e-mail: erdmandl@ornl.gov

Field Project Manager: C. David Warren
Oak Ridge National Laboratory
P.O. Box 2009, Oak Ridge, TN 37831-8050
(865) 574-9693; fax: (865) 574-0740; e-mail: warrencd@ornl.gov

Technology Development Manager: Joseph Carpenter
(202) 586-1022; fax: (202) 586-1600; e-mail: Joseph.Carpenter@ee.doe.gov
Field Technical Manager: Philip S. Sklad
(865) 574-5069; fax: (865) 576-4963; e-mail: skladps@ornl.gov

Contractor: Oak Ridge National Laboratory
Contract No.: DE-AC05-00OR22725

Objective

- Develop new experimental methods and analysis techniques to enable hybrid joining as a viable attachment technology in automotive structures. This will be accomplished by evaluating the mechanical behavior of composite/metal joints assembled using a variety of hybrid joining methods and quantifying the resultant damage mechanisms under environmental exposures, including temperature extremes and automotive fluids, for the ultimate development of practical modeling techniques that offer global predictions for joint durability.

Approach

- Characterize the structural hybrid joint to quasi-static load conditions.
- Characterize response to fatigue, creep, and environmental exposures.
- Conduct predictive analysis.

Accomplishments

- Completed fatigue tests at 85%, 70%, and 40% of ultimate load for Quantum rails.
- Evaluated GENOA for predicting the damage development.

Introduction

Weight can be reduced and fuel efficiency increased in automobiles, without compromising structural integrity or utility, by incorporating innovative designs that strategically utilize modern lightweight materials—such as polymeric composites—in conjunction with traditional structural materials such as aluminum, magnesium, and steel. Despite the advantages associated with such dissimilar or hybrid material systems, there is reluctance to adopt them for primary structural applications. In part, this reluctance can be

attributed to the limited knowledge of joining techniques with such disparate materials where traditional fastening methods such as welding, riveting, screw-type fasteners, and bolted joints may not be appropriate.

One solution to this problem is the use of hybrid joining techniques by which a combination of two or more fastening methods is employed to attach similar or dissimilar materials. One example is a mechanically fastened joint (i.e., bolted or riveted) that is also bonded with adhesive. These types of joints could provide a compromise between a familiar mechanical attachment that has proven reliability, and the reduction of problematic issues such as stress concentrations and crack nucleation sites introduced by using mechanical fasteners with polymeric composites.

The use of hybrid joining could also lead to other potential benefits such as increased joint rigidity, contributing to overall stiffness gains and a reduction of vehicle mass. Additionally, the use of adhesives in conjunction with mechanical fasteners could significantly reduce stress concentrations, which serve as locations for crack starters. Hybrid joining methods can also provide additional joint continuity to allow increased spacing between fasteners or welds.

Although numerous benefits are derived from using hybrid joining techniques and the joining of dissimilar materials is becoming a reality, little or no practical information is available concerning the performance and durability of hybrid joints. Therefore, this project has taken on the task of developing new technologies to quantify joint toughness and predict long-term durability. This will necessitate identifying and developing an understanding of key issues associated with hybrid joint performance, such as creep, fatigue, and effects of environmental exposure.

To initiate this study, it was necessary to choose a candidate hybrid joint representative of those typically encountered in automobiles. Because of their wide applicability in automotive structures, several combinations of hat-section geometries were considered. Hat sections can be incorporated into a variety of generic automotive structural components, such as crush tubes or frame rails, when they are bonded and mechanically fastened to other geometries. For the current study, the Joining Task Force selected a composite hat section bonded and riveted to a steel base, as shown in Figure 1. This selection was made on the basis of general applicability to a variety of automobile structural components. Members of the Joining Task Force identified industry partners for sources for the steel, rivets, composite hat section, and adhesive.

To determine the influences of the adhesive and the rivets on the structural performance of the rail, it was also decided to investigate bonded specimens without rivets and riveted specimens without adhesive.

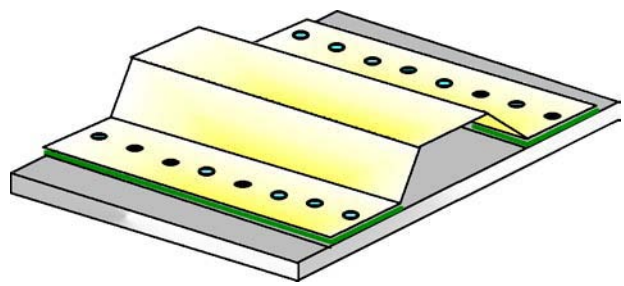

Figure 1. Hybrid joint schematic.

Fatigue Tests of Quantum Rails

Fatigue tests were performed at 85%, 70% and 40% of average ultimate static load at room temperature for both loading configurations—hat in tension and hat in compression. Three replicates of each test at 70% of ultimate load were completed. At least one data point exists for tests at 85% and 40% for all joint-load combinations. Ratio of R = 0.1 and frequency f = 1 Hz were used for tests at 85% and 70% of ultimate load. A higher frequency of 3 Hz was used for tests at 40% of ultimate load to allow for more specimens to be tested.

Several orders of magnitude scatter in number of cycles to failure, which is characteristic of fatigue tests, were observed for the Quantum rails. Inconsistency in the damage mechanisms occurred and can be attributed to previously reported scatter in material properties of Quantum composite. In spite of the scatter and inconsistencies, several trends are clearly distinguishable, and some general observations can be made.

Specimens failing at low cycle count ($N_f < \sim 10^4$) exhibit failure at the top of the hat section for hat in tension (Figure 2) and tearing of flanges for hat in compression (Figure 3). These failure mechanisms are identical to those observed in quasi-static tests.

Figure 2. Failed hat in tension—typical failure at low cycle count.

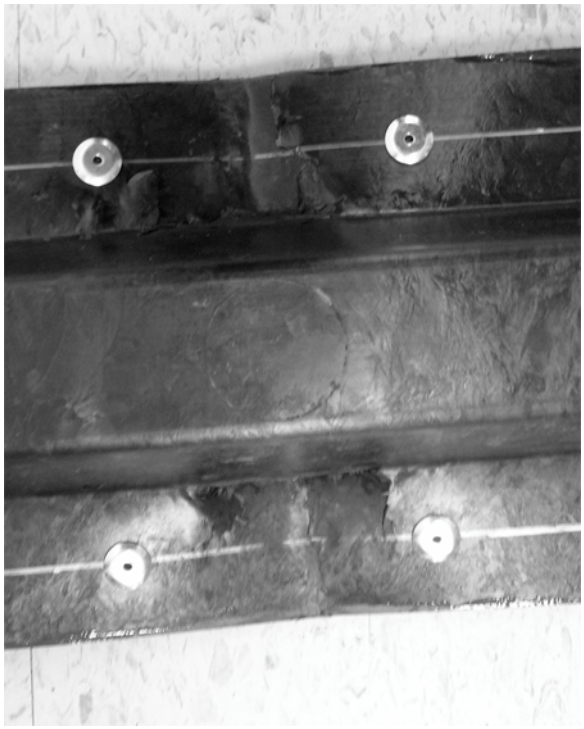

Figure 3. Failed hat in compression—typical failure at low cycle count.

Specimens reaching high cycle counts display entirely different damage, such as metal cracking and rivet failure. Specimens containing adhesive (adhesive with rivets and adhesive only) encounter cracks in the metal substrate initiating in areas of high stress concentration, such as in the vicinity of roller supports and rivet holes (Figure 4). As these cracks grow, usually in the direction perpendicular to the longitudinal axis, the load carried by the composite hat increases. Most specimens failed before the crack or cracks in the metal grew across the entire width of the specimen (Figure 5). Cracks in adhesive were never observed prior to damage or failure of either the composite hat or the metal substrate. Additionally, the adhesive contained the crack growth at the flanges (Figure 6).

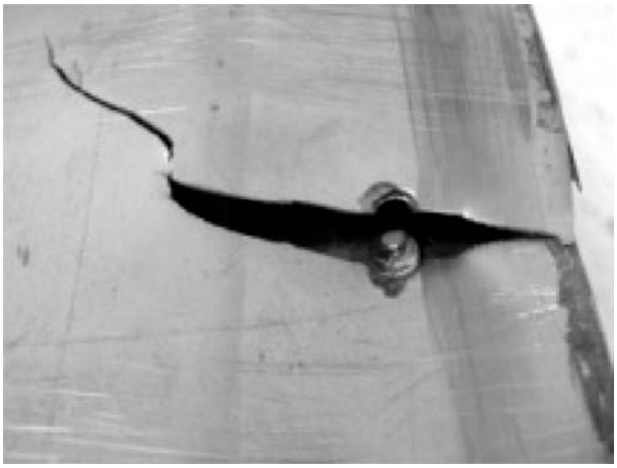

Figure 4. Crack in metal substrate initiated from rivet hole for a specimen with rivets and adhesive.

Figure 5. Cracks initiated under roller supports that grew through the substrate before final failure for hat with adhesive only.

Figure 6. Adhesive-containing crack opening—specimen with adhesive only.

Riveted specimens reaching higher cycle counts exhibited broken rivets prior to catastrophic composite failure. In some cases, all rivets ruptured on one side of the specimen, leaving no joint between the composite hat and metal substrate (Figure 7). Metal cracking as well as rivet failure can be detected from load-displacement behavior of the structure as illustrated in Figure 8. Typical S-N data are shown in Figure 9.

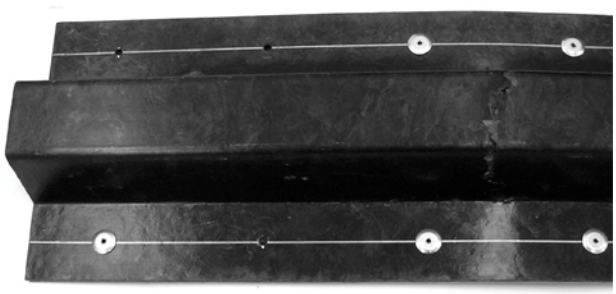

Figure 7. Half of rivets broken; some fell out during the test for specimens with rivets only.

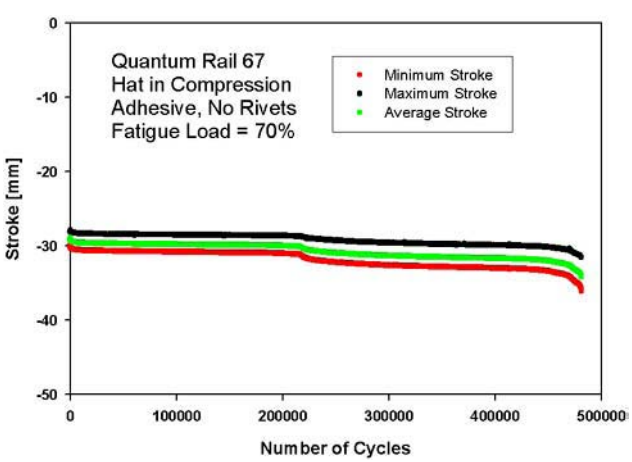

Figure 8. Crack initiation detectable at 2.2×10^5 cycles.

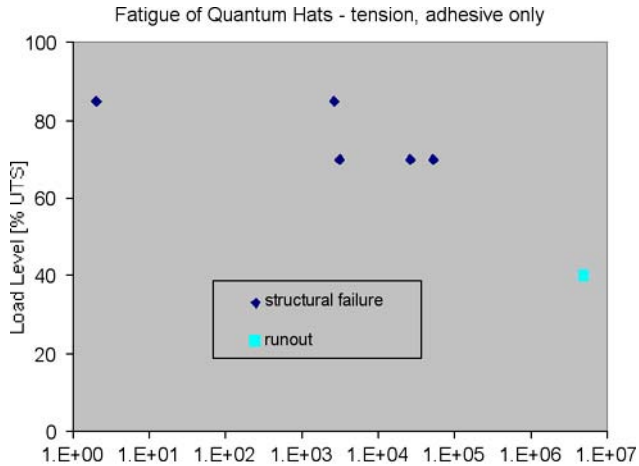

Figure 9. Typical S-N data for hat section.

Results from these fatigue tests as well as previous quasi-static tests indicate that joints containing adhesive outperform riveted joints. No damage in the adhesive joint was observed during the study prior to macroscopic cracking of either the metal substrate or the composite hat section. Under quasi-static conditions, adhesively bonded specimens reached higher ultimate loads and resulted in higher stiffness of the structure. This conclusion is further reinforced by previously reported results and analyses from environmental and creep tests.

Finite-Element Modeling

With the exception of fatigue tests with high cycle count, the hat specimens lost bearing capability due to composite failure. As a result, predictive capabilities for progressive failure of composites are critical for accurate modeling of the hat structure under consideration. A popular commercial finite-element code, ABAQUS by Hibbit & Carlsson Inc., was successfully used to predict load-displacement behavior up to the point of failure or significant damage in the composite hat. Postdamage behavior modeling with this code proved to be challenging.

GENOA code, developed by Alpha Star Corporation specifically for composites, is currently being explored, and initial results indicate that this code may provide more predictive power compared to standard finite-element codes such as ABAQUS, Nastran, and Ansys. GENOA performs stress analysis on the structure level, but instead of assuming an homogenized model for the material behavior, another finite-element analysis is performed on the fiber-matrix level for each node of

the structure model. This multiscale approach results in computationally intensive analysis through which the degradation of material properties on fiber-matrix level can be modeled (Figure 10). GENOA has been used primarily in the aerospace industry where chopped fiber composites are used scarcely if at all. Consequently, capabilities of GENOA in this area have room for improvement. It was decided that results from previously tested continuous fiber composite hat sections with T300 Mat/Urethane 420 IMR composite will be used to evaluate GENOA's capabilities. The following seven steps must be completed before obtaining results for component-level model:

- input fiber and matrix properties,
- select coupon-level experiments to be matched numerically,
- match elastic properties of composite,
- evaluate sensitivity of ultimate properties to material coefficients,
- develop models of selected coupon tests,
- calibrate material coefficients to match experimental coupon-level tests, and
- input calibrated properties into subcomponent level model.

Durability reports by J. M. Corum et al. were extensively used in this iterative material calibration process. To date, this process has been performed with the assumption of linear material behavior up to the point of ultimate failure for tension and compression coupon tests with 0/90 and ±45° fiber orientation. A comparison of experimental and numerical ultimate failure loads for hat sections with adhesive only is presented in Table 1. Predicted failure load for hat in tension matches the experimental value with remarkable accuracy.

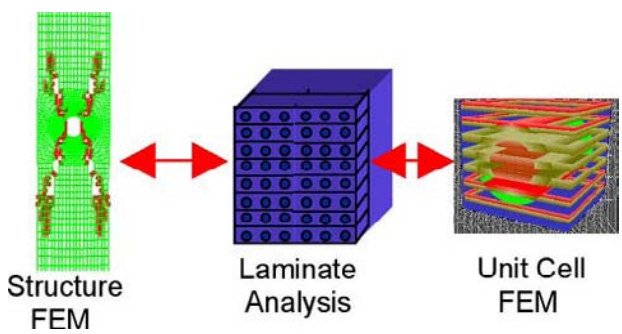

Figure 10. Scales of analysis in GENOA.

Table 1. Comparison of experimental and numerical values for hat section with adhesive only

Test configuration	Ultimate load (lb) experimental	Ultimate load (lb) GENOA
Hat in tension	4335	4340
Hat in compression	7474	4280

Results for hat in compression do not coincide as well. This can likely be attributed to the assumption of linear behavior until the point of catastrophic failure. As such, only sudden catastrophic failure, such as observed for hat in tension, can be modeled accurately. A failed model with dark v-shaped regions, designating damage in the composite, is depicted in Figure 11.

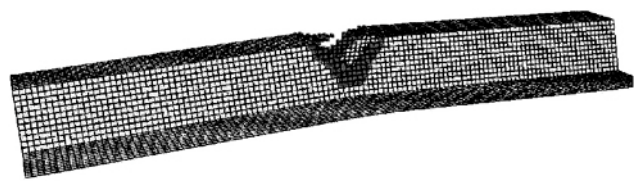

Figure 11. GENOA model of hat in tension after failure.

Nonlinear behavior of composite material used in the hat section must be captured to realistically model the response of the structure. Nonlinearity can be introduced either on the fiber-matrix level or on lamina level. Both approaches are being investigated at the present time. Plastic yielding of resin accounts for the majority of the nonlinear response of the cross-ply composite. Stress-strain response of neat resin is necessary for input on the fiber-matrix level. This information was not available from the resin manufacturer or from the durability reports. An iterative procedure was implemented in custom Python script through which the resin properties can be obtained from the response of the composite in coupon-level tests. This script repeatedly executes GENOA runs, compares the numerical results to experimental results, and adjusts the resin stress-strain curve in GENOA input to match the numerical and experimental data.

A special version of GENOA was provided by Alpha Star Corporation to enable implementation of the approach proposed by Deng, Li, Lin, and Weitsman in "The non-linear response of quasi-isotropic laminates." This paper, published in *Composite Science and Technology*, investigated

T300 Mat/Urethane 420 IMR composite with a quasi-isotropic layout.

Axial Tests

Several specimens were tested in an axial direction to assess setup in the Test Machine for Automotive Crashworthiness (TMAC). The setup is shown in Figure 12. Edges on the impact side of the specimen were filed to 45° to form a crack initiator. The energy absorption properties for all three joining techniques were compared to an aerospace-quality crush tube (Figure 13). The tube was designed specifically as an energy-absorbing member and is made of two identical aerospace-quality, continuous-fiber sections joined via adhesive bonding. The thickness of the composite section is identical for the hat and the tube (approximately 0.125 in.). The hat has 1.3 in.^{2} of composite material in the cross section and 0.3 in.^{2} of steel metal substrate. The cross-sectional area of the composite tube is 2 in.^{2}. Note that the tube in this experiment was approximately 1 in. longer in length than the hat. Energy absorbed by the structures was calculated as the area under the load-displacement curve obtained during the test (Figure 14). The total energy values as well as energy per material volume and energy per composite material crushed are compared in Table 2. It is apparent that the performance of a low-cost structural member approximately matches and possibly exceeds the performance of an aerospace-quality crush tube. The results for hats

Figure 12. Setup of axial test in TMAC.

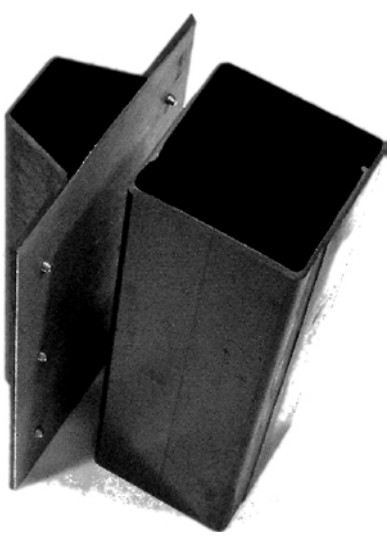

Figure 13. Hat section and crush tube.

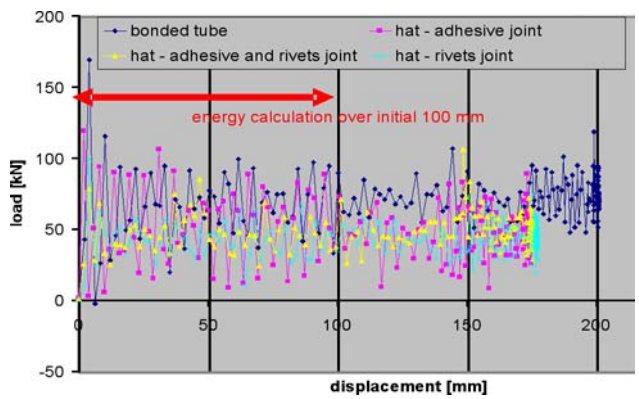

Figure 14. Superimposed test results for hybrid hat sections and bonded tube.

Table 2. Energy absorption of hybrid hat sections and bonded tube

	Total energy over 100 mm (kJ)	Energy per crushed total material volume (MJ/m^3)	Energy per crushed composite volume (MJ/m^3)
Bonded tube	6.7	51.9	51.9
Hat—adhesive	5.3	51.3	63.1
Hat—rivets	4.3	41.7	51.2
Hat—rivets and adhesive	4.7	45.5	56.0

may be statistically similar because the low-cost SMC composite exhibited significant variation in properties and only a single test was performed for each joint combination.

In Figure 15 the difference in metal substrate deformation in the initial phases of impact, which may be attributed to joining method, can be seen. It is uncertain if the joint and the substrate absorb significant levels of energy compared to the energy absorbed by the composite hat section. However, we suspect that the composite hat section is the primary energy-absorbing component of the system. Also note the difference in curvature of metal substrate for adhesively bonded joints in quasi-static (Figure 16) and the rapid 4-m/s tests (Figure 17). This difference in curvature is likely a result of time-dependent behavior of the adhesive, resulting in faster crack propagation at higher velocity. While the visco-elastic behavior of the adhesive is a likely candidate for the difference in curvature consistently observed for bonded specimens, the interaction of the metal substrate may also contribute to the overall time-dependent behavior of the structure.

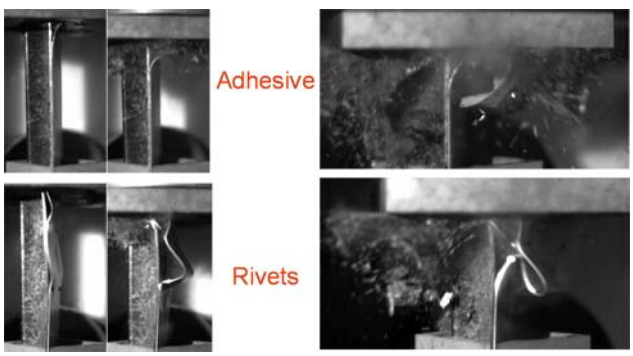

Figure 15. Initial phases of impact for bonded and riveted hat sections.

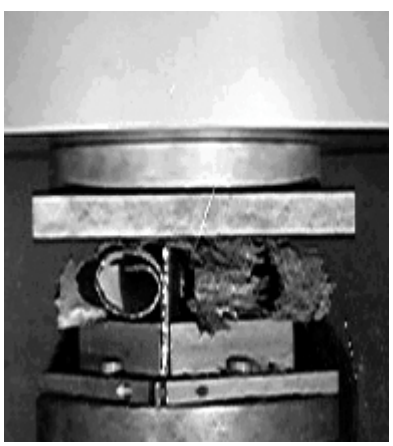

Figure 16. Specimen with adhesive only after quasi-static axial test.

Figure 17. Specimen with adhesive only after intermediate-strain-rate axial test.

Conclusions

Fatigue behavior in bending, energy absorption under axial loading, and finite-element simulation for quasi-static loading were explored for structures with a composite hat section joined to metal substrate by adhesive bonding or riveting or a combination of bonding and riveting.

Failure of specimens reaching low cycle counts in fatigue experiments was caused by damage in the composite hat section, closely resembling damage observed in quasi-static tests. Joint failure was not observed during these tests. Specimens reaching higher cycle counts exhibited cracking in the metal substrate for bonded joints and rivet failure for rivets-only joints. As a result of the damage in metallic parts of the structure, more load was carried by the composite hat section, which often lead to eventual damage of the composite and failure of the structure.

Energy absorption properties of the hat structure and aerospace-grade crush tube were compared. Low-cost hat structures approximately matched the energy absorption per volume of crushed material of the crush tube.

Progressive failure capability of GENOA software was used to model damage in the composite hat section during quasi-static tests with promising results.

K. Joining of Dissimilar Metals for Automotive Applications: From Process to Performance

Principal Investigator: Moe Khaleel
Pacific Northwest National Laboratory
P.O. Box 999/K7-36, Richland, WA 99352
(509) 375-2438; fax: (509) 375-6605; e-mail: moe.khaleel@pnl.gov

USCAR Joining Team Contact: Jim Quinn
(248) 680-4732; fax: (248) 680-2874; e-mail: james.f.quinn@gm.com

Technology Area Development Manager: Joseph A. Carpenter
(202) 586-1022; fax: (202) 586-1600; e-mail: joseph.carpenter@ee.doe.gov

Field Technical Manager: Philip S. Sklad
(865) 574-5069; fax: (865) 576-4963; e-mail: skladps@ornl.gov

---

Contractor: Pacific Northwest National Laboratory
Contract No.: DE-AC06-76RL01830

Objective

- Develop and evaluate different technologies for joining dissimilar aluminum alloys and aluminum to steel.
- Characterize the performance of these joints.
- Develop a unified modeling procedure to represent these joints in vehicle structural simulation. The steel materials include mild, high-strength low-alloy, and dual-phase steels.

Approach

- Further develop and/or enhance self-piercing rivets (SPRs) and resistance spot welding (RSW), with and without adhesives, for joining dissimilar metals.
- Develop a database for the static, dynamic, fatigue, and corrosion behavior of dissimilar material joints, consisting of different material selections and different joining techniques.
- Incorporate and represent the joint performance data into current computer-aided engineering (CAE) codes for evaluation of impact and fatigue performances of joint components.
- Develop design guidelines in the forms of tables and charts for use in joint structural and crash design.

Recent Accomplishments

- Developed a complementary experimental and analytical approach that results in a more thorough understanding of the effects of different joining methods on vehicle structural integrity and long-term performance.
- Provided knowledge regarding the selection of appropriate materials and provided the know-how for joining of dissimilar materials.
- Optimized the rivet strength by examining the effects of different manufacturing and in-service factors on the peak load and energy absorption levels of different joint configurations:
  - Effect of rivet length

  - Effect of riveting direction
  - Effect of dissimilar materials combination
  - Effect of adhesive
  - Effect of loading rate

- Investigated experimentally the static, fatigue, and dynamic behavior of the following dissimilar joints:
  - Joint ID 13A: SPR DP 600 (1.6 mm) and 5182-O (2 mm) with DOW Betamate 4601
  - Joint ID 13B: SPR DP 600 (1.6 mm) and 5182-O (2 mm) with DOW Betamate 1480
  - Joint ID 13D: SPR DP 600 (1.6 mm) and 5182-O (2 mm) exposed to 500-h salt spray

- Investigated the influence of "weld ductility" on component crash behaviors.
- Applied the fatigue analysis procedure to 14 different combinations of joined dissimilar materials.
- Conducted sequentially coupled corrosion-fatigue test on one joint population.
- Compared the influences of different structural adhesives on the strength of the bond-riveted joints.
- Documented the results of our project in terms of six topical reports and disseminated the information to the automotive industry through the U.S. Council for Automotive Research (USCAR) Web site: https://secure.uscarteams.org/VROOM/
- Completed current test populations.
- Completed validation of the proposed failure criterion.
- Transferred joint performance database to members of the joining team.
- Conducted final workshop/presentation summarizing results to the joining team.
- Completed final report.

Introduction

This project is a collaborative effort between the Department of Energy (DOE), Pacific Northwest National Laboratory, and the Metals Joining Team of the U.S. Council for Automotive Research (USCAR). The work started in April 2001.

The automotive industry envisions that an optimized vehicle, in terms of performance and cost, can be achieved only by using different materials at different vehicle locations to utilize the materials' functionalities to the fullest extent. Currently, aluminum and steel are the most important construction materials for the mass production of automotive structures. High-volume, nonsteel joining is a significant new problem to the industry. For joining dissimilar aluminum alloys, the leading candidate joining methods are spot welding and self-piercing rivets (SPRs) with or without adhesives. The major concerns with aluminum spot welding are its high-energy consumption, low electrode life (see report 7G), and structural performance concerns related to weld porosity. For joining aluminum to steel, the industry is currently comfortable with SPRs (with and without adhesives). However, there are a number of barriers to the widespread exploitation and high-volume production of the riveting technology. One of these barriers is the limited performance data relative to automotive applications.

In contrast, to shorten the vehicle development cycle, more and more computer-aided engineering (CAE) analyses are performed before the actual prototype is built. The question that the CAE researchers ask most often is how to represent the structural joints in crash simulation and fatigue simulation. Currently, there is no unified approach to representing the structural joints that works for different material combinations under multiaxial loading. This is particularly true for dissimilar material joints, where even basic performance information on the joint coupon level does not exist.

Project Summary

In this project, we have developed a complementary experimental and analytical approach that results in a more thorough understanding of the

effects of different joining methods on vehicle structural integrity and long-term performance. We have experimentally investigated the static, fatigue, and dynamic behavior of several dissimilar material joint populations (current joint studies are underlined):

- Joint ID 7: SPR 5182-O (2 mm) and 5182-O (2 mm)
- Joint ID 8: SPR 5182-O (1 mm) and 5182-O (2 mm)
- Joint ID 9: SPR 1008 (1.4 mm) and 5182-O (2 mm)
- Joint ID 10: SPR 5182-O (2 mm) and HSLA 350 (1 mm)
- Joint ID 10A: SPR 5182-O (2 mm) and HSLA 350 (1 mm) with Betamate adhesive
- Joint ID 11: SPR HSLA 350 (1 mm) and 5182-O (2 mm)
- Joint ID 11A: SPR HSLA 350 (1 mm) and 5182-O (2 mm) with Betamate adhesive
- Joint ID 12: SPR 5182-O (2 mm) and DP 600 (1.6 mm) with 6.0-mm rivet
- Joint ID 12A: SPR 5182-O (2 mm) and DP 600 (1.6 mm) with Betamate 4601 adhesive and 6.5-mm rivet
- Joint ID 12L: SPR 5182-O (2 mm) and DP 600 (1.6 mm) with 6.5-mm rivet
- Joint ID 13: SPR DP 600 (1.6 mm) and 5182-O (2 mm)
- <u>Joint ID 13A</u>: SPR DP 600 (1.6 mm) and 5182-O (2 mm) with DOW Betamate 4601
- <u>Joint ID 13B</u>: SPR DP 600 (1.6 mm) and 5182-O (2 mm) with DOW Betamate 1480
- <u>Joint ID 13D</u>: SPR DP 600 (1.6 mm) and 5182-O (2 mm) exposed to 500-h salt spray
- Joint ID 14: RSW 5182-O (2 mm) and 5182-O (2 mm)
- Joint ID 15: RSW 5182-O (2 mm) and 6111-T4 (2 mm)
- Joint ID 16: RSW 1008 (1.4 mm) and 5182-O (2 mm) with aluminum-clad steel interlayer (1.5 mm)

In characterizing the performance of these joints, we investigated the effects of different manufacturing and in-service factors on the peak load and energy absorption levels:

- effect of rivet length,
- effect of riveting direction,
- effect of dissimilar materials combination,
- effect of adhesive, and
- effect of loading rate.

We have also developed an overload failure and fatigue failure criterion from the experimental results utilizing CAE. A joint overload failure criterion was derived from the static and dynamic test results of different joint coupon configurations. Frontal and side impact simulations were performed to evaluate the impact performance of spot-welded aluminum and steel hat sections. Failure functions were monitored for each weld during the deformation processes.

Component-level joint fatigue analysis was developed using experimentally obtained master stress intensity factor (SIF) life curves. In this project, SIF was chosen to be used as the single parameter to consolidate the fatigue performance curves of different joint populations and different coupon geometries into the fatigue master SIF-life curves. The SIF was chosen because of its accuracy and computational simplicity in vehicle simulation.

The goal of this project is to provide automotive designers with more performance data for lightweight and dissimilar material joints of different choice, provide knowledge regarding the selection of appropriate materials and the joining of dissimilar materials, and to provide CAE engineers with more reliable joint properties and modeling techniques to realistically represent these structural joints in crash and durability simulations.

The following sections describe the research conducted during this reporting period.

<u>Effects of Corrosion Damage on Joint Strength</u>

Previously, salt spray corrosion tests were conducted on SPR and RSW populations evaluated

(with the exception of Joint ID 13 and 16). Specimens were exposed to salt spray/fog for 500 h according to the American Society for Testing and Materials (ASTM) B117. Scanning electron microscopy (SEM) and electron dispersive x-ray spectroscopy (EDS) were performed to determine whether corrosion was observed in the joints after being exposed to salt spray.

No pitting or crevice corrosion was observed in any of the populations analyzed. However, chloride and increased levels of oxygen were present in all SPR populations tested without adhesive in the joint. No chloride was present in the RSW joints or the SPR joints with adhesive.

Lap shear, cross tension, and coach peel coupon geometries of DP 600 and 5182-O joints (ID 13D) were exposed to 500 h of salt spray to determine the effects of corrosion on the performance of the joints; (the increased levels of oxygen observed in aluminum/steel joints are possibly due to formation of rust, Fe_2O_3). Experiments were performed to investigate the effect of salt exposure on the static and fatigue performance of the joints.

The static performance of Joint ID 13 and 13D are compared in Figures 1 and 2. It was observed that the joints exposed to salt spray yielded comparable strength characteristics for the same joint not exposed. The average peak load for lap shear coupons exposed to salt spray was approximately 9% lower than lap shear joints not exposed to salt spray. The cross-tension joints were comparable regardless of exposure.

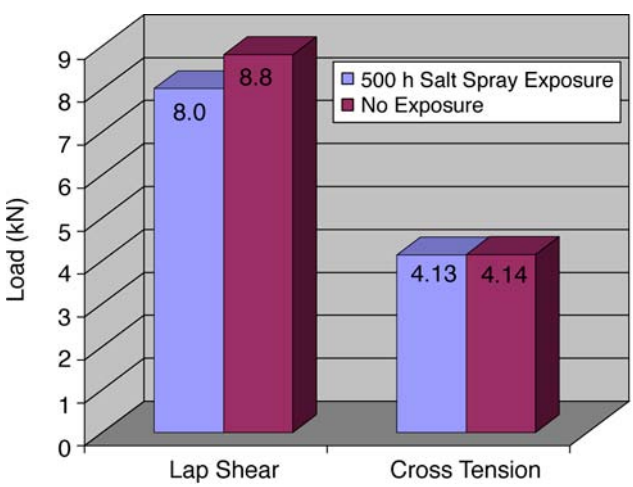

Figure 1. An illustration of static peak load results for Joint ID 13 and 13D. Results shown are representative of the average peak load observed for the specimen designs tested in each joint population.

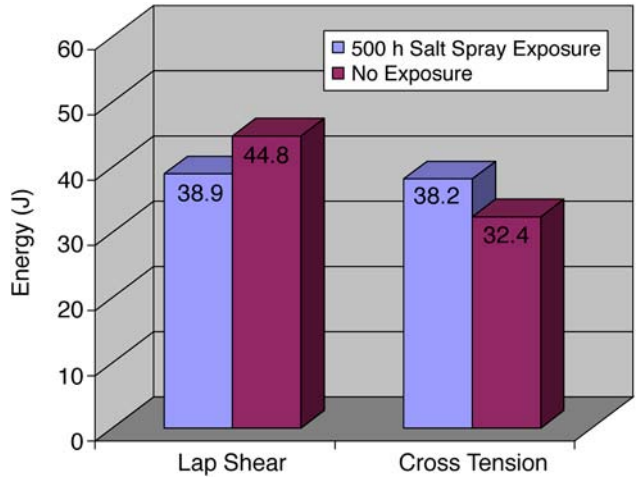

Figure 2. An illustration of the static tests energy absorption results for Joint ID 13 and 13D. Results shown are representative of the average energy absorption for the specimen designs tested in each joint population.

Cyclic fatigue tests were also performed on the joints under a tension-tension ratio of R = 0.1 for lap shear and cross-tension specimen designs. Figure 3 compares the fatigue strength of the joints. Comparable and slightly greater fatigue strengths were observed in the joints exposed to salt spray. It is thought that the corrosion products formed between the rivet and material substrates are making the joints tighter. Further investigation of the tightness of the joint and correlation of fatigue life are both needed.

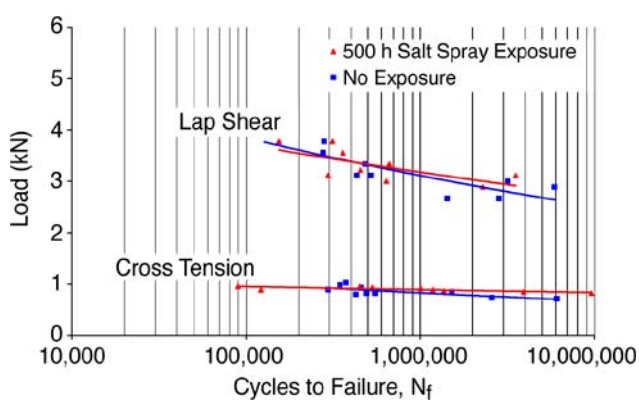

Figure 3. Fatigue test results of Joint ID 13 and 13D.

Effects of Different Structural Adhesive on Joint Strength

The effects of different structural adhesives on the static strength of two bonded-riveted populations are investigated:

- Joint ID 12A: SPR 5182-O (2 mm) and DP 600 (1.6 mm) with Dow Betamate 4601 adhesive and 6.5-mm rivet
- Joint ID 13B: SPR DP 600 (1.6 mm) and 5182-O (2 mm) with DOW Betamate 1480 adhesive

The purpose of this study is to evaluate the different adhesion levels for different adhesive systems on dissimilar metals substrates; namely, DP600 and AA5182-O. Dow Betamate 4601 is the structural adhesive currently being used in the U.S. automotive industry. Dow Betamate 1480 is currently only commercially available in the European market. Therefore, our study helps the domestic automotive industry to evaluate the structural behaviors of these two different adhesive systems. Figures 4 and 5 compare the static performance of Joint ID 12A and 13B for lap shear and cross-tension specimen designs. It was observed that the two different adhesives yielded similar strengths (first peak on load-displacement graphs).

The mode of failure for the samples was also similar. Figure 6 is a photo representative of the joints with adhesive. Both adhesive (separation at adhesive-substrate interface) and cohesive (failure within adhesive) failure modes are observed.

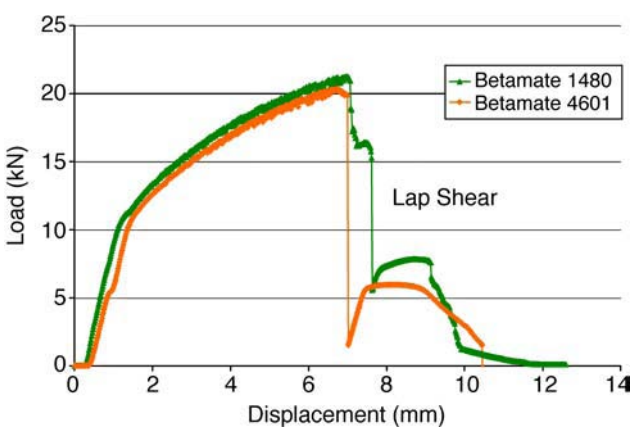

Figure 4. Static test results of ID 12A and 13B. Results shown are representative of the average peak load observed in each joint population.

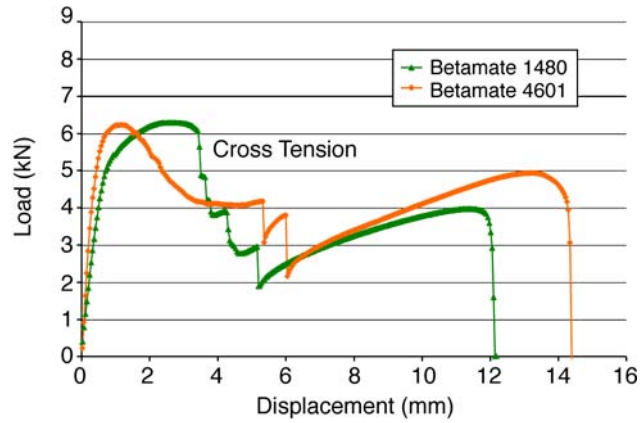

Figure 5. Static test results of ID 12A and 13B. Results shown are representative of the average peak load observed in each joint population.

Figure 6. Typical static failure mode of joints with adhesive.

Conclusions

Through the course of this project, many observations and accumulated knowledge have been documented in terms of eight topical reports. Further conclusions and technical details are documented in the following reports:

- *Joining of Dissimilar Metals for Automotive Applications—From Process to Performance* (final report)
- *Dynamic Joint Strength Evaluation under High Rate Impact Loading*
- *Characterization of Fatigue Behaviors of Dissimilar Metal Joints Part I—Experimental Studies*
- *Performance Comparisons through Weibull Analyses of Self-Piercing Rivets and Resistance Spot Welds Joining Dissimilar Metals*

- *Resistance Spot Welds of Aluminum Alloy to Steel with Transition Material: From Process to Performance*
- *Effect of Failure Modes on Strength of Aluminum Resistance Spot Welds*
- *Analytical Strength Estimator for Self-Piercing Rivets*
- *Lap Shear Coupon Design Sensitivity Study for Self-Piercing Rivets and Resistance Spot Welds*

Through experimental investigation and analytical study, the following conclusions are derived from this research:

1. The joint strength remains relatively unchanged from static to dynamic 10-mph and 20-mph tests for the dissimilar metal joint populations studied.
2. The total energy absorption for the joint samples decreases with increasing testing velocity.
3. For certain material and thickness combinations and die design, the rivet strength can be optimized through different rivet length.
4. Different piercing directions yield different strength characteristics for SPR joints. Static strength can be improved if failure occurs on the side of the stronger material.
5. Softer, more formable material at the tail end allows a better mechanical interlock between the rivet and the base material. A fatigue strength improvement is observed.
6. A mechanics model developed in this project may be used to predict SPR static joint strength given the materials and thickness combinations.
7. Application of a structural adhesive increases the static strength of riveted joints. A significant increase is observed in lap shear joints (3 ~ 5 times) and a modest increase is observed in cross tension and coach peel joints (up to 20%).
8. Application of a structural adhesive increases the static energy absorption of rivet joints, particularly, in lap shear and cross tension joints. The increase is marginal in coach peel joints.
9. Two distinct, uncoupled peaks are observed for static SPR joint samples with adhesive. The first peak is the adhesive failure; the second peak is the rivet failure.
10. Static strength of rivet bonding/weld bonding can be estimated. The rivet failure peak load is not affected by the presence of adhesive and the adhesive, failure peak load is not affected by the presence of rivets.
11. Application of a structural adhesive significantly increases the joint fatigue strength.
12. Joints exposed to salt spray yielded similar strength characteristics compared with the same joint not exposed.
13. Among the different overload failure criteria, the force based model (#2 in DYNA 970 material 100) is recommended for representing joints in vehicle crash simulation.
14. Among the different fatigue failure criteria, the stress intensity factor K-based and the structural stress-based models are recommended for representing joints in vehicle performance/ durability simulations.

A project compact disk (CD) including all topical reports, raw data, summary data, and presentations has been distributed to the Joining Task Force Team. Reports and all data have been made available to all members through the USCAR Web site: https://secure.uscarteams.org/VROOM/

Presentations and Publications

1. X. Sun, E. V. Stephens, M. A. Khaleel, H. Shao, and M. Kimchi, May 2004, "Resistance Spot Welding of Aluminum Alloy to Steel with Transition Material—From Process to Performance," *Proceedings of the Sheet Metal Welding Conference XI*.
2. X. Sun, E. V. Stephens, M. A. Khaleel, H. Shao, and M. Kimchi, June 2004, "Resistance Spot Welding of Aluminum Alloy to Steel with Transition Material—From Process to Performance, Part I: Experimental Study," *Welding Journal*, **83**(6), 188s–195s.
3. X. Sun and M. A. Khaleel, July 2004, "Resistance Spot Welding of Aluminum Alloy to Steel with Transition Material—From Process to Performance, Part II: Finite Element Analyses of Weld Nugget Growth," *Welding Journal*, **83**(7), 197s–202s.

4. X. Sun, E. V. Stephens, and M. A. Khaleel, July 2004, *Characterization of Fatigue Behaviors of Dissimilar Metal Joints Part I—Experimental Studies*, Technical Report prepared for DOE-EE-OFCVT.

5. E. V. Stephens, X. Sun, M. A. Khaleel, and R .W. Davies, September 2004, *Joining of Dissimilar Metals for Automotive Applications—From Process to Performance*, Technical Milestone Report prepared for DOE-EE-OFCVT.

6. X. Sun, E. V. Stephens, and M. A. Khaleel, September 2004, *Dynamic Joint Strength Evaluation under High Rate Impact Loading*, Technical Report prepared for DOE-EE-OFCVT.

7. X. Sun, E. V. Stephens, R. W. Davies, M. A. Khaleel, and D. J. Spinella, 2004, "Effects of Fusion Zone Size on Failure Modes and Static Strength of Aluminum Resistance Spot Welds," *Welding Journal*, **83**(11), 308s–318s.

X. Sun, E. V. Stephens, M. A. Khaleel, H. Shao, and M. Kimchi. "Resistance Spot Welding of Aluminum Alloy to Steel with Transition Material—From Process to Performance," *Sheet Metal Welding Conference XI*, *Sterling Heights, Michigan; May 12, 2004.*

M. A. Khaleel, E. V. Stephens, X. Sun, and R. W. Davies, "Joining of Dissimilar Metals for Automotive Applications—From Process to Performance," DOE-OFCVT Project Review Meeting to the USAMP Steering Committee, Southfield, Michigan; July 28, 2004.

L. Application of Thread-Forming Fasteners (TFFs) in Net-Shaped Holes

Principal Investigator: Dean M. Paxton
Pacific Northwest National Laboratory
P.O. Box 999, MSIN K2-44, Richland, WA 99352
(509) 375-2620; fax: (509) 375-2186; e-mail: dean.paxton@pnl.gov

PNNL Contract Manager: Mark T. Smith
Pacific Northwest National Laboratory
P.O. Box 999/K2-03, Richland, WA 99352
(509) 375-4478; fax: (509) 375-4448; e-mail: mark.smith@pnl.gov

Technology Area Development Manager: Joseph A. Carpenter
(202) 586-1022; fax: (202) 586-1600; e-mail: joseph.carpenter@ee.doe.gov
Field Technical Manager: Philip S. Sklad
(865) 574-5069; fax: (865) 576-4963; e-mail: skladps@ornl.gov

---

Contractor: Pacific Northwest National Laboratory
Contract No.: DE-AC06-76RLO1830

Objectives

- Move forward into the Technical Feasibility Phase applying thread-forming fasteners (TFFs) into net-shaped hole features in light alloy die castings for automotive applications as approved for FY 2005.
- Complete interim FY 2004 work scope that includes demonstrating the feasibility of applying TFFs into a cast engine alloy.

Accomplishments

- Successfully demonstrated concept feasibility for application of TFFs in net-shaped holes in FY 2003.
- Showed that clamp loads comparable to conventionally drilled holes and tapped fasteners could be achieved with TFFs in net-shaped holes.
- Completed casting and fabrication of as-cast engine alloy specimens for torque-tension mechanical testing.
- Assembled a broad-based team of contributors for moving forward with the Technical Feasibility portion of this program, including the automotive original equipment manufacturers (OEMs), fastener suppliers, assembly equipment suppliers, and manufacturers of cast components.

Future Direction

- Address, during the proposed Technical Feasibility Phase, a list of prioritized technical issues generated by the technical team:
  - casting variation
  - fastener design
  - assembling processing
  - in-service requirements
  - contamination and serviceability

Introduction

The Concept Feasibility portion of this project to investigate the use of tread-forming fasteners (TFFs) in net-shaped holes was successfully completed in 2003. The results of that phase indicated that comparable clamp loads to conventionally drilled and tapped fasteners could be achieved with TFFs in both aluminum and magnesium alloy castings. The Technical Feasibility Phase to address the highest priority technical issues resulting from the Concept Feasibility results has been proposed for FY 2005. An interim scope of work during FY 2004 was to obtain as-cast engine alloy nut and washer specimens and to perform initial torque-tension mechanical testing on these specimens.

Progress has been made in applying TFFs into machined or stamped holes featured in automotive applications for general assembly. Use of these fasteners eliminated the tapping operation and thereby reduced costs, reduced investment, and improved warranty while delivering better joint properties within an assembly. Opportunities exist to further reduce costs by using TFFs with net-shaped holes in lightweight castings by eliminating the drilling operation and associated equipment investment without sacrificing joint performance. Potential applications for using TFFs in cast components are numerous and include (1) powertrain (transmissions, engines, and rear axles); (2) chassis (control arms, suspensions); and (3) body structures that utilize large castings (inner doors, liftgates, under-hood attachments and supports).

Experimental Approach

The interim FY 2004 work scope to evaluate feasibility of applying TFFs into engine alloy cast specimens will be performed using the testing equipment and methods employed during the Concept Feasibility Phase, a summary of which is provided herein. Specimens for this testing have been cast and machined. Initial testing of these specimens will take place in early FY 2005.

To perform mechanical testing of TFFs into as-cast net-shaped holes, nut and washer plates were cast and machined into test specimens. X-radiography inspections were performed on a sampling of castings prior to final machining to verify structural integrity of the casting. The nut specimens included blind holes with 0.5° and 1.0° draft angles. A photograph and cross-section schematic of these specimens are presented in Figures 1 and 2, respectively. In addition, as-cast nut test specimens were prepared without a preset hole to allow for drilling and/or tapping of holes for comparison testing. Textron fasteners supplied 6-mm diameter (M6) Taptite fasteners with two coating types: (1) Magni 565, which is an organic coating, and (2) an electroplated zinc coating referred to as S437. Textron also provided

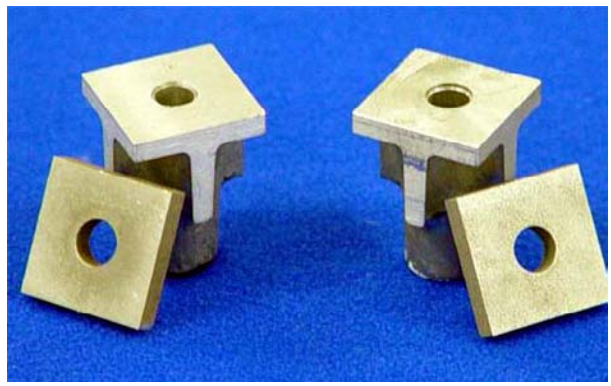

Figure 1. As-cast aluminum nut and washer specimens used for TFF torque-tension mechanical testing.

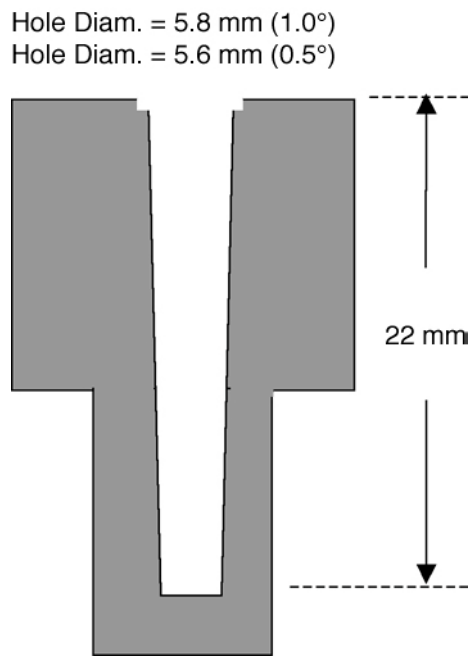

Figure 2. Cross section of nut specimen with blind hole at two draft angles (0.5° and 1.0°).

standard M6 machine screws coated with both the Magni 565 and S437 coatings for comparison testing. These fastener types were designed for use in aluminum.

The LabMaster Fastener Evaluation Test Cell was used to perform mechanical testing. This unit utilizes a slide bearing mount for the fastener drive system and mounting for the rotary torque-angle sensor and torque-tension research head. The fastener test system couples with a direct current (dc) electric nut-runner tool and controller, a rotary torque-angle transducer, a combination thread torque and clamp force transducer, and a computer control system for accurate test reproduction and data logging and reporting. The test stand equipment and nut-runner provided by Bosch Rexroth are shown in Figure 3. Individual mounting plates (Figure 4) were machined to size to hold the nut and washer specimens on either side of the load cell. The nut-runner was programmed to drive the fasteners to failure at a rundown speed of 240 rpm. During testing, the Labmaster software recorded

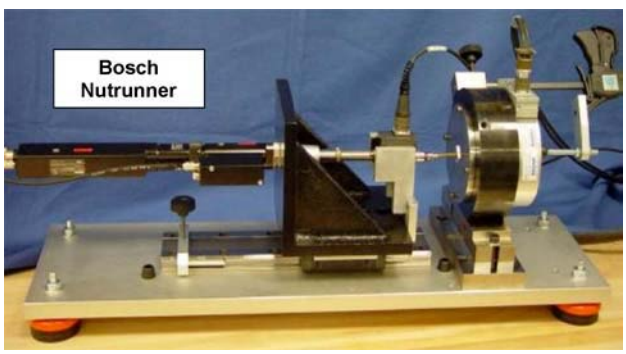

Figure 3. LabMaster Fastener Evaluation Test Cell from RS Technologies with integrated Bosch nutrunner.

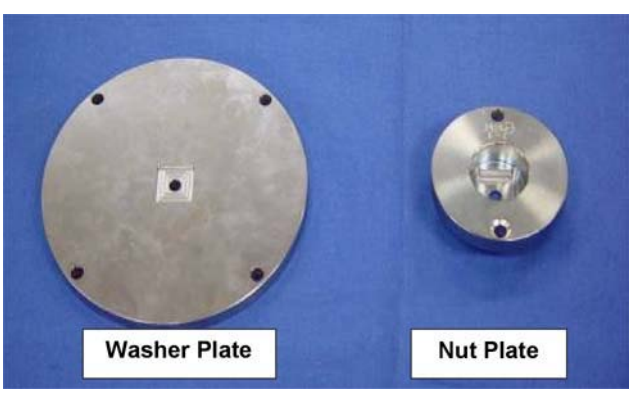

Figure 4. Washer and nut plates used with fastener test stand.

clamp load, input torque, and failure torque vs time and angular rotations of the fastener for each test.

To better understand the role of hole geometry and type (net-shape vs drilled) and to compare TFFs to standard machine screws, a parametric study was designed that also included fastener coating type and thread engagement depth. This study was focused on aluminum, although some limited testing was performed on the magnesium specimens. The variables and a symbol for each are listed in Table 1. With two coating types and four hole types, a total of eight combinations are established for each thread engagement depth; for example, M0518 and S1015.

Table 1. Summary of test matrix parameters to be applied for engine alloy TFF demonstration

Variable	Description	Symbol
Coating	Magni 565	M
	S437	S
Hole type	0.5° draft angle	05
	1.0° draft angle	10
	Drilled hole	DR
	Tapped hole	TP
Depth	18 mm	18

Future Work

The Technical Feasibility Phase has been approved for FY 2005 to resolve the highest priority technical challenge to TFF application, casting variation. The major facets of casting variation are cast hole position (shape and size) resulting from the thermal, mechanical, and metallurgical effects of the die casting process. In addition, experimentation and field measurements in production die casting facilities and computer modeling are planned. Also to be considered in this phase are the closely related in-service issues of contamination and reusability. In addition, torque-tension mechanical testing will be completed on as-cast engine alloy nut and washer specimens.

Presentation

D. M. Paxton, “Application of Thread-forming Fasteners in Net-Shaped Holes,” presented at USAMP Casting Off-Site Meeting at USCAR, Southfield, Michigan, September 29, 2004.

M. NDE Tools for the Evaluation of Laser-Welded Metals

Principal Investigator: William Charron
Ford Motor Company
17000 Oakwood
Room B154
Allan Park, MI 48101
(313) 390-3792; fax: (313) 594-1898; e-mail: wcharron@ford.com

Project Administrator: Constance J. S. Philips
National Center for Manufacturing Sciences
3025 Boardwalk
Ann Arbor, MI 48108-3266
(734) 995-7051; fax: (734) 995-1150; e-mail: conniep@ncms.org

Technology Area Development Manager: Joseph A. Carpenter
(202) 586-1022; fax: (202) 586-1600; e-mail: joseph.carpenter@ee.doe.gov
Field Technical Manager: Philip S. Sklad
(865) 574-5069; fax: (865) 576-4963; e-mail: skladps@ornl.gov

---

Contractor: U.S. Automotive Materials Partnership
Contract No.: FC26-02OR22910

Objective

- Develop fast, accurate, robust, noncontact Nondestructive Evaluation (NDE) tools and methodologies to replace current manual destructive testing of laser-welded sheet and structures in zinc-coated and uncoated steel and aluminum.
- Demonstrate accuracy and repeatability of the technologies developed or applied.
- Supplant the need for highly trained/experienced NDE operator.

Approach

- Evaluate and develop NDE tools for laser-welded steel.
- Evaluate and develop NDE tools for laser-welded aluminum.
  - Phase 1—the comprehensive assessment of existing and emerging NDE technologies for steel and aluminum, down-selection, performance testing using fabricated welded coupons in steel, correlation of NDE test results with validation test results, and NDE technology selection for Phase 2.
  - Phase 2—the specification and build of a prototype from the selected NDE methodology(ies) for
    - Steel—Conduct controlled evaluations of NDE capabilities using fabricated weld coupons and ultimately coupons made from laser-welded production parts and correlation of NDE test results with validation test results. Finally, comparison of NDE test results will be made to destructive test results obtained on production part coupons.
    - Aluminum—Conduct controlled evaluation of NDE capabilities using fabricated weld coupons and correlation of NDE test results with validation test results. Finally, comparison of NDE test results will be made to destructive test results obtained on aluminum coupons.
    - Demonstrate the selected technology with a bench prototype system in a production plant setting.

Accomplishments

- Conducted original equipment manufacturer (OEM) weld flaw characterization, selection of target laser weld application, definition of NDE system functional specifications, and assessment of NDE state-of-the-art technologies.
- Performed controlled testing of four selected NDE technologies using Coupon Set One and analyses of vendor test results.
- Defined NDE system functional specifications based on roof ditch rail application and production plant input.
- Selected of ultrasonic through-transmission technology for further testing and development.
- Evaluated ultrasonic through-transmission sensor using steel roof ditch samples fabricated on laser weld production-equal equipment, aluminum lap-weld samples fabricated on laser weld production-equal equipment, and steel roof ditch production part coupons.
- Analyzed test results for steel roof ditch samples, aluminum lap-weld samples, and steel production part coupons.
- Initiated prototype optimization based on initial plant trial performance results for roof ditch rail application.
- Redesigned aluminum coupon weld construction for NDE testing (Coupon Set Five).
- Defined plant test plan and prototype in-plant trials.

Future Direction

- Analyze the test results on (1) redesigned aluminum lap weld coupons (Coupon Set 5) and (2) additional in-plant trials using the prototype modified for the production part in steel.
- Correlate all test results from coupon and production part coupon tear-down results with the ultrasonic through-transmission signatures, C-scans, and radiographic X-ray images.

Introduction

Approved for incorporation into the United States Automotive Materials Partnership (USAMP) project portfolio in January 2001 and launched in May 2001, this project has two primary investigative missions: (1) evaluate and develop nondestructive evaluation (NDE) tools for laser-welded steel and (2) evaluate and develop NDE tools for laser-welded aluminum. The investigative approach is divided into two phases:

- Phase 1—the comprehensive assessment of existing and emerging NDE technologies for steel and aluminum, down-selection, performance testing using fabricated welded coupons in steel, correlation of NDE test results with validation test results, and NDE technology selection for Phase 2.
- Phase 2—the specification and build of a prototype from the selected NDE methodology(ies) for
  - Steel—Conduct controlled evaluations of NDE capabilities using fabricated weld coupons and, ultimately, coupons made from laser-welded production parts and correlation of NDE test results with validation test results and comparison of NDE test results to destructive test results obtained on production parts.
  - Aluminum—Conduct controlled evaluation of NDE capabilities using fabricated weld coupons and correlation of NDE test results with validation test results. Finally, comparison of NDE test results will be made to destructive test results obtained on selected aluminum coupons.

While laser welding is accepted by the automotive industry for many applications, cost factors are an issue, particularly with respect to weld discontinuities in body applications. With the high speed and high volume of laser welding coupled with the

flaw sizes of interest, finding these discontinuities can be difficult, time-consuming, and hence, expensive. If not detected before subsequent processing and/or assembly, they could cause failures during processing down line or while in use. For example, porosity in a laser-welded tailor blank can cause failure during a stamping operation, which in turn can damage dies and cause downtime for the press. To forestall this, laser welding must be accomplished with no detrimental weld discontinuities, and the process and product output must be monitored with a high degree of reliability.

A number of systems have been developed to monitor laser welding systems in real time. Generally, these systems examine the byproducts of the laser-to-metal interaction to infer the quality of the weld itself. These process monitoring methods may include examination of the frequency and intensity of the light that is given off, for example, and compare it to those parameters known to have produced an "acceptable" weld. Most of these monitoring systems use this "training" method as a basis for determining if acceptable welds or unacceptable welds were created by the laser weld process. As of this writing, such systems are being applied in the production environment to gage the process, not as a substitute for weld quality inspection or destructive testing.

Because laser welding will facilitate the use of lightweighting materials and designs, the development of NDE tools is viewed as an enabling technology for the reduction of vehicle mass through increased use of laser welding in automotive plants. Thus, this project focused on developing and using NDE for laser-welded body structures, specifically for laser stitch welds in a roof ditch rail in steel and aluminum. Demonstrations of accuracy and repeatability of the NDE system on steel and aluminum weld samples and on steel production part coupons are essential for obtaining plant acceptance and eventual implementation.

Details of Phases 1 and 2

Phase 1

AMD 303 is exploring NDE tools for use on the weld itself after creation of the weld. Of interest was the identification of progressive and emerging technologies in NDE, an assessment of the state of the art. As part of its Phase 1 effort, the AMD 303 project performed phased assessments of NDE technologies, progressively narrowing down the technologies best suited to the production application. From these assessments, specific NDE technology recommendations were reviewed and a technology chosen with the goal to have a NDE prototype ready for evaluation in a factory setting by the end of the project.

The NDE techniques included in the state-of-the-art assessment are identified in Figure 1. Commercial off-the-shelf systems were included along with emerging NDE technologies. Based on this initial assessment, four technologies were then selected for detailed evaluation using a scientifically designed and statistically controlled study. These four technologies were: ultrasonic through-transmission, ultrasonic EMAT, visual inspection—laser mapping, and resistivity. NDE performance capabilities of these four were evaluated using laboratory-fabricated weld samples simulating laser-welded roof ditch welds (Coupon Set One). See Figure 2 for an illustration of the roof ditch coupon.

To down-select further, it was determined which NDE technology offered the best array of detection capabilities and potential for conforming to the roof ditch rail geometry. All four NDE systems were found to have varying deficiencies, including false calls (reacting to a good weld as if it were flawed)

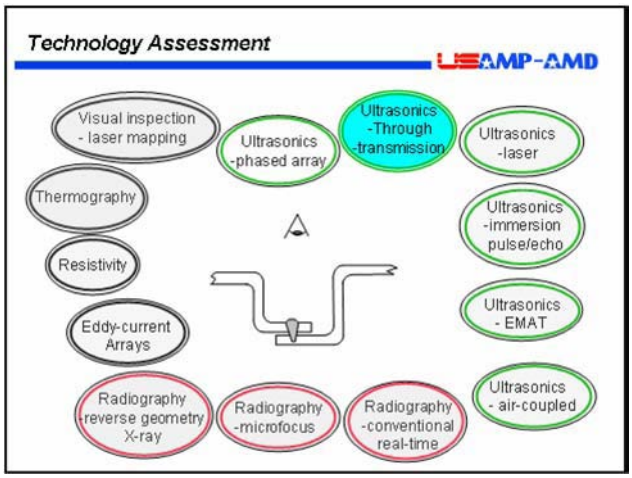

Figure 1. Phase 1 technology assessment examined the capabilities of thirteen technologies/techniques for their suitability to inspect the target weld configuration and the weld discontinuities of interest. Initial analyses identified four techniques, highlighted here in color, for detailed evaluation.

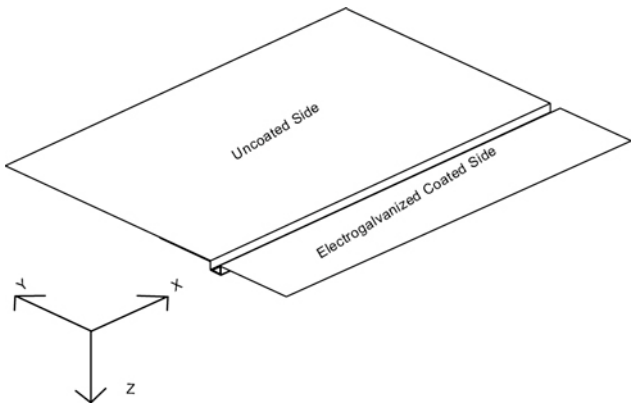

Figure 2. Overall dimensions of roof ditch weld sample: X = 400 mm; Y1 = 202 mm; Y2 = 89 mm; overall Y after bending = 287 mm; Z = 12 mm.

and missed discontinuities (not reacting to flaws known to be present), including the discontinuity of highest interest, lack of fusion. Additionally, all four tended to undersize defects.

Ultimately, two technologies were selected for their capabilities for detecting weld discontinuities judged critical by the AMD 303 Committee. The two NDE systems, one based on ultrasonic EMAT and one based on ultrasonic through-transmission, performed comparably well (albeit on some differing discontinuities). The evaluations indicated both systems required additional development and reconfiguration to perform acceptably well in the OEM production environment and on the roof ditch rail application. Finally, due primarily to cost advantages, the through-transmission ultrasonic sensor technology was selected for Phase 2 in-depth evaluation, reconfiguration, and build for the roof ditch weld application. Figure 3 illustrates a roof ditch rail in detail and the required sensor orientation to the part.

Phase 2

Specific discontinuities of interest were identified in meetings and interviews with OEM assembly plant personnel. Two high-priority detection needs were "Lack of Fusion" and "Missing Welds and Skips." Other discontinuities were rated as being of lower priority, and some were unrated, because they could be controlled with process controls or are detectable by visual means. Table 1 lists the discontinuities of interest, shows their priority classification by plant personnel, and if the discrepancy can be detected by ultrasonic through-transmission and/or ultrasonics additionally having pitch/catch capability.

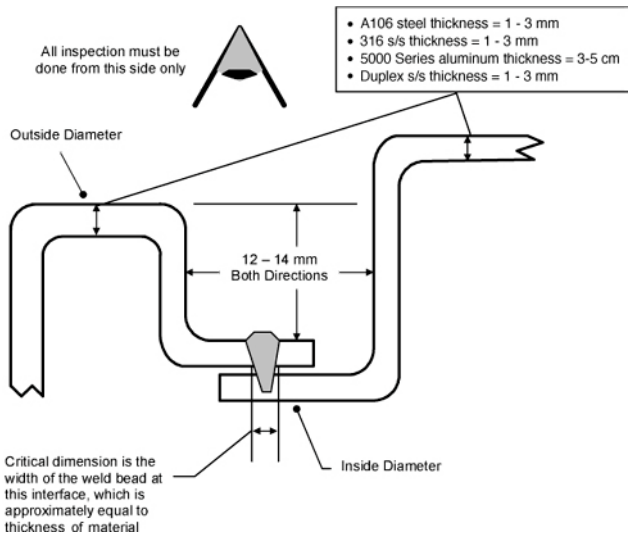

Figure 3. Laser-welded roof ditch joint details showing the sensor's field of view.

Table 1. Discrepancy detection requirements at the plant level

Discontinuity type defined in NDE-001	Plant priority	Detection table: Ultrasonics through-transmission	Detection table: Ultrasonics with pitch/catch
Lack of fusion	High	√	√
Undersize welds	Medium	√	√
Underbead cracks	Low		√
Crater cracks	Low		√
Longitudinal cracks	Low		√
Transverse cracks	Low		
Missing welds skips	High	√	√
Pore, porosity	Medium	√	√
Inclusions			√
Burn-through and holes	Medium	√	√
Top sheet through-cut			√
Undercut of underfill			√

Laser-Welded Coupons

The project has created four groups of laser-welded coupons for testing and evaluation purposes, and a fifth was designed but not yet fabricated as of this report.

Coupon Set One: EWI Roof Ditch Coupons— During Phase 1, 36 laser-welded coupons were fabricated by Edison Welding Institute in welding laboratory conditions and used in Phase 1 vendor technology evaluations. These 36 coupons form Coupon Set One.

Coupon Set Two: Roof Ditch Weld Coupons in Steel—Subsequent to the selection of the ultrasonic through-transmission technology for Phase 2, additional coupons were fabricated using production-intent welding cells built by Kuka Flexible Production Systems having a 4-kW Nd:YAG laser with robot.

Ford Motor Company, in cooperation with Kuka, laser welded 13 roof ditch weld coupons in steel. Eleven of these coupons contained lack of fusion with lengths ranging from 2.0 mm to 43.8 mm. Two coupons contained no known discrepancies.

Coupon Set Three: Lap Weld Coupons in Aluminum—Ford, in conjunction with Kuka, laser welded eight aluminum sheet coupons with a continuous lap weld. The coupons contained lack of fusion, burn through, and porosity among other discontinuities. These laser-welded coupons had distortion and configuration variances among the coupons, such as varying amounts of metal overlap, that posed additional challenges for the NDE testing. (See Figures 4 and 5.)

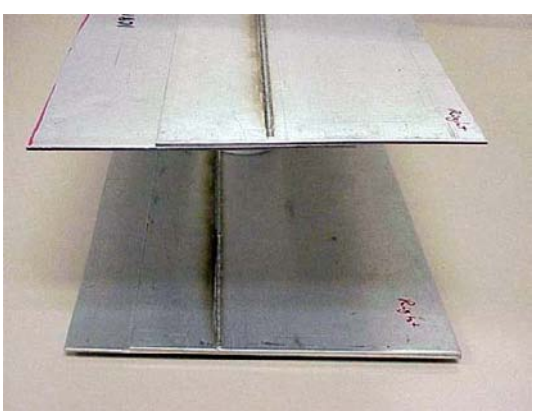

Figure 4. Lap-welded aluminum coupons using 4-kW Nd:YAG laser. The coupons illustrate the varying sizes and overlap configurations.

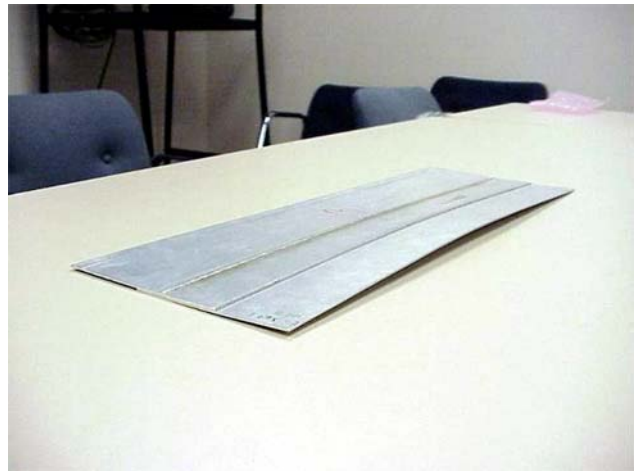

Figure 5. Aluminum coupon with distortion in the sheet caused by the laser welding process.

Coupon Set Four: Production Roof Ditch Welds in Steel—Eight production part coupons were sectioned and cut from an assembled vehicle roof produced in a production laser welding cell being readied for new model production at an OEM plant. The production parts were fabricated in steel. They exemplify the issues posed by complex part geometries in mating part contours of the roof and body sides.

Coupon Set Five: Controlled Aluminum Lap Weld Coupons—In FY 2005 General Motors Corporation (GM) will fabricate an additional set of aluminum lap weld coupons using a production equal laser welding cell at GM. This set will control the width of overlap, stitch weld length, gaps between welds, and welding parameters to control distortion.

NDE Tool: Ultrasonic Through-transmission

Ultrasonic through-transmission was found to have the following attributes:

- Through-transmission is accomplished by use of two separate transducers, which transmit and receive a 4-MHz ultrasonic wave.
- Transducers are encapsulated in dry couplant rollers that travel along in contact with the two welded sheets on both sides of the weld seam.
- Lack of fusion is indicated by drops in signal amplitude.
- "Good weld" coupons are required to calibrate and set the system gain (signal threshold).
- Encoder tracks its location along the weld as the signal is generated.

- Inspection speed determines spatial resolution.

The ultrasonic through-transmission device is capable of detecting most lack-of-fusion regions in the above test coupons, except Coupon Set Three. System noise from nonwelded contact generated by fused wax between the plates obfuscated testing. To better test the device on aluminum sheet with stitch welds, a new aluminum coupon set will be fabricated (Coupon Set Five) and the tests repeated in FY 2005. The ultrasonic through-transmission device and user interface proved to be user friendly and did not require extensive user training. The device, configured for testing of roof ditch coupons as in Coupon Set Two, is shown in Figure 6.

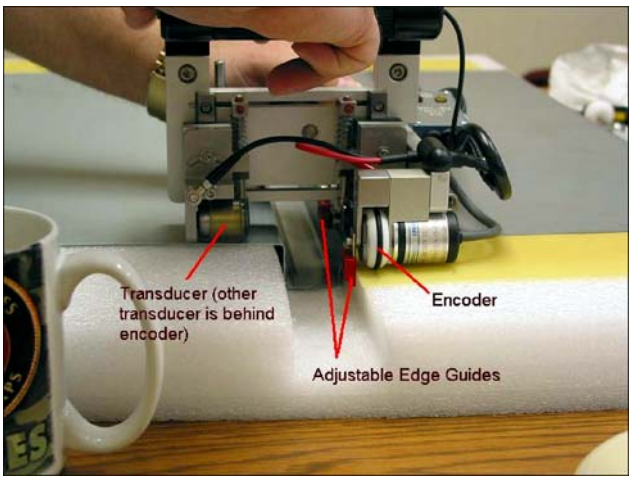

Figure 6. Ultrasonic through-transmission device shown at testing start on a steel coupon from Coupon Set Two.

NDE Test Plan

A standard test matrix was defined consisting of the following measurements:

- RMS variations,
- baseline noise,
- gage repeatability and reproducibility, and
- surface roughness.

The test plan was applied to Coupon Sets One through Four. Figure 7 shows a scan being made, and the user interface providing real-time graphic feedback to the operator representing the signature amplitude of the ultrasonic wave in response to the subject weld.

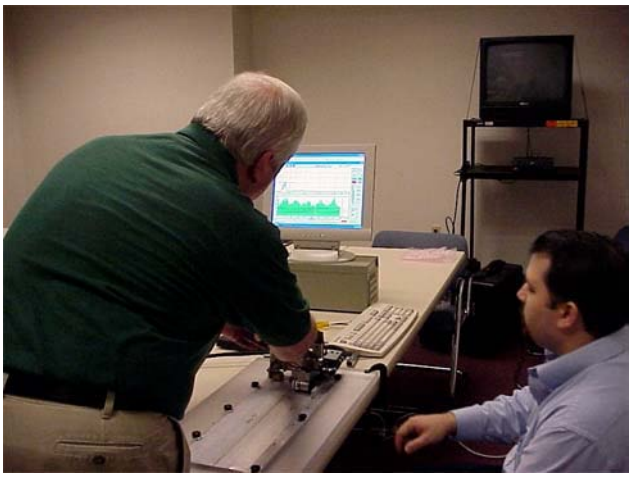

Figure 7. Ultrasonic through-transmission device testing an aluminum coupon from Coupon Set Three with the user interface displaying the signature of the ultrasonic wave in response to the weld sample.

Analyses of Test Results

Analyses of the testing results from Coupon Sets One and Two yielded the following findings:

- electronics-induced variance: 1.3% of full scale (FS)
- repeatability/scanning variance: 7.6% of FS
- total variance: 7.9% of FS
- reproducibility/operator-induced variance: 2.0% of FS

Further examination of the repeatability/scanning variance seen in these tests results focused on the rollers that encapsulate the transducers. The wheels were found to compress as the force was increased, and this had a dominant effect on the repeatability variance.

Additional analyses were conducted to determine the resolution of the scanner. Resolution is reflected in the probability of detecting a particular size gap and is dependent upon the threshold setting and the noise of the system. Using the derivative of the signal to define the beam shape, it was determined to be triangular, with a 6-db beam width of 6.5 mm. Examining the drops in amplitude of the dips between signals (equating to gaps between the stitch welds or lack of fusion) allows one to measure

the magnitude of the dip along with the variance and to calculate the probability of detection. The data analysis indicated that gaps from 2 to 6 mm in length are not able to be detected. Based on a probability plot curve, the probability of detecting gaps more than 6 mm increases until >99% probability is reached at 8 mm and larger. (See Figure 8.)

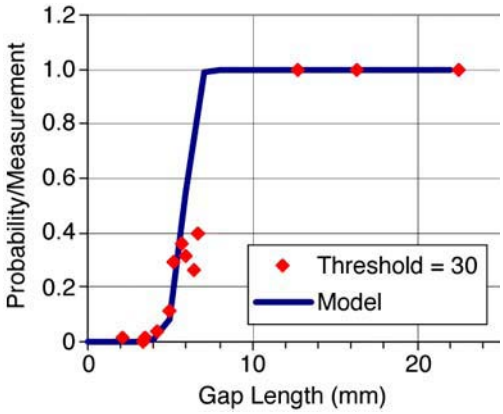

Figure 8. Graph of gap detection probability indicates the probability significantly increases for gaps exceeding 6 mm in length at a threshold setting of 30, reaching >99% probability for gaps of 8 mm or larger.

Data analyses and reporting of the test results for Coupon Set Four (production part coupons) are under way at this writing. General observations reported following the testing of Coupon Set Four using the unmodified prototype included the following:

- Maintaining dual roller contact with the geometry of the part was difficult for the operator. The part profile is a complex geometry owing to the downward slope of the body side member away from the weld location in the roof ditch.
- The time needed for data collection was adversely affected by one inexperienced operator having to back up and repeat the scan more frequently than normal.
- Electrical interference from within the plant was seen to affect the ultrasonic signal and will be reflected in the data.
- Data displayed on the prototype screen is limited to 1000 points. This number does not register sufficient data to cover a scan along the full length of the ditch rail. Thus, the part had to be marked off in sections, scanned in sections, and data collected by section. (See Figure 9.)
- Testing was done on two vehicles. Tests were performed using three operators, who switched right-hand (RH) and left-hand (LH) body sides by scanning RH from front to rear and LH by scanning from rear to front. Figure 9 illustrates the sectioning and direction of scanning by the operators.
- Eight sections cut from one vehicle (Coupon Set Four) were validated by C scan by GM and radiographic X-ray by DaimlerChrysler.
- Four welds had shims inserted in an attempt to create lack of fusion; some welds partially penetrated through the shims.

Coupon Validation

Validation tests of Coupon Set Two using radiographic X-ray and ultrasonic pulse/echo "C-scans" of the midplane in an immersion tank were completed. C-scan results were recorded for

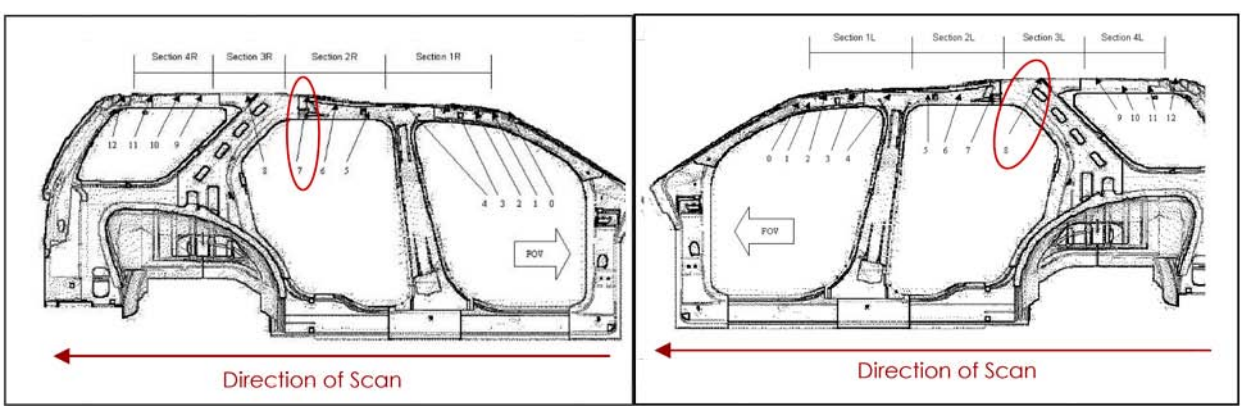

Figure 9. Illustration of scanning direction and sectioning of vehicle roof ditch for data collection purposes.

each coupon and analyzed against the ultrasonic through-transmission sensor's amplitude output data (signature) by coupon. Figure 10 is a graphic depiction of such a correlation between C-scan data and the ultrasonic through-transmission signature for Steel Coupon No. 45 from Coupon Set One. The weld is clearly visible in both the signature and the C-scan image and correlates with one another in size and position.

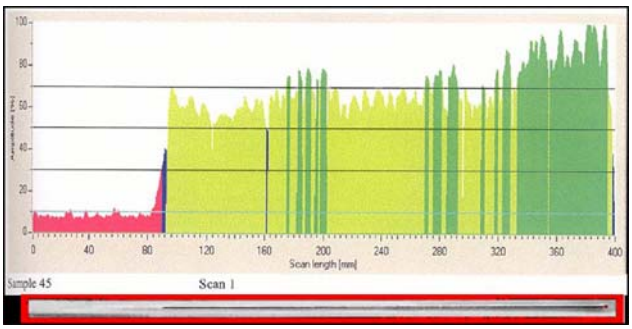

Figure 10. Ultrasonic C-scan data (bottom) and ultrasonic through-transmission signature of steel sample No. 45 from Coupon Set One.

Validation of Coupon Sets Two through Four using ultrasonic C-scans and radiographic X-ray are also complete. Production part coupons from Coupon Set Four posed particular difficulties for C-scanning as the parts were badly distorted when they were cut into sections. Weld validation data of the type shown in Figure 10 have been analyzed and will be compiled and reported in FY 2005.

A test plan for tear-down of the production part coupons is currently being implemented for Coupon Set Four, and the results will be correlated with the ultrasonic through-transmission, C-scans, and radiographic X-ray images for selected coupons. These results will be available for inclusion in the FY 2005 report. Figures 11 and 12 contain photographs of one stitch weld from Coupon Set Four, before and after tear-down. Such images will also be incorporated with the above data in the FY 2005 report.

Additional Technology Explored

Technological advancements since the beginning of this project in the areas of infrared cameras, hyper spectral imaging (3–5 μm), spectrometer

Figure 11. Photograph of production-part single stitch weld from Coupon Set Four. (Section 2R—Stitch No. 7 in Fig. 8) before tear-down.

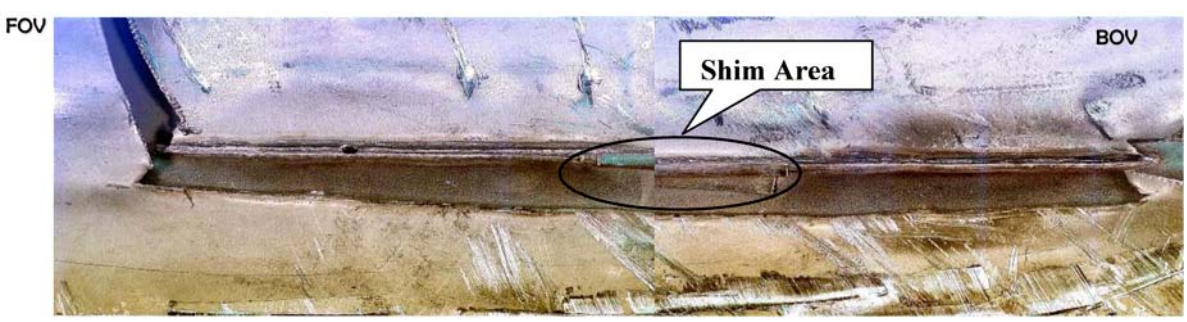

Figure 12. Picture of production-part stitch weld in Figure 11 after tear-down. (Section 2R—Stitch 7 in Fig. 8.)

capability in the ultraviolet-infrared range, high-speed capability (346 to 38,000 frames/s), high-sensitivity, and spatial resolution from 5-µm/pixel have resulted in one technology being brought back to our attention in recent months. Infrared thermography research at Oak Ridge National Laboratory by Drs. Zhili Feng and Hsin Wang has shown promise as a NDE technology now capable of detecting weld flaws without having to paint a metal part black. This possibility, which, along with the advancements cited above, could make this technology feasible for use in a production plant and was believed worthy of further investigation. Various coupons from Coupon Set One and Coupon Set Four were provided for initial feasibility experiments at ORNL. Results of these experiments will be available for inclusion in the FY 2005 report.

Conclusions

- Sufficient performance information was gained in the coupon testing conducted to date to allow performance and design guidance to be provided for prototype improvement and configuration to the ultrasonic through-transmission vendor for further production part testing in an OEM production plant.
- Additional in-plant trials are scheduled in FY 2005 to apply the prototype device modified for the roof ditch production part.
- Physical tear-down results can be correlated with the ultrasonic through-transmission signatures, C-scans, and radiographic X-ray images for selected coupons.
- Aluminum coupon testing must be repeated using coupons fabricated using thoroughly cleaned sheet stock. Results from this testing and implications for ultrasonic through-transmission inspection of aluminum laser welds will be reported in FY 2005.

N. NDE Inspection of Resistance Spot Welds in Automotive Structures Using an Ultrasonic Phased Array

Principal Investigator: Deborah Hopkins
Lawrence Berkeley National Laboratory
1 Cyclotron Road, MS 46A-1123, Berkeley, CA 94720
(510) 486-4922; fax: (510) 486-4711; e-mail: dlhopkins@lbl.gov

Technology Area Development Manager: Joseph Carpenter
(202) 586-1022; fax: (202) 586-1600; e-mail: joseph.carpenter@ee.doe.gov
Field Technical Manager: Philip S. Sklad
(865) 574-5069; fax: (865) 576-4963; e-mail: skladps@ornl.gov

Participants
U.S. Automotive Materials Partnership NDE of Welded Metals Steering Committee
Frédéric Reverdy, Ph.D., Lawrence Berkeley National Laboratory
Daniel Türler, M.S., Lawrence Berkeley National Laboratory
William B. Davis, M.S., Lawrence Berkeley National Laboratory

---

Contractor: Lawrence Berkeley National Laboratory
Contract No.: DE-AC03-765F0095

Objective

- Develop a cost-effective ultrasonic phased-array system that is sufficiently fast, accurate, and robust in manufacturing environments to be suitable for inspection of spot welds in automotive components.

Approach

- Develop a spot-weld inspection system that can be used by operators with minimal training by using state-of-the-art ultrasonic phased-array technology. The multielement probe allows the ultrasonic energy to be focused at the interface between the welded sheets and electronically scanned through the weld.
- Design a miniature mechanical scanner that will allow scanning in the direction perpendicular to the electronic scan to produce two-dimensional images of the weld. The portable system allows more than 3000 signals to be acquired in less than 4 s.
- Develop signal processing and image analysis software to distinguish satisfactory, undersized, and defective welds and provide dimensional analysis of the weld in a few seconds.
- Minimize the footprint of the probe assembly to ensure access to welds on complex components.
- Design an integrated probe housing that meets the size constraints while allowing mechanical scanning over a travel distance of 16 mm. The housing will also maintain the probe in water and must have an outer membrane that provides acoustic coupling to the part under inspection.
- Conduct plant trials to demonstrate the system's ability to characterize welds with sufficient accuracy and repeatability and to demonstrate that the integrated probe housing is rugged enough for use in a production facility.

Accomplishments

- Evaluated the performance and limitations of existing ultrasonic phased-array systems.
- Conducted a series of laboratory experiments to evaluate the performance of 5-, 10-, and 17-MHz phased-array probes for characterization of spot welds in galvanized steel.
- Developed signal-processing algorithms to distinguish between satisfactory, undersized, and defective welds.
- Developed image-processing algorithms that allow dimensional analysis of welds.
- Demonstrated the ability to acquire more than 3000 signals per weld and analyze the resulting data in a few seconds to render an estimate of weld quality.
- Demonstrated good correlation between ultrasonic measurements, measurements of weld buttons on peeled samples, and metallographic images of cross sections through welds.
- Designed a probe housing that maintains the probe in water, contains a miniature mechanical system that allows linear translation of the probe, and provides an outer membrane that confines the water column while also providing acoustic coupling to the part under inspection.

Future Direction

- Conduct laboratory experiments and plant trials to demonstrate the ability of phased-array systems to inspect spot welds with sufficient accuracy and repeatability for the full range of materials and joint configurations used in production.
- Conduct laboratory experiments to determine the concept feasibility of using ultrasonic phased arrays to inspect welds in aluminum and high-strength steel.
- Develop automated classifiers to determine weld dimensions and identify defective welds including cold welds.
- Identify and test coupling techniques that will allow existing probes to be used outside of a water tank.
- Develop a user interface in conjunction with end users to ensure ease of use and reporting of data in the most useful format for inspectors, welding engineers, and plant managers.
- Develop a fully integrated prototype system suitable for deployment and testing in a manufacturing plant.
- Perform large-scale testing and measurement system analysis.

Introduction

Development of nondestructive evaluation (NDE) techniques has been identified in both industry and government forums as an enabling technology for greater use of advanced and lightweight materials in the automotive industry. Reducing vehicle weight improves fuel efficiency and reduces emissions, and recent studies have demonstrated cost savings that derive from finding defects early in the production process and reducing waste compared to destructive testing. One of the critical technical challenges in introducing lightweight materials is developing joining technologies and inspection strategies suitable for mass production. NDE methods to assure product quality are essential for industry and consumer acceptance of new materials and manufacturing methods.

At present, the most common methods for inspecting spot welds in automotive manufacturing are pry checks and physical teardown, during which spot-welded joints are pried apart; the resulting weld buttons are visually inspected or measured with calipers. Although these methods have been used successfully for decades, destructive weld testing has several drawbacks including high costs associated with scrapped material, ergonomic injuries, and the time lag between the onset and identification of problems. In addition, pry tests and teardowns do not allow plant managers and engineers to easily collect inspection data that would allow them to identify trends and potential problems. Furthermore, these inspection techniques are not viable options for lightweight and high-strength materials. Composite structures with adhesive-bonded joints

cannot be pry checked, and aluminum is relatively expensive and more difficult to rework than steel making pry checks and teardown cost prohibitive. Welds in high-strength steel are often too strong to be pry checked or torn down, and satisfactory welds sometimes fail interfacially rather than by pulling a weld button, making it difficult for inspectors to distinguish between satisfactory and defective welds.

Advances in sensors, computing, communication, and engineering technologies have all played a role in advancing the development of NDE methods with promising automotive applications. For example, ultrasonic phased-array systems have been available since the mid-1970s, but they were prohibitively expensive. In the past decade, prices have dropped dramatically, and increased competition promises additional price reductions in the future. A recent breakthrough is the availability of portable systems that are particularly attractive for use in production environments.

Lawrence Berkely National Laboratory (LBNL) previously evaluated the adequacy of conventional, commercially available ultrasonic systems for the inspection of spot welds. Although these systems are widely used in European automotive plants, they have not gained widespread acceptance in the United States for reasons that include their dependence on trained operators to set system variables and the need to change probes frequently because of the wide range of materials and sheet thicknesses used in production vehicles. An important goal of the current project is to develop a system that is much easier to use. Plant managers also emphasize the need for intuitive user interfaces and summary reports that can be customized for welding engineers and other plant personnel.

To best advance the adoption of lightweight materials while also serving the needs of the auto industry, the current project team has adopted a strategy that strives to develop platforms that add value immediately, minimize barriers to incorporating emerging technologies at a later date, and that are as modular as possible so that they can be easily modified or adapted for new applications. Consistent with that model, the current work is focused on development of a prototype spot-weld inspection platform that integrates the best available ultrasonic phased-array technology with custom-designed signal processing and analysis software, and hardware that will allow the system to be tested and implemented in manufacturing plants as a portable stand-alone unit.

Ultrasonic Phased-Array Technology

The only commercial spot-weld inspection systems available today use conventional high-frequency, single-crystal, ultrasonic probes working in pulse-echo mode. The output from these mono-probes is a single signal that is an integrated response over an area that depends on the diameter of the probe. Different probes must be used for different sized welds. In contrast, a phased array is composed of many piezoelectric elements that are individually excited by electronic pulses at programmed delay times. As a result, phased arrays have several advantages over conventional ultrasonic probes that derive from the ability to dynamically control the acoustic beam transmitted into the structure under examination. An electronic delay can be applied separately to each electronic channel when emitting and receiving the signal. These delay laws permit constructive and destructive interference of the acoustic wavefront transmitted into the structure, allowing predefined ultrasonic beams to be formed. The acoustic energy can be focused, and delay laws can be used to steer the acoustic beam. Electronic scanning is accomplished by firing successive groups of elements in the array.

Instead of assessing weld quality based on a single signal, as is the case with mono-probes, phased arrays allow thousands of signals to be obtained for individual welds in a few seconds. The ability to perform complex scanning of the acoustic beam through the weld allows greater accuracy in sizing weld nuggets, while also improving the flaw characterization capability. These attributes of phased-array probes allow us to measure the weld-nugget diameter, locate defects, and identify misshapen and burnt welds. In addition, the same probe can be used to inspect different sized welds and welds in sheets with different thicknesses. It is also possible to electronically compensate for misalignment of the probe with respect to the sample.

Previous Work

Initial experiments were conducted using an R/D Tech ultrasonic phased-array system loaned to LBNL by the Ford Motor Company. The system consists of an electronic controller, a linear 5-MHz probe, and a data acquisition system. The system

was used to perform laboratory experiments designed to evaluate the performance of existing hardware, determine the optimal probe configuration, and to develop signal-processing and weld-classification algorithms.

An open question at the beginning of the project was the adequacy of the 5-MHz probe for the full range of materials and sheet thicknesses currently used in production. Phased-array probes are now available up to a frequency of about 20 MHz. In general, relatively high-frequency probes provide better spatial resolution than lower frequency probes, but are more expensive.

The results of the experiments conducted with the 5-MHz probe demonstrated that a central frequency of 5 MHz is too low to inspect welds in the thinnest metal sheets used in the automotive industry (thinner than 1 mm). Therefore, a new suite of experiments was carried out with leased probes with central frequencies of 10 and 17 MHz. The 10-MHz probe was a 32-element linear probe with a 0.4-mm pitch (distance between two successive elements), and the 17-MHz was a 128-element focused probe with a focal distance of 12.5 mm and a pitch of 0.28 mm. The distance between the probe and samples was held constant at 12.5 mm for all experiments to allow the same focal law to be used. The test specimens were spot-welded strips made from 1.4-mm-thick galvanized mild-steel sheet metal. Several hundred welds were inspected. Analysis of the resulting data showed that the focused 17-Mhz probe was the best choice for being able to inspect welds across the full range of sheet thicknesses used in production.

These initial experiments were performed in a water tank or using a confined water column with coupling gel between the probe and the sample. As described below, to allow measurements to be made in a production environment, a self-contained probe housing has been designed that maintains the probe in water while also providing acoustic coupling to the part under inspection.

Phased-Array Inspection Strategy

For all experiments performed to date, electronic scanning and focusing laws were combined to inspect the spot welds. The acoustic energy is focused at the interface between the two sheets by applying symmetrical delay laws to the elements (see Figure 1). The results presented here were obtained using the 17-MHz focused probe described in the previous section. Unlike the 5- and 10-MHz probes that have flat elements, the 17-MHz probe has curved elements that focus the energy with a natural focal length of 12.5 mm. When used in conjunction with the delay laws described above that focus the energy from multiple elements, the acoustic beam at the interface between the welded sheets is a circular spot that is scanned across the weld. Using a portable phased-array controller, more than 3000 signals are recorded for each weld in approximately 4 s.

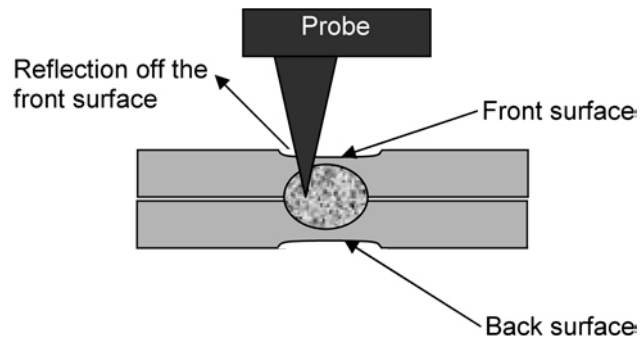

Figure 1. Schematic drawing illustrating focusing of the ultrasonic energy from several phased-array elements at the interface between two spot-welded sheets.

Scanning in one direction is performed by electronically translating the ultrasonic beam across the sample by firing a specified number of elements in sequence. For example, when eight elements are used at a time, the beam is electronically scanned across the weld in steps of one element; that is, elements one through eight are excited to generate the first signal, elements two through nine are excited to generate the second signal, and so forth. To obtain two-dimensional (2-D) images of the weld, the probe is mechanically translated across the weld in the direction perpendicular to the electronic scan.

As described above and illustrated in Figure 1, the acoustic energy generated by several adjacent elements in the probe is focused and transmitted into the test specimen. Some of the energy is reflected off the front surface as indicated in the diagram. In the welded region, the signals pass through both sheets and are reflected off the back surface. It is interesting to note that the metallurgical changes in the welded area do not cause a change in acoustic impedance large enough to create a noticeable

reflection at the boundary of the weld nugget. Outside the welded region, the signals are confined to the top sheet; that is, the acoustic waves are reflected back and forth in the upper sheet, and no energy is transferred into the lower sheet.

Signal Processing

The signals recorded while scanning through the weld are analyzed in the time and frequency domains. For a satisfactory weld, ultrasonic waves are transmitted through the weld nugget and reflected off the back surface of the lower sheet (see Figure 1). In contrast, for a cold weld, incomplete fusion at the interface between the two sheets results in partial reflection of the ultrasonic energy at the interface. This affects the periodicity of the train of echoes; that is, signals that are reflected at the interface have a shorter travel path than signals that propagate through the weld, resulting in echoes in the time domain that are closer together than echoes off the back surface.

In the frequency domain, the power spectrum captures the periodicity of the ultrasonic echoes in the time domain. Examples of the power spectra obtained from raw signals are shown in Figure 2 for the beam focused inside a satisfactory weld [(Figure 2(*a*)] and inside a cold weld [Figure 2(*b*)]. The power spectra were calculated using the data between the first backwall echo and the end of the signal. The relative magnitude of the peaks in the spectra is indicative of the amount of energy reflected at the interface. For a satisfactory weld, the ultrasonic wave propagates through the weld and reflects back and forth between the front and back surfaces resulting in a major echo [labeled 1 in Figures 2(*a*) and 2(*b*)] that corresponds to the travel path through both sheets. For a cold weld [Figure 2(*b*)], where most of the energy is reflected at the interface between the two sheets, the magnitude of echo 1 is smaller than the magnitude of echo 2, which corresponds to a travel path equal to twice the thickness of the upper sheet.

As an example of how this frequency information is used, processed images obtained for satisfactory, undersized, and defective welds are displayed in the first column of Figure 3. For each of the 3216 signals that comprise each image, the ratio of the first peak to the second peak in the power spectrum was calculated and then compared to a threshold that was used to create the binary images. White corresponds to high transmission into the lower sheet, while black indicates areas where there is complete or partial reflection off the interface between the two sheets.

The peak-ratio images allow satisfactory and undersized welds to be distinguished according to the size of the area where there is significant transmission of energy into the lower sheet. Although defective welds such as cold welds can result in a

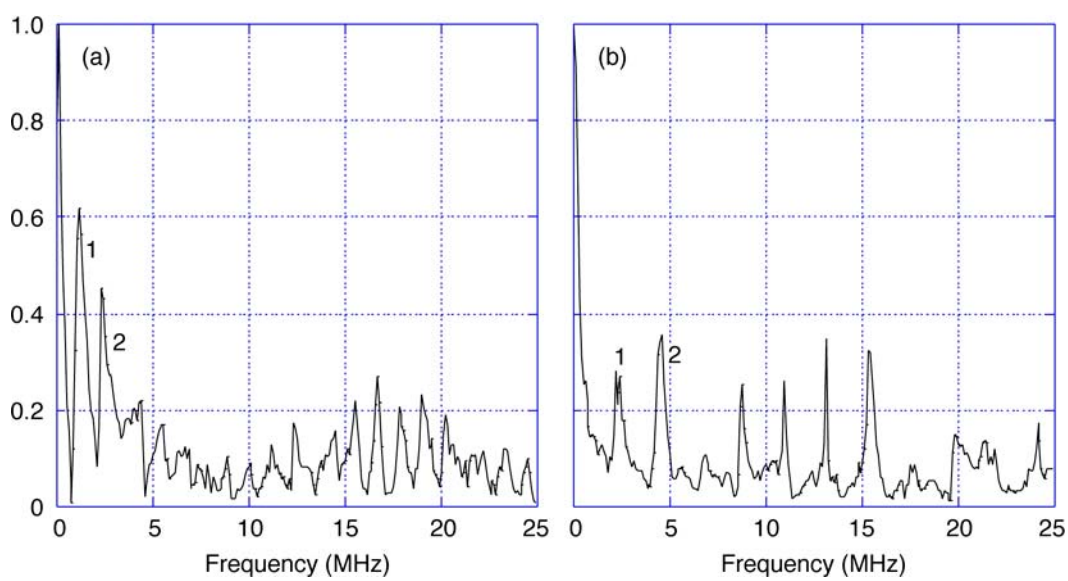

Figure 2. Fourier-based analysis showing the power spectra of individual signals obtained for a satisfactory weld (left-hand side) and a cold weld (right-hand side).

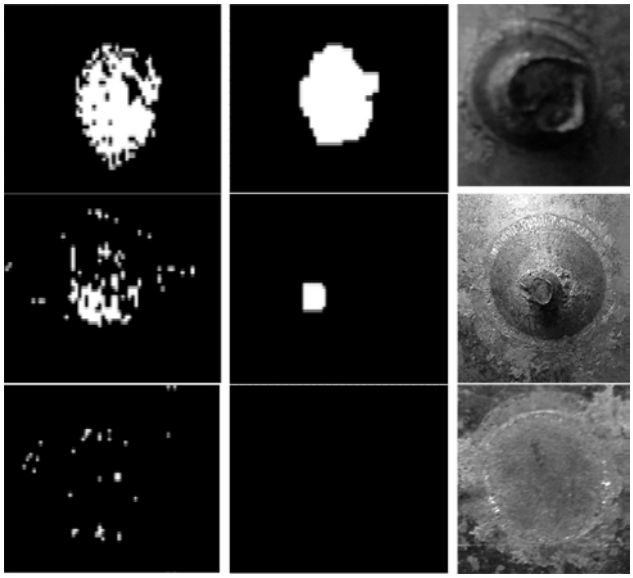

Figure 3. Binary images obtained by the Fourier peak-ratio method are displayed in the left-hand column for a satisfactory weld (top image), an undersized weld (middle image), and a defective weld (bottom image). The same images are displayed in the middle column after applying image-processing algorithms to obtain the contour of the largest zone of contiguous pixels with high transmission of acoustic energy across the interface between the two welded sheets. Photographs of the welds obtained after peeling the joints are shown in the right-hand column.

large area of ultrasonic transmission into the second sheet, the Fourier peak ratio indicates that the areas of high transmission are relatively sparse and dispersed compared to the well-defined and concentrated areas for the satisfactory and undersized welds. At present, the quality of the weld is assumed to be associated with the largest contiguous area of transmission. As described in the following sections, image-processing techniques are used to identify this area and separate it from the smaller transmission zones.

Connected Component Extraction

The first step in the process of determining whether individual pixels should be considered connected to or separate from the zone of interest is based on the operation of connected component extraction. Two points or pixels in a binary image are defined to be connected if a path can be found between them along which the characteristic function remains constant. In the examples presented here, the characteristic function is the value of the binary peak ratio. To implement this approach, it is necessary to define under what conditions two pixels are considered neighbors. For example, for four-point connectivity, only edge-adjacent pixels are considered neighbors (see Table 1). At present we are using eight-point connectivity: in this case, edge-adjacent and corner-adjacent pixels are considered neighbors.

The algorithm identifies and labels each distinct region contained within the image and associates an index to each area according to its size. The largest area is then extracted, and the smaller areas are discarded.

Table 1. Definitions of connectivity

	X
X	X
	X
X	X
O	O
X	X
	X
X	X
	X
Four-point connectivity	Eight-point connectivity

Morphological Filters of Erosion and Dilation

Morphological filters provide a wide range of operators that are commonly used for image processing. All of these operators are based on a few simple mathematical concepts from set theory, and they are particularly useful for the analysis of binary images. Common applications include edge detection, noise removal, image enhancement and image segmentation. The operations applied to the binary peak-ratio images are erosion and dilation. Erosion and dilation filters are used to add or remove pixels from the boundaries of features in order to smooth them or to join or separate portions of features. They are also used to remove isolated pixel noise from the image.

Dilation is the morphological transformation that combines two sets by using vector addition of

set elements. It is defined as the maximum of the sum of a local region of an image and a mask. The shape of the input mask (known as the structuring element, or SE) is generally chosen to emphasize or deemphasize elements in the image. Erosion is the opposite of dilation: erosion is used to smooth the boundaries between dark and light regions.

Ellipse Fitting

As discussed previously, during physical tear-down of automotive components, spot-welded joints are pried apart, and the resulting weld buttons are visually inspected or measured with calipers. To allow the results of the acoustic measurements to be compared to the size of the weld buttons, it is necessary to estimate weld dimensions from the peak-ratio images. Once the largest contiguous area of high acoustic transmission is identified and extracted, an ellipse is fit to the area as a means of estimating the size of the weld button.

Ellipse fitting is one of the classical problems in pattern recognition, and it has been the subject of considerable attention in the past 10 years because of its many applications. The technique described here is based on the method developed by M. Pilu (M. Pilu, A. Fitzgibbon, and R. Fisher "Ellipse-Specific Direct Least-Square Fitting," IEEE International Conference on Image Processing, Lausanne, September 1996).

The conic is represented as the zero set of an implicit second-order polynomial:

$$F(\mathbf{a},\mathbf{x}) = ax^2 + bxy + cy^2 + dx + ey + f \ ,$$

where **a** = [a, b, c, d, e, f] and **x** = [x^2, xy, y^2, x, y]. $F(a,x_i)$ = *dist*. is the "algebraic distance" between a point x_i and the conic $F(\mathbf{a},\mathbf{x}) = 0$. One way of fitting a conic is to minimize the algebraic distance over the set of **N** data points in the least-squares sense, that is:

$$dist. = \arg\min\left[\sum_{i=1}^{N} F\left(a, x_i\right)^2\right] \ .$$

The constraint $b^2 - 4ac = 0$ is imposed to yield elliptical solutions.

For our application, the objective is to find the edges of the largest area of ultrasonic transmission and to fit an ellipse to determine the dimensions of the major and minor axes. A simple gradient is applied to the image that has been processed using the connected-component-extraction algorithm and the morphological filters. Small anomalies in the interior of the image that occur because of small defects or a low signal-to-noise ratio are removed before applying the morphological filters. It is necessary to remove these points before applying the ellipse-fitting algorithm. Not doing so results in a low estimate of the ellipse dimensions. The boundary of the high-transmission zone is determined using the same connected-component-extraction algorithm that was used to extract the largest contiguous area (this algorithm can be improved by using a contour-tracking algorithm). The method is illustrated in Figure 4, which shows the best-fitting ellipse calculated for the processed binary peak-ratio image of a satisfactory weld.

The circumference of the satisfactory weld described above was measured to be 22 mm. The following approximation was used to calculate the circumference of the ellipse estimated using the ellipse-fitting algorithm:

$$P \approx \pi\left[3(a+b) - \sqrt{(3a+b)(a+3b)}\right] \ ,$$

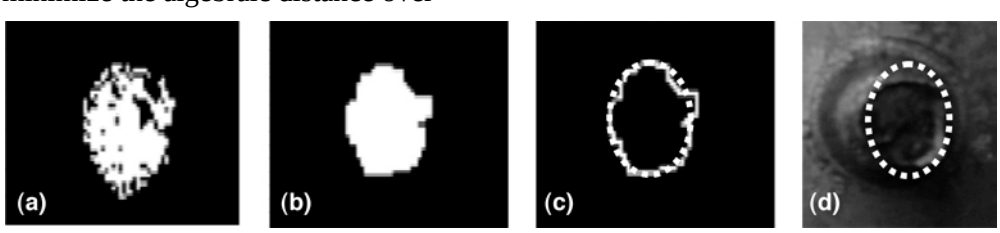

Figure 4. Binary image obtained by the Fourier peak-ratio method for a satisfactory weld (*a*), and the same image after applying image-processing techniques to obtain the contour of the zone of contiguous pixels with high transmission of acoustic energy across the interface between the two welded sheets (*b*). The dotted line in Figure (*c*) shows the ellipse fitted to the contour of the high-transmission zone. In Figure (*d*), the best-fitting ellipse is superposed on a photograph of the weld button obtained by peeling the joint.

where *a* and *b* are half the major and minor axes. The estimated perimeter of the fitted ellipse is 20.4 mm.

Metallography

While there is definitely a relationship between the size of the weld button obtained from peel tests and the size of the actual weld nugget, their dimensions are not exactly the same. To better understand this relationship, we compared the results of our signal-processing algorithms to images of cross sections through welds obtained using metallography. The samples were sectioned, polished, and etched to reveal the grain structure and the dimensions of the weld nugget. The following pictures show cross-sections through a satisfactory weld at different depths in the weld; the nugget is visible in the middle of the welded region where a characteristic dendritic grain structure is visible. The white squares denote the limit of the weld nugget as determined by visual inspection. The right-hand image shows the processed peak-ratio image obtained for this weld; the dotted lines indicate where the cross sections were made. These lines are superposed on the metallographic images to see how the algorithm performs.

Figure 5 shows the results of metallography compared to the output of the signal-processing algorithm for a satisfactory weld. The dotted lines indicate that the dimension of the processed image corresponds to the welded region visible in the metallographic image. Figure 6 shows a misshapen weld, in which there is no nugget formation in the center (see middle image in Figure 6). Although the welding parameters used in this case would normally produce a satisfactory weld, the metallographic images show that the weld nugget is actually C shaped with two separate nuggets. The processed image of the ultrasonic data also shows incomplete nugget formation and a C shape, although the small nugget on the right-hand side is not as clear on the processed peak-ratio image as it is in the metallographic images. This may be an effect of the morphological filters, which may have removed too many pixels during the erosion step. To explore this further, results obtained using erosion masks of different sizes will be compared to both metallographic images and weld buttons obtained from peel tests to determine the optimal mask size.

Probe Housing

A plant-deployable unit requires a housing for the ultrasonic probe that maintains the probe in water, contains a miniature mechanical system that allows linear translation of the probe, and that provides an outer membrane that confines the water column while also providing sufficient acoustic coupling to the part under inspection. Engineering the housing is extremely challenging because minimizing the footprint of the probe assembly is essential to ensure access to welds on complex components. The integrated probe assembly is also being

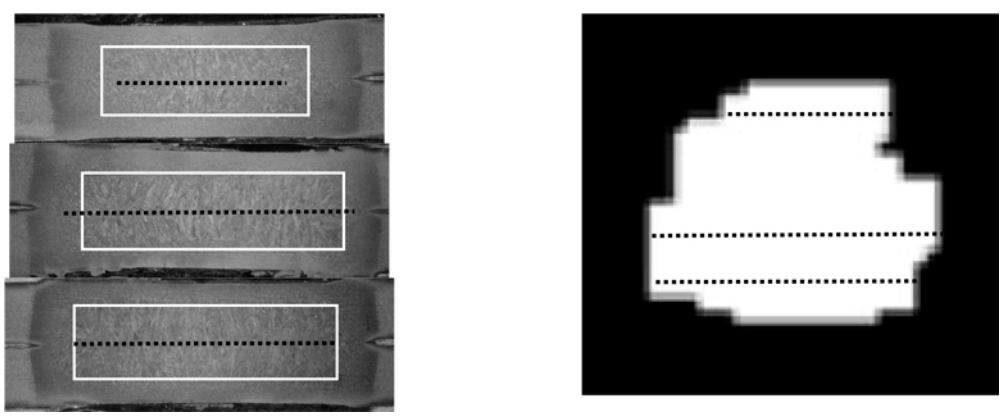

Figure 5. Metallographic images of a satisfactory weld obtained at three different depth levels in the weld (left-hand images) and the processed peak-ratio image obtained for the same weld (right-hand image). The white boxes in the metallographic images outline the boundary of the weld. The dotted lines in the right-hand image indicate the depths where cross sections of the weld were taken. These lines are superposed on the metallographic images to show the correspondence between the estimated weld diameter in the peak-ratio image and the apparent weld nugget in the metallographic images.

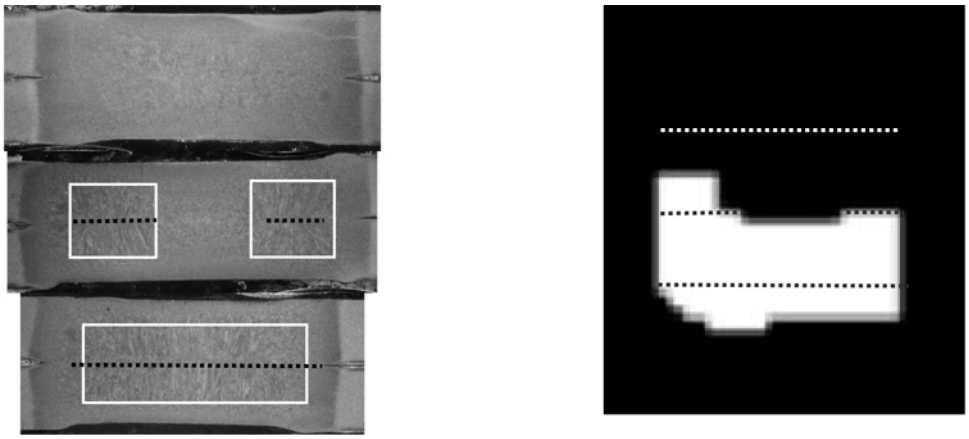

Figure 6. Metallographic images of a misshapen weld at three different depth levels in the weld (left-hand images) and processed peak-ratio image for the same weld (right-hand image). The white boxes in the metallographic images outline the boundary of the weld); note that there is no evidence of weld formation in the top image. The dotted lines in the right-hand image indicate the depths where cross sections of the weld were taken. These lines are superposed on the metallographic images to show the correspondence between the estimated weld diameter in the peak-ratio image and the apparent weld nugget in the metallographic images.

designed to allow for easy replacement of parts and troubleshooting.

For the current design, displayed in Figure 7, the overall footprint of the probe unit is 26 by 44 mm. Although the phased-array probe allows electronic scanning in one direction, mechanical scanning in the opposite direction is required to obtain 2-D images of the weld. A miniature mechanical system has been designed that allows a probe travel length of 16 mm. The small motor that will be used to drive the system has a nominal speed of 4800 rpm and is coupled to a 1:16 gearbox. The drive assembly is separated from the water column containing the probe by two slider plates and O-rings that form a watertight seal. The optimal material for the outer membrane is under investigation. Plant trials will be conducted to ensure that the integrated probe housing is rugged enough for use in a production facility.

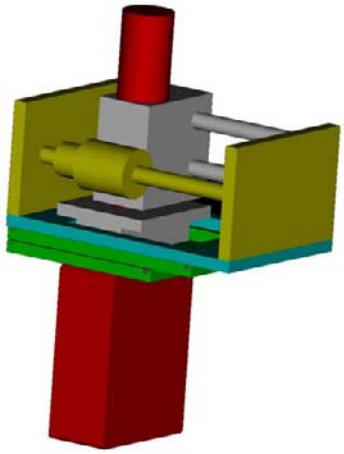

Figure 7. Mechanical drawing of the housing designed for the ultrasonic probe. The upper compartment houses the miniature mechanical system that will be used for linear translation of the probe. The lower compartment is a water chamber that contains the phased-array probe.

Conclusions

Work to date demonstrates that characterization of spot welds is possible using ultrasonic phased-array technology. Phased arrays have several advantages over mono-probes, including the ability to perform high-resolution scans that greatly increase detection and characterization capabilities. They are also less sensitive to probe placement and provide the ability to inspect a wide array of welds with a single probe. The remaining research challenge is to develop, test, and refine the techniques so that they are suitable for large-scale production facilities. Toward this end, a probe housing has been designed that will allow the system to be used in manufacturing plants. Work under way will also yield integrated real-time diagnostic tools that

operate at sufficient speed for assembly-line use. The remaining challenges include determination of resolution limits and the best diagnostic parameters for specific applications, and demonstration of robustness, accuracy, and cost-effectiveness under realistic operating conditions.

Presentations

1. C. Dasch, General Motors Corporation, "Strategic Review of Nondestructive Testing Technology," USCAR Materials Tech Team, July 21, 2004, Southfield, Michigan.
2. F. Reverdy, Lawrence Berkeley National Laboratory, "Inspection of Spot Welds Using a Portable Ultrasonic Phased-Array System," 31st Annual Review of Progress in Quantitative Nondestructive Evaluation, July 25–30, 2004, Colorado School of Mines, Golden, Colorado.
3. D. Hopkins, Lawrence Berkeley National Laboratory, "Development of an Ultrasonic Phased-Array System for Nondestructive Evaluation of Resistance Spot Welds," United States Automotive Materials Partnership (USAMP)—Automotive Materials Division (AMD) Offsite, December 2, 2004, Southfield, Michigan.

O. Technical Cost Modeling

Principal Investigator: Sujit Das
National Transportation Research Center
2360 Cherahala Boulevard
Knoxville, TN 37932-6472
(865) 946-1222; fax: (865) 946-1314; e-mail: dass@ornl.gov

Technology Area Development Manager: Joseph A. Carpenter
(202) 586-1022; fax: (202) 586-1600; e-mail: joseph.carpenter@ee.doe.gov
Field Technical Manager: Philip S. Sklad
(865) 574-5069; fax: (865) 576-4963; e-mail: skladps@ornl.gov

Contractor: Oak Ridge National Laboratory
Contract No.: DE-AC05-00OR22725

Objectives

- Address the economic viability of new and existing lightweight materials technologies.
- Develop technical cost models to estimate the cost of lightweight materials technologies.

Approach

- Address the economic viability of lightweight materials technologies supported by the ALM.
- Use cost modeling to estimate specific technology improvements and major cost drivers that are detrimental to the economic viability of these new technologies.
- Derive cost estimates based on a fair representation of the technical and economic parameters of each process step.
- Provide technical cost models and/or evaluations of the "realism" of cost projections of lightweight materials projects under consideration for ALM funding.
- Examine technical cost models of lightweight materials technologies that include (but are not limited to) aluminum sheet; carbon fiber precursor and precursor processing methods; fiber-reinforced polymer composites; and methods of producing primary aluminum, magnesium, and titanium and magnesium alloys with adequate high-temperature properties for powertrain applications.

Accomplishments

- Assessed comparative cost of alternative manufacturing technologies for the composite-intensive body-in-white (BIW) structures.
- Assessed lightweighting opportunities for fuel cell vehicles.
- Assessed carbon-fiber-reinforced polymer (CFRP) matrix composites potential for the automotive industry.

Future Direction

- Estimate the impacts of the ALM for the fiscal years FY 2000–2004 and also aid in the formulation of mid-term and long-term goals for the ALM.
- Continue individual project-level cost modeling to identify specific technology improvements and major cost drivers that are detrimental to the economic viability of these technologies.

Comparative Cost Assessment of Alternative Carbon-Fiber-Reinforced Composite BIW Manufacturing Technologies

This task focused on the relative cost-effectiveness of competing carbon-fiber-reinforced, polymer (CFRP) composite, BIW manufacturing technologies. The part under consideration was an upper dash panel weighing about 1.9 kg. Of a total of six competing manufacturing technologies under consideration, three were based on the compression molding and long fiber injection (LFI) processes. The process by Krauss-Maffei was selected as the LFI process. Two carbon-fiber sheet molding compound (SMC) materials for the compression molding process considered were Quantum composites and HexMC by Hexcel Corporation. The former carbon-fiber, sheet molding, SMC material has recently been used in Dodge Viper for the windshield surround, inner door panels, and fender support system applications. Of the three remaining manufacturing technologies, fabric preforms using CompForm technology and prepregs besides the programmable powder preform process (P4)/structural reaction injection molding (SRIM) process were considered.

With the limited data available directly from the suppliers where most of these technologies are still in the development stage, LFI appears to be the most cost-effective technology among the six competing technologies considered here. As shown in Figure 1, the costs of parts produced by the six technologies range from $28.12 to $129.18, and the cost-effectiveness of various technologies, in decreasing order, is as follows: LFI, P4/SRIM, Quantum, CompForm, HexMC, and prepreg. The high scrap rate (i.e., 10–30%) of material that costs $20/lb causes HexMC and prepreg technologies to be the least cost-effective among the technologies considered here. The part cost per pound ranges from $6.45 to $35.29, considerably higher than the weight savings premium of $1–$4/lb accepted by the industry. Material dominates the overall part cost distribution in all cases, followed by labor, capital,

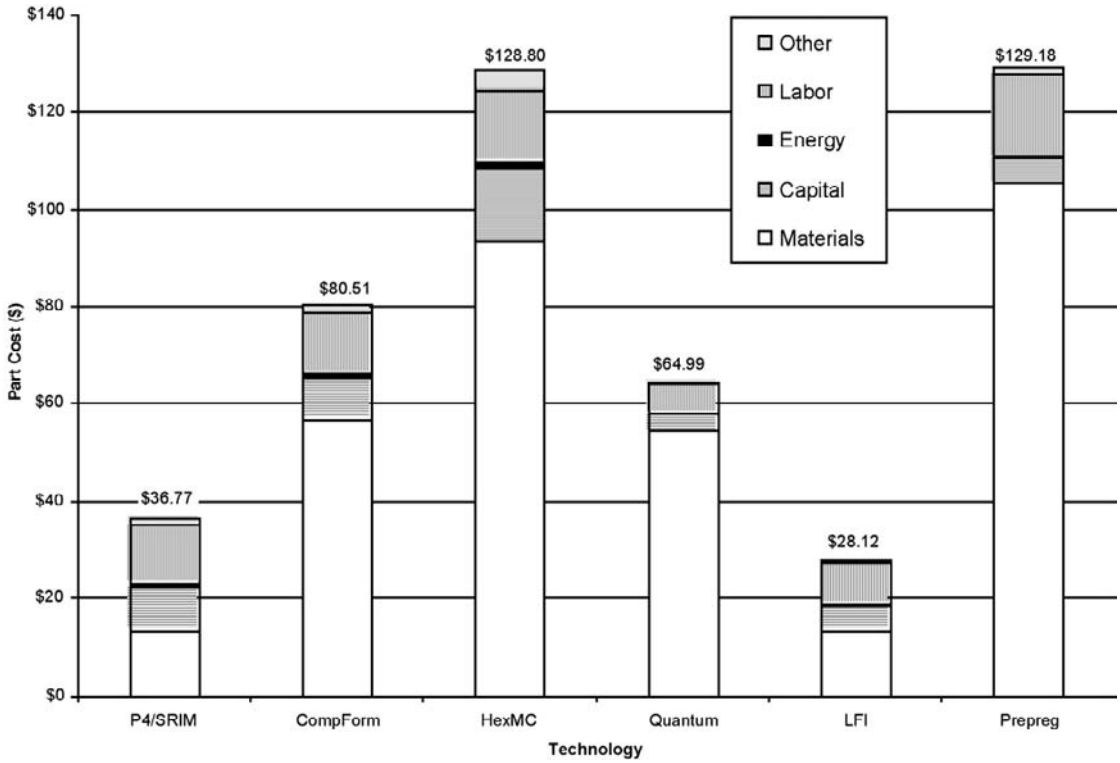

Figure 1. Baseline upper dash panel cost distribution.

and energy, where the last component is comparatively less significant to overall part cost. The share of material to part cost was found to be in the range of 37% to 84%, where the lower- and upper-end values correspond to P4/SRIM and Quantum technologies, respectively. Capital cost is greatest for HexMC technology due its 13-min-long molding cycle and the high molding pressure used. The labor costs of P4/SRIM, CompForm, HexMC, and prepreg technologies are higher than the other two technologies and similar to one another because of these technologies' higher cycle times at the charge preparation/preforming step.

It appears that significant technology enhancements, beyond drastic carbon fiber material cost reductions, will be necessary for the four non-chopped carbon fiber technologies to be cost-effective. For example, LFI's automated single-step operation, low molding pressure, and chopped carbon fiber use cause it to be most the cost-effective technology. Even with significant increases in major baseline parameter values, this technology was still found to be economically superior to five other technologies. With its capital costs higher than LFI's and its performing cycle time, P4/SRIM is the second most cost-effective technology. Quantum's lower cycle time gives it the potential to be competitive, but it would require a significant reduction in carbon fiber material cost. Quantum's part cost is estimated to decrease by $4.20 per $1/lb decline in carbon fiber material cost. The main drawback to the CompForm technology is its high preforming cost—higher than P4—due to its higher fabric cost and preform scrap rate. A 44% reduction in carbon fabric cost can lower part cost by 30% using this technology. High material cost, charge preparation scrap rate, and molding cycle time are some of the potential drawbacks of HexMC technology. Currently under development are polyester-based HexMC materials requiring no staging and a significant lower molding cycle time of 1.5 min, which will likely improve its cost-effectiveness. Advantages of low-cost press molding of prepregs can only be cost-effective with significant reductions in prepreg cost and charge preparation scrap rate. The use of cheaper, unidirectional carbon material of more than 24K will significantly lower the prepreg cost.

Lightweighting Opportunities for Fuel Cell Vehicles

This task examined the lightweighting opportunities for midsize passenger, direct hydrogen, fuel cell vehicles to determine whether this would facilitate the early commercialization of fuel cell vehicles. The current fuel cell powertrain is heavy and expensive, so it is interesting to examine whether at the expense of lightweight BIW materials alone, the fuel cell vehicle penetration rate can be enhanced. The commercial viability of fuel cell vehicles is examined in the context of several advanced lightweight BIW material options [i.e., ultra light steel autobody (ULSAB), stainless steel spaceframe, aluminum unibody, aluminum spaceframe, glass fiber reinforced polymer composites, and CFRP composites] alone, as well as in combination with improvements in the fuel cell powertrain. A detailed 35+ vehicle components level automotive system cost model was used to estimate the lightweighting opportunities for fuel cell vehicles.

A midsize direct hydrogen fuel cell vehicle cost is estimated to be 3.88 times higher than the conventional vehicle. A heavier powertrain in fuel cell vehicles causes an increase in the body subsystem weight by 22% and contributes to 3.34-fold increase in the vehicle cost. It is estimated that the weight and cost of current fuel cell vehicles need to be reduced by 41% and 74%, respectively, for the vehicles to be competitive with the conventional vehicle today. Several lightweight BIW materials not in widespread use today have vehicle-weight-reduction potential in the range of 4–17%, considerably less than the desired goal. The lower- and upper-end of this weight reduction range correspond to ULSAB and CFRP BIW material, respectively. Even CFRP, having the greatest weight savings potential, will reduce vehicle costs only by 11%, far less than the 74% cost reduction needed to achieve commercial viability.

As one would expect, improvements in fuel cell parameters such as specific power and cost would have greater impacts than lightweight materials. Alone, a reduction in fuel cell cost by 78% ($200/kW today vs $45/kW 2010 DOE target), would lower the current cost of fuel cell vehicles by 57%, whereas a 60% BIW weight savings with

CFRP would lower vehicle cost by 12%. Only a substantial vehicle weight reduction can be achieved with the improvements in fuel cell specific power. A 40% improvement in fuel cell specific power is necessary to achieve the 2010 DOE target, but this level of improvement will result in vehicle weight and cost reductions estimated to be 24% and 17%, respectively. Although lightweight materials alone may not be able to achieve the desired vehicle weight and cost goals, they are definitely anticipated to aid in the early commercialization of fuel cell vehicles by imposing less restrictive requirements in fuel cell improvements. For example, for a 30% reduction in vehicle cost, necessary fuel cell cost improvements can be reduced by 3.5% and 10% with the use of ULSAB and CFRP BIW materials, respectively. Impacts of lightweight materials were significantly higher in the case of fuel cell specific power because both are directly related to weight. For example, for a 15% reduction in vehicle cost, necessary fuel cell specific power improvements can be reduced by 7.6% and 24% with the use of ULSAB and CFRP BIW materials, respectively.

Vehicle weight reduction will definitely help but alone may not be sufficient for early commercialization of fuel cell vehicles. The role of lightweighting for fuel cell vehicles is anticipated to be at least very similar to that observed for conventional vehicles in maintaining weights despite the introduction of various weight-adding vehicle technologies during the past two decades. The research and development in vehicle lightweighting will be more critical for fuel cell vehicles—extending well beyond the powertrain components—because vehicle weight and cost challenges pose a serious hurdle for the commercialization of fuel cell vehicles today.

Potential of Automotive Carbon Fiber Reinforced Polymer Composites

CFRP composites, with weight reduction potential of 50–70% and a considerably higher strength-to-weight ratio compared to conventional steel, provide a tremendous potential in automotive applications. To date, the use of this material has been limited to upper-end, high-performance, price-premium, niche vehicles limited to a production volume of less than a thousand per year in most applications. Several concurrent research and development projects are currently under way, but it is not clear when, or whether, this material, will find widespread use in commercial automotive applications. Manufacturing cost is one of the major concerns for original equipment manufacturers (OEMs) considering any material substitution, and this, along with the material's ability to meet long-term technical requirements and its manufacture for the automotive environment, is cited as the most significant challenge for its automotive application today. Consequently, this task examined the existing cost studies of CFRP and explored the factors associated with the high cost of material to determine under what circumstances and at what future point this material may become suitable to be used widely in automotive applications.

Most cost studies to date have focused on the BIW application at large-scale production volumes, comparable to conventional steel, where part consolidation is maximized to make the part at least cost. These studies confirm that cost-effectiveness of BIW can be achieved at a production volume less than 100,000 parts/year, and material cost and cycle times are detrimental to the economic viability of CFRP today. High material cost is the main factor at a larger production volume, and carbon fiber is the main contributor to material cost. Lowering carbon fiber cost would not only improve CFRP competitiveness in terms of per-part cost at a given annual production volume, but it would also increase the annual production volume range at which it stays competitive. At a production volume range of less than 125,000 parts/year, carbon fiber price in the range of $3–$5/lb will be sufficient to reach cost effectiveness. ALM work to develop new carbon fiber manufacturing technologies suggests that these price targets are achievable. Carbon fiber prices of less than $3/lb, a requirement indicated by several studies, may not be necessary to achieve the CFRP cost-effectiveness at a relatively large production volume if optimized designs offering a significantly higher level of weight reduction can be achieved.

Most fabrication technologies for CFRP are anticipated to be similar to those used for glass-fiber-reinforced polymer composites (GFRP), but they are yet to be demonstrated. Most of these technologies are not effective at scaled-up production volumes with high cycle times, posing one of the major barriers to their scale-up and, thus, cost-effectiveness. A recent ORNL cost assessment of six competing high-volume processing methods (as discussed above) indicates a manufacturing cost range of $6.45 to $35.39/lb, significantly higher than

the $2.50/lb needed to be in contention with aluminum in certain automotive applications. The popularity of GFRP SMCs has been recently demonstrated for CFRP as well, but these finished carbon-fiber-based materials technologies appear to be more expensive than direct-chopped fiber technologies and do not provide any major subsequent processing benefits. A recent study has rightly pointed out that a significant reduction in process costs that is achieved through a high degree of automation at all stages of manufacturing and that reduces the number of intermediate products in the process chain, can do much more to change the current viability of CFRP than a decrease in carbon fiber prices. The key to bringing CFRP into automotive usage is to advance today's enabling process technologies and improve the vertically integrated supplier structure.

Due to higher weight reduction potential in assembled BIWs, CFRP is competitive at significantly higher production levels when considered system-wide than when considered in part-by-part substitution. Because it is relatively less risky, the part-by-part substitution is likely to continue in the foreseeable future, and the industry will gain experience needed to feel comfortable with this material. It will be at least a decade or more before one will find CFRP in any large-scale commercialization of automotive BIW structures. However, the focus of past cost studies on the viability of CFRP structures at large production volumes may be contrary to the latest trends of platform sharing and low-production-volume vehicle models. Of all vehicle models manufactured in 2003, 72% (or 2.1 million units) of car models and 69% (2 million units) of truck models were in the production volume range of less than 100,000 vehicles/year. These trends have allowed the mixing of lower-volume "differentiating" technologies with higher-volume "standardized" technologies to increase market attractiveness and lower costs. CFRP is definitely a promising candidate for differentiating standardized vehicle platforms.

Consideration of life-cycle costs that appropriately assess the cost-effectiveness of lightweight materials is not prevalent in the automobile industry's materials selection. It is, nevertheless, imperative to consider in this analysis the parameters that affect vehicle operation stage costs, for example, fuel economy improvements and fuel costs due to vehicle lightweighting. The sensitivity analysis of major parameters indicates that on a life-cycle cost basis, the cost-effectiveness of CFRP at a higher volume of 250,000 parts/year can be attained within the first vehicle life in all cases, unlike on the basis of manufacturing cost alone. As shown in Figure 2, a fuel price increase to $3/gal (100% increase from the base price) will allow the life-cycle cost equivalence to conventional BIW steel achieved at about 7 years; however, the fuel price as high as $4.50/gal (about 200% increase from the today's price) would not provide the cost-effectiveness of CFRP on the basis of manufacturing cost alone. Lower carbon fiber price of $3.3/kg or CFRP manufacturing cost decline by 25% at a large production volume will facilitate in achieving the life-cycle cost equivalence to steel within the first 10 years of vehicle life. The weight reduction factor of CFRP is critical, a lower 55% BIW weight reduction potential than optimized 67% weight reduction potential design at a production volume of 100,000 parts/year would move the cost-effectiveness from the first year of vehicle life to beyond 12 years of vehicle operation. Life-cycle cost consideration would allow not only to determine when the life-cycle cost equivalence can be achieved but also extends the annual production volume range of the CFRP cost-effectiveness. Whether material suppliers, component suppliers, and automakers must respond to life-cycle cost issues remains to be determined. Ultimately, their

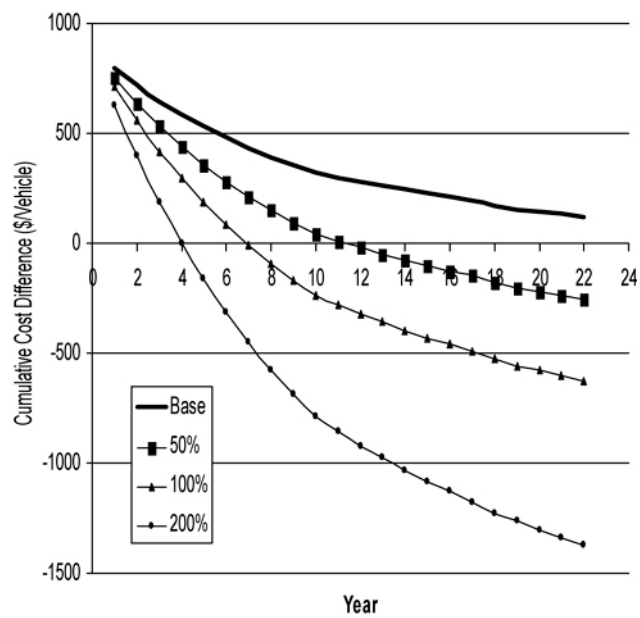

Figure 2. A comparison of CFRP BIW cumulative life cycle cost impacts of different fuel price scenarios.

response will depend on their ability to benefit from these savings combined with consumer demand and the legislative environment.

It is unlikely that the large-scale commercialization of automotive CFRP parts will happen any time in the near future due to high material cost and a lack of high-volume processing technologies; challenges that the industry faces comparatively are more for the higher production volume range. Until then the product differentiation aspect of the platform-sharing will promote the CFRP material substitution in niche, low-volume, premium performance vehicles. The performance market segment of the aftermarket industry continues to grow by providing the customization preference to the consumers to compete with the entrance of so many newer vehicles equipped with modern engine and handling technology into this segment. The low-production-volume market size appears to be large enough to maintain the viability of the CFRP industry during the initial market penetration phase. There are several other competing lightweight materials such as GFRP and aluminum, including high-strength steels with the industry experience comparatively high on the learning curve, which would pose obstacles in the large-scale penetration of CFRP automotive applications. Unless there is a demand for lower vehicle weight with higher strength-to-weight ratio precipitated by events such as an extremely high fuel price increase, high fuel efficiency and low emissions standards, and alternative powerplant technologies (e.g., fuel cells) requiring a considerable reevaluation of complementary lightweight bodies, it would be difficult to justify CFRP purely on the economic perspective alone. This material could produce a major change in automotive engineering in the future, but major sociopolitical shifts will be needed to bring about a carbon fiber-based synergistic change.

Publications

1. "Magnesium for Automotive Applications: Primary Production Cost Assessment," *Journal of Metals* (November 2003).

2. "Life Cycle Impacts of Automotive Liftgate Inner," accepted for publication in *Resources, Conservation and Recycling*.

8. HIGH-STRENGTH STEELS

A. Evaluations of the Effects of Manufacturing Processes and In-Service Temperature Variations on the Properties of Transformation-Induced Plasticity (TRIP) Steels

Principal Investigator: Moe Khaleel
Pacific Northwest National Laboratory
P.O. Box 999/K7-36, Richland, WA 99352
(509) 375-2438; fax: (509) 375-6605; e-mail: moe.khaleel@pnl.gov

PNNL Contract Manager: Mark T. Smith
Pacific Northwest National Laboratory
P.O. Box 999/K2-03, Richland, WA 99352
(509) 375-4478; fax: (509) 375-4448; e-mail: mark.smith@pnl.gov

Technology Area Development Manager: Joseph A. Carpenter
(202) 586-1022; fax: (202) 586-1600; e-mail: joseph.carpenter@ee.doe.gov
Field Technical Manager: Philip S. Sklad
(865) 574-5069; fax: (865) 576-4963; e-mail: skladps@ornl.gov

---

Contractor: Pacific Northwest National Laboratory
Contract No.: DE-AC06-76RL01830

Objective

- Develop an understanding of the effects of typical automotive manufacturing processes, such as welding and forming, on the retained properties of advanced transformation-induced plasticity (TRIP) steels.
- Evaluate the effects that in-service temperature variations have on the retained properties and energy absorption characteristics of TRIP steels.
- Compare the range of TRIP steel grades to determine their mechanical property sensitivity to thermal histories and manufacturing conditions.

Approach

- Develop a mechanical property vs in-service temperature relationship for the available grades of TRIP steels to determine their suitable vehicle applications and allowable thermal processing histories for manufacturing and vehicle performance. A temperatures range of –40°F to 200°F will be considered. Room temperature mechanical properties will be obtained from steel suppliers.
- Determine the effects of welding and forming on the retained mechanical properties of different grades of TRIP steels; tensile samples will be cut out from formed parts and welded parts. Tensile tests will then be done at three different rates to determine the effects of forming and welding on the static and dynamic strength of TRIP steel.
- Develop a database for the static, dynamic, fatigue, and corrosion behavior of dissimilar material joints, consisting of different material selections and different joining techniques.

Accomplishments

- Held project kick-off meetings with original equipment manufacturer (OEM) participants.
- Identified TRIP 800 as the initial material grades to be studied.
- Identified three TRIP steel suppliers from the United States, Europe, and Japan.
- Started materials acquisition processes from three material suppliers.
- Started experimental evaluation of 304 stainless steel as high-alloy TRIP steel.
- Began base material chemistry composition analysis on 304 stainless steel.
- Began Marciniak cup-stretch forming test on 304 stainless steel.

Future Direction

- Complete current tests on 304 stainless steel.
- Complete temperature- and prestrain-dependent material evaluations for all three populations of low-alloy TRIP steels.
- Transfer material performance database to U.S. Automotive Materials Partnership (USAMP) and OEM participants.

Introduction

This project is a collaborative effort between the Department of Energy (DOE), Pacific Northwest National Laboratory, and the U.S. Automotive Materials Partnership (USAMP) of the U.S. Council for Automotive Research (USCAR). The work started in July 2004.

Because of the excellent strength and formability of transformation-induced plasticity (TRIP) steels, they offer the potential to reduce vehicle weight and improve vehicle crash performance. The presence of retained austenite in TRIP steels enhances ductility at a particular strength level by means of TRIP. Because the enhanced ductility is the result of a phase transformation, thermal cycling, forming, and welding could be expected to impact the final microstructure and, thus, final material properties. Although the combination of strength and energy-absorbing capabilities of TRIP steels make them attractive, their sensitivity to thermal processing and in-service temperature variations has not been sufficiently established. To introduce TRIP steels into critical areas of the body structure (such as crash energy management areas), the automotive original equipment manufacturers (OEMs) must know what the retained properties of the material are after exposure to a range of manufacturing and in-service conditions.

This project will examine key aspects of the manufacturing process that TRIP steels would be exposed to, and it will systematically evaluate how the forming and thermal histories affect final strength and ductility of the material. The project will also evaluate in-service temperature variations, such as under-hood and hot/cold cyclic conditions, to determine whether these conditions influence final strength, ductility, and energy absorption characteristics of several available TRIP steel grades. As part of the manufacturing thermal environment evaluations, stamping process thermal histories will be included in the studies. As part of the in-service conditions, different loading rates will also be included. At the completion of the study, a thermal history/materials property relationship will be established over a full range of expected thermal histories and selected loading rates. Establishing these relationships will then allow OEM designers to select TRIP steels for proper vehicle applications and to specify manufacturing process conditions that yield reliable final material property levels.

Project Deliverables

The project deliverables include the following:

- Mechanical properties, that is, strength and ductility, vs in-service temperature relationship for the selected grades of TRIP steel to

determine their suitable vehicle applications and allowable thermal processing histories for manufacturing and vehicle performance. A temperatures range of –40°F to 200°F will be considered.

- Effects of prestraining on the retained mechanical properties of different grades of TRIP steels. Tensile samples will be cut out from prestrained sheets. Tensile tests will then be done at three different temperatures to determine the effects of forming on the static strength of TRIP steel under different temperatures.
- Formability of TRIP steel using LDH and Marciniak type forming tests under different stamping temperatures.
- Axial crush and energy absorption characteristics of TRIP steel hexagonal columns under different loading rates.

Technical Approach

We will follow the standard American Society for Testing and Materials (ASTM) tensile-test procedures to conduct our materials characterization at different temperatures. Tensile samples will be cut from the steel sheet stock along the rolling directions. The following procedures will be followed to ensure the testing temperature:

Heating. Heating the tensile specimens will be done in a furnace that encompasses the entire specimen and grips. This furnace has a maximum temperature output of 450°F, so the required test temperature of 200°F can be set and reached easily by the controller for the furnace. This furnace is an air-circulating furnace. Thermocouples will be placed on the bottom and top grip (and on the specimen if necessary) to monitor the temperature. Once 200°F is reached, a soak time of 5 min will be needed before testing can begin. Temperature will be maintained throughout the test. Temperature will be recorded using an analog output temperature indicator, and it will be taken by the computer that is monitoring other test data such as load, displacement, and time.

Cooling. Cooling for the tensile specimens will be done in an enclosure that encompasses the entire specimen and grips. This enclosure will be cooled with liquid nitrogen that will be circulated by a fan to promote the even distribution of temperature. Thermocouples will be placed on the bottom and top grip (and on the specimen if necessary) to monitor the temperature. Once –40°F is reached, a soak time of 5 min will be needed before testing can begin. Temperature will be maintained throughout the test. Temperature will be recorded using an analog output temperature indicator, and it will be taken by the computer that is monitoring other test data such as load, displacement, and time.

Recent Accomplishments

- Held project kick-off meetings with OEM participants.
- Identified TRIP 800 as the initial material grades to be studied.
- Identified three TRIP steel suppliers from the United States, Europe, and Japan.
- Started material acquisition processes from three material suppliers.
- Started experimental evaluation of 304 stainless steel as high-alloy TRIP steel.
- Began base material chemistry composition analysis on 304 stainless steel.
- Began Marciniak cup-stretch forming test on 304 stainless steel.

Conclusions

- Material acquisitions of TRIP steel continue to be very difficult.
- TRIP steels are performance-based steels; therefore, different suppliers have different chemistries and surface coatings on the same steel grade. OEMs need to pay particular attention to the tolerance of yield strength and ultimate strength from the steel supplier. In general, the common perception that “the higher the strength, the better” is not necessarily true.

B. High-Strength Steel Stamping Project

Principal Investigator: Jack Noel
Auto/Steel Partnership
2000 Town Center, Suite 320, Southfield, MI 48075-1123
(248) 945-4778; fax: (248) 356-8511; e-mail: JNoel@a-sp.org

James Fekete, Co-chairman
General Motors Corp.—Metal Fabricating Division
2000 Centerpoint Parkway, Pontiac, MI 48341
(248) 753-5324; fax: (248) 753-4810; e-mail: Jim.Fekete@gm.com

Changqing Du, Co-chairman
DaimlerChrysler Corporation
800 Chrysler Drive, Auburn Hills, MI 48326
(248) 576-5197; fax: (248) 576-7910; e-mail: CD4@DCX.com

Technology Area Development Manager: Joseph A. Carpenter
(202) 586-1022; fax: (202) 586-1600; e-mail: joseph.carpenter@ee.doe.gov
Field Technical Manager: Philip S. Sklad
(865) 574-5069; fax: (865) 576-4963; e-mail: skladps@ornl.gov

---

Contractor: U.S. Automotive Materials Partnership
Contract No.: FC26-02OR22910

Objectives

- Determine how to accurately predict and/or control the amount of springback and other deviations from the desired stamping geometry for parts made from high-strength steel (HSS) and advanced high-strength steel (AHSS) prior to the construction of the production tooling.
- Develop part design and manufacturing process guidelines that can be recommended to automotive design and manufacturing engineers for the purpose of reducing springback and other part distortions common to the manufacture of higher strength steel stampings.

Approach

- Improve HSS stamping springback predictability through more accurate applications of finite-element analysis (FEA). This will require that we achieve a better understanding of residual stresses resulting from each combination of AHSS material, part geometry and deformation process.
- Achieve HSS stamping springback control by developing knowledge of part design geometries that reduce flange springback and die processes that control springback. Several different types of dies have been constructed or are on loan to the Auto/Steel Partnership for the stamping process development.

Accomplishments

- Identified processes to control springback, sidewall curl, and panel twist.
- Modified our research tooling for stretch-forming processes of AHSS automotive body structural components to neutralize the residual stresses that cause springback and sidewall curl. Good results have been shown for HSLA 350 and DP 600. General Motors and DaimlerChrysler representatives state that this information is now being used in their AHSS manufacturing process planning.

- Designed and built a new multiprocess master die (Figure 1) that is capable of producing a variety of part shapes and processes by adding subdies for specific part shapes. The master die has a high-pressure hydraulic cushion that can be programmed for various process control features (Figure 2). Two new subdies have been designed and constructed to provide data on AHSS stamping characteristics. These data will be used to develop additional AHSS design and manufacturing guidelines.

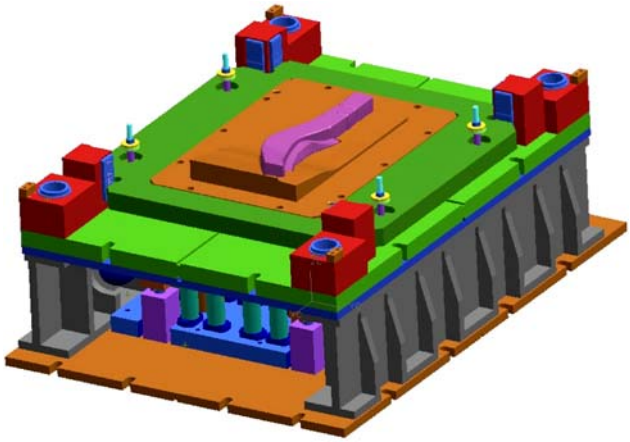

Figure 1. Multiprocess master die.

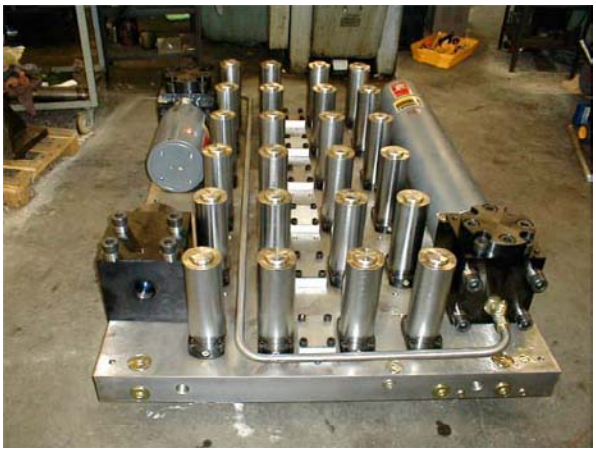

Figure 2. High-pressure hydraulic press cushion.

Future Direction

- Begin stamping experiments with our new multiprocess master die and programmable hydraulic cushion. This die is designed as a master die set and pressure system that will accept subdie inserts to produce a variety of AHSS structural parts and/or stamping processes.
- Focus on stamping AHSS thin gauge automotive structural members to replace the thicker gauge components in the body structure. Future possibilities for weight reduction also exist in the thinner gauge large panels, such as doors and fenders.

Introduction

Due to the mechanical properties of high-strength steels (HSSs), the springback after forming and the geometric dimensional control of the stamped parts has been a critical issue in stamping tool construction and in stamping production. Because the actual dimensions of HSS stampings off the tooling are unpredictable with current tools and

technology, the average die face remachining may be four to six times normal and result in 2 to 3 months of tryout time.

Computer simulation technology has been widely applied in the stamping industry and has been recognized as a common virtual stamping tool to identify formability issues and evaluate solutions before the actual stamping dies are made. Although computer simulation provides accurate prediction for splits and buckles, experience has shown that computer simulation data have not been reliable in predicting the amounts and modes of the springback, twist, or side-wall curl.

Springback and other distortions in HSS stampings may be controlled by innovative stamping processes that neutralize residual stresses resulting from the metal deformation. These processes will involve some type of stretch forming to give the stamping "shape set." The work of this project team is to determine the most effective means of researching and applying these "shape set" processes. Computer simulation is also being analyzed to improve the data input for accurate formability prediction.

In addition to the formability issues, there are other concerns regarding energy requirements and stamping press capabilities when forming higher strength sheet steels. Increased mechanical press flywheel energy and cushion pressures may be required to effectively work with AHSS. This project team will also focus its attention on manufacturing methods that minimize the energy requirements for working with the higher strength materials.

Deliverables

1. Improve the capability of computer simulation for predicting stamped part deviations, such as springback, from nominal.
2. Develop part design and manufacturing process guidelines to control or neutralize residual stresses that cause dimensional deviations in the stampings of AHSS.
3. Determine energy requirements and safe operating parameters to avoid damage to stamping presses when producing AHSS stampings.

Progress Toward Meeting Deliverables

1. All experimental stamped panels will be laser scanned for dimensional data. These data are then subject to data analysis, and the results for each series of experiments are provided in a written report to computer simulation programmers at the automotive companies. This information is then used to update their finite-element analysis (FEA) programs for AHSS.
2. Part design features and manufacturing processes that minimize dimensional variation are recorded and will be included in the revised High Strength Steel Stamping Design Manual. Part shapes that contribute to forming difficulties and dimensional variation will be identified for the product engineer's consideration.
3. Stamping presses used for these experiments are being instrumented to provide data on total tonnage requirements at impact and at bottom dead center. The impact loads are a major concern for press damage and flywheel energy dissipation. Press tonnage monitors will be used for recording the total tonnage requirements. Press signature analysis equipment will be used to monitor the impact loads.

Conclusions

The project team is currently proceeding with final tryout of the new stamping research dies and a high-pressure hydraulic cushion system. Installation and calibration of the press monitoring instrumentation is near completion, and the acquisition of sheet steels in the gauges and grades necessary to complete the design of experiments is under way. It is expected that collected data from these experiments will greatly enhance our knowledge for working with these materials and contribute to the increased application of lighter weight AHSS in future automotive products.

C. Strain Rate Characterization

Project Manager: Pat V. Villano
Auto/Steel Partnership
2000 Town Center Drive, Suite #320
Southfield, MI 48075-1123
(248) 945-4780; fax: (248) 356-8511; e-mail: pvillano@a-sp.org

Chairman: David J. Meuleman
General Motors Corporation-Metal Fabricating Division
2000 Centerpoint Parkway
Pontiac, MI 48341
MC (483) 520-266
(248) 753-5334; fax: (248) 753-4810; e-mail: david.meuleman@gm.com

Lead Scientist: Srdjan Simunovic
Oak Ridge National Laboratory
Oak Ridge, TN 37831-6359
(865) 241-3863; fax: (865) 574-7463; e-mail: simunovics@ornl.gov

Technology Area Development Manager: Joseph A. Carpenter
(202) 586-1022; fax: (202) 586-1600; e-mail: Joseph.Carpenter@ee.doe.gov
Field Technical Manager: Philip S. Sklad
(865) 574-5069; fax: (865) 576-4963; e-mail: skladps@ornl.gov

Contractor: U.S. Automotive Materials Partnership
Contract No.: FC26-02OR22910

Contractor: Oak Ridge National Laboratory
Contract No.: DE-AC05-00OR22725

Objectives

- Develop new experimental setups for characterization of crashworthiness and strain-rate sensitivity of both high-strength steels (HSSs) and structural designs.
- Replicate impact conditions that occur in automotive impact by simpler and more manageable experiments to generate meaningful data for computer modeling.

Accomplishments

- Developed experimental setup procedures for new crashworthiness characterization test based on parallel-plates buckling (procedure was developed at the University of Dayton Research Institute).
- Developed and conducted constant-velocity crash experiments on circular tubes made of dual-phase (DP) and transformation-induced plasticity (TRIP) steels.

Future Direction

- Develop experiments for characterizing strain and strain-rate history in tubular components (circular and rectangular tube crush tests).
- Provide high-quality data for material and finite-element method (FEM) modeling development.

Introduction

Crashworthiness characterization of high-strength steel (HSS)[1] requires testing of materials and structures under increased strain rates, large plastic strains, and large displacements that are characteristic of actual impact events. Aside from providing a physically quantitative measure of crashworthiness, the experiments also provide benchmarks for verification of finite-element method (FEM) models that are used for automotive design and analysis. Typical crashworthiness experiments involve crushing of tubular objects, such as circular or rectangular tubes.[2] Because of a combination of relatively high velocities and force levels required for progressive crushing, the experiments are usually conducted in inertia-based equipment, such as drop towers or impact sleds. For example, in a drop tower, the drop height and the drop mass can be adjusted to generate desired crush force and length. However, there are practical limits on the mass and the velocity that can be used in a drop tower. The kinetic energy of the impact must be such that it can be expended in the deformation of the specimen and the safety restraints in order not to damage the testing equipment. Vibrations of the falling mass are practically impossible to eliminate, and the lateral forces are not easily measured, nor controlled. The velocity of impact cannot be kept constant and gradually reduces from the onset of impact.

The objective of this project is to develop and conduct coupon- and component-level experiments for characterization of crashworthiness of HSS. The project will also provide high-quality data for development of material and structural FEM models, and, therefore, enable more accurate modeling and design of lightweight crashworthy vehicles.

Design of Experiments

Parallel-Plate Impact Test

A new coupon-level test based on parallel-plate drop tower test by Tam and Calladine[3] has been developed for the servo-hydraulic testing machine. The University of Dayton Research Institute (UDRI) was contracted to perform double-hinge buckling tests at different strain rates as part of the Auto/Steel Partnership (A/SP) work to develop structures for the automotive industry that will improve passenger safety in crashes. Results from drop tower tests were used to develop a model of energy absorption. The results from the servo-hydraulic test will be used for characterization of material under impact and bending. The tests under three different crush speeds have been conducted during 2004.

The test is developed with the objective to replicate deformation history of automotive structures made of polygonal tubular components that occurs during impact. The simplicity of the specimen allows for semianalytical extraction of data and simple correlation with the FEM experiments. The instrumentation includes force cell, strain gages, and a digital camera that will be used to correlate the measurements. The fixture design is shown in Figure 1.

Up to eight strain gages are used to record strain history for a test. Gages are arranged as seen in Figure 2, with gages 4, 5, and 6 placed back-to-back with 1, 2, and 3.

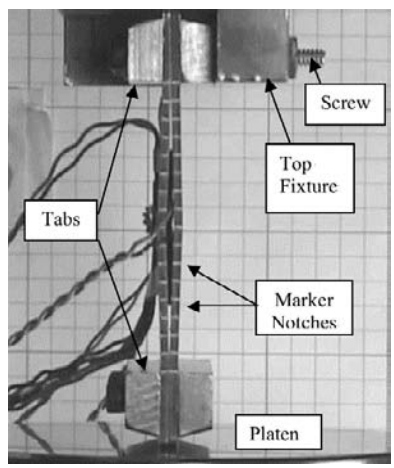

Figure 1. Parallel-plate impact specimen.

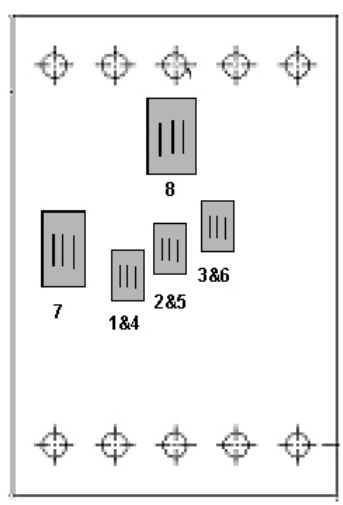

Figure 2. Strain gage locations.

Gage equipment was calibrated to record up to 10% or 20% strain as appropriate. Results from a successful high-rate test setup are shown in Figure 3.

A typical record of experimental data is shown in Figure 4, where left and right ordinates denote the impact force (lb) and strain gage data, respectively.

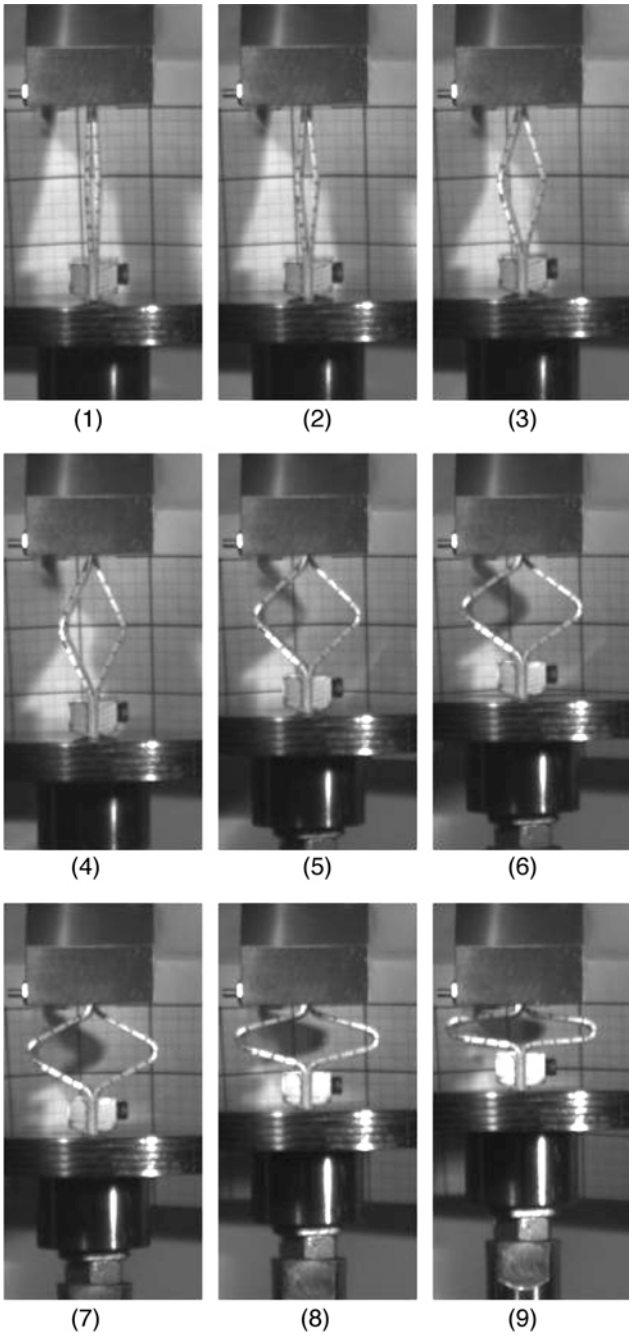

Figure 3. Double-plate test (numbers below the photographs denote the relative time sequence).

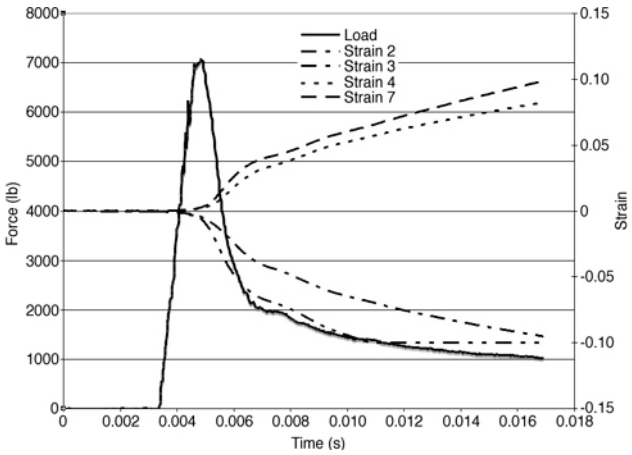

Figure 4. Double-plate test experimental data.

Data from the test are used to develop information about material rate sensitivity and deformation during early impact and formation of plastic hinges. The data are also used for correlation with the modification of the computational FEM models.

Tube Crush Experiments

To improve experimental investigations of the material and structural behavior for automotive impact, the Oak Ridge National Laboratory (ORNL) and the Automotive Composites Consortium (ACC) of the U.S. Council for Automotive Research (USCAR) have developed a new integrated virtual and physical test system for hydraulic, high-force, high-velocity crashworthiness experiments of automotive materials and structures. This unique system, the test machine for automotive crashworthiness (TMAC), permits controlled, progressive crush experiments at programmable velocity profiles and high-force levels. More details about the TMAC system can be found on http://www.ntrc.org.

The tube crush experiments were conducted at the National Transportation Research Center user facility in Oak Ridge, Tennessee. The TMAC system is shown in Figure 5.

The ability to control displacement (velocity) and large lateral stiffness of the machine allows for strain-history measurements[4] that are not practical in drop tower equipment.

Experimental tube specimens were supplied by the Auto/Steel Partnership. A relatively large diameter provides better bonding with the strain gages and relatively tight manufacturing tolerances

Figure 5. TMAC.

alleviate uncertainties due to imperfection sensitivity of the circular tubes. Geometry of the tube specimens is defined by tube length 178 mm (7 in.), diameter 50 mm (2 in.), and wall thickness 1.6 mm (0.063 in.).

The objective of the project is to investigate the strain-rate histories that material experiences during the crush in order to improve predictive capabilities of the numerical models. The principal tools for strain-rate-history measurement are electric resistance strain gages. Materials experience large strains during progressive crush, and therefore, high elongation gages have to be used. Different aspects of gage placement, bonding, and data acquisition were studied to maximize the amount of data from the experiments. Several bonding materials and gage types were considered. The tube force was measured by a set of load cells and a load washer.

Different modes of deformation can be triggered with appropriate modifications of tube geometries[5,6] and boundary conditions.[7] Axially symmetric crush of a mild steel tube is shown in Figure 6.

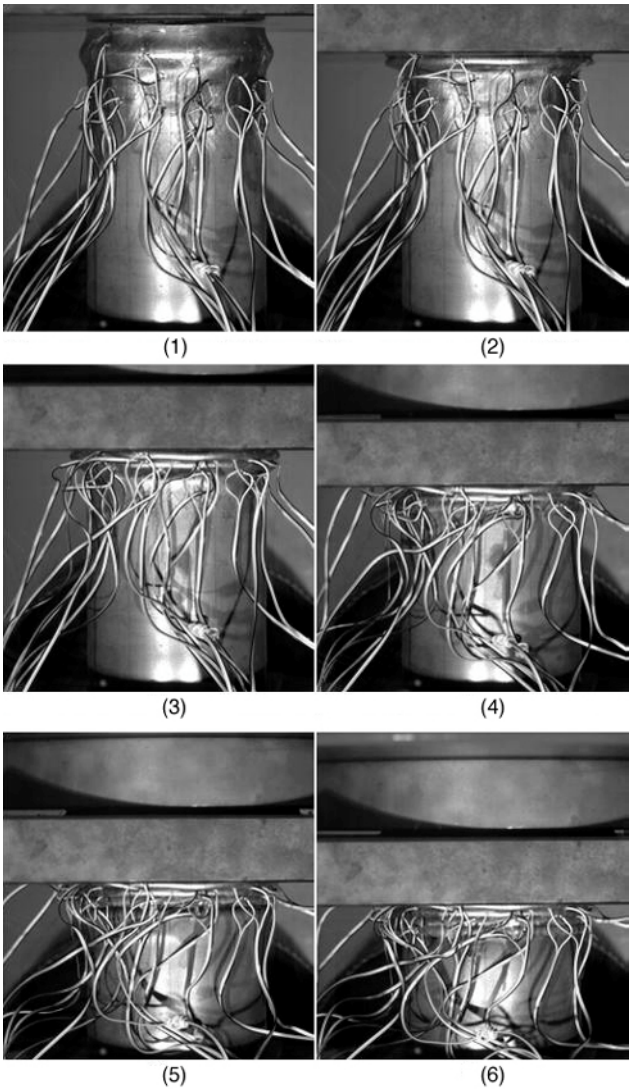

Figure 6. Progressive crush of a mild steel tube under constant velocity of 2 m/s (numbers below the photographs denote the relative time sequence).

An asymmetric crush of a high-strength low-alloy steel (HSLA) tube is shown in Figure 7.

The ongoing research involves investigations of different load measurement techniques in crashworthiness. The data from load sensors, displacement trace, and high-speed camera are synchronized and together provide comprehensive information about the progressive crush, and crashworthiness.

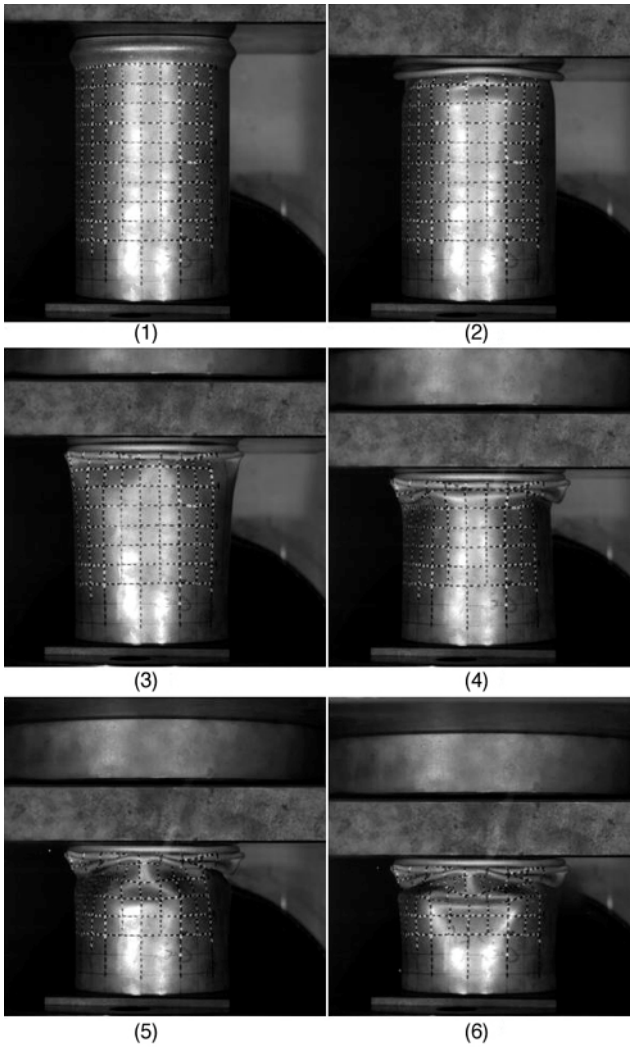

Figure 7. Progressive crush of a HSLA tube under constant velocity of 2 m/s (numbers below the photographs denote the relative time sequence).

Current efforts involve fixture modifications, calibration of high-speed camera equipment, and development of test procedures and test parameter tolerances.

Conclusions

Two new experimental setups have been developed for characterization of crashworthiness of HSS. The experiments are based on hydraulic-based testing systems. The systems provide unique, tightly controlled testing environments for structural and material characterization. The experimental data are used for validation and evaluation of modeling approaches and for development of modeling guidelines for HSS materials and structures under impact loads.

Acknowledgments

The tubes for preliminary crush experiments were donated by U.S. Steel Corporation. Support from the Auto/Steel Partnership-Strain Rate Characterization Team is acknowledged.

Future Work

The future work on the project will focus on two remaining topics:

1. conducting circular tube crush experiments in TMAC test machine, and
2. development of experimental setup for crushing of rectangular tubes in the TMAC test machine.

References

1. "Constitution and Properties of Steels," ed. F. B. Pickering, *Materials Science and Technology*, Vol. **7**, VCH, New York, 1992.
2. N. Jones, *Structural Impact*, Cambridge University Press, 1989.
3. L. L. Tam and C. R. Calladine, "Inertia and strain-rate effects in a simple plate-structure under impact loading," *International Journal of Impact Engineering*, **11**(3), 349–377 (1991).
4. M. Avalle and G. Belingardi, "Experimental evaluation of the strain field history during plastic progressive folding of aluminum circular tubes," *International Journal of Mechanical Sciences*, **39**(5), 575–583 (1997).
5. J. Singer, T. Weller, and J. Arbocz, "Basic Concepts, Columns, Beams and Plates," *Volume 1, Buckling Experiments: Experimental Methods in Buckling of Thin-Walled Structures*, John Wiley & Son Ltd., 1998.
6. J. Singer, T. Weller, and J. Arbocz, Buckling Experiments: Experimental Methods in Buckling of Thin-Walled Structures: Shells, Built-Up Structures and Additional Topics, John Wiley & Son, Ltd., 2002.
7. A. Copa, "Effect of end conditions on buckling of cylindrical shells under axial compression impact," in *Test Methods for Compression Members*, ASTM Tech. Pub. No. 419, pp. 115–136, 1966.

D. Development of Advanced Tools for Energy Management

Co-Principal Investigator: Srdjan Simunovic
Oak Ridge National Laboratory
P.O. Box 2008, Oak Ridge, TN 37831-6359
(865) 241-3863; fax: (865) 574-7463

Co-Principal Investigator; J. Michael Starbuck
Oak Ridge National Laboratory
P.O. Box 2009, Oak Ridge, TN 37831-8048
(865) 576-3633; fax: (865) 574-8257; e-mail: starbuckjm@ornl.gov

Technology Area Development Manager: Joseph A. Carpenter
(202) 586-1022; fax: (202) 586-1600; e-mail: joseph.carpenter@ee.doe.gov
ORNL Technical Program Manager: Philip S. Sklad
(865) 574-5069; fax: (865) 576-4963; e-mail: skladps@ornl.gov

---

Contractor: Oak Ridge National Laboratory
Contract No.: DE-AC05-00OR22725

Objectives

- Develop numerical modeling guidelines to realistically assess the influence that the properties of strain-rate-dependent materials exert in crashworthiness computations.

Approach

- Model the dynamic loading problems using diverse combinations of modeling approaches (submodels) that are essential in describing strain-rate sensitivity in computational simulations. Submodels examined include finite-element method (FEM) formulations, constitutive materials models, material properties under different strain rates and loading conditions, contact conditions, etc, as well as material property changes caused by component processing.

Accomplishments

- Investigated effects of stress transients for high-strength steel (HSS) and their effects on peak impact force.
- Developed experimental setup for new crashworthiness characterization test based on parallel-plates buckling (test under way at the University of Dayton Research Institute).
- Developed program for analysis of history of strain-rate calculations.
- Analyzed history of strain rates in unsymmetric crushing.
- Determined modeling effects on strain-rate history in unsymmetric crushing.
- Develop new constitutive models for HSS to account for strain-rate history and transients.
- Investigated forming and welding effect on steel tube crashworthiness.
- Developed model for tube roll-forming and validated it against manufacturing process.

Future Direction

- Develop new constitutive models for modeling of damage and tearing of HSS during impact.
- Conduct and analyze crush experiments (parallel-plates and tube crush).
- Develop experimental guidelines based on the two tests above.
- Determine optimal FEM formulations for modeling of crushing of rectangular tubes.
- Develop experimental program for crushing of rectangular tubes.
- Develop modeling guidelines for rectangular tubes.

Introduction

The objective of the project is to develop numerical modeling guidelines for strain-rate-dependent materials in crashworthiness computations. The scope of the project is to study specific structural problems in automotive impact, develop new experimental and analytical techniques for characterization of strain-rate sensitivity of high-strength steel (HSS) and modeling of complex strain and strain-rate histories. The dynamic loading problems are modeled using diverse combinations of modeling approaches (submodels) that are essential in describing strain-rate sensitivity in computational simulations. Submodels to be examined include finite-element formulations, constitutive materials models, and contact conditions. The trends, influences, and direct effects of employed modeling techniques will be identified and documented. The relative significance of employed submodels is established, particularly in relation to the strain-rate effect resulting from the material constitutive models.

The research project is conducted as a team effort between the Oak Ridge National Laboratory (ORNL) and the Auto/Steel Partnership Strain Rate Characterization Group (see 8.C).

The Effect of Stress Transients on Impact Peak Force

Impact experiments with steel tubes and coupons have shown a pronounced force peak for some types of steels that cannot be accounted for with existing strain-rate-dependent constitutive models. These same steels in coupon-level strain rate experiments show pronounced stress transients with increasing strain rate. These transients are usually discarded in development of constitutive models because presence of softening regions in stress-strain relation brings about significant problems with FEM formulation and uniqueness of the results. However, when strain-rate sensitivity is present in the model, and when it is evaluated in certain fashion, these problems are to a large extent eliminated, and stress transients during initial impact and strain rate variations can be taken into account. Figure 1 shows modified stress-strain data where stress transients based on experimental data were added from rate 0.1/s.

When this model is used for simulation of tube crush, an excellent agreement with the initial force peak is found. The comparison of the simulation and the model is shown in Figure 2.

The softening regions of the stress-strain curves do not severely affect the uniqueness of the solution if the material model is based on plastic strain rate. Together with strain-rate sensitivity, this introduces a characteristic length scale, stabilizes the model evaluation, and alleviates spurious mesh sensitivity.

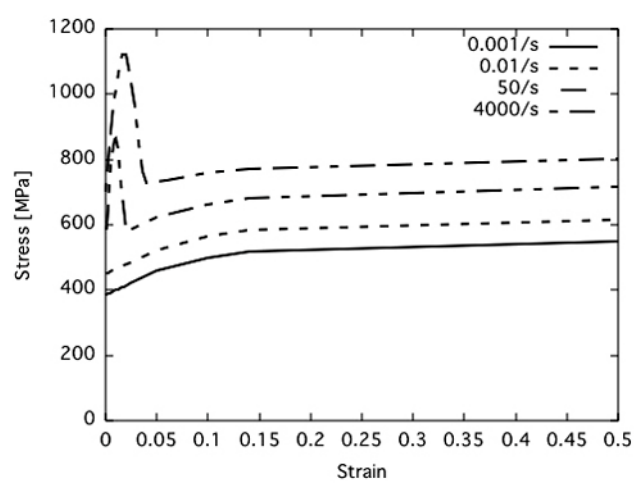

Figure 1. Modified high-strength low-alloy (HSLA) constitutive model with stress transients.

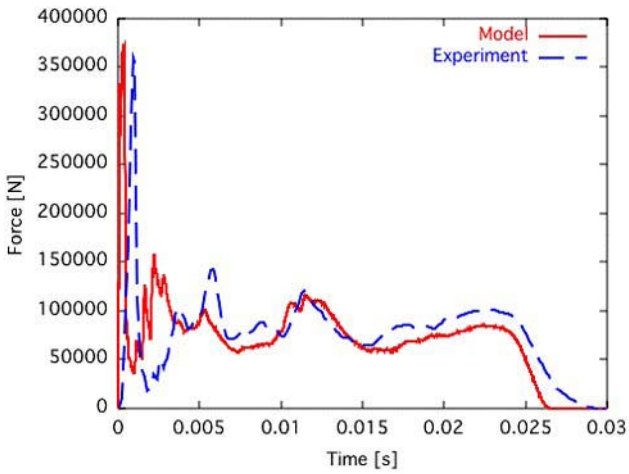

Figure 2. Modified HSLA constitutive model with stress transients.

The stress transients are dependent on strain-rate history, and the above treatment is just a first-order approximation of the phenomena. A more fundamental approach is described in the following section and is a subject of a journal publication under preparation.

Development of New Material Model for Stress Transients in Impact

Preliminary tube crush experiments were conducted at the ORNL Test Machine for Automotive Crashworthiness (TMAC) equipment described in 7C of the overall report. Tubes made of DP590 and TRIP590 steels were crushed at various speeds. Imperfection was introduced by making the top edge of the tube at a prescribed angle with the actuator, as shown in Figure 3.

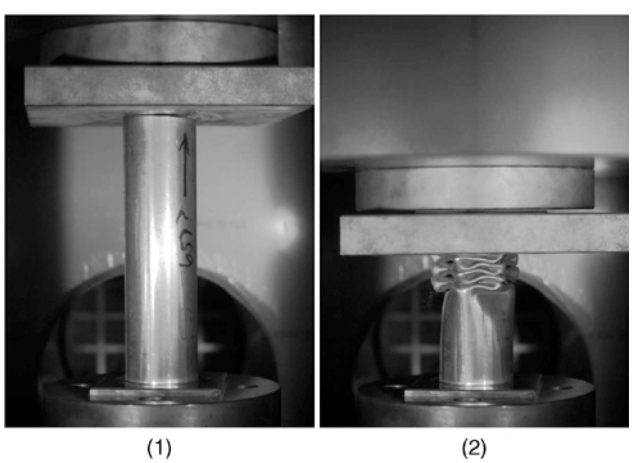

Figure 3. TMAC tube test.

The experiments were simulated using an isotropic plasticity and strain-rate dependency described by piecewise linear-plasticity model. The simulation was conducted for dual-phase (DP) steel tube under constant crush velocity of the actuator of 0.6 m/s. Figure 4 shows the comparison between the experiment and the model. Data have not been filtered.

The model correctly predicts the initial stiffness of the tube, but fails to achieve experimental peak. The origins of the peak impact force have so far been difficult to isolate because of the coupling between the test specimen and testing equipment and inertia of the measurement devices. The current results indicate that the peak value is not an artifact of testing but that such force is really experienced by the specimen. The actuator rigidity and inertia together with the measurements from the load washer at different constant loading velocities, imply that the origin of the peak force is in the material behavior. The material model would, therefore, have to be modified to include strain-rate history effects. Strain-rate history effects had been investigated in the past, but have not yet found a wide acceptance in the engineering practice.

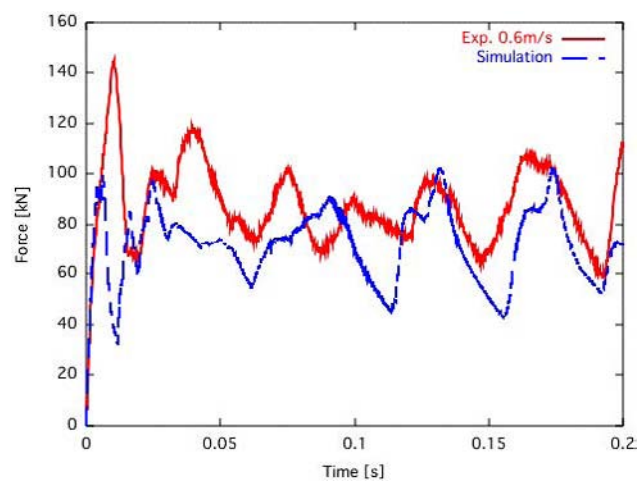

Figure 4. DP tube crush force; crush velocity 0.6 m/s.

Model Background

The complexity of material characterization under dynamic loading[1] is compounded with the difficulties of and filtering of equipment artifacts from the genuine material behavior. This filtering is especially difficult for materials that exhibit pronounced transient effects during the onset of yielding or rapid change in loading rate.

The transient effects during the loading rate change have been subject of research over the last several decades. In general, two theories were put forward for addressing the transient material response under sudden changes in loading rate. The first theory attributes the transient behavior to the stiffness of the testing equipment and the sample, whereas the second theory characterizes the observed material response as the fundamental property of the material. Experimental results obtained on very stiff testing equipment with feedback control favor the later explanation. Earlier results with shocked material[2] and dynamic torsion bars[1] also support the notion of significant material microstructure evolution during the loading rate jumps. The delay-yield phenomenon and its rate dependence also fall in the same general category. These phenomena have been satisfactorily explained by dislocation theory,[3] which was used in engineering simulations to improve modeling of the peak impact forces.

In the earlier studies,[4] strain-rate history effects in face-centered cubic (FCC) and body-centered cubic (BCC) metals have been studied based on the concept of fading memory. Based on this concept, the material loses its memory of the previous strain rate gradually within the duration of the current loading rate. Other models that are based on dislocation mechanics account for the strain-rate history through evolution of its internal variables. Because many use the strain-rate jump tests for investigation of superposition of strengthening mechanisms and strain-rate sensitivity evolution with the strain, they incorporate strain-rate history effect although not as their primary scope. Recent investigation[5] of the ability of modern micromechanics-based material models to simulate the strain rate jump tests found that the models could not accurately fit all the transients.

Transient Stresses in BCC Metals

Several major differences between the deformation characteristics of FCC and BCC alloys exist.[6] Contrary to the FCC metals, the primary short-range obstacle to dislocation motion is the Peierls-Nabarro frictional stress, and the stored dislocations behave as long-range obstacles; thus the hardening rate is not strongly affected by the strain rate. Experiments on BCC metals[7,8] indicate that the slip becomes finer and that mobile dislocation density increases with increasing strain rate. In the BCC metals, the mobile dislocation density increases rapidly with the applied strain and reaches an equilibrium state that gives the lowest stress at a given strain rate. This implies the existence of an attractor state for each applied strain rate toward which the current material state will eventually evolve if the loading is continued. In other words, the consequence of the existence of an attractor state is that there exists a unique characteristic strain rate for which the material microstructural state would be in equilibrium.

The material model proposed in this paper introduces a new scalar internal state variable (ISV), r_{ISV}, associated with the characteristic strain rate of the material microstructural state. The stress due to the strain-rate transition is superimposed onto the base stress that would otherwise be obtained if the strain-rate changes were not accounted for. Stress enhancement due to the difference between the applied and characteristic strain rate ISV is modeled by a viscous rheological element, and is based on the transients observed in experiments. The evolution law of the strain-rate ISV is such that it will eventually saturate to the applied strain rate according to the fading memory rule.

Model Formulation

Figure 5 presents the model's rheological scheme.

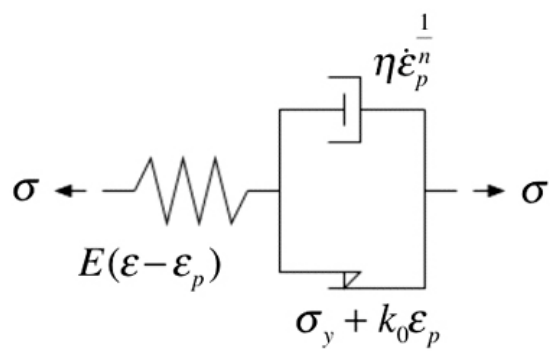

Figure 5. Elasto-visco-plastic material.

The stress balance is written in the form of a linear differential [Eq. (1)] that can be solved in closed form.

$$\eta \dot{\varepsilon}^{1/n} \left(\frac{d\varepsilon_p}{d\varepsilon} \right)^{1/n} + \sigma_y + k_0 \varepsilon_p - E\left(\varepsilon - \varepsilon_p \right) = 0$$

$$\varepsilon_p \left(\frac{\sigma_y}{E} \right) = 0 \quad . \quad (1)$$

The associated stress-strain curves corresponding to Eq. (1) for different constant strain rate tests are shown in Figure 6.

The material response in Figure 2 indicates that Eq. (1) is not suitable for modeling the effect of stress transients during the early loading.

Figure 7 presents the scheme of the proposed model, where a new element has been introduced to account for the evolution of internal microstructural state that accommodates the strain-rate jump.

As mentioned earlier, in BCC metals, the material's structure responsible for accommodating the imposed strain rate will gradually transition between its current equilibrium state described by r_{ISV} to the state that corresponds to the imposed external strain rate. For simplicity, we have used the imposed total strain rate as the target rate. Variable r_{ISV} represents the characteristic strain-rate variable for the current material state. The element resembles a viscous element as it is proportional to a difference of two rate terms. The new equilibrium equation is

$$\eta \dot{\varepsilon}_{p(ISV)}^{1/n} + \sigma_y + k_0 \varepsilon_p + k_2 \left(\dot{\varepsilon} - r_{ISV} \right) - E\left(\varepsilon - \varepsilon \right) = 0 \ ,$$

$$\varepsilon_p \left(\frac{\sigma_y}{E} \right) = 0 \quad . \quad (2)$$

The initial value for r_{ISV} can be estimated from the experimental data as the highest constant strain rate that does not produce noticeable stress transients (overshoots) and is denoted as r_{ISV}^0. The evolution law for r_{ISV} (fading of memory of the previous strain rate) is assumed to be in the exponential form with a time relaxation constant τ:

$$\dot{r}_{ISV} = -\frac{1}{\tau} \left(r_{ISV} - \dot{\varepsilon} \right) \quad . \qquad (3)$$

We restrict the analysis only to the initial loading so that we can integrate Eq. (3) analytically:

$$r_{ISV} = \dot{\varepsilon} + \left(r_{ISV}^0 - \dot{\varepsilon} \right) e^{-t/\tau} \quad . \qquad (4)$$

Parameter τ in Eq. (3) can be estimated based on the duration of the transients in experiments. Another obvious choice for the evolution law would be to base it on plastic strain increment. However, in the present study, Eq. (2) is selected because it can be analytically solved. Figure 8 presents the

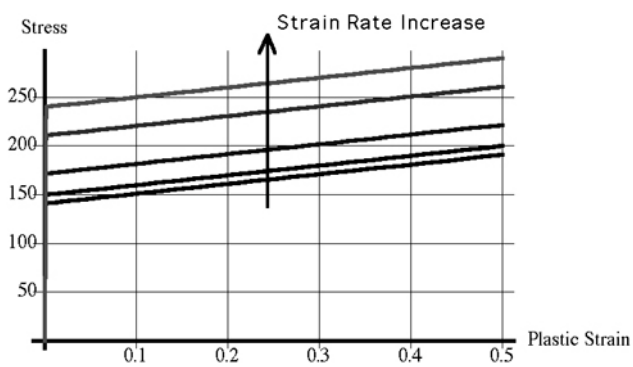

Figure 6. Stress-strain curves (strain rates 0.1, 1, 10, 50, 100/s, stress in MPa).

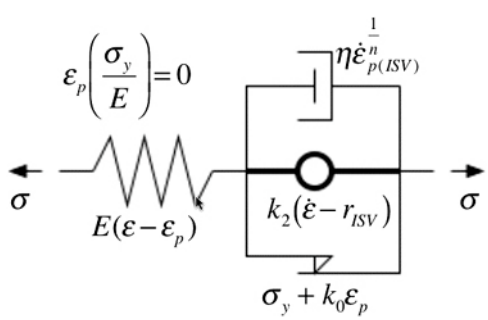

Figure 7. Elasto-visco-plastic material with strain rate history effect.

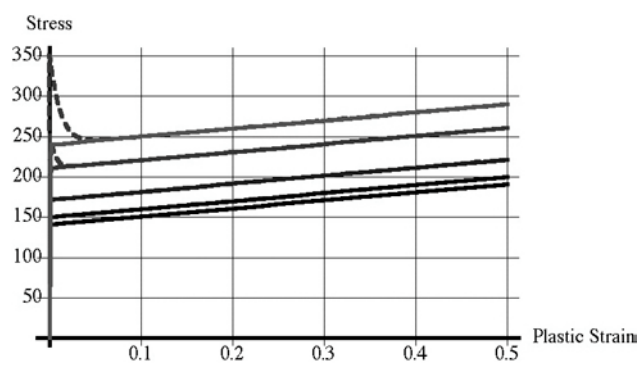

Figure 8. Stress-strain curves for model with strain rate history effect (strain rates 0.1, 1, 10, 50, 100/s).

solutions for imposed constant strain rate tests assuming that $r_{ISV}^0 = 0$.

The grey curves correspond to classical solution, whereas the dashed curves include the stress enhancements due to the transition of the internal state component responsible for strain rate accommodation. The overall trends in Figure 8 correspond favorably to the trends observed in experiments. The duration, shape, and magnitude of the transients can be modified using a different evolution law for r_{ISV} and more complicated rheological element.

Model Summary

We propose a new internal state variable corresponding to the characteristic strain rate associated with the material's current microstructural state for describing the strain-rate history effects. The new ISV is added to the classical elasto-visco-plastic model to illustrate its ability to model the jumps in the applied strain rate. The new model has been documented in an article submitted to a peer-reviewed conference.

Modeling of Forming Effects on HSS Tube Crash Performance

An FEM model has been developed to simulate roll forming of HSS tubes used in TMAC testing at ORNL. The model uses piecewise linear-plasticity material model. The tube forming includes spring-back simulation after forming that brings tube to its desired radius. The model was verified against manufacturing conditions. The formed tube information is transferred to the crush model using the initial plastic strains through the tube thickness. Figure 9 shows the comparison between the crush force of a DP tube using models with and without incorporated forming effects for an HSLA tube.

It can be seen that the incorporation of roll-forming effects does not impart significant difference onto the crush force and energy dissipation. The differences may mainly occur through the change of crush folding mode.

We have also incorporated laser weld effects through the modification of material parameters in the weld region based on measured hardness levels. The effect of welding was also found to be marginal except for triggering of the folding pattern.

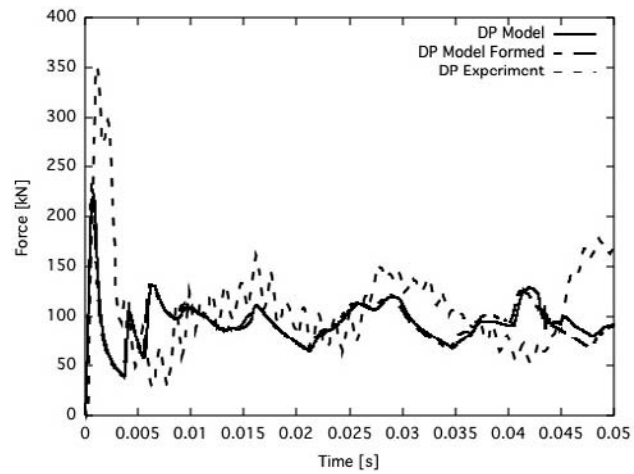

Figure 9. Tube crush force for models with and without forming effects. Green dotted line denotes experimental result.

Conclusions

The current project concentrates on investigation of different FEM modeling approaches for modeling of impact in HSS structures. The research is performed in collaboration with an experimental program on characterization of HSS under impact (8.C). The modeling is also used for development of new high-strain-rate material and structural characterization tests. The results of the project are used for development of more accurate modeling approaches for automotive design. The research results are also applicable in high-strain-rate forming operations.

Future Work

The future work on the project will focus on four topics:

1. Support of the strain-rate experiments on coupon and component level.
2. Development and validation of material models and modeling techniques.
3. Modeling of HSS rectangular tubes.
4. Development of models and experiments for damage and fracture of HSS in a crash.

The remaining most important aspects to address from the modeling of HSS crashworthiness are the methods to model the crush of tubes with rectangular (polygonal) cross section, modeling of damage that the HSS experiences during the deformation, and incorporation of processing into the models.

Acknowledgments

The research was performed at the Oak Ridge National Laboratory (ORNL), which is managed by UT-Battelle, LLC for the U.S. Department of Energy under contract DE-AC05-00OR22725. The tubes for the TMAC experiments were donated by the U.S. Steel Corporation. The support of Auto/Steel Partnership Strain Rate Characterization Team is acknowledged.

References

1. J. D. Campbell, *Dynamic Plasticity of Metals*. New York: Springer, 1972.
2. R. C. Smith, "Studies of effect of dynamic preloads on mechanical properties of steel," *Exp. Mech*., 153–159 (1961).
3. W. G. Johnston, "Yield points and delay times in single crystals," *J. Appl. Phys.* **33**(9), 2716–2730 (1962).
4. J. R. Klepaczko, "A general approach to rate sensitivity and constitutive modeling of FCC and BCC metals," in Ammann et al. (eds.), *Impact: Effects of Fast Transient Loadings*, Rotterdam, Balkema, 1988.
5. A. B. Tanner, R. D. McGinty, and D. L. McDowell, "Modeling temperature and strain rate history," *OFHC Cu. Int. J. of Plasticity* **15**, 575–603 (1999).
6. K. Miura, S. Takagi T. Hira, and O. Furukimi, "High strain rate deformation of high strength sheet steels for automotive parts," SAE Paper 980952 (1998).
7. J. Shiori and K. Satoh, "An ultrasonic wave study of the behaviour of dislocations under high strain rate deformations," *Inst. Phys. Conf. Ser.*, **21**, 154–162 (1978).
8. *Plastic Deformation and Fracture of Materials*, vol. ed. H. Mughrabi, *Materials Science and Technology*, Vol. 6, VCH, New York (1992).

E. Lightweight Front Structures

Project Manager: Pat V. Villano
Auto/Steel Partnership
2000 Town Center Drive, Suite #320
Southfield, Michigan 48075-1123
(248) 945-4780; fax: (248) 356-8511; e-mail: pvillano@a-sp.org

Co-Chairman: John Catterall
General Motors Corporation
Body Systems Center
Engineering West
Mail Code 480-111-W23
30200 Mound Road
Warren, MI 48090
(586) 986-354; fax: (586) 986-4184; e-mail: john.1.catterall@gm.com

Co-Chairman: Jody Shaw
5850 New King Court
Troy, Michigan 48098-2608
(248) 267-260; fax: (248) 267-2581; e-mail: jrshaw@uss.com

Technology Area Development Manager: Joseph A. Carpenter
(202) 586-1022; fax: (202) 586-1600; e-mail: Joseph.Carpenter@ee.doe.gov
Field Technical Manager: Philip S. Sklad
(865) 574-5069; fax: (865) 576-4963; e-mail: skladps@ornl.gov

---

Contractor: U.S. Automotive Materials Partnership
Contract No.: FC26-02OR22910

Objectives

- Benchmark, develop, and document proven solutions that will balance the interaction of material, manufacturing, and performance. The initial phase of the study focused on the automotive front-end system solutions that address high-volume manufacturing and assembly. Furthermore, example solutions were manufactured, and physical testing was performed to evaluate the advanced high-strength steel (AHSS) designs.
- Provide choices and consequences via the AHSS solutions that address real world challenges faced in the vehicle development process. A comprehensive knowledge-base design tool was developed to capitalize on a set of robust AHSS automotive design guidelines relating choices to consequences.

Approach

- Retrofitted an existing front rail system from a donor vehicle with AHSS dual-phase (DP) 800 to save 22% mass. In addition, a front bumper made from DP 980 replaced the existing bumper.
- Manufactured and tested the AHSS designed rail system and bumper to compare performance with the conventional design it replaced.
- Carried out analytical and physical testing on both the original and the redesigned rail system.
- Draw comparisons and document recommended practices.

Accomplishments: Additional Phase 2 Deliverables

- Provided team selection of stamped design.
- Obtained final optimized stamped rail and bumper designs.
- Completed formability simulation of the stamped design.
- Generated computer-aided design (CAD) data for manufacturing of the new stamped rail and bumper designs.
- Developed prototype tools for manufacturing rails and bumper stampings.
- Manufactured prototype dies for rails, rail extensions, and bumper.
- Developed new welding schedules for AHSS joining.
- Used static/dynamic stiffness design of experiment (DoE) finite-element (FE) models.
- Examined static stiffness DoE response surface.
- Examined dynamic stiffness DoE response surface.
- Stamped rails and bumpers and welded as assemblies.
- Prepared donor vehicle to receive the new rails and bumper.
- Welded new AHSS rails and bumper and installed into the vehicle.
- Conducted a successful (certified) Insurance Institute for Highway Safety (IIHS) 35-mph crash test of the retrofitted vehicle and recorded the results.

Future Direction

- Compare correlation of the vehicle crash (test) data with analytical results.
- Update Proteus, a knowledge base tool, with the findings of this project.
- Publish a final report detailing all of the findings of this project, including lessons learned.
- Complete roll-out application methodology communications package.

Phase 2 Summary (October 2003 through September 2004)

The project team selected the concept 2 stamped design for the final vehicle build. This stamped design consisted of octagonal Dual-Phase (DP) 780, three-piece, tailor-welded rail inner and rail outer stampings with symmetric flanges and tapered front section. This concept included a three-piece tailor-welded rail extension design with reinforcement. The rail curvatures were modified in side (XZ) and plan (XY) views. The original bumper from the donor vehicle was replaced with a DP980 two-piece double-box design incorporating energy-absorbing features.

Selection of Concept for Final Design

A comparison of the stamped design from concept 2 and the hydroformed design from concept 3 was prepared to select the most suitable design that could then be further optimized for mass reduction. A table detailing the comparison of the two designs appears as Table 1.

Although the hydroformed design had the potential for more mass savings, the stamped design provided the option with less manufacturing concerns and a higher chance for acceptance in the production environment. The team thus selected the stamped design for further development and prototyping. The final optimization determined the steel grades and gages of the rail design as shown in Table 2.

Table 1. Design comparison—stamped vs hydroformed rails

	Stamped design	Hydroformed design
Mass reduction	31%	31%
Performance	NCAP meets target, and IIHS performance did not meet the target, but the team felt that this could be achieved	NCAP meets target and acceptable IIHS performance
Manufacturing	— Use of tailor-welded blanks well established — Tailor-welded blanks can complicate stampings — Springback is a major issue — Small holes can be a problem	— Manufacturing tailor-welded tubes could be an issue — Prebending and hydroforming tailor-welded tubes could present significant problems — Springback is controllable — Small holes can be a problem
Assembly	— Welding DP980 with DP980 could be an issue — Spot welding rails to attached parts is not an issue	— No assembly welding required — Single-sided welding of rails with attached parts would be problematic
Production	Acceptance of stamped design in production environment is not an issue	Acceptance of hydroformed design in production environment is difficult

Table 2. Final stamped rail design optimization

Components	Baseline		Optimized	
	Grade	Gauge	Grade	Gauge
Bumper beam	DP980	1.0	DP980	1.0
Rail front outer	DP800	1.0	DP800	1.0
Rail front inner	DP800	1.0	DP800	1.0
Rail mid-outer	DP800	1.4	DP800	1.2
Rail mid-inner	DP800	1.4	DP800	1.2
Rail rear outer	DP800	2.0	DP800	1.4
Rail rear inner	DP800	2.0	DP800	1.4
Rail extension front	DP800	2.0	DP800	2.0
Rail extension rear	DP800	1.3	DP800	1.2
Rail extension reinforcement	DP800	2.0	DP800	1.4
Rail inner reinforcement	DP800	2.0	DP800	2.0
Total mass		34.460		30.458
Mass reduction (kg)		4.77		8.77
% Mass reduction		12.16		22.36

Formability Simulation of the Final Stamped Design

Formability simulations were conducted for the bumper and rail subassemblies. Bumper formability analyses were undertaken for the two-piece DP980 double-box design with incorporated energy-absorbing features. Both the inner and outer bumper components showed thinning below the target of 11%, thus indicating that the bumper is a formable design. The formability analysis results for the bumper components are shown in Figures 1 and 2.

The rail extension was fabricated using a three-piece tailor-welded DP780 design. The rail

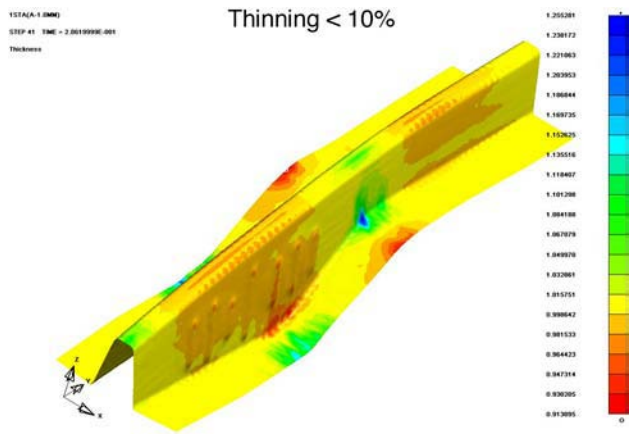

Figure 1. Bumper inner thinning.

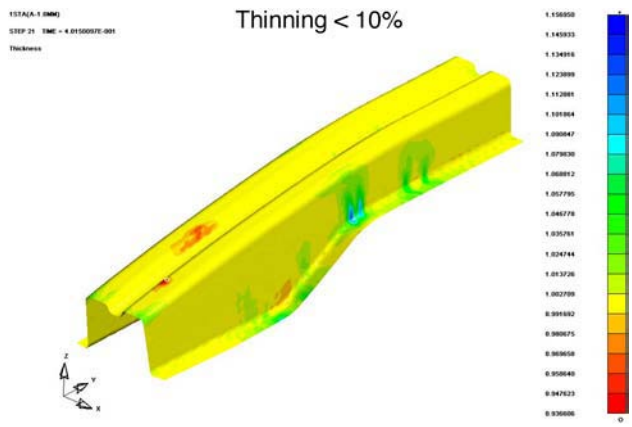

Figure 2. Bumper outer thinning.

extension reinforcement was also designed using DP780 steel. The rail extension and the rail extension reinforcement yielded a thinning of 15% and 13%, respectively. The formability analysis results for each of these parts are shown in Figures 3 and 4. Although the actual thinning was greater than

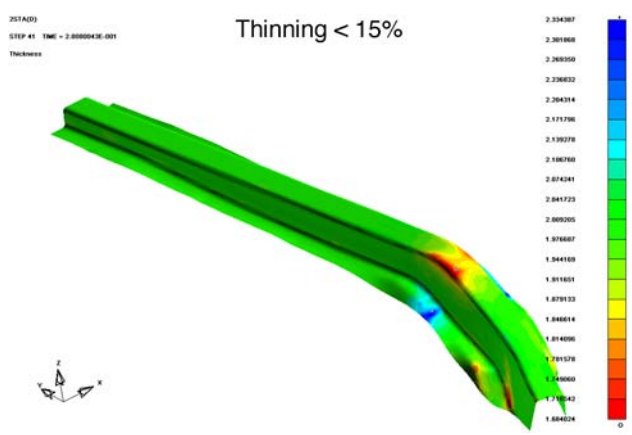

Figure 3. Rail extension thinning.

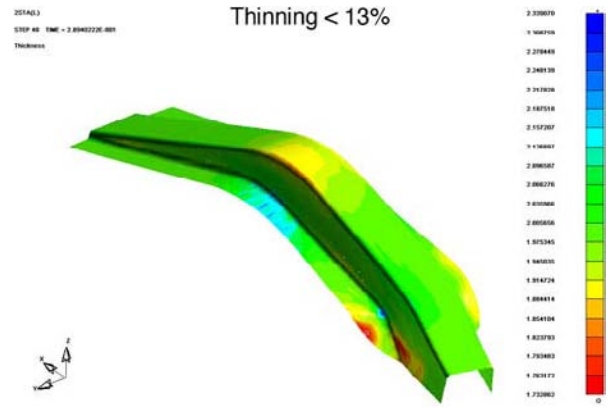

Figure 4. Rail extension reinforcement thinning.

the target of 11%, it was determined that the condition could be alleviated by rounding selected corners. The rail extension and the rail extension reinforcement were thus considered formable.

Generation of CAD Data

The computer-aided design (CAD) data for manufacturing the new rail and bumper system designs were generated, and the blank sizes of the components were also developed. These images appear as Figures 5, 6, and 7.

Development of Prototype Tools

The development of the required prototype tools for the rail and bumper subassemblies was completed and fabrication followed. Examples of selected tools and stamped parts follow as Figures 8 through 12.

Vehicle Retrofit/Reassembly

Following the fabrication and assembly of the front rails, rail extensions, and rail extension reinforcement, these and the bumper subassemblies were retrofitted onto the donor vehicle. It was also necessary to modify certain of the original donor vehicle mating parts to accommodate the new assemblies. Figures 13 through 15 depict select tooling as well as vehicle modifications.

Crash (Validation) Test

The New Car Assessment Program (NCAP) 35-mph Crash Test of the donor vehicle retrofitted with the AHSS rails and bumper was performed at the Transportation Research Center (TRC) in East Liberty, Ohio, on September 21, 2004.

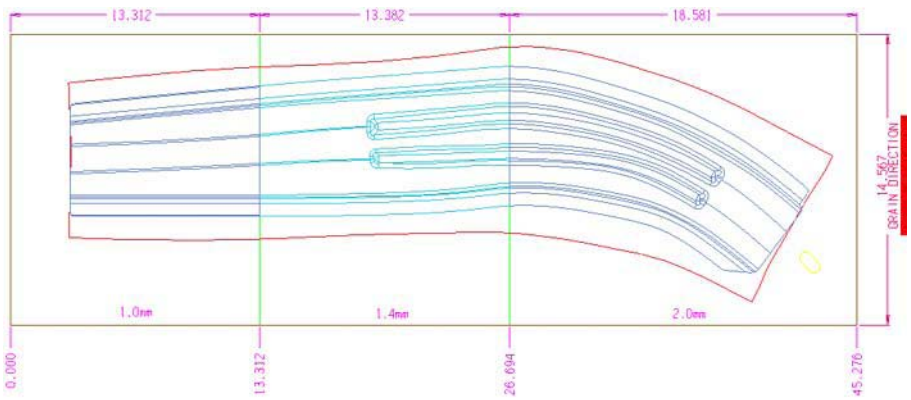

Figure 5. CAD-developed blank size for front rail outer.

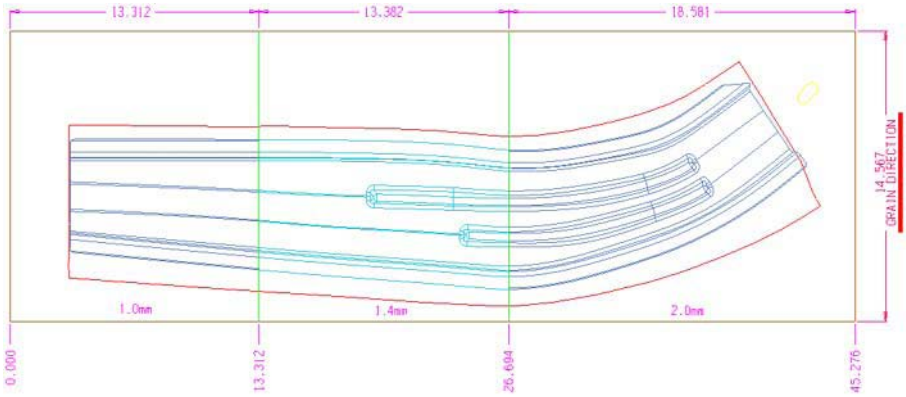

Figure 6. CAD-developed blank size for front rail inner.

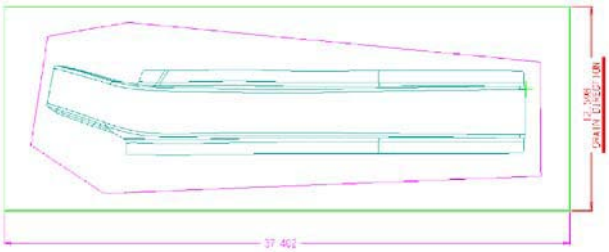

Figure 7. CAD-developed blank size for rail extension.

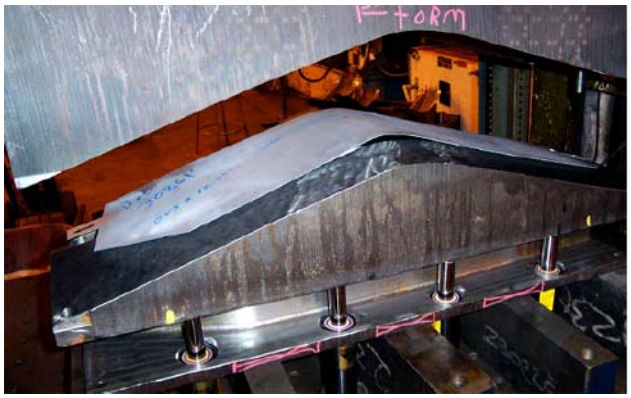

Figure 8. LH rail extension reinforcement—first form.

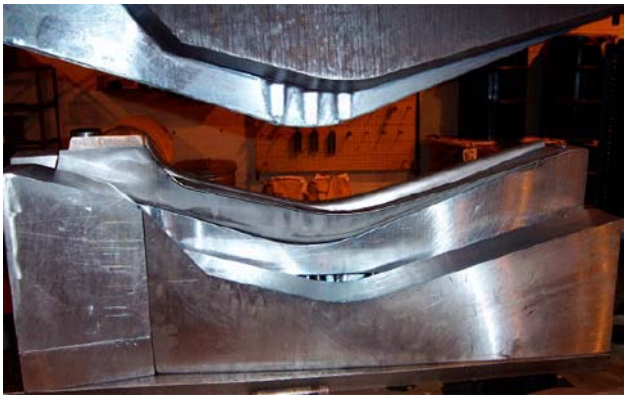

Figure 9. LH rail extension reinforcement—second form.

Figure 10. Formed LH rail extension reinforcement.

Figure 11. Bumper assembly fixture—combined.

Figure 12. Bumper assembly complete.

Figure 13. Complete rail assembled.

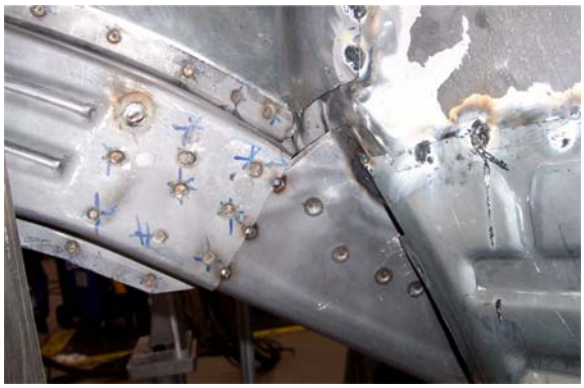

Figure 14. Weld connection between front rail and rail extension.

Figure 15. Custom parts fabricated, welded, and bonded as on the original vehicle.

Conclusions/Observations

Preliminary observations following the crash test indicated positive results were achieved (Figure 16). Only upon detailed analysis of the test data can specific conclusions be drawn. Final results are expected early in FY 2005, at which time the final project report will be completed.

Figure 16. Posttest three-fourths front view—right.

F. Hydroform Materials and Lubricants Project

Principal Investigator: Gene Cowie
Auto/Steel Partnership
2000 Town Center, Suite 320, Southfield, MI 48075-1123
(248) 945-4779; fax: (248) 356-8511; e-mail: gcowie@a-sp.org

Ronald Hughes, Temporary Chairperson
Severstal North America, Inc.
3001 Miller Road, Dearborn, MI 48121-1699
(313) 390-1400; fax: (313) 390-4100; e-mail: Rhughes@severstalna.com

Technology Area Development Manager: Joseph A. Carpenter
(202) 586-1022; fax: (202) 586-1600; e-mail: joseph.carpenter@ee.doe.gov

Field Technical Manager: Philip S. Sklad
(865) 574-5069; fax: (865) 576-4963; e-mail: skladps@ornl.gov

---

Contractor: U.S. Automotive Materials Partnership
Contract No.: FC26-02OR22910

Objectives

- Develop mechanical test procedures and forming limit diagrams (FLDs) for tubes.
- Improve the accuracy and confidence in finite-element modeling of tubular hydroforming.
- Develop an understanding of steel and lubricant requirements for hydroforming using a combination of experiments and finite-element modeling.

Approach

- Determine the forming limits of various grades and gauges of steel tubing in free expansion and corner fill processes using several types of lubricant to provide (FLDs) for each set of parameters. The work has been divided into six phases:
  Phase 1—Free expansion and corner fill characteristics
  Phase 2—Effects of end feeding and prebending on hydroforming limits
  Phase 3—Optimizing prebending parameters for the hydroforming process
  Phase 4—Optimizing bending parameters for advanced high-strength steel tubing
  Phase 5—The experimental forming limits of steel tubes
  Phase 6—Empirical prediction of tube FLDs and analysis of hydroforming data

  Delays in obtaining sheet stock and tubes caused Phases 3 and 4 to follow 5 and 6.

Accomplishments

- Evaluated the validity of the traditional forming limit curve for sheet metal stamping as it relates to tubing.
- Developed forming limit correction factors for tubular hydroforming of straight tubes.
- Developed forming limit curves for tubular hydroforming of straight tubes.
- Modified compression test tooling and prepared test samples to permit tension as well as compression of tubing during pressurization, allowing us to collect data for both sides (draw and stretch-form) of the FLD for quasi-linear strain paths for 0.79 IF-GA, 0.79 AKDQ, and 0.79 DP 600 steel tubes.

- Completed and published on the Auto/Steel Partnership (A/SP) Web site a summary report of Phases 5 and 6, performed at the Industrial Research and Development Institute (IRDI).

Future Direction

- Complete Phases 3 and 4.
- Evaluate tailor-welded tubes in free expansion and corner fill processes to determine the integrity of the laser welds under internal pressurization.

Introduction

Hydroformed steel tubes have been used in the automotive industry to form components that meet structural objectives, particularly strength and rigidity, at optimal mass. One of the most significant advantages of tubes is that they are monolithic closed sections and, as such, exhibit many times more stiffness in torsion than conventional open sections, such as "C" and "hat" shapes. Their use is limited largely by a lack of knowledge about the capabilities of hydroforming processes and the effects of the processes on the tubes.

This project was undertaken to investigate and quantify the capabilities and effects of various hydroforming processes so that automotive designers and engineers can utilize the tube configurations that are available and predict the performance of components made by hydroforming. Hydroforming tubes made from high-strength and advanced high-strength steels is of particular interest because of the potential reduction of mass associated with materials of higher strength.

Discussion

Hydroforming is a process in which a tube is placed into a die, which is shaped to develop the desired configuration of the tube. Water is introduced into the tube under very high pressures, causing the tube to expand into the die. The tube ends can be held stationary or moved during the process to induce either compression or tension.

The process has two distinct stages, shown in Figure 1. The first stage is free expansion, [Figure 1(*a*)]. It continues until the tube contacts the die wall [Figure 1(*b*)]. In the second stage, corner filling, the tube is in contact with the surface of the die, which constrains subsequent deformation [Figure 1(*c*)]. During this stage, the tube expands into the corners of the cavity, accomplishing corner fill. A tube that has been hydroformed is shown with the die in Figure 2. Note that the test was continued until the tube failed.

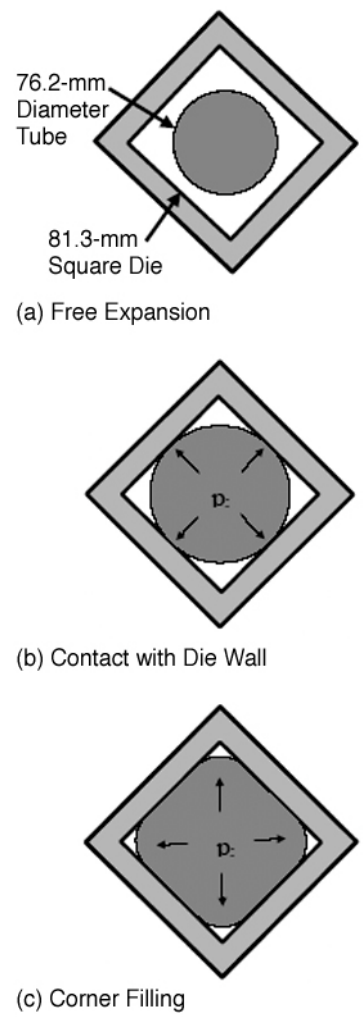

Figure 1. (*a*–*c*) The hydroforming process.

During corner fill, the tube slides against the die; therefore friction between the tube and die affects the process, and the lubricant used in the process becomes a significant parameter.

Figure 2. A hydroformed tube and die.

During both stages, the tube undergoes plastic strain. The amount of plastic strain that can occur before the material fractures is predicted in stamping processes that utilize flat sheet steel, by using a forming limit diagram (FLD). The FLD is determined by the properties of the material. The hydroforming process is preceded by tube forming and sometimes prebending of the tube, both of which induce strains in the material and alter its properties. Before an FLD can be developed for the hydroforming process, the strain history, that is, the strain induced in the material prior to hydroforming, must be known.

An FLD is required for any successful computer simulation of hydroforming. Therefore, in addition to experiments with tube expansion to determine the effects of axial compression and tension in combination with internal pressurization, the effects of prebending and preforming on subsequent formability were addressed. Collected data were used to develop FLDs for tubular hydroforming of straight tubes. These data will be used to develop guidelines for optimizing bending operations.

Presently, the formability limit for prebent steel in tubular hydroforming is poorly understood. The effect of prior strain induced in the tube conversion and tube bending processes that precede the hydroforming operation has been ignored. Accuracy needs to be assessed and improved to allow optimum application of tubular hydroforming in the lightweighting of vehicles.

Future Work

Tube bending, phases 3 and 4, which were delayed while obtaining the selected sheet steel and converting to tube, will begin in November 2004. The bending tests comprehend three variables: material, lubricant and bending speed. The materials are interstitial free (IF) and dual-phase (DP600); a water-based and a mineral-oil-based lubricant have been selected. Bending speeds have not yet been finalized. The results will be evaluated to determine the effects of these variables on tube surface quality and hydroforming formability. Bending services have been procured to perform this phase of the work.

The Hydroforming Materials and Lubricants Project Team is considering a proposal to evaluate the potential of tailor-welded tubes for the hydroforming process. Structural members fabricated from this type of tubing have the potential for mass reduction and improved crash energy absorption. The Team has tentatively selected two grades and thicknesses of steel that are representative of those that will be used in forthcoming applications and are currently available.

Conclusions

Analysis of tests run to date indicates the following:

- Tensile testing in the longitudinal direction is sufficient to adequately characterize the mechanical properties of tubes having a diameter of 76 mm or larger.
- Free expansion tests helped to determine stress and strain behavior as well as formability limits for tubes pressurized in free space.
- Limit strains for low carbon steel tubes can be predicted from the tube mechanical properties.
- Free expansion tests of bent tubes highlighted the existence of an area along the bending neutral axis in which deformation tends to localize when the bent tube is pressurized.
- Material formability has much more influence on the expansion into a corner than friction or end feed conditions. However, friction has a

very significant influence on thickness uniformity in the wall of the hydroformed part.

- Different benchmark tests were also carried out to determine tube behavior under internal pressure.

G. High-Strength Steel Joining Technologies Project

Project Manager: Thomas D. Mackie
Auto/Steel Partnership
2000 Town Center, Suite 320, Southfield, MI 48075-1123
(248) 945-4781; fax: (248) 352-1740; e-mail: Tmackie@a-sp.org

Chairman: James Dolfi
Dolfi AWS LLC
16883 Shrewsbury, Livonia, MI 48154
(734) 427-8117; fax: (734) 427-1827; e-mail: dolfi@www.net.com

Technology Area Development Manager: Joseph A. Carpenter
(202) 586-1022; fax: (202) 586-1600; e-mail: Joseph.Carpenter@ee.doe.gov
ORNL Technical Program Manager: Philip S. Sklad
(865) 574-5069; fax: (865) 576-4963; e-mail: skladps@ornl.gov

---

Contractor: U.S. Automotive Materials Partnership
Contract No.: FC26-02OR22910

Objective

- Facilitate the increased use of the advanced high-strength steels (AHSSs) in the Auto/Steel Partnership (A/SP) lightweighting projects through the development of weld parameters and weld schedules that will produce quality welds in various grades of these advanced steels. Consider resistance welding as well as laser and metal inert gas (MIG) welding processes.

Approach

- Evaluate weld lobe under peel test conditions to determine the optimum welding time and current. Test for properties such as hardness, tensile shear, metallographic, impact, and fatigue.
- Evaluate weld bonding of three of the AHSSs and compare to straight welded joints.
- Evaluate properties of tensile shear, impact, and fatigue for various welding practices and weld bonded joints.
- Document fracture characteristics of resistance welds and compare to the weld strengths in the development of a standard for partial-thickness fractures.
- Perform a design of experiment (DoE) analysis of relationships of weld parameters to physical properties.
- Work in coordination with the Lightweight Front Structures Group to determine the weld parameters in welding DP-980 and DP-800 steels (various thicknesses) to make and crash a predesigned front structure (for optimum light weight).
- Determine the welding parameters to produce optimum welds and statistically test welds produced with these parameters. Tensile shear and hardness will be evaluated (complete).
- Conclude the American Iron and Steel Institute/Edison Welding Institute (AISI/EWI) tempering project that addresses the effect of tempering welds made with dual-phase, Martensitic, and transformation-induced plasticity (TRIP) steels. This AISI/EWI project is also in concert with the DOE (complete).
- Secure the various material grades in sufficient quantities to complete the resistance welding and the materials planned for laser and MIG welding (complete).

- Write the test plan and procedures for the SWSG project (Statement of Work).
- Weld coupons and test accordingly (in process).
- Report results (in process).
- Develop a Standard of Acceptance for welds with inner-facial fractures that meet the strength requirements of welds or pull the traditional nugget. Develop into a weld standard by the American Welding Society (in process).

Accomplishments

Weld Lobe Study:

- Established procedure for weld lobe study, testing, and machine characterization.
- Characterized two machines, scissor gun and C gun, regarding rigidity and weldability.
- Secured the samples for all 12 materials, 200 ft^2 of each, at Roman Engineering, Inc. Material sheared into coupons and welded for weld lobe study, tensile shear, impact, and fatigue testing.
- Completed weld lobe study on all 12 materials (Figure 1).

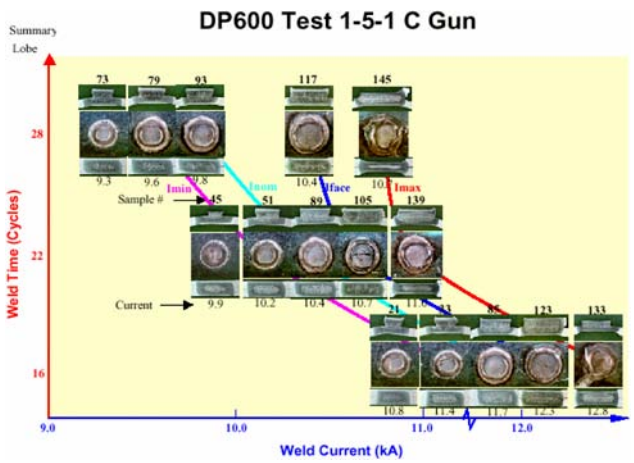

Figure 1. Sample of welding curves and welds produced. 1 of 24 weld charts.

- Completed impact tests and microhardness traverse tests on all 12 materials (Figures 2 and 3).
- Completed the design, produced, and tested fatigue test coupons (Figure 4).
- Designed, produced, and tested weld bonded coupons (Figure 5).
- Performed tensile shear tests on all material iterations (Figure 6).
- Developed acceptance criteria document and submitted same to Division 8 of American Welding Society (AWS), standards writing body of the AWS.
- Completed testing of weld study coupons (impact, tensile, and fatigue).
- Writing of final report on weld lobe study is in progress (first draft written by J. Dolfi).

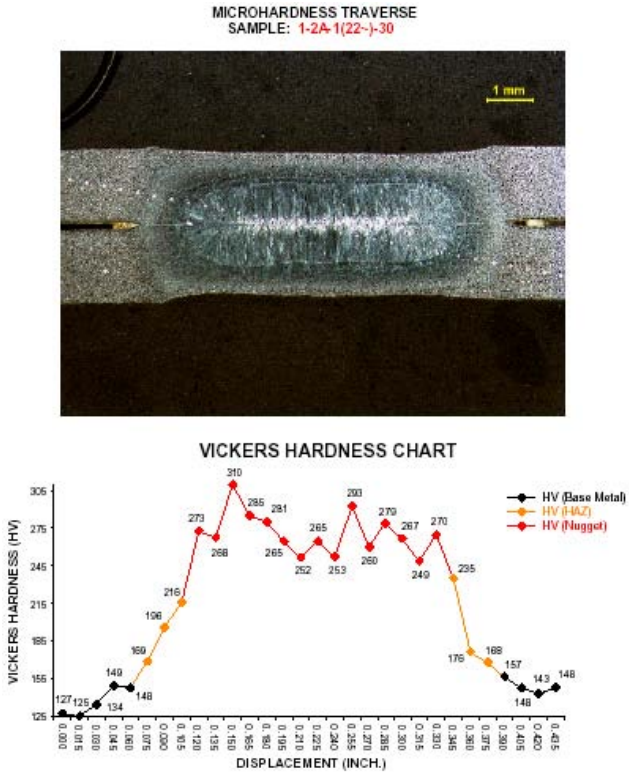

Figure 2. Photomicrograph and microhardness traverse of weld.

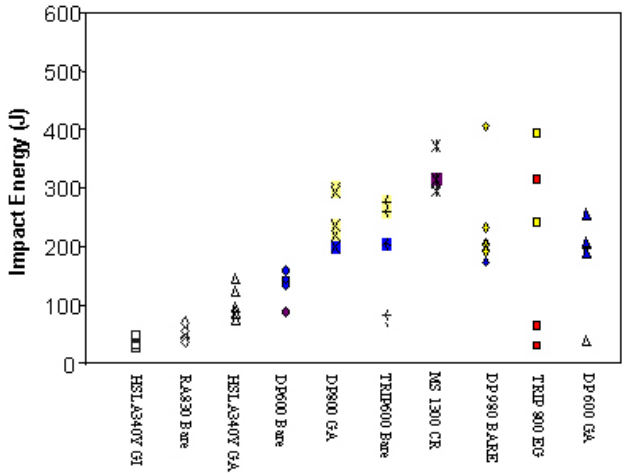

Figure 3. Impact data comparison of ten steels. Large welds and long hold time.

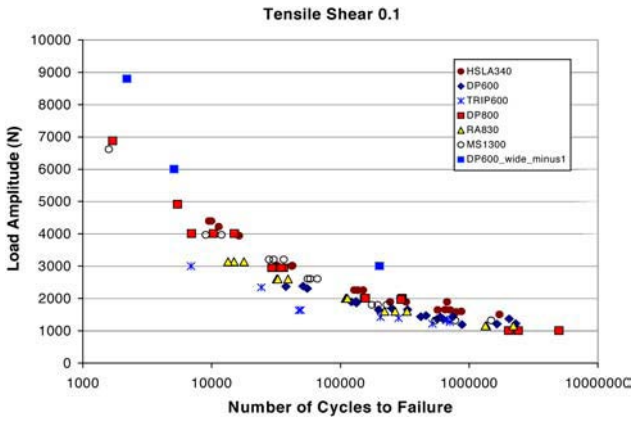

Figure 4. Load amplitude vs cycles to failure on seven materials.

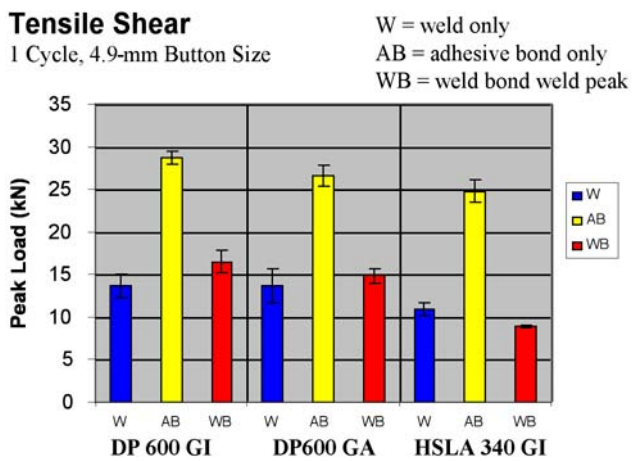

Figure 5. Tensile shear comparison of three materials: welded vs bonded vs weld bonded.

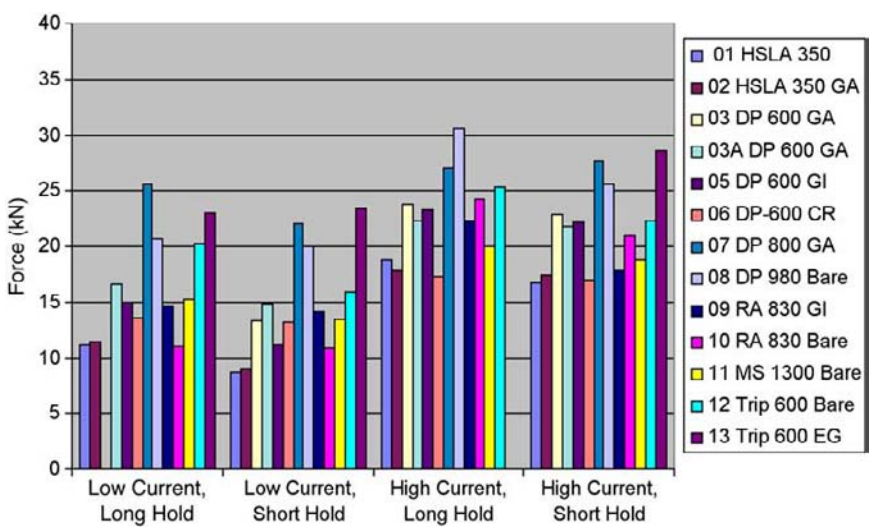

Figure 6. Tensile shear results as peak force vs weld setup for all 13 materials.

EWI/AISI Temper Study:

- Completed work on the EWI/AISI Temper Study Project. Report is published and on "A/SPsteel" Web page.

LWFS Weldability Study (resistance welding):

- Redeveloped material matrix to test DP-800 and DP-980 materials only.
- Secured materials of different thicknesses for Lightweight Front Structure (LWFS) tests.
- Tested for weld parameters for making welds with various materials.
- Supervised the welding of prototype parts for crash tests using weld parameter data.
- Built and tested two crash models via LWFS group.
- Evaluated weld performance on tested crash structures via joining team.

Structural Welding Subgroup Project (SWSG):

- Developed test matrix for MIG and laser welding of various AHSS materials.
- Secured nine test materials for testing.
- Initiated contract to weld and test according to test matrix.

Other

- Secured three AHSS materials for CanMet project. CanMet to run surface tension transfer tests on several AHSS steels at no cost.

Future Direction

- Develop a DoE analysis to determine relationships between current, hold time , electrodes, welding gun type to produce suitable properties of strength, hardness, impact, and fatigue.
- Complete testing of MIG and laser-welded joints made with HSLA baseline material and compared to Dual-Phase 600, 800, and 980 materials.
- Evaluate if a ductile/brittle transition exists by impacting joints at extremely low temperatures.
- Evaluate fractures and correlate to mechanical properties and determine the predictability of failures.
- Evaluate the weldability of projection welded fasteners to AHSSs.

Introduction

The purpose of this project is to evaluate the weldability of the new advanced high-strength steels (AHSSs) currently being considered by the automotive companies as a solution to lightweighting without compromising cost or structural strength. We are to evaluate various grades, thicknesses, and joining processes. Initially, resistance welding was evaluated, but subsequent tests extended to metal inert gas (MIG) and laser joining processes. The joining processes were to be validated by welding a front-end assembly using AHSSs, and subsequently, crash testing the assembly.

Issues that needed to be resolved in the weld lobe study before extensive welding of coupons follow:

1. weld coupon design,
2. weld tip conditioning,
3. weld gun design,
4. interfacial fractures, and
5. ultrasonic evaluation.

Weld Coupon Design

Weld coupon design was considered important because a narrow coupon (38 mm) when tensile tested, exhibited a rotational load on the weld nugget, resulting in less than optimum tensile shear strength. After discussion of a variety of ways to avoid this rotation, the coupon was designed with extra width (125 mm) and validated with comparative tests.

Weld Tip Conditioning

It was determined that an electrode stabilization procedure at 16, 22, and 28 cycles was needed to determine the weld window between no-weld and expulsion. This process was used to develop the weld lobe to meet minimum requirements (6-mm diameter).

Weld Gun Design

Two weld gun designs, one a "C" straight acting gun, and one pivot/scissor gun, with electrode movement typically used in production were used. These were characterized by gun arm deflection and overall affect on weld performance, and the nature of weld tip contact with the sheet. Tests were subsequently run with both guns for comparison.

Interfacial fractures

Sheet steels that exhibit interfacial or partial facial fractures in spot welds have been unacceptable to automotive companies for many years for various reasons (mostly because the welds with interfacial fracture usually exhibited low tensile shear strength). However, it was found by proper weld schedule, welds of this type passed all the tensile, impact, and fatigue requirements. Comparisons of the fractures with tensile, impact, and fatigue strengths, led to the construction of acceptance criteria, which eventually will lead to an industry standard.

Ultrasonic Evaluation

Consideration was given to evaluation of weld size using Ultrasonic Testing. An ultrasonic B-scanner was used to provide inspection of various welds produced using DP-600 material. Welds of various sizes were produced, including unfused internal structures. Comparisons between ultrasonic measurements and cross-sectioning measurements revealed that nugget width can be predicted to within 10% of actual width.

Peel Test

Welds were made at three cycle settings (16, 22, and 28) at various currents from no-weld to expulsion. Subsequent welds were all peel tested to fracture the welds. The calibrated peel test was determined not reliable. Welds were selected from the matrix and examined by microstructure and hardness. Sample welded coupons were made for tensile shear tests, impact tests, and fatigue tests.

Weld Conditions

All welding was performed with weld cap 4 as defined in AWS/SAE D8.9 standard. This weld cap (electrode) is fabricated from RWMA class 2 copper. It has a 45° truncated cone having a flat diameter of 7 mm and a body diameter of 19 mm. Weld force was maintained at 1500 lb. Water flow was 3.8 L/min (1 gpm), at a temperature of 81°F. Unless otherwise stated, electrode face and weld size stabilization procedures were used for all welds. Weld hold times were 30 cycles for all weld lobes.

Other Discussion—Weld Lobe Study

In the weld lobe study, all the weld data and subsequent test results were recorded on run sheets, which could be later tabulated and compared via computer program such as Minitab. Material properties such as yield and tensile, elongation, hardness, along with complete chemistries were made and tabulated also. There were 13 combinations of material, strength level, and coatings tested, all in the 1.5-mm-thickness range.

Plans are to write an executive summary similar to the attached, do a DoE on all the variables to determine their relationships, and to make available a disc of all the data for independent evaluation.

Lightweight Front Structures Work

The LFSG of the Auto/Steel Partnership needed assistance in welding a lightweight design from Dual-Phase 600, 800, and 980 materials. After obtaining the various materials, the Joining Team proceeded to evaluate the weldability of these materials, and to test weld the combinations prescribed

for a front end structure. The Joining Team established the weld parameters, and assisted the prototype source in making the structure. After crash test of the front structure, the Joining Team proceeded to examine the welded assembly. Weld parameters were delivered to the Structures Team along with mechanical and chemical properties of the test materials.

EWI/AISI Temper Study Project

The EWI/AISI Temper project is one where Edison Welding and American Iron and Steel were cooperating in a project with the Department of Energy in 2002 and 2003, in an investigation using AHSSs by posttempering after welding, to produce tough welds. Since the Joining team was interested as a possible fallback position, we joined them. Edison Welding has concluded its investigation in welding and tempering dual-phase steels, TRIP steels, and martensitic steels. They concluded that tempering after welding or spike tempering during the weld cycle does reduce the hardness of the weld and improves the ductility. Quench and temper maps were produced for all the materials. A complete report is on the A/SP web site under the Joining Team reports section (www.a-sp.org).

SWSG MIG/Laser Project (Structural Welding Subgroup)

The structural welding subgroup originated out of the Joining Technologies Team in an effort to evaluate the welding of AHSSs by MIG, laser and laser-assisted MIG welding processes. Three grades of dual-phase and HSLA (baseline) materials were considered. These were materials of various thicknesses and coatings considered for frame and rail applications. All the materials for test have been secured. A test matrix was developed, and test coupons were designed. The contractor will be making and testing various combinations and reporting the results. This project should conclude by September 2005.

Low-Temperature Impact

Preliminary tests on impacting one HSS indicated a potential problem with a ductile/brittle transition at low-temperature. An investigation has been defined for low-temperature impact testing with several of the AHSSs (dual phase, martensitic, and TRIP, and using HSLA as a benchmark). The impact testing used on the weld lobe study will serve as a basis for comparison. Completion of this study is predicted by June 2005.

Several other welding issues will be addressed during 2005, guided by various members of the Team, mostly funded as in-kind.

H. Sheet Steel Fatigue Characteristics

Principal Investigator: Gene Cowie
Auto/Steel Partnership
2000 Town Center, Suite 320, Southfield, MI 48075-1123
(248) 945-4779; fax: (248) 356-8511; e-mail: gcowie@a-sp.org

Chairman: John Bonnen, Ph.D.
Ford Motor Company, Ford Research Laboratory
20000 Rotunda Drive, Dearborn, MI 48121-2053
(313) 322-9127; fax: (313) 390-0514; e-mail: jbonnen@ford.com

Technology Area Development Manager: Joseph A. Carpenter
(202) 586-1022; fax: (202) 586-1600; e-mail: joseph.carpenter@ee.doe.gov
Field Technical Manager: Philip S. Sklad
(865) 574-5069; fax: (865) 576-4963; e-mail: skladps@ornl.gov

---

Contractor: U.S. Automotive Materials Partnership
Contract No.: FC26-02OR22910

Objective

- Compile the test data generated in the previous phases of the program into a user-friendly database so that it can be used in all phases of design and structural analysis of sheet-steel vehicle bodies.
- Investigate the fatigue life of joints formed by spot welding, adhesive bonding, and weld bonding (a combination of welding and adhesive bonding).
- Explore the parameters for testing metal inert gas (MIG) and laser-welded joints.

Approach

- Investigate the fatigue characteristics of spot welding, a fusion process in which the metal being joined is melted and resolidified, forming an alloy with a distinctly different microstructure than that of the metals that are joined. In addition, the weld nugget, or button, may contain discontinuities, which can become sites at which fatigue cracks form. The amount and type of discontinuities are affected to a considerable extent by the welding process. The microstructures of the joined metals are also refined in the area adjacent to the weld, which is known as the heat affected zone (HAZ).
- Investigate the fatigue characteristics of adhesive bonding, which introduces an entirely different material into the load path. The adhesive must adhere to the metals being joined and resist fatigue failure at the areas of contact and within itself.
- Investigate the fatigue characteristics of weld bonding, a combination of adhesive bonding and spot welding.
- Investigate the previously unknown, or at best little known, factors that are expected to improve durability and facilitate modeling and simulation.
- Investigate the fatigue characteristics of MIG welding, a fusion process, which also forms alloy microstructures different from the metals being joined.

Accomplishments

- Defined parameters of the sheet-steel fatigue database and engaged a contractor to perform the work. The database has been constructed and has undergone several evaluations by team members. Work is expected to be complete by the end of 2004.
- Selected 27 combinations of steel grade and coating for joint fatigue testing. Of the combinations, 22 were spot welded, and all are completed. Two of the combinations were weld bonded, and both have been completed. Three of the combinations were bonded, with all three in process.
- Contacted several consultants, invited them to present proposals for fatigue testing MIG welds, and selected one to develop a test program.

Future Direction

- Analyze the data from spot weld fatigue tests (882 specimens).
- Verify the accuracy of the information and determine the fatigue performance of the advanced high-strength steels tested.
- Ensure that the information will be made available on the Auto/Steel Partnership Web site and in published form through SAE.
- Begin fatigue testing of MIG welds.

Introduction

In the era when vehicle mass was not a drawback and, in fact, was sometimes considered an advantage, the primary concern in body design was rigidity. More recently, the need to reduce body mass to comply with mandated corporate average fuel economy (CAFE) while improving the levels of occupant protection in a crash or rollover, caused design engineers to reexamine design procedures and materials. High-strength steels, judiciously selected and applied, emerged as potential low-cost (compared with aluminum and plastics), reliable materials for meeting these mandates. As structural components are optimized and thinner gauge, higher strength materials are assessed, fatigue life of the component and the areas where loads are transferred become considerations. To assess the performance of a component in the design phase, the fatigue characteristics of the base material and the areas where loads are transferred must be known. This project has completed a significant amount of testing of various grades of steel and is currently addressing joining methods most commonly used in vehicle bodies made from sheet steel.

Discussion

The three participating auto companies have been investigating the fatigue characteristics of spot welds, but there remains a need for a joint effort to evaluate the fatigue characteristics of welded and weld-bonded joints. Because spot welding is by far the most common welding process used in automotive steel bodies, initial efforts focused on this process.

The effort began in the 2002 fiscal year with presentations by key researchers on the current state of the work at DaimlerChrysler Corporation, Ford Motor Company, and General Motors Corporation. Based on these presentations, the Sheet Steel Fatigue Project Team was able to develop parameters for a test program that would produce results beneficial to all three companies. Early in the planning, the Auto/Steel Partnership (A/SP) Joining Technologies Team was consulted, and it was agreed that the Joining Technologies Team would prepare the samples to be tested. This interaction ensured that the samples would be joined using procedures that were properly controlled and in adherence to the best current practices in sheet metal joining.

The following test parameters were developed and agreed on in the planning stage:

1. There will be two modes of testing: tensile shear (Figure 1) and coach peel (Figure 2).
2. Weld fatigue performance is independent of metal thickness for mild steels and high-strength low-alloy (HSLA) grades; therefore, tests on these grades will utilize only one metal thickness (1.6 mm).
3. Because no such data are yet available for advanced high-strength steel (HSS), several grades in this class will be tested at two thicknesses (1.6 mm and 0.7 mm).
4. Testing will be done at two R ratios: 0.1 and 0.3. R is the stress ratio, defined as the ratio of the minimum stress to the maximum stress in the test cycle. Maximum and minimum values are algebraic, with tension designated as positive and compression negative.
5. Eight steel grades were originally selected for testing. The number was subsequently increased to 11.

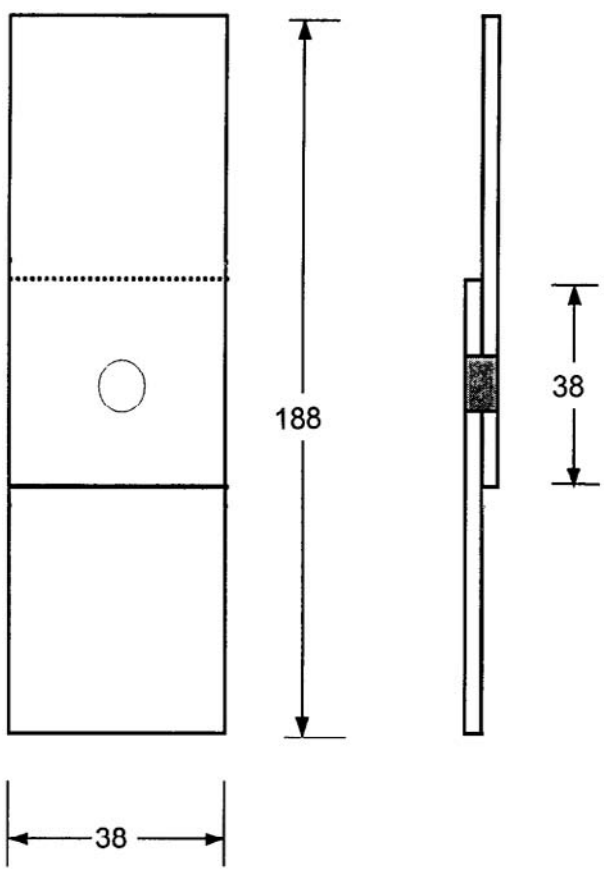

Figure 1. Lap shear test specimen.

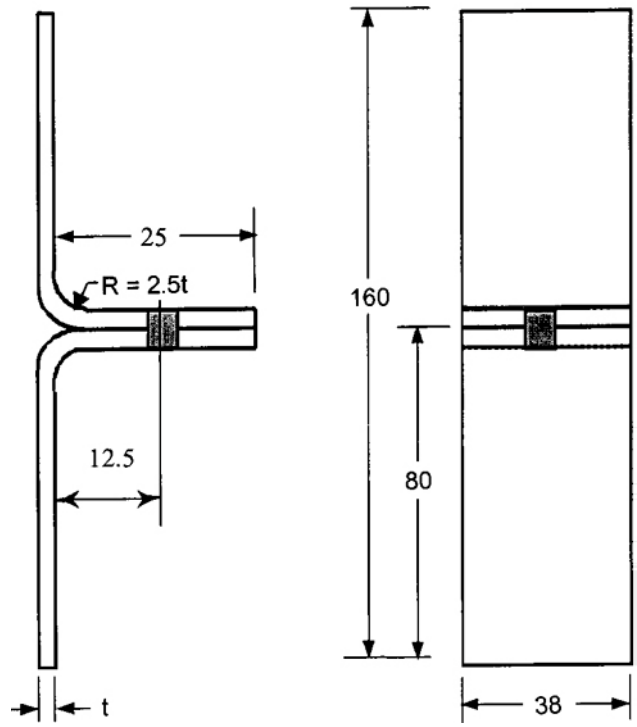

Figure 2. Coach peel test specimen.

6. Testing was originally planned for spot-welded and weld-bonded joints. Several tests on joints that were bonded only were added.

The team prepared a statement of work and sent it to nine testing laboratories known to have capabilities in this type of testing and invited them to submit proposals.

- The University of Alabama, Tuscaloosa, Alabama
- Colorado School of Mines, Advanced Steel Processing and Products Research Center, Golden, Colorado
- University of Dayton Research Institute—Dayton, Ohio
- University of Missouri—Columbia, Missouri
- University of Nevada—Reno, Nevada
- University of South Carolina—Columbia, South Carolina
- University of Toledo—Toledo, Ohio
- University of Waterloo—Waterloo, Ontario, Canada
- Westmoreland Mechanical Testing and Research, Inc.—Youngstown, Pennsylvania

All nine responded with acceptable proposals. The project team reviewed the proposals based on technical competency, qualifications of key personnel, demonstrated experience, understanding of the project requirements and price. Two were selected to perform the work: The University of Missouri in Columbia, Missouri, and Westmoreland Mechanical Testing and Research, Inc., in Youngstown, Pennsylvania.

As the testing progressed, and results were analyzed, the following tests were added for comparison purposes.

1. Testing at specified R ratios means that the maximum and minimum loads are constant throughout the test. This process is valuable for establishing baseline data. However, in the real world, loads can be expected to vary. For this reason, two sets of spectrum loading tests, run at predetermined load variations, were scheduled.
2. Two tests are in progress on samples with a different welding schedule that produced a smaller weld button.
3. Three tests were scheduled with samples joined by adhesive bonding only.
4. At the request of the Joining Technologies Team, three tests were scheduled using wide samples (125 mm vs the standard 38 mm). The wider samples minimize twisting of the weld under load.

Conclusions

Preliminary analysis of results received to date indicates that the fatigue performance of a spot weld is independent of the materials being welded. This finding supports the initial understanding that the melting and resolidifying processes (see Approach) form new alloys and make the properties and coating of the material(s) being joined and the welding parameters, insignificant contributors to fatigue performance. This conclusion will be verified or negated when the analysis of the work is completed during the next fiscal year.

I. Tribology

Project Manager: Pat V. Villano
Auto/Steel Partnership
2000 Town Center Drive, Suite #320
Southfield, MI 48075-1123
(248) 945-4780; fax: (248) 356-8511; e-mail: pvillano@a-sp.org

Project Chairman: Alan Pearson
General Motors Corporation
Metal Fabricating Division
2000 Centerpointe Pkwy., Mail Code 483-520-042
Pontiac, MI 48341
(248) 753-2056; fax: (248) 753-2344; e-mail: alan.pearson@gm.com

Technology Area Development Manager: Joseph Carpenter
(202) 586-1022; fax: (202) 586-1600; e-mail: Joseph.Carpenter@ee.doe.gov
Field Technical Manager: Philip S. Sklad
(865) 574-5069; fax: (865) 576-4963; e-mail: skladps@ornl.gov

---

Contractor: U.S. Automotive Materials Partnership
Contract No.: FC26-02OR22910

Objectives

- Conduct stamping simulation tests to study the effects of tribological conditions on the stamping performance of advanced high-strength steels (AHSS). Stamping performance in this project is defined as minimizing die wear and maximizing dimensional stability. The understanding of the contribution of lubricants to errors in springback prediction when using finite-element analysis (FEA) will also improve dimensional performance.
- Include these ultimate benefits:
  - Improve test procedure to simulate springback and die wear.
  - Improve control of springback and die wear.
  - Optimize lubricant/die combinations for AHSS.
  - Maintain common lubricants among automotive companies and steel suppliers.
  - Conduct a study to examine wear rates of different die materials.

Approach

- Compare the die wear rate with various HSS, AHSS, and lubricants.
- Correlate other process indicators such as restraining force, temperature, and contact area to wear on the draw beads.
- Correlate the data with the friction test results from Phase 1.
- Build on the extended knowledge gained in Phase 1 and Phase 2. Phase 2 established a baseline of wear data from three sheet steel materials, and two lubricants, with one die material.

Accomplishments

- Completed Phase 1 report "Enhanced Stamping Performance of High Strength Steels with Tribology."
- Completed Phase 2 report "Effect of Stroke Length and Penetration on Die Wear."

- Used steel coils of galvannealed AKDQ, HSLA340, and DP600 supplied by partner companies. The material is used in the wear tests for Phase 3.
- Collected data for the eight test conditions.
- Completed Phase 3 report "Enhanced Stamping Performance of High Strength Steels with Tribology—Report on Phase 3 Testing."

Future Direction

- Develop wear rate model to predict die life.
- Gather wear test data to substantiate model.
- Correlate model with production data as AHSSs come into production.

Progress Report

Phase 3 of this study examines die wear for three different sheet steel materials on three die surface treatments to understand how die life will be affected with advanced high-strength steels (AHSS).

Stamping die design, development, and buyoff represents a considerable portion of the cost and time in product development for the automotive industry. Yet, after the dies go into production, little is known of how die wear affects part quality and production costs. Because die wear is mainly a function of die temperature and contact stress, previous work by this project team suggests that die wear with AHSS will bring production issues to the forefront. Indeed, early experiences implementing DP500 and DP600 show that die wear will need to be addressed.

Findings in Phase 1 (2001) and Phase 2 (2002) of this project highlighted potential issues with the stamping of AHSS. Drawbead tests revealed much higher restraining forces and elevated temperatures with DP600 over aluminum-killed draw quality (AKDQ) and high-strength low alloy (HSLA). How will the higher contact stress and elevated part temperature associated with AHSS affect die life? How will part geometry be affected? What process changes such as lubricants and die treatments can be used to increase die life and improve process capability?

The Die Wear Test was developed by TribSys, Inc., to measure die wear at production volumes and rates. Phase 2 showed measurable and significant wear rates for different process variables (sliding distance and bead penetration). The Phase 3 plan was to compare die wear of DP600 with HSLA and AKDQ galvannealed sheet steels. For each test, one coil, or the equivalent of 9,000 parts, was processed.

Data collection and analysis on this scale of experiment poses many challenges. The experimentalist must balance the "purity" of the laboratory with the "reality" of the production environment. Environmental factors, test interruptions, and material variability are factors that are representative of production. These factors raise statistical variance and complicate analysis.

Temperature and restraining force data were gathered throughout the tests and compared to wear indicators on the dies. The die temperatures obtained should not be considered absolute measurements because many factors will affect heat buildup in a die. Rather, these data can be used to evaluate relative effects of changes in sheet materials and dies.

Restraining force was highest for the DP600 sheet, particularly on the flame-hardened dies where restraining force measurements were 27% greater than the AKDQ and HSLA. Die surface treatment had a significant effect on restraining force with the DP600 and HSLA showing opposite trends (see Figure 1). The opposite trends may be related to differences in the galvannealed coating. The HSLA (and AKDQ) galvannealed produced more powder on the dies, while the DP600 galvannealed coating tended to pickup, rather than form, powder. This difference would be a critical consideration when drawing conclusions from the results.

The higher restraining force was accompanied by a corresponding increase in sheet and die temperature. Interestingly, die temperature and strip exit temperature varied inversely. This was observed where poor heat transfer conditions prevented the

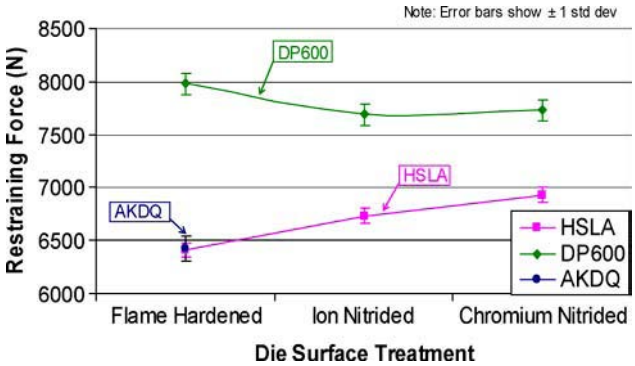

Figure 1. Average restraining force vs different die surface treatment and steel sheets.

heat in the strip from moving to the die. The resistance to heat transfer appeared to result from the chromium nitride coating (a ceramic) or zinc pick-up that prevented continuous contact of the sheet with the die.

Contact area on the strip and die were measured. Strip contact area measurements with the galvannealed coatings were difficult and unreliable. Die contact was clear, and significant differences in contact between the sheet material types were observed.

As strip strength increased, contact decreased (see Figure 2). This decrease has several sometimes opposite effects on lubrication and die wear:

1. Contact stress increases—increasing tendency for wear.
2. Heat transfer decreases—however local temperatures that drive thermal stress may increase and heat in part is not dissipated.
3. Lubricant performance should improve with the reduced sliding distance and the opportunity for lubricant replenishment.

The extended testing (18,000 parts) on the chromium nitrided dies (the best performing surface treatment) with the DP600 sheet shows the

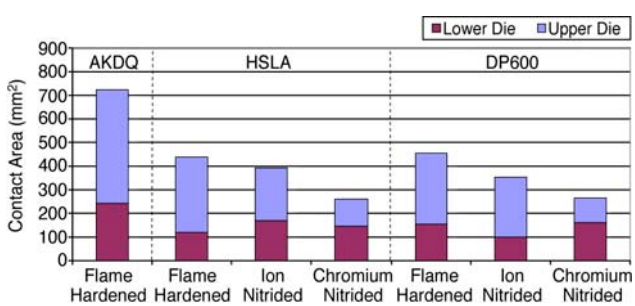

Figure 2. Contact area on die surface.

restraining force initially decreasing and then increasing after 14,000 parts (see Figures 3 and 4). This rise suggests the coating may be beginning to wear at this point. Further examination with the scanning electron microscope would confirm this hypothesis.

Strip curl is a good indicator of potential for sidewall curl and, in some cases, springback. The greatest variation in strip curl was between materials with DP600 showing much higher strip curl than either the AKDQ or the HSLA (see Figure 5). Strip curl varied throughout the tests with changing die conditions and could be related directly to changes in restraining force brought about by changes in die radius or friction. The most dramatic change was with the AKDQ on the flame-hardened dies where curl changed from a 600-mm radius to 300-mm radius. This change was attributed to the change in die radius as a result of wear. These results confirm findings in Phase 1 where strip curl in the drawbead simulator was observed and measured for a large number of materials, lubricants, and die surface treatments.

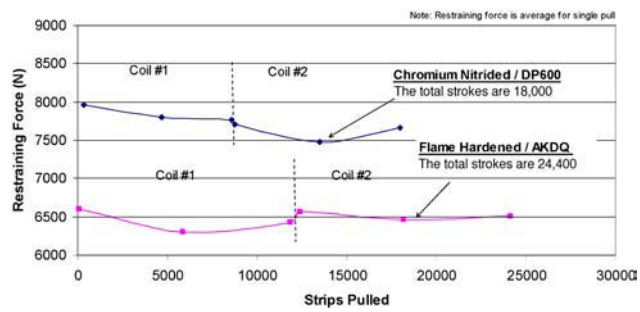

Figure 3. Extended die wear test—restraining force.

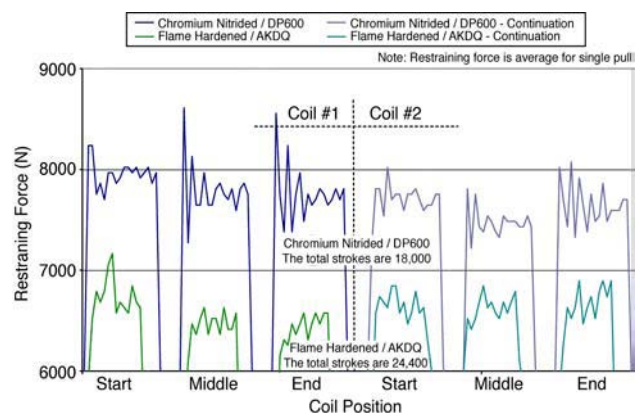

Figure 4. Extended die wear test—restraining force profiles.

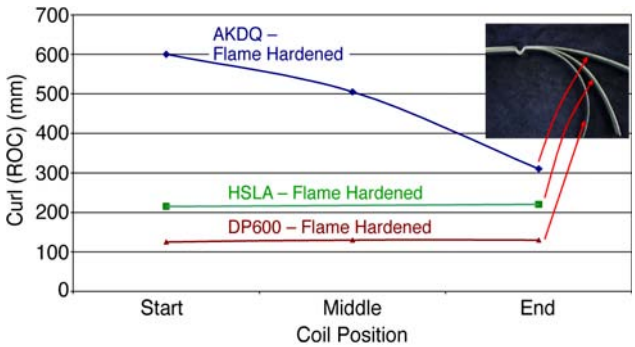

Figure 5. Strip curl with AKDQ, HSLA, and DP600 on flame-hardened dies.

Analysis of the data shows that die wear and process conditions with DP600 differs dramatically from HSLA and AKDQ (Figure 6 and Figure 7). This difference will affect AHSS implementation

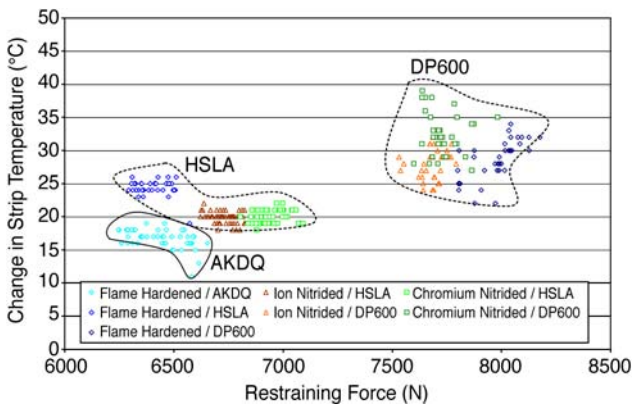

Figure 6. Restraining force vs the changes of strip temperature.

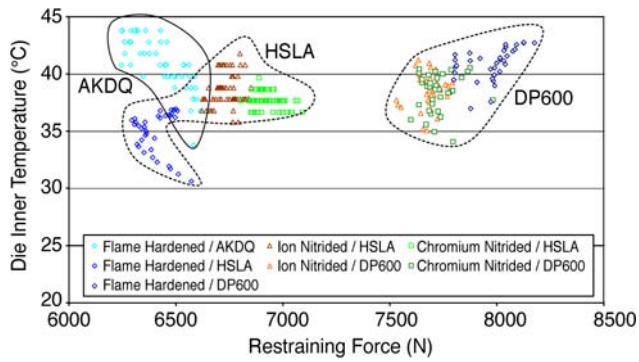

Figure 7. Restraining force vs die inner temperature.

from die design to production. Further, the analysis shows that die life, process capability, and part geometry will be affected by process factors such as sheet material choice, die material and surface treatment, and production run size.

The results of Phase 1 indicated that lubricant was a significant factor in process control. A logical question arises from Phase 3 results: how would choice of lubricant affect die life and process capability?

Future Work

The plan for 2005 includes a study to investigate wear behavior of AHSS with the goal of developing a basic wear model. Key parameters have been identified, and the choice of die materials and coatings has been completed. The Department of Energy will examine 6 variables at 2 levels for a total of 16 tests.

J. Lightweight Closure Panels Project

Principal Investigator: Gene Cowie
Auto/Steel Partnership
2000 Town Center, Suite 320, Southfield, MI 48075-1123
(248) 945-4779; fax: (248) 356-8511; e-mail: gcowie@a-sp.org

Chairman: Paul Geck
Ford Motor Company, Scientific Research Laboratory
2101 Village Road, Dearborn, MI 48124
(313) 323-0014; fax: (313) 390-0514; e-mail: pgeck@ford.com

Technology Area Development Manager: Joseph A. Carpenter
(202) 586-1022; fax: (202) 586-1600; e-mail: joseph.carpenter@ee.doe.gov
Field Technical Manager: Philip S. Sklad
(865) 574-5069; fax: (865) 576-4963; e-mail: skladps@ornl.gov

---

Contractor: U.S. Automotive Materials Partnership
Contract No.: FC26-02OR22910

Objectives

- Reduce the mass of a vehicle door outer panel by 20% at a maximum cost increase of $0.70/lb ($1.55/kg) of mass saved.
- Compare the results of computer-aided engineering (CAE) formability studies with the results of stamping try-outs.
- Develop a "tool kit" to guide in the design of door and body panels, which currently use mild steels, to use steels that have higher strength but lower formability.

Approach

- Select several grades of steel that could potentially meet the objectives.
- Run CAE studies on the base material and the selected grades in several thicknesses. The CAE tests include formability and performance criteria such as stiffness and dent resistance.
- Build soft tooling and perform stamping trial runs.
- Assemble the outer panels to inner panel assemblies for stiffness and dent testing for those grades and thicknesses that produce satisfactory panels.

Accomplishments

- Completed CAE simulations and selected two grades of steel: BH250 (bake hardenable) and DP500 (dual phase).
- Built "soft" (Kirksite, zinc-based alloy) tooling and an assembly fixture (hem buck).
- Performed stamping trials and compared the results with the CAE analyses.
- Identified acceptable panels that are being assembled to inner panel assemblies for subsequent painting and dent testing.

Future Direction

No additional work is scheduled for this project. A final report documenting and summarizing the results of all experiments related to the use of specific grades and gages of door outer materials, including various surface coatings, will be complete by the December 31, 2004. Reporting will be completed by April 1, 2005.

Introduction

In 2000, the Auto/Steel Partnership started the Lightweight Closures Project team with the goal of reducing the door-in-white mass by 25%, while incurring a cost penalty of less than a $0.70/lb of mass reduced ($1.55/kg) and retaining steel as the primary structural material. The new Jeep Liberty front door, which at that time was still in the preproduction phase, was chosen as the baseline. It was chosen because (1) it represented the state of the art in that it used a laser-welded blank for the inner panel, (2) all of the component designs were well-optimized, (3) the overall door architecture was fairly conventional when compared with other candidate doors in the industry, and (4) it was for a sport utility vehicle where mass reductions are particularly desirable.

The two largest mass contributors to the structure of an automotive door are the inner panel (45%) and the outer panel (33%). Significant efforts by the automotive industry to reduce the mass of the door inner panel have led to a de-facto standard tailor-welded blank (TWB). This construction eliminates or minimizes the need for reinforcements at the front of the door by substantially increasing the thickness of the leading edge of the door inner while the remainder of the door inner panel remains at traditional gages.

Most of the initial effort was focused on innovative changes to the door inner architecture. This effort led to the conclusion that, while door inner mass reductions could be achieved in the range of 15 to 20%, the reductions were accompanied by cost increases in the $2.00/lb ($4.40/kg) range.

Preliminary calculations on the door outer panel indicated a potential to reduce its mass by 20% while incurring no additional cost by using advanced high-strength steels, with associated latest generation CAE tools and stamping technology. Therefore the project team redirected its efforts to address the outer panel. The team selected seven of the most capable body design and manufacturing companies in southeastern Michigan to submit quotations. The project team reviewed the proposals based on technical competency, qualifications of key personnel, demonstrated experience, and understanding of the project requirements, qualifications of named subcontractors, and price. Oxford Automotive, which had participated in the door inner panel study, was selected to perform the work.

Discussion

The Lightweight Closure Panels Project Team was selected to include members of auto producers and steel producers with extensive experience in forming sheet steel body panels. This membership enabled the team to narrow the selection of steel grades for the outer panel study to two: BH250 (bake hardenable) and DP500 (dual phase). Both grades have been developed to give strengths significantly higher than mild steels, which are commonly used in body panels, while retaining a high degree of formability. Both grades had been laboratory tested extensively so that all of the material properties essential to forming operations were documented.

The existing production panel is being made from mild steel with a thickness of 0.74 mm (0.0291 in.). Three thicknesses were selected for the test materials: 0.7 mm (0.0275 in.), 0.65 mm (0.0255 in.) and 0.6 mm (0.0235 in.). Several different types of corrosion-resistant surface treatment were analyzed, because surface treatment affects formability.

The computer-aided engineering (CAE) forming analyses began with the baseline material to confirm the parameters of the CAE process. When the higher strength materials were run, several areas of the panel with “crisp” styling features (sharp radii) were identified as potential trouble spots. The major problems occurred at the beltline (immediately below the window opening) and mirror pocket (slight recess into which the outside mirror fits). To relieve these problems, the team agreed on two minor changes: an increase in the bending radius on

the beltline feature and a reduction in the depth of the mirror pocket. The beltline modification constituted a minor styling change. The mirror pocket could result in no styling change by slightly modifying the mirror.

Numerous tests were run and discussed by the team at regular meetings. When the simulations indicated that there was a reasonable chance for several of the test materials to be formed, soft tools (Kirksite, zinc alloy) were built, and the work was transferred to a subcontractor who specializes in die try-out. This company's expertise enabled them to identify problem areas on the panels and recommend appropriate modifications to the stamping process to correct the problems.

The panels were visually inspected by all involved parties and checked for springback. Those that were considered acceptable were set aside for assembly, painting, and display. A typical panel that was successfully formed is shown in Figure 1.

When panels were not successfully formed in the baseline design, the die was successively modified to the design variations agreed upon by the project team and rerun.

In addition to the soft tooling, a hem buck was prepared to assemble the outer panel to production inner panels, which were an in-kind contribution by DaimlerChrysler Corporation. The acceptable panels were subsequently assembled to form a complete door structure (minus glass, window regulator, trim, etc). The assemblies are scheduled for painting and dent testing, which will conclude the build-and-test portion of the program.

Figure 1. Typical door outer panel before trimming.

Conclusions

- Two grades of steel, BH250 (bake hardenable) and DP500 (dual phase) can be successfully formed into door outer panels in gauges less than 0.74 mm (0.029 in.).
- CAE programs can be used as first-order analysis tools to guide the selection of sheet steel grades (material, thickness, and surface coating) to be formed in stamping dies.

Appendix A. ACRONYMS AND ABBREVIATIONS

A/SP	Auto/Steel Partnership
ABP	acrylobenzophenone
ABS	acrilonitrile-batadiene-styrene
ACAP	Automotive Corrosion and Prevention Committee
ACC	Automotive Composites Consortium
ADFG	advanced drive file generation
AES	auger electron spectroscopy
AFS	American Foundry Society
AHSS	advanced high-strength steel
AISIS	American Iron and Steel Institute
AKDQ	aluminum-killed draw-quality
Al	aluminum
ALCOA	Aluminum Company of America
ALM	Automotive Lightweighting Materials
ALTC	Automotive and Light Truck Committee
AMD	Automotive Metals Division
AN	acrylonitrile
ANL	Argonne National Laboratory
APAW	aluminum plasma arc welding
APC	American Plastics Council
ARC	Automotive Research Consortium
AS	adaptive simulation
ASTM	American Society for Testing and Materials
BCC	body-centered cubic
BCF	Bead Correction Factor
BH	Bake Hardening
BH	blank holder
BHF	blank holder force
BIW	body-in-white
BLR	bolt load retention
CAD	computer-aided design
CAE	computer-aided engineering
CAFE	corporate average fuel economy
CANMET	National Resources Canada
CD	compact disk
CFC	carbon-fiber composite
CFD	computational fluid dynamics
CFRPMCs	carbon-fiber-reinforced polymer-matrix composites
CGR	circle grid analysis
CHIP	CIP/sinter/HIP
CIP	cold isostatic pressing
CLM	cast light metal
COV	coefficient of variability
CP	cold pressed
CRADA	cooperative research and development agreement
CVD	chemical vapor deposited

CWRU	Case Western Reserve University
CWT	Changing World Technologies
DAQ	data acquisition
dc	direct current
DCB	double-cantilever beam
DNS	double-notch shear
DOC	depth of cut
DOE	design of experiment
DOE	U.S. Department of Energy
DP	dual phase
DPF	direct powder forging
DQSK	drawing quality special-killed
DRIFT	Direct Reinforcement Fabrication Technology
DSC	dispersion strengthened copper
DTUL	deflection temperature under load
E	experimental
EDS	electron dispersive x-ray spectroscopy
EDS	energy-dispersive spectroscopy
EDX	energy dispersive x-ray
EFLC	enhanced forming limit curve
EFLD	enhanced forming limit diagram
EGN	exfoliated graphite nanostructure
ELV	end-of-life vehicle
EMF	electromagnetic forming
ENF	end-notch flexure
EWI	Edison Welding Institute
FBL	feedback linearization
FCVT	FreedomCAR and Vehicle Technologies
FE	finite element
FEA	finite-element analysis
FEM	finite-element method
FLC	forming-limit curve
FLD	forming-limit diagram
FP2	Focal Project 2
FP3	Focal Project 3
FY	fiscal year
GASP	grazing angle surface polarimeter
GM	General Motors
HAZ	heat affected zone
HDG	hot dip galvanized
HDPE	high-density polyethylene
HIP	hot isostatic pressing
HIPS	high-impact polystyrene
HPDC	high-pressure die casting
HSLA	high-strength low-alloy
HSS	high-strength steel

HTML	High Temperature Materials Laboratory
HVSC	Huron Valley Steel Corporation
ICS	Industrial Ceramic Solutions
IF	interstitial free
IFU	University of Stuttgart
IIW	International Institute of Welding
ipr	inches per rotation
IR	infrared
IRDI	Industrial Research and Development Institute
ISRM	intermediate strain rate machine
ITP	Industrial Technologies Program
ITP	International Titanium Powders, Inc.
LANL	Los Alamos National Laboratory
LBNL	Lawrence Berkeley National Laboratory
LCCF	low-cost carbon fiber
LFI	long fiber injection
LIBS	laser-induced breakdown spectroscopy
LLDPE	linear low-density polyethylene
LLNL	Lawrence Livermore National Laboratory
LPPM	low-pressure permanent mold
LWFS	lightweight front structure
MA	methylacrylate
MAP	microwave-assisted plasma
MFR	melt flow rate
MIG	metal inert gas
MIT	Massachusetts Institute of Technology
MMB	mixed-mode bending
MMC	metal matrix composite
MMCC	metal matrix cast composites
MOT	maximum operating temperature
MPCC	magnesium powertrain cast components
MPUL	mass per unit length
NAT	N. A. Technologies
NCC	National Composites Center
NCF	noncrimped fabric
NDE	nondestructive evaluation
NDT	nondestructive test
NIST	National Institute of Standards and Technology
NMR	nuclear magnetic resonance
NRCAN	Natural Resources of Canada
NTRC	National Transportation Research Center
NVH	noise vibration harshness
NWR	nuclear magnetic imaging
ODS	oxygen dispersion strengthened
OEM	original equipment manufacturer
OFC	oxygen-free copper

OPT	optimization
ORNL	Oak Ridge National Laboratory
P&S	press and sintering
P4	programmable powder preform process
PAN	polyacrylonitrile
PBDE	polybrominated diphenyl ether
PC	personal computer
PCB	polychlorinated biphenyl
PCD	polycrystalline diamond
PE	polyethylene
PID	proportional integral derivative
PM	powder metallurgy
PMC	polymer matrix composite
PMPRA	powder metallurgy particle-reinforced aluminum
PNNL	Pacific Northwest National Laboratory
PP	polypropylene
PPS	poly (phenylene sulfide)
PRA	particle-reinforced aluminum
PUF	polyurethane foam
PVB	polyvinyl butyral
PVC	polyvinyl chloride
R&D	research and development
RH	relative humidity
ROI	return on investment
ROM	read-only memory
RSW	resistance spot welding
RT	room temperature
RUC	representative unit cell
RVE	representative volume element
SA/RD	sales and administrative/research and development
SAE	Society of Automotive Engineers
SAMPE	Society for the Advancement of Material and Process Engineering
SC	sand casting
SCMD	structural cast magnesium development
SE	structuring element
SEA	specific energy absorption
SEM	scanning electron microscope
SENB	single-edge notch bend
sfm	surface feet per minute
SG	specific gravity
SHT	solution heat treatment
SIF	stress-intensity factor
SIMS	secondary-ion mass spectroscopy
SLS	single-lap shear
SMC	sheet molding compound
SNL	Sandia National Laboratories
SOC	substance of concern
SOM	solid-oxygen-conducting membrane

SPR	self-piercing rivet
SRI	Southern Research Institute
SRIM	structural reaction injection molding
STL	sound transmission loss
SUV	sport utility vehicle
TCM	technical cost model
TDM	Troy Design and Manufacturing
TEM	transmission electron spectroscopy
TGA	thermo-gravimetric
TMAC	Test Machine for Automotive Crashworthiness
TPI	Troy Polymers, Inc.
TRIP	transformation-induced plasticity
TWB	tailor-welded blank
UDRI	University of Dayton Research Institute
ULSAB	ultralight steel auto body
UM	University of Michigan
USAMP	U.S. Automotive Materials Partnership
USCAR	U.S. Council for Automotive Research
UT	University of Tennessee
UTS	ultimate tensile strength
UV	ultraviolet
VRP	Vehicle Recycling Partnership
WF	warm forming
XPS	x-ray photoelectron spectroscopy
YS	yield strength
YSZ	yttria-stabilized zirconia

This document highlights work sponsored by agencies of the U.S. Government. Neither the U.S. Government nor any agency thereof, nor any of their employees, makes any warranty, express or implied, or assumes any legal liability or responsibility for the accuracy, completeness, or usefulness of any information, apparatus, product, or process disclosed, or represents that its use would not infringe privately owned rights. Reference herein to any specific commercial product, process, or service by trade name, trademark, manufacturer, or otherwise does not necessarily constitute or imply its endorsement, recommendation, or favoring by the U.S. Government or any agency thereof. The views and opinions of authors expressed herein do not necessarily state or reflect those of the U.S. Government or any agency thereof.

Printed on recycled paper

A Strong Energy Portfolio for a Strong America

Energy efficiency and clean, renewable energy will mean a stronger economy, a cleaner environment, and greater energy independence for America. Working with a wide array of state, community, industry, and university partners, the U.S. Department of Energy's Office of Energy Efficiency and Renewable Energy invests in a diverse portfolio of energy technologies.

For more information contact:
EERE Information Center
1-877-EERE-INF (1-877-337-3463)
www.eere.energy.gov